BRNO UNIVERSITY OF TECHNOLOGY
VYSOKÉ UČENÍ TECHNICKÉ V BRNĚ

FACULTY OF MECHANICAL ENGINEERING
FAKULTA STROJNÍHO INŽENÝRSTVÍ

INSTITUTE OF MACHINE AND INDUSTRIAL DESIGN
ÚSTAV KONSTRUOVÁNÍ

TOP-OF-RAIL PRODUCTS IN RAIL TRANSPORT

TOP-OF-RAIL PRODUKTY
V KOLEJOVÉ DOPRAVĚ

HABILITATION THESIS
HABILITAČNÍ PRÁCE

AUTHOR
AUTOR

Ing. Radovan Galas, Ph.D.

BRNO 2024

The important thing is to never
stop questioning.

Albert Einstein

ABSTRACT AND KEYWORDS

Friction in the wheel-rail interface is crucial for the efficiency and safety of railway transport. Two traditional friction management methods, sanding and wheel-flange lubrication, are widely used to address low adhesion, wear, and noise issues. Although these methods have proven effective over decades, issues like corrugation, squeal noise, and rolling contact fatigue still remain. These issues can be mitigated by the top-of-rail friction management approach, which is the focus of this habilitation thesis. The research examines the frictional behaviour of various top-of-rail products under different dosing conditions, their performance under varying operational and environmental conditions, and their behaviour in the presence of water contamination. The findings provide valuable insights into both the advantages and limitations of the top-of-rail friction management approach, offering practical guidelines for optimising this method. Building on these insights, a multi-phase testing methodology was developed to enable comprehensive performance evaluation and enhance result transferability. This methodology also includes the study of track performance parameters under laboratory conditions, which helps reduce the number of time- and cost-intensive field experiments. The findings of this thesis have been published in fifteen peer-reviewed journal articles.

railway; wheel-rail interface; friction modification; top-of-rail products; adhesion

ABSTRAKT A KLÍČOVÁ SLOVA

Tření mezi kolem a kolejnicí je jedním z klíčových faktorů pro efektivitu a bezpečnost kolejové dopravy. V praxi se běžně využívají metody pískování a mazání okolku, které řeší problémy spojené s nízkou adhezí, opotřebením a hlukem. Ačkoliv jsou tyto metody efektivní a prověřené desítkami let praxe, stále existují další výzvy, které je třeba řešit, jako například vlnkovitost, kvílivý hluk nebo kontaktní únava. Pro zmírnění těchto nežádoucích projevů se využívá metoda řízení tření na temeni kolejnice, což je hlavním tématem této habilitační práce. Výzkum se zaměřuje na chování různých typů produktů pro řízení tření na temeni kolejnice v závislosti na aplikovaném množství, jejich výkonnost v různých provozních a environmentálních podmínkách a jejich chování při kontaminaci vodou. Tyto poznatky poskytují přehled o výhodách a omezeních tohoto přístupu a mohou být využity k jeho optimalizaci. Na základě těchto poznatků byla vyvinuta vícefázová metodika testování, která umožňuje komplexní posouzení jejich výkonnosti a zajišťuje přenositelnost výsledků mezi různými pracovišti. Metodika zahrnuje také hodnocení traťových parametrů výkonnosti produktů, což napomáhá snížit počet časově a finančně náročných traťových testů. Výsledky této práce byly publikovány v patnácti odborných článcích ve vědeckých časopisech s recenzním řízením.

železnice; rozhraní kolo-kolejnice; modifikace tření; produkty pro temeno kolejnice; adheze

ACKNOWLEDGEMENT

I would like to sincerely thank Prof. Martin Hartl, Prof. Ivan Křupka, and Dr. Milan Omasta for their invaluable support, guidance, and collaboration throughout my research. I am also very grateful to my colleagues in the Wheel-rail research group at Brno University of Technology for their assistance and involvement. I would like to extend my thanks to all the students I had the pleasure of working with, especially my master's students, for their hard work and dedication.

Special thanks go to the Tribology Research Institute at Southwest Jiaotong University, particularly to Prof. Wen-jian Wang and Assoc. Prof. Haohao Ding, for the opportunity to collaborate with their team and for the time I spent at their institute.

I would also like to acknowledge the many authors of scientific publications whose work has been a significant source of inspiration for my research.

Finally, I am deeply grateful to my girlfriend, Klára, for her unwavering support, motivation, and patience.

AUTHOR'S DECLARATION OF ORIGINALITY

I hereby declare that this habilitation thesis, entitled **'TOP-OF-RAIL PRODUCTS IN RAIL TRANSPORT'**, is my own original work, except where specific references have been made and properly cited.

.....

Author's signature

CONTENT

1	**INTRODUCTION**	**1**
2	**TOP-OF-RAIL PRODUCTS AND THEIR PERFORMANCE**	**3**
2.1	Introduction	3
2.2	The effect of TOR products on frictional properties	4
2.3	The effect of TOR products on corrugation, wear, and RCF	7
2.4	The effect of TOR products on curve squeal	9
2.5	Summary of the literature review and research gaps	12
2.6	Author's contribution	13
3	**TOP-OF-RAIL PRODUCTS IN AN OPEN TRIBOLOGICAL SYSTEM**	**27**
3.1	Introduction	27
3.2	Contaminants Affecting wheel-rail contact	28
3.3	Interaction of Top-of-Rail Products with Contaminants	31
3.4	Summary of the literature review and research gaps	34
3.5	Author's contribution	35
4	**APPROACHES FOR TESTING TOP-OF-RAIL PRODUCTS**	**43**
4.1	Introduction	43
4.2	Rigs for wheel-rail contact research	44
4.3	Laboratory testing of TOR products	44
4.4	Field testing of TOR products	47
4.5	Summary of the literature review and research gaps	50
4.6	Author's contribution	52
5	**CONCLUSIONS AND FUTURE WORK**	**62**
6	**LIST OF FIGURES AND GRAPHS**	**65**
7	**REFERENCES**	**68**
8	**LIST OF ABBREVIATIONS**	**80**
9	**RESEARCH PAPERS**	**81**

1

INTRODUCTION

Railway transportation is crucial for moving goods and passengers over medium distances and within urban areas worldwide. Moreover, with the development of high-speed rail lines, railways have become more competitive even for long-distance travel. This mode of transport offers several key advantages, including environmental friendliness, energy efficiency, and reliability **[1]**. Despite these benefits, several challenges must be addressed to ensure the sustainable development of railway transportation, such as increasing demands for speed, rising axle load requirements, noise issues, and climate change. The interaction between wheel and rail is one of the keys to overcoming these challenges.

Two important contact regions between the wheel and rail are identified: the wheel tread/rail head and the wheel flange/rail gauge corner. Additionally, a third contact region sometimes occurs between the field sides of the wheel and rail, although it is less frequent. These regions operate under significantly different conditions, particularly in terms of slip and contact pressure, each requiring a specific level of friction. For example, a low friction value is desired at the wheel flange/rail gauge corner to minimise wear. Conversely, a medium friction level is preferred at the wheel tread-rail head to enhance traction and braking capabilities.

To achieve these requirements, two conventional friction management methods are widely used: **wheel flange lubrication** and **sanding**, see **Fig. 1.1**. The first method reduces friction at the contact between the wheel flange and the rail gauge during curve negotiation. In contrast, the second method addresses low friction between the wheel tread and rail, typically caused by weather and contamination. Both methods have been tested over decades, proving to be cost-effective, easy to operate, and environmentally friendly.

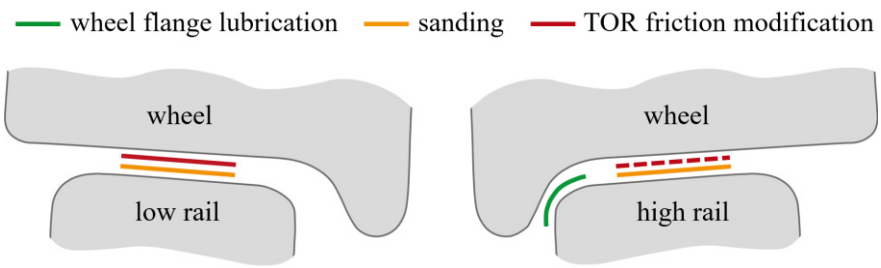

Fig. 1.1 Overview of friction management methods (modified from **[2]**)

Building on these traditional methods, **top-of-rail (TOR) friction management** was introduced in the late 1980s and early 1990s to address short-pitch corrugation issues **[3]**. This innovative approach not only adjusts but also manages friction between the wheel tread and the railhead, maintaining it within the desired intermediate range. Today, various TOR products and application strategies are implemented in rail transport to achieve several benefits, including extended service

life of rails and wheels, which helps reduce maintenance costs **[4]-[6]**. However, the effectiveness of these products is affected by environmental conditions, contaminants, and operational parameters, which significantly vary across railway systems.

Understanding how these factors influence the performance of TOR products is essential for optimising TOR friction management methods. This habilitation thesis, written as a collection of scientific articles published by the author, is structured into three main chapters to expand the knowledge about the TOR friction management approach from multiple perspectives. The first chapter focuses on the different types of TOR products and their effectiveness in areas such as frictional performance, wear reduction, and noise mitigation. The second chapter examines the impact of weather conditions on TOR product performance, and the final chapter introduces a newly developed multi-phase methodology for TOR product testing.

2

TOP-OF-RAIL PRODUCTS AND THEIR PERFORMANCE

2.1 Introduction

As mentioned in the previous chapter, TOR friction management was initially developed to address short-pitch corrugation and the associated noise issues **[3]**. That pilot study employed a solid TOR product, hereafter referred to as **solid sticks**, which was applied from the vehicle to the wheel treads. Subsequently, several types of liquid TOR products were developed. In contrast to solid sticks, these liquid products can be applied in two different ways: directly from a vehicle, similarly to solid sticks, or using track-mounted systems. These track-mounted systems are usually installed in areas where issues such as corrugation and squealing noise frequently occur. In such cases, TOR products with higher viscosity or a higher NLGI grade are generally preferred. Liquid TOR products can be classified based on their base medium into two groups: **friction modifiers** (water-based products) and **TOR lubricants** (oil- or grease-based products) **[7]**. The second group also includes the so-called **TOR hybrids**, which have both a water and oil base. However, in this thesis, TOR hybrids are considered as a third, separate group to avoid confusion between oil- and grease-based products (TOR lubricants) and TOR hybrids.

Another key aspect of TOR products is their composition, which typically includes several types of solid particles **[8]-[10]**. These include particles for friction modification (PFM), such as magnesium silicate or zinc oxide, as well as solid lubricants like molybdenum disulfide or graphite. Other solid particles, such as talc, are used as rheological control or binding agents in friction modifiers. The most significant difference between friction modifiers and TOR lubricants lies in the role of the base medium. In the case of friction modifiers, water primarily acts as a transport medium, which is necessary for dosing and spreading the product along the track. Once the water evaporates, a thin, dry, frictional layer of solid particles remains on the surfaces. In contrast, the oil or grease contained in TOR lubricants remains on the surfaces with solid particles **[11]**.

Because of these differences, friction modifiers and TOR lubricants are often referred to as **drying** and **non-drying materials**, respectively **[7]**. A boundary lubrication regime typically occurs for drying materials and solid sticks, while both boundary and mixed lubrication regimes can occur for non-drying materials, as depicted in **Fig. 2.1(a)**. It is important to note that full-film lubrication can occur under certain operating conditions, especially when an excessively high amount of non-drying materials is applied **[11]**. As a result, accurate dosing is required to prevent undesired full-film lubrication, as this regime can lead to a significant drop in friction.

Although various types of TOR products exist and have different application and dosing requirements, they should all provide similar frictional properties. According to **[12]**, TOR products

should meet two key frictional properties to achieve the expected benefits of TOR friction modification:

- Provide an intermediate level of friction, typically around 0.35. The value may vary depending on rail characteristics and the type of contaminants present. For example, the intermediate range in **[13]** is defined from 0.2 to 0.4.
- Exhibit a positive creep curve beyond the saturation point, meaning the coefficient of friction (CoF) increases with rising sliding velocity or creep (slip), as shown in **Fig. 2.1(b)**.

Achieving these frictional properties is crucial for obtaining the expected benefits, such as noise mitigation **[14]**, reduced or suppressed corrugation development **[15]**, decreased wear and rolling contact fatigue (RCF) **[6]**, and fuel savings **[16]**.

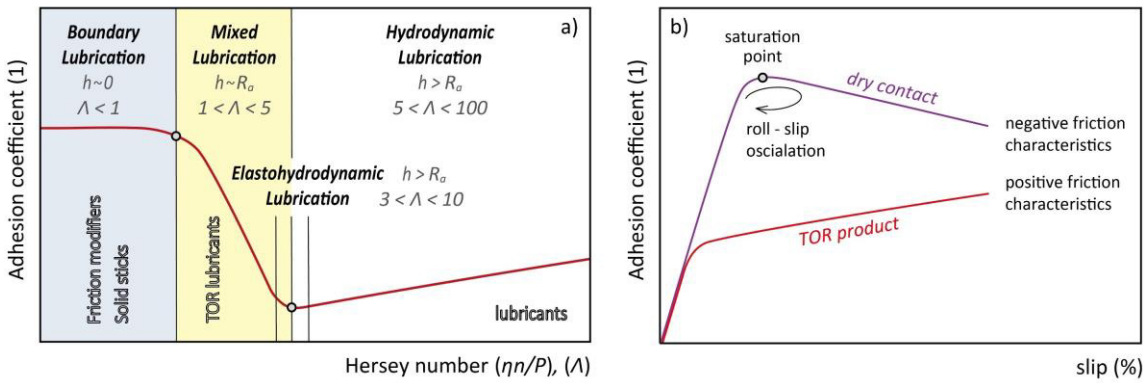

Fig. 2.1 Expected behaviour of TOR products in terms of **(a)** lubrication regimes and **(b)** creep curve (modified from **[2]**)

2.2 The effect of TOR products on frictional properties

In 2002, Japanese researchers published pilot studies investigating the ability of friction modifiers to provide an intermediate level of friction and a positive trend in the creep curve **[17],[18]**. Matsumoto et al. **[17]** used a scaled roller stand to examine creep curves in both longitudinal and lateral directions under dry conditions and with the application of a friction modifier. While a negative trend in the creep curve was observed in both directions under dry conditions, the presence of the friction modifier changed this negative slope to a positive one in both directions. Based on these findings, the authors concluded that this friction management approach may be suitable for reducing noise and corrugation.

In the same year, Tomeoka et al. **[18]** used a two-roller-rig machine to investigate the effect of a friction modifier on the creep curve and its development with an increasing number of test cycles. Additionally, two different application strategies were tested: painting and spraying. Both strategies demonstrated that the tested friction modifier could produce a positive trend in the creep curve and maintain an intermediate level of friction. However, low friction values (around 0.1) were observed during the initial test cycle, particularly when the friction modifier was applied by painting, as depicted in **Fig. 2.2(a)**. These low friction values were almost avoided when the friction modifier was applied by spraying, as the CoF was low only for low slip values, as shown in **Fig. 2.2(b)**. Based on these findings, the authors developed an on-board system, which was subsequently tested on both tangent tracks and tight curves. In these field tests, the friction modifier was sprayed onto

the rail using nozzles mounted on the last bogie of the trains. The results showed that the friction modifier substantially reduced tangential and vertical forces on the tested curve sections.

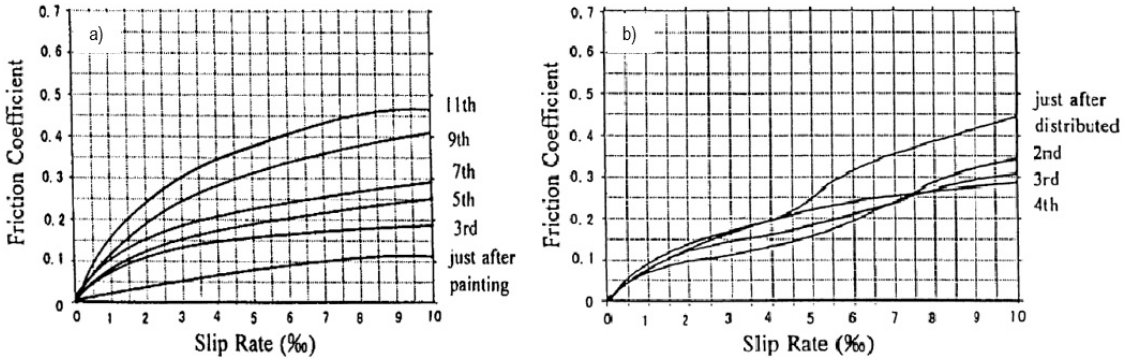

Fig. 2.2 Effect of a friction modifier on creep curve for **(a)** painted and **(b)** sprayed application **[18]**

Later studies also confirmed the ability of friction modifiers to provide an intermediate level of friction **[19]** and a positive creep curve trend **[20]**. In addition to research testing the frictional performance of commercial friction modifiers, a study conducted by Galas et al. **[22]** focused on the effect of friction modifier composition on adhesion. The results revealed that even non-complex substances (two- or three-component substances) could provide the desired frictional behaviour. Furthermore, the study compared the performance of different compositions in both wet and dry states, as this factor is important for friction modifiers that need to perform effectively under both conditions. The study also highlighted the importance of drying, showing that a sharp drop in adhesion can occur during the transition between wet and dry friction layers. This comparison further showed that substances with a suitable chemical composition did not cause low adhesion issues in the dry state. Additionally, it was found that friction modifiers, whether wet or dry, are less dependent on the amount applied compared to TOR lubricants, as described below.

These findings have been recently confirmed by a study that employed both experimental and numerical approaches to investigate the performance of friction modifiers for several applied amounts **[23]**. The simulation results showed that the peak coefficient of traction (CoT) decreased from 0.21 to approximately 0.08 as the applied amount increased from 16 mL/mile to 2048 mL/mile, representing an overdosing situation. These results indicate that even when an extremely large amount of friction modifier is applied, the CoT does not drop as critically as for TOR lubricants (described below).

In contrast to the extensive research conducted on friction modifiers, studies on TOR lubricants have mainly received attention in recent years. Galas et al. **[24]** published one of the first studies on TOR lubricants, examining the performance of two commercial products using a ball-on-disc tribometer. The study revealed that TOR lubricants can provide an intermediate level of friction when applied in optimal amounts, as shown in **Fig. 2.3(a)**. However, TOR lubricants had a negligible effect on the coefficient of adhesion (CoA) when the applied amount was below the optimal, while larger amounts resulted in low adhesion conditions. These results indicate that the frictional behaviour of TOR lubricants is highly dependent on the amount applied. The risk of low adhesion conditions with excessive TOR lubricant amounts was confirmed using Stribeck tests, as depicted in **Fig. 2.3(b)**. At very low speeds, the CoA fell within the range of 0.03 to 0.09; at higher speeds, it was even below 0.02.

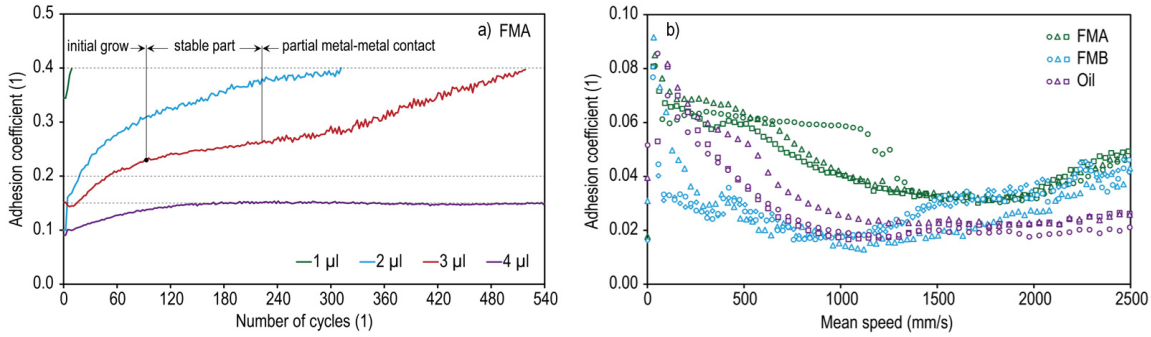

Fig. 2.3 (a) Effect of TOR lubricant amount on the friction curve; **(b)** Stribeck curves for excessive amounts of TOR lubricants and oil **[24]**

Oomen et al. **[25]** reached similar conclusions while studying the effect of three oil-based TOR products on CoA under varying speeds using a horizontal twin-disc machine. As speed increased, CoA dropped sharply to values below 0.02, indicating a transition to a different lubrication regime. Even at low speeds and high slips, CoA remained significantly reduced for several cycles after product application. The risk of low adhesion was further confirmed by Liu et al. **[26]** and Sanchez et al. **[27]**, who examined the impact of TOR lubricants on CoA. While their findings demonstrated the ability to mitigate a negative creep curve trend, CoA values remained below 0.1, even at maximum slip levels, as shown in **Fig. 2.4**. In contrast, Seo et al. **[28]** demonstrated that both key parameters, a positive trend of the creep curve and an intermediate level of friction, can be achieved with the proper application of a TOR product. However, it is important to note that the study used a TOR hybrid containing both water and oil.

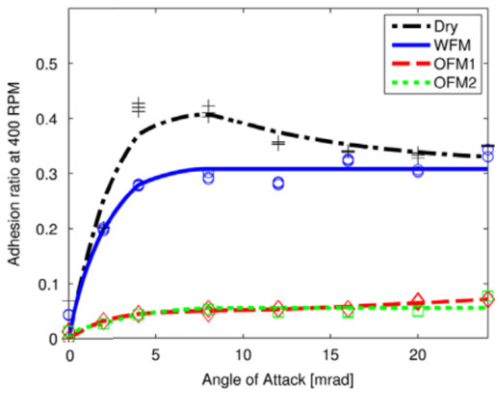

Fig. 2.4 Creep curves for dry contact, contact treated with the friction modifier, and contact treated with TOR lubricants **[26]**

One of the most recent and comprehensive studies, published by Gutsulyak et al. **[29]**, examined the performance of three different types of TOR products using a twin-disc machine. This study specifically tested two friction modifiers, a hybrid TOR product and a TOR lubricant. The findings align with previous research, showing that low adhesion conditions were observed when the contact was treated with the TOR lubricant, whereas an intermediate adhesion level was achieved for the other tested products.

In the case of field studies, Galas et al. **[30]** conducted a series of tram braking tests to evaluate the effect of different amounts of TOR lubricant on braking distance. They found that applying a small amount, less than that recommended by the manufacturer, resulted in a negligible change in braking distance. However, with larger amounts, a significant increase in braking distance was

observed. Additionally, these braking conditions were accompanied by wheel sliding, causing the formation of flat spots on the wheels, which are highly undesired as they increase vibration and noise levels **[31]**. The tendency toward low adhesion conditions following the application of a TOR product was later confirmed by another field study conducted by Khan et al. **[32]**, who reported a reduction in braking capacity. Furthermore, tests conducted with excessive amounts of the product led to a significant drop in friction measured by a hand push tribometer.

Since 1992, when Kalousek et al. **[3]** published a pioneering study on solid sticks, only a limited number of studies have focused on the performance of these solid products. Examples of these studies are investigations from the University of Sheffield, which aimed to determine whether the application of a solid stick poses risks to wheel-rail isolation **[33],[34]**. The findings showed that the tested solid stick did not increase contact impedance, suggesting it would not negatively affect the functionality of track circuits used to detect vehicles. Additionally, the results of this study demonstrated that a solid stick can provide an intermediate level of friction without causing an initial sharp drop in the CoF, as shown in **Fig. 2.5**. The ability of solid sticks to provide an intermediate level of friction was later demonstrated by Velez et al. **[35]**, who compared the performance of a commercial product with two custom-made solid sticks. Although some tested solid sticks exhibited a positive creep curve, this positive trend was also observed under dry contact conditions, suggesting that the results may not provide clear information about the shape of the creep curve.

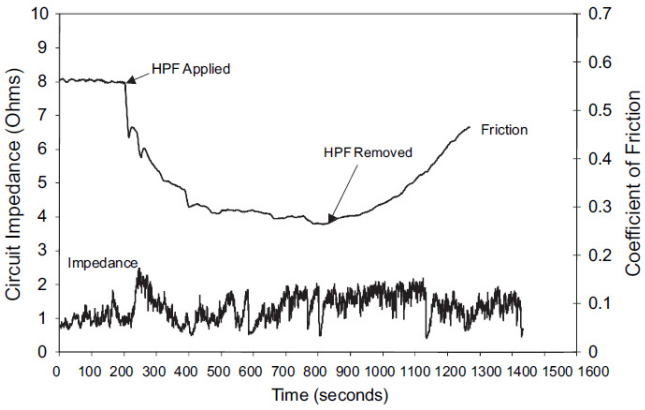

Fig. 2.5 Effect of a solid stick on impedance and CoF **[33]**

2.3 The effect of TOR products on corrugation, wear, and RCF

The field study conducted by Kalousek et al. **[3]** demonstrated that the application of a solid stick can suppress the development of short-pitch corrugation. This phenomenon was extensively studied between 2000 and 2010, with several studies confirming the positive effects of friction modifiers in reducing corrugation development across various railway systems **[36]-[38]**. Egana et al. **[36]** applied a friction modifier using a wayside system near a curved section of a commuter line where the inner rail was corrugated. In this study, the rail was first ground, and then a friction modifier was applied for 19 months. During this period, no corrugation development was observed. However, once the friction modifier application was stopped, the corrugation amplitude increased almost immediately. Over the next 22 months, without the friction modifier application, the peak corrugation amplitude increased from 0.05 mm to nearly 0.18 mm. These results demonstrated the ability of the friction modifier to suppress or at least significantly mitigate corrugation

development. Supporting these findings, two comprehensive studies by Eadie et al. **[37]**,**[38]** investigated the impact of friction modifiers on short-pitch corrugation, with experiments conducted on various railway systems, including metro, tram, and light rail. These studies were carried out on tracks with different conditions, such as new, corrugated, and worn tracks, as well as on various types of track structures, including concrete sleepers with ballast and embedded tracks. The results showed that applying a friction modifier could significantly reduce or even completely suppress corrugation growth across all systems. An example of these results from a metro system is shown in **Fig. 2.6**.

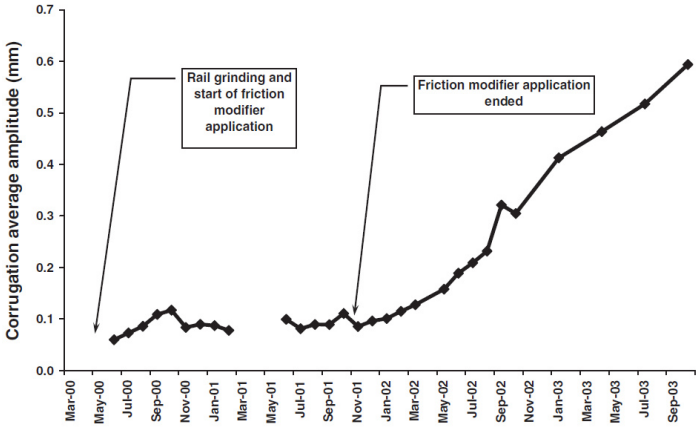

Fig. 2.6 Corrugation development in Metro Bilbao **[37]**

Reducing wear and RCF is another important aspect of using TOR products. Unlike studies on corrugation, research on these effects has primarily been conducted in laboratory conditions. Two of the most relevant studies on this topic were conducted by Eadie et al. **[39]** and Stock et al. **[40]**, which utilised a full-scale wheel test rig to investigate wear and RCF under dry conditions and with the friction modifier application at various intervals. The former study **[39]** revealed that by applying a friction modifier, rail wear was eliminated on both the gauge corner and the top of the rail, as shown in **Fig. 2.7(a)**. Surface analyses indicated a significant reduction in RCF crack formation, with the rail surface becoming significantly smoother compared to untreated conditions, as evidenced by **Fig. 2.7(b)**. These results were supported by modelling, which demonstrated that peak pressure shifted from the ratcheting regime to the elastic shakedown zone when the friction modifier was used. Additionally, sub-surface analyses showed a significant reduction in the depth of the deformed surface layer. The later study **[40]** showed similar positive effects associated with using the friction modifier when a premium rail was used. Additionally, it was found that the application of the friction modifier had no negative impact on the growth of pre-existing cracks.

Hardwick et al. **[41]** later investigated the impact of various materials on pre-existing cracks and wear. The materials tested included both drying and non-drying materials, such as water, friction modifier, low-viscosity TOR lubricant, high-viscosity TOR lubricant, TOR hybrid, and gauge face lubricant. Water and low-viscosity TOR lubricant showed the highest mass loss, whereas the other materials exhibited significantly lower wear rates. Regarding the effect on RCF, the friction modifier performed best, as this drying product did not accelerate crack growth. In contrast, the high-viscosity TOR lubricant, TOR hybrid, and gauge face lubricant slightly interacted with existing cracks, leading to spalling. The low-viscosity TOR lubricant caused the worst surface deterioration, with significant material loss, faster crack growth, and surface delamination. These results suggest that non-drying materials should be avoided in track sections with pre-existing RCF

damage to prevent further crack growth and spalling. In contrast, friction modifiers can be used, as these products minimally impact crack propagation and surface wear due to their quick-drying behaviour.

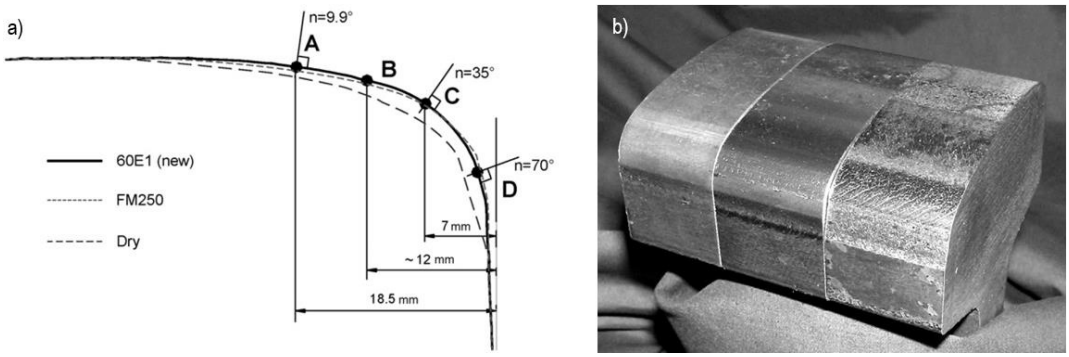

Fig. 2.7 (a) Comparison of rail wear profiles for dry and friction modifier conditions; **(b)** rail surface images (left to right) for new, friction modifier, and dry conditions **[39]**

The articles by Sanchez et al. **[27]** and Seo et al. **[28]** later confirmed and expanded the findings from Hardwick et al. **[41]**. Sanchez et al. **[27]** compared the performance of two TOR lubricants in terms of frictional behaviour (as described in the previous subchapter) and their impact on wear and surface damage. Their analyses revealed that a combination of high slips and the presence of TOR lubricants between the contact bodies caused ratcheting and delamination, suggesting a crack pressurisation mechanism. Seo et al. **[28]** reported similar findings for the TOR hybrid material. The TOR hybrid reduced wear compared to dry conditions; however, the wear rate was higher than in water-lubricated conditions. Concerning surface damage, the most significant damage occurred with the shortest spraying time of the TOR hybrid, representing the lowest applied amount. The authors described this phenomenon as a mixed environment where both wet and dry conditions coexist. In this scenario, traction forces in dry conditions initiate crack formation, while fluid entrapment mechanisms, typical of water conditions, accelerate crack growth.

2.4 The effect of TOR products on curve squeal

Several noise sources are distinguished in railways, including rolling noise, curve squeal, bridge noise, ground vibration noise, aerodynamic noise, and impact noise **[42]**. Curve squeal is one of the most disturbing noises, occurring when a vehicle negotiates sharp curves. High-frequency noise from light rail systems, trams, and subways is a major problem in urban areas, often disturbing nearby residents. Curve squeal can be divided into TOR squeal and flanging noise, with typical frequency ranges of 1000–5000 Hz and 5000–10,000 Hz, respectively **[43]**. The latter is often referred to as grinding noise, as it occurs when the wheel flange rubs against the gauge face of the rail. Two hypotheses have been proposed to explain the generation of TOR squeal: the falling friction mechanism **[44]** and the more recent mode coupling mechanism **[45],[46]**. The paragraphs below provide a brief overview of research focused on reducing TOR squeal, as it is one of the most frequently mentioned benefits of TOR friction management.

The effect of TOR products on TOR squeal has been extensively studied by Eadie et al. **[12],[37],[47]**, who published several papers on this topic. In a 2002 review article **[47]**, they highlighted the importance of the rheological properties of the interfacial layer, which directly influence the trend of the creep curve. They noted that changing the creep curve trend from negative

to positive can prevent roll-slip oscillation, thereby reducing related vibrations and noise. This change was demonstrated using an elastic-plastic rheological model previously published by Hou et al. **[48]**. The study also included a comparison of the noise frequency spectrum for trains passing with and without the application of a solid stick product on the wheel tread. This comparison revealed a significant sound level reduction in the 800-6000 Hz frequency range, including the range of TOR squeal, with noise reductions of up to 20 dB and an average noise reduction between 5 and 10 dB.

The ability of friction modifiers to reduce TOR squeal noise was effectively demonstrated with friction modifiers applied using a trackside applicator **[12]**. Two case studies focused on a light rail system in the USA and a tram line in Japan. In the light rail system, applying the friction modifier through the trackside applicator resulted in an average noise reduction of 12.8 dB, while manual application achieved an even greater reduction of 14.3 dB, as illustrated in **Fig. 2.8**. This reduction was observed at a frequency of 1600 Hz, but noise reduction was evident across the entire monitored frequency range (100-8000 Hz). In contrast, the Japanese tram line showed a significantly lower average noise reduction. The authors attributed this lower reduction to lower speeds during measurements than typical operational speeds. The results highlighted the importance of the application process, as the experiments included two scenarios: applying the friction modifier on both rails or the inner rail only. When applied to both rails, the average noise reduction reached 5.1 dB, while applying the friction modifier only to the inner rail achieved a reduction of just 3.5 dB. The greater noise reduction achieved by lubricating both rails was due to a decrease in flanging noise caused by reduced flanging forces on the high rail.

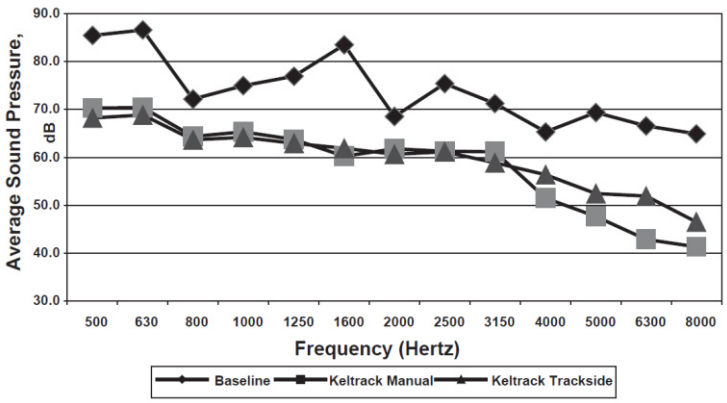

Fig. 2.8 Average sound pressure level vs. frequency for dry and FM conditions **[12]**

Eadie et al. **[37]** published a comprehensive study on the effects of friction modifiers on noise across five European railway systems, including metro, light rail, and tram systems. The study examined variations in track structure, track conditions, curve radius, and operating conditions. Two application strategies for friction modifiers were used: automatic trackside application and manual application. In all cases, a gauge face lubrication system was also employed, either on-board or trackside. The overall results showed noise reductions ranging from 6.3 to 22.8 dB, with an average reduction of 12 dB. The largest reduction was observed in a recently opened tram system, where severe squeal and flanging noise had been identified, while the smallest reduction was recorded in a heavily corrugated metro system. Baseline data (without friction modifier) indicated that gauge face lubrication alone is ineffective at combating noise in curves. In contrast, applying friction modifiers was observed to reduce both TOR squeal and flanging noise in some systems.

Recent field research includes studies carried out in Australia **[49],[50]**. Kwong et al. **[49]** demonstrated the effectiveness of TOR friction management in a high-density tram network in Melbourne, with noise reductions ranging from 11 to 18.5 dB. This corresponds to an approximate 50% reduction in perceived loudness. In contrast, Curley et al. **[50]** revealed unexpected findings that question established theories. Their seven-month study focused on gauge face lubrication and TOR friction modification to reduce noise from freight and passenger trains. This extensive research involved various experiments in which gauge face lubrication and TOR friction modification were applied separately or together on the inner rail, outer rail, or both. The results showed that gauge face lubrication significantly affected tonal wheel squeal rather than the expected impact of TOR friction modification. Additionally, applying friction modifier or TOR lubricant only to the inner rail was proven to be ineffective in mitigating noise.

There are only a limited number of laboratory studies on the impact of TOR products on noise compared to the extensive field studies. The pioneering laboratory study on TOR squeal was published by Liu et al. **[26]**, who used a twin-disc machine to investigate the effect of a friction modifier and two TOR lubricants using a twin-disc machine. This machine allowed for adjustments in the angle of attack (AoA), enabling the study of the creep curve trend. The experiments revealed that squeal noise was not eliminated in all measurements despite the tested TOR lubricants preventing the negative trend in the creep curve observed under dry conditions. Squeal noise persisted, especially at higher speeds and greater AoA values. Based on these findings and the modelling included in the study, the authors suggested that squeal noise may not be suppressed due to the positive slope of the creep curve but rather by reducing the lateral vibration forces that excite the wheel squeal mode. However, at higher speeds and larger AoA, an instantaneous negative creep curve can still exist (see **Fig. 2.9**), which may explain the occurrence of squeal noise under these conditions. The authors mentioned that this phenomenon can also be explained by the mode coupling theory, previously summarized by Pieringer et al. **[51]**.

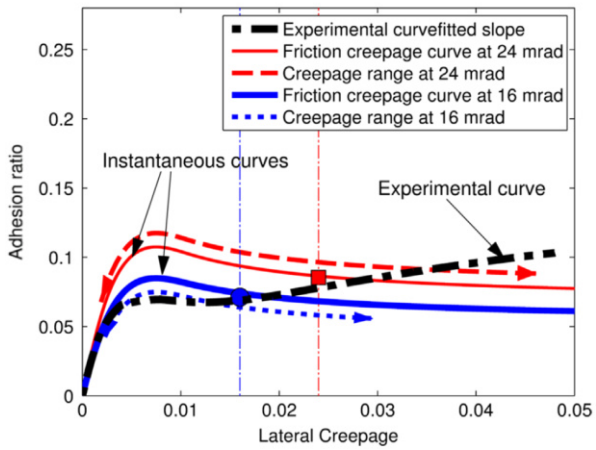

Fig. 2.9 Creep curves and instantaneous behaviour **[26]**

The subsequent study published by Galas et al. **[30]** examined the performance of a commercial TOR lubricant on sound pressure levels using a twin-disc machine. The study tested varying application amounts and an extreme AoA of 4°, simulating conditions in a tram loop. Their investigation demonstrated a significant noise reduction from approximately 100 dBA under dry conditions to 70 dBA with the TOR lubricant application. Furthermore, a strong correlation was found between noise levels and friction data.

The significance of the mode coupling theory was demonstrated in a recent study by Liu et al. **[52]**, who employed a twin-disc rolling contact test rig capable of adjusting both the contact angle and AoA. The findings revealed that the frequency and amplitude of squeal noise closely align with the analytical predictions of the mode coupling model.

2.5 Summary of the literature review and research gaps

Since the first study on friction management was published in 1992 **[3]**, numerous articles have explored the benefits of TOR friction modification. The literature primarily focuses on the behaviour and advantages of friction modifiers, while other types of TOR products have received considerably less attention. These water-based substances provide the desired frictional behaviour **[17]-[20]**, specifically an intermediate level and a positive slope of the creep curve beyond saturation. This behaviour has also been confirmed for TOR lubricants **[22],[25],** TOR hybrids **[28],[29]**, and partially for solid sticks **[33],[34]**. However, many studies indicate that TOR lubricants can cause low adhesion **[22],[29]**,**[53],** which may lead to braking issues **[32]** and extended braking distances **[30]**. This phenomenon is not yet fully understood but may result from overdosing **[32]** or could be related to the composition of TOR lubricants **[24],[54]**. Overdosing can also occur with friction modifiers, although the optimal dose must be exceeded significantly **[23]**. Adhesion issues may arise immediately after application **[20],[55],** as also seen with TOR lubricants, or due to the drying of friction modifiers, particularly during transitions from semi-dry to dry friction layers **[22]**.

One of the main benefits of applying TOR products is the reduction of corrugation and wear. While many field studies have demonstrated the positive effects of friction modifiers in minimising corrugation growth across various railway systems **[36]-[38]**, findings on wear and RCF reduction differ by product type. A decrease in wear was observed across different TOR products **[20],[24],[28],[35],** but their impact on pre-existing cracks was inconsistent. No adverse effects were found for friction modifiers **[41]**, whereas RCF crack growth was noted with TOR hybrids **[28]** and especially with low-viscosity TOR lubricants **[41]** due to the oil wedge effect previously described and observed for other liquids **[56]-[58]**.

Other studies have demonstrated a positive effect of TOR products on noise reduction. Many studies have shown this effect for friction modifiers across different railway systems with varying track and operating conditions **[12],[37],[50]**. The most significant noise reduction was observed on recently opened or unworn tracks, where noise from corrugation did not contribute to the overall noise level **[37]**. These findings also suggested that gauge face lubrication alone can be ineffective in noise mitigation, as TOR friction modification can effectively reduce both squeal and flanging noise **[14],[37]**. However, this contrasts with Curley et al. **[50]**, who found that gauge face lubrication of the outer rail impacts squeal noise levels more than TOR friction modification. Additionally, it was shown that applying a TOR product only to the inner rail was ineffective or less effective for noise reduction **[12]**. Regarding the squeal noise reduction mechanism, the study by Liu **[26]** found that squeal noise may persist even with a positive creep curve, attributing this to an instantaneous negative creep curve or mode coupling theory **[51],[52]**.

Based on this literature summary, the following research gaps (RGs) have been identified:

- **RG1:** While the impact of friction modifier composition was studied in **[22]**, the effect of TOR lubricant composition on frictional behaviour remains unclear, as most studies have utilised commercial TOR lubricants. A clearer understanding of these findings could help

explain several phenomena related to TOR lubricants, including mechanisms that lead to a sharp drop in adhesion following TOR lubricant application **[25]**. Additionally, further exploration of the relationship between frictional performance and the applied amount of TOR lubricants is needed **[24]**. This knowledge could support the development of new TOR lubricants with enhanced frictional properties and lower sensitivity to dosage accuracy.

- **RG2:** Although various studies have compared the performance of different types of TOR products **[29],[41]**, a comprehensive study examining their frictional properties across varying application amounts has not yet been published. As discussed above, the applied amount is crucial for achieving the desired frictional properties **[22],[24]**.
- **RG3:** The effect of solid sticks on wear and surface damage remains unclear, as previous studies have primarily focused on wheel-rail contact impedance **[33],[34]**. The study by Vélez et al. **[35]** partially addresses these issues, providing insights into the impact of solid sticks on wear; however, their effect on RCF has not yet been explored. It should be noted that the findings of Vélez et al. **[35]** were published after this RG was formulated and were unavailable during our research.
- **RG4:** Many studies have explored the performance of various TOR products, focusing on aspects such as retentivity **[20]** and minimum adhesion after application **[55]**. However, these experiments were typically conducted under fixed operating conditions, including specific pressure and slip parameters. This approach does not address how variations in these conditions might influence the performance of TOR products in terms of frictional properties, wear, and surface damage.
- **RG5:** In relation to **RG4**, the impact of temperature on the frictional properties of TOR products and on wear and surface damage has not been fully explored despite their use in environments with a wide range of temperatures.
- **RG6:** The performance of friction modifiers in reducing noise has been extensively investigated in numerous field studies conducted on various tracks **[37],[50]**. However, these studies primarily utilised commercial friction modifiers, so the effect of specific compositions on noise reduction remains unclear. The study **[22]** explored the performance of various water-based substances on adhesion and demonstrated that even simple, non-complex substances can provide the desired frictional behaviour. This raises the question of whether such simple TOR products or even water alone might provide the required friction properties while simultaneously reducing noise.

2.6 Author's contribution

The author of this thesis has been working on the topic of TOR friction modification since 2016, when he published his first article focusing on the behaviour of oil-based TOR products **[24]**. Since then, he has released several articles that expand knowledge about various types of TOR products from multiple perspectives. The eight articles **[59]-[66]** included in this chapter directly build on previous research and fully or partially address the research gaps described above. However, it should be noted that additional research gaps exist that are not mentioned here but are covered in the fifth chapter of the thesis as suggestions for future research directions.

The first article **[59]** contributes to the field by introducing an asperity-based model specifically designed to predict CoA in rolling-sliding contact. This model effectively combines friction from

both asperity contacts and liquids, enabling accurate predictions across various lubrication regimes. The accuracy of the model is validated by a comparison with experimental data for dry and water-contaminated contacts, underscoring its reliability. While the article does not directly address previously identified research gaps, it serves as a valuable tool in subsequent studies **[60],[61]** aimed at predicting CoA in rolling-sliding contact in different lubrication regimes.

The second article **[60]** makes a significant contribution by exploring how the composition of TOR lubricants affects their frictional properties, directly addressing **RG1**. This research develops custom-made TOR lubricants aimed at minimising the initial drop in CoA after application while maintaining a desired friction level for a wider range of applied amounts. This work is crucial for addressing the common issue of frictional performance dependence on applied amounts observed in commercial TOR lubricants. Furthermore, the study enhances understanding of the mechanisms behind the initial CoA drop and the subsequent development of the friction curve by employing the asperity-based model **[59]**.

The third article **[61]** contributes to the field by examining the frictional performance of various TOR products across a wide range of applied amounts, which addresses **RG2**. Additionally, it investigates the effects of elevated temperatures, thus contributing to **RG5** as well. By combining shear properties obtained from torsion rheometer measurements with the asperity-based model **[59]**, the study allows for the prediction of creep curves for different TOR products. This predictive capability is valuable for vehicle dynamic simulations and improves the understanding of the physical processes occurring at the wheel-rail contact.

The fourth article **[62]** contributes to understanding solid stick products by investigating their frictional properties and effects on wear, surface damage, and the generation of RCF cracks, thus addressing **RG3**. By comparing the mechanisms that lead to RCF crack formation in both liquid and solid TOR products, this study enhances knowledge in this area.

The contribution of the fifth article **[63]** lies in understanding how operating conditions affect the performance of the friction modifier, focusing on factors such as contact pressure, slip, and applied amount. The resulting contour diagrams illustrate both potential adhesion risks and changes in product retentivity based on the operating parameters, providing valuable insights for optimising the application of friction modifiers in the field. Furthermore, it highlights the necessity of careful consideration when applying friction modifiers to rails with pre-existing surface damage under heavy haul conditions, as improper use may worsen existing issues. This article addresses **RG4**, although it focuses on only one type of TOR product.

The sixth article **[64]** contributes by providing insights into how temperature changes influence the performance of the friction modifier, specifically regarding retentivity, wear, and the formation of RCF cracks. By examining ambient conditions and extreme temperatures of -40 °C, the study simulates typical and severe conditions in the coldest regions where the TOR friction modification approach is applied. This understanding highlights the limitations of this friction management method, particularly at very low temperatures and in the presence of pre-existing cracks. This article contributes to addressing **RG5**.

The seventh article **[64]** contributes by expanding on the previous work of the author **[22]**, which investigated how the composition of friction modifiers influences their frictional behaviour. This research reveals the relationship among the chemical compositions of friction modifiers, their frictional performance, and their effectiveness in reducing noise generated from contact. Importantly, the study identifies a significant bi-linear correlation between adhesion and noise data, providing valuable insights for managing the application process of friction modifiers based on

actual noise levels. Furthermore, it proposes that spraying water could be an environmentally friendly method for mitigating squeal noise, enhancing the overall strategy for noise reduction in rail systems. This article contributes to addressing **RG6**.

The last article **[66]** contributes to the exploration of water as an eco-friendly lubricant for noise mitigation. It investigates how water can effectively lower noise levels without negatively impacting traction and braking capabilities. However, the research also suggests that more frequent applications may be necessary in field conditions to maintain this effectiveness. By examining these factors, this article addresses **RG6** and enhances the understanding of the role of water in noise management strategies.

The author has contributed to the following papers[1]:

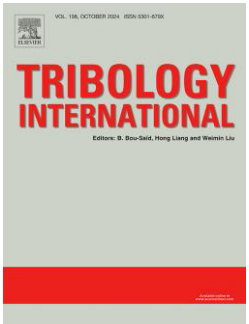

[59] Kvarda D, **Galas R**, Omasta M, Shi L, Ding H, Wang W, et al. Asperity-based model for prediction of traction in water-contaminated wheel-rail contact. Tribology International 2021;157.

Author's contribution	19%
Journal impact factor (2021)	5.620
JIF/AIS Quartile	Q1/Q1
Citations (WoS/Scopus/Google Scholar)	18/20/19

[60] Kvarda D, Skurka S, **Galas R**, Omasta M, Shi L, Ding H, et al. The effect of top of rail lubricant composition on adhesion and rheological behaviour. Engineering Science And Technology, An International Journal 2022;35:796-805.

Author's contribution	20%
Journal impact factor (2022)	5.597
JIF/AIS Quartile	Q1/Q2
Citations (WoS/Scopus/Google Scholar)	15/18/19

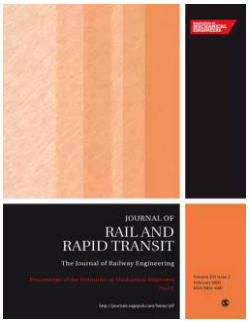

[61] Kvarda D, **Galas R**, Omasta M, Hartl M, Krupka I, Dzimko M, et al. Shear properties of top-of-rail products in numerical modelling. Proceedings Of The Institution Of Mechanical Engineers, Part F: Journal Of Rail And Rapid Transit 2023;237:796-805.

Author's contribution	24%
Journal impact factor (2023)	1.741
JIF/AIS Quartile	Q3/Q2
Citations (WoS/Scopus/Google Scholar)	5/3/5

[1] All listed articles are listed in Chapter 9.

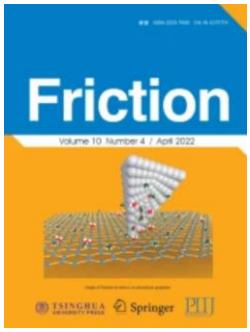

[62] Song J, Shi L, Ding H, **Galas R**, Omasta M, Wang W, et al. Effects of solid friction modifier on friction and rolling contact fatigue damage of wheel-rail surfaces. Friction 2022;10:597-607.

Author's contribution	20%
Journal impact factor (2022)	4.924
JIF/AIS Quartile	Q1/Q1 (D1)
Citations (WoS/Scopus/Google Scholar)	18/17/23

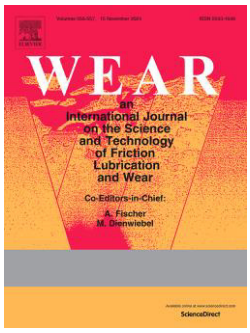

[63] Wang W, Li S, Ding H, Lin Q, **Galas R**, Omasta M, et al. Wheel/rail adhesion and damage under different contact conditions and application parameters of friction modifier. Wear 2023;523.

Author's contribution	15%
Journal impact factor (2022)	5.3
JIF/AIS Quartile	Q1/Q1
Citations (WoS/Scopus/Google Scholar)	7/9/10

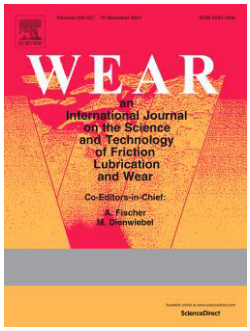

[64] Li J, Wu B, Ding H, **Galas R**, Omasta M, Wen Z, et al. Wear and damage behaviours of wheel and rail materials: Effects of friction modifier and environmental temperature. Wear 2023;523.

Author's contribution	15%
Journal impact factor (2022)	5.3
JIF/AIS Quartile	Q1/Q1
Citations (WoS/Scopus/Google Scholar)	8/8/11

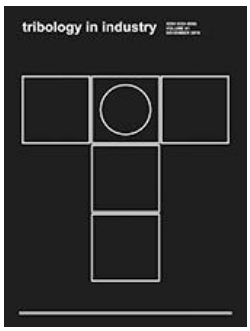

[65] Navrátil V, **Galas R**, Klapka M, Kvarda D, Omasta M, Shi L, et al. Wheel Squeal Noise in Rail Transport: The Effect of Friction Modifier Composition. Tribology In Industry 2022;44:361-373.

Author's contribution	22%
Journal impact factor (2022)	not relevant
JIF/AIS Quartile	not relevant
Citations (WoS/Scopus/Google Scholar)	-/3/4

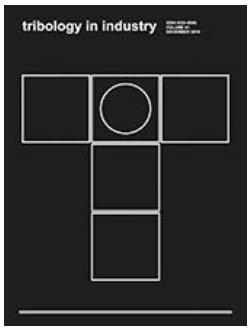

[66] Navrátil V, **Galas R**, Klapka M, Kvarda D, Omasta M. Wheel Squeal Mitigation Under Water Lubrication. Tribology In Industry 2024; 3:418-431.

Author's contribution	25%
Journal impact factor (2024)	not relevant
JIF/AIS Quartile	not relevant
Citations (WoS/Scopus/Google Scholar)	-/0/0

2.6.1 Asperity-based model for prediction of traction in water-contaminated wheel-rail contact [59]

The aim of the first article was to develop a numerical model to predict CoA in the rolling-sliding contact across various lubrication regimes, from boundary to elastohydrodynamic lubrication (EHL). The resulting CoF includes both the CoF associated with surface asperity contact (μ_{BL}) and the CoF related to the lubrication film (μ_{EHL}). Moreover, the dimensionless loads carried by the asperities and by the EHL film are calculated according to Greenwood and Tripp's theory **[67]**, as shown in **Fig. 2.10**.

Friction in asperity contact was calculated using Kalker's simplified theory implemented into the FASTSIM algorithm **[68]**, with the influence of asperities and contaminants modelled as a change in the flexibility parameter, following Rovira et al. **[69]**. Instead of using a limiting CoF, Voce's hardening law was employed to model the contact interface **[70]**. This approach enabled the calculation of the CoF associated with surface asperity contact (μ_{BL}).

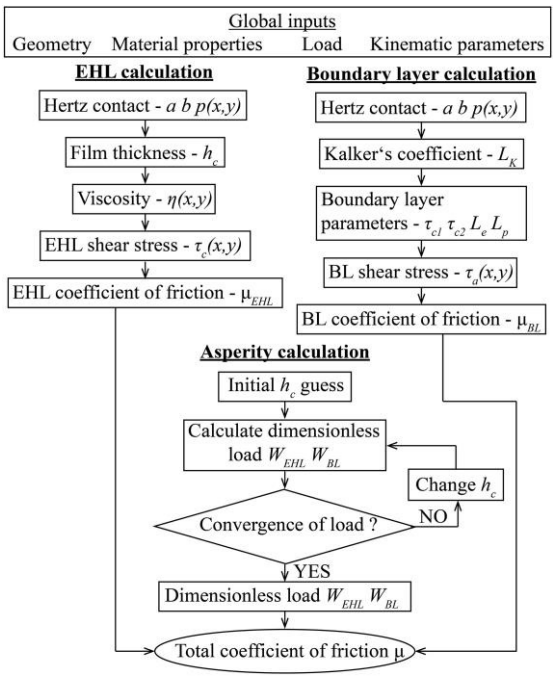

Fig. 2.10 Schematic representation of the proposed model

For fluid film lubrication, the film thickness and viscosity of the liquid are required. The film thickness was determined using a formula for the iso-viscous regime **[71]**, assuming Newtonian liquid behaviour, as the water was used to validate the model experimentally. Once the film thickness was known, the CoF for the lubrication film (μ_{EHL}) was calculated.

Numerical data were compared with experimental results obtained for water-contaminated contact to assess the accuracy of the model. A ball-on-disc tribometer with optical interferometry was used to measure both the CoF and film thickness. The comparison between model predictions and experimental data is shown in **Fig. 2.11**. This figure shows the relationship between film thickness and speed (**Fig. 2.11(a)**), and it also includes typical creep curves (**Fig. 2.11(b)**). These results support the accuracy of the proposed model.

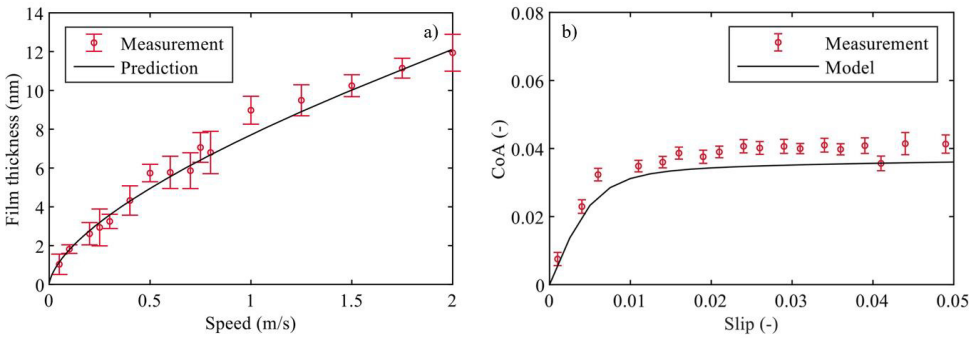

Fig. 2.11 Comparison between predictions and experiments for water-contaminated contact: **(a)** film thickness vs. speed, **(b)** creep curves

2.6.2 The effect of top of rail lubricant composition on adhesion and rheological behaviour: The effect of environmental conditions on adhesion in rolling-sliding contact [60]

The second study focused on optimising the composition of TOR lubricants to maintain a desired friction level for as long as possible. The goals included preventing a significant initial drop in CoA after application and reducing the product performance dependence on the applied amount, thereby mitigating the risk of contact overdosing. Additionally, the study aimed to identify the lubrication regime responsible for the frictional behaviour of TOR lubricants at various stages of the experiments, given that CoA varies significantly during the tests.

For this purpose, both experimental and numerical approaches were employed. The experimental part involved investigating the frictional performance of custom-made and commercial TOR lubricants using a tribometer in a ball-on-disc configuration. Additionally, rheological properties were assessed through experiments conducted with a high-pressure torsion (HPT) apparatus, which enables the investigation of the boundary layer parameters necessary for predicting CoA using the boundary friction model described in **[59]** and illustrated in **Fig. 2.10**. For EHL friction, a previously developed model was adjusted from an iso-viscous to a piezo-viscous regime **[72],[73]** as oil-based products were tested. Unlike **[59]**, this study did not consider the mixed lubrication regime.

The results regarding the composition of TOR lubricants revealed that PFM particles have a dominant effect on their frictional behaviour, with particle hardness as a key property. As shown in **Fig. 2.12(a)-(c)**, the best-performing custom-made substances exhibited stable frictional performance across a wide range of applied amounts. This indicates their resistance to overdosing, which helps avoid long periods of critically low adhesion, a problem commonly found in commercial TOR lubricants. This suggests that a suitable chemical composition can effectively address potential overdosing issues often seen with TOR lubricants. However, even these well-performing substances could not prevent the initial drop in CoA.

A deeper analysis of the results, using the model and data from HPT tests, revealed that the initial drop in CoA results from the EHL regime and an excessive amount of TOR lubricant in contact. This aligns with a previous study **[24]** suggesting that the effect of oil dominates over the influence of particles under fully flooded conditions. Under these conditions, most PFM particles are expected not to enter the contact area. Subsequently, contact starvation begins, causing an increase in CoA

until saturation is reached (0.22 in **Fig. 2.12(c)**). This study found that this saturation value corresponds to the CoA observed in boundary lubrication tests conducted with the HPT apparatus, as indicated by the boundary line (BL Subs. AZ in **Fig. 2.12(d)**), which falls within the desired friction level. The result for the commercial product (TOR A) also corresponds with the predicted values; however, its behaviour is not desirable for this larger amount.

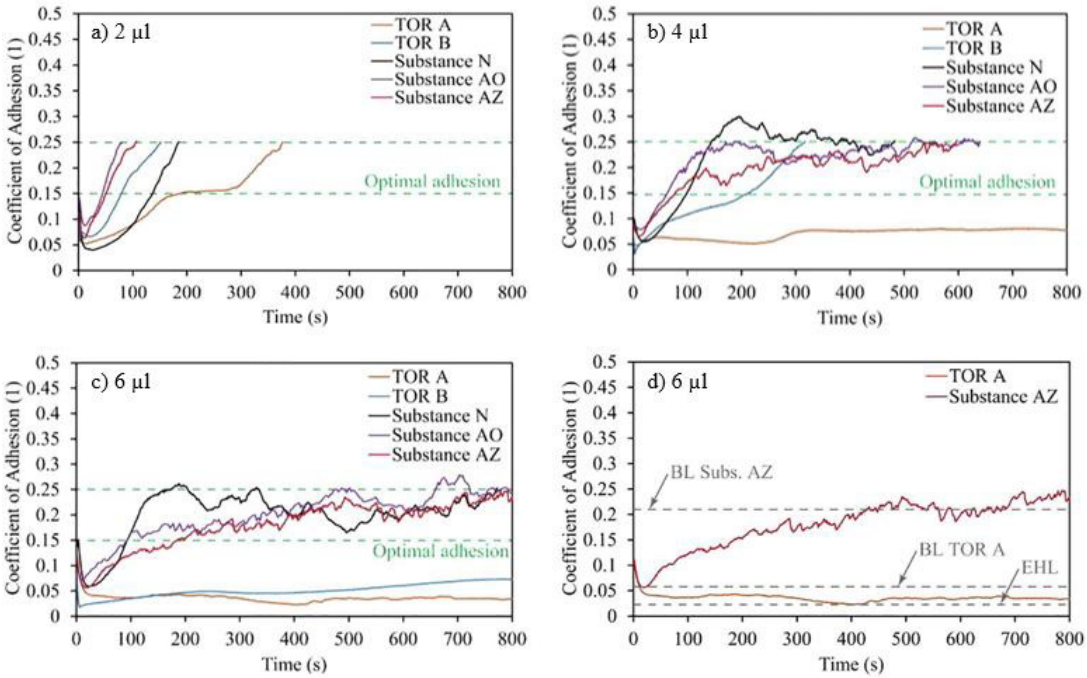

Fig. 2.12 (a)-(c) Comparison of custom-made and commercial TOR lubricants for different application amounts; **(d)** experimental vs. predicted results (dashed line)

2.6.3 Shear properties of top-of-rail products in numerical modelling [61]

This study aimed to compare the performance of various TOR products, specifically focusing on friction modifiers in different states, two TOR lubricants, and a solid stick. The evaluation also considered the effects of applied amount and temperature. All experiments were conducted using the HPT apparatus under pure sliding conditions. The experimental data served as input parameters for the boundary model **[59]** to predict creep curves.

Fig. 2.13(a) summarizes the performance of different TOR products across various applied amounts. Significant sensitivity to the applied amount was observed for all TOR products except the friction modifier in the wet state. While this sensitivity was anticipated for the TOR lubricants (OFM1 and OFM2), unexpected results were noted for the friction modifier in the dry state and the solid stick.

In the case of the dry friction modifier film, the results differ from those reported in **[22]**, where low sensitivity to the applied amount was found. The unexpected drop in the CoF occurred due to a uniform thick layer covering the entire contact area of the specimens, indicating low shear strength. This scenario is unlikely to occur on the track unless a bulk quantity of the product dries at the application point before the first vehicle passes over it.

For the solid stick, the results were likely influenced by the application method. In this study, the solid stick was crushed to a fine powder and then applied. Although this method allowed for precise application, it appears unsuitable, as it may lead to different results compared to applying the product in its original stick form pressed against the surface. These findings suggest that further exploration is needed to fully understand its frictional behaviour in relation to the applied amount.

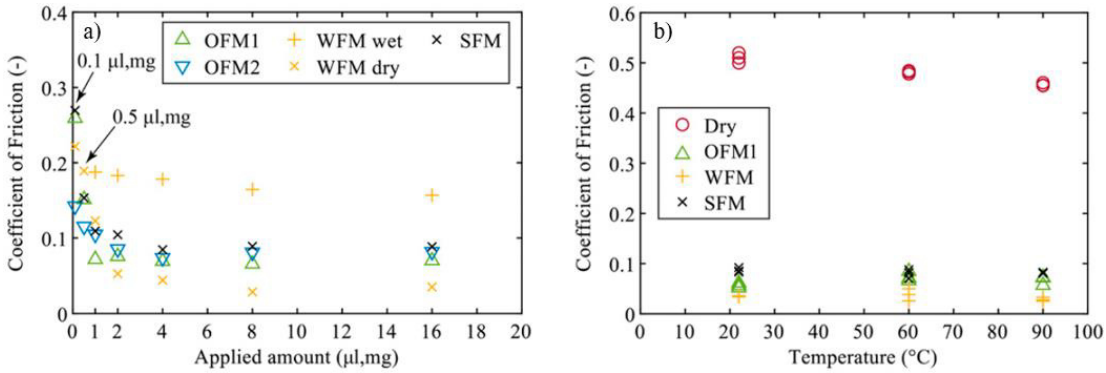

Fig. 2.13 Effect of applied amount **(a)** and temperature **(b)** on CoF

Fig. 2.13(b) illustrates the effect of increasing temperature on CoF. It was observed that CoF decreases with increasing temperature for dry contact, consistent with studies **[74],[75]** that employed similar specimen material. In contrast, a negligible change in CoF was observed for contact treated with TOR products. The experimental data were utilised as input for the boundary model **[59]** to predict a set of creep curves at a speed of 10 m/s, as shown in **Fig. 2.14**. These curves demonstrate the potential application of laboratory test results combined with the developed boundary model.

The results in **Fig. 2.14** align with the literature on CoF values **[26]**, indicating that TOR lubricants typically provide lower CoF than friction modifiers, while the solid stick shows an intermediate CoF **[34]**. A negative slope was expected for dry contact; however, the absence of a positive trend in the creep curves with TOR products may result from lower sliding speeds compared to those typical in the field. At higher sliding speeds, TOR products are removed more quickly, leading to a potential positive trend in the creep curve.

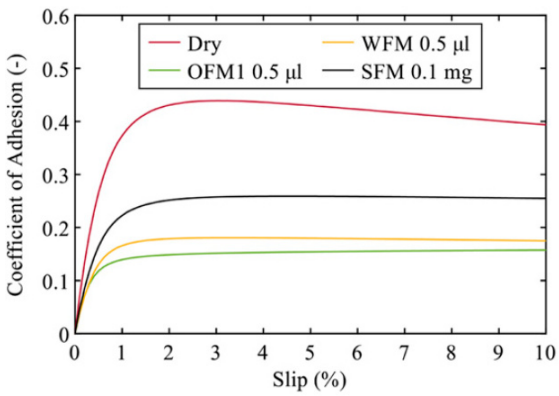

Fig. 2.14 Predicted creep curves for dry contact and contact treated with TOR products

2.6.4 Effects of solid friction modifier on friction and rolling contact fatigue damage of wheel-rail surfaces [62]

The objective of this article was to investigate the effect of a solid stick on adhesion, wear, and surface damage using a twin-disc machine that allows for the adjustment of various slip conditions. A custom-made solid stick was formulated with polytetrafluoroethylene (PTFE), molybdenum disulphide, talcum, and carbon fibre. The study was divided into two types of experiments: (1) focusing on frictional behaviour and (2) examining wear and surface damage.

Fig. 2.15(a) shows the friction curves for different slip values. Unlike liquid TOR products **[20],[24]**, the tested solid stick did not cause a significant initial drop in CoF. Based on these friction curves, the creep curve for the solid stick product was plotted, demonstrating that an intermediate level of friction was achieved, as shown in **Fig. 2.15(b).**

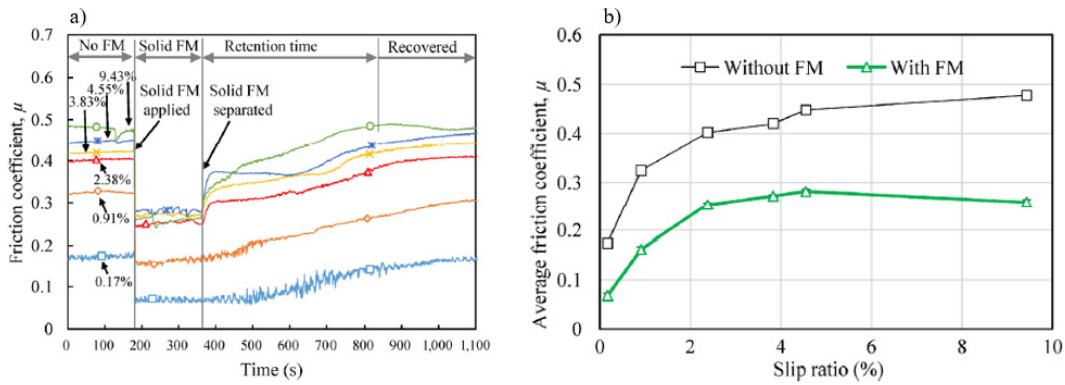

Fig. 2.15 (a) Friction curves for a solid stick at different slip values; **(b)** creep curves with and without the solid stick application

The second type of experiment revealed that applying a solid stick reduces the wear rate of both wheel and rail discs and decreases both the thickness of the plastic deformation layer and the surface hardness, as illustrated in **Fig. 2.16**. Surface and subsurface analyses demonstrated that the solid stick prevented the initiation of subsurface cracks observed under dry conditions and also reduced the length and depth of RCF cracks. This study suggests that applying a solid stick can suppress the acceleration of RCF crack growth typically associated with liquid TOR products **[58]**.

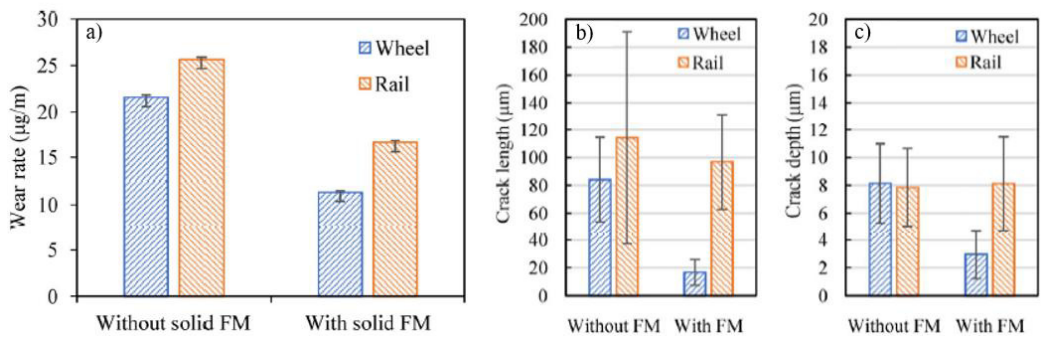

Fig. 2.16 Comparison of conditions with and without solid stick application:**(a)** wear rate, **(b)** crack length, **(c)** crack depth

2.6.5 Wheel/rail adhesion and damage under different contact conditions and application parameters of friction modifier [63]

This study aimed to investigate how changes in operating conditions affect the performance of friction modifiers applied in varying amounts from 5 to 80 µL. The study evaluated the performance of friction modifiers from two perspectives: frictional performance and the ability to reduce wear and surface damage. Frictional performance was evaluated by measuring two parameters: the minimum CoA and retentivity (holding time), while wear rate, crack length, and crack depth were measured to evaluate surface damage. Operating conditions varied by adjusting creepage from 0.3 to 5% and contact stress from 800 to 1500 MPa to simulate typical conditions for both light rail and heavy haul systems. All experiments were conducted using a twin-disc machine with a line contact configuration.

The experimental results on frictional performance were used to plot a set of contour diagrams for different applied amounts. As shown in **Fig. 2.17(a)-(c)**, each diagram shows how the minimum CoA varies with creepage and contact stress, with colours representing the corresponding minimum CoA values across various operating conditions. Another set of contour diagrams was created to depict the dependency of retentivity (holding time) on creepage and contact stress, as illustrated in **Fig. 2.17(d)-(f)**. These contour graphs enable the determination of a suitable application amount to maximise product retentivity while ensuring that the minimum adhesion value reaches the necessary levels for traction and braking.

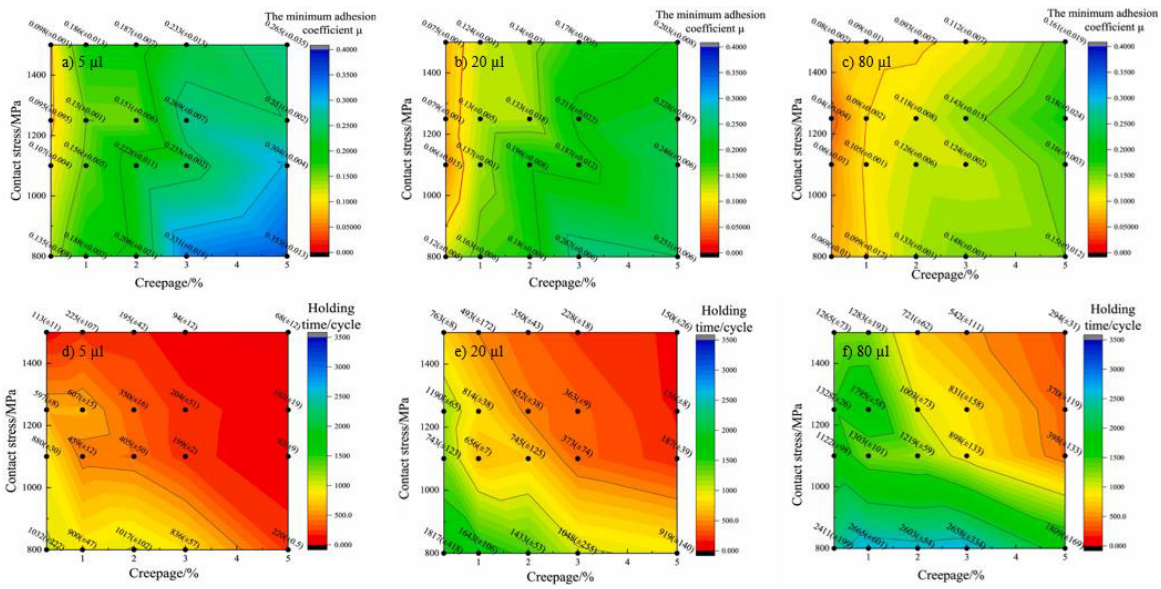

Fig. 2.17 (a)-(c) Contour diagrams of minimum CoA across different operating conditions; **(d)-(f)** contour diagrams of retentivity (holding time) across different operating conditions

The wear rate was determined under dry conditions and with the application of a friction modifier. For the friction modifier application, two different scenarios were considered: (1) application after the pre-worn phase and (2) application without the pre-worn phase. The pre-worn phase was conducted under dry conditions to create more representative surface damage typical for actual operation.

The results in **Fig. 2.18** indicate that under low and medium contact stress levels (900 and 1100 MPa), a significant reduction in the wear rate was achieved, particularly in the test without

the pre-worn phase. In contrast, a rapid increase in the wear rate and rail crack length and depth was observed for the rail disc at a high contact stress of 1500 MPa with the application of the friction modifier. This behaviour can be attributed to the oil wedge effect **[58]**, where the combination of a liquid medium and high contact pressure promotes crack propagation. Therefore, caution is advised when applying friction modifiers directly to rails with pre-existing surface damage, as it may worsen rather than alleviate the issue.

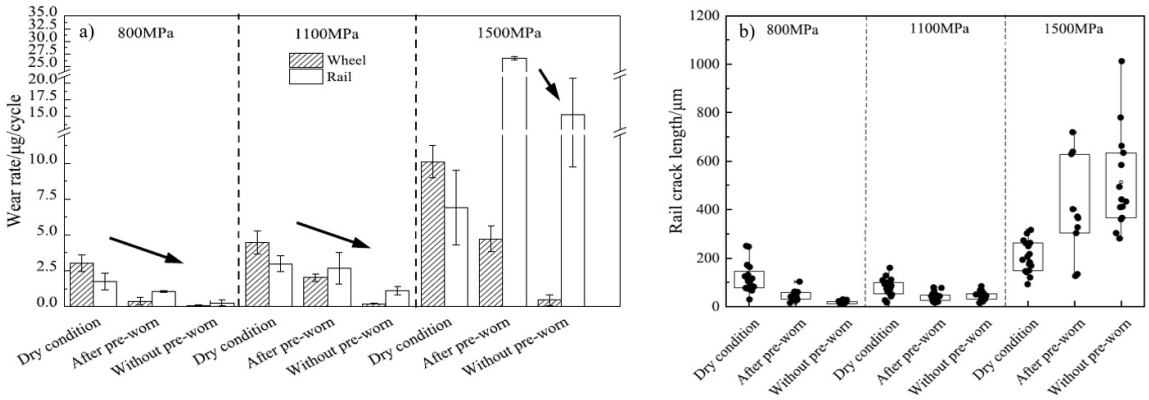

Fig. 2.18 (a) Wear rate of specimens under different application conditions; **(b)** rail crack length under different application conditions

2.6.6 Wear and damage behaviours of wheel and rail materials: Effects of friction modifier and environmental temperature [64]

The study aimed to investigate the effect of a friction modifier on wear and damage behaviour in a cold environment. For this purpose, a twin-disc machine equipped with a cooling system was used. Experiments were conducted at 25 °C (ambient), 0 °C, and -40 °C. All tests began with a pre-worn phase at room temperature and dry conditions for 5,000 cycles to create surface damage representative of actual operation, following the procedure used in the previous study **[63]**.

Fig. 2.19(a) illustrates how temperature affects the CoA and retentivity (lasting effect), while **Fig. 2.19(b)-(c)** show the changes in wear rate with decreasing temperature for dry conditions and with the friction modifier, respectively. The results indicate that the application of the friction modifier reduced the wear rate at all tested temperatures. It should be noted that different trends in the overall wear rate were observed between dry and friction modifier conditions. Under friction modifier conditions, the wear rate corresponded with the changes in CoA values.

However, surface and sub-surface analyses revealed that applying friction modifiers at temperatures lower than ambient led to the growth of fatigue cracks and an increase in their depth, as shown in **Fig. 2.20**. Moreover, at -40 °C, a very deep fatigue crack with a distinct 'C-shaped' propagation was observed, **see Fig. 2.20(d)**. Based on these findings, it can be concluded that the friction modifier effectively controls wear rate and surface damage and maintains the minimum CoA at levels sufficient for traction and braking only at ambient temperature. In contrast, severe RCF damage to the rail specimens was observed at temperatures lower than ambient.

Significant RCF damage at low temperatures occurred due to the material transitioning from a ductile to a brittle state as the temperature dropped below -15 °C, which increased its brittleness **[76],[77]**. At -40°C, the pearlite structure became shorter and more irregular **[78]**, leading to

subsurface cracks that easily merged with surface cracks, forming larger fatigue cracks and resulting in severe RCF damage. Additionally, the friction modifier penetrated these cracks, intensifying the oil wedge effect **[79]** and further aggravating RCF damage, especially in the rail specimens. This effect is further intensified as the lasting effect of the friction modifier shortens **(Fig. 2.19(a))** at low temperatures, requiring more frequent reapplication. Overall, this study has demonstrated that applying friction modifiers at very low temperatures to surfaces with pre-existing cracks can lead to severe RCF damage, showing a limitation of this TOR friction modification approach.

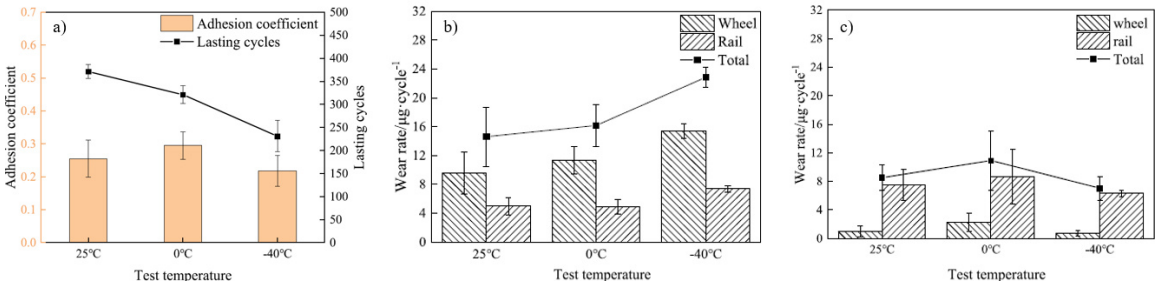

Fig. 2.19 (a) Effect of temperature on CoA and retentivity (lasting cycles) for contact treated with the friction modifier; **(b)** wear rate under dry conditions; **(c)** wear rate with friction modifier application

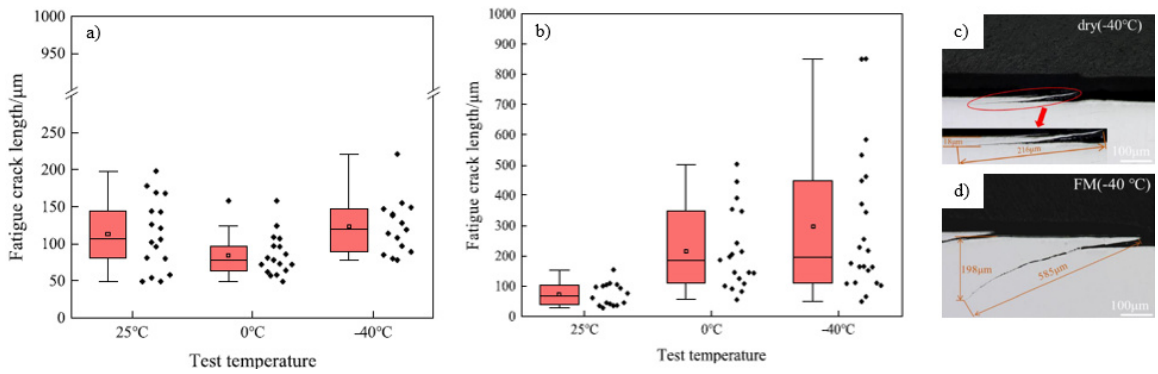

Fig. 2.20 Fatigue crack length under **(a)** dry conditions and **(b)** friction modifier application; crack depth under **(c)** dry conditions and **(d)** friction modifier application

2.6.7 Wheel Squeal Noise in Rail Transport: The Effect of Friction Modifier Composition [65]

The objective of this study was to investigate the effect of friction modifier composition on CoA and squeal noise levels. Ten compositions, including pure water as a reference, were prepared with varying complexity based on a previous study **[22]**. Their performance was evaluated in both dry and wet states, as they are all drying products. Experiments were conducted using a scaled-down twin-disc machine at an AoA of 4° to simulate extreme curve conditions in tram loops. The sound pressure level (SPL) was measured in the range of 20 Hz to 18,000 Hz. Based on the friction curves, several parameters were determined to evaluate the frictional properties of the compositions.

The results revealed that only complex substances (containing a base medium, binding agent, PFM, and solid lubricant) provided long retentivity. It was found that retentivity increases with a higher solid lubricant content; however, it can also cause a more significant initial drop in CoA. Based on the results for both dry and wet films, the most suitable composition was one containing a base medium, binding agent, soft talc particles, and a low concentration of solid lubricant (2 wt%), as it provided the required frictional properties in both conditions. Aside from these complex substances, good results were also achieved when water was used as a TOR product, suggesting it as a potential eco-friendly option.

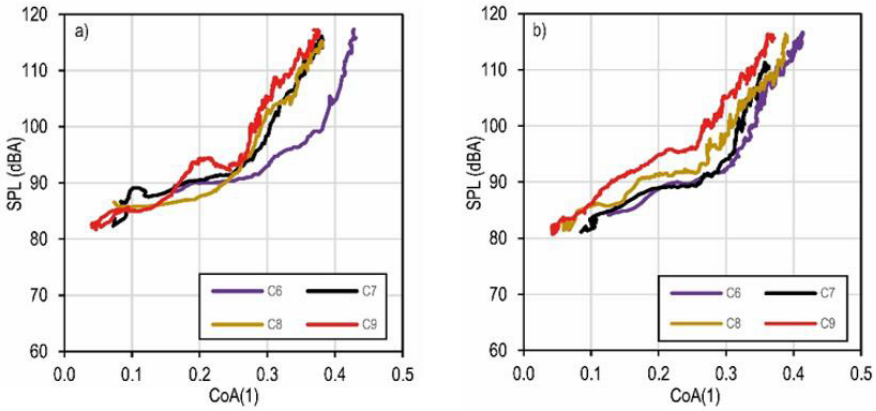

Fig. 2.21 Dependence between CoA and SPL for **(a)** wet and **(b)** dry films

For the best-performing substances, the relationship between CoA and SPL for both wet and dry films is shown in **Fig. 2.21**, indicating a bilinear dependence in both conditions. The graphs clearly indicate that there is a specific CoA value above which a sharp increase in SPL occurs; in this study, this value was found to be approximately 0.25. This finding can be used to manage the friction modifier application process using wayside systems based on actual noise levels in the nearby area.

2.6.8 Wheel Squeal Mitigation Under Water Lubrication [66]

The aim of this study was to build on previous research and further investigate the potential of using water as a TOR product to mitigate unpleasant squeal noise. For this purpose, a full-scale twin-disc machine was developed, equipped with a tram wheel and an adjustable AoA to simulate curve conditions **[80]**; see **Fig. 2.22(a)**. This setup allows for the measurement of vertical and lateral forces, enabling the determination of CoA in the lateral direction. The device is also equipped with a sound meter to record noise data from 20 Hz to 20 kHz. Additionally, a laser Doppler vibrometer was used to identify the frequencies at which noise is generated solely by the wheel, and these frequencies were subsequently compared with the results of FEM modal analysis.

Six dominant frequencies corresponding to wheel vibration modes were identified using measurements (**Fig. 2.22(b)**) and then verified with FEM modal analyses. The most significant vibration mode under both dry and wet conditions was found at 1087 Hz, as shown in **Fig. 2.22(b)** and **(c)**. Subsequently, creep curves for both dry and wet conditions were measured at 2 and 4 m/s, with SPL recorded simultaneously; see **Fig. 2.23(a)-(b)**. The experiments revealed a significant decrease in SPL when water was applied, with reductions of 11–17 dB at 2 m/s and 9–11 dB at 4 m/s, while CoA was maintained at the desired intermediate friction level.

The final set of experiments investigated the effect of the applied amount on retentivity, noise, and CoA reduction, as depicted in **Fig. 2.23(c)**. It was found that increasing the applied amount significantly extended retentivity, while both CoA and SPL showed minimal change. It should be emphasised that for all tested amounts, the CoA drop was no more than 0.1 (from 0.48 to 0.38), while noise was reduced by around 10 dB (from 107 to 97 dB). These results suggest that water application is an effective way to combat squeal noise without risking low adhesion conditions. However, the results were obtained on perfectly cleaned surfaces, indicating that further research is needed.

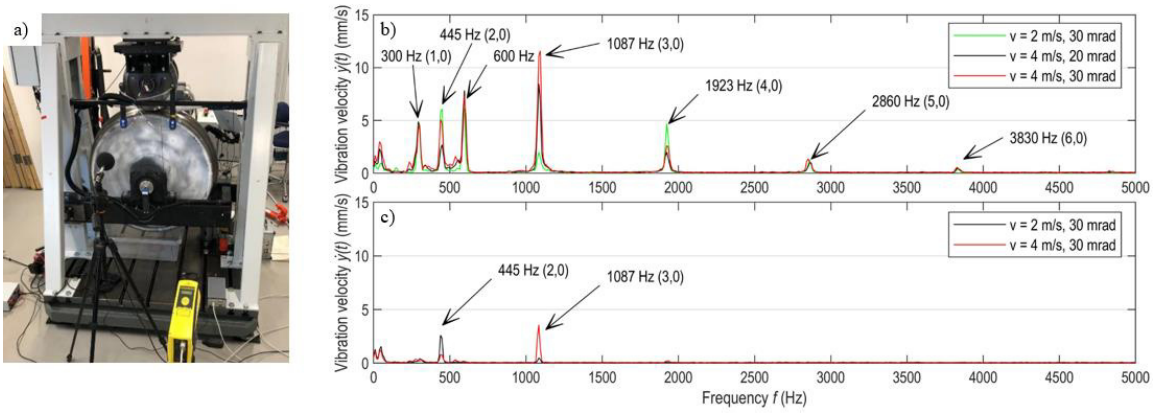

Fig. 2.22 (a) Developed full-scale twin-disc machine; **(b)** vibration frequency composition under dry conditions; **(c)** vibration frequency composition under wet conditions

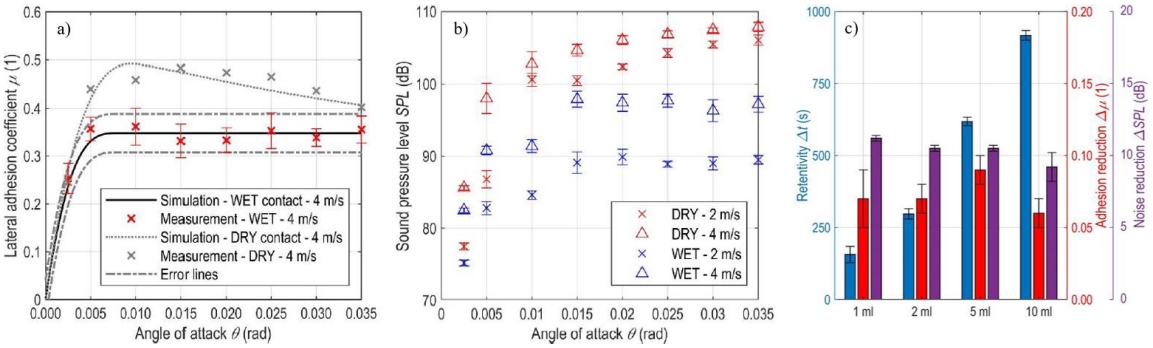

Fig. 2.23 (a) Measured vs. predicted creep curves under wet and dry conditions; **(b)** SPL development with increasing speed and AoA; **(c)** effect of water on retentivity, CoA, and SPL reduction

3

TOP-OF-RAIL PRODUCTS IN AN OPEN TRIBOLOGICAL SYSTEM

3.1 Introduction

The previous chapter provides a detailed overview of the benefits of TOR friction modification. While these studies offer valuable insights into the behaviour of TOR products from multiple perspectives, most of them were conducted without considering the effects of environmental conditions, including contaminants and changing weather conditions. However, these conditions can significantly affect adhesion at the wheel-rail interface, as it is an open tribological system **[81]**.

Various contaminants affect adhesion at the wheel-rail interface, such as water, oil or grease, and solid particles like wear debris, oxides, and sand. Among these, crushed fallen leaves represent one of the most discussed contaminants, as they cause the seasonal low adhesion problem, leading to delays, platform overruns, and even collisions. This condition is commonly referred to as the 'wet-rail' phenomenon **[82]** or 'wet-rail' syndrome **[83]**. Although this phenomenon is often attributed to fallen leaves, it must be highlighted that many low-adhesion incidents in operation were reported as non-contaminated **[84]**. According to **[85]**, there is a high probability of low adhesion occurring in the morning or night hours, likely due to the dew effect leading to water condensation. This small amount of water wets the leaf layer or interacts with other third-body particles, resulting in low adhesion conditions.

Although the wet-rail phenomenon is not fully understood, the interaction between small amounts of water and other materials is believed to play a key role **[86]**. This situation is inevitable even with the application of TOR products during rainy or dew conditions. This issue can be particularly critical for TOR lubricants, as they are oil-based, and it is well known that the interaction between oil and water can result in extremely low adhesion levels **[87]-[90]**. In contrast, for friction modifiers, water contamination can disrupt the drying process, which may also significantly affect product performance. Besides water contamination, other natural contaminants, such as leaves and oxide particles, as well as artificial contaminants like oil and grease, can substantially affect the performance of TOR products. Therefore, understanding how TOR products behave under contaminated conditions can help optimise their application strategy and prevent potential risk scenarios associated with product contamination.

3.2 Contaminants Affecting wheel-rail contact

3.2.1 Water as a lubricant

Water is the most common natural contaminant, as it comes from the atmosphere and can appear anywhere, unlike contaminants such as oil, which are usually limited to specific areas. Water can be present on the track in various forms, including heavy rain, drizzle, dew, frost, or mist, each of which can lead to different levels of adhesion, especially when interacting with other contaminants. Significant research has focused on the impact of water contamination on adhesion between the wheel and rail. Numerous studies have examined the effect of bulk water, simulating continuous rain, on wheel-rail adhesion. In such conditions, large amounts of water wash away solid railhead contaminants, creating a boundary lubrication regime where water acts as a lubricant **[91]**. Both experimental **[92],[93]** and numerical studies **[94],[95]** have shown that adhesion in water-contaminated contact is influenced by surface roughness, with higher surface roughness resulting in a higher CoA. In addition to surface roughness, surface orientation also affects adhesion; however, published results are contradictory **[96],[97]**. Although the CoA varies between 0.1 and 0.45 **[98]-[104]** depending on the test conditions, critically low adhesion usually does not happen when a large amount of water lubricates the contact. However, as speed increases, the situation can change, leading to a drop in adhesion due to the transition from the boundary to a fully lubricated regime. This drop becomes significant at speeds exceeding 150 km/h, where adhesion can fall below 0.1, and at 200 km/h, where it can decrease to 0.05 **[92],[105]**, as depicted in **Fig. 3.1**. Moreover, a further decrease in the CoA can occur as the water temperature decreases **[106]**.

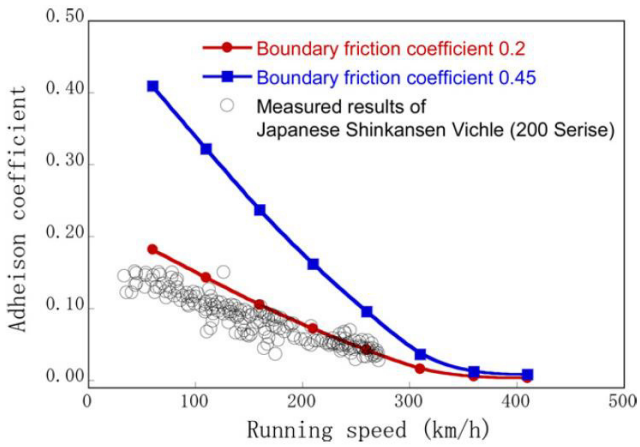

Fig. 3.1 Relationship between CoA and speed: comparison of field data and simulations **[92]**

3.2.2 Water in interaction with other contaminants

A more serious situation can occur when water interacts with other contaminants on the railhead. As mentioned earlier, critically low adhesion that compromises braking and traction capabilities can occur when water mixes with operating fluids, such as grease and oils, on the top of the rails **[87]-[90]**. This issue can be prevented or at least mitigated by proper flange lubrication to minimise lubricant migration and by maintaining vehicles in good technical condition to avoid lubricant leaks.

Another risky situation regarding low adhesion occurs when solid particles on the rail, such as wear debris or surface rust, are wetted and mixed with a small amount of water, typically from dew or light rain. As this mixture dries, a non-Newtonian viscous paste can form between the surfaces **[107]**. This lubricating paste can lead to extremely low adhesion, as low as 0.05 (see **Fig. 3.2**), particularly when the water-to-particle ratio is small **[107]**, as the viscosity of the paste increases exponentially **[108]**. Although this phenomenon was first mentioned in 1974 by Broster et al. **[91]**, and despite numerous laboratory studies addressing it **[86],[109],[110]**, it remains not fully understood. The difficulty lies in experimentally observing this phenomenon on real tracks, as it occurs within a very narrow window of conditions because it is highly transient **[86]**. While this phenomenon is generally believed to be responsible for many low-adhesion incidents, some results suggest that these incidents are not always associated with solid railhead contaminants **[111]**.

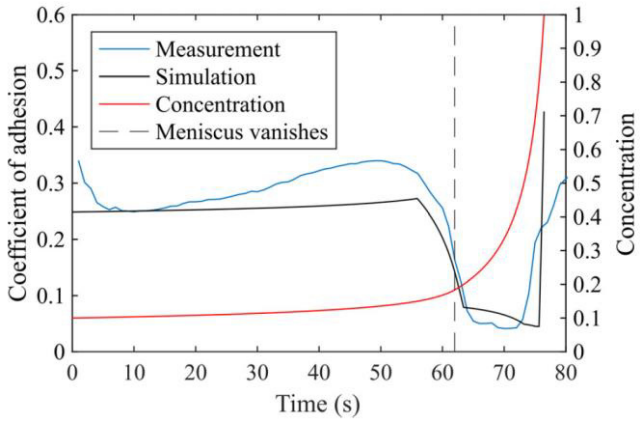

Fig. 3.2 Friction test with water-particle mixture demonstrating a drop in CoA **[109]**

3.2.3 Leaves on the line

Leaves on the track are a frequently discussed issue, often leading to low adhesion conditions during autumn **[112]**. When crushed on the railhead, fallen leaves form a layer that can significantly reduce adhesion, sometimes dropping below 0.1, as observed in both field **[113]-[114]** and laboratory conditions **[115]-[118]**. In some instances, the CoA dropped as low as 0.02 **[113]**, particularly when a wet film was present. This layer is commonly called the 'black leaf film', believed to form due to a chemical reaction between organic materials from the leaves and inorganic components like iron oxide. A study by Zhu et al. **[119]** supports this explanation using electron spectroscopy, which revealed a high carbon content of approximately 48% in the tarnished leaf layer. Furthermore, the study identified three types of leaf-contaminated surfaces: with a residual leaf layer, with a tarnished layer, and without any obvious layer. The existence of the last category may explain some low-adhesion incidents where the rail appears visually clean. This is supported by studies **[120],[121]** showing that leaf extract, which contains some typical leaf components mixed with water, can significantly reduce adhesion.

3.2.4 Humidity and oxidation

Relative humidity and temperature are additional factors that are not controlled in the open tribological system and affect friction. Beagley et al. **[122]** investigated the effect of relative humidity on CoF using the Amsler machine. The results showed that relative humidity directly influences friction; specifically, the CoF varied between 0.57 and 0.22 as relative humidity decreased from 100% to 15%. That study also disproved the theory of long-term oxide growth, as a change in the humidity was quickly followed by a change in the CoF. At 100% relative humidity, condensation occurred, leading to a more significant drop in the CoF. This drop was attributed to the formation of a paste, and the rate of this decline depends on the water/solid ratio. Other researchers later found similar trends in the field **[91]** and in the laboratory for both sliding **[123]** and rolling-sliding conditions **[124]**.

A friction value is influenced, among other factors, by iron oxides (rust) covering surfaces due to humidity, as well as both ambient temperature and the temperature within the contact. Various types of anhydrous and hydrated iron oxides, differing in colour, hardness, and crystalline structure, can be found on rails **[125]**. Moreover, the thickness of a formed layer can range from a few microns to tens of microns **[126]**. Suzumura et al. **[127]** analysed oxides on rail segments exposed to atmospheric conditions typical for tunnels. Analysis using a portable X-ray diffractometer with integrated X-ray fluorescence revealed that most rust consisted of red rust (γ-FeOOH and α-FeOOH) and magnetite (Fe_3O_4), as depicted in **Fig. 3.3**. According to **[128]**, other common oxides and oxy-hydroxides, specifically Fe_2O_3 and β-FeOOH, may also be found on rail surfaces depending on atmospheric conditions. For instance, in the submarine railway tunnel on the Shinkansen line, β-FeOOH was formed, causing a significant reduction in the CoF and leading to rail corrugation **[129]**.

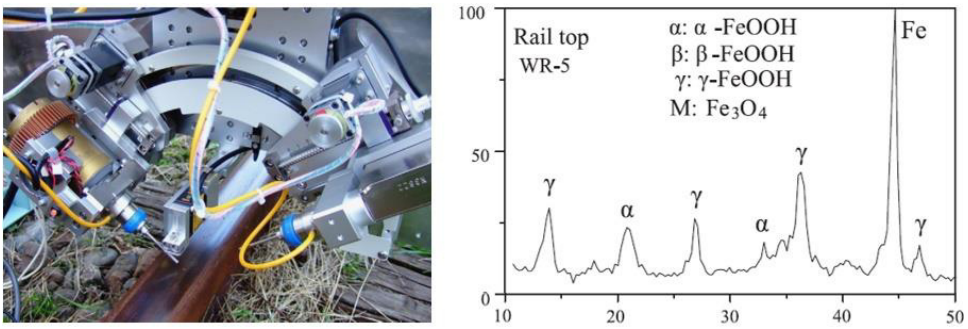

Fig. 3.3 Portable system for oxide analysis with example results from the railhead **[127]**

Several laboratory studies investigated the effect of oxide layers on the CoF. Nakahara et al. **[130]** used a twin-disc machine to measure friction curves (relationship between friction and time/sliding distance) under both dry and wet conditions. Each experiment was stopped at different stages, and the oxide layer was analysed using various spectroscopic techniques to determine its composition. A comparison of friction data and spectroscopic analysis revealed that a rapid increase in the CoT under both dry and wet conditions is associated with an increase in hard α-Fe_2O_3 in the thin oxide layer. Conversely, the formation of softer Fe_3O_4 appears to reduce the increase in the CoT. It was observed that oxides increased the CoT only at the beginning of the test, which is typical for non-run-in specimens. The CoT then reached an intermediate value of 0.3 at sliding distances of 0.5 m and 1 m for dry and wet conditions, respectively, with friction continuing to increase in both cases. These results partially align with the findings of Zhu et al. **[131]**, who tested

pre-treated oxide layers with varying thickness and initial roughness of specimens. Their findings indicate that low friction conditions are unlikely when an oxide layer is present under dry conditions. In contrast to **[130]**, Zhu et al. **[131]** reported a more significant drop in the CoA for wet conditions, where the saturated adhesion varied between 0.14 and 0.17 depending on the thickness of the layer and roughness.

Besides water-contaminated contact, Zhu et al. **[132],[133]** conducted two studies exploring the effect of pre-created oxides under dry, wet, and varying RH and temperature conditions using a pin-on-disc tribometer equipped with a climate chamber. Both studies found that increasing RH led to a sharp decrease in the CoF due to lubrication by water molecules. The CoF stabilised at an RH of 65%, with no further decrease observed as the RH increased. This behaviour was explained as a balance between water molecule lubrication and the increasing effect of hematite formed on the surfaces, as illustrated in **Fig. 3.4**. It should be pointed out that the CoF did not fall below 0.4 for any of the tested conditions, including dry and rusted specimens. The only exceptions were conditions involving leaves, glycol/water mixture, or a combination of both, with the lowest recorded value being approximately 0.1 **[133]**.

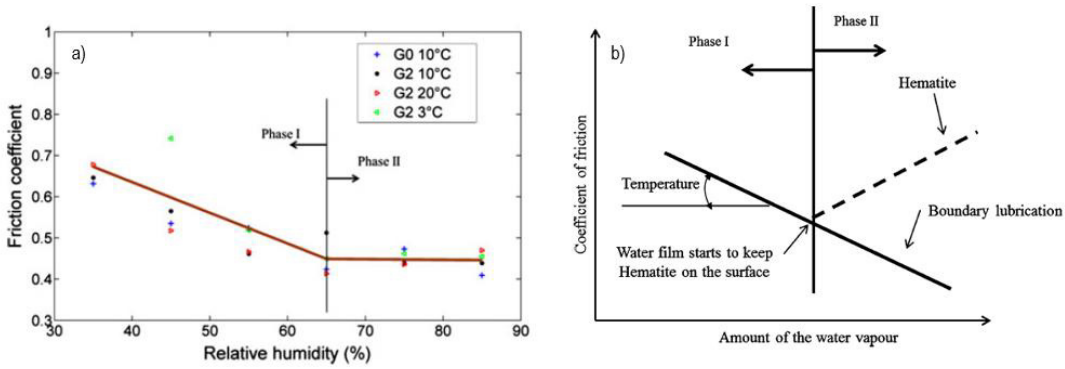

Fig. 3.4 **(a)** CoF vs. relative humidity; **(b)** CoF vs. amount of water vapour **[132]**

3.3 Interaction of Top-of-Rail Products with Contaminants

A pilot study on the interaction of TOR products with other materials was published by Lu et al. in 2005 **[134]**. This study examined the interaction of friction modifiers with iron oxide (Fe_2O_3) and grease. The experiments were conducted using two different methods: a pin-on-disc rheometer and a disc-on-disc Amsler tester. For the mixture of friction modifier and iron oxide, it was found that friction modifier particles primarily controlled the friction value. Even at a high concentration of oxide, the frictional behaviour was still primarily controlled by the smaller amount of friction modifier, as shown in **Fig. 3.5(a)**. This aligns with predictions based on the wear model **[135]**, which suggests that behaviour mainly depends on the volume fraction of particles and their wear resistance, as particles with higher wear resistance dominate the CoF. In contrast, grease contamination significantly affected the performance of the friction modifier, lowering the CoF and disrupting the adhesion between the friction modifier layer and the steel surface of the specimens, as shown in **Fig. 3.5(b)**. In the case of light grease contamination, the trend of the creep curve did not change and remained positive, as observed for the uncontaminated friction modifier. The article suggests three hypotheses to explain the mechanism behind the positive creep curve.

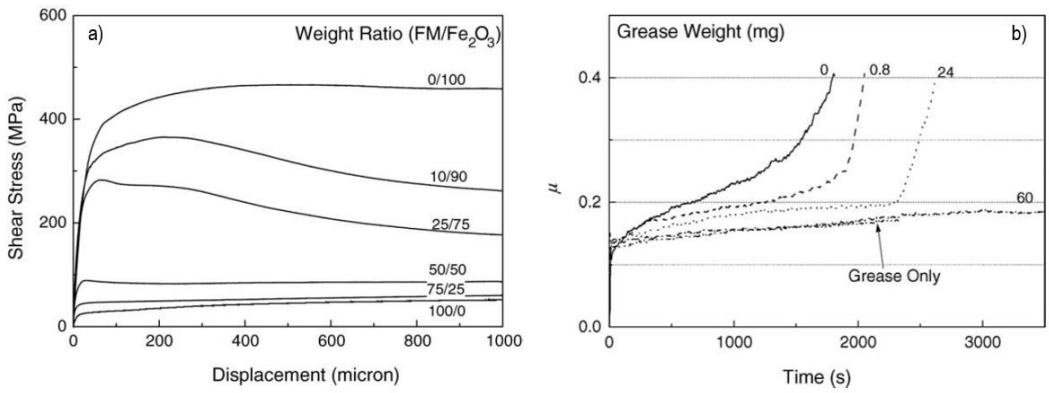

Fig. 3.5 (a) Shear strength vs. displacement for a friction modifier and oxides mixture; **(b)** interaction between friction modifier and grease **[134]**

In 2009 and 2010, two studies on the performance of friction modifiers under wet and leaf contamination were carried out **[20],[136]**. Although both tested TOR products were categorised as friction modifiers, they were used in these studies more as friction enhancers, as their performance was primarily evaluated based on their ability to restore adhesion under contaminated conditions. The fact that these are special types of TOR products is evident from their composition, as both products contained much larger particles than is typical for common friction modifiers. Moreover, both products were previously tested on the track specifically to overcome low adhesion conditions. The first product, FMA, was tested at a train depot in Japan to address adhesion issues caused by rain. The second product, FMB, was applied during autumn on British and Dutch railways to combat problems caused by wet leaves on the tracks. On the other hand, the trend of the creep curve was another evaluated parameter, typically assessed for friction modifiers. For this purpose, experiments at various slip values were performed using the twin-disc machine.

The first study **[20]** showed that both TOR products provided a positive creep curve, while a negative trend was observed under dry conditions. Under dry conditions, the product with smaller particles, FMA, demonstrated better performance compared to the second product. In contrast, FMB showed better performance in wet conditions, where results for FMA indicated potential traction issues. Regarding wear rate and surface damage, the large, hard particles in FMB caused severe surface damage, such as indentations and scratches, whereas FMA showed no significant surface damage. These results align with the second study **[136]**, which reported similar wear and surface damage under leaf-contaminated conditions. On the other hand, the large, hard particles in FMB ensured fast adhesion recovery, as they could break up the leaf layer. The results of both studies highlight that the hardness and size of particles play a key role in improving adhesion under contaminated conditions.

One of the most relevant articles on TOR product interaction with other materials was carried out by Lewis et al. **[137]**. The study explored how red and black iron oxides affect friction modifier performance under varying atmospheric conditions. The experiments were conducted using a pin-on-disc tribometer equipped with an environmental chamber (see **Fig. 3.6(a)**), simulating typical underground and tunnel conditions at temperatures of 10 °C and 20 °C and relative humidity levels between 40% and 90%. For this purpose, the friction modifier and iron oxide mixtures in concentrations of 25%, 35%, and 45% were tested. Results indicated that friction levels were primarily controlled by relative humidity and the concentration of iron oxide in the mixtures. It was observed that at humidity levels above 70%, friction remained consistently low throughout the test. At lower humidity levels (40%), friction increased with sliding distance due to the evaporation of

water within the friction modifier, as shown in **Fig. 3.6(b)**. These findings led to the conclusion that low friction occurs when the mixture of iron oxide and friction modifier remains wet, as this prevents the formation of a dry frictional layer required to achieve desired friction levels. Another key finding was that mixtures with higher oxide concentrations (45%) retain water within the friction modifier, maintaining undesirably low friction levels.

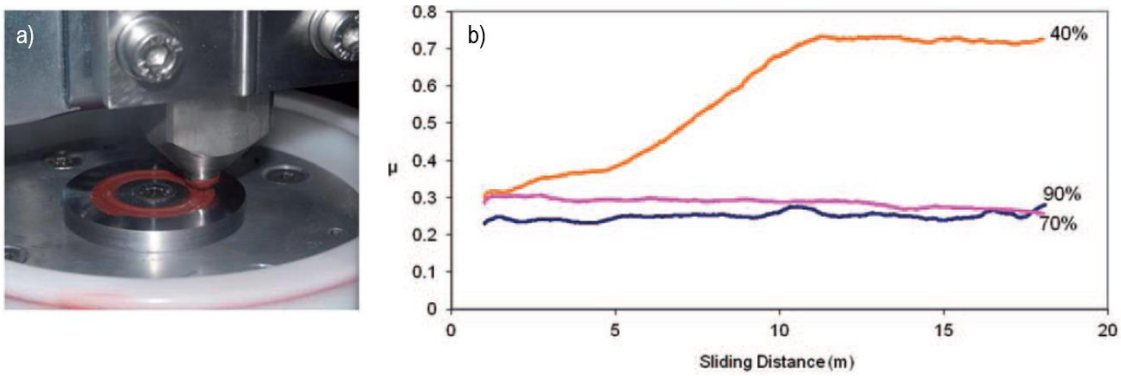

Fig. 3.6 (a) Pin-on-disc tribometer test of friction modifier and red oxide mixture; **(b)** effect of relative humidity on CoF of friction modifier and black oxide mixture **[137]**

Following these controlled laboratory experiments, two field studies were conducted to evaluate the performance of TOR products under actual operating conditions **[138],[139]**. The first study, by Oldknow et al. **[138]**, measured the lateral-to-vertical force ratio (L/V ratio) on a 300 m radius curve under heavy-haul conditions. Measurements were carried out under four conditions: dry, wet, with an applied friction modifier, and with a friction modifier under precipitation conditions. Results indicated that applying a friction modifier in dry conditions produced a narrow L/V distribution with a peak value 0.2. However, a notable change in this distribution was observed when precipitation was combined with the friction modifier. Under these combined conditions, the peak distribution value shifted gradually. Initially, it was at levels typical for wet conditions, then it progressed to levels where the friction control was not yet fully effective, and finally reached a value characteristic of the friction modifier alone. The final peak was slightly below 0.2 due to contamination of the friction modifier by precipitation.

The second field study focused on the interaction between TOR products and various materials **[139]**. The experiments involved braking tests conducted under both dry and wet conditions at a speed of 40 km/h, with several products applied to the inner rail surface. Initially, tests were conducted without product application to establish reference values for dry and wet conditions. The products tested included one water-based product, one oil-based product, and two solid sticks. Results showed that, depending on the product used, braking distance increased by 2.1% to 16.8% under dry conditions and by 7.2% to 20.9% under wet conditions compared to the reference values. Under both tested conditions, the most significant increases in braking distance compared to the reference values were observed with the non-specific water-based product.

3.4 Summary of the literature review and research gaps

The literature review above focused on the open wheel-rail tribological system to identify conditions where low, and particularly very low, adhesion can occur. It has been demonstrated that water plays a dominant role in both untreated contacts and contacts treated with TOR products. Several mechanisms illustrate how water can reduce adhesion in an untreated contact. The first mechanism is associated with heavy rain, where a large amount of water is present on the track. These conditions can cause low adhesion only at very high speeds, resulting in an EHL or hydrodynamic lubrication regime **[92],[105]**. In contrast, no low-adhesion incidents occur at lower speeds where water acts as a boundary lubricant **[98]-[104]**. Additionally, large amounts of water wash away other contaminants from the railhead, which may prevent the second mechanism **[82]**.

The second mechanism describes a small amount of water, such as light precipitation or dew conditions, interacting with free solid particles on the railhead **[91]**. Several studies have shown that such mixtures can cause a significant drop in adhesion **[86],[109],[110]**, depending on the water-to-solid ratio **[107]**. In critical cases, adhesion can drop to values as low as 0.05 **[107]**. This phenomenon has been observed in both field **[108]** and laboratory experiments **[109]**.

Besides the direct effect of water on adhesion, water on the railhead or in the air can accelerate the formation of oxides, which also affects adhesion **[140]**. While some types of oxides increase friction, others reduce it, potentially causing additional issues such as rail corrugation **[129]**. It is important to note that oxide layers may have a short lifespan on the railhead **[128]**, which makes reproducing them in laboratory conditions difficult **[110]** and their effects challenging to study. Furthermore, as these layers are removed, oxide debris is left on the surface, potentially forming the paste under light precipitation.

Water also plays an important role during autumn, when numerous low-adhesion incidents are reported due to fallen leaves **[85]**. Water softens the formed leaf layer, leading to lower adhesion conditions compared to dry crushed leaves **[113]**. Additionally, water can mix with oils released from the leaves, forming a substance similar to an oil-water emulsion. This liquid, termed leaf extract in the literature, can cause critically low adhesion values as low as 0.06 **[120]**.

Only a few publications address the performance of TOR products under contaminated conditions. Furthermore, two of them tested products that should be categorised as friction enhancers rather than friction modifiers **[20],[136]**. Studies have investigated the effect of water on contacts treated with TOR products, showing that water-contaminated products increase braking distances for various product types **[139]** and cause changes in the L/V ratio distribution in curves for contacts treated with the friction modifier **[138]**.

When examining interactions between TOR products and other contaminants, it was demonstrated that the behaviour of the mixture of friction modifier and iron oxides strongly depends on the wear resistance of the particles **[134]**, following the wear model published in **[135]**. This indicates that even when friction modifier particles are present in smaller proportions than oxides, they can still control friction. However, such mixtures on the track can contain up to 90% oxides **[134]**, suggesting that the friction modifier may not provide the required frictional properties under these conditions. Lewis et al. **[137]** studied these mixtures and found that higher relative humidity can keep a friction modifier layer mixed with oxide particles wet, which leads to low friction values. Additionally, higher oxide concentrations can retain water in the mixture, similarly resulting in low adhesion conditions.

Although many studies show a decrease in adhesion when the contact is contaminated, these drops often do not reach critical values typical of low-adhesion incidents. Furthermore, there are some contradictory findings regarding the effect of relative humidity on adhesion. Several studies report that no further significant decrease in adhesion occurs when relative humidity exceeds 60-70% **[132],[133]**. However, other studies reported a continuous decrease in adhesion with rising relative humidity, with a sharp additional drop when dew conditions are reached **[91],[122]**. This discrepancy may be due to several factors, with one key factor potentially related to the experimental configuration. While the experiments in **[132]** and **[133]** were conducted under pure-sliding conditions, the experiments described in **[91]** and **[122]** were carried out under rolling-sliding conditions.

Based on this literature summary, the following RGs have been identified:

- **RG1:** Although several studies address the low adhesion phenomenon, only a few of them found critically low adhesion values **[107],[113]**. Additionally, none of these studies provide comprehensive findings across various environmental conditions. As mentioned above, many studies employed a pin-on-disc tribometer **[132],[133]**, which is not representative of wheel-rail contact and may not be suitable for studying critically low adhesion conditions. A comprehensive study focusing on low adhesion conditions under rolling-sliding conditions is lacking.
- **RG2:** Only little is known about the performance of TOR products under contaminated conditions. Several possible contaminants could be investigated; however, even the effect of water, as the most common contaminant, on the behaviour of TOR products has not been explored in depth. Unlike untreated contact, both small and large amounts of water may pose risks when interacting with TOR products. In particular, larger volumes may lead to low adhesion conditions, especially when combined with TOR lubricants, as a similar effect to oil-water mixtures can be expected **[87]-[90]**. It should also be noted that water can be present on the track in various forms. Therefore, this gap is divided into two parts: the first deals with TOR products contaminated by directly applied water (**RG2.1**), while the second focuses on TOR products interacting with water from condensation (**RG2.2**).

3.5 Author's contribution

The authors contribute to the topic of adhesion in wheel-rail contact under contaminated conditions with three articles **[141]-[143]**. The first article focuses on untreated contact **[141]**, while the other two examine the interaction between water and commercial TOR products **[142],[143]**. All studies utilise the same experimental approach, a ball-on-disc tribometer, to ensure consistency and accurately simulate rolling-sliding conditions typical for wheel-rail contact. It should be noted that these articles do not address all possible contaminants, as the scope is extensive. Therefore, potential future directions in this area are described in the fifth chapter of this thesis.

The first article **[141]** significantly contributes to the understanding of the conditions that lead to low, and particularly very low, adhesion in rolling-sliding contact, specifically addressing **RG1**. It highlights how various environmental factors, including liquid contaminants such as water and leaf extract, as well as a solid pre-created leaf layer, affect adhesion. Furthermore, the study explores the influence of temperature and humidity variations. Based on these data, formulas for predicting adhesion in rolling-sliding contact under different temperature and humidity conditions were derived. By providing a comprehensive overview of these conditions and predictive models,

the article enhances our understanding of how low and very low adhesion can occur in rolling-sliding contact, which is crucial for improving strategies to mitigate low adhesion issues.

The second article **[142]** provides valuable insights into the effects of water contamination on the behaviour of TOR products under simulated precipitation conditions, thereby addressing **RG2.1**. By applying different water volumes directly to the contact, the study identifies how varying precipitation levels interact with existing TOR product layers, potentially leading to low or very low adhesion. A key contribution of this research is the identification of specific conditions that increase the risk of low adhesion due to the interaction between TOR products and water. These findings can help improve application strategies for existing TOR products and assist in developing new products to prevent adhesion issues caused by water contamination.

The last article **[143]** contributes to the understanding of the effects of water contamination on TOR products, specifically under dew conditions. Unlike the previous study **[142]**, which involved direct water application, this research simulates dew formation by allowing water to enter the contact through controlled relative humidity and temperature changes. By addressing **RG2.2**, the study enhances the understanding of the behaviour of TOR lubricants in conditions commonly found in the morning, evening, or within tunnels, particularly regarding water and TOR product interaction. Together with findings from the previous study **[142]**, these insights can be utilised to optimise the dosing strategies of TOR products, thereby helping to prevent adhesion issues associated with water contamination.

The author has contributed to the following papers[2]:

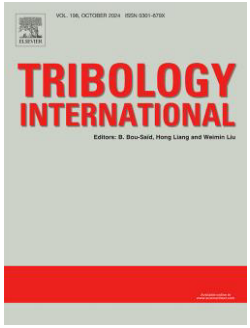

[141] Galas R, Omasta M, Shi L, Ding H, Wang W, Krupka I, et al. The low adhesion problem: The effect of environmental conditions on adhesion in rolling-sliding contact. Tribology International 2020;151.

Author's contribution	40%
Journal impact factor (2020)	4.872
JIF/AIS Quartile	Q1/Q1
Citations (WoS/Scopus/Google Scholar)	23/28/27

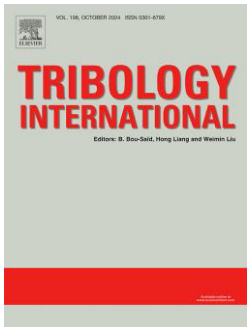

[142] Skurka S, **Galas R**, Omasta M, Wu B, Ding H, Wang W, et al. The performance of top-of-rail products under water contamination. Tribology International 2023;188.

Author's contribution	30%
Journal impact factor (2023)	6.052
JIF/AIS Quartile	Q1/Q1
Citations (WoS/Scopus/Google Scholar)	2/3/4

[2] All listed articles are listed in Chapter 9.

[143] Skurka S, **Galas R**, Omasta M, Ding H, Wang W, Krupka I, et al. Assessing the Performance of TOR Lubricants in Humid Environments and Under Dew Conditions. Tribology Letters 2024;72.

Author's contribution	30%
Journal impact factor (2023)*	2.858
JIF/AIS Quartile*	Q2/Q2
Citations (WoS/Scopus/Google Scholar)	0/0/0

*The data for the year 2024 are not yet available.

3.5.1 The low adhesion problem: The effect of environmental conditions on adhesion in rolling-sliding contact [141]

The aim of the first article was to investigate the conditions that lead to low and very low adhesion under contaminated conditions. The initial section explores the effects of water and leaf extract (a mixture of water and lubricants released from leaves) as potential liquid contaminants of the contact. It is important to note that some experiments were prolonged to study the effect of oxide formation. The second section investigates how variations in temperature (1-50 °C) and relative humidity (8-100%) influence the CoA. These experiments were conducted with both clean discs and discs with a pre-created leaf layer. All experiments were carried out using the Mini-Traction machine (MTM2) in a ball-on-disc configuration.

The results of the first part showed that a large amount of water does not significantly decrease adhesion; however, a notable drop occurred when an oxide layer formed on the surfaces due to the action of water, as shown in **Fig. 3.7(a)**. In the most critical case, the CoA dropped below 0.05, which is considered the threshold for very low adhesion. When a small amount of water was applied, the adhesion dropped to an intermediate value of around 0.4. Before adhesion fully recovered, a secondary drop related to surface drying was observed (see **Fig. 3.7(b)**), consistent with observations in **[87],[107]**. A similar trend in the friction curves was observed for the contact with leaf extract, which exhibited a second adhesion drop. However, both the first and second adhesion drops were more significant, with CoA falling below 0.1.

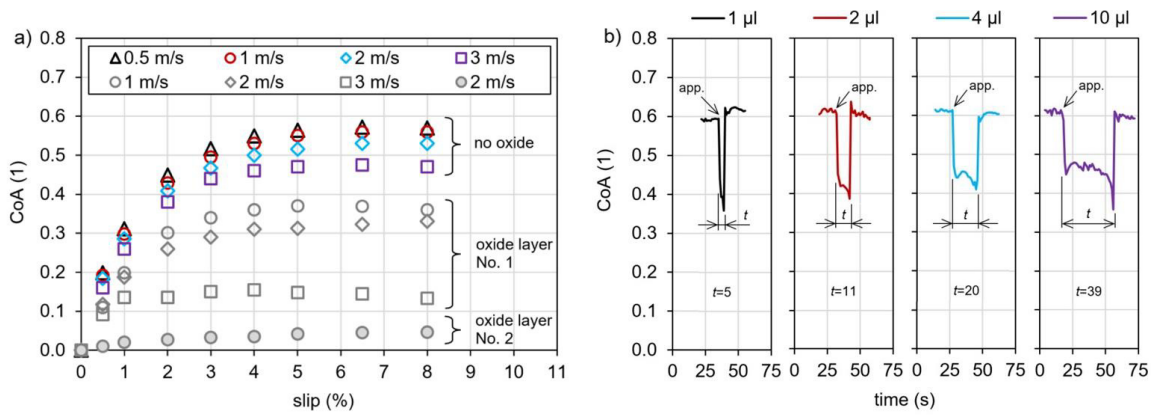

Fig. 3.7 (a) Creep curves for water-contaminated contact operating under fully-flooded conditions; **(b)** effect of a small amount of water on CoA

The results of the second part showed that relative humidity significantly affects adhesion values, particularly at lower temperatures, as depicted in **Fig. 3.8**. Unlike findings from pin-on-disc studies **[132],[133]**, a substantial drop in adhesion was observed when relative humidity exceeded 70% due to water condensation, consistent with observations in **[122]**. The lowest recorded adhesion values were below 0.15 for clean discs and even below 0.05 for contaminated discs. Based on these results, equations predicting the CoA for contact operating under rolling-sliding conditions were derived for both clean and leaf-contaminated specimens.

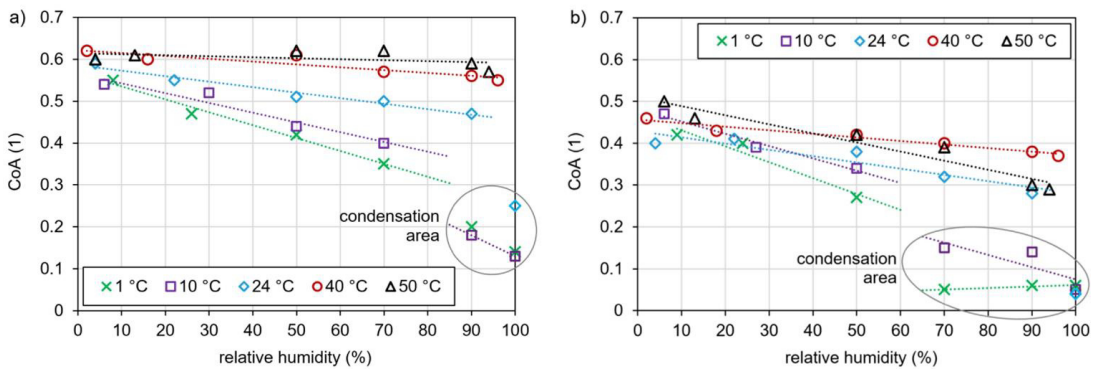

Fig. 3.8 Effect of relative humidity on CoA for **(a)** a clean disc and **(b)** a disc with pre-created leaf layer

The results overview depicted in **Fig. 3.9** shows when low and very low adhesion conditions occur. It can be seen that very low adhesion conditions can be simulated when specimens covered with an oxide layer are exposed to wet conditions or when dew point conditions are reached, causing a small amount of water to mix with the leaf layer. In general, it can be concluded that very low adhesion conditions are always a result of the presence of water. The second important conclusion is that a rolling-sliding configuration is a more suitable experimental approach than other configurations for studying low adhesion phenomena, as it reproduces the severe adhesion drops observed in the field. This conclusion is supported by **Fig. 3.14**, where the results obtained using several experimental approaches are compared.

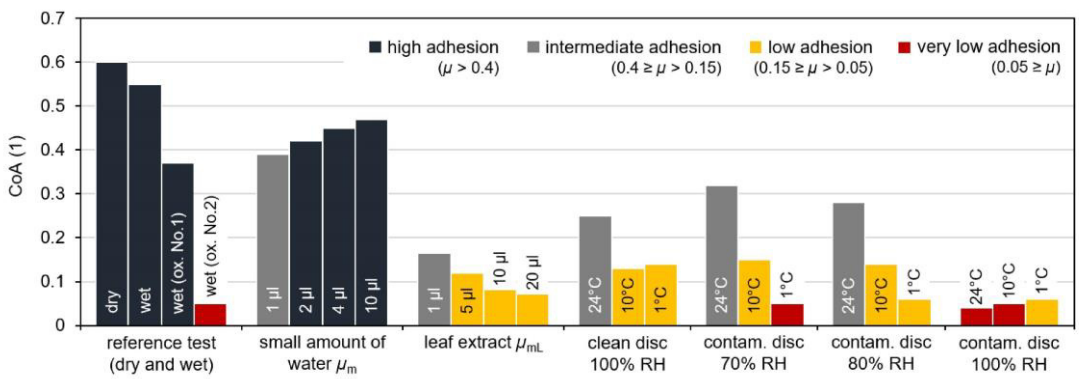

Fig. 3.9 Overview of the tested conditions with highlighted adhesion values

3.5.2 The performance of top-of-rail products under water contamination [142]

The aim of the second study was to explore the interaction between water and TOR products and determine what happens when a TOR product layer is contaminated with water. Experiments were conducted using the MTM2 in a ball-on-disc configuration. Initially, three commercial TOR products, including two TOR lubricants and one friction modifier, were tested under varying conditions without water contamination to identify the most appropriate amounts for subsequent experiments. These experiments included testing of four specific application amounts: 2 µL, 8 µL, 32 µL, and 2 mL. In the case of water contamination, water was applied at three specific moments (T1, T2, T3; see **Fig. 3.10**) to simulate different track conditions, contaminating the TOR product layer at various stages of the friction curve: shortly after applying the TOR product (T1), during the intermediate stage of the friction curve (T2), and when the product had become ineffective (T3).

The results in **Fig. 3.10** show that a small amount of water causes a sudden drop in adhesion; however, this is followed by the immediate sharp increase, suggesting that this situation is not risky in terms of low adhesion. In contrast, a different scenario occurs when a large amount of water is applied, as shown in **Fig. 3.10(b)** and **Fig. 3.10(d)**. The application of a large amount of water significantly affects both the TOR lubricant and the friction modifier. For the TOR lubricant, the water application results in extremely low adhesion values, dropping below 0.04 and remaining almost unchanged until the end of the experiment. This undesired behaviour can be explained by the water-oil emulsion lubrication theory, which covers various lubrication regimes, from the fluid-film regime to the mixed regime. However, further research is necessary to verify these hypotheses.

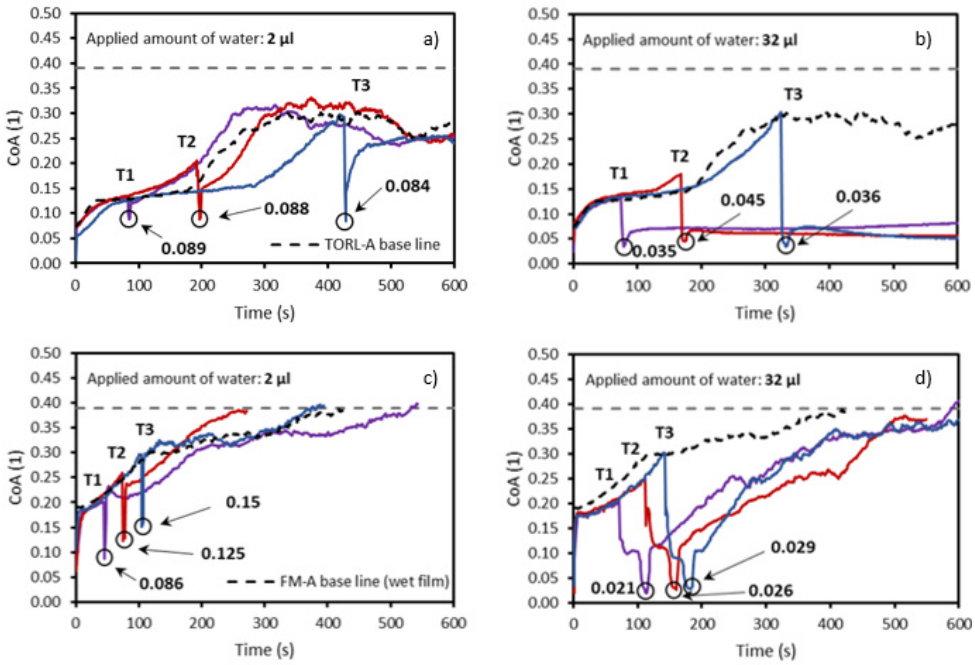

Fig. 3.10 Interaction of water with TOR lubricant **(a)**,**(b)** and with friction modifier **(c)**,**(d)**

In the case of the friction modifier, a large amount of water also caused a significant drop in adhesion, reaching approximately 0.1, followed by a further drop to values lower than 0.03. This behaviour is characteristic of the viscous paste formed when a small amount of water mixes with solid particles **[22]**. These results indicate that this low adhesion phenomenon can occur even when

the contact is treated with a friction modifier. On the other hand, no additional adverse effects were observed when the friction modifier interacted with water. The experiments also included a scenario where a dry friction modifier layer was contaminated with water. In this case, the frictional behaviour was similar to that observed for the friction modifier before the base medium evaporated.

Fig. 3.11 shows the duration of low adhesion conditions for different TOR products and various amounts of water. The data indicate that low or critically low adhesion is most likely when a large amount of water contaminates a TOR lubricant. For the friction modifier, low adhesion can also occur; however, it persists only for a short duration, as is typical for water-debris mixtures. When the largest amount of water was applied, the friction modifier was washed off the surfaces, and no further adverse effects were observed.

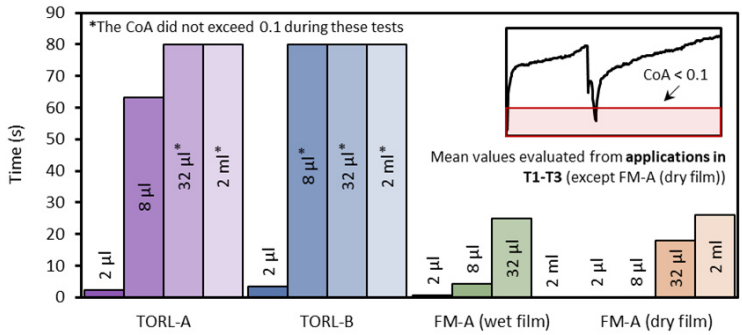

Fig. 3.11 Duration of low-adhesion periods for various TOR products and water amounts

3.5.3 Assessing the Performance of TOR Lubricants in Humid Environments and Under Dew Conditions [143]

The third study aimed to investigate how changes in relative humidity affect the performance of TOR products. It focused especially on dew conditions, which often occur in the morning and evening and are associated with many reported low-adhesion incidents. Moreover, these conditions are common in tunnels. Based on the results of the previous study, this study focused only on TOR lubricants, as they are more prone to causing low adhesion conditions when contaminated with water. For this purpose, the MTM2 in a ball-on-disc configuration was equipped with a climate chamber that supplied moist air from a humidification unit. The performance of two commercial TOR lubricants was evaluated at different levels of relative humidity (34%, 70%, and 100%) and two specimen temperatures (22 °C and 12 °C). Unlike the previous article, all experiments were conducted as traction tests following the I-OLF methodology, specifically designed to assess TOR product performance. This methodology is introduced in detail in Chapter 4.6.1.

Fig. 3.12 shows the results of experiments for six sets for one of the tested TOR lubricants (TORL-A). Each graph includes several creep curves, illustrating the behaviour of the product from its application (typically represented by the lowest curve) until the point where the effect of the TOR product becomes negligible (the highest curve meeting the criterion). In the corner of each graph (except the first), information about the measured condensate water volume on the disc is provided. It should be noted that calculations indicate that only approximately 4% of this water volume was directly on the contact path. The results show that the number of curves rapidly increased with rising water amounts, particularly in or near the red traction zone, representing the critical area where very low adhesion occurs.

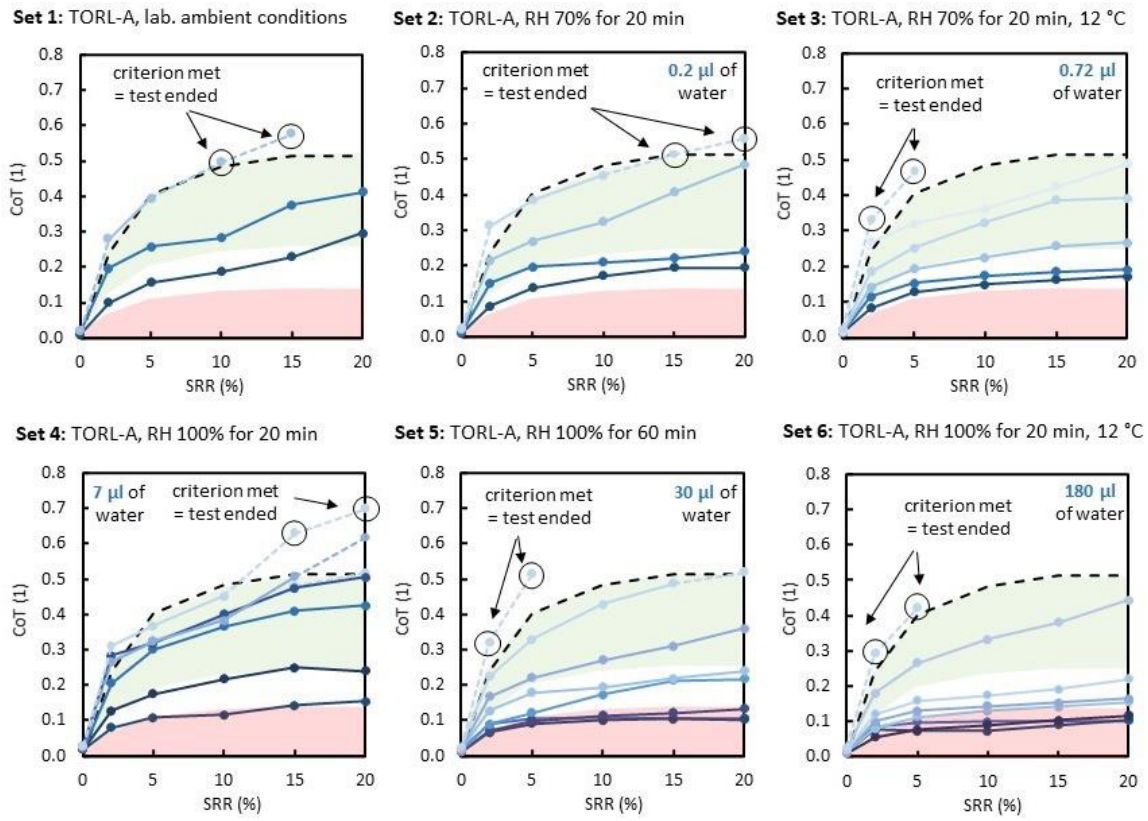

Fig. 3.12 Effect of relative humidity, specimen temperature, and humidification duration on the performance of the TOR lubricant (TORL-A) tested using the I-OLF methodology

The data from **Fig. 3.12** were then used to create a performance map, as shown in **Fig. 3.13**. The performance map categorises TOR products into four performance classes, ranging from Q1 to Q4. Arrows on the graphs show how the performance of TORL-A varies with increasing condensate levels. The best result (Q2) was observed when a minimal amount of water was present (set no. 2), while the poorest result (Q3) was seen in set no. 8, where the highest water volume interacted with the TOR lubricant. Under these conditions, 1 µL of TOR lubricant interacted with approximately 7 µL of water. The results for the second tested TOR lubricant (TORL-B) followed a similar trend as observed for TORL-A.

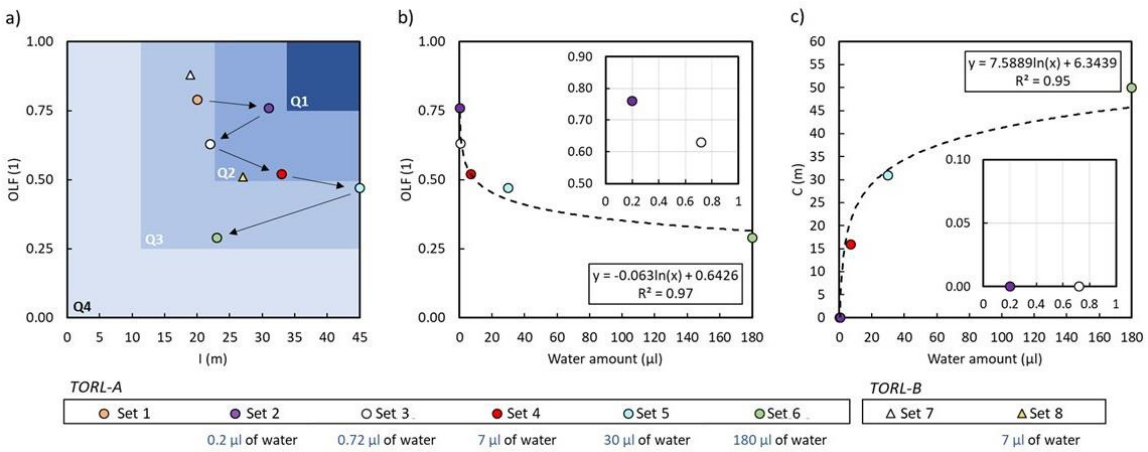

Fig. 3.13 (a) Performance map; **(b)** dependence of OLF on water amount for TORL-A; **(c)** dependency of the C parameter on water amount for TORL-A

The findings show that TOR lubricant performance remains relatively stable with changes in relative humidity, but significant changes arise under dew conditions, potentially leading to low or very low adhesion, as shown in **Fig. 3.14**. This figure also includes data from two earlier studies (references 27 and 31 in **Fig. 3.14**). The combined insights from the three studies introduced in this chapter **[141]-[143]** can be utilised to manage the application strategy of TOR products, considering environmental factors.

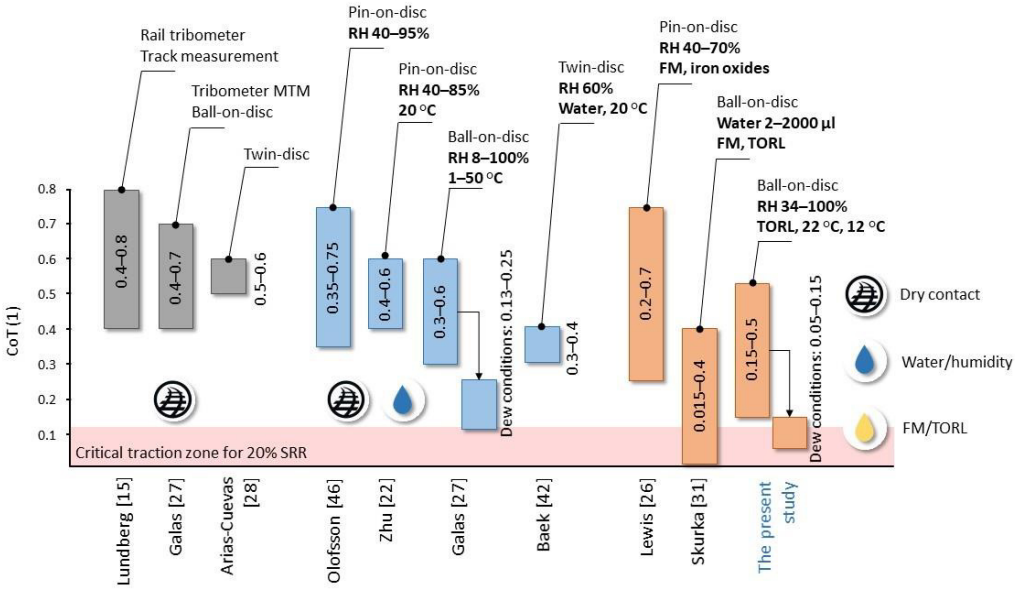

Fig. 3.14 Comparison of friction/adhesion results measured using different experimental approaches under various environmental conditions

4

APPROACHES FOR TESTING TOP-OF-RAIL PRODUCTS

4.1 Introduction

Several types of TOR products are currently on the market **[7],** with new ones continuously being developed. Developing a new product or selecting a suitable TOR product and its application strategy for a specific track or operator can be highly challenging, as their performance can be evaluated from multiple perspectives. The frictional properties are among the most important aspects of TOR products and should always be considered, as they are crucial for achieving the expected benefits associated with TOR friction modification. Experimental approaches for investigating these frictional properties can be classified into laboratory and field testing.

Field testing using an instrumented vehicle may be the most accurate approach; however, significant limitations, including cost, must be considered. One major limitation is the open nature of the system, which leads to constantly changing environmental conditions that affect the composition of the natural third body layer. Additionally, experiments can be complicated by variability in the thickness of the TOR product layer. When applying the TOR product using a wayside system, passing vehicles spread a puddle of the product along the track. This means that the thickness of the layer on the rail, typically less than one micron **[144]**,**[145]**, decreases with distance from the point of application. Additionally, it is further reduced as it is gradually consumed by passing vehicles. Considering factors such as changes in surface topography and varying vehicle operating conditions, quantifying the performance of an individual TOR product in the field is challenging, and comparing the performance of several TOR products is even more difficult. Therefore, field testing with an instrumented vehicle should be seen as a final step rather than a routine test, for which laboratory testing is more suitable.

Laboratory testing provides the benefit of conducting experiments under controlled conditions and is typically less time-consuming and more cost-effective, depending on the device used. A primary challenge remains in transferring laboratory results to actual wheel-rail contact, which can be partially addressed by using full-scale devices or portable devices for field testing. Selecting a suitable experimental device and carefully designing the experiment to match the specific phenomenon under study is essential for achieving reliable and representative results.

4.2 Rigs for wheel-rail contact research

Many different experimental rigs are used to study wheel-rail friction properties. These rigs can be categorised based on various aspects. The most straightforward way to organize them is by rig scale, distinguishing between full-scale and reduced-scale rigs. Note that the terminology used in this subchapter has been partially adapted from **[146]**. Full-scale rigs can be further classified into three groups based on their complexity: vehicle/bogie rigs **[147],[148]**, wheel-on-roller rigs **[149],[150]**, and wheel-on-straight track rigs (sometimes referred to as 'linear' rigs) **[40],[151]**. Vehicle/bogie rigs and wheel-on-roller rigs offer significant advantages, enabling high speeds, reaching up to 500 km/h **[152]**, and closely simulating the dynamic behaviour of the system. In contrast, wheel-on-straight track rigs operate at much lower rolling speeds. However, they provide non-repeated contact conditions, which can be useful when studying the formation process and transfer mechanisms of applied products, such as in evaluating traction gels **[153]**.

Reduced-scale rigs are divided into three sub-groups in this work. The first sub-group consists of rigs specifically designed for studying wheel-rail contact. This sub-group includes wheel-on-roller rigs (with single or multiple contacts) **[154],[155]**, twin-disc machines **[156],[157]**, wheel-on-rail track rings **[158],[159]**, and wheel-on-straight rail rigs **[160],[161]**. The second sub-group contains commercial tribometers in various configurations, which enable the simulation of a range of tribological contacts and systems, including wheel-rail contact. Since these tribometers typically offer various testing modules, both rolling-sliding and pure-sliding conditions can be achieved; for example, the MTM2 allows for both configurations **[120],[162]**. The last sub-group includes portable devices, such as pendulums **[163],[164]** and tribometers **[165],[166]**, which can be used in both laboratory and field conditions to evaluate railhead frictional properties.

The devices in the first and second sub-groups typically do not reach the high speeds typical for full-scale devices; however, they generally provide better control of conditions and greater repeatability. Additionally, the small sample sizes enable both surface and subsurface analysis and allow for easy sample exchange, making these devices suitable for studying rolling contact wear and fatigue. Devices in the third sub-group are mainly useful for comparing laboratory and field data.

4.3 Laboratory testing of TOR products

In 2002, two pioneering studies on the frictional properties of TOR products were published by Japanese researchers **[17],[18]**. Matsumoto et al. **[17]** examined the frictional performance of a commercial friction modifier using a scaled wheel-on-roller rig (1:5 scale) developed specifically for this purpose. Their objective was to determine whether this TOR product could produce a positive creep curve. The results showed that the friction modifier changed the negative creep curve trend observed under dry conditions to a positive one in both lateral and longitudinal directions.

A similar finding was reported by Tomeoka et al. **[18]**, who studied the behaviour of the friction modifier in both the laboratory and the field. Moreover, their study includes a complex laboratory experiment in which a friction modifier layer was subjected to several consecutive tests, simulating repeated vehicle passes over the same location, as was shown in **Fig. 2.2**. During these tests, the desired positive trend of the creep curve was consistently observed, with the CoF increasing after each test until dry conditions were reached.

Since Matsumoto et al. and Tomeoka et al. **[17],[18]** published their pioneering studies, numerous articles investigating the performance of TOR products under laboratory conditions have followed. These studies tested different types of TOR products using various experimental approaches to examine different performance parameters. As this chapter focuses on the development of testing methodology for TOR products, key findings from laboratory studies are summarized into points to provide a comprehensive overview rather than describing detailed results of individual studies.

- The most common type of experiment to investigate the frictional behaviour of TOR products is a friction test, which shows the development of the CoA over time (or the number of cycles) at a constant slip value. Based on this experiment, two parameters are often determined: the minimum adhesion level **[168]**, typically observed immediately after product application, and retentivity, also referred to as the lasting effect or holding time **[20],[24],[63]**, as shown in **Fig. 4.1**. Retentivity is defined as the number of cycles during which a TOR product influences adhesion in the contact, measured from the point of application until its effect becomes negligible (reaching a specified friction threshold) **[169]**. This experimental approach is widely used as it allows straightforward comparison of different TOR products **[25],[136],[167]**. Although some studies did not directly quantify retentivity, it was generally considered when comparing TOR product performance.

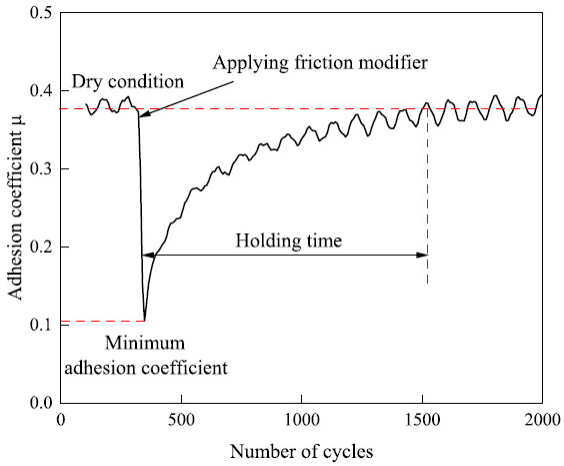

Fig. 4.1 Friction test with commonly evaluated parameters **[63]**

- The data from the friction tests mentioned above, measured for various slip values, are often used to evaluate creep curves to reveal whether a tested TOR product provides the required positive trend, as shown in **Fig. 4.2**. This method is applied because most experimental devices do not allow direct measurement of the creep curve in a traction regime. Using this approach, a positive effect has been consistently observed across different TOR product types, including friction modifiers **[20]**, TOR lubricants **[24]**, TOR hybrids **[29]**, and solid sticks **[35]**. However, in some cases, a neutral **[26]** or even negative slope **[35]** has been observed in contacts treated with TOR products. Additionally, certain creep curves consistently exhibited the CoF below 0.1, **[26],[27],[54]**, significantly under the target intermediate friction level.

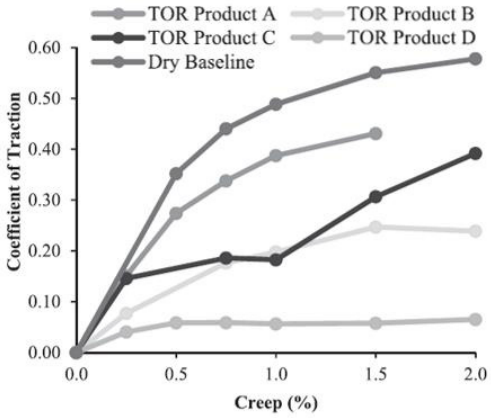

Fig. 4.2 Creep curves generated based on friction tests **[29]**

- As described in the second chapter of this thesis and shown in **Fig. 2.3(a)**, the performance of TOR products depends significantly on the applied amount **[60],[63]**. Therefore, this factor is often considered when investigating the performance of TOR products **[170],[171]** to ensure that their frictional behaviour is evaluated at an optimal amount. In cases where an excessive amount is applied, extremely low adhesion values can occur, and the frictional behaviour is then similar to that of oil/grease rather than a TOR product, as demonstrated by Stribeck tests in **[24]**. This amount-dependent effect is especially evident for TOR lubricants due to their oil-based composition **[142]**.
- Other frequently evaluated parameters of TOR products relate to wear and surface damage. These aspects can be studied using two test strategies, referred to here as common and specialised tests. Common tests assess fundamental parameters such as wear rate, RCF, and subsurface damage **[28],[168]**. Twin-disc machines are commonly used to evaluate these parameters, with contact bodies made from wheel and rail materials to simulate wheel-rail contact accurately. In contrast, specialised tests focus on specific parameters, such as changes in rail profile, and require specialised testing rigs **[39],[40].** Experiments focusing on wear rate and fatigue are not typically part of the friction tests described above but are conducted separately due to differing test parameters.
- Impedance is another key parameter in rail transport, as any material applied between the wheel and rail can impact shunting. This process is crucial for accurate signal transmission and to prevent potential safety issues within the railway network. Studies on this effect have focused on solid TOR products **[34],[172],** using a twin-disc machine with a simplified electrical circuit to enable impedance evaluation. An example of this experiment is shown in **Fig. 2.5**.
- When TOR products are applied between two surfaces in relative motion under high contact pressure, it is crucial to evaluate the released particles, especially ultra-fine particles **[173]**, as they can pose a health risk **[174]**.
- The behaviour of TOR products is influenced by their transfer mechanisms, which should be considered when evaluating their performance. According to **[175]**, three key transfer mechanisms are identified: pick-up, carry-on, and consumption. The first mechanism, pick-up, describes the amount of product the wheel picks up from the puddle on the rail, as shown in **Fig. 4.3(a)**. The second mechanism, carry-on, refers to the subsequent transfer of the product from the wheel back to the rail, as depicted in **Fig. 4.3(b)**. Finally,

the consumption mechanism involves the removal of the product layer from the contact surfaces, which can be quantified using the retentivity parameter described above. Lee et al. **[176]** used a linear full-scale rig to study these transfer mechanisms, emphasising the importance of application quantity and the role of product tackiness, which can be assessed with an HPT tribometer following the methodology in **[177]**.

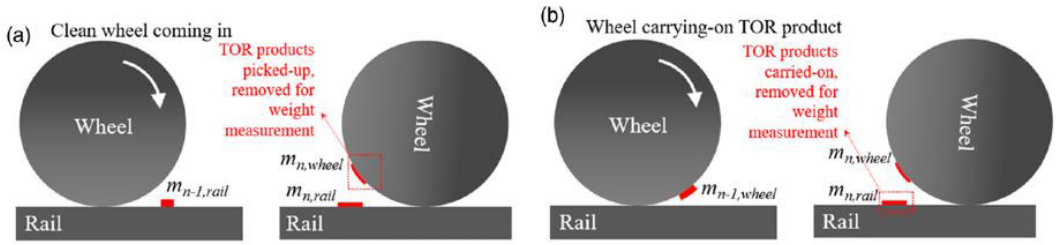

Fig. 4.3 (a) Pick-up mechanism; **(b)** carry-on mechanism **[176]**

- Based on the literature review, several key aspects important for testing TOR products have been identified. They should be considered when designing experiments to evaluate their performance, as these aspects can significantly affect the results. These aspects mainly involve the wear-in and run-in processes, the type and conditions of experiments, the application method of TOR products, the range of tested amounts, and friction values used as thresholds, all of which are critical for accurate evaluation.
- One key literary source is the recently published standard CEN/TS 15427–2–2:2021, Railway Applications - Wheel/Rail Friction Management - Part 2–2: Properties and Characteristics - Top of Rail Materials **[178]**. This standard specifies methods for testing and evaluating TOR products using a twin-disc machine and the MTM tribometer in the ball-on-disc configuration. In particular, twin-disc tests outline procedures for assessing product retentivity and creep curves, while MTM tests use a series of traction tests to compare a tested product with a single threshold obtained for a commercial TOR product already approved for use in operations.

4.4 Field testing of TOR products

As introduced in the first chapter of this thesis, a pilot field study on TOR friction modification, focusing on corrugation issues and friction modification by solid sticks, was published by Kalousek and Johnson in 1992 **[3]**. Following this, several scientific articles and field reports were released. In 1998 and 1999, the U.S. Department of Transportation published two comprehensive reports utilising trains with the same on-board lubrication system **[179],[180]**. These studies provided valuable insights into the performance and benefits of TOR lubrication. The findings demonstrated that optimal dosing of TOR products could reduce lateral curving loads, energy consumption, and fuel use without negatively affecting braking distance, train handling, or speed control. However, these studies also identified certain risks linked to TOR products, such as wheel slip occurrence due to improper application rates.

Several subsequent field studies have demonstrated the ability of TOR products to reduce lateral curving loads **[170], [181]** and mitigate corrugation development **[36],[38]**. In addition to a lateral load reduction, Tomeoka et al. **[18]** reported a reduction in tangential force on two tested tight curves treated with a TOR product sprayed onto the rails from the vehicle. However, this reduction

led to a significant drop in the F/P ratio (tangential force/wheel load), from 0.31 and 0.23 under dry conditions to 0.13 and 0.07 with a TOR application. Areiza et al. **[182]** compared the effects of two TOR products and a flange lubricant at two different contact pressure values. Their findings showed that both TOR products reduced the CoT, with one achieving excessively low values comparable to values measured for the flange lubricant. Additionally, their study observed a positive trend in the creep curve for both TOR products, which was also unexpectedly seen under dry conditions, where a negative trend is generally expected.

Other researchers have also observed a tendency for low friction conditions after applying TOR products. Lundberg et al. **[144]** reported that the CoT highly depends on the amount of TOR product used, specifically the friction modifier, which was manually applied to the rails. When a larger amount of this friction modifier was applied, unacceptably low CoT values (0.13-0.16) were recorded, as shown in **Fig. 4.4**. Moreover, this conclusion was validated using two measurement methods: a handheld tribometer and an instrumented train. This method comparison revealed that the actual CoT measured by the train was lower than that obtained from the tribometer. It could be useful information for other studies when designing their experiments or interpreting obtained results. Similar findings have been reported by Khan et al. **[32]**, who investigated the effect of a friction modifier using a hand-push tribometer. They found that an excessive amount can cause low friction conditions for tens of meters from the application point. Conversely, repeated applications of a smaller amount of friction modifier achieved the desired friction level without the occurrence of low friction conditions.

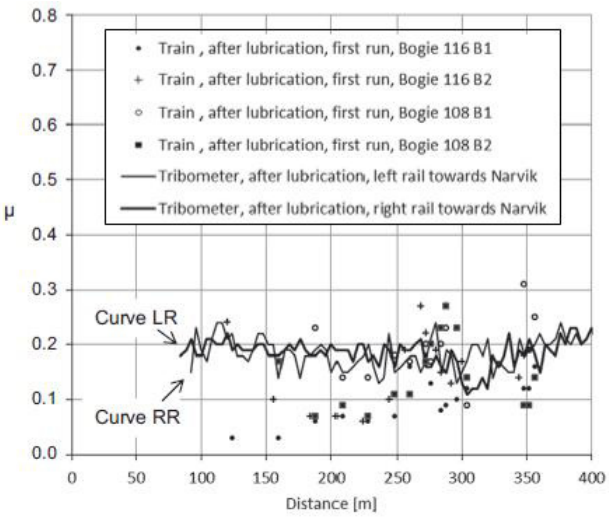

Fig. 4.4 CoF as a function of distance under lubricated conditions **[144]**

As a consequence of low adhesion conditions, braking or traction issues can occur. A series of tram braking tests with varying amounts of the TOR lubricant applied using a wayside system on both rails were conducted in **[30]**. Results showed that with the smallest amount, braking distance was unaffected, but no noise reduction was observed. When the amount of TOR product was increased, the distance was extended by up to 66%, and braking was accompanied by wheel skidding. Similarly, a study by Khan et al. **[32]** reported a roughly 20% reduction in braking capacity and occurrences of wheel slippage when the TOR product was applied. In contrast, Ibrahim et al. **[183]** found no negative effect of a TOR product on the braking distance of a maintenance vehicle. In this case, a roller was used to apply a uniform, 100-meter layer of product on both rails.

The application strategy of a TOR product and the product itself plays a key role in achieving the expected benefits without any negative impacts described above. As previously mentioned, a high-performance TOR product can provide a positive creep curve and an intermediate level of friction; however, it should also be spread along the track as far as possible and remain effective for as long as possible. The distance over which a TOR product remains effective is referred to in the literature as the carry distance (sometimes also called carry-on distance) **[175]**, while the retentivity parameter indicates the duration for which the TOR product maintains its effectiveness **[169]**. Despite their significance, only a few field studies have focused on these two important parameters.

Different methods have been used to investigate the carry distance, as it cannot be assessed with the naked eye **[145]**. Chen et al. **[139]** studied the carry distance of five products (not only typical TOR products) using a compact rail tribometer operating under pure-sliding conditions. Their findings indicated that the carry distance varied between 18 and 125 meters. Additionally, they observed that increasing the application amount from 2 to 5 mL did not significantly affect the carry distance for most of the products tested. Khan et al. **[184]** proposed an alternative approach, using cotton swabs to collect the third body layer from the rail at various distances from the application point. The collected samples were analyzed using energy-dispersive X-ray, based on which the carry distance was then determined.

This technique was used to investigate the carry distance of two TOR products on an actual track at two locations. One location was equipped with a wayside system, while the other used a manual application method to demonstrate the difference between drying and slowly drying TOR products **[184]**. When applied via the wayside system, the maximum carry distances were 70 m for drying products and 450 m for slowly drying products. At the second location, the carry distances were shorter, measuring 65 m and 320 m, which were significantly lower than those claimed by the manufacturers. The study also analysed how far the TOR products remained in the contact band on the wheel, revealing that they remained effective up to 100 m for drying products and 340 m for slowly drying products. However, both TOR products were found on the sides of the wheel contact band over 3 km from the application point.

These observations align with **[185]**, where the carry distance was assessed by detecting a friction modifier containing a dye using the laser-induced fluorescence method. The friction modifier was detected on the tangent track up to 200 m; however, in the contact band, the distance was limited to 70 m due to the inability of the product to withstand high pressure in the contact zone, as shown in **Fig. 4.5(b)**. In addition, **Fig. 4.5(a)** shows that the friction modifier reappeared in the curves, detected up to 2 km from the application point. This reappearance occurred because some of the product initially squeezed out to the sides of the wheel contact band returned to the contact area. This re-entry was due to the lateral movement of the wheelsets when the vehicle was curving. These findings provide evidence that the carry distance does not need to be continuous, as the initially squeezed TOR product can re-enter the contact band, thereby affecting frictional conditions several kilometres away from the application point. This phenomenon, termed the 'phantom applicator' effect, was identified by Mast et al. **[186]** during their studies on carry distance using various optical methods.

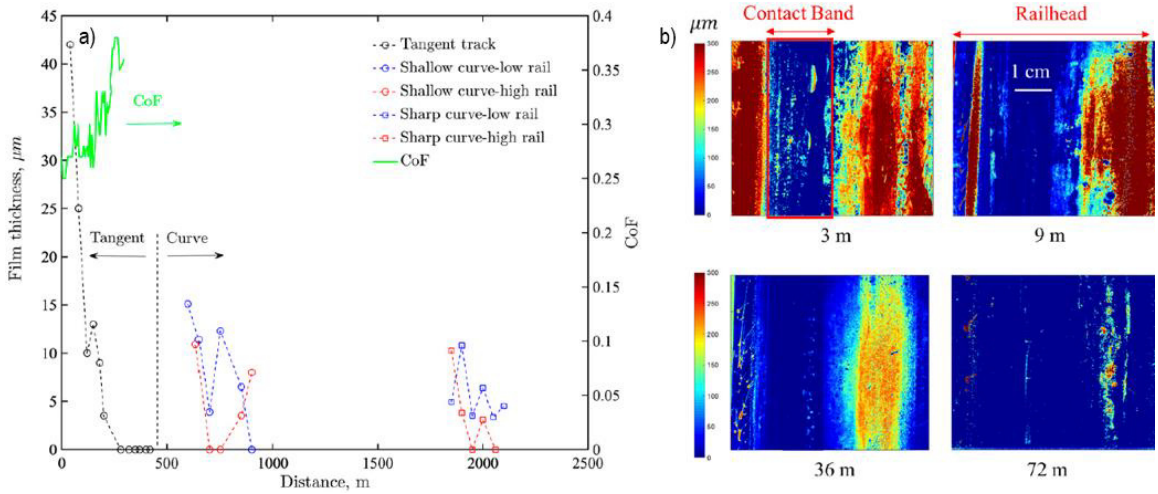

Fig. 4.5 **(a)** Film thickness of friction modifier and CoF as a function of distance in various track sections; **(b)** deposited frictional layer of friction modifier on the railhead **[185]**

Although carry distance is often assumed to be continuous in models **[175]**, the findings above suggest it can vary, particularly due to the phantom applicator effect. Additionally, the CoT can fluctuate significantly over distance, even on tangent track sections **[144]**. This variation is crucial for examining the retentivity parameter, emphasising the importance of selecting appropriate locations for its assessment. An example is the study by Fukagai et al. **[188]**, which investigated how the CoF changed with the increasing number of axles passing through a tested curve treated with the TOR product.

4.5 Summary of the literature review and research gaps

Many scientific studies focusing on wheel-rail tribology, including TOR product testing, have been conducted in laboratory environments using small-scale devices, primarily twin-disc machines **[187]**. These studies address key aspects of TOR product performance, such as creep curve trends **[20]**,**[62]**, product retentivity **[30]**,**[55]**, wear **[53]**,**[63]**, and surface damage **[28]**,**[64]**. A significant issue arises from the use of various experimental devices that are often custom-made and have differing testing parameters across studies, which makes it challenging to compare results. Additionally, the effect of the TOR product application amount is not always considered, potentially leading to inconsistent or misleading results.

While custom-designed experiments can be used to investigate various phenomena related to TOR products, e.g. studying the film thickness of the TOR product layer, a universal tool for straightforward comparisons of their general frictional performance is lacking. It should be noted that the CEN/TS 15427–2–2:2021 standard **[178]** partially addresses this gap. Although tests conducted according to this standard provide valuable information on whether a TOR product may lead to insufficiently low friction conditions, other critical aspects, such as retentivity and the ability to achieve an intermediate friction level, are not considered in the section focusing on testing using the MTM. In other words, a more comprehensive performance assessment of TOR products is needed. Furthermore, the standard does not adequately emphasise the need to test different application amounts of TOR products, even though performance can be strongly dependent on the amount used **[24]**,**[176]**. This effect is especially important when testing TOR products on

scaled devices **[169]**, making it reasonable to consider application amount as a standard parameter in TOR product testing.

Another part of the literature focuses on the performance of TOR products under field conditions or in settings that closely simulate these conditions. While many field studies have investigated the effect of TOR products on noise **[12]**,**[37]** and corrugation reduction **[36]-[38]**, as described in detail in Chapter 2, only a few publications have been focused on their frictional properties. A limited number of articles have addressed research on carry distance **[184]**,**[185]**, as it is a highly challenging parameter to study under field conditions and even more under laboratory conditions. Various methods have been employed to evaluate the carry distance in the field **[139]**[**184]**,**[185]**; however, these methods typically do not include friction measurements, meaning that the investigated carry distance may not accurately represent the distance over which the desired frictional properties are delivered. Even less information has been reported from field studies on retentivity and creep curves.

Track performance parameters, such as retentivity and carry distance, have not been extensively studied, likely due to the demanding methodology required for field experiments and limitations in available devices. Track tribometers appear to be the most suitable choice for this purpose; however, a primary limitation is that most do not allow for investigation of 'local' friction properties over a short distance. Given this limitation, these devices are hardly suitable for assessing retentivity at a specific track section (measuring over a short distance). For similar reasons, this approach is difficult to use in laboratory studies focusing on carry distance. Additionally, tribometers typically lack the capability to measure creep curves over a short distance and tend to overestimate CoT results **[144]**, making it challenging to investigate the frictional properties of a TOR layer on a real track.

On the other hand, some portable tribometers, such as the model described in **[189]**, allow for an evaluation of the CoT over short distances. In the case of this device, a partial creep curve, up to 16% slip, can also be investigated by adjusting various angles of attack. This method can be effectively applied in both laboratory and field testing of TOR products. Another promising approach for studying track performance parameters under laboratory conditions has been introduced by Lee et al. **[176]**, who used a full-scale linear rig to evaluate the pick-up, carry-on, and consumption mechanisms of two friction modifiers. Similarly, the study **[161]** proposed the concept of a scaled-down 'linear' rig, which presents another potential option for such investigations.

Based on this literature summary, the following research RGs have been identified:

- **RG1:** A comprehensive methodology to compare TOR products based on frictional performance is currently lacking. Testing TOR products in varying amounts should be an integral part of this methodology, as numerous studies emphasise its importance **[24]**,**[63]**,**[176]**. In addition, the proposed methodology should ensure the transferability of results between laboratories.
- **RG2:** Knowledge about the track performance parameters of TOR products, including carry distance, retentivity, and creep curve shape, remains limited. This is largely due to the complexity of both laboratory and field experiments and the high demands on test equipment. No study has yet defined a comprehensive methodology for investigating these track performance parameters in both laboratory and field conditions. Published studies often focus on a single parameter rather than providing a comprehensive assessment. The following three sub-gaps have been identified to address this important RG:

- **RG2.1:** Develop a portable tribometer that enables evaluation of the CoT and the creep curve, specifically for measurements conducted over short distances on the rail.
- **RG2.2:** Propose a laboratory methodology for evaluating track performance parameters of TOR products, primarily focusing on carry distance and retentivity.
- **RG2.3:** Develop a field methodology for assessing track performance parameters in actual operational conditions.

4.6 Author's contribution

Building on experience from previous work and addressing identified research gaps, the authors developed a multi-phase methodology for testing TOR products, as shown in **Fig. 4.6**. This comprehensive methodology consists of several testing phases that can be applied either individually or in combination. This approach reduces the number of field experiments needed when evaluating the performance of a TOR product before deployment to operation or during the development of a new TOR product. The development of this methodology includes four articles **[190]-[193]** published in peer-reviewed journals.

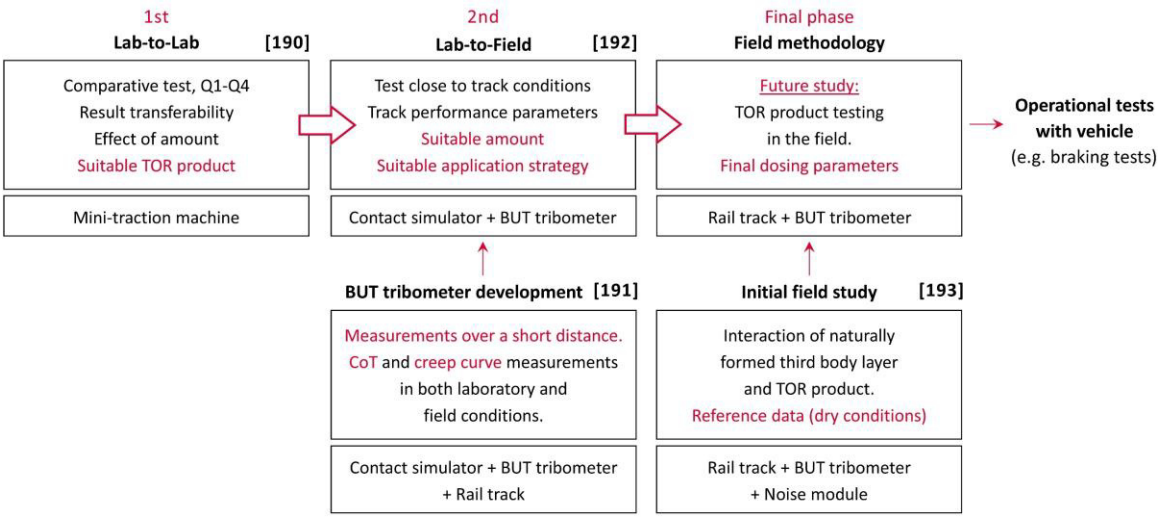

Fig. 4.6 Proposed multi-phase methodology for testing TOR products

The contribution of the first study **[190]** lies in the development of the initial phase of a benchmarking methodology, depicted in **Fig. 4.6**, which addresses **RG1**. This methodology allows for the assessment and comparison of the frictional performance of TOR products under laboratory conditions. A key feature includes testing various applied amounts for each TOR product, providing a comprehensive understanding of their performance. This methodology ensures full transferability of results among laboratories, as is typical for international standards; therefore, it is referred to as the Lab-to-Lab methodology. As a result, it serves as a universal tool for selecting the most suitable TOR product for further evaluation.

The second study **[191]** contributes to the field by developing a portable tribometer designed for measuring friction on the top of the rail. This tribometer (referred to as the BUT tribometer) is important for two phases of the multi-phase methodology, as shown in **Fig. 4.6**, and fully addresses **RG2.1**. A key advantage is its ability to investigate the frictional properties of both the third body layer and the TOR product layer over a short distance, which is essential for determining TOR product performance. This capability allows the tribometer to be used for both laboratory and field research, enabling direct data comparison. Additionally, the tribometer can assess a complete creep curve over short distances and measure very low values of CoT, which is useful when studying frictional properties of leaf layers, for example.

The third study **[192]** presents the second step of the multi-phase methodology, which involves further testing of the TOR product identified as the best-performing according to the Lab-to-Lab methodology **[190]**. The main contribution of this second phase lies in its ability to study typical track performance parameters of TOR products, such as carry distance and retentivity, under laboratory conditions that closely simulate actual track conditions. Referred to as the Lab-to-Field methodology, this step serves as a 'bridge' between laboratory and field testing of TOR products. As shown in **Fig. 4.6**, this approach also enables the determination of the optimal amount and application strategy, which are challenging to study effectively using small-scale devices. The results obtained using this Lab-to-Field methodology can serve as preliminary inputs for field testing, thus reducing the number of demanding field tests. In addition, the methodology enables the determination of the transfer behaviour of a tested product and employs a predictive model simulating product redistribution, which is useful for modelling. This study fully addresses **RG2.2**.

The fourth study **[193]** represents the initial field step of the multi-phase methodology, aimed at assessing the suitability of a newly developed tribometer for field experiments. A key contribution of this phase is the examination of the frictional properties of the natural third-body layer (without applying a TOR product), providing valuable insights into how weather conditions influence dry friction. The findings will be used in future research focused on evaluating the friction properties of a TOR product in the field. Furthermore, the study revealed a significant relationship between CoT and noise duration. This phase partially addresses **RG2.3**, as a comprehensive field-testing methodology for TOR products has yet to be developed.

The author has contributed to the following papers[3]:

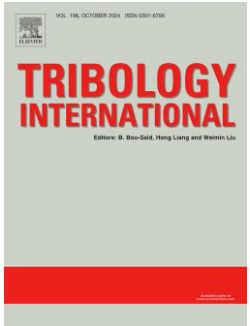

[190] Galas R, Skurka S, Valena M, Kvarda D, Omasta M, Ding H, et al. A benchmarking methodology for top-of-rail products. Tribology International 2023;189.

Author's contribution	35%
Journal impact factor (2023)	6.052
JIF/AIS Quartile	Q1/Q1
Citations (WoS/Scopus/Google Scholar)	2/3/3

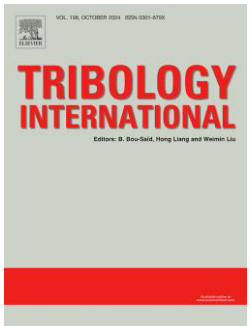

[191] Valena M, Omasta M, Kvarda D, **Galas R**, Krupka I, Hartl M, et al. An approach for the creep-curve assessment using a new rail tribometer. Tribology International 2024;191.

Author's contribution	17%
Journal impact factor (2023)*	6.052
JIF/AIS Quartile*	Q1/Q1
Citations (WoS/Scopus/Google Scholar)	2/2/2

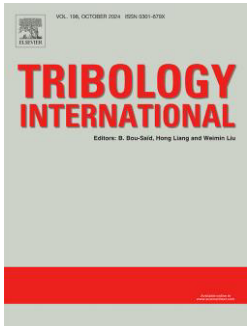

[192] Galas R, Valena M, Jordan T, Kvarda D, Omasta M, Skurka S, et al. A benchmarking methodology for top-of-rail products: Carry distance and retentivity. Tribology International 2024;197.

Author's contribution	45%
Journal impact factor (2023)*	6.052
JIF/AIS Quartile*	Q1/Q1
Citations (WoS/Scopus/Google Scholar)	1/1/1

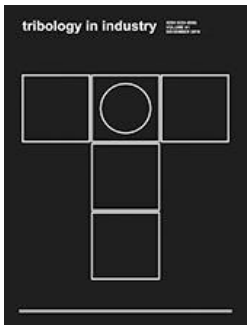

[193] Valena M, Omasta M, Klapka M, **Galas R**, Navratil V, Krupka I, et al. Case study: Correlations between Curve Squeal, Weather Conditions, and Traction in a Tram Loop. Tribology In Industry, Article in press.

Author's contribution	13%
Journal impact factor (2023)	not relevant
JIF/AIS Quartile	not relevant
Citations (WoS/Scopus/Google Scholar)	-/0/0

*The data for the year 2024 are not yet available.

[3] All listed articles are listed in Chapter 9.

4.6.1 A benchmarking methodology for top-of-rail products [190]

This study introduced the Lab-to-Lab methodology for comparing the frictional performance of TOR products. This methodology was designed for a commercial tribometer, the MTM2, in a ball-on-disc configuration to ensure result transferability and to achieve typical rolling-sliding conditions. Investigating the frictional performance of each TOR product for a specific amount requires five performance tests using the same specimens. As shown in **Fig. 4.7(a)**, each performance test includes six steps that define the procedure for both the preparation and measurement phases. A key step, S4, specifies the traction test procedure, which is repeated until the stopping criterion is met, after which the next performance test begins from step S1. A similar experimental approach was used in **[18],[178]**.

When the five performance tests are completed, the evaluation phase begins with steps S7 to S9, as shown in **Fig. 4.7(b)**. This process is based on three traction zones (red, green, and blue), which represent areas of insufficient adhesion, optimal adhesion, and retentivity. Based on these zones, three performance parameters (C, I, and R) are calculated to express the cumulative sliding distance during which contact operated within each zone. These parameters are then used to calculate the Over-Lubrication Factor (OLF), indicating whether a tested TOR product, for a given amount, is likely to cause low adhesion issues. A lower OLF value, ranging from 0 to 1, indicates a higher risk of low adhesion issues.

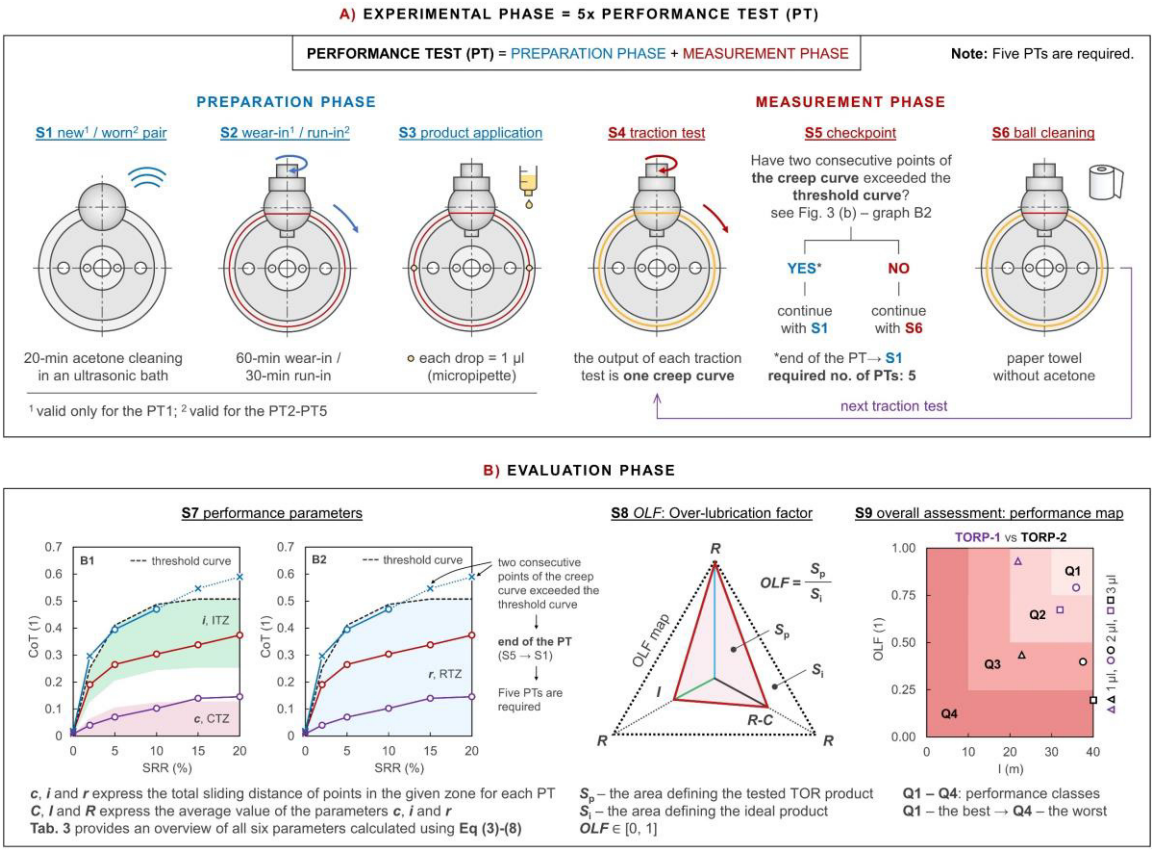

Fig. 4.7 (a) Experimental phase and **(b)** evaluation phase of the Lab-to-Lab methodology

Based on the OLF and the I parameter, which expresses 'effective' retentivity (indicating that the contact operates in the desired traction zone), a performance map is created to categorise TOR products into four performance classes. For each tested TOR product, multiple points are plotted

on this map, each representing a different tested amount. When comparing multiple TOR products, the one with the highest performance class or the best overall performance across the tested amounts is selected as the optimal product for further testing in a more representative configuration, as introduced in the second phase of the methodology: the Lab-to-Field methodology **[192]**.

This study includes a case study in which the frictional performance of several products was investigated using the proposed Lab-to-Lab methodology to demonstrate its applicability and suitability. The results shown in **Fig. 4.8** indicate that, in terms of the OLF, the sensitivity of TOR lubricants (labelled as TORL-A and TORL-B) to the applied amount is significantly higher than that observed for the tested friction modifier (labelled as FM). This suggests that increasing the amount of friction modifier is unlikely to cause any traction or braking issues. However, this water-based product provides significantly shorter effective retentivity, as expressed by the I parameter, compared to TOR lubricants. The results for TORL-A and its bleed oil further validate the methodology, as the TOR lubricant achieved higher performance than its bleed oil. Based on the overall results in **Fig. 4.8**, two TOR products, specifically TORL-B and FM, have been selected as the best-performing TOR products for further testing.

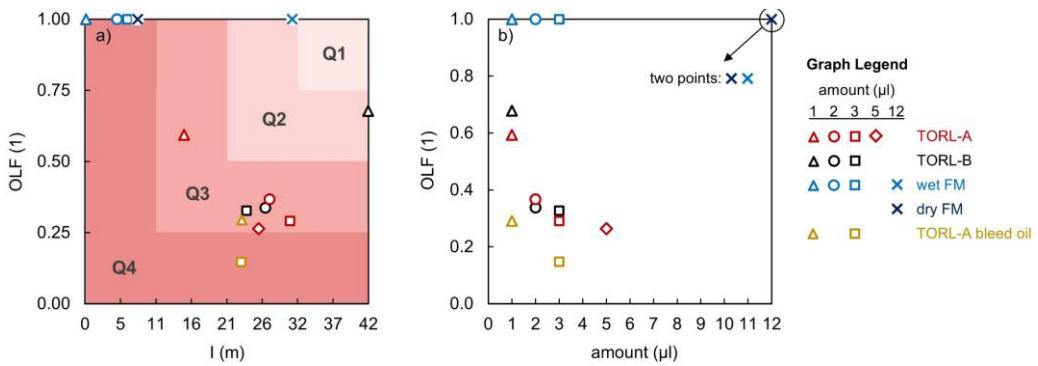

Fig. 4.8 (a) Performance map; **(b)** dependence of OLF on applied amount

4.6.2 An approach for the creep-curve assessment using a new rail tribometer [191]

The second study introduced a newly developed portable tribometer for measuring rail head friction in both laboratory and field conditions, allowing for a direct comparison of these results. The tribometer, shown in **Fig. 4.9**, was designed to operate in a traction regime that closely simulates actual wheel-rail contact conditions. This design provides precise control of the braking torque on the measuring wheel, enabling the creation of various slip values in the wheel-rail contact based on the frictional properties of the third body layer. The rapid changes in braking torque, which induce different slip values, enable the full creep curve to be obtained over short distances. This capability is essential for examining the frictional properties at specific points on the rail, which is especially important when analysing TOR product imprints.

The tribometer provides three measuring modes, each suitable for different experiments depending on the frictional layer to be analysed. Moreover, it enables the analysis of extremely low values of the CoT, as low as 0.02. These features allow for the analysis of various frictional layers, such as oxide, leaf, and TOR product layers, within just a few passes of the measuring wheel over the layer. In some cases, the experiment can be conducted even in a single pass. As a result, the findings are not significantly influenced by changes in the frictional layer during the measurement process.

Consequently, both the current frictional performance of the layer and its wear resistance can be effectively investigated. Parameters for plotting creep curves are assessed using three methods: the median method, Polach's analytical model **[59]**, and the modified FASTSIM model **[194]**.

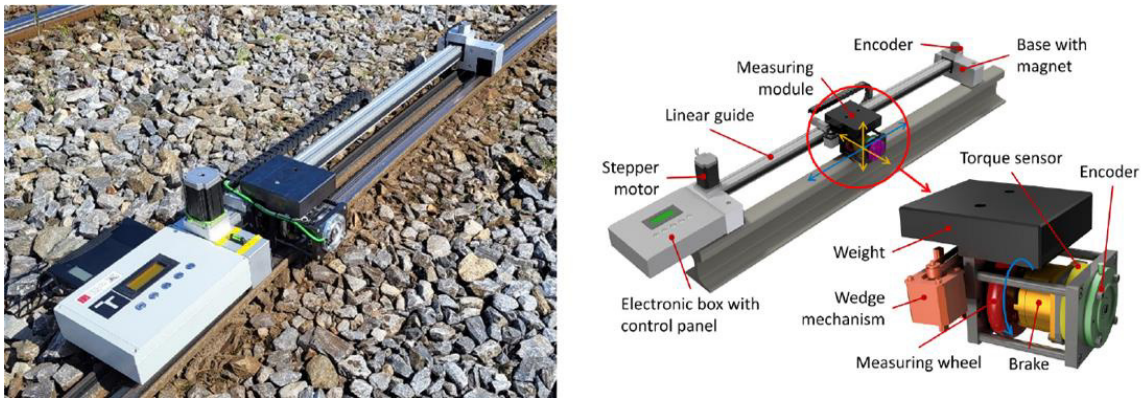

Fig. 4.9 Design of the portable tribometer

The initial experiment presented in this study compared the frictional conditions for contact before and after the run-in process, water-contaminated contact, and contact treated with TOR lubricant. The results, including both the values and shapes of the creep curves, are consistent with the literature, where a similar experimental approach was used, as shown in **Fig. 4.10(a)**. Finally, the experiment with oil demonstrated a high level of repeatability, as depicted in **Fig. 4.10(b)**.

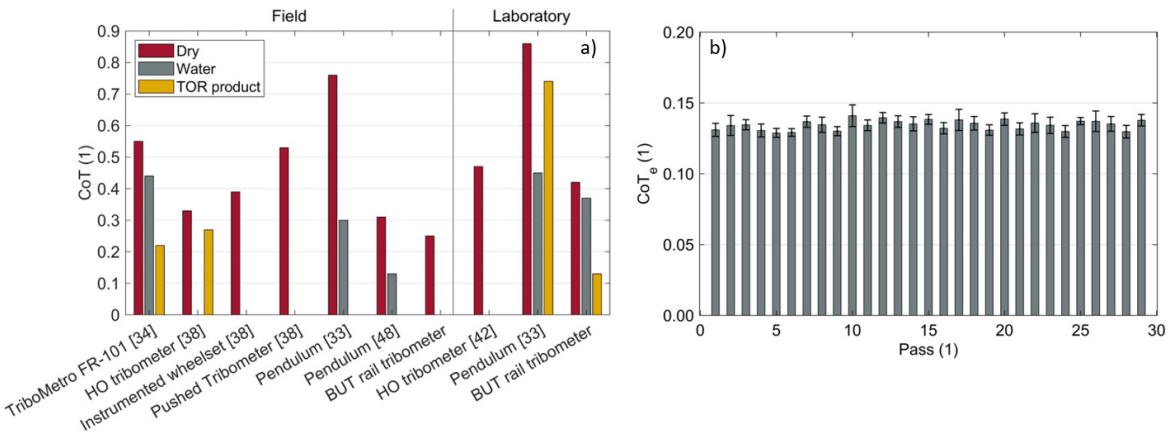

Fig. 4.10 (a) Comparison of experimental approaches; **(b)** measurement repeatability

4.6.3 A benchmarking methodology for top-of-rail products: Carry distance and retentivity [192]

The third study introduces the second phase of the proposed multi-phase methodology for TOR product testing, aiming to investigate key track performance parameters, specifically carry distance and retentivity. Two custom-made devices were utilised to achieve representative track conditions: a contact simulator (a linear rig) for creating representative TOR product imprints on the rail and a newly developed portable tribometer **[191]** for analysing these imprints.

The carry distance was evaluated based on the number of TOR product imprints (see **Fig. 4.11**) that provided a CoT value below the selected threshold, indicating the transition from treated to untreated contact. The same threshold was used to evaluate TOR product retentivity; however, only the imprint at the application point was analysed in this case. Several dozen passes were conducted over this imprint using the contact simulator, with friction analysis performed periodically using the portable tribometer. Upon test completion, retentivity was determined as the total number of passes before reaching the threshold. The data from the retentivity tests were then used to calculate the OLF and plot creep curves (see **Fig. 4.12**), showing the development of these curves with increasing passes.

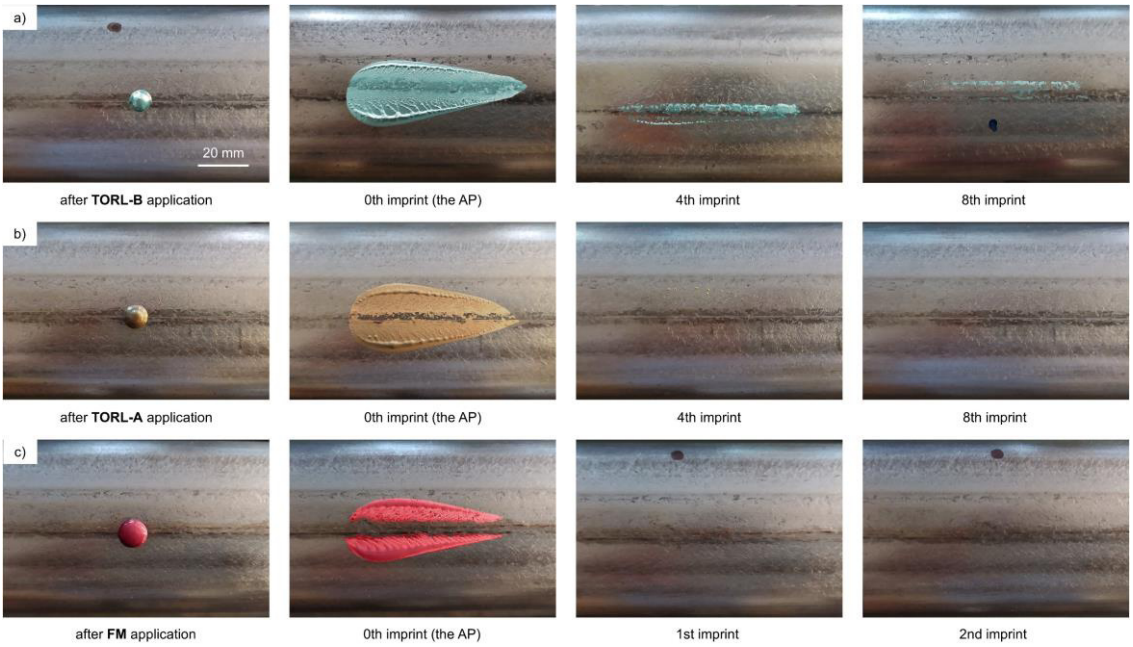

Fig. 4.11 Imprint development at the application point for different TOR products

As mentioned earlier, the primary goal of this Lab-to-Field methodology is to determine the optimal amount and application strategy for the TOR product identified as the best-performing one using the Lab-to-Lab methodology **[190]**. However, the case study presented here instead focuses on investigating the frictional performance of the same TOR products tested in the Lab-to-Lab methodology rather than on determining the optimal dosing conditions for these products. Although the effect of the applied amount was studied for the best-performing TOR lubricant (TORL-B), the impact of various application strategies was not included. This approach was chosen because the primary objective of this initial study was to compare the friction performance of the tested TOR products using both laboratory phases of the multi-phase methodology, which allowed for their validation.

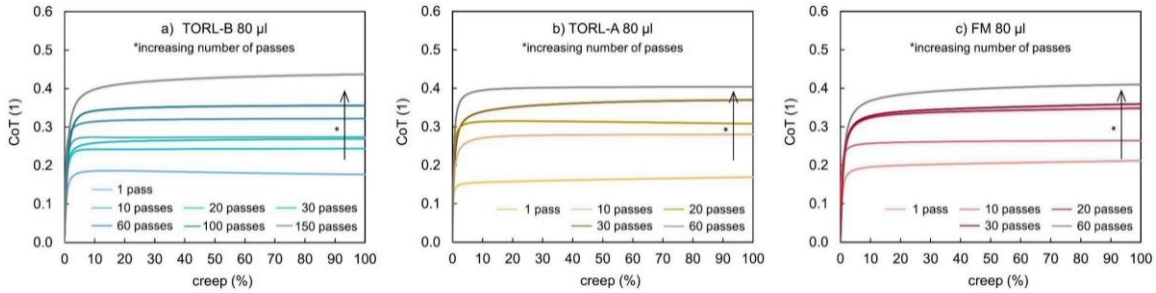

Fig. 4.12 Development of creep curves for different TOR products

From this perspective, results obtained using both methodology phases showed good agreement, as the same TOR product was identified as the best-performing in terms of retentivity, see **Fig. 4.8(a)** and **Fig. 4.13**. Additionally, both methodologies revealed that the tested TOR lubricants had significantly lower OLF values than those found for the friction modifier. The results from the Lab-to-Field methodology further indicated that carry distance is the most limiting parameter for TOR products, particularly for friction modifiers, which aligns with the existing literature **[184],[185]**. These experiments also showed that carry distance cannot be assessed visually because a surface that appeared free of the TOR product still provided the desired level of CoT, indicating that it was lubricated. Moreover, these experiments allowed for the study of the transfer mechanisms of TOR products, based on which a predictive model simulating the redistribution of the best-performing TOR product was developed.

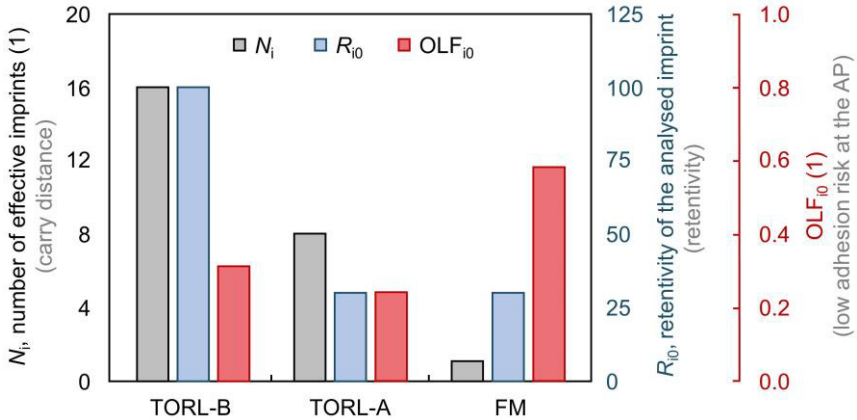

Fig. 4.13 Overall assessment of the tested TOR products using the Lab-to-Field methodology

4.6.4 Case study: Correlations between Curve Squeal, Weather Conditions, and Traction in a Tram Loop [193]

The objective of the last study was to demonstrate the suitability of a newly developed tribometer for field testing, as this approach is anticipated for use in the final step of the multi-phase methodology prior to vehicle-based testing. However, the initial study focused on investigating the frictional properties of a natural third-body layer rather than a TOR product layer. This approach was chosen because it was necessary first to describe how the CoT in dry conditions develops throughout the day due to changes in weather conditions. These findings are intended to serve as reference input values for a subsequent study examining the interaction between TOR product performance and a natural third-body layer. Additionally, friction data obtained from the tribometer were compared with noise data from a stationary noise model, which distinguishes between squeal and flanging noise based on frequency characteristics.

The experiments were conducted on a tram line loop (as shown in **Fig. 4.14**) with a radius of 21 meters due to ongoing complaints from residents regarding elevated noise levels, indicating that future use of the TOR product on this section of the track is needed. The CoT was measured at three points in the loop, labelled S1-S3 in **Fig. 4.14**, to obtain representative data on the frictional properties of the natural third-body layer. Noise data were collected and analysed in the vicinity of the sharpest track section, near point S1.

The measurements revealed that the CoT decreases with rising temperatures, as shown in **Fig. 4.15**, consistent with previously published studies **[137],[195]**. However, an unexpected result was observed in the relationship between CoT and relative humidity, where CoT increased with rising relative humidity. Although this finding does not align with existing literature **[137],[141]**, the trend was consistently observed at all three measurement points. A hypothesis has been proposed to explain this behaviour, which will be the subject of future research. In addition, a comparison of friction data revealed a correlation between CoT and squeal noise duration. As a result of these findings, the noisiest trams were removed from service on this line. Additionally, the results of this study can be used to control the dosing of TOR products using a track-mounted system.

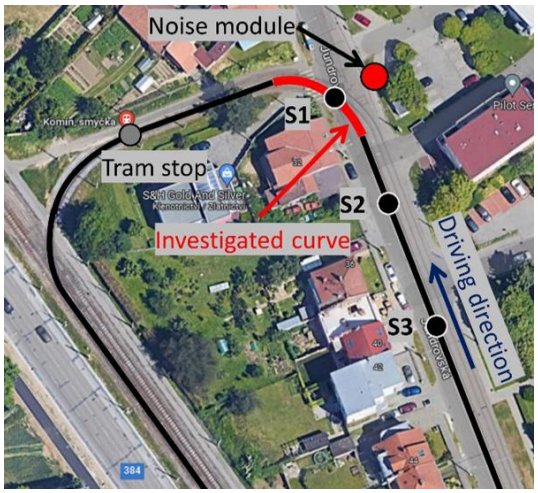

Fig. 4.14 Tram loop used for experimental testing

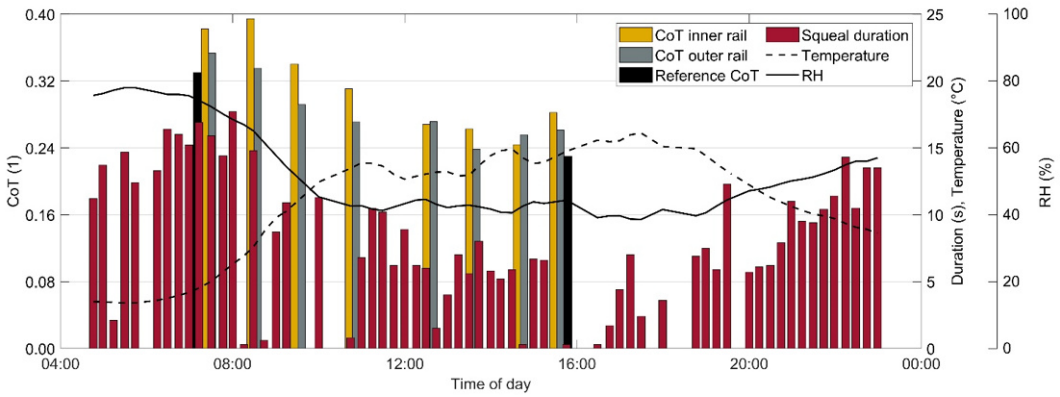

Fig. 4.15 Development of CoT, squeal duration, and weather conditions throughout the day

5

CONCLUSIONS AND FUTURE WORK

Since the initial use of TOR products to address corrugation issues, the field of TOR friction management has made significant progress, leading to the development of various products and applications. Scientific effort has focused on understanding the potential benefits of this approach, such as reducing noise, wear, corrugation, and RCF. While many studies have confirmed the positive effects of TOR products, some negative impacts, such as traction and braking issues or the inability to reduce noise, have also been identified. However, these negative effects cannot always be attributed to the products themselves and can result from improper dosing, testing methodology, or the influence of operating and environmental conditions and contaminants.

This habilitation thesis provides **insights into three areas of TOR friction modification**, detailed in **Chapters 2 to 4**. The first area covers the behaviour of various TOR products under different dosing and operating conditions. The second area deals with the effect of contaminants on both untreated and treated contacts with a TOR product. The third area addresses the development of a multi-phase testing methodology for TOR products. Each of these chapters began with a general introduction, followed by a review of the state of the art, which led to the identification of research gaps. An overview of the studies that addressed these gaps was provided, with a summary of the author's contributions to each study. Finally, the content of each paper was briefly described (all described papers are attached in Chapter 9). This habilitation thesis includes a total of fifteen papers, all published in peer-reviewed journals. Twelve of these articles were published in journals with an impact factor indexed in the Web of Science database, while three were released in journals indexed in the Scopus database.

The first research area, **Chapter 2**, consists of eight papers, each contributing to various aspects of TOR friction management. The first study presented an asperity-based model that enables a prediction of CoA across various lubrication regimes under rolling-sliding conditions. This model was then employed in two subsequent studies, which focused on two important phenomena related to TOR products, especially TOR lubricants: a sharp CoA drop that occurs after product application and a significant dependency of product performance on the applied amount. The combination of experimental and numerical approaches provided valuable insights into both these phenomena and highlighted the limitations of TOR lubricants in terms of the initial CoA drop. Further limitations of TOR products, specifically friction modifiers, were revealed by two studies that tested friction modifiers under a wide range of operating conditions, including high contact pressure and extremely low temperatures. The research showed that applying water-based products can present risks, particularly when pre-existing cracks are present, and the highest risk occurs under heavy haul conditions and low temperatures.

In addition to wear and RCF, another study focused on the ability of friction modifiers to reduce noise. Unlike most studies, this study tested non-commercial friction modifiers, investigating the effect of friction modifier composition on CoA and noise and their relationship. A significant

bi-linear correlation was found, which provides a valuable tool for managing the application of wayside systems based on a current noise level. Moreover, it was revealed that water itself could be a promising solution for combating squeal noise. This hypothesis was then tested by a study that employed a full-scale device to examine the effect of water on CoA and noise under conditions simulating vehicle curving. The findings showed that water could significantly reduce the level of noise without significantly impacting CoA; however, more frequent applications are required than for common TOR products.

The second research area, **Chapter 3**, examined the effect of contaminants on both treated and untreated contact. While many studies on low adhesion have been published, only a few have addressed critically low adhesion values. Many of these studies were conducted under pure-sliding conditions, which did not accurately represent wheel-rail contact. The first study in this chapter investigated how contaminants and environmental conditions, such as temperature and relative humidity, affected adhesion. The main contribution of this study was identifying the conditions that led to extremely low adhesion values, as well as the proposal of formulas for predicting CoA under rolling-sliding conditions. The second and third studies investigated the interaction between contaminants and TOR products, specifically examining water as the most common contaminant. These studies have shown that water contamination poses a particular risk for TOR lubricants, especially under dew conditions or when there is a significant amount of water in the contact area, such as during rainfall.

Chapter 4 focused on testing methods for TOR products. Comparing the results of studies testing TOR products is challenging, as different custom-made devices were used to evaluate various performance parameters. Therefore, a multi-phase methodology for TOR product testing was developed and was described in four articles. The first article introduced the Lab-to-Lab methodology, which categorised TOR products into four performance classes. By using a commercial tribometer (the MTM2) and clearly defined steps, this methodology ensured the transferability of results across different laboratories. The outcome of this first phase was the identification of the most suitable TOR product for further testing.

Another article described the second phase of the methodology, the Lab-to-Field methodology, where experiments are performed under conditions that closely simulate track conditions. This phase serves as a bridge between laboratory and field conditions because this setup enables the creation of realistic TOR product imprints on the rail using a simple contact simulator. These imprints are then analysed with a unique tribometer developed specifically for this purpose, as described in one of the papers included in Chapter 4. Notably, this tribometer allows for the measurement of the entire creep curve over a short distance. Due to this capability, each imprint can be analysed separately, enabling the evaluation of typical track performance parameters, such as retentivity and carry distance. The latter has rarely been studied under laboratory conditions as it is a challenging task. Using this methodology, the optimal amount and application method can be identified, thereby minimising the number of field experiments required when deploying a new TOR product into operation.

The final study employed the developed tribometer in the field, at a tram loop, to investigate how adhesion changed due to relative humidity and temperature variations throughout the day. Additionally, the occurrence and intensity of squeal noise were monitored using a noise module, and these data were compared with the adhesion data obtained from the tribometer to identify potential correlations. This study was conducted as the initial field test using the developed tribometer, which will be followed by the final step of the methodology, which aims to evaluate the performance of TOR products in field conditions prior to vehicle-based testing. The results of

this initial field test were also used to identify the noisiest trams of the Brno City Transport Company, which were subsequently removed from service on this line.

The overall contribution of this thesis lies in identifying the benefits and limitations of TOR products under various operational and environmental conditions, providing guidance for optimising the TOR friction management approach. Additionally, a comprehensive multi-phase methodology for testing TOR products was developed, offering a practical tool for assessing existing TOR products and enabling faster, cost-effective development of new, higher-performing TOR products.

There are still several challenges in TOR friction management that could significantly improve its effectiveness. One example is squeal noise, which remains a significant issue and is not yet fully understood. This thesis presents a novel approach that utilises water application to reduce squeal noise; however, further research is required, particularly in conditions where water interacts with other contaminants and could potentially cause low adhesion issues. Another example of a future research direction is the study of the interaction between TOR products and other contaminants, as this thesis focused only on the effect of water. Additionally, further research can focus on the transfer mechanisms of TOR products, which are important inputs when modelling TOR layers. Lastly, the number of released particles should be considered when evaluating the performance of TOR products.

6

LIST OF FIGURES AND GRAPHS

Fig. 1.1 Overview of friction management methods 1

Fig. 2.1 Expected behaviour of TOR products in terms of **(a)** lubrication regimes and **(b)** creep curve 4

Fig. 2.2 Effect of a friction modifier on creep curve for **(a)** painted and **(b)** sprayed application .. 5

Fig. 2.3 **(a)** Effect of TOR lubricant amount on the friction curve; **(b)** Stribeck curves for excessive amounts of TOR lubricants and oil 6

Fig. 2.4 Creep curves for dry contact, contact treated with the friction modifier, and contact treated with TOR lubricants 6

Fig. 2.5 Effect of a solid stick on impedance and CoF 7

Fig. 2.6 Corrugation development in Metro Bilbao 8

Fig. 2.7 **(a)** Comparison of rail wear profiles for dry and friction modifier conditions; **(b)** rail surface images (left to right) for new, friction modifier, and dry conditions 9

Fig. 2.8 Average sound pressure level vs. frequency for dry and FM conditions 10

Fig. 2.9 Creep curves and instantaneous behaviour 11

Fig. 2.10 Schematic representation of the proposed model 17

Fig. 2.11 Comparison between predictions and experiments for water-contaminated contact: **(a)** film thickness vs. speed, **(b)** creep curves 18

Fig. 2.12 **(a)-(c)** Comparison of custom-made and commercial TOR lubricants for different application amounts; **(d)** experimental vs. predicted results (dashed line) 19

Fig. 2.13 Effect of applied amount **(a)** and temperature **(b)** on CoF 20

Fig. 2.14 Predicted creep curves for dry contact and contact treated with TOR products 20

Fig. 2.15 **(a)** Friction curves for a solid stick at different slip values; **(b)** creep curves with and without the solid stick application 21

Fig. 2.16 Comparison of conditions with and without solid stick application:**(a)** wear rate, **(b)** crack length, **(c)** crack depth 21

Fig. 2.17 **(a)-(c)** Contour diagrams of minimum CoA across different operating conditions; **(d)-(f)** contour diagrams of retentivity (holding time) across different operating conditions 22

Fig. 2.18 **(a)** Wear rate of specimens under different application conditions; **(b)** rail crack length under different application conditions 23

Fig. 2.19 **(a)** Effect of temperature on CoA and retentivity (lasting cycles) for contact treated with the friction modifier; **(b)** wear rate under dry conditions; **(c)** wear rate with friction modifier application 24

Fig. 2.20 Fatigue crack length under **(a)** dry conditions and **(b)** friction modifier application; crack depth under **(c)** dry conditions and **(d)** friction modifier application 24

Fig. 2.21 Dependence between CoA and SPL for **(a)** wet and **(b)** dry films 25

Fig. 2.22 **(a)** Developed full-scale twin-disc machine; **(b)** vibration frequency composition dry conditions; **(c)** vibration frequency composition under wet conditions 26

Fig. 2.23 **(a)** Measured vs. predicted creep curves under wet and dry conditions; **(b)** SPL development with increasing speed and AoA; **(c)** effect of water on retentivity, CoA, and SPL reduction 26

Fig. 3.1 Relationship between CoA and speed: comparison of field data and simulations 28

Fig. 3.2 Friction test with water-particle mixture demonstrating a drop in CoA 29

Fig. 3.3 Portable system for oxide analysis with example results from the railhead 30

Fig. 3.4 **(a)** CoF vs. relative humidity; **(b)** CoF vs. amount of water vapour 31

Fig. 3.5 **(a)** Shear strength vs. displacement for a friction modifier and oxides mixture; **(b)** interaction between friction modifier and grease 32

Fig. 3.6 **(a)** Pin-on-disc tribometer test of friction modifier and red oxide mixture; **(b)** effect of relative humidity on CoF of friction modifier and black oxide mixture 33

Fig. 3.7 **(a)** Creep curves for water-contaminated contact operating under fully-flooded conditions; **(b)** effect of a small amount of water on CoA 37

Fig. 3.8 Effect of relative humidity on CoA for **(a)** a clean disc and **(b)** a disc with pre-created leaf layer 38

Fig. 3.9 Overview of the tested conditions with highlighted adhesion values 38

Fig. 3.10 Interaction of water with TOR lubricant **(a)**,**(b)** and with friction modifier **(c)**,**(d)** 39

Fig. 3.11 Duration of low-adhesion periods for various TOR products and water amounts 40

Fig. 3.12 Effect of relative humidity, specimen temperature, and humidification duration on the performance of the TOR lubricant (TORL-A) tested using the I-OLF methodology 41

Fig. 3.13 **(a)** Performance map; **(b)** dependence of OLF on water amount for TORL-A; **(c)** dependency of the C parameter on water amount for TORL-A 41

Fig. 3.14 Comparison of friction/adhesion results measured using different experimental approaches under various environmental conditions 42

Fig. 4.1 Friction test with commonly evaluated parameters 45

Fig. 4.2 Creep curves generated based on friction tests 46

Fig. 4.3 **(a)** Pick-up mechanism; **(b)** carry-on mechanism 47

Fig. 4.4 CoF as a function of distance under lubricated conditions 48

Fig. 4.5 **(a)** Film thickness of friction modifier and CoF as a function of distance in various track sections; **(b)** deposited frictional layer of friction modifier on the railhead 50

Fig. 4.6 Proposed multi-phase methodology for testing TOR products 52
Fig. 4.7 **(a)** Experimental phase and **(b)** evaluation phase of the Lab-to-Lab methodology 55
Fig. 4.8 **(a)** Performance map; **(b)** dependence of OLF on applied amount 56
Fig. 4.9 Design of the portable tribometer 57
Fig. 4.10 **(a)** Comparison of experimental approaches; **(b)** measurement repeatability 57
Fig. 4.11 Imprint development at the application point for different TOR products 58
Fig. 4.12 Development of creep curves for different TOR products 59
Fig. 4.13 Overall assessment of the tested TOR products using the Lab-to-Field methodology ... 59
Fig. 4.14 Tram loop used for experimental testing 60
Fig. 4.15 Development of CoT, squeal duration, and weather conditions throughout the day 61

7

REFERENCES

[1] Giunta M. Trends and Challenges in Railway Sustainability: The State of the Art regarding Measures, Strategies, and Assessment Tools. Sustainability 2023;15.

[2] Galas R. Friction modification within wheel-rail contact. Dissertation Thesis. 2017.

[3] Kalousek J, Johnson K. An Investigation of Short Pitch Wheel and Rail Corrugations on the Vancouver Mass Transit System. Proceedings Of The Institution Of Mechanical Engineers, Part F: Journal Of Rail And Rapid Transit 1992;206:127-135.

[4] Khan S, Lundberg J, Stenström C. Life cycle cost analysis for the top-of-rail friction-modifier application: A case study from the Swedish iron ore line. Proceedings Of The Institution Of Mechanical Engineers, Part F: Journal Of Rail And Rapid Transit 2021;235:83-93.

[5] Elvidge D, Stock R, Hardwick C, Oldknow K. The Effect of Freight Train Mounted TOR-FM on Wheel Life and Defects. Proceedings of the Third International Conference on Railway Technology: Research, Development and Maintenance, Stirlingshire, Scotland: Civil-Comp Press; 2016.

[6] Lu X, Makowsky T, Eadie D, Oldknow K, Xue J, Jia J, et al. Friction management on a Chinese heavy haul CoAl line. Proceedings Of The Institution Of Mechanical Engineers, Part F: Journal Of Rail And Rapid Transit 2012;226:630-640.

[7] Harmon M, Lewis R. Review of top of rail friction modifier tribology. Tribology Materials Surface Interfaces 2016;10:150-162.

[8] Chiddick K. Solid lubricants and friction modifiers for heavy loads and rail applications. USA patent No. 6,136,757 A, 2000.

[9] Cotter J. Friction control composition with enhanced retentivity. USA patent No. 6,759,372 B2, 2004.

[10] Chiddick K. Solid lubricants and friction modifiers for heavy loads and rail applications. EP patent No. 0 946 693 B1, 2005.

[11] Stock R, Stanlake L, Hardwick C, Yu M, Eadie D, Lewis R. Material concepts for top of rail friction management – Classification, characterisation and application. Wear 2016; 366-367:225-232.

[12] Eadie D, Santoro M, Powell W. Local control of noise and vibration with KELTRACK™ friction modifier and Protector® trackside application: an integrated solution. Journal Of Sound And Vibration 2003;267:761-772.

[13] Kalousek J, Magel E. Modifying and managing friction. Railway Track & Structures 1997;93(5):31-X4.

[14] Eadie D, Santoro M, Powell W. Wheel Squeal Control With Keltrack Liquid Friction Modifier and Protector Trackside Application: Theory and Practice. Rail Transportation 2001:149-155.

[15] Beck M, Stock R, Temple B. Rail corrugation growth in curves – Friction management as a sustainable solution. The Dynamics of Vehicles on Roads and Tracks, Graz: CRC Press; 2016, pp. 1269-1279.

[16] Davis K, Stickland W. Evaluation of a Top-of-rail Lubrication System 1999:1–120.

[17] Matsumoto A, Sato Y, Ono H, Wang Y, Yamamoto M, Tanimoto M, et al. Creep force characteristics between rail and wheel on scaled model. Wear 2002;253:199-203.

[18] Tomeoka M, Kabe N, Tanimoto M, Miyauchi E, Nakata M. Friction control between wheel and rail by means of on-board lubrication. Wear 2002;253:124-129.

[19] Zakharov S, Goryacheva I, Krasnov A, Yudin A, Morozov A, Markov D, et al. Tribological studies for developing friction modifiers in the wheel–rail system. Journal Of Friction And Wear 2015;36:468-475.

[20] Arias-Cuevas O, Li Z, Lewis R, Gallardo-Hernández E. Rolling–sliding laboratory tests of friction modifiers in dry and wet wheel–rail contacts. Wear 2010;268:543-551.

[21] Yang Z, Zhang P, Moraal J, Li Z. An experimental study on the effects of friction modifiers on wheel–rail dynamic interactions with various angles of attack. Railway Engineering Science 2022;30:360-382.

[22] Galas R, Kvarda D, Omasta M, Krupka I, Hartl M. The role of constituents contained in water–based friction modifiers for top–of–rail application. Tribology International 2018;117:87-97.

[23] Evans M, Lee Z, Harmon M, Six K, Meierhofer A, Stock R, et al. Top-of-rail friction modifier performance assessment: High pressure torsion testing; creep force modelling and field validation. Wear 2023;532-533.

[24] Galas R, Omasta M, Krupka I, Hartl M. Laboratory investigation of ability of oil-based friction modifiers to control adhesion at wheel-rail interface. Wear 2016;368-369:230-238.

[25] Oomen M, Bosman R, Lugt P. Characterization of Friction and Wear Behavior of Friction Modifiers used in Wheel-Rail Contacts. International Journal Of Prognostics And Health Management 2017;8.

[26] Liu X, Meehan P. Investigation of squeal noise under positive friction characteristics condition provided by friction modifiers. Journal Of Sound And Vibration 2016; 371:393-405.

[27] Sanchez J, Jaramillo J, Santa J, Toro A. Twin-disc assessment of the effect of top-of-rail friction modifiers on the tribological response of R8-R370HT pairs for use in wheel-rail systems. Revista Latinoamericana De Metalurgia Y Materiales 2019;39:1-14.

[28] Seo J, Jun H, Kwon S, Lee D. Effect of Friction Modifier on Rolling Contact Fatigue and Wear of Wheel and Rail Materials. Tribology Transactions 2017;61:19-30.

[29] Gutsulyak D, Stanlake L, Qi H. Twin disc evaluation of third body materials in the wheel/rail interface. Tribology - Materials, Surfaces & Interfaces 2021;15:115-126.

[30] Galas R, Omasta M, Klapka M, Kaewunruen S, Krupka I, Hartl M. Case Study: the Influence of Oil-based Friction Modifier Quantity on Tram Braking Distance and Noise. Tribology In Industry 2017;39:198-206.

[31] Kukėnas V, Jasevičius R, Petrenko V, Kilikevičius A, Vainorius D. Analysis of Sound Power Level Changes Caused by Wheel with Flat Spot Using Numerical and Physical Experiment. Applied Sciences 2021;11.

[32] Khan S, Rantatalo M, Asplund M. Wheel-rail squeal sound reduction using top of rail friction modifier: a case study. International Journal Of Comadem 2020;23:69-76.

[33] Lewis R, Gallardo E, Cotter J, Eadie D. The effect of friction modifiers on wheel/rail isolation. Wear 2011;271:71-77.

[34] Hardwick C, Lewis S, Lewis R. The effect of friction modifiers on wheel/rail isolation at low axle loads. Proceedings Of The Institution Of Mechanical Engineers, Part F: Journal Of Rail And Rapid Transit 2014;228:768-783.

[35] Vélez J, Cornelio J, Sierra R, Santa J, Hoyos-Palacio L, Nevshupa R, et al. Development of a composite friction modifier with carbon nanotubes for applications at the wheel–rail interface. Advanced Composites Letters 2020;29.

[36] Egana J, Vinolas J, Gil-Negrete N. Effect of liquid high positive friction (HPF) modifier on wheel-rail contact and rail corrugation. Tribology International 2005;38:769-774.

[37] Eadie D, Santoro M. Top-of-rail friction control for curve noise mitigation and corrugation rate reduction. Journal Of Sound And Vibration 2006;293:747-757.

[38] Eadie D, Santoro M, Oldknow K, Oka Y. Field studies of the effect of friction modifiers on short pitch corrugation generation in curves. Wear 2008;265:1212-1221.

[39] Eadie D, Elvidge D, Oldknow K, Stock R, Pointner P, Kalousek J, et al. The effects of top of rail friction modifier on wear and rolling contact fatigue: Full-scale rail–wheel test rig evaluation, analysis and modelling. Wear 2008;265:1222-1230.

[40] Stock R, Eadie D, Elvidge D, Oldknow K. Influencing rolling contact fatigue through top of rail friction modifier application – A full scale wheel–rail test rig study. Wear 2011;271:134-142.

[41] Hardwick C, Lewis R, Stock R. The effects of friction management materials on rail with pre existing rcf surface damage. Wear 2017;384-385:50-60.

[42] Thompson D. Curve Squeal Noise, in: Railway Noise And Vibration 2009:315-342.

[43] Stock R, Santoro M, Makowsky T, Elvidge D, Xia P. Friction Management as a Sustainable Solution for Controlling Noise at the Wheel-Rail Interface. Noise And Vibration Mitigation For Rail Transportation Systems 2018:723-734.

[44] Rudd M. Wheel/rail noise—Part II: Wheel squeal. Journal Of Sound And Vibration 1976;46:381-394.

[45] Hoffmann N, Fischer M, Allgaier R, Gaul L. A minimal model for studying properties of the mode-coupling type instability in friction induced oscillations. Mechanics Research Communications 2002;29:197-205.

[46] Hoffmann N, Gaul L. Effects of damping on mode-coupling instability in friction induced oscillations. Zamm - Journal Of Applied Mathematics And Mechanics / Zeitschrift Für Angewandte Mathematik Und Mechanik 2003;83:524-534.

[47] Eadie D, Kalousek J, Chiddick K. The role of high positive friction (HPF) modifier in the control of short pitch corrugations and related phenomena. Wear 2002;253:185-192.

[48] Hou K, Kalousek J, Magel E. Rheological model of solid layer in rolling contact. Wear 1997;211:134-140.

[49] Kwong M, Frossinakis R, Makowsky T, Yu M, Lu X, O'Grady J, et al. Wayside Top of Rail Friction Control: An Embedded Track Solution in a High Density Tram Network. Ausrail Plus 2019 2019:1-14.

[50] Curley D, Anderson D, Jiang J, Hanson D. Field Trials of Gauge Face Lubrication and Top-of-Rail Friction Modification for Curve Noise Mitigation. Noise and Vibration Mitigation for Rail Transportation Systems, Berlin, Heidelberg: Springer Berlin Heidelberg; 2015, pp. 449-456.

[51] Pieringer A. A numerical investigation of curve squeal in the case of constant wheel/rail friction. Journal Of Sound And Vibration 2014;333:4295-4313.

[52] Liu S, De Silva U, Chen D, Leslie A, Meehan P. Investigation of wheel squeal noise under mode coupling using two-disk test rig experiments. Wear 2023;530-531.

[53] Sánchez J, Jaramillo J, Santo J, Toro A. Twin-disc assessment of the effect of top-of-rail friction modifiers on the tribological response of er8-r370ht pairs for use in wheel-rail systems. Revista Latinoamericana De Metalurgia Y Materiales 2019;39:2-15.

[54] Leiva-Mateus J, Santa-Marín J, Buitrago-Sierra R, Mesa Grajales D, Geffroy E. Rheological and tribological evaluation of friction modifiers for wheel-rail applications. Lubrication Science 2022;34:537-546.

[55] Wu B, Shi L, Li J, Ding H, Galas R, Omasta M, et al. Rheological and tribological performance of top-of-rail friction modifiers with different viscosities. Wear 2024;538-539.

[56] Bogdański S, Lewicki P, Szymaniak M. Experimental and theoretical investigation of the phenomenon of filling the RCF crack with liquid. Wear 2005;258:1280-1287.

[57] Kaneta M, Yatsuzuka H, Murakami Y. Mechanism of Crack Growth in Lubricated Rolling/Sliding Contact. A S L E Transactions 2008;28:407-414.

[58] Wang W, Lewis R, Evans M, Liu Q. Influence of Different Application of Lubricants on Wear and Pre-existing Rolling Contact Fatigue Cracks of Rail Materials. Tribology Letters 2017;65.

[59] Kvarda D, Galas R, Omasta M, Shi L, Ding H, Wang W, et al. Asperity-based model for prediction of traction in water-contaminated wheel-rail contact. Tribology International 2021;157.

[60] Kvarda D, Skurka S, Galas R, Omasta M, Shi L, Ding H, et al. The effect of top of rail lubricant composition on adhesion and rheological behaviour. Engineering Science And Technology, An International Journal 2022;35.

[61] Kvarda D, Galas R, Omasta M, Hartl M, Krupka I, Dzimko M. Shear properties of top-of-rail products in numerical modelling. Proceedings Of The Institution Of Mechanical Engineers, Part F: Journal Of Rail And Rapid Transit 2023;237:796-805.

[62] Song J, Shi L, Ding H, Galas R, Omasta M, Wang W, et al. Effects of solid friction modifier on friction and rolling contact fatigue damage of wheel-rail surfaces. Friction 2022;10:597-607.

[63] Wang W, Li S, Ding H, Lin Q, Galas R, Omasta M, et al. Wheel/rail adhesion and damage under different contact conditions and application parameters of friction modifier. Wear 2023;523.

[64] Li J, Wu B, Ding H, Galas R, Omasta M, Wen Z, et al. Wear and damage behaviours of wheel and rail materials: Effects of friction modifier and environmental temperature. Wear 2023;523.

[65] Navrátil V, Galas R, Klapka M, Kvarda D, Omasta M, Shi L, et al. Wheel Squeal Noise in Rail Transport: The Effect of Friction Modifier Composition. Tribology In Industry 2022;44:361-373.

[66] Navrátil V, Galas R, Klapka M, Kvarda D, Omasta M. Wheel Squeal Mitigation Under Water Lubrication. Tribology In Industry 2024;3:418-431.

[67] Greenwood J, Tripp J. The Contact of Two Nominally Flat Rough Surfaces. Proceedings Of The Institution Of Mechanical Engineers 1970;185:625-633.

[68] Kalker J. Three-dimensional elastic bodies in rolling contact. Dordrecht: Kluwer Academic Publishers; 1990.

[69] Rovira A, Roda A, Lewis R, Marshall M. Application of Fastsim with variable coefficient of friction using twin disc experimental measurements. Wear 2012;274-275:109-126.

[70] Six K, Meierhofer A, Müller G, Dietmaier P. Physical processes in wheel–rail contact and its implications on vehicle–track interaction. Vehicle System Dynamics 2015;53:635-650.

[71] Esfahanian M, Hamrock B. Fluid-Film Lubrication Regimes Revisited. Tribology Transactions 1991;34:628-632.

[72] Barus C. Isothermals, isopiestics and isometrics relative to viscosity. American Journal Of Science 1893;s3-45:87-96.

[73] Roelands C. Correlational Aspects of the Viscosity-Temperature Pressure Relationship of Lubricating Oils. PhD Thesis. 1966.

[74] Milan J, Carvalho M, Xavier R, Franco S, De Mello J. Effect of temperature, normal load and pre-oxidation on the sliding wear of multi-component ferrous alloys. Wear 2005;259:412-423.

[75] Pearson S, Shipway P, Abere J, Hewitt R. The effect of temperature on wear and friction of a high strength steel in fretting. Wear 2013;303:622-631.

[76] Valtonen K, Ratia V, Ramakrishnan K, Apostol M, Terva J, Kuokkala V. Impact wear and mechanical behavior of steels at subzero temperatures. Tribology International 2019;129:476-493.

[77] Lyu Y, Bergseth E, Olofsson U. Open System Tribology and Influence of Weather Condition. Scientific Reports 2016;6.

[78] Ma L, Guo J, Liu Q, Wang W. Fatigue crack growth and damage characteristics of high-speed rail at low ambient temperature. Engineering Failure Analysis 2017;82:802-815. https://doi.org/10.1016/j.engfailanal.2017.07.026.

[79] Lyu Y, Bergseth E, Olofsson U. The Effect of Subzero Temperature and Snow on the Tribology of Wheel-Rail Contact. Proceedings of the Third International Conference on Railway Technology: Research, Development and Maintenance, Stirlingshire, Scotland: Civil-Comp Press; 2016, pp. 153-165.

[80] Omasta M, Navrátil V, Gabriel T, Galas R, Klapka M. Design and Development of a Twin Disc Test Rig for the Study of Squeal Noise from the Wheel – Rail Interface. Applied Engineering Letters: Journal Of Engineering And Applied Sciences 2022;7:10-16.

[81] Olofsson U, Lyu Y. Open System Tribology in the Wheel–Rail Contact—A Literature Review. Applied Mechanics Reviews 2017;69.

[82] White B, Lewis R. Simulation and understanding the wet-rail phenomenon using twin disc testing. Tribology International 2019;136:475-486.

[83] Buckley-Johnstone L, Trummer G, Voltr P, Meierhofer A, Six K, Fletcher D, et al. Assessing the impact of small amounts of water and iron oxides on adhesion in the wheel/rail interface using High Pressure Torsion testing. Tribology International 2019;135:55-64.

[84] White B, Watson M, Lewis R. A year-round analysis of railway station overruns due to low adhesion conditions. Proceedings Of The Institution Of Mechanical Engineers, Part F: Journal Of Rail And Rapid Transit 2023;237:458-469.

[85] Ishizaka K, Lewis S, Lewis R. The low adhesion problem due to leaf contamination in the wheel/rail contact: Bonding and low adhesion mechanisms. Wear 2017;378-379:183-197.

[86] White B, Kempka R, Laity P, Holland C, Six K, Trummer G, et al. Iron Oxide and Water Paste Rheology and Its Effect on Low Adhesion in the Wheel/Rail Interface. Tribology Letters 2022;70.

[87] Wang W, Zhang H, Wang H, Liu Q, Zhu M. Study on the adhesion behavior of wheel/rail under oil, water and sanding conditions. Wear 2011;271:2693-2698.

[88] Wang W, Liu T, Wang H, Liu Q, Zhu M, Jin X. Influence of friction modifiers on improving adhesion and surface damage of wheel/rail under low adhesion conditions. Tribology International 2014;75:16-23.

[89] Moreno-Ríos M, Gallardo-Hernández E, Vite-Torres M, Peña-Bautista A. Field and laboratory assessments of the friction coefficient at a railhead. Proceedings Of The Institution Of Mechanical Engineers, Part F: Journal Of Rail And Rapid Transit 2016;230:313-320.

[90] Lewis R, Gallardo-Hernandez E, Hilton T, Armitage T. Effect of oil and water mixtures on adhesion in the wheel/rail contact. Proceedings Of The Institution Of Mechanical Engineers, Part F: Journal Of Rail And Rapid Transit 2009;223:275-283.

[91] Broster M, Pritchard C, Smith D. Wheel/rail adhesion: its relation to rail contamination on british railways. Wear 1974;29:309-321.

[92] Chen H, Ishida M, Namura A, Baek K, Nakahara T, Leban B, et al. Estimation of wheel/rail adhesion coefficient under wet condition with measured boundary friction coefficient and real contact area. Wear 2011;271:32-39.

[93] Zhu Y, Olofsson U, Persson K. Investigation of factors influencing wheel–rail adhesion using a mini-traction machine. Wear 2012;292-293:218-231.

[94] Chen H, Ban T, Ishida M, Nakahara T. Adhesion between rail/wheel under water lubricated contact. Wear 2002;253:75-81.

[95] Wang H, Wang W, Liu Q. Numerical and experimental investigation on adhesion characteristic of wheel/rail under the third body condition. Proceedings Of The Institution Of Mechanical Engineers, Part J: Journal Of Engineering Tribology 2016;230:111-118.

[96] Chen H, Ban T, Ishida M, Nakahara T. Experimental investigation of influential factors on adhesion between wheel and rail under wet conditions. Wear 2008;265:1504-1511.

[97] Wu B, Wen Z, Wu T, Jin X. Analysis on thermal effect on high-speed wheel/rail adhesion under interfacial contamination using a three-dimensional model with surface roughness. Wear 2016;366-367:95-104.

[98] Lewis S, Lewis R, Richards P, Buckley-Johnstone L. Investigation of the isolation and frictional properties of hydrophobic products on the rail head, when used to combat low adhesion. Wear 2014;314:213-219.

[99] Wang W, Shen P, Song J, Guo J, Liu Q, Jin X. Experimental study on adhesion behavior of wheel/rail under dry and water conditions. Wear 2011;271:2699-2705.

[100] Wang W, Wang H, Wang H, Guo J, Liu Q, Zhu M, et al. Sub-scale simulation and measurement of railroad wheel/rail adhesion under dry and wet conditions. Wear 2013;302:1461-1467.

[101] Chen H, Namura A, Ishida M, Nakahara T. Influence of axle load on wheel/rail adhesion under wet conditions in consideration of running speed and surface roughness. Wear 2016;366-367:303-309.

[102] Shi L, Wang C, Ding H, Kvarda D, Galas R, Omasta M, et al. Laboratory investigation on the particle-size effects in railway sanding: Comparisons between standard sand and its micro fragments. Tribology International 2020;146.

[103] Baek K, Kyogoku K, Nakahara T. An experimental investigation of transient traction characteristics in rolling–sliding wheel/rail contacts under dry–wet conditions. Wear 2007;263:169-179.

[104] Wang C, Shi L, Ding H, Wang W, Galas R, Guo J, et al. Adhesion and damage characteristics of wheel/rail using different mineral particles as adhesion enhancers. Wear 2021;477.

[105] Chen H, Yoshimura A, Ohyama T. Numerical analysis for the influence of water film on adhesion between rail and wheel. Proceedings Of The Institution Of Mechanical Engineers, Part J: Journal Of Engineering Tribology 1998;212:359-368.

[106] Chen H, Ban T, Ishida M, Nakahara T. Effect of water temperature on the adhesion between rail and wheel. Proceedings Of The Institution Of Mechanical Engineers, Part J: Journal Of Engineering Tribology 2006;220:571-579.

[107] Beagley T, Pritchard C. Wheel/rail adhesion — the overriding influence of water. Wear 1975;35:299-313.

[108] Beagley T. The Rheological Properties of Solid Rail Contaminants and their Effect on Wheel/Rail Adhesion. Proceedings Of The Institution Of Mechanical Engineers 1976;190:419-428.

[109] Kvarda D, Meierhofer A, Six K. Testing and modelling of transient adhesion phenomena in rolling-sliding contacts. Friction 2024;12:1016-1027.

[110] Kempka R, Falconer R, Gutsulyak D, Lewis R. Effects of oxide and water on friction of rail steel – new test method and friction mapping. Tribology - Materials, Surfaces & Interfaces 2020;15:80-91.

[111] Investigation into the effect of moisture on rail adhesion: T1042. Rail Safety and Standards Board; 2014.

[112] Fulford C. Review of Low Adhesion Research. Rail Safety and Standards Board; 2004.

[113] Arias-Cuevas O, Li Z. Field investigations into the adhesion recovery in leaf-contaminated wheel–rail contacts with locomotive sanders. Proceedings Of The Institution Of Mechanical Engineers, Part F: Journal Of Rail And Rapid Transit 2011;225:443-456.

[114] Chen H, Furuya T, Fukagai S, Saga S, Ikoma J, Kimura K, et al. Wheel slip/Slide and low adhesion caused by fallen leaves. Wear 2020;446-447.

[115] Arias-Cuevas O, Li Z, Lewis R. A laboratory investigation on the influence of the particle size and slip during sanding on the adhesion and wear in the wheel–rail contact. Wear 2011;271:14-24.

[116] Jaffe J, White B, Lanigan J, Lewis R. “A novel methodology for developing ultra-low adhesion leaf layers on a full-scale wheel/rail rig.” Proceedings Of The Institution Of Mechanical Engineers, Part F: Journal Of Rail And Rapid Transit 2024;238:736-741.

[117] Lewis R, Trummer G, Six K, Stow J, Alturbeh H, Bryce B, et al. Leaves on the line: Characterising leaf based low adhesion on railway rails. Tribology International 2023;185.

[118] Kumar N, Radmehr A, Ahmadian M. Experimental Evaluation of Effect of Leaves on Railroad Tracks in Loss of Braking. Machines 2024;12.

[119] Zhu Y, Olofsson U, Nilsson R. A field test study of leaf contamination on railhead surfaces. Proceedings Of The Institution Of Mechanical Engineers, Part F: Journal Of Rail And Rapid Transit 2014;228:71-84.

[120] Cann P, Stoeterau R, Ferrer B, Zuin A, Biazon Cavalcanti L, Cousseau T. The ”leaves on the line” problem—a study of leaf residue film formation and lubricity under laboratory test conditions. Tribology Letters 2021;24:151-158.

[121] Omasta M, Machatka M, Smejkal D, Hartl M, Křupka I. Influence of sanding parameters on adhesion recovery in contaminated wheel–rail contact. Wear 2015;322-323:218-225.

[122] Beagley T, McEwen I, Pritchard C. Wheel/rail adhesion — the influence of railhead debris. Wear 1975;33:141-152.

[123] Olofsson U, Sundvall K. Influence of leaf, humidity and applied lubrication on friction in the wheel-rail contact: Pin-on-disc experiments. Proceedings Of The Institution Of Mechanical Engineers, Part F: Journal Of Rail And Rapid Transit 2004;218:235-242.

[124] Shen M, Li J, Li L, Li S, Ma C. Adhesion and Damage Behaviour of Wheel–Rail Rolling–Sliding Contact Suffering Intermittent Airflow with Different Humidities and Ambient Temperatures. Tribology Letters 2024;72.

[125] Zhu Y. The influence of iron oxides on wheel–rail contact: A literature review. Proceedings Of The Institution Of Mechanical Engineers, Part F: Journal Of Rail And Rapid Transit 2018;232:734-743.

[126] Berthier Y, Descartes S, Busquet M, Niccolini E, Desrayaud C, Baillet L, et al. The role and effects of the third body in the wheel-rail interaction. Fatigue & Fracture of Engineering Materials & Structures 2003;27:423-436.

[127] Suzumura J, Sone Y, Ishizaki A, Yamashita D, Nakajima Y, Ishida M. In situ X-ray analytical study on the alteration process of iron oxide layers at the railhead surface while under railway traffic. Wear 2011;271:47-53.

[128] Chen H. Review of various influencing factors and improvement measures on wheel-rail adhesion. Wear 2024;550-551.

[129] Ishida, M., Aoki F, Sone Y, Ban T, Shirouzu K. Rail corrugations caused by low coefficient of friction in a submarine railway tunnel. In: Proceedings of WTC 2005 World Tribology Congress III, Washington, D.C., USA: 2005, pp. 931-932.

[130] Nakahara T, Baek K, Chen H, Ishida M. Relationship between surface oxide layer and transient traction characteristics for two steel rollers under unlubricated and water lubricated conditions. Wear 2011;271:25-31.

[131] Zhu Y, Chen X, Wang W, Yang H. A study on iron oxides and surface roughness in dry and wet wheel−rail contacts. Wear 2015;328-329:241-248.

[132] Zhu Y, Olofsson U, Chen H. Friction Between Wheel and Rail: A Pin-On-Disc Study of Environmental Conditions and Iron Oxides. Tribology Letters 2013;52:327-339.

[133] Zhu Y, Lyu Y, Olofsson U. Mapping the friction between railway wheels and rails focusing on environmental conditions. Wear 2015;324-325:122-128.

[134] Lu X, Cotter J, Eadie D. Laboratory study of the tribological properties of friction modifier thin films for friction control at the wheel/rail interface. Wear 2005;259:1262-1269.

[135] Axén N, Hutchings I, Jacobson S. A model for the friction of multiphase materials in abrasion. Tribology International 1996;29:467-475.

[136] Li Z, Arias-Cuevas O, Lewis R, Gallardo-Hernández E. Rolling–Sliding Laboratory Tests of Friction Modifiers in Leaf Contaminated Wheel–Rail Contacts. Tribology Letters 2009;33:97-109.

[137] Lewis S, Lewis R, Olofsson U, Eadie D, Cotter J, Lu X. Effect of humidity, temperature and railhead contamination on the performance of friction modifiers: Pin-on-disk study. Proceedings Of The Institution Of Mechanical Engineers, Part F: Journal Of Rail And Rapid Transit 2013;227:115-127.

[138] Oldknow K, Eadie D, Stock R. The influence of precipitation and friction control agents on forces at the wheel/rail interface in heavy haul railways. Proceedings Of The Institution Of Mechanical Engineers, Part F: Journal Of Rail And Rapid Transit 2013;227:86-93.

[139] Chen H, Fukagai S, Sone Y, Ban T, Namura A. Assessment of lubricant applied to wheel/rail interface in curves. Wear 2014;314:228-235.

[140] Hardwick C, Lewis R, Olofsson U. Low adhesion due to oxide formation in the presence of salt. Proceedings Of The Institution Of Mechanical Engineers, Part F: Journal Of Rail And Rapid Transit 2014;228:887-897.

[141] Galas R, Omasta M, Shi L, Ding H, Wang W, Krupka I, et al. The low adhesion problem: The effect of environmental conditions on adhesion in rolling-sliding contact. Tribology International 2020;151.

[142] Skurka S, Galas R, Omasta M, Wu B, Ding H, Wang W, et al. The performance of top-of-rail products under water contamination. Tribology International 2023;188.

[143] Skurka S, Galas R, Omasta M, Ding H, Wang W, Krupka I, et al. Assessing the Performance of TOR Lubricants in Humid Environments and Under Dew Conditions. Tribology Letters 2024;72.

[144] Lundberg J, Rantatalo M, Wanhainen C, Casselgren J. Measurements of friction coefficients between rails lubricated with a friction modifier and the wheels of an IORE locomotive during real working conditions. Wear 2015;324-325:109-117.

[145] Eadie D, Oldknow K, Maglalang L, Makowsky T, Reiff R, Sroba P, et al. Implementation of Wayside Top of Rail Friction Control on North American Heavy Haul Freight Railways. In Proceedings of the 7th World Congress on Railway Research, Montreal, Canada: 2006, pp. 4.8.

[146] Naeimi M, Li Z, Petrov R, Sietsma J, Dollevoet R. Development of a New Downscale Setup for Wheel-Rail Contact Experiments under Impact Loading Conditions. Experimental Techniques 2018;42:1-17.

[147] Matsumoto A, Sato Y, Nakata M, Tanimoto M, Qi K. Wheel-rail contact mechanics at full scale on the test stand. Wear 1996;191:101-106.

[148] Jin X, Wen Z. Rail corrugation formation studied with a full-scale test facility and numerical analysis. Proceedings Of The Institution Of Mechanical Engineers, Part J: Journal Of Engineering Tribology 2007;221:675-698.

[149] Liu B, Bruni S. A method for testing railway wheel sets on a full-scale roller rig. Vehicle System Dynamics 2015;53:1331-1348.

[150] Chang C, Chen B, Cai Y, Wang J. Experimental investigation of high-speed wheel-rail adhesion characteristics under large creepage and water conditions. Wear 2024;540-541.

[151] Buckley-Johnstone L, Harmon M, Lewis R, Hardwick C, Stock R. A comparison of friction modifier performance using two laboratory test scales. Proceedings Of The Institution Of Mechanical Engineers, Part F: Journal Of Rail And Rapid Transit 2019;233:201-210.

[152] Liang Y, Zeng J, Wang Q, Mao R. Dynamic performance study of railway vehicle on half-vehicle roller rig. International Journal Of Dynamics And Control 2023;11:473-481.

[153] White B, Hyland-Knight J, Lewis R. Assessing the effectiveness of traction gels using full-scale and field testing. Proceedings Of The Institution Of Mechanical Engineers, Part F: Journal Of Rail And Rapid Transit 2021;235:690-699.

[154] Voltr P, Lata M. Transient wheel–rail adhesion characteristics under the cleaning effect of sliding. Vehicle System Dynamics 2015;53:605-618.

[155] Bosso N, Magelli M, Zampieri N. Investigation of adhesion recovery phenomenon using a scaled roller-rig. Vehicle System Dynamics 2021;59:295-312.

[156] Gallardo-Hernandez E, Lewis R. Twin disc assessment of wheel/rail adhesion. Wear 2008;265:1309-1316.

[157] Shu K, Wang W, Ding H, Lin Q, Meli E, Guo J, et al. Influence of sand transport rate on rolling wear and damage behaviors of wheel/rail in Gobi and desert windblown sand environments. Tribology International 2022;172.

[158] Zhang P, Li Z. Experimental study on the development mechanism of short pitch corrugation using a downscale V-Track test rig. Tribology International 2023;180.

[159] Zhu J, Thompson D, Jones C. On the effect of unsupported sleepers on the dynamic behaviour of a railway track. Vehicle System Dynamics 2011;49:1389-1408.

[160] Temple P, Harmon M, Lewis R, Burstow M, Temple B, Jones D. Optimisation of grease application to railway tracks. Proceedings Of The Institution Of Mechanical Engineers, Part F: Journal Of Rail And Rapid Transit 2018;232:1514-1527.

[161] Tayer P, Stoeterau R, Ferrer B, Zuin A, Cavalcanti L, Cousseau T. Laboratory test rig to measure carry-down, retentivity, splash and pickup of lubricant in wheel-rail lubrication system. Proceedings Of The 26Th International Congress Of Mechanical Engineering 2021.

[162] Ploss M, Tian Y, Yoshikawa S, Westbroek R, Leckner J, Glavatskih S. Tribological Performance of Non-halogenated Phosphonium Ionic Liquids as Additives to Polypropylene and Lithium-Complex Greases. Tribology Letters 2020;68.

[163] Lewis S, Lewis R, Olofsson U. An alternative method for the assessment of railhead traction. Wear 2011;271:62-70.

[164] Harmon M, Santa J, Jaramillo J, Toro A, Beagles A, Lewis R. Evaluation of the coefficient of friction of rail in the field and laboratory using several devices 2020;14:119-129.

[165] Harrison H, McCanney T, Cotter J. Recent developments in coefficient of friction measurements at the rail/wheel interface. Wear 2002;253:114-123.

[166] Bernal E, Spiryagin M, Oldknow K, Wu Q, Rahaman M, Camacho D, et al. Hand operated tribometer versus twin disc dry friction characteristics measurements. Wear 2024;540-541.

[167] Xavier Y, Rezende A, Fonseca S, Jun Kina E, Mei P. Study of the Initial Cycles Number Influence on the Retentivity of a Commercial Friction Modifier Using the Twin-disk Test. Tribology Transactions 2024;67:212-221.

[168] Wu B, Shi L, Ding H, Guo J, Liu Q, Zhou Z, et al. Influence of different solid particles in friction modifier on wheel-rail adhesion and damage behaviours. Wear 2023;522.

[169] White B, Lee Z, Lewis R. Towards a Standard Approach for the Twin Disc Testing of Top-Of Rail Friction Management Products. Lubricants 2022;10.

[170] Matsumoto K, Suda Y, Fujii T, Komine H, Tomeoka M, Satoh Y, et al. The optimum design of an onboard friction control system between wheel and rail in a railway system for improved curving negotiation. Vehicle System Dynamics 2006;44:531-540.

[171] Pan Y, Radmehr A, Ahmadian M. Experimental evaluation of amount and repeated applications of top of rail friction modifiers on wear and adhesion. International Journal Of Rail Transportation 2023;11:855-871.

[172] Ishida M, Ban T, Iida K, Ishida H, Aoki F. Effect of moderating friction of wheel/rail interface on vehicle/track dynamic behaviour. Wear 2008;265:1497-1503.

[173] Abbasi S, Olofsson U, Zhu Y, Sellgren U. Pin-on-disc study of the effects of railway friction modifiers on airborne wear particles from wheel–rail contacts. Tribology International 2013;60:136-139.

[174] Fruhwirt D, Sturm P, Nöst T, Leonhardt P, Bode G, Michael S, et al. PM emissions from railways – Results of tests on a wheel-rail test bench. Transportation Research Part D: Transport And Environment 2023;122.

[175] Trummer G, Lee Z, Lewis R, Six K. Modelling of Frictional Conditions in the Wheel–Rail Interface Due to Application of Top-of-Rail Products. Lubricants 2021;9.

[176] Lee Z, Trummer G, Harmon M, White B, Six K, Lewis R. Studying the transfer mechanisms of water based top-of-rail products in a wheel/rail interaction. Proceedings Of The Institution Of Mechanical Engineers, Part F: Journal Of Rail And Rapid Transit 2024;238:164-174.

[177] Harmon M, Lewis R. New laboratory methodologies to analyse the top of rail friction modifier performance across different test scales. Proceedings Of The Institution Of Mechanical Engineers, Part F: Journal Of Rail And Rapid Transit 2021;235:191-200.

[178] CEN/TS 15427–2-2:2021. Railway applications - Wheel/Rail friction management - Part 2–2: Properties and Characteristics - Top of Rail materials, 2021.

[179] Reiff R, Gage S, Kumar S. Top-of-rail lubrication energy test. 1998.

[180] Davis K, Strickland W, Sherrock E. Evaluation of a top-of-rail lubrication system. 1999.

[181] Suda Y, Iwasa T, Komine H, Tomeoka M, Nakazawa H, Matsumoto K, et al. Development of onboard friction control. Wear 2005;258:1109-1114.

[182] Areiza Y, Garcés S, Santa J, Vargas G, Toro A. Field measurement of coefficient of friction in rails using a hand-pushed tribometer. Tribology International 2015;82:274-279.

[183] Ibrahim A, Loke J, Ahmad J, Ismail B, Rosli M. Noise and braking tests on permanent way at Bukit Mertajam, Pulau Pinang using top-of-rail friction modifier (TOR FM) 2023:060005.

[184] Khan S, Lundberg J, Stenström C. Carry distance of top-of-rail friction modifiers. Proceedings Of The Institution Of Mechanical Engineers, Part F: Journal Of Rail And Rapid Transit 2018;232:2418-2430.

[185] Rahmani H, Gutsulyak D, Stanlake L, Stoeber B, Green S. Carrydown of liquid friction modifier. Proceedings Of The Institution Of Mechanical Engineers, Part F: Journal Of Rail And Rapid Transit 2022;236:1124-1134.

[186] Mast T, Pan Y, Holton C, Ahmadian M. Intermediate Distance Testing of Optical Top-of Rail (TOR) Lubricity Sensors on a Remote-Controlled Rail Cart. 2021 Joint Rail Conference 2021.

[187] Rocha R, Ewald H, Rezende A, Fonseca S, Mei P. Using twin disc for applications in the railway: a systematic review. Journal Of The Brazilian Society Of Mechanical Sciences And Engineering 2023;45.

[188] Fukagai S, Ban T, Ogata M, Ishida M, Namura A. Development of Wheel/Rail Friction Moderating System (FRIMOS). Quarterly Report Of RTRI 2008;49:26-32.

[189] Persson I, Spiryagin M, Casanueva C. Influence of non-dry condition creep curves in switch negotiation. Vehicle System Dynamics 2023;61:892-904.

[190] Galas R, Skurka S, Valena M, Kvarda D, Omasta M, Ding H, et al. A benchmarking methodology for top-of-rail products. Tribology International 2023;189.

[191] Valena M, Omasta M, Kvarda D, Galas R, Krupka I, Hartl M. An approach for the creep-curve assessment using a new rail tribometer. Tribology International 2024;191.

[192] Galas R, Valena M, Jordan T, Kvarda D, Omasta M, Skurka S, et al. A benchmarking methodology for top-of-rail products: Carry distance and retentivity. Tribology International 2024;197.

[193] Valena M, Omasta M, Klapka M, Galas R, Navratil V, Krupka I, et al. Case study: Correlations between Curve Squeal, Weather Conditions, and Traction in a Tram Loop. Tribology In Industry; Article in press.

[194] Polach O. Creep forces in simulations of traction vehicles running on adhesion limit. Wear 2005;258:992-1000. https://doi.org/10.1016/j.wear.2004.03.046.

[195] Baek K, Kyogoku K, Nakahara T. An experimental study of transient traction characteristics between rail and wheel under low slip and low speed conditions. Wear 2008;265:1417-1424.

8

LIST OF ABBREVIATIONS

AoA	Angle of attack
CoA	Coefficient of adhesion
CoF	Coefficient of friction
CoT	Coefficient of traction
EHL	Elastohydrodynamic lubrication
FEM	Finite element method
HPT	High-pressure torsion
L/V	Lateral-to-vertical force ratio
MTM	Mini-Traction machine
NLGI	National Lubricating Grease Institute
OLF	Over-Lubrication Factor
PFM	Particles for friction modification
PTFE	Polytetrafluoroethylene
RCF	Rolling contact fatigue
RG	Research gap
SPL	Sound pressure level
TOR	Top-of-rail

9

RESEARCH PAPERS

Tribology International 157 (2021) 106900

Contents lists available at ScienceDirect

Tribology International

journal homepage: http://www.elsevier.com/locate/triboint

Asperity-based model for prediction of traction in water-contaminated wheel-rail contact

Daniel Kvarda [a,*], Radovan Galas [a], Milan Omasta [a], Lu-bing Shi [b,c], Haohao Ding [b], Wen-jian Wang [b], Ivan Krupka [a], Martin Hartl [a]

[a] Faculty of Mechanical Engineering, Brno University of Technology, Technicka 2896/2, 616 69, Brno, Czech Republic
[b] Tribology Research Institute, State Key Laboratory of Traction Power, Southwest Jiaotong University, Chengdu, 610031, China
[c] Zhengzhou Research Institute of Mechanical Engineering Co., Ltd., Zhengzhou, 450001, China

ARTICLE INFO

Keywords:
Adhesion coefficient
Water
Low adhesion
Rail–wheel tribology

ABSTRACT

The wheel-rail contact is subjected to various environmental contaminations, while one of the most common is water. A numerical model has been used to evaluate friction in water-contaminated contact. The Greenwood and Tripp theory is used to calculate the load carried by asperities and liquid film. This model uses Kalker's simplified theory with an implemented third body layer to determine the frictional values of asperity contact and elasto-hydrodynamic theory for friction generated by liquid. The results are compared with experiments on two types of surface roughness. The results show the difference between elastic and plastic asperity deformation model, where the plastic model predicts more accurate transition in mixed lubrication regime. The plastic deformation model was used to predict traction curves.

1. Introduction

As an open tribological system, the wheel-rail contact is subject to many kinds of environmental influences. It is crucial to ensure safe and reliable operation of railway vehicles under those conditions. Contaminants such as water, oil and products used to manage wheel-rail friction (top-of-rail lubricants, flange lubricants) change the frictional behaviour of the contact interface. These substances influence the friction in both boundary and elastohydrodynamic (EHL) regimes where solid shear strength and viscosity define the frictional behaviour, respectively.

Water is the most common contaminant and contamination can happen on a rainy day or as a dew condensate from humid air. As a dew condensate, low amounts of water mixed with wear debris on contact surfaces create a film with low shear strength [1,2] and high viscosity [2] that can cause low adhesion [2,3]. On a rainy day, the water floods the contact and at very high speeds, a surface separation can lead to low adhesion [4]. The degree of adhesion in wheel-rail contact is commonly expressed by the adhesion coefficient, which is defined as the ratio between tangential frictional force and normal load. Depending on the slip value, this coefficient takes value from 0 to the value representing the coefficient of friction. Under dry conditions, the typical coefficient of friction is between 0.5 and 0.8 [5]. A low adhesion means that the tangential frictional force is not sufficient to provide the required force for traction or braking. In terms of coefficient of adhesion, the low adhesion is generally considered with values lower than 0.1 [6]. Studies report that with increasing speed the coefficient of adhesion is decreasing [7–11]. The rate of decrease depends on the change in film thickness and roughness profile. Increasing the roughness causes the contact to shift closer to the boundary regime and thus increasing the coefficient of adhesion [8,9,12,13].

The friction generated in liquid separating two surfaces can be predicted by means of hydrodynamic theory. One key variable is a surface separation, which can be calculated from the Reynolds equation or analytical formulas [14]. The resulting shear stress is then solved using Newton's law of viscosity. The friction generated by solid asperity contact is mostly simplified by using a fixed value of the coefficient of friction [4,9,13,15] or by varying based on defined parameters such as slip and rolling speed [16,17]. Studies set this value based on experimental data of dry contact conditions. To determine this value numerically, Kalker's simplified theory can also be used [18]. This approach and its modifications are widely used [16,17,19] since it provides good accuracy and fast computational time compared to more accurate and demanding exact theory implemented in CONTACT [20]. The coefficient of friction in real contact depends on conditions such as material

* Corresponding author.
E-mail address: Daniel.Kvarda@vut.cz (D. Kvarda).

https://doi.org/10.1016/j.triboint.2021.106900
Received 11 November 2020; Received in revised form 15 January 2021; Accepted 25 January 2021
Available online 27 January 2021
0301-679X/© 2021 Elsevier Ltd. All rights reserved.

properties, contamination and roughness. This is taken into account by Kalker [21] as another layer that adds displacement and changes the flexibility coefficient.

A lot of numerical work has been done showing ways to address the problem of predicting coefficient of adhesion in mixed lubrication regime. The main problem is determining the magnitude of asperity contact. One of the first analytical solutions to model asperity contact was done by Greenwood and Tripp [22], which was applied by the following publications [4,9,15,19,23]. This approach uses the statistical distribution of asperity heights and defined geometry of asperity peaks. Using such a stochastic method allows for fast solution of asperity contact status. Once it is known what portion of the contact area is realized through asperity contact and interfacial fluid, the resulting coefficient of friction can be determined. New approaches to prediction of asperity contact were published [24–28] with different ways to tackle the effect of elasto-plastic asperity behaviour. These models are mathematically and computationally more complex than the approach of Greenwood and Tripp [22]. The main differences are in the way plasticity is considered by the model.

Many recent studies deal with the problem of water contamination and model prediction [1,12,29–33]. Publication [1] uses a high pressure torsion device and friction model, which is similar to previous publication by Beagley [2]. This model is used to assess the boundary shear properties of water and iron oxide particles mixture. However, this does not consider the EHL effect and transition in mixed lubrication regime. Studies [30,31] use a parametrised model based on laboratory experiments to estimate the coefficient of adhesion. Such models are good for fast evaluation based on the contact conditions but are not built on physical processes and material properties of the contact interface. Lastly, the work of Chen [4,13,23] uses EHL model to predict the surface separation and fluid friction. To evaluate the change in coefficient of adhesion, this model uses a fixed value of coefficient of adhesion for boundary friction based on experimental data.

The presented approach aims to use the fundamental solid shear and viscosity properties of the interfacial layer. The bulk liquid responds to the rate of displacement in EHL regime which is accounted for by the EHL solver. The solid shear responds to surface displacement alone in boundary regime and that is implemented using Kalker's simplified theory with contamination accounted for. This frees the solution from knowing the boundary coefficient of adhesion, but rather uses the fundamental properties of solid interface shearing. Both procedures are connected in mixed lubrication regime by asperity contact calculation. This approach allows the prediction of Stribeck and traction curves simultaneously across all lubrication regimes. With this, we can identify the train running conditions that can lead to severe loss of adhesion based on the physical properties of the contact interface, making such model very versatile. It also allows for the prediction of coefficient of adhesion in many conditions with materials of different properties. Such an advantage is valuable in wheel-rail contact, where many different materials and conditions may occur.

Further use of this model is beneficial in problems such as design and testing of products applied into the wheel-rail contact and the use in dynamic simulations to prevent the generation of wheel squeal noise. Using a numerical approach makes it easy to implement any shear dependency such as pressure, temperature, shear-thinning and others. The presented study is limited to pure water contamination to assess the feasibility of this modelling approach. This is due to the experimental methods used which are not suited for non-transparent substances such as water and oxide mixture. Transparent water allows us to control the main parameters of the model simultaneously – film thickness and coefficient of adhesion.

2. Material and methods

Contact area of two bodies with interfacial fluid can be separated into partly contact of asperities and partly into areas where the fluid is separating both surfaces as shown in Fig. 1. When there is a relative motion of contacting surfaces, shear stresses arise creating a reaction opposite to the direction of relative motion. Considering the concept of fluid entrapped between contact asperities, the shear stress can either result from asperity interaction or hydrodynamic processes in areas separated by fluid. Solids react to deformation, while fluids react to the rate of deformation. Combining the fundamentally different shear stress mechanism is a problem of finding the portion of shear taken up by asperities and a portion taken up by fluid. For that, an asperity contact model based on the previous work of Greenwood and Tripp [22] can be deployed. This model presents both elastic and plastic predictions. It is simpler and might not be as accurate for some conditions as more recent models for elasto-plastic asperity contact. However, for the current study we found that the Greenwood and Tripp model was accurate enough and allowed us to compare elastic and plastic asperity contact. It also allowed for faster calculation of each iteration algorithm, which is convenient since calculating Stribeck and traction curves requires varying both slip and speed parameters.

2.1. Asperity contact model

For the calculation of load carried by asperities and fluid a theory developed by Greenwood and Tripp is used [22]. A similar algorithm to the one published by Chen [4] is applied in this study as described in Fig. 2. Calculation of load carried by the lubricating film and asperity contact is compared to the total load applied to get the error of calculation. The solution is acquired by minimizing this error value by Newton-Raphson method.

The defining parameter for calculating resulting mean asperity pressure is separation of surface reference planes. In lubricated rolling-sliding contact, this is represented as the thickness of lubricant film. In this work, water is used as lubricant and thus Newtonian behaviour with respect to shear rate is assumed and there is no change in viscosity with change of pressure. For the separation of surfaces, a film thickness formula assuming iso-viscous behaviour is used [14]:

$$h_c = 5.08 U^{0.66} W_{EHL}{}^{-0.21} r \tag{1}$$

where the non-dimensional parameters are defined as:

$$U = \frac{\eta_0 v}{Er} \tag{2}$$

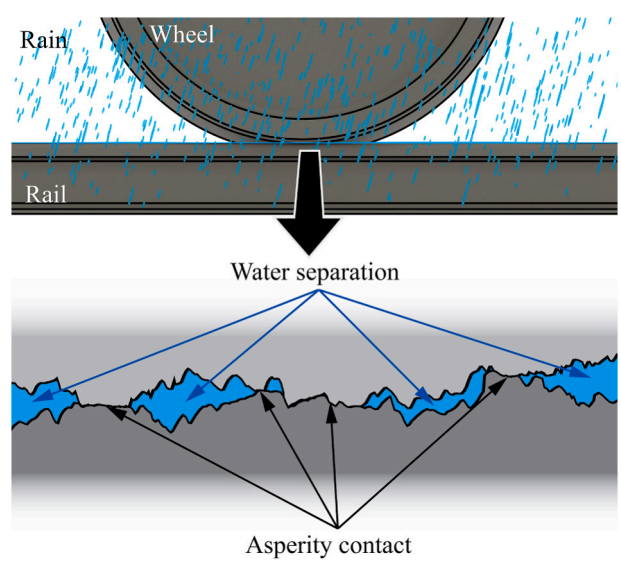

Fig. 1. Wheel-rail asperity contact illustration.

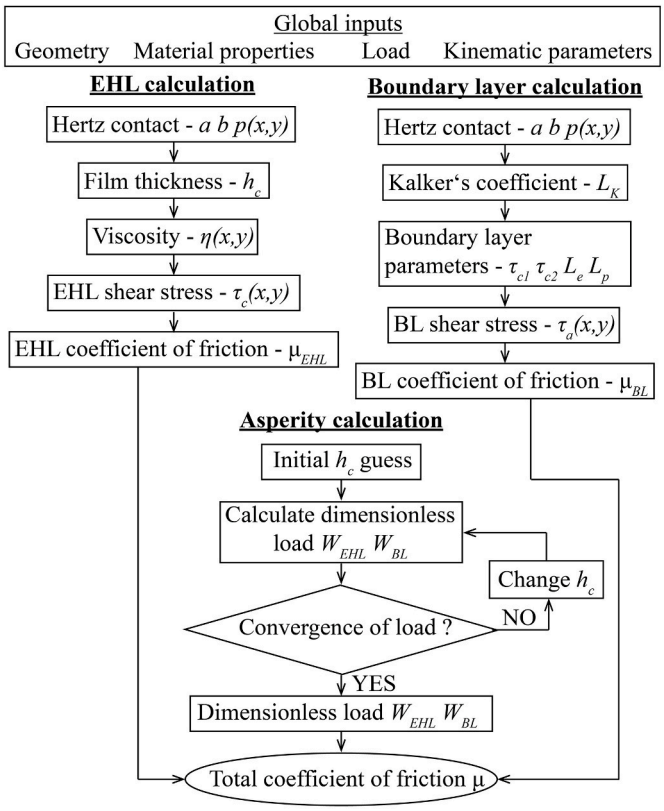

Fig. 2. Solution algorithm.

$$W_{EHL} = \frac{F_{EHL}}{Er^2} \tag{3}$$

The value of load carried by lubrication film F_{EHL} in the first iteration of calculation is equal to the total load applied to the contact F. Each other subsequent iteration uses Eq. (1) to evaluate the nondimensional load parameter of fluid film.

Calculation of central film thickness is used as surface separation in the mean asperity pressure p_a evaluation. In the current study, two approaches from Greenwood and Tripp theory [22] are used for comparison. The first approach described by Eq. (4) assumes paraboloidal asperity and elastic deformations. The asperities follow Gaussian distribution and are defined by three parameters: standard deviation σ, curvature of asperity peak β and density of asperity peaks ρ. Here we define $K = \sigma\beta\rho$ to compare different cases of surface topography. The function $F_{3/2}$ for Gaussian distribution is calculated from Eq. (5) given by Greenwood and Williamson [34]. For good accuracy of the numerical integration, the integral's upper limit is set to 30 with 1000 steps between integral bounds.

$$p_a = \frac{4}{3}\frac{K}{2}EF_{3/2}\left(\frac{h_c}{\sigma}\right)\sqrt{\frac{\sigma}{\rho}} \tag{4}$$

$$F_n(h) = \frac{1}{\sqrt{2\pi}}\int_h^{\infty}(u-h)^n e^{-u^2/2}\mathrm{d}u \tag{5}$$

The second approach to mean asperity pressure differs by assuming conical asperities and plastic deformation. The parameters of paraboloidal asperities are used by inscribing the cone into equivalent paraboloid. Greenwood and Tripp then give:

$$p_a = \frac{2}{3}\pi^2 HK^2 F_4\left(\frac{h_c}{\sigma}\right) \tag{6}$$

Where H is mean pressure related to the hardness. A good estimation can be made that the value of H equals to approximately 6x yield stress in shear [35].

For the case of numerical calculation, the asperity load from mean asperity pressure is given by non-dimensional parameter:

$$W_{BL} = \frac{p_a \pi a^2}{Er^2} \tag{7}$$

The non-dimensional loads of hydrodynamic film and asperity contact are then compared to give the error of calculation:

$$\varepsilon = \left|\frac{W^2 - (W_{EHL} + W_{BL})^2}{W^2}\right| \tag{8}$$

$$W = \frac{F}{Er^2} \tag{9}$$

The terminating condition is that the error should be lower than 0.1%. In the first iteration, when this condition is not met, the surface separation h_c is changed by step of $h_c/1000$. Subsequent steps and changes in separation are controlled by the numerical method. Each new step recalculates the hydrodynamic load W_{EHL}, mean asperity contact pressure p_a and asperity load W_{BL} with new surface separation h_c until the condition of maximum error is satisfied.

Dividing by the non-dimensional total load, the numbers W_{EHL}/W and W_{BL}/W represent a portion of load carried by lubricant film and asperity contact respectively. If we assume that the frictional forces are governed by Coulomb's law, then based on the coefficients of friction for hydrodynamic film μ_{EHL} and asperity contact μ_{BL} we get Eq. (10). The resulting coefficient of friction μ is:

$$\mu = \frac{\mu_{EHL}W_{EHL} + \mu_{BL}W_{BL}}{W_{EHL} + W_{BL}} \tag{10}$$

The parameters μ_{EHL} and μ_{BL} are defined in the following sections based on EHL theory and Kalker's simplified theory.

2.2. Friction in fluid film lubrication

To calculate the traction force and coefficient of friction in EHL, a basic simplification used in most analyses is made. For the purpose of calculating both EHL and asperity contact traction, the contact area is discretized into n by m areas as shown in Fig. 3. This discretization is not necessary for iso-viscous EHL calculation, because all variables for

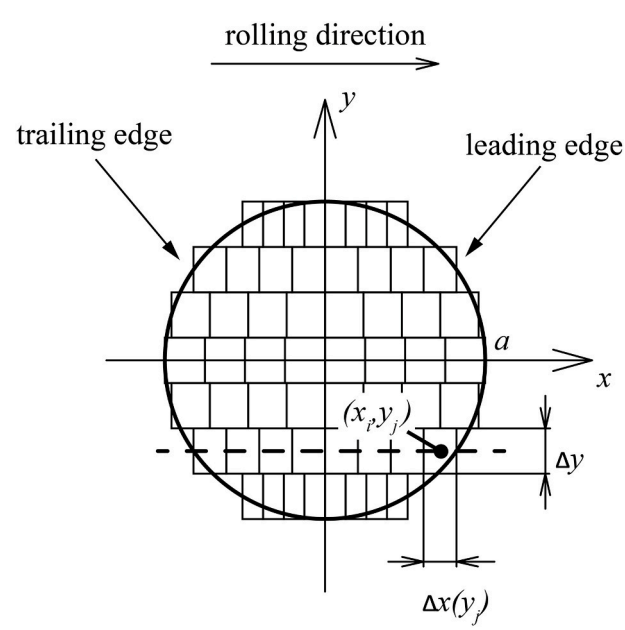

Fig. 3. Contact area discretization.

calculating traction force are constant across the contact patch. However other regimes as well as asperity contact require discrete mesh for calculation and thus for the convenience of changing regimes it is used here. Moreover, the discretization along the axis of rolling is variable, depending on the length of the contact at specific y coordinate. The model was set up in such a way, that each strip is divided into same number of discrete points. This increases the resolution at the side edges of the contact area.

The contact pressure of circular contact at each coordinate is described by semi-ellipsoid distribution given by Hertz:

$$p(x_i, y_j) = \frac{3F}{2\pi a^2}\left(1 - \left(\frac{x_i}{a}\right)^2 - \left(\frac{y_j}{a}\right)^2\right) \tag{11}$$

Since iso-viscous lubricant is assumed, there is no change in viscosity due to the Hertzian distribution of pressure in contact. Thus we assume viscosity distribution $\eta(x,y) = \eta_0$. Using Newtonian fluid with viscosity η between sliding surfaces separated by h_c with sliding speed equal to entrainment velocity v times slip ratio s. The shear stress is given by the equation:

$$\tau_{EHL}(x_i, y_j) = \eta(x_i, y_j)\frac{vc}{h_c} \tag{12}$$

The resulting coefficient of friction is calculated assuming Coulomb's law by the following equation:

$$\mu_{EHL} = \frac{\boldsymbol{\tau_{EHL}}}{\boldsymbol{p}} \tag{13}$$

2.3. Friction in asperity contact

Calculation of friction in asperity contact is based on Kalker's simplified theory implemented into FASTSIM algorithm [18]. We assume the influence of asperity and contamination as a change in the flexibility parameter as suggested by previous studies [16]. Instead of using a limiting coefficient of friction, the interface is modelled as a material following Voce's hardening law as mentioned in the study by Six. et al. [36]. The influence of pressure and temperature is neglected in the current study.

Imagining a particle on the surface entering contact at the leading edge, this is represented in Fig. 3 on the right side of the ellipse. At the leading edge the particle is undeformed, and no shear or normal stress is acting upon it from contact interaction. As the time progresses, the particle moves along the axis of rolling direction into the contact from the leading edge towards the trailing edge. As it passes through the contact area, stresses and relative motion are applied to it. The normal stress is defined by Eq. (11). To work towards the shear stress, we first define the slip velocity w. For the steady-state case, the interfacial slip velocity is given by kinematic equations:

$$w = c - (\partial u / \partial x)v \tag{14}$$

where c is rigid creep velocity and u is surface displacement. The simplified theory presumes that the displacement of each point on the surface is only affected by the shear stress at this point. The slip velocity w is equal to zero at the leading edge and only gains non-zero values in points where the surface displacements exceed the elastic capability of contact. Given this presumption, the simplified theory introduces load-displacement law where surface displacements and shear stresses are connected by a flexibility parameter L.

$$u = L\tau \tag{15}$$

Combining Eq. (14) and Eq. (15) and applying them to the previously described discretization of the contact area, as shown in Fig. 3, gives the shear stress in each elastically deformed point of contact.

$$\tau_{BL}(x_i, y_j) = \tau_{BL}(x_{i-1}, y_j) - \frac{2a(y_j)}{vm}\frac{c}{L} \tag{16}$$

The flexibility L is originally defined for clean contact and ideal geometry of contact bodies. In reality, the contact is influenced by surface condition and third body materials in the interface. To represent real surfaces closer to reality, the elasto-plastic behaviour of contact is introduced. During the elastic deformations, the shear stress is calculated by Eq. (16) where the flexibility L is calculated from Kalker's flexibility coefficient L_K and flexibility coefficient representing real contact conditions L_e (Eq. (17)).

$$L = L_K + L_e \tag{17}$$

When the surface deformations exceed the elastic limit, the shear stress is calculated from the plastic part of Voce's hardening material model [37] described by Eq. (18). The surface deformation u in this equation is calculated by discretizing Eq. (14).

$$\tau_{BL} = \tau_{c1} + (\tau_{c2} - \tau_{c1})\left(1 - e^{\left(-u + \tau_{c1}L_e\right)/L_p}\right) \tag{18}$$

The parameters τ_{c1} and τ_{c2} separate the regions where shear stress behaves elastically and plastically as shown in Fig. 4. Parameter L_e defines the slope of initial elastic region. The shape of plastic region is defined by parameter L_p.

Since pressure distribution in contact area changes at each point as represented by Eq. (11), also the shear stress needs to follow pressure changes. Assuming a simplification with linear relationship between shear stress and pressure, the parameters of Eq. (18) can be obtained by introducing new parameters μ_{c1}, μ_{c2}, $L_{\mu e}$ and $L_{\mu p}$ in such a way that:

$$\tau_{c1} = \mu_{c1}p \tag{19}$$

$$\tau_{c2} = \mu_{c2}p \tag{20}$$

$$L_e = L_{\mu e}/p \tag{21}$$

$$L_p = L_{\mu p} \tag{22}$$

The asperity contact coefficient of friction μ_{BL} is calculated using the same relationship for μ_{EHL} as shown in Eq. (23):

$$\mu_{BL} = \frac{\boldsymbol{\tau_{BL}}}{\boldsymbol{p}} \tag{23}$$

2.4. Experimental validation

The verification experiments were conducted using ball-on-disc tribometer with the capability of using optical interferometry to measure lubricant film thickness. Measured values of film thickness were acquired from thin-film interferometry evaluation software [38]. The ball specimen with 25.4 mm diameter resulting in circular contact. The ball was made from bearing steel AISI 52100 and had measured

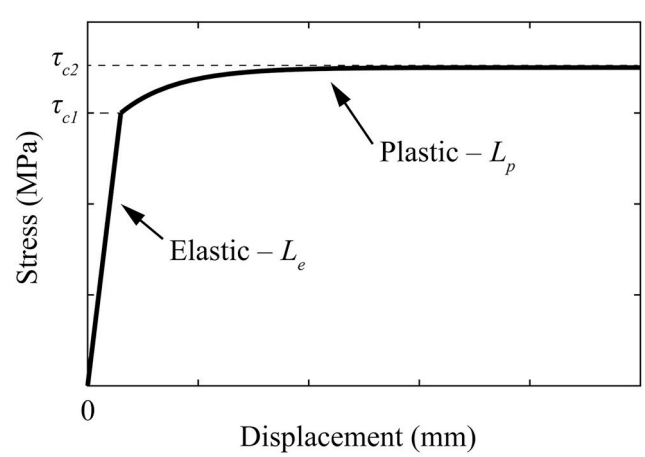

Fig. 4. Parameters of Voce's hardening material model.

hardness 53HRC (standard deviation 0.3HRC) which corresponds to a mean pressure related to the hardness of approximately 6 GPa. A smooth surface of the ball specimen was prepared by polishing with diamond paste. A rough surface was prepared by 5-minute dry run-in test with maximum Hertzian pressure of 0.75 GPa, 5% slip and 500 mm/s entrainment speed. Surface parameters were measured by optical profilometer Bruker Contour GTX and are stated in Table 1. The steel ball was loaded against the glass disc with a thin chromium coating that allows the partial reflection of light, creating an interferometric image together with reflection from the ball surface. The glass disc had roughness lower than 1 nm and because of this low roughness, the calculation neglects the effect of glass disc surface topography. A schematic of the test rig is shown in Fig. 5.

The ball-on-disc tribometer uses servo motors to separately drive the ball and disc to achieve set speed and slip. However, to ensure precise values the slip and speed were calculated from measured true rotations of both ball and disc drive shafts. Shaft with an attached ball is connected through a torque transducer that records at sampling frequency 1 kHz. Based on the measured radius of the ball and its position with regards to the disc's rotational axis, the true speeds of both surfaces in contact and the resulting slip is calculated. Coefficient of adhesion (marked as CoA in figures) is calculated from the loading force, torque and radius of the ball specimen.

The applied water used in this study was previously distilled to guarantee its pureness and stable properties during tests. The viscosity of distilled water is taken from the following study [39] based on ambient temperature during measurement. Application of water was done directly into contact through a syringe with a needle.

Film thickness measurements were done at 0% slip with a speed range from 0 to 2 m/s. Stribeck curves were measured at 5% slip with a sequence of increasing speed from 0 m/s up to 2 m/s and then decreasing back to 0 m/s. Dry traction and traction curve measurements were done by increasing the slip values from negative to positive slip (see Table 2). Assuming a symmetrical behaviour of slip, the negative values were transformed into the first quadrant to make sure there is no shift of the traction curve with regards to 0% slip. Each point of coefficient of adhesion was measured by averaging a 4 s long reading from torque transducer at the set speed and slip.

The roughness of the ball specimen was measured after each test to guarantee minimal deviation from the parameters stated in Table 1. However, higher deviations of roughness parameters (more than 15%) were seen after traction tests with smooth surface at lower speeds. This might have been because of longer time spent at saturated values of traction curves in the mixed lubrication regime. Such behaviour was not observed with Stribeck tests due to only a few measured points being in the mixed lubrication regime. Because of this, only rough surface traction measurements were evaluated.

3. Results and discussion

3.1. Determining the parameters for model

Prior to the main experiments comparing rough and smooth surfaces contaminated with water, the unknown parameters of the Voce's hardening model had to be determined. The relationship between surface deformation and resulting shear stresses can be acquired by slow relative movement of two surfaces while measuring the relative displacement and resulting frictional force. This type of experiment has been previously used to identify the influence of small amounts of water and iron oxide mixture on adhesion in wheel-rail contact [1]. However, in this study it was not feasible to conduct such experiment with the specimens used. Because of this, the stress-displacement relationship had to be determined based on the traction measurements. Subsequently, a model fit and identification of main parameters was done.

Table 1
Surface parameters.

Surface condition	Roughness standard deviation σ (nm)	Asperity peak curvature β (mm)	Asperity peak density ρ (1/mm^2)	K (−)
Smooth	8.3	0.301	24200	0.0605
Rough	9.56	0.373	21500	0.0767

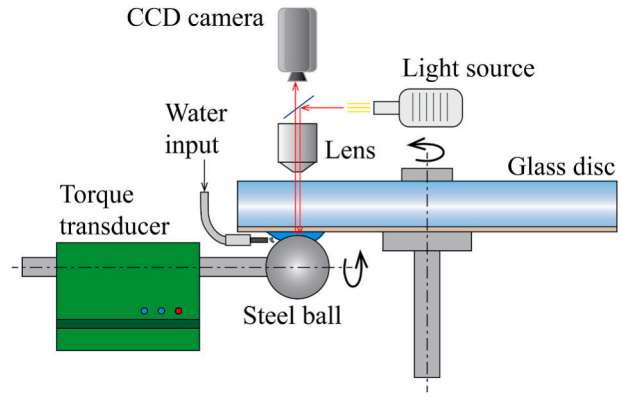

Fig. 5. Scheme of ball-on-disc tribometer.

Results of traction curve measurement under dry conditions are shown in Fig. 6. The measured values of the coefficient of adhesion show an initial increase up to 0.01 slip. To determine the exact shape of traction curve around saturation point, more measurements were done around this slip value. In terms of wheel-rail contact, the saturation at 0.01 slip is a good representation as suggested by other experimental [7,8] and numerical [16,19] studies. Even though some studies with similar geometry show much later onset of saturation [12]. At the coefficient of adhesion value 0.16 saturation is reached and only a slight positive change with a further increase of slip is achieved. The saturated values converge around the coefficient of adhesion 0.18. Such low values are the result of glass contact specimen used with different material properties of glass and chromium layer compared to steel. Moreover, the glass disc with negligible roughness and the steel ball with polished surface do not provide strong enough surface interaction to overcome the coefficient of adhesion values higher than 0.2, which is quite low compared to steel–steel contact. Conducting experiments under dry conditions also causes excessive wear of the chromium layer, which can change surface properties and makes the wear path unusable for further study of film thickness. The fitted traction curve and corresponding parameters for model prediction are also noted in Fig. 6. These parameters were used throughout this whole study.

3.2. Film thickness

For a correct prediction of load carried by asperities, the film separation predicted by the model needs to correspond to experimental measurement. The measured values of average central film thickness and standard deviation are shown in Fig. 7. The prediction in this figure corresponds to iso-viscous regime defined by Eq. (1). At speeds lower than 100 mm/s the measured film thickness values run into the resolution limit of coloric interferometry method. At film thickness of 1.25 nm at 50 mm/s the error due to a resolution limit (0.5 nm) is 40% of the measured value. These values at low speed should thus be interpreted with caution. However, with increasing speed the film thickness follows the same trend as predicted values. At speeds higher than 1 m/s the standard deviation almost always crosses the predicted value.

These results show that using iso-viscous elastic film prediction formula yields accurate values compared with experimental measurement for the measured conditions. Interferograms for selected speeds can be seen in Fig. 8. Visible contact areas show the different hue for specified film thickness. Due to the monochromatic nature of

Table 2
Experimental conditions and type of experiment.

Test type	Roughness type	Speed (m/s)	Slip (%)	Max. Hertz. pressure (MPa)	Fig. No
Dry traction	Rough	0.5	−10 – 10	750	6
Film thickness	Smooth	0–2	0	750	7,8
Stribeck	Smooth	0.1–2	5	750	9
Stribeck	Rough	0.1–2	5	750	10
Traction	Rough	0.25, 0.5, 1, 1.5, 2	−5–5	750	13

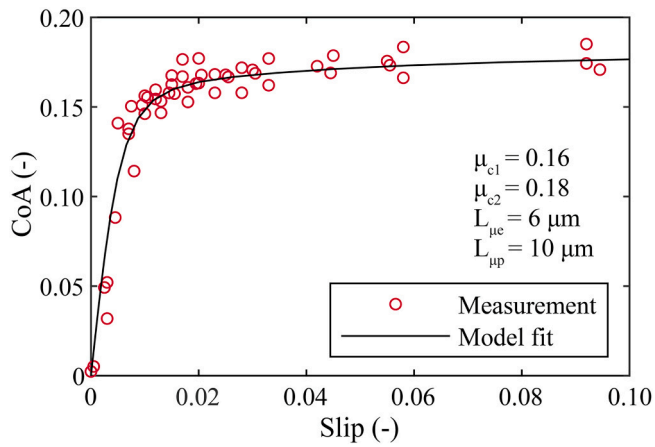

Fig. 6. Traction curve under dry conditions.

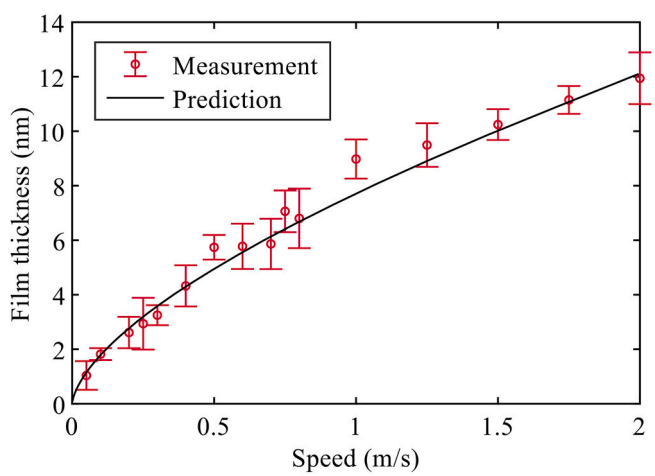

Fig. 7. Water film thickness measurement compared with prediction.

interferograms, the precise calibration before and after each set of speed sequence had to be done. This ensured that the calibration scale was stable throughout the whole experiment. The chromatic layer was not uniform as can be seen from the interferograms. This can be as a result of prior damage from contact interaction since the direction of non-uniformity is the same as the direction of rolling. However, this has negligible influence on the average film thickness. The film was mostly uniform across the whole contact area. No visible side lobes or minimum film thickness regions occur making it easier for evaluation.

3.3. Friction and model prediction

The Stribeck experiment with smooth surface indicates some discrepancy compared with the presented model, see Fig. 9. *Measurement 1* represents sequence with increasing speed, while *Measurement 2* was done by decreasing speed. Minimal changes between the direction of speed change are present. The initial slope of the coefficient of adhesion with increased speed is low, which suggests that the contact is at the mixed lubrication regime and the roughness parameters do not allow the transition to boundary regime. This is also validated by low values of the coefficient of adhesion in comparison with values for dry contact. The lowest measured value of coefficient of adhesion was 0.007 with a standard deviation of 0.004. With the speed increasing from 1 m/s to 2 m/s the coefficient of adhesion changed only about 30%.

Looking at the prediction models, the elastic formula for asperity contact predicts extremely low values at lower speeds. With a range of speed 1 mm/s to 2 m/s the coefficient of adhesion changes from 0.0033 to 0.0004. Such low values would indicate that almost no load is carried by asperity peaks and the regime of lubrication fluid dominated. This does not represent well the experimental data at lower speeds, even

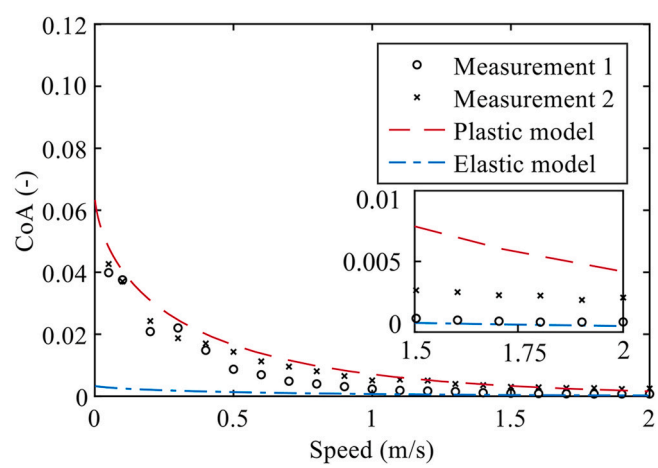

Fig. 9. Stribeck curve for smooth surface.

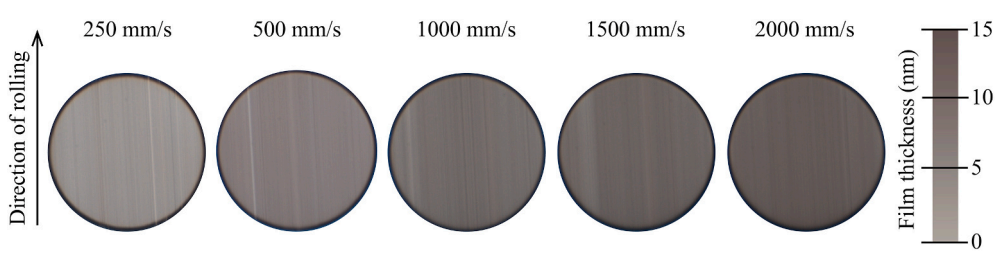

Fig. 8. Water film thickness interferograms.

though a big part of past research published on the topic of using Greenwood and Tripp theory [22] works with the elastic formula [4,9,15,23]. However, new approaches to elasto-plastic behaviour of contact asperities have been studied [10,19,40]. The simple plastic asperity model used in this study suggests much clearly the change in coefficient of adhesion with increasing speed compared to the elastic model. It can be seen that the experimental data show similar trend to the predicted values. This implies that the roughness is close to the one measured by the optical profilometer.

From the interference images obtained during the experiment it was obvious that the increase of wear on the chromatic layer has happened during the test sequence. Because of this the film thickness measurement was impossible to perform. The wear of the chromatic layer caused inhomogeneous reflection intensity across the contact area. This meant that it would be much more complicated to evaluate the true film thickness due to changes in calibration across the taken interference image. However, a qualitative assessment could be made to make sure that the film thickness is within expected values and no contamination of water happened during the experiment.

The effect of increased roughness parameters is depicted in Fig. 10. As in the test with a smooth surface, the direction of speed change has a negligible effect on the coefficient of adhesion. The initial slope at lower speed is much steeper in comparison with the smooth surface experiment and reaches higher values. This corresponds well with the plasticity based predictive model used, where higher roughness causes higher mean asperity pressure for the same separation h_c/σ as reported by other studies [4,13,19,41,42]. Thus, the contact is located closer to the boundary lubrication regime. For the lowest measured speeds, there was no saturation of measured values, which would suggest boundary lubrication regime. Moreover, the highest measured value of coefficient of adhesion was 0.085 with a standard deviation of 0.009. This value is closer to dry contact conditions than the smooth surface experiment. The lowest value at 2 m/s was 0.015 with a standard deviation of 0.0003. A similar order of values were measured using Mini Traction Machine [12] with a polished steel specimen at speed 1.5 m/s with roughness almost equivalent to the specimens used in this study. Other numerical studies also suggest such a low coefficient of adhesion for either an extremely smooth surface or high enough speed to separate contact bodies [10,23,42].

The predictive formula for elastic deformation of asperities gives extremely low values of the coefficient of adhesion similarly to smooth surface conditions. Increasing the roughness parameters had no significant influence on the elastic model prediction. Higher predicted coefficient of adhesion was acquired with increased roughness of the rough surface. At lower speed, the increased roughness caused 60% higher values of coefficient of adhesion compared with the smooth surface. This happened even though the parameter K had only a small change going from smooth to rough surface. This can be explained by the sensitivity of predictive model to the change in roughness on a scale where film thickness and roughness are of the same order. The fact that small changes in surface roughness parameter can cause significant changes in the coefficient of adhesion was previously studied numerically [4,19], however it is important to distinguish the scale of roughness and speed on which this is studied. The roughness studied in this paper are not representative of real wheel-rail contact. For the case of rough surface, it is clearly visible that the plastic model predicts a slightly lower coefficient of adhesion than experimental data throughout the whole range of speeds. Around 1.2 m/s, it is clear that the measurement slowly saturates at the lowest measured value while the plastic model prediction continues a decreasing trend.

The changes in lubrication regime are controlled by the surface asperity distribution function in Eq. (5). A more accurate representation of the Stribeck curve might be achieved with a specific surface function to the measured surface topography. Previous studies [43] show that the functions F_n with Gaussian distribution might not have satisfiable precision and it is recommended to use surface-specific functions which better represent the true geometrical asperity distribution. It should also be noted that because of the method used to prepare a smooth surface of the ball specimen, there might be some dominant direction of asperities. Some research [10,13] shows that the coefficient of adhesion can change depending on the angle between the direction of rolling and the roughness orientation. However, this effect should become predominant at higher speeds rather than the lower speeds that reach the mixed lubrication regime in this study.

The film thickness defines surface separation which is key to determining the asperity load and coefficient of adhesion. Since the presented model uses iterative algorithm of changing the film thickness to obtain a solution, it is of interest to compare the iterative solution to analytical iso-viscous elastic formula, see Fig. 11. These results show the change difference in calculated film thickness compared to the analytical prediction by Esfahanian and Hamrock [14]. For both simulated surface conditions with the plastic model, the error is decreasing with the increase of speed. The smooth surface shows smaller changes in film thickness difference, which was also reported by Chen et al. [44]. However, the highest difference values mean only an order of a tenth of a nanometre, which is insignificant compared to the overall roughness. Higher speed makes the difference drop slightly under 0% and the iterative prediction slowly converges to around −4% in the observed range of speeds. This says that the lower the speed, the higher the surface separation needs to be. And thus, the asperity load is smaller than if the analytical film thickness was used.

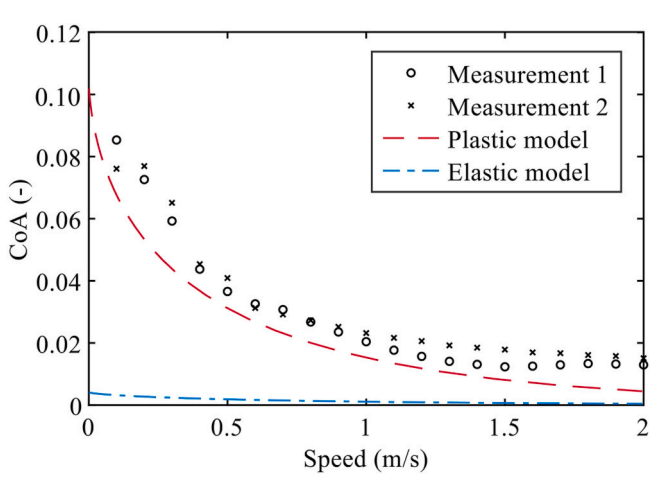

Fig. 10. Stribeck curve for rough surface.

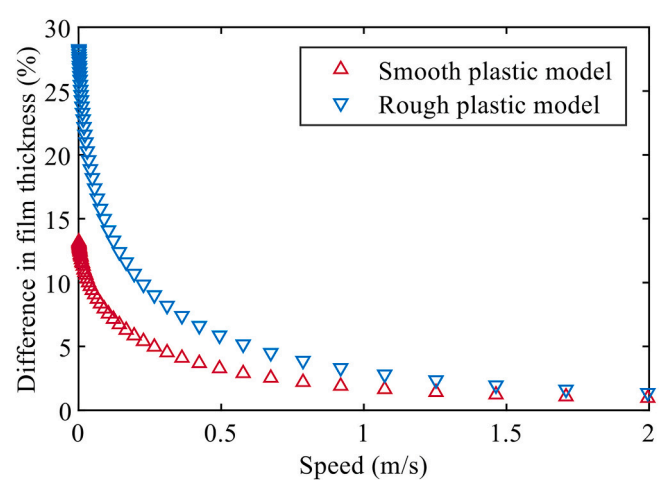

Fig. 11. Difference in film thickness acquired in comparison with analytical prediction.

Looking at the predicted values of load carried by asperities as shown in Fig. 12, the boundary regime can be clearly seen. The transition point from the boundary to mixed lubrication regime is located around 10e-2 to 10e-1 m/s. Asperity load proportion for the boundary regime increases with increased roughness of the contact surface. Using the data from dry experiment we can assume that the coefficient of adhesion for boundary regime of rough surface should be around 0.126 while for smooth surface 0.08. Further increasing the roughness should allow the contact to carry the full load by asperities in boundary regime. This would result in achieving a maximal coefficient of adhesion limited by dry contact. For the roughness cases used in this study, it would be optimal to accurately study the speed from 1 mm/s to 10 m/s to represent all three lubrication regimes: boundary, mixed and elastohydrodynamic. It is evident that such range of speed is not reachable with the used tribometer. For a future study on a larger scale experimental device, the operating conditions should be adequately chosen to allow the experiment to represent the whole range of Stribeck curve where the regime changes. For the real wheel-rail contact, the mixed lubrication regime should be between 50 and 200 m/s depending on the specific roughness based on previously conducted studies [4,7,8,23].

3.4. Traction measurements

Traction curves for the selected speeds are shown in Fig. 13. The initial part of traction curve before reaching the saturation point conveys the same trend for both measured and predicted values. The saturation point should be reached around 0.01 slip as suggested by the model, which is well correlated with the measured data. After reaching the saturation point there is only a small increase in the coefficient of adhesion with increasing slip as represented by both the model and experiment. The only exception is the lowest measured speed in Fig. 13a. At this speed, the trend of traction curve after saturation is decreasing. Other speeds measured do not exhibit this behaviour. This difference compared with other measurements might be because of higher values of the coefficient of adhesion influencing the asperity interaction and temperature changes. For real wheel-rail materials, it is expected that the coefficient of adhesion should drop with large slip values as reported by Refs. [7,11,45]. The largest discrepancy between model and experiment is present at a higher speed. For 1 m/s (Fig. 13c) the experiment shows higher values than the model prediction with still increasing values of the coefficient of adhesion. Similarly, the highest speed of 2 m/s (Fig. 13e) also shows higher measured values at higher slips. As seen from the Stribeck curves (Fig. 10), the model seems to predict decreasing values of adhesion coefficient even after 2 m/s. While the experiments show that around 1.5 m/s the lowest values are reached, and no further decrease is happening with increased speed. The measured values in Fig. 10 for speed 2 m/s and the corresponding values at 0.005 slip in Fig. 13e show a small discrepancy. The Stribeck curve measurement showed higher values of coefficient of adhesion in comparison with traction measurement. However, the difference is not too significant and most importantly, the trend with regards to the prediction model is the same.

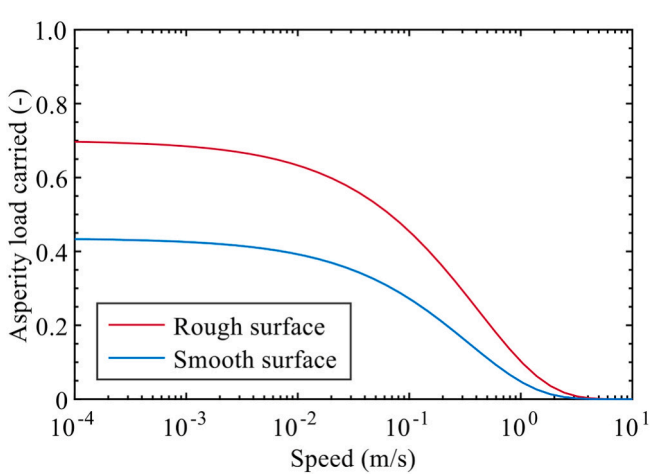

Fig. 12. Asperity load portion carried for different surface conditions.

3.5. Limitations and further development

Due to this study being conducted on a scaled apparatus with different materials of contact specimen, there are some aspects of the model that should be considered for future work. The material and roughness are far from the wheel-rail interface. However, for model validation the harder bearing steel and low roughness allow us to maintain stable surface conditions and work in the mixed lubrication regime. Also, these specimens prevent excessive wear to chrome layer which is important to determine film thickness which is a key parameter of the model. The generation of heat and its influence on lowering the coefficient of adhesion with an increase of slip [7,10,11,45] should be taken into consideration. A solution to this is using a temperature calculation across the contact area. A simple temperature calculation model using slip-velocity generated heat [46] can be used to give enough accuracy of temperature rise. The temperature influences not only the solid contact of materials [47,48] but also the behaviour of interfacial liquid [4,41]. For oil-based contaminants, a non-Newtonian property might also be expected at higher shear rates. Such a study [49] was previously conducted for shear-thinning properties of oil on a similar scale as this paper.

Another phenomenon that the presented model neglects is the dependence on pressure. Assuming iso-viscous water in the model means that viscosity does not change with pressure. However, liquids in general will increase viscosity with such pressure as in wheel–rail contact and this should be implemented accordingly as studied before [10,15,42]. For solid to solid contact, the pressure also influences the coefficient of adhesion. For dry contact, the increase in pressure causes a decrease in the coefficient of adhesion [1,7,16,19]. The calculated mean pressure from asperity contact defines the region of lubrication for set parameters. A more precise calculation can be done by using a more sophisticated modelling approach to plasticity [24–28,35,40]. These models could more accurately represent wheel-rail material and different types of contact conditions where the plasticity effect might be negligible or more dominant than what was observed in the current study. Moreover, the surface specific functions (Eq. (5)) can be defined more precisely [43], due to modern methods for roughness measurement.

4. Conclusions

The interfacial shear-based model together with ball-on-disc apparatus has been used to study the applicability of this model on rolling-sliding frictional contact contaminated with water. The asperity contact models studied are based on a simple formula for elastic or plastic deformation of asperities. The friction from asperity contact is based on Kalker's simplified theory, while the friction from liquid uses general EHL theory. For experimental validation, a tribometer with the capability to measure film thickness and coefficient of adhesion is used.

- For the studied conditions, the elastic model predicts a significantly lower coefficient of adhesion than the plastic model. The experimental data are in line with the plastic model. However, a difference in the trend at higher speed was found in an experiment with a rough surface. A deeper consideration should be taken when determining which asperity model to use for specific cases.
- The minimum coefficient of adhesion reached with water-contaminated smooth surface was equal to 0.4% of dry contact. Using a rough surface, the value increased to 7.2% of dry contact.

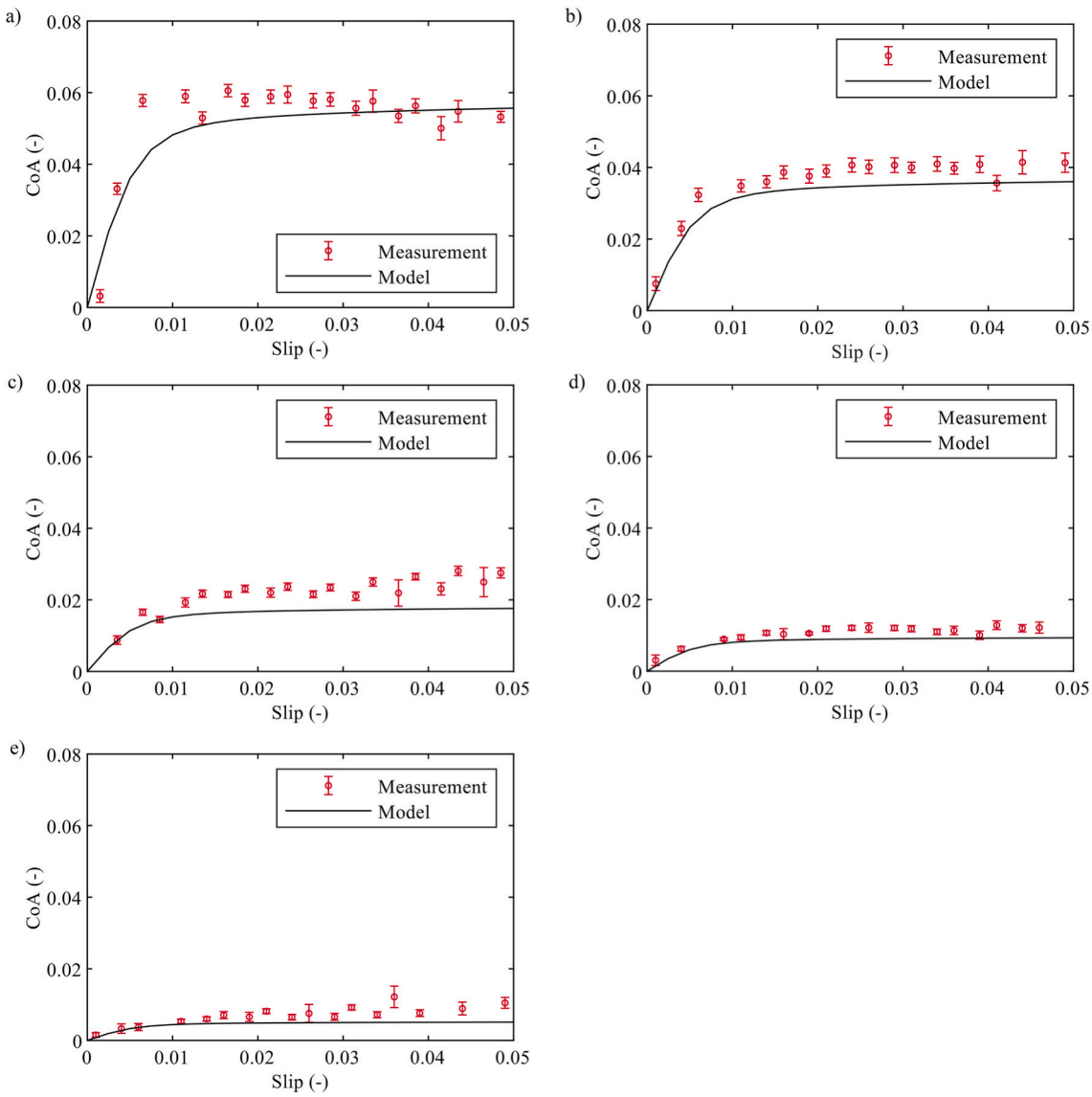

Fig. 13. Traction curves for speed: a) 0.25 m/s, b) 0.5 m/s, c) 1 m/s, d) 1.5 m/s, e) 2 m/s.

Such a difference was achieved with only 15% of change in roughness standard deviation σ.

- The shape of predicted Stribeck curves does not seem to fully correspond with measurement, especially at higher speed for the rough surface. The presented model predicts a more gradual decrease of coefficient of adhesion with an increase of speed. More accurate prediction of asperity load might be achieved with a surface specific function instead of Gaussian surface distribution. In addition, a more refined elasto-plastic asperity contact model can improve the estimation of mean asperity pressure.
- The presented model shows a good accuracy in predicting traction curves. Small differences between the experiment and model were observed. However, the trend of change with increasing speed and values of coefficient of adhesion is well within satisfiable accuracy.

The presented model gives a different approach for predicting friction in rolling–sliding contact. Using Kalker's FASTSIM algorithm frees the solution from using a set value for asperity friction. This comes into more of importance in the real wheel–rail contact where the real friction in contact is not easy to precisely determine. However, further development is necessary to increase the accuracy of the model and to experimentally determine the properties of the contact interface.

CRediT authorship contribution statement

Daniel Kvarda: Conceptualization, Methodology, Investigation, Data curation, Writing - original draft. **Radovan Galas:** Conceptualization, Methodology, Investigation, Writing - review & editing. **Milan Omasta:** Conceptualization, Investigation, Methodology, Writing - review & editing, Project administration. **Lu-bing Shi:** Data curation, Writing - review & editing, Visualization. **Haohao Ding:** Writing - review & editing, Visualization. **Wen-jian Wang:** Conceptualization, Data curation, Writing - review & editing, Project administration. **Ivan Krupka:** Data curation, Writing - review & editing. **Martin Hartl:** Supervision, Funding acquisition.

Declaration of competing interest

The authors declare that they have no known competing financial interests or personal relationships that could have appeared to influence the work reported in this paper.

Acknowledgments

This research was supported by the Czech Science Foundation

(Project No. 20-23482S). The authors also thank the support by National Key R&D Program Intergovernmental Key Items for International Scientific and Technological Innovation Cooperation (No.2018YFE0109400) and Sichuan Science and Technology Program (No.2020YFH0057).

Appendix A. Nomenclature

Nomenclature

a	Radius of contact area (m)
c	Rigid slip (m/s)
E	Effective elastic modulus ($1/E = 1/2((1-\upsilon_1^2)/E_1 + (1-\upsilon_2^2)/E_2)$, Pa)
E_1, E_2	Elastic modulus of body 1 and body 2 (Pa)
F	Total load applied to the contact (N)
F_{EHL}	Load carried by EHL film (N)
F_n	Surface function (−)
H	Mean pressure related to the hardness (Pa)
h_c	Central film thickness (m)
K	Surface roughness parameter (−)
L	Kalker's contact flexibility (mm^3/N)
L_e	Elastic flexibility of asperity contact (mm^3/N)
L_K	Kalker's contact flexibility (mm^3/N)
L_p	Plasticity parameter (m)
p	Contact pressure (Pa)
p_a	Average pressure carried by asperity (Pa)
r	Rolling radius (m)
U	Dimensionless speed parameter (−)
u	Surface displacement (m)
v	Rolling velocity (m/s)
W	Dimensionless load (−)
w	Slip velocity (m/s)
W_{BL}	Dimensionless load carried by asperity (−)
W_{EHL}	Dimensionless load carried by EHL film (−)
x	x coordinate in rolling direction (m)
y	y coordinate in lateral direction (m)
β	Asperity peak radius of curvature (m)
ε	Error tolerance for calculation convergence (−)
η	Viscosity of water at operating conditions (Pa s)
η_0	Viscosity of water at room temperature and ambient pressure (Pa s)
μ	Total coefficient of friction (−)
μ_{BL}	Coefficient of friction related to the asperity contact (−)
μ_{EHL}	Coefficient of friction related to the lubrication film (−)
υ_1, υ_2	Poisson ratio of body 1 and body 2 (−)
ρ	Density of asperity peaks ($1/m^2$)
σ	Standard deviation of roughness (m)
τ	Shear stress (Pa)
τ_{BL}	Shear stress in asperity contact (Pa)
τ_{c1}	Elasticity limiting shear stress (Pa)
τ_{c2}	Plasticity limiting shear stress (Pa)
τ_{EHL}	Shear stress in lubricant film (Pa)

References

[1] Buckley-Johnstone LE, Trummer G, Voltr P, Meierhofer A, Six K, Fletcher DI, et al. Assessing the impact of small amounts of water and iron oxides on adhesion in the wheel/rail interface using High Pressure Torsion testing. Tribol Int 2019;135:55–64.
[2] Beagley TM. The rheological properties of solid rail contaminants and their effect on wheel/rail adhesion. Proc Inst Mech Eng - Part F J Rail Rapid Transit 1976;190:419–28.
[3] White B, Lewis R. Simulation and understanding the wet-rail phenomenon using twin disc testing. Tribol Int 2019;136:475–86.
[4] Chen H, Ban T, Ishida M, Nakahara T. Adhesion between rail/wheel under water lubricated contact. Wear 2002;253:75–81.
[5] Stock R, Stanlake L, Hardwick C, Eadie DT, Lewis R. Material concepts for top of rail friction management – classification , characterization and application. In: Proceedings of 10th International Conference on Contact Mechanics and Wear of Rail/Wheel Systems; 2015. p. 1–8.
[6] Harmon M, Lewis R. Review of top of rail friction modifier tribology. Tribol Mater Surface Interfac 2016;5831:1–13.
[7] Wang WJ, Shen P, Song JH, Guo J, Liu QY, Jin XS. Experimental study on adhesion behavior of wheel/rail under dry and water conditions. Wear 2011;271:2699–705.
[8] Chen H, Ban T, Ishida M, Nakahara T. Experimental investigation of influential factors on adhesion between wheel and rail under wet conditions. Wear 2008;265:1504–11.
[9] Wang H, Wang W, Liu Q. Numerical and experimental investigation on adhesion characteristic of wheel/rail under the third body condition. Proc IME J J Eng Tribol 2016;230:111–8.
[10] Wu B, Wen Z, Wu T, Jin X. Analysis on thermal effect on high-speed wheel/rail adhesion under interfacial contamination using a three-dimensional model with surface roughness. Wear 2016;366–367:95–104.
[11] Zhang W, Chen J, Wu X, Jin X. Wheel/rail adhesion and analysis by using full scale roller rig. Wear 2002;253:82–8.
[12] Zhu Y, Olofsson U, Persson K. Investigation of factors influencing wheel-rail adhesion using a mini-traction machine. Wear 2012;292–293:218–31.
[13] Chen H, Ban T, Ishida M, Nakahara T. Influential factors on adhesion between wheel and rail under wet conditions. Q Rep RTRI 2012;53:223–30.
[14] Esfahanian M, Hamrock BJ. Fluid-film lubrication regimes revisited. Tribol Trans 1991;34:628–32.
[15] Wu B, Wen Z, Wang H, Jin X. Numerical analysis on wheel/rail adhesion under mixed contamination of oil and water with surface roughness. Wear 2014;314:140–7.
[16] Rovira A, Roda A, Lewis R, Marshall MB. Application of Fastsim with variable coefficient of friction using twin disc experimental measurements. Wear 2012;274–275:109–26.
[17] Jin XS, Zhang WH, Zeng J, Zhou ZR, Liu QY, Wen ZF. Adhesion experiment on a wheel/rail system and its numerical analysis. Proc IME J J Eng Tribol 2004;218:293–303.
[18] Kalker JJ, Johnson KL. Three-dimensional elastic bodies in rolling contact, vol. 60. Eisenbahntechnische Rundschau; 1993.
[19] Tomberger C, Dietmaier P, Sextro W, Six K. Friction in wheel-rail contact: a model comprising interfacial fluids, surface roughness and temperature. Wear 2011;271:2–12.
[20] Kalker JJ. On the rolling contact of two elastic bodies in the presence of dry friction. Delft University of Technology; 1967.
[21] Kalker JJ. Survey of Wheel–Rail rolling contact theory. Vehicle system dynamics. Int J Veh Mech Mobil 1979;8:317–58.
[22] Greenwood JA, Tripp JH. The contact of two nominally flat rough surfaces. Proc Inst Mech Engrs 1970;185:625–33.
[23] Chen H, Yoshimura A, Ohyama T. Numerical analysis for the influence of water film on adhesion between rail and wheel. Proc IME J J Eng Tribol 1998;212:359–68.
[24] Kogut L, Etsion I. Elastic-plastic contact analysis of a sphere and a rigid flat. J Appl Mech Trans ASME 2002;69:657–62.
[25] Jackson RL, Green I. A statistical model of elasto-plastic asperity contact between rough surfaces. Tribol Int 2006;39:906–14.
[26] Li L, Etsion I, Talke FE. Contact area and static friction of rough surfaces with high plasticity index. J Tribol 2010;132:1–10.
[27] Jackson RL, Green I. A finite element study of elasto-plastic hemispherical contact against a rigid flat. J Tribol 2005;127:343–54.
[28] Cohen O, Kligerman Y, Etsion I. A model for contact and static friction of nominally flat rough surfaces under full stick contact condition. J Tribol 2008;130:1–9.
[29] Buckley-Johnstone LE, Trummer G, Voltr P, Six K, Lewis R. Full-scale testing of low adhesion effects with small amounts of water in the wheel/rail interface. Tribol Int 2020;141:105907.
[30] Galas R, Omasta M, Shi LB, Ding H, Wang WJ, Krupka I, et al. The low adhesion problem: the effect of environmental conditions on adhesion in rolling-sliding contact. Tribol Int 2020;151:106521.
[31] Trummer G, Buckley-Johnstone LE, Voltr P, Meierhofer A, Lewis R, Six K. Wheel-rail creep force model for predicting water induced low adhesion phenomena. Tribol Int 2017;109:409–15.
[32] Shi LB, Wang C, Ding HH, Kvarda D, Galas R, Omasta M, et al. Laboratory investigation on the particle-size effects in railway sanding: comparisons between standard sand and its micro fragments. Tribol Int 2020;146:106259.
[33] Galas R, Kvarda D, Omasta M, Krupka I, Hartl M. The role of constituents contained in water–based friction modifiers for top–of–rail application. Tribol Int 2018;117:87–97.
[34] McCool JI. Comparison of models for the contact of rough surfaces. Wear 1986;107:37–60.
[35] Bhushan B. Contact mechanics of rough surfaces in tribology: multiple asperity contact. Tribol Lett 1998;4:1–35.
[36] Six K, Meierhofer A, Muuller G, Dietmaier P. Physical processes in wheel-rail contact and its implications on vehicle-track interaction. Veh Syst Dyn 2015;53:635–50.
[37] Voce E. The relationship between stress and strain for homogeneous deformation. J Inst Met 1948;74:537–62.
[38] Hartl M, Krupka I, Poliscuk R, Liska M. An automatic system for real-time evaluation of EHD film thickness and shape based on the colorimetric interferometry. Tribol Trans 1999;42:303–9.
[39] Eisenberg D, Kauzmann W. The structure and properties of water. Oxford University Press; 2007.

[40] Zhao Y, Marietta DM, Chang L. An asperity microcontact model incorporating the transition from elastic deformation to fully plastic flow. J Tribol 2000;122:479–80.
[41] Tanimoto H, Chen H. Influence of surface roughness and temperature on wheel/rail adhesion in wet conditions. Q Rep 2015;56:206–11.
[42] Wu B, Wu T, An B. Numerical investigation on the high-speed wheel/rail adhesion under the starved interfacial contaminations with surface roughness. Lubric Sci 2020;32:93–107.
[43] Morris N. Asperity contact modelling for measured surfaces. 11th Int. Tribol. Conf. SAIT Tribol. 2015 0–7.
[44] Chen H, Namura A, Ishida M, Nakahara T. Influence of axle load on wheel/rail adhesion under wet conditions in consideration of running speed and surface roughness. Wear 2016;366–367:303–9.
[45] Gallardo-Hernandez EA, Lewis R. Twin disc assessment of wheel/rail adhesion. Wear 2008;265:1309–16.
[46] Ertz M, Knothe K. A comparison of analytical and numerical methods for the calculation of temperatures in wheel/rail contact. Wear 2002;253:498–508.
[47] Baek KS, Kyogoku K, Nakahara T. An experimental study of transient traction characteristics between rail and wheel under low slip and low speed conditions. Wear 2008;265:1417–24.
[48] Ertz M, Bucher F. Improved creep force model for wheel/rail contact considering roughness and temperature. Veh Syst Dyn 2002;37:314–25.
[49] Morgado PL, Otero JE, Lejarraga JBSP, Sanz JLM, Lantada AD, Munoz-Guijosa JM, et al. Models for predicting friction coefficient and parameters with influence in elastohydrodynamic lubrication. Proc IME J J Eng Tribol 2009;223:949–58.

Engineering Science and Technology, an International Journal 35 (2022) 101100

HOSTED BY

ELSEVIER

Contents lists available at ScienceDirect

Engineering Science and Technology, an International Journal

journal homepage: www.elsevier.com/locate/jestch

The effect of top of rail lubricant composition on adhesion and rheological behaviour

Daniel Kvarda [a,*], Simon Skurka [a], Radovan Galas [a], Milan Omasta [a], Lu-bing Shi [b,c], Haohao Ding [b], Wen-jian Wang [b], Ivan Krupka [a], Martin Hartl [a]

[a] Faculty of Mechanical Engineering, Brno University of Technology, Technicka 2896/2, 616 69 Brno, Czech Republic
[b] Tribology Research Institute, State Key Laboratory of Traction Power, Southwest Jiaotong University, Chengdu 610031, China
[c] Zhengzhou Research Institute of Mechanical Engineering Co., Ltd., Zhengzhou 450001, China

ARTICLE INFO

Article history:
Received 5 August 2021
Revised 4 January 2022
Accepted 23 January 2022
Available online 7 February 2022

Keywords:
Coefficient of adhesion
Top of rail lubrication
Wheel-rail tribology
Rheology
Numerical model

ABSTRACT

The effect of top of rail lubricant composition on adhesion has been investigated using a laboratory ball-on-disc tribometer. Rheological properties were analysed using viscosimeter and high pressure torsion device. As a base medium, a biodegradable ester oil with bentonite thickener was selected. Added particles for friction modification were aluminium oxide, zinc oxide, copper sulfide and solid lubricants molybdenum disulfide and graphite. The effect of these components in the base medium on adhesion was evaluated. It was found that the most dominant component was the solid particles for friction modification. Based on the results, top of rail lubricant substances were prepared and tested. The best performing substances provided the optimal level of adhesion. These substances also showed resilience to overdosing, which caused commercial products to provide very low adhesion conditions. The rheological investigation confirmed the very low adhesion is controlled by elastohydrodynamic regime while the stable values are a result of transition to boundary lubrication.
© 2022 Karabuk University. Publishing services by Elsevier B.V. This is an open access article under the CC BY license (http://creativecommons.org/licenses/by/4.0/).

1. Introduction

Railway transportation runs into high demands in terms of energy efficiency, safety and reliability. A key role in train operation is played by the contact between wheel and rail where traction and braking forces are transferred. In recent decades, the application of top of rail (TOR) products to manage wheel-rail friction was thoroughly studied and employed by many train operators all over the world.

The TOR products can be divided into three main categories: oil-based (TOR lubricants), water-based (friction modifiers) and solid stick. Their use and positive effects have been reported by several laboratory and field studies. The main idea is to reduce the coefficient of friction to an intermediate level (around 0.3) and provide a positive slope of frictional characteristic [1]. One of the main resulting benefits is the reduction of wear [2,3] as well as head checks [4] which can be completely eliminated. Field studies also demonstrated the benefits in reducing short pitch corrugation [5–7] and suppressing its evolution. If the application of TOR product is stopped, the corrugation starts to grow [6]. In city transportation systems, the impact of friction modification goes beyond the vehicle and track itself when noise emission in urban areas is an unpleasant problem. Stick-slip phenomena causing a noise generation can be minimized [8–10] by the positive slope of friction curve provided by TOR products. This has been supported by numerical works [11,12]. Other typical benefits can be achieved with respect to reducing lateral forces [13,14] and rolling contact fatigue [4]. However, TOR lubricant studies [1,2,15] suggest that it is important to correctly set the applied quantity. Overdosing the contact can lead to very low adhesion. This can also happen for friction modifiers [3] when the water base does not dry out. When these low adhesion conditions occur, the braking performance of the train can be significantly reduced [9]. The overdosing effect is more dominant for TOR lubricants [1], where lower values of coefficient of friction can arise.

Study of commercial TOR lubricants [2] showed that different products can lead to varying frictional behaviour after application. Also, under fully flooded conditions the coefficient of adhesion dropped as low as 0.02 for one of the tested products. However, because the products are commercial with no detailed specification, it is not easy to draw conclusions about the influence of the composition. In experiments with wheel-rail products [16], the

* Corresponding author.
E-mail address: Daniel.Kvarda@vut.cz (D. Kvarda).
Peer review under responsibility of Karabuk University.

https://doi.org/10.1016/j.jestch.2022.101100
2215-0986/© 2022 Karabuk University. Publishing services by Elsevier B.V.
This is an open access article under the CC BY license (http://creativecommons.org/licenses/by/4.0/).

Nomenclature

CoA	Coefficient of adhesion (-)
D	Ellipticity parameter (-)
F_N	Normal force (N)
F_T	Frictional force (N)
G	Dimensionless materials parameter (-)
h_c	Central film thickness (m)
p	Contact pressure (Pa)
r	Rolling radius (m)
r_{ball}	Radius of ball specimen (m)
r_{disc}	Radius of disc specimen (m)
SRR	Slide to roll ratio (-)
U	Dimensionless speed parameter (-)
W	Dimensionless load parameter (-)
z	Roelands pressure-viscosity coefficient (Pa-1)
α	Barrus pressure-viscosity coefficient (Pa-1)
η	Viscosity at operating conditions (Pa•s)
η_0	Viscosity at room temperature and ambient pressure (Pa•s)
ω_{ball}	Rotational velocity of ball specimen (rad•s)
ω_{disc}	Rotational velocity of disc specimen (rad•s)

TOR lubricant performed similarly to grease and gauge face lubricant and did not provide adhesion levels required for friction management as suggested by study [1]. As in the previous study, the composition of tested TOR lubricant is not known. Other frictional studies [9,15,17,18] suggest that TOR lubricants can achieve very low levels of coefficient of adhesion, especially after initial application or overapplication. The solution to prevent these low levels of adhesion is to optimize the application process either by changing the amount applied or by improving the application process. Because only commercial products are used, studies do not focus on the effect of the TOR composition and its possible influence on overdosing the contact. Study [3] showed that using not only different solid lubricant, but also hard particles for friction modification, can improve the performance of friction modifier and prevent low adhesion conditions. However, this study is focused on friction modifiers, which are water-based substances. TOR lubricants work differently as described in [1], which means that a study on the composition of these oil-based substances can provide new information and possible ways to suppress the effect of overapplication. Due to the complexity of the problem and its use in railway systems, modelling approaches have been employed in many fields such as contact mechanics, dynamics and wear simulations.

Modelling wheel-rail contact is an important approach to demonstrate or prove a tool and concept without additional costs of experiments and field testing. Significant contributions to exact and simplified models have been made by Kalker and can be found in his book [19]. Studies mainly build upon the simplified algorithm FASTIM. To accurately represent the experimental results for dry and contaminated contact calculation, the changes in traction curve, such as lower initial slope and decreasing coefficient of adhesion at high slips, had to be implemented. This has been done by introducing velocity/slip dependent frictional characteristics by different authors [20–24]. This was applied to contact contaminated with oil and leaves as well as friction enhancers [21]. With this approach, the authors worked backwards to identify the model parameter based on the twin-disc experimental data. This method does not use or provide information on the rheological properties of interfacial layer. Rheological elasto-plastic material characteristics measured by high pressure torsion [25] implemented in FASTSIM calculation model were demonstrated in dry, wet and sanded conditions. These models using FASTSIM algorithm do not account for elastohydrodynamic (EHL) effects where surface separation can cause a decrease in coefficient of friction, as was demonstrated in water-contaminated contact [26,27] with a constant coefficient of friction.

Previous studies point to the right direction where the rheological properties of the interfacial layer can be used to improve wheel-rail contact models. Considering TOR lubricants, the pure boundary model is not satisfiable as the EHL regime can be present with oil based substances as suggested by study [2]. Additionally, the effect of frictional heating can be considered [28] to account for decrease in coefficient of adhesion at higher slips. However, a direct comparison between the rheological properties used for modelling and frictional response was not thoroughly investigated. Despite several improvements in the model predictions, an approach for both boundary and EHL friction of TOR lubricant has not been studied yet. To achieve this, the interfacial layer needs to be characterized by rheological properties for both the boundary and the EHL friction. In the boundary regime, the shear stresses arise from surface displacements while the EHL regime responds to the rate of displacement.

The studies mentioned above are primarily focused on the use of commercial products. However, the composition of these products is crucial in terms of the desired behaviour after application. Commercial products do not list specific components, and thus it is not easy to assess the effect of different materials used. A study looking into water-based friction modifiers was already published [3]. However, a deeper analysis of TOR lubricant composition is still an unexplored area. Especially because of the sensitivity to application [1], which could be suppressed by changing the substance composition. This article aims to investigate the role of different components in TOR lubricant on adhesion behaviour. Selected compositions are then compared with commercial products. The boundary and EHL frictional properties are then compared with a numerical model to assess the lubrication regime and validate the model for complex TOR substances.

2. Materials and Methods

2.1. Adhesion tests

In this study, a ball-on-disc tribometer Mini Traction Machine (MTM) from PCS Instruments was used for coefficient of adhesion evaluation. Scheme of the apparatus can be seen in Fig. 1. The normal force is measured by force transducer attached to the ball loading system. The frictional force is calculated from the measured torque by transducer attached to the disc shaft. Data acquisition software is provided by the device manufacturer. All sensor data are acquired with a sampling frequency of 1 Hz. However, this 1 Hz signal is a result of averaging a higher frequency input signal that the manufacturer does not specify. The measurement system uses a feedback loop to actively control the driving parameters. Ball and disc of diameters 19.05 mm and 46 mm respectively are loaded against each other and driven by individual servomotors, thus SRR (slide-to-roll ratio) can be controlled and determined by the following equation:

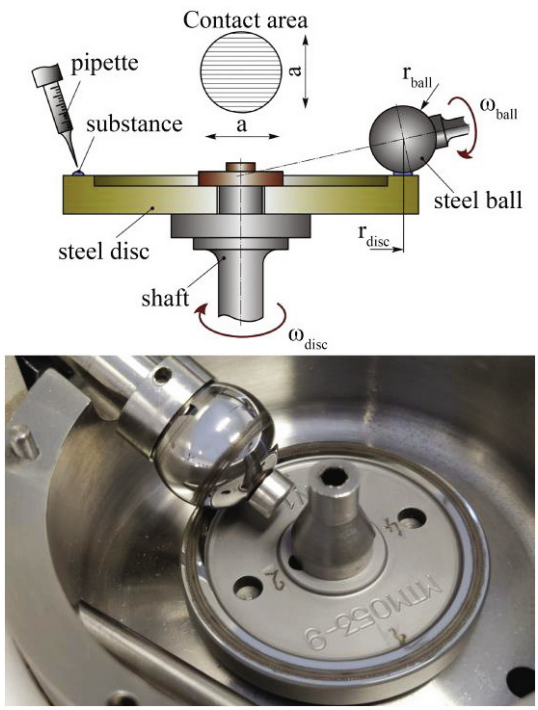

Fig. 1. Scheme of MTM apparatus [3] with picture after experiment.

$$SRR = \frac{\omega_{ball} * r_{ball} - \omega_{disc} * r_{disc}}{\omega_{ball} * r_{ball} + \omega_{disc} * r_{disc}} * 200\% \quad (1)$$

Where ω_{ball} and ω_{disc} are angular velocities of ball and disc respectively, and r_{ball} and r_{disc} stands for specimen's radii. The normal force F_N and the friction force F_T are measured simultaneously and the coefficient of adhesion (CoA) is evaluated using the following formula:

$$CoA = \frac{F_T}{F_N} \quad (2)$$

The material of both specimens is AISI 52,100 bearing steel with Vickers macro-hardness of 800–920 HV (ball) and 720–780 HV (disc). Hardened bearing steel is not a typical rail material [29], and it was used to reduce excessive wear losses and changes in surface topography during the adhesion test. This ensures similar contact conditions for all tests, which is desirable for quantitative comparison of the tested substances and suppressing the effect of surface wear debris. A similar approach has been already used in studies [2,3,9,30].

The parameters for the tests were as follows: normal force of 18 N (≈800 MPa maximum Hertzian contact pressure), mean rolling speed of 1000 mm/s and 2 % SRR. The parameters for normal load were selected to represent the contact pressure of a light-rail tram system. The rolling speed was set based on analysis of a lambda lubrication parameter. The study [31] compares the lambda parameter of MTM conditions with a commuter train where the mean rolling speed 1 m/s of MTM corresponds to approximately 60 km/h for the train. The mean speed of MTM also has a limitation due to displacement of the applied composition by centrifugal force, which had to be taken into account. The SRR was set to represent realistic conditions of wheel and rail contact. Higher values would also promote wear that changes surface conditions during the experiment.

The duration of each experiment was 20 min to provide enough time for the compositions to exceed the optimal levels of adhesion or show an overlubricating effect. Longer test times could also cause excessive wear of the contacting surfaces, resulting in a change of experimental conditions. There was also an initial run-in phase before each experiment with a duration of 10 min, after which the roughness of both specimens was measured. The purpose of the run-in phase was to stabilize the roughness of the surface in 0.1–0.3 μm interval, so similar surface conditions and thus the lubrication regime could be maintained before each experiment. Both specimens were cleaned in acetone before each test.

The amount of lubricant applied for the adhesion test was 4 μl. The solid particles in dry contact were applied by mixing with ethanol and drying out before the start of the experiment. The applied amount was 0.5 ml with particles representing 1/7 of the total weight. The results are reported in the form of a time chart of coefficient of adhesion or as a bar chart showing the mean value of coefficient of adhesion calculated as an average from the last 100 s of the experiment. For data interpretation, the optimal value of coefficient of adhesion is considered 0.15 – 0.25. This value is based on the lower SRR of 2 % and the lower measured coefficient of adhesion in dry conditions than suggested by study [1].

2.2. Rheological tests

To obtain information about the lubrication regime, a set of rheological tests were conducted. These tests were designed to identify the boundary and EHL properties of the tested substances. The measured parameters are used as input to the prediction model. The viscosity and pressure-viscosity coefficient of the base oil were measured using a custom-made high pressure viscosimeter. This viscosimeter allows to measure pressures up to 0.3 GPa. It is built on the principle of a falling cylinder element where the position of the falling element is measured by a linear variable differential transformer sensor. Based on the velocity of the falling element, the viscosity is calculated. For viscosity measurements, the oil separated from the base medium was used. Viscosity was measured at 50 MPa steps up to 300 MPa at an ambient temperature of 25 °C.

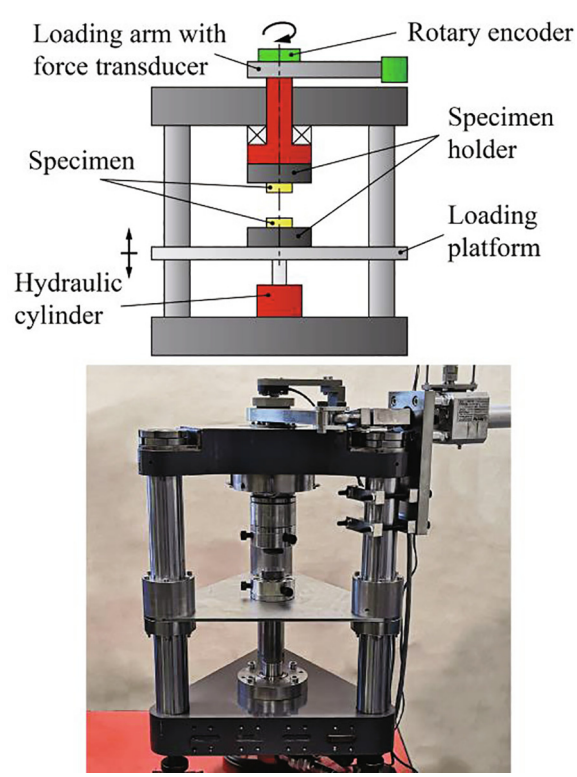

Fig. 2. High pressure torsion rig.

The boundary layer parameters were measured by a high pressure torsion (HPT) apparatus as seen in Fig. 2. The HPT apparatus provides information about the relationship between surface displacements and coefficient of friction. This is used in the boundary regime calculation to estimate the shear stresses by multiplying the local normal stress and the coefficient of friction for local surface displacement, as measured by HPT.

This HPT device consists of a hydraulic cylinder that loads the lower specimen against the upper specimen by a set normal force. The maximum normal loading force capability is 100 kN. The normal force is measured using a pressure gauge. The torque is applied by a loading arm with a worm jack driven by a stepper motor. Between the loading arm and the worm jack, there is a 2 kN force transducer that is used for calculation of the applied torque. The transducer has a sensitivity error of 0.25%. The maximum allowable torque is limited by the nominal rated force of the transducer to 400 Nm. The coefficient of friction is calculated as the measured torque divided by the loading force and the effective radius of contact area. The rotational displacement of the upper specimen is measured by a rotary encoder. The displacement resolution at the effective radius of the specimen is 20 nm. The acquisition of data from all sensors was done by a measurement card with sampling frequency of 100 Hz.

All HPT tests were carried out at 750 MPa normal pressure and displacement speed 1 μm/s. The specimens were made from DIN 100CrMn6 which is similar to the specimen used in MTM tests. The contact surface is an annulus with an inner radius of 3 mm and an outer radius of 6 mm. These contact dimensions result in an effective radius of 4.66 mm. Each substance was applied to the contact surface by a micropipette. The amount applied was 8 μl to ensure that the entire contact surface was covered. To simulate a small amount of slip distance, as in the ball-on-disc tribometer, a preliminary run-in was done. This consisted of a shear displacement of 60 mm at a pressure of 500 MPa. After this phase, the pressure was increased to 750 MPa for the main test. The maximum shear displacement was set to 0.1 mm where all tested substances reached saturation in coefficient of friction.

2.3. Tested components and substances

The focus of this study is on oil-based TOR lubricants. They dominantly consist of oil-based medium, friction modifier particles and solid lubricants. No other additives were used in this study. A grease based on synthetic ester oil with bentonite thickener was used as a base medium. Alumina particles of two different sizes, zinc oxide and copper sulfide were used as friction modifier particles. Graphite and molybdenum disulfide were used as solid lubricant. For more details, see Table 1. All components were weighted using an analytical laboratory balance and then mixed by a shaft mixer for two hours before each test to ensure homogeneity of the composition.

For comparison, two commercial oil-based TOR lubricants were selected. These lubricants are referred to as TOR A and TOR B. Both are biodegradable high pressure resistance lubricants that are water repulsive. The main benefits of using these lubricants are reducing wear and elimination of squeal noise in curves.

Table 1
Components for TOR lubricant.

Category	Name	Particle size (μm)	Mohs hardness (–)
Oil-base medium	Synthetic ester with bentonite thickener	–	–
Friction modifier particles	Aluminium oxide	10, 44 (D99)	9
	Zinc oxide	5 (D99)	4.5
	Copper(I) sulfide	≈5	2.5
Solid lubricants	Graphite	7 (D90)	1–2
	Molybdenum disulfide	4.2 (D50)	1–1.5

2.4. Numerical model

The motivation for the use of a numerical model is to validate a tool to predict the adhesion behaviour of TOR lubricants. Such a tool is helpful when assessing a variety of running conditions without the need for excessive experimental effort. The numerical results can be further built upon with the use of dynamic simulations focusing on vehicle-track interaction. Another utilization is to predict the consumption of the applied product and its redistribution by assessing the time for reapplication and the amount of lubricant needed. The idea behind the model is to use the rheological properties of the interfacial layer. This provides a clear and direct algorithm without any ambiguous parameters. Another motivation is to understand the functioning of TOR lubricants. These substances are more complex than TOR FMs due to the contribution of the EHL lubrication regime.

The frictional model, which is closely described in [32], is composed of two main calculation algorithms: boundary friction and EHL friction. The mixed lubrication regime using the asperity contact model is not used due to the starvation effect and complicated interaction with solid particles in contact. This is due to the oil-base content being slowly consumed by the contact resulting in an increase of coefficient of adhesion due to starvation which promotes the boundary lubrication effect. As such, the prediction would need to include a time-dependent starvation model in combination with mixed lubrication to accurately estimate the transition between EHL and the boundary regime during the rolling-sliding test. This is a complex problem that is considered for future work and development of the model.

The boundary friction model is based on Kalker's FASTIM [33] routine to calculate surface displacements. Based on the calculated displacements and elasto-plastic shear behaviour from HPT tests, the coefficient of friction in the boundary lubrication regime is determined. The model is used to provide information on the frictional properties of the TOR lubricant in different regimes. Validation of the model with experimental data can help with future transfer of the results to real wheel-rail contact. Its use can bring benefits to dynamic models, wear estimation and design of TOR products.

The inputs are geometry, material properties, loading, kinematics and rheological properties. The contact area is divided into a discrete grid, where at each point the calculation is realized. The EHL calculation uses viscosity and pressure-viscosity coefficient together with analytically determined film thickness to calculate the EHL shear stress. The boundary calculation uses the FASTSIM algorithm to determine surface displacements. Based on the calculated surface displacements and friction-displacement relationship from HPT test the boundary shear stresses in contact area can be determined. Using the calculated shear stress and normal stress from Hertz theory, the coefficient of adhesion is determined as a ratio between shear and normal stress for both the boundary and the EHL regime.

The shear stresses generated by the EHL film are the result of lubricant viscosity and shear rate. The change in viscosity with pressure is described by Barus [34] and Roelands [35] equations as described by Eq. (3) and Eq. (4). Eq. (3) is used to determine the pressure-viscosity coefficient α that is important in determining the surface separation. The Eq. (4) is more precise for high pressures and is used in the main calculation of shear stress by Newton's law of viscosity. This means that no changes in viscosity with shear rate is considered.

$$\eta = \eta_0 e^{\alpha p} \tag{3}$$

$$\eta = \eta_0 e^{[ln\eta_0 + 9.67]\left\{\left(1+5.1\cdot 10^{-9}p\right)^z - 1\right\}} \tag{4}$$

The model is altered to be suitable for piezo-viscous liquids where the central film thickness is calculated by Eq. (5). Parameters G, W and U represent the nondimensional material, load and speed respectively. Parameter D is equal to 1 for circular contacts and r is equal to the rolling radius for the ball-on-disc apparatus.

$$h_c = 2.69U^{0.67}G^{0.53}W^{-0.067}(1 - 0.61e^{-0.73D})r \tag{5}$$

3. Results and discussion

3.1. Adhesion tests

The first set of experimental results in Fig. 3 show the adhesion behaviour of separate components in dry conditions and mixed in base medium. The particles in the base medium were represented by 10 wt% for graphite and MoS_2, 30 wt% for Cu_2S and 15 wt% for oxides. The coefficient of adhesion for dry contact at run-in phase was measured 0.39. We can clearly see that the particles of alumina and zinc oxide are very close to dry contact. Solid lubricant MoS_2 and graphite can achieve a coefficient of adhesion equal to or lower than 0.1. The particles of Cu_2S achieved a coefficient of adhesion 0.24 which is closer to dry conditions. The results of zinc oxide are in line with a previous study [3]. Similarly, the fact that larger particles provide a slightly lower coefficient of adhesion and larger deviations correspond with study [36]. With larger particles, we can expect higher resulting surface roughness and abrasive wear as a result of a more significant crushing process [37].

When mixed with the oil-base medium, only the aluminium oxides can provide an increased coefficient of adhesion. The increase is greater compared to the study [38], which might be due to the different particle size. Similarly, a lower coefficient of adhesion for zinc oxide compared to aluminium oxide under wet conditions was found in study [39]. Compared to the coefficient of adhesion of the base medium in Fig. 4, the particles of ZnO and Cu_2S provided some increases in adhesion, but the increments are not significant enough to be considered for optimal level of adhesion between 0.15 and 0.25. These results show that for the particle sizes used, only aluminium oxide is a suitable material for friction modification particles.

The effect of the weight content of the alumina particles is shown in Fig. 4. There is an increasing trend with higher amounts of particles. Only a slight inconsistency is shown for 15 wt% of

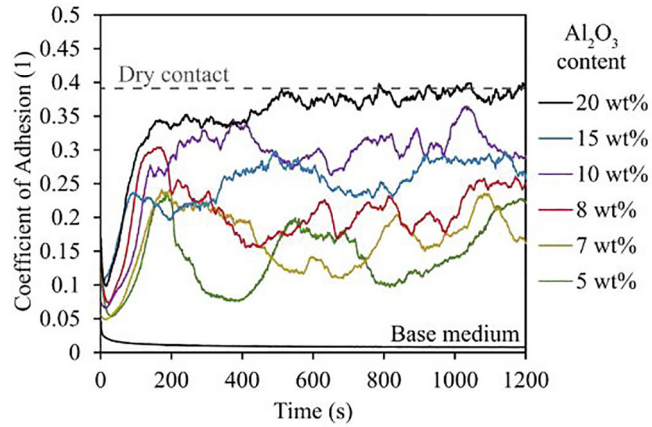

Fig. 4. Effect of aluminium oxide (10 μm) content in oil-base medium.

Al_2O_3, which could be caused by the particles not entering the contact sufficiently. This is indicated by the initial increase being similar to 20 wt% but suddenly deviating around coefficient of adhesion 0.23. This fact means that the initial crushing and stabilization process plays an important role for the substance of base oil and particles for friction modification. Above 20 wt%, the results indicate close to dry levels of adhesion. For all tested contents, the time tests show significant time variability, especially at lower Al_2O_3 contents. This suggests a complex interaction between the particles and the base surface. The saturation point of 20 wt% can be correlated to a similar study [36], where increasing the feed rate of alumina particles increased the coefficient of adhesion until a plateau is reached. Similar results are achieved with sand particles in water [37]. The coefficient of adhesion inconsistency with time might be result of the high ball and disc hardness. When a real wheel/rail specimen and continuous application are used [37,38], much smoother results are acquired.

To further increase the complexity of the substance, a solid lubricant was added in the form of molybdenum disulfide and graphite particles. The base composition consists of the base medium and 10 wt% of Al_2O_3 (10 μm). The results of these compositions are shown in Fig. 5. Increasing the amount of solid lubricant in the composition does not result in a steep coefficient of adhesion reduction. However, one would expect a much larger adhesion drop, as suggested by the use of a solid lubricant without Al_2O_3 in Fig. 3. Both lubricants are able to reduce the coefficient of adhesion to values between 0.2 and 0.3 with the presence of Al_2O_3. Substances with 5, 10 and 30 wt% of MoS_2 give an average coefficient

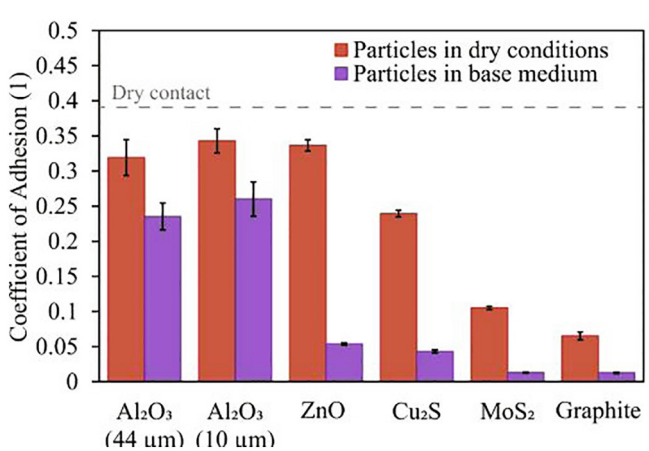

Fig. 3. Solid particles in dry conditions and mixed with oil-base medium.

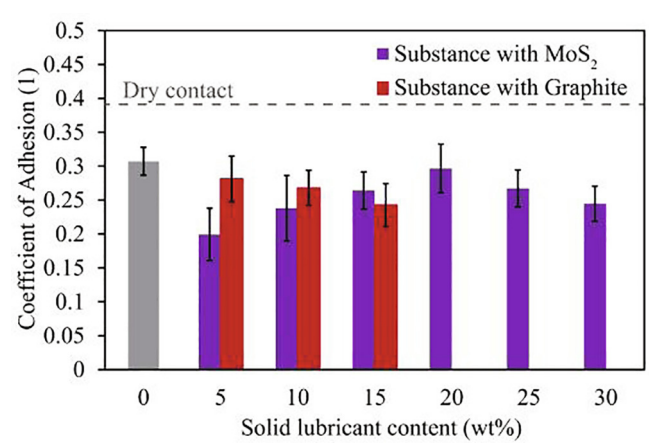

Fig. 5. Effect of solid lubricant in oil-base with 10 wt% Al_2O_3 (10 μm).

of adhesion below 0.25. The same applies for the substance with 15 wt% graphite.

The main finding is that a higher solid lubricant content creates a paste-like substance. At such a state, it is not feasible to add more particles while maintaining a homogeneous mixture. This was achieved at 20 wt% of graphite and 35 wt% of MoS_2. This thick state of the composition is also not suitable, as it creates difficulties with application and promotes starvation of the contact. Similar paste-like forming and related problems with application were found in studies [3,40].

These results suggest that the increased content of MoS_2 and graphite does not help reduce the coefficient of adhesion. The key to achieving intermediate adhesion seems to be mainly in using the correct amount of friction modification particles. The total amount of solid particles can be altered to result in a suitable viscosity of the substance with respect to the application and adherence to the surface.

Based on these results, several substances were prepared and tested to assess the adhesion performance. The two main evaluated parameters were the time after application where very low adhesion conditions occur (<0.1) and the effective time between the optimal coefficient of adhesion of 0.15 – 0.25. Some of the substances show good performance in terms of optimal adhesion but with a substantial and prolonged drop in adhesion after application. Only three of the best performing substances are further compared. The composition of the selected substances is described in Table 2.

Adhesion tests for the selected compositions are shown in Fig. 6. The lower and upper bound of the optimal level of adhesion is represented by dashed lines. It is evident that the application can be divided into two areas: (I) drop after application with a steep slope of the coefficient of adhesion, (II) effective part of the adhesion curve with a slow gradual increase in the coefficient of adhesion. This initial drop and then a slow increase in the coefficient of adhesion can also be found in previous studies [2,3,9,41]. It is beneficial to shorten the length or even eliminate these initial low adhesion conditions to prevent their negative impact, such as increased braking distance [9]. The substance N, which is characterized by a lower amount of particle portion, overshoots the initial increase in coefficient of adhesion. This was observed in a similar fashion with all repeated tests of substance N, but not by the other two substances. However, all three substances exhibit very similar behaviour in the initial drop of adhesion and its time length. Around 400 s, all three substances followed a similar trend, and around 1000 s the upper limit of optimal adhesion is reached.

The selected compositions were also tested with different applied amounts together with commercial TOR lubricants for comparison. The applied amounts were 2, 4 and 6 μl based on previous experiments with TOR lubricants. The results are shown in Fig. 7. It is evident that an increased amount of TOR lubricant applied extends the effective time of the substance. For the 2 μl applied, all compositions exhibited a similar behaviour. After application, a coefficient of adhesion below 0.1 is reached and then increases towards dry conditions. The commercial substance TOR A has the longest part of optimal adhesion at this applied amount. However, increasing the amount to 4 μl causes TOR A to overlubricate the contact. Throughout the 800 s measured, the coefficient of

Table 2
Composition of selected substances.

Name	Friction modification particles	Solid lubricant
N	3 wt% Al_2O_3 (10 μm)	7 wt% Cu_2S 1 wt% MoS_2
AO	10 wt% Al_2O_3 (10 μm)	30 wt% MoS_2
AZ	10 wt% Al_2O_3 (10 μm)	15 wt% Graphite

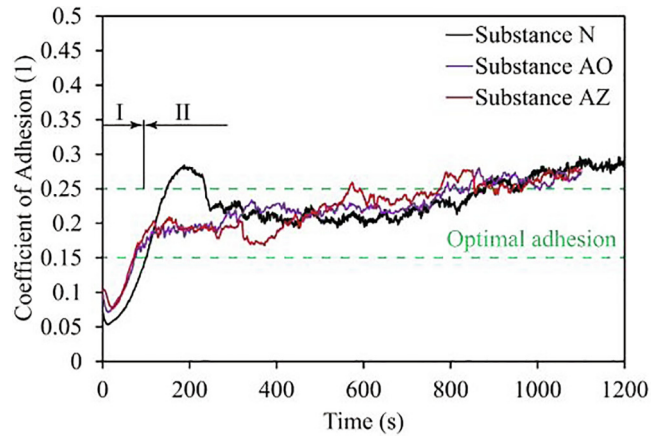

Fig. 6. Effect of aluminium oxide (10 μm) content in oil-base medium.

adhesion is constantly between 0.05 and 0.1, which could be unacceptable for railway application. The other commercial product TOR B performs well at 4 μl with short duration below the coefficient of adhesion of 0.1. The duration before reaching the upper limit of optimal adhesion is around 300 s. The prepared substances provide a longer lasting effect. Substance N exceeds the optimal level after the initial rising of coefficient of adhesion. The other two substances, AO and AZ, provide around 600 s long-lasting effect and the initial drop of adhesion after application is the shortest of all tested substances. Especially the substance AZ shows a desirable trend of slowly increasing adhesion. For 6 μl applied, both commercial TOR lubricants overlubricate the contact. Substance N seems to be very unstable even though it satisfies the optimal adhesion. Substances AO and AZ provide very good behaviour for TOR lubricant.

Comparing with commercial TOR products, the overdosing effect was not observed with the prepared substances. Based on the adhesion curves, we can assume that commercial products use different types and amounts of friction modifier particles. The measured curves for commercial TOR lubricants are very smooth with minimal instability. Nevertheless, this might be the reason why very low adhesion conditions were measured with a higher applied amount of TOR lubricant. Based on the SEM photographs of commercial products [2], we can assume that they are composed of smaller and more flake-like metal particles. These particles may be less prone to being crushed or cause abrasion that would transfer forces compared to rounder Al_2O_3 particles in the prepared substances. This high sensitivity to the applied quantity was also observed for commercial TOR products in other studies [2,9,15]. It should be noted that this high sensitivity might be a result of the used scaled tribometer. For real wheel-rail, contact a less sensitive behaviour might be expected.

3.2. Rheological properties

Based on available information, both commercial TOR lubricants use ester oil as a base medium with thickener. Because of this, the results for viscosity measurements are used for all tested products with similar base oil. The measured viscosity of the base oil at ambient conditions was η_0 = 0.09 Pa•s. Based on the model fit to the viscosity measurements at higher pressures we get α = 13.5 GPa^{-1} and z = 0.468. The calculated film thickness (Eq. (5)) for experimental conditions is 360 nm. This value is slightly above the range of surface roughness 0.1 – 0.3 μm which the adhesion tests were conducted in. Accounting for the effect of hard particles in the contact, we can assume that the lubrication is in the range of mixed to boundary regime. The resulting EHL coefficient of adhe-

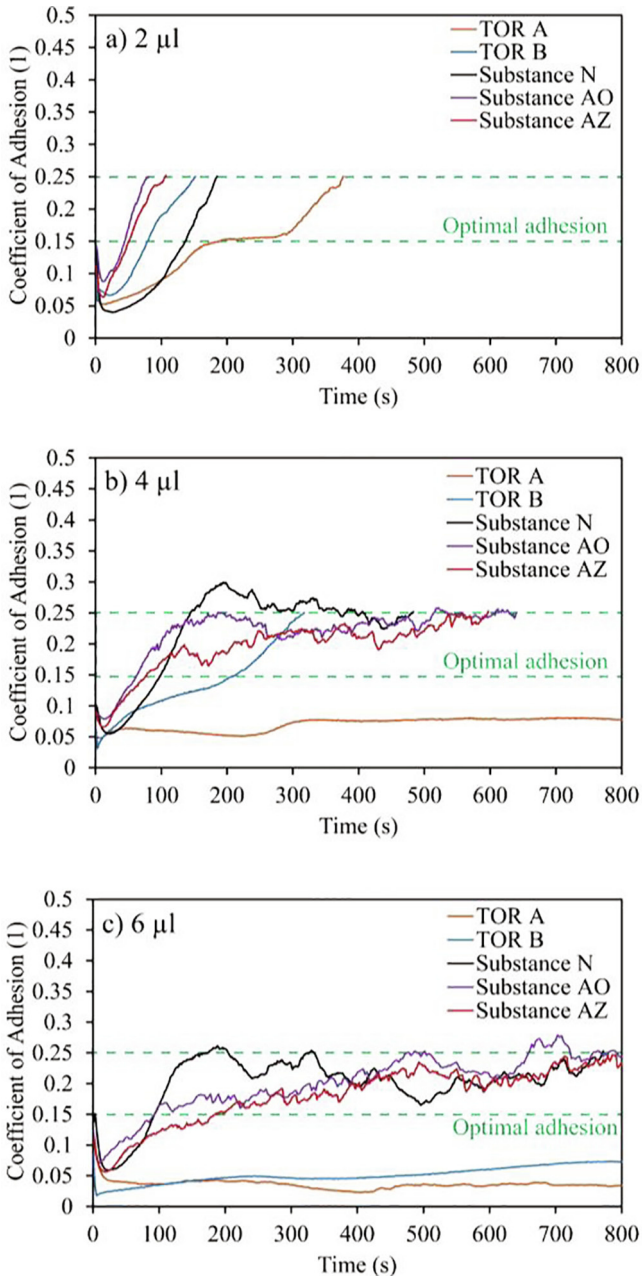

Fig. 7. Adhesion tests with different applied amounts.

sion predicted by the model for base oil and the parameters used in the adhesion tests is 0.027. If we consider a temperature influence and shear-thinning properties on lubricant, this value could be even lower as suggested by study [42].

The boundary friction properties of the tested substances are shown in Fig. 8. The TOR A substance showed the lowest coefficient of friction after reaching plastic deformation shearing. The initial elastic region represents a situation where the surfaces with the applied substance between asperities are in locked state with no macroscopic slip with an increase of shear load. After the shear stress exceeds the ability of the surfaces and interfacial substance to carry the shearing load, a relative movement between surfaces occurs resulting in a plastic deformation. Surprisingly, all three prepared substances have a similar trend in the initial elastic and plastic parts of the curve. The maximum coefficient of friction occurs at the displacement distance 0.01 mm. After reaching the

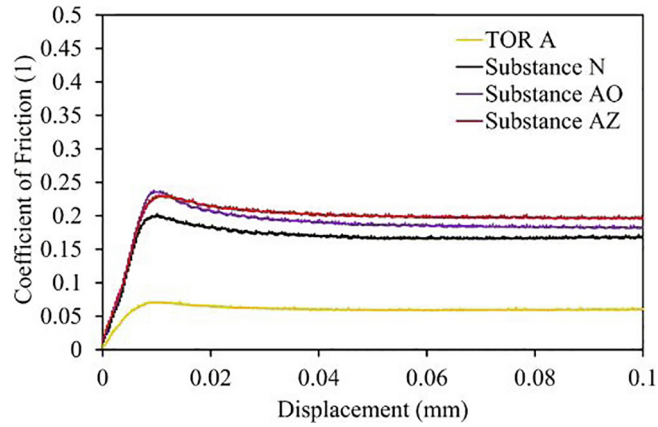

Fig. 8. High pressure torsion tests of selected substances.

maximum, it slightly falls and reaches stable values around 0.2 for all three substances. The values for the commercial TOR product correspond to previous measurements by HPT rig with a larger contact surface [43]. The initial elastic part shows a slightly uneven increasing trend with a lower slope compared to the results in [43].

3.3. Numerical model results

The results were parametrized based on the hardening model as suggested by [32]. This hardening model describes the pseudo-elasto-plastic behaviour seen in the HPT experiments using four parameters. This parametric model smoothly fits any data and provides a faster calculation time. Using these results as input to the boundary calculation predicted a too low coefficient of adhesion around 0.03 for the substance AZ. This is a result of the calculation predicting too low displacements in the ideal small point contact area in combination with the measured elastic part having an uneven slope. For the ideal contact geometry, the maximum calculated contact displacement is 4 µm while the average is about 1.7 µm. In reality, wear of the contact surfaces would change the true contact area and geometry of the specimen, resulting in different contact conditions and increase in surface displacements. The fact that the FASTIM algorithm was mainly used for larger contacts also introduces an error to the calculation. Using the results of HPT device for this boundary model is not reliable for such a small point contact compared to the HPT contact area and would need further investigation. Based on the previous MTM results of commercial TOR products [2], we can see that under the experimental conditions of the adhesion tests the boundary layer displacement is close to the frictional peak (as seen in Fig. 8). Based on this, the value for coefficient of adhesion is taken from the end of the elastic part of the measured curve.

The results of the model are coefficient of adhesion values for the EHL regime of the base oil and coefficient of adhesion values for the boundary regime of the selected complete substances. The substance AZ is used for comparison with the commercial TOR product as it provides the most stable coefficient of adhesion from the three selected substances N, AO and AZ. The experimental results for TOR A and the substance AZ with an applied amount of 6 µl (from Fig. 7c) were selected for comparison with the model that predicts EHL and boundary coefficient of adhesion. This quantity shows a stable behaviour, which is the most representative of the HPT results. As seen in Fig. 9, the coefficient of adhesion of TOR A is between the predicted values of both the boundary and EHL regime. Since the predicted values are close together, it is evident that unless starvation occurs the substance should result in coeffi-

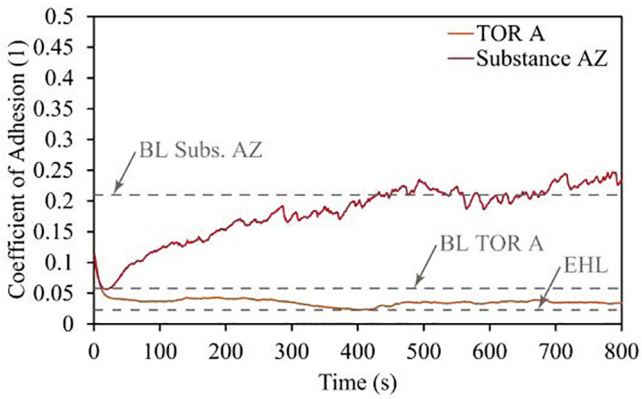

Fig. 9. Comparison of prediction (dashed lines) and experiments with 6 μl.

cient of adhesion between 0.02 and 0.05. This starvation effect was most evident at the applied amount of 2 μl as seen in Fig. 7a. The coefficient of adhesion of the substance AZ initially drops to 0.05, suggesting that the hard particles of Al_2O_3 are not able to interact between the contact surfaces. Assuming the film thickness of 360 nm, the roughness is about 200 nm and the particle size in order of micrometres, it might be the case that only small and fragmented particles are able to enter the contact. This is in contradiction with study [44], but the high hardness of contact surfaces could promote particle fragmentation and prevent the larger particles to be embedded to the surface. The oil starvation causes an increase in coefficient of adhesion and the smooth curve transitions to a rough progression caused by particle interaction. A stable value was reached around the coefficient of adhesion 0.2 and running the test for longer time would cause the particles to be depleted and coefficient of adhesion to increase back to dry conditions. The boundary prediction for substance AZ shows that the saturation occurs at the same values as the HPT results.

The transitioning behaviour of starvation and subsequent rise to dry conditions is hard to predict by the used numerical model due to the complex interaction between particles and contacting surfaces. The surface conditions also play a key role in determining the lubrication regime. Studying the influence of surface parameters and the interaction between solid particles in the contact area is the next step in understanding the TOR substances. Developing a model to explain the starvation behaviour that leads to dry contact conditions would also help with determining the correct application dosages.

4. Conclusions

A laboratory experimental device was used to study the properties and composition of oil-based top of rail lubricants. Adhesion tests were conducted to evaluate the effect of different solid particles in TOR composition.

It was found that the friction modification particles have a dominant effect on the adhesion behaviour in base medium. The hardness of the particles seems to be the key factor in increasing the coefficient of adhesion. Particles of aluminium oxide were the only ones that could increase the coefficient of adhesion above 0.1 in combination with oil-based medium. Zinc oxide and copper sulfide with less than half of the hardness of Al_2O_3 were unable to have a significant effect. The addition of solid lubricant managed to decrease the coefficient of adhesion by 30 % at maximum. Increasing the amount of solid lubricant did not yield any more reduction. Moreover, there is a limit to how much solid lubricant can be homogenously dispersed in the oil-based medium. Increasing the amount also changes the consistency to more paste-like, which can be of importance in the application of the substance.

The tested custom substances showed resilience against overdosing which caused very low adhesion conditions in commercial TOR lubricants. This can prevent problems with traction and braking of a railway vehicle. However, such a behaviour might not be expected in real wheel/rail contact, where the contact geometry differs from the used laboratory device. For further validation, an experimental device with a larger contact area should be used. Moreover, in laboratory experiments the contact always runs on the same path every rotation of the specimen. The high sensitivity to the applied amount of commercial product can also be the result of making the substance cost effective in terms of its consumption. The results suggest that the developed compositions could be suitable for use in the field with added benefits of overdosing resilience and stable frictional behaviour at doses that would cause very low adhesion conditions for a commercial product. However, before application to the field, an investigation on the wear properties should be conducted. Higher doses can cause unwanted surface damage due to hard particles. Especially the initiation of rolling contact fatigue, which could be accelerated by the oil entrapment in cracks causing them to grow. Lastly, compatibility with application units should be confirmed. The particle content could cause abrasion of key parts of the application units. Such a scenario is unsuitable for long term use.

An analysis of the lubrication regime based on the base oil properties and the substance shear behaviour measured by high pressure torsion was carried out. At the maximum application amount of 6 μl, the commercial TOR lubricant behaved in an interval between the predicted boundary and EHL regime. The prepared substance AZ appeared to have more EHL tendency after application. However, after about 400 s the coefficient of adhesion increased to the values predicted by boundary lubrication HPT tests. This suggests a more complex interaction where starvation of the oil promotes more solid particles and asperity interaction. Future studies will focus on the time-dependance of coefficient of adhesion that is caused by the product consumption from starvation of the base oil. The use of HPT results for such small point contacts does not seem to be reliable and a more thorough investigation needs to be carried out. This will involve using both a larger scale rolling-sliding contact and a smaller HPT contact area. This will provide understanding of the transfer of experimental data between various scales of laboratory devices and real wheel and rail contact.

Declaration of Competing Interest

The authors declare that they have no known competing financial interests or personal relationships that could have appeared to influence the work reported in this paper.

Acknowledgments

The work was supported by the project LTACH19001 with financial support from the Ministry of Education, Youth and Sports of the Czech Republic. The authors also thank the support by National Key R&D Program Intergovernmental Key Items for International Scientific and Technological Innovation Cooperation (No.2018YFE0109400) and Sichuan Science and Technology Program (No.2020YFH0057).

References

[1] R. Stock, L. Stanlake, C. Hardwick, M. Yu, D. Eadie, R. Lewis, Material concepts for top of rail friction management – Classification, characterisation and

application, Wear. 366–367 (2016) 225–232, https://doi.org/10.1016/j.wear.2016.05.028.
[2] R. Galas, M. Omasta, I. Krupka, M. Hartl, Laboratory investigation of ability of oil-based friction modifiers to control adhesion at wheel-rail interface, Wear. 368–369 (2016) 230–238, https://doi.org/10.1016/j.wear.2016.09.015.
[3] R. Galas, D. Kvarda, M. Omasta, I. Krupka, M. Hartl, The role of constituents contained in water–based friction modifiers for top–of–rail application, Tribol. Int. 117 (2018) 87–97, https://doi.org/10.1016/j.triboint.2017.08.019.
[4] D.T. Eadie, D. Elvidge, K. Oldknow, R. Stock, P. Pointner, J. Kalousek, P. Klauser, The effects of top of rail friction modifier on wear and rolling contact fatigue: Full-scale rail-wheel test rig evaluation, analysis and modelling, Wear. 265 (9-10) (2008) 1222–1230, https://doi.org/10.1016/j.wear.2008.02.029.
[5] D.T. Eadie, M. Santoro, K. Oldknow, Y. Oka, Field studies of the effect of friction modifiers on short pitch corrugation generation in curves, Wear. 265 (9-10) (2008) 1212–1221, https://doi.org/10.1016/j.wear.2008.02.028.
[6] J.I. Egana, J. Vinolas, N. Gil-Negrete, Effect of liquid high positive friction (HPF) modifier on wheel-rail contact and rail corrugation, Tribol. Int. 38 (8) (2005) 769–774, https://doi.org/10.1016/j.triboint.2004.11.006.
[7] J. Kalousek, K.L. Johnson, An investigation of short pitch wheel and rail corrugations on the Vancouver mass transit system, Proc. Inst. Mech. Eng. Part F J. Rail Rapid Transit. 206 (2) (1992) 127–135, https://doi.org/10.1243/PIME_PROC_1992_206_226_02.
[8] D.T. Eadie, M. Santoro, Top-of-rail friction control for curve noise mitigation and corrugation rate reduction, J. Sound Vib. 293 (3-5) (2006) 747–757, https://doi.org/10.1016/j.jsv.2005.12.007.
[9] R. Galas, M. Omasta, M. Klapka, S. Kaewunruen, I. Krupka, M. Hartl, Case study: The influence of oil-based friction modifier quantity on tram braking distance and noise, Tribol. Ind. 39 (2017) 198–206, https://doi.org/10.24874/ti.2017.39.02.06.
[10] D.T. Eadie, M. Santoro, W. Powell, Local control of noise and vibration with KELTRACK friction modifier and Protector trackside application: An integrated solution, J. Sound Vib. 267 (3) (2003) 761–772, https://doi.org/10.1016/S0022-460X(03)00739-9.
[11] X. Liu, P.A. Meehan, Investigation of squeal noise under positive friction characteristics condition provided by friction modifiers, J. Sound Vib. 371 (2016) 393–405, https://doi.org/10.1016/j.jsv.2016.02.028.
[12] P.A. Meehan, X. Liu, Modelling and mitigation of wheel squeal noise under friction modifiers, J. Sound Vib. 440 (2019) 147–160, https://doi.org/10.1016/j.jsv.2018.10.025.
[13] D.T. Eadie, K.D. Oldknow, L. Maglalang, T. Makowsky, R. Reiff, P. Sroba, W. Powell, Implementation of wayside Top of rail friction control on north american heavy haul freight railways, in: Proc. Seventh World Congr. Rail- W. Res., 2006: pp. 2–11.
[14] A. Matsumoto, Y. Sato, H. Ohno, M. Tomeoka, K. Matsumoto, T. Ogino, M. Tanimoto, Y. Oka, M. Okano, Improvement of bogie curving performance by using friction modifier to rail/wheel interface Verification by full-scale rolling stand test, Wear. 258 (7-8) (2005) 1201–1208, https://doi.org/10.1016/j.wear.2004.03.063.
[15] K. Matsumoto, Y. Suda, T. Iwasa, T. Fujii, M. Tomeoka, M. Tanimoto, Y. Kishimoto, T. Nakai, A Method to Apply Friction Modifier in Railway System, in, JSME Int. J. Ser. C 47 (2) (2004) 482–487, https://doi.org/10.1299/jsmec.47.482.
[16] C. Hardwick, R. Lewis, R. Stock, The effects of friction management materials on rail with pre existing rcf surface damage, Wear. 384–385 (2017) 50–60, https://doi.org/10.1016/j.wear.2017.04.016.
[17] X. Lu, J. Cotter, D.T. Eadie, Laboratory study of the tribological properties of friction modifier thin films for friction control at the wheel/rail interface, Wear. 259 (7-12) (2005) 1262–1269, https://doi.org/10.1016/j.wear.2005.01.018.
[18] M. Tomeoka, N. Kabe, M. Tanimoto, E. Miyauchi, M. Nakata, Friction control between wheel and rail by means of on-board lubrication, Wear. 253 (1-2) (2002) 124–129, https://doi.org/10.1016/S0043-1648(02)00091-1.
[19] J.J. Kalker, Three-Dimensional Elastic Bodies in Rolling Contact, Springer, Netherlands, Dordrecht (1990), https://doi.org/10.1007/978-94-015-7889-9.
[20] J. Piotrowski, Kalker's algorithm Fastsim solves tangential contact problems with slip-dependent friction and friction anisotropy, Veh. Syst. Dyn. 48 (7) (2010) 869–889, https://doi.org/10.1080/00423110903178495.
[21] A. Rovira, A. Roda, R. Lewis, M.B. Marshall, Application of Fastsim with variable coefficient of friction using twin disc experimental measurements, Wear. 274–275 (2012) 109–126, https://doi.org/10.1016/j.wear.2011.08.019.
[22] M. Spiryagin, O. Polach, C. Cole, Creep force modelling for rail traction vehicles based on the Fastsim algorithm, Veh. Syst. Dyn. 51 (11) (2013) 1765–1783, https://doi.org/10.1080/00423114.2013.826370.
[23] J.G. Giménez, A. Alonso, E. Gómez *, Introduction of a friction coefficient dependent on the slip in the FastSim algorithm, Veh. Syst. Dyn. 43 (4) (2005) 233–244, https://doi.org/10.1080/00423110412331282913.
[24] B. Croft, C. Jones, D. Thompson, Velocity-dependent friction in a model of wheel-rail rolling contact and wear, Veh. Syst. Dyn. 49 (11) (2011) 1791–1802, https://doi.org/10.1080/00423114.2010.543138.
[25] K. Six, A. Meierhofer, G. Müller, P. Dietmaier, Physical processes in wheel-rail contact and its implications on vehicle-track interaction, Veh. Syst. Dyn. 53 (5) (2015) 635–650, https://doi.org/10.1080/00423114.2014.983675.
[26] H. Chen, A. Yoshimura, T. Ohyama, Numerical analysis for the influence of water film on adhesion between rail and wheel, Proc. Inst. Mech. Eng. Part J J. Eng. Tribol. 212 (5) (1998) 359–368, https://doi.org/10.1243/1350650981542173.
[27] H. Chen, T. Ban, M. Ishida, T. Nakahara, Adhesion between rail/wheel under water lubricated contact, Wear. 253 (1-2) (2002) 75–81, https://doi.org/10.1016/S0043-1648(02)00085-6.
[28] C. Tomberger, P. Dietmaier, W. Sextro, K. Six, Friction in wheel-rail contact: A model comprising interfacial fluids, surface roughness and temperature, Wear. 271 (1-2) (2011) 2–12, https://doi.org/10.1016/j.wear.2010.10.025.
[29] Y. Hu, L. Zhou, H.H. Ding, R. Lewis, Q.Y. Liu, J. Guo, W.J. Wang, Microstructure evolution of railway pearlitic wheel steels under rolling-sliding contact loading, Tribol. Int. 154 (2021) 106685, https://doi.org/10.1016/j.triboint.2020.106685.
[30] R. Galas, M. Omasta, L.-B. Shi, H. Ding, W.-J. Wang, I. Krupka, M. Hartl, The low adhesion problem: The effect of environmental conditions on adhesion in rolling-sliding contact, Tribol. Int. 151 (2020) 106521, https://doi.org/10.1016/j.triboint.2020.106521.
[31] Y. Zhu, U. Olofsson, K. Persson, Investigation of factors influencing wheel-rail adhesion using a mini-traction machine, Wear. 292–293 (2012) 218–231, https://doi.org/10.1016/j.wear.2012.05.006.
[32] D. Kvarda, R. Galas, M. Omasta, L.-B. Shi, H. Ding, W.-J. Wang, I. Krupka, M. Hartl, Asperity-based model for prediction of traction in water-contaminated wheel-rail contact, Tribol. Int. 157 (2021) 106900, https://doi.org/10.1016/j.triboint.2021.106900.
[33] J.J. Kalker, A Fast Algorithm for the Simplified Theory of Rolling Contact, Veh. Syst. Dyn. Int. J. Veh. Mech. Mobil. 11 (1982) 1–13.
[34] C. Barus, Isothermals, isopiestics and isometrics relative to viscosity, Am. J. Sci. s3-45 (266) (1893) 87–96, https://doi.org/10.2475/ajs.s3-45.266.87.
[35] C. Roelands, Correlational Aspects of the Viscosity-Temperature Pressure Relationship of Lubricating Oils, PhD Thesis. (1966) 495.
[36] X. Cao, W.L. Huang, C.G. He, J.F. Peng, J. Guo, W.J. Wang, Q.Y. Liu, M.H. Zhu, The effect of alumina particle on improving adhesion and wear damage of wheel/rail under wet conditions, Wear. 348–349 (2016) 98–115, https://doi.org/10.1016/j.wear.2015.12.004.
[37] L.B. Shi, C. Wang, H.H. Ding, D. Kvarda, R. Galas, M. Omasta, W.J. Wang, Q.Y. Liu, M. Hartl, Laboratory investigation on the particle-size effects in railway sanding: Comparisons between standard sand and its micro fragments, Tribol. Int. 146 (2020) 106259, https://doi.org/10.1016/j.triboint.2020.106259.
[38] W.J. Wang, T.F. Liu, H.Y. Wang, Q.Y. Liu, M.H. Zhu, X.S. Jin, Influence of friction modifiers on improving adhesion and surface damage of wheel/rail under low adhesion conditions, Tribol. Int. 75 (2014) 16–23, https://doi.org/10.1016/j.triboint.2014.03.008.
[39] C. Wang, L.B. Shi, H.H. Ding, W.J. Wang, R. Galas, J. Guo, Q.Y. Liu, Z.R. Zhou, M. Omasta, Adhesion and damage characteristics of wheel/rail using different mineral particles as adhesion enhancers, Wear. 477 (2021) 203796, https://doi.org/10.1016/j.wear.2021.203796.
[40] B. White, R. Lewis, Simulation and understanding the wet-rail phenomenon using twin disc testing, Tribol. Int. 136 (2019) 475–486, https://doi.org/10.1016/j.triboint.2019.03.067.
[41] Z. Li, O. Arias-Cuevas, R. Lewis, E.A. Gallardo-Hernández, Rolling-Sliding Laboratory Tests of Friction Modifiers in Leaf Contaminated Wheel-Rail Contacts, Tribol. Lett. 33 (2) (2009) 97–109, https://doi.org/10.1007/s11249-008-9393-3.
[42] P.L. Morgado, J.E. Otero, J B Sánchez.-P. Lejarraga, J.L.M. Sanz, A.D. Lantada, J.M. Munoz-Guijosa, H.L. Yustos, P.L. Wiña, J.M. García, Models for predicting friction coefficient and parameters with influence in elastohydrodynamic lubrication, Proc. Inst. Mech. Eng. Part J J. Eng. Tribol. 223 (7) (2009) 949–958, https://doi.org/10.1243/13506501JET599.
[43] M. Evans, W.A. Skipper, L. Buckley-Johnstone, A. Meierhofer, K. Six, R. Lewis, The development of a high pressure torsion test methodology for simulating wheel/rail contacts, Tribol. Int. 156 (2021) 106842, https://doi.org/10.1016/j.triboint.2020.106842.
[44] R.S. Dwyer-Joyce, J. Heymer, The entrainnient of solid particles into rolling elastohydrodynamic contacts, in, Tribol. Ser. (1996) 135–140, https://doi.org/10.1016/s0167-8922(08)70777-6.

Check for updates

Article

Institution of MECHANICAL ENGINEERS
Journal of RAIL AND RAPID TRANSIT

Proc IMechE Part F:
J Rail and Rapid Transit
2022, Vol. 0(0) 1–10
© IMechE 2022
Article reuse guidelines:
sagepub.com/journals-permissions
DOI: 10.1177/09544097221138374
journals.sagepub.com/home/pif
SAGE

Shear properties of top-of-rail products in numerical modelling

Daniel Kvarda[1], Radovan Galas[1], Milan Omasta[1], Martin Hartl[1], Ivan Krupka[1] and Marian Dzimko[2]

Abstract

Top-of-rail product assessment in terms of frictional properties plays a key role in the evaluation of desired benefits for wheel-rail contact. In this study, a high-pressure torsion device is used to study the friction-displacement properties of three types of top-of-rail products. The effects of applied amount and increased temperature were investigated. All tested products were very sensitive to the amount applied. For the water-based substance, the evaporation of water created a solid-like film that provided very low friction. The increase in temperature lowered the coefficient of friction for dry contact but had a negligible effect on the applied products. A FASTSIM-based numerical model is used to demonstrate the application of these results.

Keywords

Adhesion coefficient, top-of-rail product, friction, rail–wheel tribology, adhesion model

Date received: 6 April 2022; accepted: 25 October 2022

Introduction

The tribology of wheel-rail contact has been the main focus of studies for many decades. This is due to the processes in the small contact area that influence the comfort, reliability and safety of railway transport. The friction in the wheel-rail interface is key in managing the safe braking characteristics, wear of surfaces, noise emission and energy consumption. For these reasons, friction management solutions are deployed in rail vehicles and infrastructure. The main idea is to apply top-of-rail product (TOR) to the contact interface. This changes the frictional characteristics to satisfy the aforementioned demands.

The positive effects of these products have been mainly linked to the ability to achieve intermediate levels of coefficient of adhesion. Normally, these values for high slip rate are in the range of 0.3–0.4[1] compared to lubricated conditions (<0.2) and dry conditions (>0.5). However, depending on the experimental device, the frictional values measured can vary[2] for both TOR products and dry conditions. The reduction of coefficient of adhesion to intermediate levels by means of top of rail friction management has been shown in many studies.[2–8] The positive slope of coefficient of adhesion with increasing slip rate suppresses the stick-slip oscillations that initiate the generation of noise[9,10] and corrugation wear.[11,12] Some disadvantages can arise with the incorrect use of these products. Especially for oil-based products, the amount of application is the key to not overlubricate the contact,[1] which can cause low adhesion levels and an increase in braking distance.[13] This is not the case for water-based products, where water is used as a carrying medium and is supposed to evaporate. However, if evaporation does not occur and water is present, low adhesion conditions may occur.[14] Solid stick products for wheel tread have advantages in an easy application system and no liquid base that would be needed to spread the substance across the rail. The friction values for the solid stick are reported[15–17] to be around 0.3.

Previously, to describe the behaviour of rolling-sliding in real conditions a third body layer containing natural and artificial materials was proposed. This layer between contacting surfaces is under pressure and shear stresses that control the frictional characteristics of wheel-rail contact. The layer can be described by its elastoplastic rheological properties.[18] To study contaminants, a rotational rheometer that measures the coefficient of friction as a function of displacement was previously used.[18] In combination with the third body layer model, the results can predict the coefficient of adhesion in the wheel-rail contact. The same type of experimental device was also used[19] to demonstrate different frictional properties of TOR products and the effect of contamination.[20] Recently, a high-pressure torsion (HPT) testing[21,22] was used to study the shear-displacement properties of contact interface in combination with wheel-rail contact modelling. These studies show coefficient of

[1]Faculty of Mechanical Engineering, Brno University of Technology, Brno, Czech Republic
[2]Faculty of Mechanical Engineering, University of Zilina, Zilina, Slovak Republic

Corresponding author:
Daniel Kvarda, Faculty of Mechanical Engineering, Brno University of Technology, Technicka 2896/2, Brno 616 69, Czech Republic.
Email: Daniel.Kvarda@vut.cz

friction for dry conditions around 0.55[22] and even up to 0.8.[21] This suggest that the surface conditions such as removal of oxides by cleaning and the roughness of the specimen can vary the resulting frictional values. Small amount of water caused drop in coefficient of friction down to 0.2.[22] The use of friction modifier in a dry state[21] reduced coefficient of friction below 0.3 and with increasing dosage down to 0.1. An overapplication of friction modifier caused coefficient of friction lower than 0.05. During this overapplication the drying of base medium had negligible effect on the frictional behaviour.

Analytical and numerical tools for the frictional behaviour of rolling-sliding contact help understand and predict the traction forces in contact but are also integral part in vehicle dynamic simulations. Kalker's FASTSIM algorithm[23] has been widely used and built on due to its simplicity and fast calculation times compared to exact solutions such as Kalker[24]'s CONTACT. The original theory assumes ideal bodies, but in reality the adhesion conditions change based on factors such as contamination, wear, surrounding environment and also the application of TOR products.[25] To accommodate for such changes, the implementation of slip-dependent friction has been used.[26–29] This can resolve issues of the original theory, where after reaching saturation point of adhesion there is no change with higher slip. In addition, changes in contact flexibility have been implemented in the initial part of the traction curve.[29] Both these phenomena are the result of elasto-plastic response of material to shearing which was previously also implemented in FASTSIM.[30] The decrease in coefficient of adhesion at higher slips is attributed to the increase in temperature, which can be calculated analytically and numerically.[31] The use of temperature-dependent friction[30] can then be used instead of slip-dependent friction to accurately represent contact conditions.

Although many studies test the performance of these products on different scales and conditions, the comparison of frictional properties is not easy to make. The different scales and specimen geometries do not allow quantitative comparison of published studies. The focus of this study is to experimentally describe the frictional properties of TOR products and use the measured data as an input to a numerical model for prediction of friction in rolling-sliding contact. The effect of increased temperature is also taken into account. To achieve these results, a high-pressure torsion rheometer is used. The acquired experimental data are then used as an input to predict the traction curves using a modified FASTSIM algorithm to demonstrate the practical applicability of this approach. The results from torsion rheometer provide a connection between the surface displacements calculated in the numerical model and the coefficient of friction in rolling-sliding contact. This applicability includes parametric studies of different running conditions, use in dynamic simulations and understanding the physical processes in contact interface. The novelty of this paper lies in simultaneous evaluation of different TOR products on a simple frictional device and the use of experimental data for implementation in prediction model for further analysis. The effect of applied amount of different TOR products with regards to the contact area as well as temperature influence bring a new insights into the workings of different types of TOR products.

Materials and methods

Torsion rheometer

A torsion rheometer shown in Figure 1 was used to study the shear strength of films created in the contact of solid bodies. The purpose of the torsion rheometer is to study third-body layers under very high loads. Two specimens are pressed against each other and a slow rotational motion is applied. This rotational motion causes displacement of the surfaces and shear stresses arise. The displacement creates elastic behaviour in the first micrometres, after that a pseudo-plastic region occurs. Due to the small surface displacements taking place on an anulus surface far from the axis of rotation, the shear stress is recalculated into a form of one-dimensional sliding motion. The results are in the form of coefficient of friction, which is defined as the ratio between shear stress and normal pressure, changing with displacement distance.

The rheometer uses a hydraulic cylinder to apply normal load to the specimen. The maximal normal loading force is 100 kN. The lower specimen is fixed on a loading platform that can move up or down by loading the hydraulic cylinder. The upper specimen is mounted on a rotational shaft with an axial ball bearing. To ensure parallel initial position during the experiment and constant pressure throughout the contact area, both specimens were aligned prior to the experiment. The contact area alignment is evaluated by pressing against a copper sheet that is analysed by an optical profilometer. The even deformation of the imprint indicates parallelism of

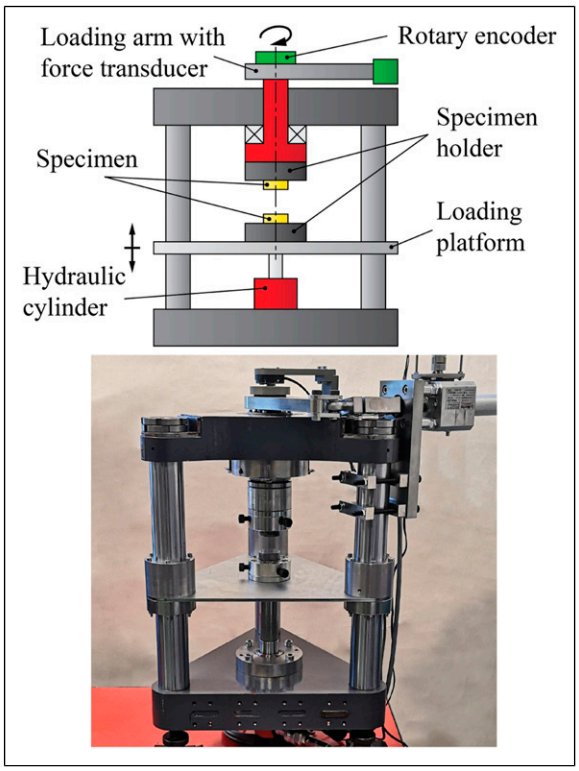

Figure 1. Torsion rheometer.

the contacting surfaces. A loading arm is fixed at the end of the shaft with a force transducer that is used to measure the loading torque with a maximum of 400 Nm. The force transducer used has a 0.02% repeatability error which results in a measurement uncertainty of 0.08 Nm, corresponding to an error in coefficient of friction of 0.0002. The loading arm uses a screw jack with a stepper motor to provide slow and precise rotation of the shaft. The arm angle resolution controlled by the motor is 0.00045°. This uncertainty corresponds to 20 nm of displacement for the specimens at the effective radius. A rotary encoder is used to measure the precise angle of the shaft with upper specimen to determine the true displacement. The combination of the motor position control and the rotary encoder results in a displacement accuracy of 1 μm at the effective radius.

Both specimens are made of bearing steel with a hardness of 60HRC. This choice of material does not represent real wheel-rail contact, however the justification for it is the more stable and comparable surface conditions for each experiment. Compared to the steel used for wheels and rails, the hardness of the specimen used can be twice as high.[32] Different hardness can cause a change in wear regime, wear rate and interaction with solid particles. The study[32] shows that different hardness and normal load do not significantly change the coefficient of friction and only slightly change the wear rate. Additionally, because of the very low sliding distances in HPT testing, these processes are negligible compared to rolling-sliding tests. Due to the lower wear rate of bearing steel samples, the change in surface roughness during the test is less significant and the results are more stable. This configuration is more suitable for testing the properties of applied layer, as is suggested by studies.[8,14] This means that the experimental data will be representative of the added TOR product and will not be greatly influenced by the material and surface condition of the specimens. Both specimens have a 40 mm large diameter that fits the specimen holder. The lower specimen has a flat surface and the upper specimen has an annulus with outer diameter of 12 mm and inner diameter of 6 mm. These contact dimensions result in a contact area of 85 mm^2. This value is similar to the real wheel-rail contact, where an area of around 100 mm^2 is expected. Based on the dimensions of the specimen, the maximal achievable contact pressure with the torsion rheometer is 1.2 GPa. The initial surface roughness root mean square height (Rq) for both specimens is 0.15 μm ± 0.02 μm. However, after the initial run-in process before the experiment, the value increases and stabilizes at 0.3 μm ± 0.05 μm.

Due to the normal loading force, a contact pressure p (Equation (1)) is applied to the contact surfaces. When exerting a torque, shear stresses τ (Equation (2)) arise in the shearing plane. Due to the difference between inner and outer radius, the shear stress is not uniform across the width of the contact. As such, an effective radius r_e (Equation (3)) needs to be incorporated at which the shear stress is calculated. This inconsistency in shear stress across contact does not influence the results due to the difference being small enough and averaged by the effective radius. Thus, a uniform shear stress is assumed across the contact. The instantaneous coefficient of friction μ at the effective radius is then defined as the tangential shear stress divided by the normal contact pressure, see (Equation (4)). All displacement values of the HPT results in this paper are at the effective radius.

$$p = \frac{F}{S} \tag{1}$$

$$\tau = \frac{M_k}{r_e S} \tag{2}$$

$$r_e = \frac{2\left(r_2^3 - r_1^3\right)}{3\left(r_2^2 - r_1^2\right)} \tag{3}$$

$$\mu = \frac{\tau}{p} \tag{4}$$

TOR products

The shear properties of four TOR products were evaluated. These four products are oil-based (OFM), water-based (WFM) and solid stick (SFM) for wheel tread. This represents the current products available and used in the railway industry. Both oil-based TOR lubricants (OFM1 and OFM2) contain ester oil, solid lubricant and metallic particles. The thickener used is organic in case of OFM1 and inorganic for OFM2. The NLGI grade for product consistency (determined by the cone penetration test) according to ISO 6743-9 is 0 for OFM1 and 00 for OFM2. Water-based friction modifier (WFM) contains water, thickener, solid lubricant and solid particles. Solid stick (SFM) is made of a polymeric base with solid lubricant and particles for friction modification.

Experimental procedure

The initial phase of the experiments consisted of contact surface run-in. This was carried out by subsequent dry tests at a contact pressure of 750 MPa and a displacement rate of 1 μm/s. This procedure ensured that initial changes in surface roughness were avoided in the main measurement. The target surface roughness for the main experiments was Rq 0.3 μm. The roughness profile was evaluated after each test and if it exceeded Rq 0.4 μm a surface repolishing procedure was performed to obtain the initial roughness. This run-in procedure was performed by torsional loading in one direction and unloading the normal force after completing the effective radius displacement distance of 0.4 mm.

In the main experiments, the application of liquid TOR product was done by micropipette. The liquid substance was then spread out on the contact area of the HPT specimen. The drying process for WFM was accelerated by a heat gun set to 60°C. The solid stick was crushed to a fine powder (particle size around 50 μm) and the precise amount applied was measured by laboratory balance. This ensures control over the amount applied to the contact. This application methodology for solid stick was used mainly because the same application method as in railway vehicle by pressing the stick against a sliding surface would not give us precise information about the mass of the solid stick

removed. After the application, the specimens were loaded with normal force, resulting in a set pressure. Rotational displacement started with a 1 μm/s displacement rate and 400 μm maximum displacement distance. These parameters were selected based on preliminary tests and findings in study,[21] where the low displacement rate provides stable friction. The displacement limit of 0.4 mm provides enough room for the pseudo-plastic regime to stabilize. After each test, the specimens were unloaded. The tests under dry conditions and with applied amount were carried out under 750 MPa contact pressure.

In wheel and rail contact, the contact temperature rises due to frictional heating of the contact surfaces under high loads and sliding velocities. Flash temperature can be in order of hundreds of degrees.[31,33] In HPT tests, the frictional power is too low to cause a substantial temperature increase. Thus, the experiments under increased contact temperature were done by heating the lower specimen with an aluminium block and cartridge heating elements. During the heating procedure, both specimens are kept in contact to provide heating of the lower and upper contact surfaces. The specimens are unloaded only when a surface temperature measurement is taken in the centre of the lower specimen surface. The maximum achievable temperature for current configuration is 100°C. The temperatures used for measurements were 90°C, 60°C and an ambient temperature of 22°C. These experiments were carried out with 16 μL and 16 mg product applied to ensure a complete contact coverage, so temperature parameters are not influenced by the asperity contact. These tests were carried out under 750 MPa contact pressure, 1 μm/s displacement rate, and stopped after 0.2 mm displacement at the effective radius.

Mathematical model

To demonstrate the use of these results, a boundary model as described in[34] is used. The model uses FASTSIM algorithm to predict contact surface tractions. The equations that define the surface tractions in the discretized contact area grid are equation (5) for the elastic region and equation (6) for the pseudo-plastic region. The contact area is divided into m by n discrete points in x and y directions, respectively. The elastic region has upper shear stress limit defined by τ_{c1} and the pseudo-plastic region shear stress is between τ_{c1} and τ_{c2}. The contact elasticity parameter L is the sum of the Kalker's elasticity coefficient L_K and the elasticity parameter of third body represented by the initial elastic slope L_e in the surface shearing measured by the torsion rheometer, as suggested by.[26] Plasticity behaviour is calculated using Voce's hardening law[35] as is used in the study.[30] The model[34] uses an elliptical contact area and the parameters for limiting elastic (τ_{c1}) and plastic (τ_{c2}) shear stress are extended to incorporate temperature dependence, see equation (7). The model is simplified to assume that the coefficient of friction is independent of contact pressure. The elliptical contact area uses a semi-ellipsoid pressure distribution with semiaxes contact dimensions at the major axis a and the minor axis b. The temperature influence is modelled as a two-parameter exponential decrease. This represents the exponential decrease in coefficient of adhesion with increasing slip in wheel-rail contact. Similar exponential decrease was suggested by studies.[29] The complete formula for limiting shear stress is described by equation (7).

$$\tau_{BL}(x_i,y_j) = \tau_{BL}(x_{i-1},y_j) - \frac{2a(y_j)}{vm}\frac{s}{L} \tag{5}$$

$$\tau_{BL}(x_i,y_j) = \tau_{c1}(x_i,y_j) + (\tau_{c2}(x_i,y_j) - \tau_{c1}(x_i,y_j)) \left(1 - e^{\left(-u+\tau_{c1}(x_i,y_j)L\right)/L_p}\right) \tag{6}$$

$$\tau_{ck}(x_i,y_j) = \mu_{ck}p(x_i,y_j)\cdot exp(k_k(T(x_i,y_j) - T_A)) \tag{7}$$

Index k in equation (7) refers to either elastic (1) or plastic (2) limiting shear stress. Parameter T_A is the ambient temperature so the parameters μ_{ck} can be set from measurements at ambient temperature. The parameter $p(x_i,y_j)$ is the contact pressure at each discrete calculation point and k_k defines the trend of exponential change. Negative values of k_k mean decreasing coefficient of friction with increasing temperature. The calculation of temperature distribution is done by using an iterative process where calculated shear stress is used to estimate the temperature. Based on the calculated temperature, the limiting shear stresses are recalculated with changes described by equation (7) and a new temperature solution is acquired. This process is stopped after the temperature change between iterations is less than 0.1°C. The temperature distribution in equation (8)[33] is based on the frictional heat power dissipation rate $q(x_i,y_j) = \tau(x_i,y_j)v_s$ generated by friction. Here, $\tau(x_i,y_j)$ is the shear stress in corresponding point of contact and v_s is sliding velocity.

$$T(x_i,y_j) = \frac{2}{\sqrt{\lambda\rho c}}\sqrt{\frac{a(y_j)}{\pi v}}\sum_{h=1}^{i}\dot{q}(x_i,y_j)\left(\sqrt{x_i - x_{h-1}} - \sqrt{x_i - x_h}\right) \tag{8}$$

To demonstrate the applicability of the HPT results, the model is applied to rolling sliding contact of half-axis dimensions $a = 3.7\ mm$ and $b = 3.3\ mm$. These dimensions are approximately related to an unworn tram wheel with a longitudinal radius of 350 mm and a rail profile S49. The normal load is 20 kN, resulting in a maximum contact pressure of 790 MPa. The created contact area is 38 mm^2, which is about half the contact area of the HPT test specimen. The parameters of the interfacial layer are based on the HPT experiments. Due to different material of the specimen used in HPT testing it is not possible to directly correlate the results to real application, however, a qualitative comparison between dry conditions and the effect of TOR products on adhesion can be made. Different slip conditions are examined to show the effect of temperature increase. The parameters are summarized in Table 1. The thermal parameters are valid for dry contact but are also used for TOR products to simplify the case.

Table 1. Calculation parameters.

	Value	Unit
Longitudinal semi-axis a	3.7	mm
Lateral semi-axis b	3.3	mm
Rolling radius r	350	mm
Running velocity v	10	m/s
Normal force F	20	kN
Maximum Hertzian pressure p_0	790	MPa
Thermal conductivity λ [36]	50	W/Km
Density ρ	7850	kg/m^3
Specific heat capacity c [36]	450	J/kgK

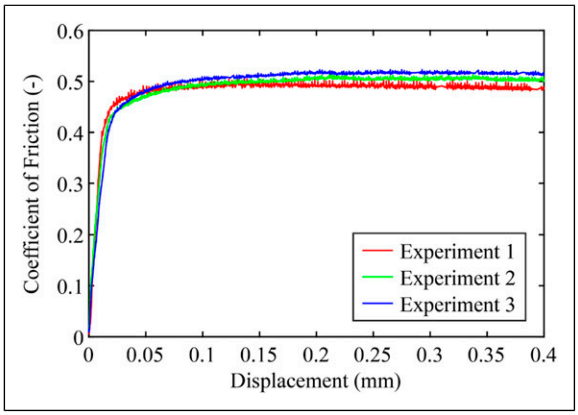

Figure 2. Dry contact conditions.

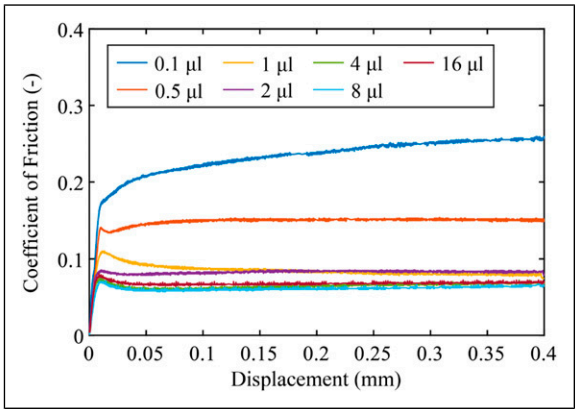

Figure 3. OFM1: the influence of applied amount.

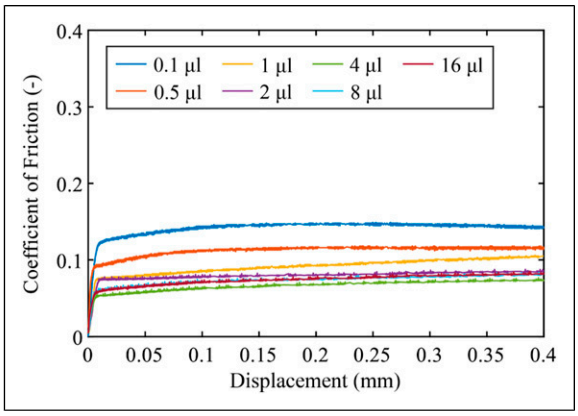

Figure 4. OFM2: the influence of applied amount.

Results and discussion

Dry contact conditions

The first set of experiments was aimed at investigating the coefficient of friction in dry conditions. As shown in Figure 2, three experiments were conducted to evaluate the repeatability. The results show good repeatability of the cleaning and run-in procedure. For all tests, the transition between elastic and plastic deformation starts at coefficient of friction 0.45. The linear part of the elasticity ends with displacement of around 15 µm. When comparing the results with a real wheel-rail material,[21,22] the bearing steel shows a considerably more linear progression of the elastic part, while the real material has a gradually decreasing slope. The plastic part of the measurement slowly saturates and from around 0.2 mm displacement does not show any change with increasing displacements. The average value of the coefficient of friction at 0.4 mm displacement was 0.502 with standard deviation of 0.018. These saturated values correspond well with HPT study using real wheel rail material[22] after run-in procedure. However, a higher values above 0.7 were measured in[21] with wheel and rail material. The differences in coefficient of friction can be caused by the material and surface conditions such as roughness, oxidation and cleaning method. As the coefficient of friction measurement uncertainty is in the order of 10^{-4}, it has very little influence on the evaluation of results. Higher influence of measurement uncertainty is introduced with random variations resulting from cleaning process and small changes in roughness between experiments.

Lubricated contact conditions

Figure 3 shows the influence of OFM1 amount. With an increasing amount from 0.1 µL to 16 µL the maximum coefficient of friction decreases. The highest coefficient of friction at 0.4 mm displacement reached 0.257 at 0.1 µL applied. For this amount, the coefficient of friction started saturating around 0.4 mm displacement. A possible explanation could be an uneven distribution of the applied product, where a stable frictional layer is formed in later stages of shearing. Amounts larger than 1 µL slowly converge to a coefficient of friction of 0.07. Above 2 µL there is no significant change, and the measured curves behave the same. The applied amount has a negligible effect on the slope of initial elastic part. The saturation point is reached between 7 and 14 µm.

The results of the amount applied for the second oil-based TOR lubricant OFM2 tested are shown in Figure 4. Similarly to OFM1, the initial elastic part has a comparable increasing slope for all amounts tested. The maximum peak of the elastic part is reached at 9 µm displacement for 0.1 µL down to 4 µm for 16 µL. For 0.1 µL applied the plastic part starts at a coefficient of friction of 0.125 and reaches a maximum of 0.15. Above 2 µL the curves have a similar trend as was observed for OFM1 with a converging trend to the coefficient of friction of 0.08. The 1 µL and 2 µL amounts have the same initial elastic part, but with increasing displacement distance the 1 µL amount increases coefficient of friction while 2 µL stays the same.

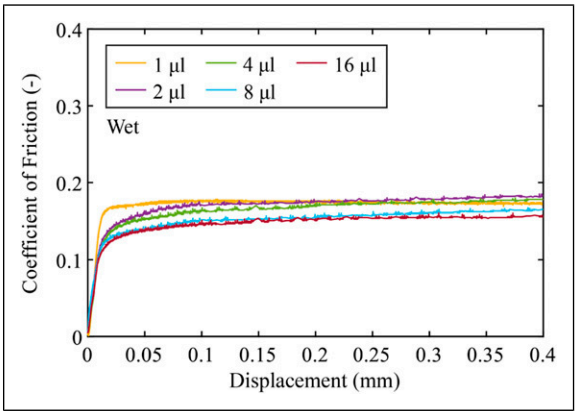

Figure 5. WFM: the influence of applied amount in wet state.

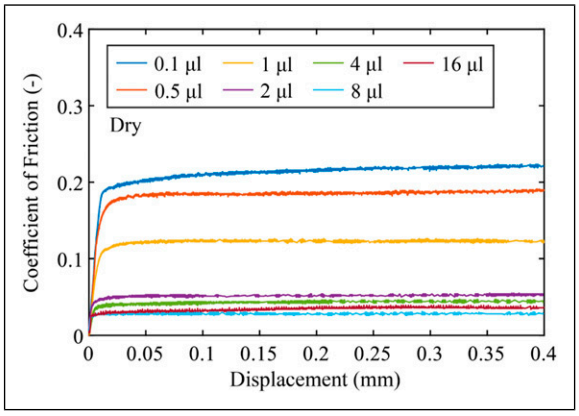

Figure 6. WFM: the influence of applied amount in dry state.

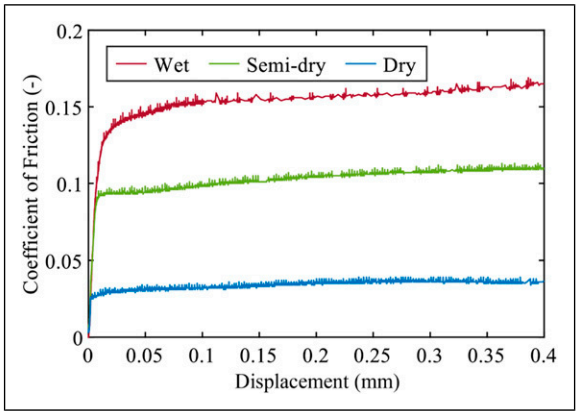

Figure 7. WFM: the influence of drying the substance (16 µL).

In combination with the OFM1 results, this suggests that there is a transition phase where the overlubricating effect starts between 1 and 2 µL. The lowest applied amount of OFM2 only reached coefficient of friction of 0.15 while OFM1 reached 0.25. Application of 1 µL seem to be the saturating amount for both oil-based products. Also, a difference is seen in the transition between the elastic and plastic parts of the curve. For OFM1, the transition exhibits a peak value that quickly drops and stabilizes. This peak part is not evident in OFM2, where the transition is smoother. This behaviour with the peak transition was already observed with the testing of friction modifiers[20] where the introduction of grease contamination suppressed the peak to a more bilinear transition.

The effect of the amount of water-based friction modifier applied in the wet state is seen in Figure 5. In this type of measurement, an amount less than 1 µL dried out too quickly in open air to be counted as a "wet" state. For 1 µL applied the shape of the curve still suggests a semi-dried state. For the rest of the amounts tested, the measurements do not show a significant discrepancy or dependence on the applied amount. The maximum coefficient of friction for 1 µL and 16 µL was 0.175 and 0.157, respectively. This shows insensitivity to the amount applied for wet conditions. The initial elastic part of all measurements had a similar trend, whereas the plastic part is very stable with only a slight increasing trend with higher displacement.

Experiments in the dry state of WFM are shown in Figure 6. The effect of the applied amount is very evident for this state. Increasing the applied amount causes a decrease in coefficient of friction. The turning point is between 0.5 µL and 2 µL where the coefficient of friction drops from 0.19 to 0.05. Above 2 µL the dried substance creates a solid thick film. This film separation is what causes the low friction values for 2 µL and more. The lowest value of coefficient of friction at 0.4 mm displacement was 0.027 with 8 µL applied. The difference between 8 µL and 16 µL starts at around 0.05 mm displacement and can be caused by random variance during the experiment. This is based on the fact that such large volumes of WFM already cover the entire contact area. Any excessive amount will be squeezed out and with that, different amounts of particles can be trapped in the contact area. With increase in displacement, the curves for these two applied amounts diverge with difference in coefficient of friction of 0.008 at 0.4 mm displacement. The very low values phenomenon is caused by the solid dry state of the substance being unable to be squeezed out of contact, as is possible in the wet state. Thus, the film causes a thick separation layer that causes a low coefficient of friction. Such conditions could be replicated on track only by drying the substance before it is spread out along the rail. As suggested by other studies,[1,14,19] water-based products are designed to be carried along the rail when the base medium is present. When the base medium dries out, the particles adhere to the surface, and no further material transfer occurs.

To test the change in shear properties under the effect of drying the applied film, a semidried state measurement was carried out with 16 µL applied to ensure total contact coverage and enough time in semi-dried state, where lower amounts dried too quickly. Semi-dried state was achieved by stopping the drying process when half of the applied amount still had water present, seen as a darker shade of the applied film. In the fully dry state, the applied film appeared to have a rubber-like consistency. As seen in Figure 7 the drying process caused a substantial drop in the coefficient of friction. This suggests that the dry film creates a separation layer with low shear strength, while in the wet state the more dispersed particles promote asperity interaction. In reality, the applied substance would be spread along the rail and undergo substantial sliding before drying out. This would create a much thinner and more spread-out film that would not cause such low friction conditions as seen with higher applied amounts in Figure 6.

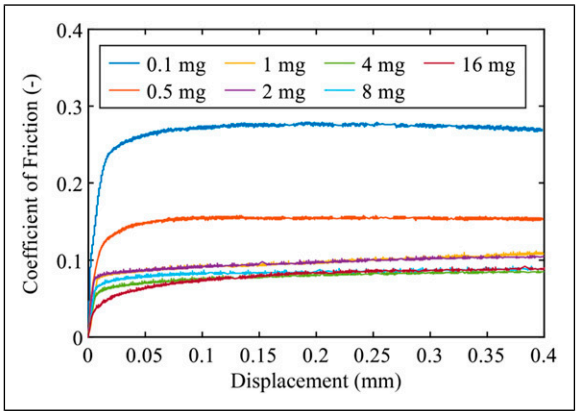

Figure 8. SFM: the influence of applied amount.

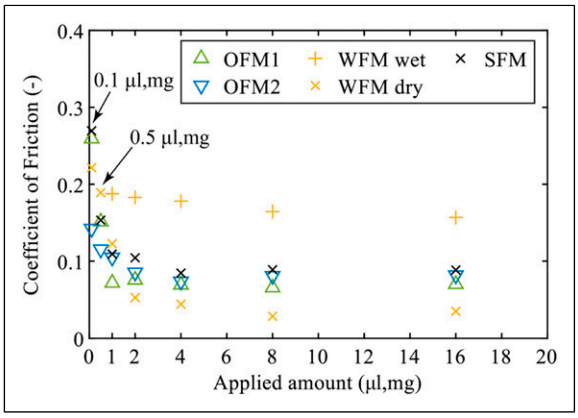

Figure 9. The effect of applied amount on the coefficient of friction at 0.4 mm displacement.

The results for the applied amount of SFM are shown in Figure 8. As with OFM2 and WFM, increasing the amount applied decreased the coefficient of friction. The highest values for 0.1 mg applied and 0.4 mm displacement reached 0.28 while the lowest was 0.09 at 16 mg. The transition phase of coefficient of friction was between 0.1 mg and 1 mg. Amounts larger than 1 mg slowly converged to the coefficient of friction 0.09. The high applied amounts created a thick film, similar to dry WFM, which persisted even through high pressure and shear loading of the contact. Since studies do not focus on the application methodology of solid FMs it is not possible to estimate if such conditions are achievable in rolling-sliding conditions. When used in railway vehicles, the solid stick is pressed against the rotating wheel and the film is transferred to the wheel tread. The different application methodology in this study is what might have caused such low friction conditions. Studies[15,37] suggest coefficients of friction up to 0.3, which is in line only with the amount applied around 0.1 mg.

Summarizing the results for applied amount, it is evident that OFM1, OFM2 and SFM behave very similarly in the range of 1 µL or 1 mg applied and above as seen in Figure 9. Below 1 µL the OFM1 quickly increases to similar values as SFM. OFM2 provides the lowest coefficient of friction in the lower applied amount range compared to other tested products. At higher applied amounts of 2 µL and above, the dry WFM causes the lowest coefficient of friction. These results correspond well with publication[21] where the lowest

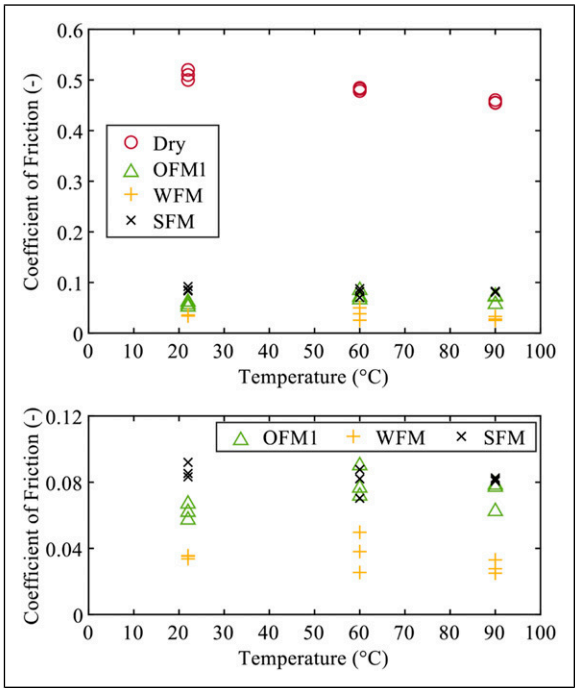

Figure 10. The effect of temperature on the coefficient of friction at 0.2 mm displacement.

applied amount of dry FM caused coefficient of friction of about 0.25–0.3. Increasing the applied amount lowered the friction values below 0.1 and even down to 0.05 with excessive overapplication. This comparison points to the fact, that using bearing steel when TOR product drives the frictional behaviour does not significantly invalidate the results.

For the higher applied amounts, only WFM in the wet state caused higher levels of friction above 0.15. Assuming that the WFM composition will always be spread along the rail before drying out, the rail will be covered in thin film regardless of the initial applied amount as a result of the spreading and squeezing out. The case where a low coefficient of friction is achieved with the dry film is representative if the substance is not carried by wheels and dries locally.

The results presented are well in agreement with the study[1] where oil-based substances show a high sensitivity to the amount applied. The coefficients of friction measured in this study are lower, which could be caused by the different specimen material and application method. The results suggest that the overapplication of SFM could also lead to low coefficients of friction. However, this is the impact of the application methodology. Vehicle application systems press the solid stick against the wheel tread, preventing the creation of a thick film due to the removal of material being realized through asperities. In this study, a fine powder was applied which caused a thick separation film between testing specimens because the powder is not able to squeeze out of contact.

The last set of experiments tested the increase in temperature, as shown in Figure 10. For dry conditions, the increase in temperature caused a decrease in coefficient of friction. A similar gradual decrease was observed with AISI 52 100 against HSS[38] as well as experiments with high-

Table 2. Interfacial layer parameters for model calculation.

	Dry	OFM1 0.5 μL	WFM dry 0.5 μL	SFM 0.1 mg
μ_{c1} (−)	0.4	0.14	0.12	0.18
μ_{c2} (−)	0.51	0.152	0.19	0.27
L_{ep} (μm)	30	60	60	50
L_p (μm)	30	40	10	15
k_1, k_2 (1/°C)	−0.0016	0.0005	−0.001	−0.0005

strength alloy steel.[39] The mean coefficient of friction at 0.2 mm displacement from a set of three experiments at ambient temperature, 60°C and 90°C was 0.51, 0.482 and 0.457, respectively. The main difference in the measured curves was the value of the coefficient of friction where plasticity begins. No significant changes were observed in the slope of initial elastic deformation or the trend in the plastic deformation. None of the tested products showed a considerably changing trend in the coefficient of adhesion with an increase in temperature. OFM1 and SFM show comparable values of coefficient of friction at higher temperatures, while WFM provided lower values between 0.03 and 0.04. The results for WFM are taken in the dry state of the substance since it dried quickly at increased contact temperature. The results from three measurements for each condition in Figure 10 show a good repeatability of the measurement.

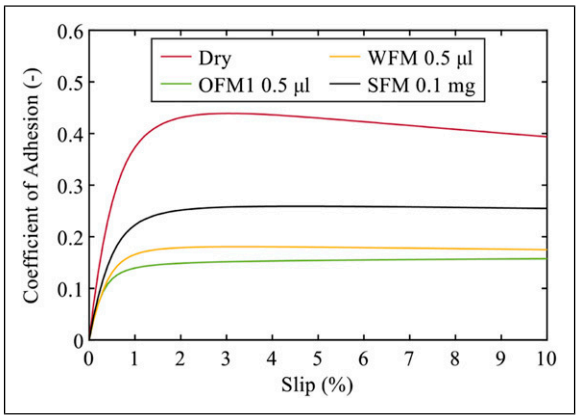

Figure 11. Traction curves for dry conditions and TOR products.

Model prediction

Based on the results of HPT tests, the parameters of the interfacial model were identified. The amounts applied for the model were selected based on the realistic friction values, as well as the assumption that SFM should in practice have less total consumption per distance applied. These parameters, as described in equation (7) and previous publication,[34] are summarized in Table 2. The temperature coefficients k_1 and k_2 have the same value due to a similar trend in the change of the limiting elastic and plastic coefficient of friction. Experimental measurements reached only 90°C for which the coefficients were fitted. However, the gradual decrease fitted to the experimental data of dry conditions is comparable to previous study of steel-steel friction, where temperatures up to 600°C were reached.[38] A similar assumption is made in study,[40] where at 400°C the coefficient of friction is half of the value as in ambient conditions, which corresponds well to the fitted data in this study. As seen from Figure 10, the TOR products have negligible change in friction with increased temperatures. This results in a very small temperature coefficient and, for OFM1, even positive values. Note that the WFM values were taken from dry substance experiments, as discussed previously. The L_{ep} and L_p parameters are taken from ambient temperature conditions, as the increasing temperatures did not have effect on these values. Parameter L_{ep} defines the slope of initial elastic increase, and to get the true L_e a formula $L_e=L_{ep}/p$ applies. Higher values of L_{ep} cause a slower increase in the coefficient of adhesion with increasing slip ratio. Parameter L_p defines the nonlinear increase in the region of plastic deformation. Higher values of L_p cause a slower increase in the of coefficient of friction with displacement until the limiting friction is reached.

Prediction of traction curves for the tested substances at rolling velocity of 10 m/s is shown in Figure 11. Using OFM1, WFM or SFM reduces the coefficient of adhesion. The lowest adhesion values at 10% slip are predicted for OFM1 that reached coefficient of adhesion 0.15. The water-based product WFM provides a slight increase to 0.18 and the highest coefficient of adhesion was for SFM at 0.26. As suggested by HPT tests, the trend of traction curves is very similar for all evaluated products. This is due to very fast transitions between elastic and plastic parts and subsequent stabilization of measured HPT curves. However, in field or laboratory rolling-sliding experiments, the higher total sliding distances would promote removal of the layer and thus decreasing the amount of TOR product which would increase the coefficient of adhesion at higher slip, as seen in studies.[6,7,19] This would produce a more positive trend of traction curve.

Under dry conditions at 10% slip, the maximum contact temperature is 250°C, while with SFM the temperature drops to 175°C. Reducing friction further by a solid film of WFM causes a maximum temperature of 125°C. OFM1 has the lowest peak temperature close to WFM at 118°C. However, these results assume the temperature properties of steel and neglect any thermal properties that a thin film of the TOR product might have.

OFM1 and WFM perform very similarly as suggested by Figure 9. Compared to other studies on different scales[2,5,6] the coefficient of adhesion range between 0.1 and 0.2 seems to be very typical for rolling-sliding tests with moderate

amounts applied. The results for SFM are in line with studies,[15,17] which suggest a coefficient of adhesion of around 0.3. Aside from the dry WFM, all these results can differ depending on the application amount, as was discussed with Figure 9. Also, the different application methodology for solid stick can distort the interpretation of higher application amounts presented in this work.

Conclusions

High-pressure torsion tests were carried out to evaluate the boundary friction behaviour of three different types of TOR products. These products were investigated for the influence of applied amount and temperature. The results of these tests are used in a frictional model based on Kalker's FASTSIM algorithm. The results of the model show traction curves for selected applied amounts and the influence of increased temperature.

- For OFMs and dry WFM, the amount greater than 1–2 μL causes a very low coefficient of friction, which is not recommended for use of the TOR product. The trend of application amount for OFMs and wet WFM replicates well the data presented in the study[1] in terms of oil-based products being very sensitive to the application amount.
- The effect of WFM drying should be considered in the case where the substance is not spread out on the surface. Large amounts in dry state caused the lowest coefficient of friction measured across all tests.
- The selected amounts and predicted traction curves show a similar behaviour for tested products as suggested by the measured HPT curves, that did not show differences in the transition between elastic and plastic deformation. The level of adhesion changes primarily on the basis of the amount applied.
- The predictions show that dry contact exhibits a decreasing adhesion coefficient with increasing slip. The TOR products did not show any changes in the slope of traction curve due to a lower temperature coefficient in combination with lower contact temperatures.

Declaration of conflicting interests

The author(s) declared no potential conflicts of interest with respect to the research, authorship, and/or publication of this article.

Funding

The author(s) disclosed receipt of the following financial support for the research, authorship, and/or publication of this article: This work was supported by the GA20-23482S project with financial support from the Czech Science Foundation.

ORCID iDs

Daniel Kvarda https://orcid.org/0000-0002-5386-2486
Radovan Galas https://orcid.org/0000-0001-7364-899X
Marian Dzimko https://orcid.org/0000-0003-3401-1018

References

1. Stock R, Stanlake L, Hardwick C, et al. Material concepts for top of rail friction management – classification, characterisation and application. *Wear* 2016; 366–367: 225–232.
2. Areiza YA, Garcés SI, Santa JF, et al. Field measurement of coefficient of friction in rails using a hand-pushed tribometer. *Tribol Int* 2014; 82: 274–279.
3. VanderMarel J, Eadie DT, Oldknow KD, et al. A predictive model of energy savings from top of rail friction control. *Wear* 2014; 314: 155–161.
4. Arias-Cuevas O, Li Z, Lewis R, et al. Rolling-sliding laboratory tests of friction modifiers in dry and wet wheel-rail contacts. *Wear* 2010; 268: 543–551.
5. Lundberg J, Rantatalo M, Wanhainen C, et al. Measurements of friction coefficients between rails lubricated with a friction modifier and the wheels of an IORE locomotive during real working conditions. *Wear* 2015; 324–325: 109–117.
6. Matsumoto K, Suda Y, Iwasa T, et al. A method to apply friction modifier in railway system. *JSME Int J Ser C* 2004; 47: 482–487.
7. Tomeoka M, Kabe N, Tanimoto M, et al. Friction control between wheel and rail by means of on-board lubrication. *Wear* 2002; 253: 124–129.
8. Galas R, Omasta M, Krupka I, et al. Laboratory investigation of ability of oil-based friction modifiers to control adhesion at wheel-rail interface. *Wear* 2016; 368–369: 230–238.
9. Eadie DT, Kalousek J and Chiddick K. The role of high positive friction (HPF) modifier in the control of short pitch corrugations and related phenomena. *Wear* 2002; 253: 185–192.
10. Eadie DT, Santoro M and Kalousek J. Railway noise and the effect of top of rail liquid friction modifiers: changes in sound and vibration spectral distributions in curves. *Wear* 2005; 258: 1148–1155.
11. Eadie DT, Santoro M, Oldknow KD, et al. Field studies of the effect of friction modifiers on short pitch corrugation generation in curves. *Wear* 2008; 265: 1212–1221.
12. Egana JI, Vinolas J and Gil-Negrete N. Effect of liquid high positive friction (HPF) modifier on wheel-rail contact and rail corrugation. *Tribol Int* 2005; 38: 769–774.
13. Galas R, Omasta M, Klapka M, et al. Case study: the influence of oil-based friction modifier quantity on tram braking distance and noise. *Tribol Indust* 2017; 39: 198–206.
14. Galas R, Kvarda D, Omasta M, et al. The role of constituents contained in water–based friction modifiers for top–of–rail application. *Tribol Int* 2018; 117: 87–97.
15. Kalousek J and Johnson KL. An investigation of short pitch wheel and rail corrugations on the Vancouver mass transit system. *Proc Inst Mech Eng F: J Rail Rapid Transit* 1992; 206: 127–135.
16. Hardwick C, Lewis S and Lewis R. The effect of friction modifiers on wheel/rail isolation at low axle loads. *Proc Inst Mech Eng Part F: J Rail Rapid Transit* 2014; 228: 768–783.
17. Song J, Shi L, Ding H, et al. Effects of solid friction modifier on friction and rolling contact fatigue damage of wheel-rail surfaces. *Friction* 2021; 10.
18. Hou K, Kalousek J and Magel E. Rheological model of solid layer in rolling contact. *Wear* 1997; 211: 134–140.

19. Harrison H, McCanney T and Cotter J. Recent developments in coefficient of friction measurements at the rail/wheel interface. *Wear* 2002; 253: 114–123.
20. Lu X, Cotter J and Eadie DT. Laboratory study of the tribological properties of friction modifier thin films for friction control at the wheel/rail interface. *Wear* 2005; 259: 1262–1269.
21. Evans M, Skipper WA, Buckley-Johnstone LE, et al. The development of a high pressure torsion test methodology for simulating wheel/rail contacts. *Tribol Int* 2021; 156: 106842.
22. Buckley-Johnstone LE, Trummer G, Voltr P, et al. Assessing the impact of small amounts of water and iron oxides on adhesion in the wheel/rail interface using high pressure torsion testing. *Tribol Int* 2019; 135: 55–64.
23. Kalker JJ. A fast algorithm for the simplified theory of rolling contact. *Vehicle Syst Dyn Int J Vehicle Mech Mobil* 1982; 11: 1–13.
24. Kalker JJ. *Three-dimensional elastic bodies in rolling contact*, 2. Dordrecht: Springer Netherlands, 1990.
25. Vollebregt EAH, Six K and Polach O. Challenges and progress in the understanding and modelling of the wheel–rail creep forces. *Vehicle Syst Dyn* 2021; 59: 1026–1068.
26. Rovira A, Roda A, Lewis R, et al. Application of fastsim with variable coefficient of friction using twin disc experimental measurements. *Wear* 2012; 274–275: 109–126.
27. Piotrowski J. Kalker's algorithm fastsim solves tangential contact problems with slip-dependent friction and friction anisotropy. *Vehicle Syst Dyn* 2010; 48: 869–889.
28. Giménez JG, Alonso A and Gómez E. Introduction of a friction coefficient dependent on the slip in the FastSim algorithm. *Vehicle Syst Dyn* 2005; 43: 233–244.
29. Spiryagin M, Polach O and Cole C. Creep force modelling for rail traction vehicles based on the fastsim algorithm. *Vehicle Syst Dyn* 2013; 51: 1765–1783.
30. Six K, Meierhofer A, Muuller G, et al. Physical processes in wheel-rail contact and its implications on vehicle-track interaction. *Vehicle Syst Dyn* 2015; 53: 635–650.
31. Ertz M and Knothe K. A comparison of analytical and numerical methods for the calculation of temperatures in wheel/rail contact. *Wear* 2002; 253: 498–508.
32. Liu J, Jiang W, Chen S, et al. Effects of rail materials and axle loads on the wear behavior of wheel/rail steels. *Adv Mech Eng* 2016; 8: 1–12.
33. Knothe K and Liebelt S. Determination of temperatures for sliding contact with applications for wheel-rail systems. *Wear* 1995; 189: 91–99.
34. Kvarda D, Galas R, Omasta M, et al. Asperity-based model for prediction of traction in water-contaminated wheel-rail contact. *Tribol Int* 2021; 157: 106900.
35. Voce E. The relationship between stress and strain for homogeneous deformation. *J Inst Met* 1948; 74: 537–562.
36. Gupta V, Hahn GT, Bastias PC, et al. Calculations of the frictional heating of a locomotive wheel attending rolling plus sliding. *Wear* 1996; 191: 237–241.
37. Lewis R, Gallardo EA, Cotter J, et al. The effect of friction modifiers on wheel/rail isolation. *Wear* 2011; 271: 71–77.
38. Milan JCG, Carvalho MA, Xavier RR, et al. Effect of temperature, normal load and pre-oxidation on the sliding wear of multi-component ferrous alloys. *Wear* 2005; 259: 412–423.
39. Pearson SR, Shipway PH, Abere JO, et al. The effect of temperature on wear and friction of a high strength steel in fretting. *Wear* 2013; 303: 622–631.
40. Ertz M and Bucher F. Improved creep force model for wheel/rail contact considering roughness and temperature. *Vehicle Syst Dyn* 2002; 37: 314–325.

Appendix 1

Nomenclature

a	Longitudinal half-axis dimension (m)
b	Lateral half-axis dimension (m)
c	Specific heat capacity (J/kgK)
F	Normal load applied to the contact (N)
k_1	Temperature coefficient of elastic limiting shear stress (−)
k_2	Temperature coefficient of plastic limiting shear stress (−)
L	Contact elasticity parameter ($L = L_K + L_e$, mm^3/N)
L_e	Elasticity parameter of third body (mm^3/N)
L_K	Kalker's elasticity parameter (mm^3/N)
L_p	Plasticity parameter (m)
m	Contact discretization in x direction (−)
M_k	Torque (Nm)
n	Contact discretization in y direction (−)
p	Contact pressure (Pa)
q	Frictional heat power dissipation rate (W/m^2)
r	Rolling radius (m)
r_1	Inner radius of contact area (m)
r_2	Outer radius of contact area (m)
r_e	Effective radius (m)
S	Contact area (mm^2)
s	Rigid slip (m/s)
T	Temperature (°C)
T_A	Ambient temperature (°C)
u	Surface displacement (m)
v	Running velocity (m/s)
v_s	Sliding speed (m/s)
x	Position in longitudinal direction (m)
y	Position in lateral direction (m)
λ	Thermal conductivity (W/Km)
μ	Coefficient of friction (−)
ρ	Density (kg/m^3)
τ	Shear stress (Pa)
μ_{c1}	Elasticity limiting coefficient of friction (−)
τ_{c1}	Elasticity limiting shear stress (Pa)
μ_{c2}	Plasticity limiting coefficient of friction (−)
τ_{c2}	Plasticity limiting shear stress (Pa)

Friction
https://doi.org/10.1007/s40544-021-0521-5
ISSN 2223-7690
CN 10-1237/TH
RESEARCH ARTICLE

Effects of solid friction modifier on friction and rolling contact fatigue damage of wheel-rail surfaces

Jingdong SONG[1,2], Lubing SHI[1], Haohao DING[1,*], Radovan GALAS[3], Milan OMASTA[3], Wenjian WANG[1], Jun GUO[1], Qiyue LIU[1], Martin HARTL[3]

[1] *Tribology Research Institute, State Key Laboratory of Traction Power, Southwest Jiaotong University, Chengdu 610031, China*

[2] *School of Mechanical Engineering, Xi'an Jiaotong University, Xi'an 710049, China*

[3] *Faculty of Mechanical Engineering, Brno University of Technology, Brno 616 69, Czech Republic*

Received: 18 July 2020 / Revised: 14 December 2020 / Accepted: 19 April 2021

© The author(s) 2021.

Abstract: In railway network, friction is an important factor to consider in terms of the service behaviors of wheel-rail system. The objective of this study was to investigate the effect of a solid friction modifier (FM) in a railway environment. This was achieved by studying the friction, wear, and rolling contact fatigue (RCF) damage on the wheel-rail materials at different slip ratios. The results showed that when a solid FM was applied, the friction coefficient decreased. After the solid FM was separated from the wheel-rail interface, the friction coefficient gradually increased to its original level. With the application of the solid FM, the wear rates of the wheel-rail decreased. In addition, the thickness and hardness of the plastic deformation layers of the wheel-rail materials were reduced. The worn surfaces of the wheel-rail were dominated by pits and RCF cracks. Without the FM, RCF cracks ranged from 84 to 120 μm, and subsurface cracks were generated. However, with the FM, RCF cracks ranged from 17 to 97 μm and no subsurface cracks were generated. These findings indicate possible methods of improving the performance of railway rolling stock by managing friction, and reducing wear and permanent RCF damage affecting both the wheels and rails.

Keywords: wheel-rail; solid friction modifier (FM); friction; wear; rolling contact fatigue (RCF) damage

1 Introduction

In railway network, an appropriate friction level can accelerate and decelerate a train. However, low friction can cause serious safety problems [1, 2]. Meanwhile, the initiation and propagation of rolling contact fatigue (RCF) cracks on railway wheels are serious problems in the field [3, 4]. Experiments and calculation models for degraded friction [5] and wear and RCF [6] have been studied recently. The friction level at the wheel-rail interface played a significant role in traction and braking.

A friction coefficient of the wheel-rail interface that is too low (less than 0.1) causes poor friction for trains during braking, which can result in safety issues by increasing the braking distance [7]. However, a high friction coefficient under dry conditions (0.5–0.8) could have a negative effect on train operations when braking and accelerating, or cause surface damage (RCF or wear) [8]. Friction modifiers (FMs) can be applied to the top surface of the rail to achieve intermediate friction coefficient (0.3–0.4) in the third body layer. This reduces wear and surface damage by reducing the traction forces without compromising the braking or friction functions. Furthermore, a FM can be used in some critical sections (such as curves) to reduce the friction coefficient, however they would not be applied at inclines where higher friction levels would be needed for traction and braking. Friction control at the top of the rail has been used in

* Corresponding author: Haohao DING, E-mail: haohao.ding@swjtu.edu.cn

railway maintenance using liquid or solid FMs at the wheel-rail interface to reduce the friction coefficient, thereby reducing the wheel-rail wear, damage, and noise [9–13].

FMs can be applied by trackside applicators or from train-mounted systems, which are popular because no access to the track is required and the amount of FM used can be easily controlled. Considering the classification, top-of-rail FMs are available in the form of solid sticks, liquids/solutions, foam, and gels [14]. In addition, FMs for applications are divided into passenger transit (conventional trains), high-speed railways, freight corridors, and mixed traffic. The solid form of FM, often referred to as high positive friction (HPF) [14, 15], is provided with the active components embedded in a thermoset polymeric matrix, and the HPF sticks are applied directly to the wheel tread. Then, under load via a constant force spring, the HPF stick material is transferred to the wheel, and the resin material oxidizes under high temperatures at the wheel-rail interface. This leaves a thin film of the dry solid FM, which plays a role in managing the friction coefficient at the wheel-rail interface.

Third bodies applied to the rail head or wheel tread surfaces, such as deliberately applied sand, can compromise the wheel-rail electrical contact and result in loss of train detection owing to the resistance of third body layers in wheel-rail contact (wheel-rail isolation) [16]. However, the HPF solid modifier does not cause wheel-rail isolation [14].

Water-based friction management has some disadvantages [17], including quicker vaporization in high-contact-temperature scenarios, such as high axle loads, hot weather, and tight curves. Furthermore, Eadie et al. [13] studied a water-based suspension called Keltrack and found that the FM application had a very small pass effect compared to dry conditions. There is an optimum amount of FM and increasing application beyond this amount has no extra benefits. FMs can be used to increase or decrease the friction level at wheel-rail interfaces. Many FMs have been used to increase the friction level at the wheel-rail interface [18, 19], and Lewis et al. [14] summarized that FMs could also been applied to decrease the high friction coefficient (0.6–0.7) to an intermediate level (0.3–0.4), in ways that will improve the braking or accelerating process.

RCF is one of the most common types of damage occurring on wheel-rail surfaces [20, 21]. RCF damage is influenced by many parameters, including wheel-rail materials, loading pressure, lubrication, and running conditions [8, 22]. Meanwhile, the wear and RCF mutually affect each other [23, 24]. Through simulations and experiments, Donzella et al. [25] and Guo et al. [26] found that wear could eliminate RCF cracks on wheel-rail surfaces. A sensitivity analysis showed that the probability of fatigue failure was dependent on the fatigue strength and material defect distribution [27]. The application of a developed criterion for predicting the crack growth for different loading states showed good agreement with the experimental results [28]. It should be noted that the improper application of liquid media (such as liquid lubrication or liquid FM) to the wheel-rail surfaces might accelerate the development of RCF cracks and damage [29, 30] due to hydro-pressurization. Hardwick and Lewis [31] studied the effects of liquid FMs on pre-existing RCF damage cracks and found that a lower viscosity caused faster crack growth. Solid FMs are attracting increasing attention owing to their convenient installation and application. However, the effect of a solid FM on RCF damage has not yet been systematically explored.

In this study, a solid FM is developed. The wheel-rail rolling-sliding tests were conducted with and without solid FM on the MMS-2A rolling-sliding test machine. The effect of a solid FM on friction, wear, and damage was studied. Meanwhile, the RCF surface cracks and subsurface cracks were explored in detail using microscopic methods.

2 Experimental

All tests were performed under dry conditions using an MMS-2A rolling-sliding test machine (Jinian Yihua Tribology Testing Technology Co., Ltd., China), which was previously used in the wheel-rail contact studies [18, 32], as shown in Fig. 1. The upper specimen (wheel roller, 7 in Fig. 1) and lower specimen (rail roller, 6 in Fig. 1) were powered and controlled by the direct-current motor (DC motor, 1 in Fig. 1) through the transmission gears. Different rotational speeds of the

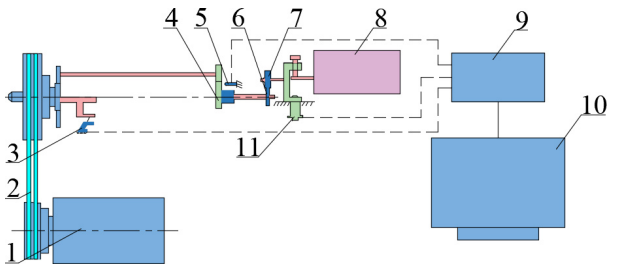

Fig. 1 MMS-2A rolling-sliding test machine. 1-DC motor; 2-belt; 3-torque sensor; 4-driving shaft gear; 5-revolution sensor; 6-lower specimen (rail roller); 7-upper specimen (wheel roller); 8-driven shaft gear; 9-controller; 10-computer; 11-normal force sensor.

upper and lower specimens were achieved by changing the gear pairs. There are six gear pairs to perform six different slip ratios, 0.17%, 0.91%, 2.38%, 3.83%, 4.55%, and 9.43%, respectively. The upper roller is fixed in a swinging bracket, to which a normal force can be applied by a compressed spring. The tangential and normal forces at the wheel-rail interface were measured and recorded automatically on a computer using a torque sensor (3 in Fig. 1, TQ-660, Beijing Shitongkechuang Technology Co., Ltd., China, 0–15 N·m) and a load sensor (11 in Fig. 1, LC-7, Putianshi Hongfei Sensor Co., Ltd., China) (0–2 kN, measurement error ±5%). The test apparatus monitors the parameters of vertical load, friction moments, and friction coefficient in the entire process via a computer program (10 in Fig. 1) and records the parameter variation in real time.

The diameters of the wheel-rail rollers were 40 mm, with a contact width of 5 mm (Fig. 2). Wheel-rail rollers were cut from the CL60 wheel tread and the U75V rail head, respectively. The chemical compositions of the wheel-rail materials are listed in Table 1. The solid FM investigated in this study was developed by us. The composition and production processes are as follows. The composition was polytetrafluoroethylene (PTFE, 40 wt%) + molybdenum (MoS_2 100–300 mesh, 30 wt%) + talcum (10 wt%, 100–300 mesh) + carbon fiber (20 wt%). The production processes were as follows: PTFE, MoS_2, talcum, and carbon fiber powders were mixed, dried for 10–15min at 60–90 °C, and then pressed into a solid cylinder (3–5 MPa, 20–30 min).

Table 1 Chemical compositions of wheel-rail materials (wt%).

Material	C	Si	Mn	P	S
Wheel	0.67–0.77	0.15–1.00	0.60–0.90	≤ 0.03	0.005–0.040
Rail	0.71–0.80	0.50–0.80	0.70–1.50	≤ 0.03	≤ 0.03

During the test, the rotational speed of the rail roller, v_{rail}, was 200 rpm. The rotational speed of the wheel roller, v_{wheel}, was lower than that of the rail roller. The slip ratios ($(v_{rail}-v_{wheel})/v_{rail}$) were 0.17%, 0.91%, 2.38%, 3.83%, 4.55%, and 9.43%, respectively. A normal force of 1,100 N was loaded on the wheel roller, leading to a contact pressure of 900 MPa between the wheel-rail rollers. The solid FM was pressed on the wheel surface with a dead weight (Fig. 3). The contact force between the solid FM and the wheel roller was 10 N.

Two groups of tests were conducted. The first group, Group 1, was designed to study the effect of the solid FM on the friction coefficient. Tests were carried out under dry conditions without the FM for 3 min, and then the solid FM was pressed on the wheel roller for a further 3 min. The solid FM was then separated from the wheel surface and the tests were continued for approximately 15 min. The second group, Group 2, was designed to explore the effect of the solid FM on the wear and damage of the whee-rail materials. Tests were conducted under dry conditions without the FM for 100 min, and then the solid FM was pressed on the wheel surface and tests were continued for a further 200 min. For the tests in Group 2, the slip ratio was 0.91%.

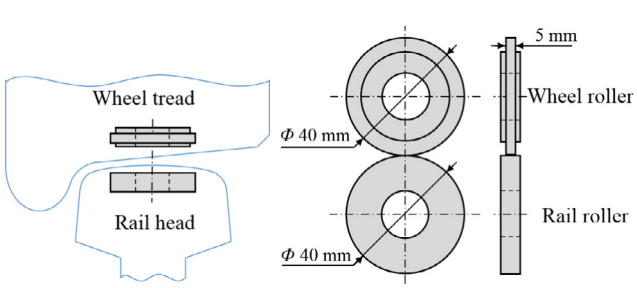

Fig. 2 Geometries and sampling positions of wheel-rail rollers.

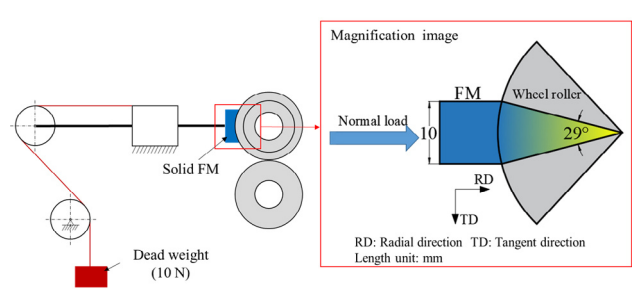

Fig. 3 Feeding method of solid FM on wheel-rail interface.

The wheel-rail rollers were ultrasonically cleaned in ethanol, dried, and weighed using an electronic balance (TG328A, Shangtian Precision Instrument Co., Ltd., China, measurement accuracy: 0.0001 g) before and after testing. The wear rate of the wheel-rail roller was defined as the ratio of weight loss to rolling distance (μg/m). The hardness of the wheel-rail rollers was measured using a Vickers hardness instrument (MVK-H21, Akashi, Japan). The worn surfaces and RCF cracks were inspected using an optical microscope (OM, BX60M, Olympus, Japan) and a scanning electron microscope (SEM, JSM-7001F, JEOL Ltd., Japan).

3 Results

3.1 Friction coefficient

Figure 4 shows the changes in the friction coefficient from the tests in Group 1. In the first 3 min of contact under dry conditions for the six different slip ratios, some tiny cracks were generated in the new wheel-rail rollers. This closely resembles the service state of the wheel-rail surfaces in the field. Conversely, if a solid FM is applied to a new wheel-rail interface, it is difficult to initiate surface damage. Hardwick et al. [31] has demonstrated the benefits of pre-existing RCF cracks for this solid FM friction management experimental study. The friction coefficients were relatively high. When the solid FM was applied after 3 min, all the friction coefficients decreased. After the solid FM was separated after 6 min, the friction coefficient increased gradually to its previous level.

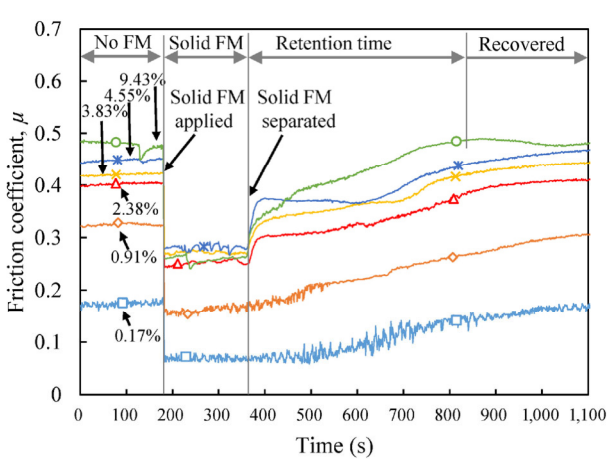

Fig. 4 Friction coefficient as a function of time.

Based on the friction coefficient curves (Fig. 4), the average friction coefficients under dry conditions without any FM (0–3 min) and with the solid FM applied (3–6 min) could be obtained, as shown in Fig. 5. It is clear that as the slip ratio increases, the friction coefficient increases sharply when the slip ratio is less than approximately 1%, and then remains relatively stable when the slip ratio is greater than 1%. When a solid FM was applied, the stable friction coefficient decreased from the range of 0.4–0.5 to 0.2–0.3.

As shown in Fig. 4, after the FM was separated from the wheel surface, the friction coefficient remained relatively low and then increased gradually, which means that the FM continued to work at least partially, for a period of time. The time before the friction coefficient recovered to the level before the application of the FM was defined as the retention time. Figure 6 shows the retention time for different slip ratios. It is clear that as the slip ratio increases, the retention time of the solid FM decreases.

3.2 Wear of wheel-rail materials

To explore the effect of the solid FM on the wear and damage of wheel-rail materials, tests were performed

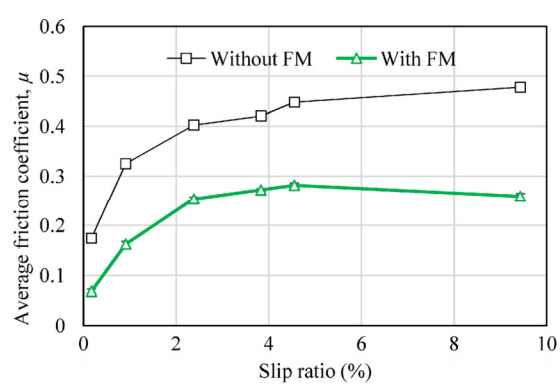

Fig. 5 Average friction coefficient as a function of slip ratio.

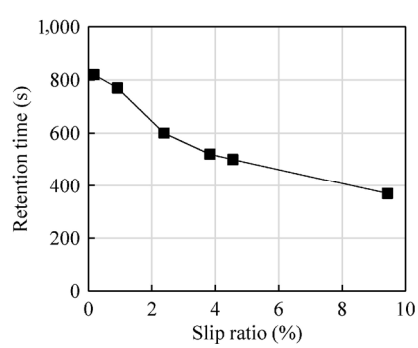

Fig. 6 Retention time as a function of slip ratio.

without the FM for 100 min, and then continued for 200 min with or without the FM at a slip ratio of 0.91%. Figure 7 shows the wear rates of the wheel-rail rollers. The wear rate γ in the test was defined by the following equation:

$$\gamma = \frac{\gamma_a - \gamma_b}{L} \tag{1}$$

where γ_a and γ_b are the sums of the weights of the wheel-rail rollers before and after the wear tests, respectively, and L is the rolling contact distance between the wheel-rail rollers. With FM, the wear rates of wheel-rail were decreased to 50% and 65% of those without FM.

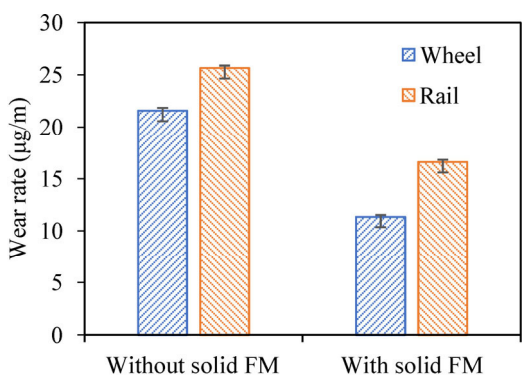

Fig. 7 Wear rates of wheel-rail.

3.3 Surface and subsurface damages

Under dry conditions without the FM, the worn wheel surface was relatively smooth with some pits. The surface damage of the rail was more severe than that of the wheel surface. Figure 8 shows OM images of the worn surfaces on the wheel-rail rollers under dry conditions with the FM. The OM observations indicate that the application of the solid FM had no apparent effect on the wheel damage, and only a few small pits were observed, however there was slight rail damage.

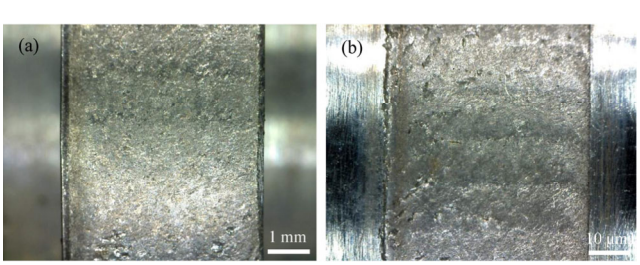

Fig. 8 OM images of worn surfaces with solid FM applied: (a) wheel and (b) rail.

Figure 9 shows the hardness of the cross sections of the wheel-rail rollers. With the solid FM, the surface hardness values of the wheel-rail rollers were clearly lower than those under the dry conditions without the FM. Meanwhile, the hardness gradually decreased with depth increasing. Furthermore, with the solid FM, the decrease in hardness was sharper. Thus, the hardening layers on the wheel-rail rollers with the application of solid FM were thinner than those without FM. Figure 10 shows the plastic deformation of the wheel-rail materials. With the solid FM, the thicknesses of the plastic deformation layers of the wheel-rail materials (60–70 μm) were smaller than those under the dry conditions without the FM (80–100 μm). The plastic deformation and hardening behaviors are closely related to the friction coefficient. Under cyclic rolling-sliding tests, the friction force led to the plastic flow of the wheel-rail materials. The microstructures

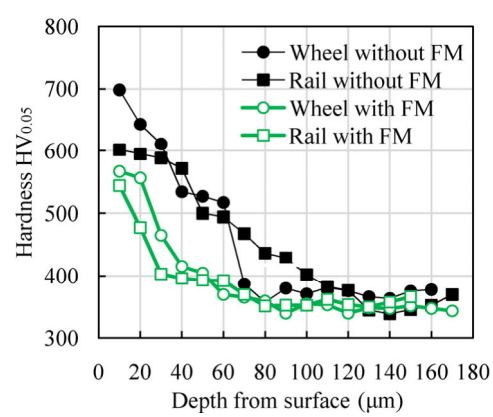

Fig. 9 Hardness of wheel-rail as a function of depth.

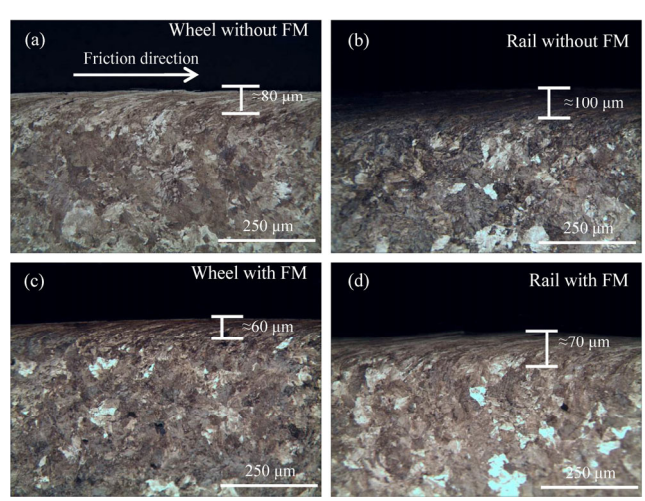

Fig. 10 Plastic deformation without FM applied: (a) wheel and (b) rail; with solid FM applied: (c) wheel and (d) rail.

were deformed, broken, and refined under cyclic loads, resulting in work hardening. With the application of the FM, the friction coefficient was lower; thus, the plastic deformation layer and hardness value were also lower.

Figure 11 shows the OM images of the RCF cracks on the cross sections of the wheel-rail roller. With the solid FM, Figs. 11(a) and 11(b) show that fewer cracks were generated than those without FM. Meanwhile, as shown in Fig. 11(b), more cracks were generated on the rail roller than on the wheel roller. The length, depth, and angle of the RCF cracks were measured, as shown in Fig. 12. The depth of the cracks decreased on the wheel rollers, but there was almost no change on the rail rollers. Under cyclic normal and friction forces, plastic deformation accumulates. When the surface shear stress exceeded the strain limit of the wheel-rail materials, cracks were initiated and developed further.

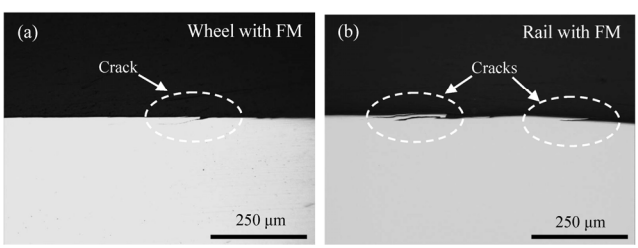

Fig. 11 OM images of RCF cracks on cross sections with solid FM applied: (a) wheel and (b) rail.

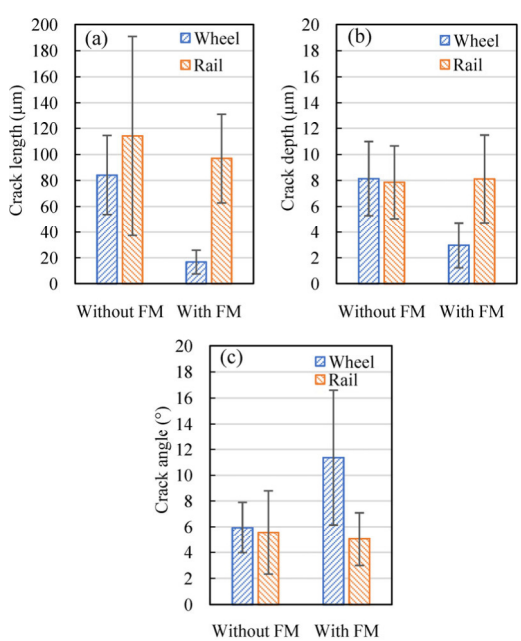

Fig. 12 RCF cracks: (a) length, (b) depth, and (c) angle.

In the current study, under dry conditions without the FM, the cracks tended to propagate along the plastic deformation line. Subsurface cracks were also generated. Figure 13 shows SEM images of RCF cracks on the wheel-rail roller with the FM application. It can be seen that the RCF crack fractured under cyclic loads, leading to wear loss of the material. With the solid FM applied as shown in Figs. 13(a) and 13(b), the RCF damage was milder and no subsurface cracks were observed. Owing to the friction force, the maximum stress occurred at the subsurface. Without the FM, the friction force was high, which promoted the generation of subsurface cracks. With the FM, the friction force was low; thus, cracks tended to initiate at the surface.

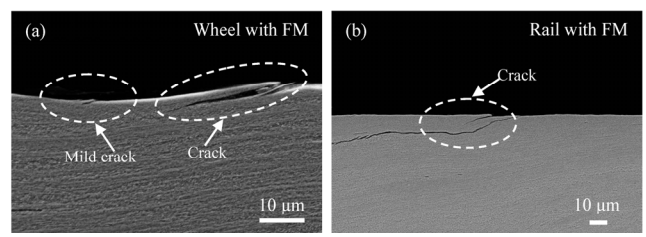

Fig. 13 SEM images of RCF crack with solid FM applied: (a) wheel and (b) rail.

4 Discussion

4.1 Effect of solid FM on friction

It is clear that the FM caused the friction coefficient to decrease (Figs. 4 and 5). The decrease rates were approximately 61%, 50%, 37%, 35%, 37%, and 46% for the slip ratios of 0.17%, 0.91%, 2.38%, 3.83%, 4.55%, and 9.43%, respectively. The reduction in the friction coefficient was due to the lubrication properties of PTFE and MoS_2, which were the main compositions of the solid FM. After the solid FM was separated from the wheel roller, the friction coefficient did not return to a high level immediately. It remained relatively low and then gradually increased (Fig. 4). This is because when the FM was separated, the FM material remained on the wheel-rail surfaces or trapped in the micro-concaves as shown in Fig. 14(b). The residual material decreases the friction for a period of time (the retention time). This means that solid FM can be applied periodically. With an increase in the slip ratio, the friction force (Fig. 5) increased and the

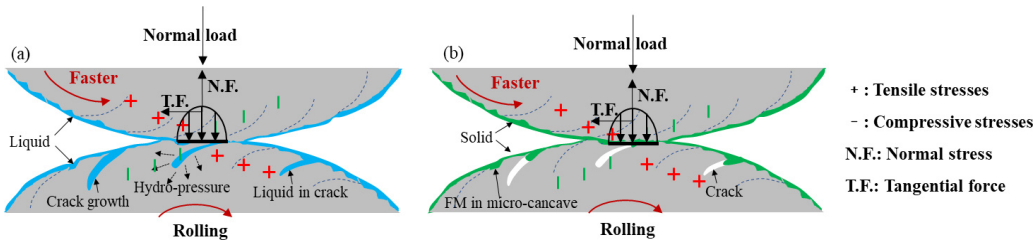

Fig. 14 Effect of FM on RCF cracks: (a) liquid and (b) solid.

wear of the wheel-rail surfaces increased as well [26]; therefore, the residual FM was removed more rapidly as the slip ratio increased and the retention time decreased accordingly (Fig. 6).

4.2 Effect of solid FM on RCF damage

The RCF of the wheel-rail materials is mainly caused by cyclic loading on the wheel-rail interface. Under the condition of cyclic contact loading, each cycle of the rolling contact load causes plastic deformation and material hardening. The plastic flow and strain hardening of wheel materials can accumulate up to failure, which can lead to the generation of fatigue cracks and even RCF failures [33]. Thus, thin flakes of material were detached, causing wear of wheel-rail materials [34–36]. With the increase in cumulative plastic deformation, tiny fatigue cracks may initiate on the roller surface if the stress in the contact zone exceeds the elastic shakedown limit of the wheel-rail materials. In addition, the maximum shear force occurs on the contact surface of the wheel-rail under dry conditions. FMs can be applied to the top of the rail to achieve an intermediate friction coefficient in the third body layer. This reduces the traction forces without compromising the braking or friction.

In the current study, compared with the wheel-rail interface without FM, the tangential force (i.e., the friction coefficient multiplied by the constant normal force) with the solid FM decreased by approximately 50% (under a slip ratio of 0.91%, Fig. 5). Thus, the plastic deformation (Fig. 10) and hardening (Fig. 9) were milder. The average length of the RCF cracks decreased (Figs. 12 and 13), and the wear rates of the wheel-rail materials decreased (Fig. 7). Thus, the application of the solid FM decreases the friction coefficient and alleviates the wear and RCF damage of the wheel-rail materials.

Both liquid and solid FMs are used on trains. In our previous studies, we found that the liquid FMs (or liquid lubricants) could decrease the friction coefficient, but they might lead to severe RCF damage to the wheel-rail surfaces if improperly applied [37]. This is because the liquid can easily flow into the cracks, as shown in Fig. 14(a). When one surface moved against the crack opening direction in the other surface, the crack mouth was first closed, and then the trapped liquid caused a high hydro-pressure under the normal force that accelerated the growth of RCF cracks. For the solid FM as shown in Fig. 14(b), the FM does not easily flow into the cracks; thus, severe RCF damage can be avoided during the rolling-sliding condition. Therefore, solid FMs should have more suitable applications in the field because of the reduction in both friction and RCF damage.

From the results, it can be seen that using the new FM can effectively decrease the wear and RCF of wheel-rail surfaces. Simultaneously, the FM is also a third-body medium (like other foreign objects, such as sand, leaves, and contaminants). Our study can be used to support the wheel-rail contact model considering friction and RCF under a third-body medium. This would be helpful to further understand the phenomenon of wheel-rail friction coefficient in the presence of a third medium.

5 Conclusions

1) The friction coefficient was dependent on the slip ratio and solid FM. With an increase in the slip ratio, the friction coefficient increased sharply when the slip ratio was below 1% and then remained stable. When solid FM was applied, the friction coefficient decreased. After the solid FM was separated from the wheel-rail interface, the friction coefficient increased gradually, and the retention time decreased with the slip ratio.

2) With the application of the solid FM, the wear rates of the wheel-rail were decreased to 50% and 65%, respectively, of those without FM at a slip ratio of 0.91%. The thicknesses of the plastic deformation layers of the wheel-rail were reduced from 80–100 μm to 60–70 μm. The surface hardness of the wheel-rail decreased from 600–700 $HV_{0.05}$ to approximately 550 $HV_{0.05}$.

3) The worn surfaces of the wheel-rail were dominated by pits and RCF cracks. With the application of the solid FM, the average lengths of cracks were reduced from 84–120 μm to 17–97 μm. Meanwhile, subsurface cracks were generated in the absence of the FM, but no subsurface cracks were observed with the application of the solid FM.

Acknowledgements

This study was supported by the National Key R&D Program Intergovernmental Key Items for International Scientific and Technological Innovation Cooperation (No. 2018YFE0109400), Sichuan Science and Technology Program (No. 2020YFH0057), and Fundamental Research Funds for the Central Universities (No. 2682020CX29). The study was also carried out under the Project 8JCH1042 with financial support from the Ministry of Education, Youth and Sports of the Czech Republic.

Open Access This article is licensed under a Creative Commons Attribution 4.0 International License, which permits use, sharing, adaptation, distribution and reproduction in any medium or format, as long as you give appropriate credit to the original author(s) and the source, provide a link to the Creative Commons licence, and indicate if changes were made.

The images or other third party material in this article are included in the article's Creative Commons licence, unless indicated otherwise in a credit line to the material. If material is not included in the article's Creative Commons licence and your intended use is not permitted by statutory regulation or exceeds the permitted use, you will need to obtain permission directly from the copyright holder.

To view a copy of this licence, visit http://creativecommons.org/licenses/by/4.0/.

References

[1] Buckley-Johnstone L E, Trummer G, Voltr P, Six K, Lewis R. Full-scale testing of low adhesion effects with small amounts of water in the wheel/rail interface. *Tribol Int* **141**: 105907 (2020).

[2] Galas R, Omasta M, Shi L, Ding H, Wang W, Krupka I, Hartl M. The low adhesion problem: The effect of environmental conditions on adhesion in rolling-sliding contact. *Tribol Int* **151**: 106521 (2020).

[3] Zeng D, Xu T, Wang J, Lu L, Meng W, Jiang B, Zou Q. Investigation of the crack initiation of subsurface rolling contact fatigue in railway wheels. *Int J Fatigue* **130**: 105281 (2020).

[4] Shahani A R, Babaei M. The crack propagation path for a system of surface and subsurface cracks and their interactions due to rolling contact fatigue. *Acta Mech* **231**(5): 1751–1764 (2020).

[5] Meacci M, Shi Z Y, Butini E, Marini L, Meli E, Rindi A. A local degraded adhesion model for creep forces evaluation: An approximate approach to the tangential contact problem. *Wear* **440–441**: 203084 (2019).

[6] Butini E, Marini L, Meacci M, Meli E, Rindi A, Zhao X J, Wang W J. An innovative model for the prediction of wheel–Rail wear and rolling contact fatigue. *Wear* **436–437**: 203025 (2019).

[7] Olofsson U. A multi-layer model of low adhesion between railway wheel and rail. *Proc Inst Mech Eng F*: *J Rail Rapid Transit* **221**(3): 385–389 (2007)

[8] Seo J W, Jun H K, Kwon S J, Lee D H. Effect of friction modifier on rolling contact fatigue and wear of wheel and rail materials. *Tribol Trans* **61**(1): 19–30 (2018)

[9] Stock R, Stanlake L, Hardwick C, Yu M, Eadie D, Lewis R. Material concepts for top of rail friction management-classification, characterisation and application. *Wear* **366–367**: 225–232 (2016)

[10] Eadie D T, Santoro M, Powell W. Local control of noise and vibration with KELTRACK™ friction modifier and Protector® trackside application: An integrated solution. *J Sound Vib* **267**(3): 761–772 (2003)

[11] Eadie D T, Kalousek J, Chiddick K C. The role of high positive friction (HPF) modifier in the control of short pitch corrugations and related phenomena. *Wear* **253**(1–2): 185–192 (2002)

[12] Suda Y, Iwasa T, Komine H, Tomeoka M, Nakazawa H, Matsumoto K, Nakai T, Tanimoto M, Kishimoto Y. Development of onboard friction control. *Wear* **258**(7–8): 1109–1114 (2005)

[13] Eadie D T, Elvidge D, Oldknow K, Stock R, Pointner P, Kalousek J, Klauser P. The effects of top of rail friction modifier on wear and rolling contact fatigue: Full-scale rail-wheel test rig evaluation, analysis and modelling. *Wear* **265**(9–10): 1222–1230 (2008)

[14] Lewis R, Gallardo E A, Cotter J, Eadie D T. The effect of friction modifiers on wheel/rail isolation. *Wear* **271**(1–2): 71–77 (2011)

[15] Hardwick C, Lewis S, Lewis R. The effect of friction modifiers on wheel/rail isolation at low axle loads. *Proc Inst Mech Eng F: J Rail Rapid Transit* **228**(7): 768–783 (2014)

[16] Lewis R, Dwyer-Joyce R S, Lewis J. Disc machine study of contact isolation during railway track sanding. *Proc Inst Mech Eng F: J Rail Rapid Transit* **217**(1): 11–24 (2003)

[17] Abbasi S, Olofsson U, Zhu Y, Sellgren U. Pin-on-disc study of the effects of railway friction modifiers on airborne wear particles from wheel-rail contacts. *Tribol Int* **60**: 136–139 (2013)

[18] Wang W J, Liu T F, Wang H Y, Liu Q Y, Zhu M H, Jin X S. Influence of friction modifiers on improving adhesion and surface damage of wheel/rail under low adhesion conditions. *Tribol Int* **75**: 16–23 (2014)

[19] Arias-Cuevas O, Li Z, Lewis R, Gallardo-Hernández E A. Rolling-sliding laboratory tests of friction modifiers in dry and wet wheel-rail contacts. *Wear* **268**(3–4): 543–551 (2010)

[20] Hu Y, Guo L C, Maiorino M, Liu J P, Ding H H, Lewis R, Meli E , Rindi A, Liu Q Y, Wang W J. Comparison of wear and rolling contact fatigue behaviours of bainitic and pearlitic rails under various rolling-sliding conditions. *Wear* **460–461**(4): 203455 (2020)

[21] Hu Y, Zhou L, Ding H H, Tan G X, Lewis R, Liu Q Y, Guo J, Wang W J. Investigation on wear and rolling contact fatigue of wheel-rail materials under various wheel/rail hardness ratio and creepage conditions. *Tribol Int* **143**: 106091 (2020)

[22] Khalladi A, Elleuch K. Effect of surface topography with different groove angles on tribological behavior of the wheel/rail contact using alternative machine. *Friction* **4**(3): 238–248 (2016)

[23] Deters L, Proksch M. Friction and wear testing of rail and wheel material. *Wear* **258**(7–8): 981–991 (2005)

[24] Wang W J, Guo J, Liu Q Y, Zhu M H, Zhou Z R. Study on relationship between oblique fatigue crack and rail wear in curve track and prevention. *Wear* **267**(1–4): 540–544 (2009)

[25] Donzella G, Faccoli M, Ghidini A, Mazzù A, Roberti R. The competitive role of wear and RCF in a rail steel. *Eng Fract Mech* **72**(2): 287–308 (2005)

[26] Guo L C, Zhu W T, He C G, Ma L, Wang W, Liu Q. Analysis on wear and damage characteristics of $U_{75}V$ rail under different slip ratio conditions. *J Mech Eng* **54**(4): 167–175 (2018)

[27] Sandström J. Subsurface rolling contact fatigue damage of railway wheels-a probabilistic analysis. *Int J Fatigue* **37**: 146–152 (2012)

[28] Sajjadi S H, Salimi-Majd D, Ostad Ahmad Ghorabi M J. Development of a brittle fracture criterion for prediction of crack propagation path under general mixed mode loading. *Eng Fract Mech* **155**: 36–48 (2016)

[29] Spiryagin M, Sajjad M, Nielsen D, Sun Y Q, Raman D, Chattopadhyay G. Research methodology for evaluation of top-of-rail friction management in Australian heavy haul networks. *Proc Inst Mech Eng F: J Rail Rapid Transit* **228**(6): 631–641 (2014)

[30] Lu X, Makowsky T W, Eadie D T, Oldknow K, Xue J L, Jia J Z, Li G B, Meng X H, Xu Y D, Zhou Y. Friction management on a Chinese heavy haul coal line. *Proc Inst Mech Eng F: J Rail Rapid Transit* **226**(6): 630–640 (2012)

[31] Hardwick C, Lewis R. The effects of alternative top of rail friction materials on pre-existing rolling contact fatigue cracks. In *Proceedings of the Second International Conference on Railway Technology: Research, Development and Maintenance*, Civil-Comp Press, Stirlingshire, UK, Paper 181, 2014.

[32] Wang W J, Hu J, Guo J, Liu Q Y, Zhu M H. Effect of laser cladding on wear and damage behaviors of heavy-haul wheel/rail materials. *Wear* **311**(1–2): 130–136 (2014)

[33] Kapoor A. Wear by plastic ratchetting. *Wear* **212**(1): 119–130 (1997)

[34] Suh N P. The delamination theory of wear. *Wear* **25**(1): 111–124 (1973)

[35] Hu Y, Zhou L, Ding H H, Lewis R, Liu Q Y, Guo J, Wang W J. Microstructure evolution of railway pearlitic wheel steels under rolling-sliding contact loading. *Tribol Int* **154**: 106685 (2021)

[36] Wang Y, Ding H, Zou Q, Xiao F, Zhang X, Wang W, Guo J, Liu Q. Research progress on rolling contact fatigue of railway wheel treads. *Surf Tech* **49**(5): 120–128 (2020).

[37] Wang W J, Lewis R, Evans M D, Liu Q Y. Influence of different application of lubricants on wear and pre-existing rolling contact fatigue cracks of rail materials. *Tribol Lett* **65**(2): 1–15 (2017)

Jingdong SONG. He received his B.S. degree in transportation from Ludong University, China, in 2013. He received his M.S. degree in vehicle engineering from Southwest Jiaotong University, China, in 2019. He is studying at the Institute of Aeronautics Engine, School of Mechanical Engineering, Xi'an Jiaotong University as a Ph.D. student. He is now focusing on the wheel-rail tribology and surface engineering.

Lubing SHI. He received his B.S. degree in industrial engineering in 2013 from Xi'an Polytechnic University, China. He is studying at the Tribology Research Institute, State Key Laboratory of Traction Power, Southwest Jiaotong University, as a Ph.D. student. He is now focusing on the adhesion of wheel and rail.

Haohao DING. He received his Ph.D. degree in materials science from Ecole Centrale de Lyon, France, in 2018. Then he joined the Tribology Research Institute, State Key Laboratory of Traction Power, Southwest Jiaotong University, China. His current position is an assistant professor. His research interests include the wheel-rail tribology, laser surface treatment, coating, etc.

Radovan GALAS. He received his B.S., M.S., and Ph.D. degrees in mechanical engineering from Brno University of Technology, Czech Republic, in 2011, 2013, and 2018, respectively. His current position is an assistant professor and a member of Railway Research Group at Institute of Machine and Industrial Design, Faculty of Mechanical Engineering, Brno University of Technology. His research focuses on wheel-rail tribology, especially on friction management methods.

Milan OMASTA. He received his B.S., M.S., and Ph.D. degrees in mechanical engineering from Brno University of Technology, Czech Republic, in 2007, 2009, and 2013, respectively. His current position is an assistant professor and the head of Railway Research Group at Institute of Machine and Industrial Design, Faculty of Mechanical Engineering, Brno University of Technology. His research areas cover friction and lubrication between wheel and rail and elastohydrodynamic lubrication.

Wenjian WANG. He received his Ph.D. degree in mechanical design and theory from Southwest Jiaotong University, China, in 2008. Then he continued to work at the Tribology Research Institute, State Key Laboratory of Traction Power, Southwest Jiaotong University. His current position is a researcher. His research interests include the wheel-rail friction control technology, wheel-rail wear and damage evaluation technology, laser surface treatment, etc.

Jun GUO. He received his Ph.D. degree in mechanical design and theory from Southwest Jiaotong University, China, in 2007. Then he continued to work at Southwest Jiaotong University. His current position is a researcher. His research interests include the rail grinding technology, wheel-rail wear, rolling contact fatigue, etc.

Qiyue LIU. He received his Ph.D. degree in mechanical design and theory from Southwest Jiaotong University, China, in 1999. Then he continued to work at the Tribology Research Institute, State Key Laboratory of Traction Power, Southwest Jiaotong University. His current position is a professor. His research interests include the tribology, wheel-rail service and reliability, mechanical engineering, etc.

Martin HARTL. He received his M.S. and Ph.D. degrees in mechanical engineering from Brno University of Technology, Czech Republic, in 1990 and 1997, respectively. His current position is a professor and the head of Institute of Machine and Industrial Design, Faculty of Mechanical Engineering, Brno University of Technology. His research areas cover the boundary, mixed and elastohydrodynamic lubrication, roughness effect, and biotribology.

Wear 523 (2023) 204870

Contents lists available at ScienceDirect

Wear

journal homepage: www.elsevier.com/locate/wear

Wheel/rail adhesion and damage under different contact conditions and application parameters of friction modifier

Wenjian Wang [a], Shengjie Li [a], Haohao Ding [a], Qiang Lin [a,*], Radovan Galas [b], Milan Omasta [b], Enrico Meli [c], Jun Guo [a], Qiyue Liu [a]

[a] Tribology Research Institute, Traction Power State Key Laboratory, Southwest Jiaotong University, Chengdu, 610031, China
[b] Faculty of Mechanical Engineering, Brno University of Technology, Technicka 2896/2, 616 69, Brno, Czech Republic
[c] Department of Industrial Engineering, University of Florence, Via S. Marta 3, 50139, Firenze, Italy

ARTICLE INFO

Keywords:
Friction modifier
Application parameter
Adhesion coefficient
Wheel/rail damage

ABSTRACT

Friction modifier (FM) is a newly developed third medium to control the service performance of wheel/rail. The wheel/rail performance is influenced by the wheel/rail contact conditions and FM application parameters. Therefore, the effects of FM application parameter and the wheel/rail contact parameters on the adhesion and damage behaviors of wheel and rail materials should be explored. In this study, the influences of application amount of FM, the wheel/rail contact stress and the creepage on the adhesion and damage behaviors were studied using a twin-disc machine. Results indicated that the increase in contact stress would reduce the wheel/rail minimum adhesion coefficient and effective holding time of FM. The increase in the creepage would increase the adhesion coefficient and reduce the holding time. Under the wheel/rail contact stresses of 800 and 1100 MPa, the application of FM could reduce wheel/rail wear and damage. But under 1500 MPa, FM could cause serious rail surface damages. Moreover, the surface crack propagation process of rail mainly included three stages: initial stage, transition stage and rapid propagation stage. The "oil wedge effect" was the main mechanism for aggravating the surface damages of rail under 1500 MPa.

1. Introduction

Railway occupies an important role in the economic development of various countries in the world. With the rapid development of railway transport, the daily operation and maintenance of the wheel/rail system are facing new technical challenges [1,2]. Especially for the freight railways and urban rail systems with small curve radii, wheel/rail wear (wheel polygonal wear, rail corrugation, rail side wear, etc.), surface damages and friction noise have become key issues for affecting running safety and passenger comfort [3–6]. The solutions to the above problems mainly include wheel/rail material optimization and wheel/rail friction modification strategies [7].

In recent years, wheel/rail friction modification technologies and related products have gradually been widely developed and applied in field. The wheel/rail friction modification can be divided into two categories: rail side lubrication and top-of-rail (TOR) friction modification. Through spraying oil, grease or other lubricants on the rail side or the wheel flange, the friction coefficient could reach 0.1 or smaller, so as to solve the problems of rail side wear and friction noise [8]. Unlike the rail side lubrication, TOR friction modification is to apply lubricating material (TOR friction modifier) on the rail top surface directly [9]. In order to avoid affecting the safety of train operation, TOR friction modifiers should have a "medium friction coefficient level", that is, the friction (adhesion) coefficient of the wheel tread/railhead interface is controlled to the range of 0.1–0.3 [10]. So, the TOR friction modification technology not only decreases the friction, but also meets the adhesion coefficient requirement for normal traction and braking of trains [11]. The TOR friction modification related products have been developed and used since the 1990s. They were first applied to the Vancouver urban rail system to solve the problem of corrugation of small-radius curved rails [12], and were gradually promoted to North America, New Zealand, Europe, China freight railways and the field of urban rail transit. Nowadays, the TOR friction modification has become an important friction reduction technology to prolong the service life of rails and reduce the cost of railway operation and maintenance.

The friction modifiers (FMs) currently developed and used mainly

* Corresponding author.
E-mail address: linqiang@swjtu.edu.cn (Q. Lin).

https://doi.org/10.1016/j.wear.2023.204870
Received 18 September 2022; Received in revised form 1 February 2023; Accepted 3 February 2023
Available online 31 March 2023
0043-1648/© 2023 Elsevier B.V. All rights reserved.

include solid, oil-based and water-based FMs. In the early 1990s, solid FMs began to be used in the Vancouver rail transit system [13]. Field application found that this kind of FM could effectively suppress the corrugation of small-radius curved rails, but the disadvantage was that it was not easy to control its application amount. Galas et al. [14] found that the application of oil-based FMs could significantly reduce the adhesion coefficient. Compared with the dry condition, the wear and contact surface roughness of the wheel/rail samples could be significantly reduced. But the "oil wedge effect" occurred when it was applied improperly. Moreover, when the application amount of oil-based FM was too large, the low adhesion phenomenon of wheel/rail contact interface would occur. In order to better adjust the adhesion coefficient of the TOR, water-based FMs were developed and used in the late 1990s [15]. The constituent materials of these water-based FMs were designed according to the required adhesion level. Generally, water-based FMs contained water, solid lubricants, binders, FM granules, and wetting agents, etc. [16]. After the water-based friction was applied to the wheel/rail contact interface, the internal dispersion medium such as water would volatilize, a solid lubricating film (similar to the solid FMs) was formed on the wheel/rail contact interface which was not easy to be carried and transmitted with the running of the locomotive comparing with the oil-based FM. Since the late 1990s, in order to better understand the effect of water-based FMs, a large number of laboratory and field studies were conducted. Stock et al. [17] proved via laboratory tests that water-based FMs could effectively reduce wheel/rail wear and rolling contact fatigue damages. Tomeoka et al. performed laboratory and field experiments and demonstrated the positive effect of water-based FMs on decreasing derailment possibility and noise of railway systems in different countries' railway systems [18]. Besides noise reduction, the effect of FMs on the formation and development of rail corrugation have been intensively studied [19,20]. The results showed that the application of FMs on the TOR could reduce or completely avoid the development of rail corrugation. Egana et al. [21] used a water-based FM to the curved line in the field, and concluded that the FM could greatly reduce the vertical and lateral accelerations of the wheel/rail system, thereby inhibit the development of rail corrugation.

The effects of TOR FMs, such as modifying wheel/rail friction coefficient [22], suppressing wear [23,24] and surface damages [25–28], alleviating rail corrugation [29], reducing friction noise [30,31], improving bogie curving performance [32] etc., have been extensively studied. Also, the related reasons have been preliminarily explained. The studies found that the application amount of FM and the wheel/rail operating parameters would have significant impacts on the wheel/rail adhesion coefficient and damages. Moreover, in the previous works, the research mainly focused on the effect of application amount of FM on the wheel/rail adhesion coefficient, and the wheel/rail contact conditions were relatively simple. However, the application of FM under different contact conditions is a significant issue for its field application [33–35]. In order to obtain the optimal friction modification performance of FMs, the effects of different FM application parameter (application amount) and wheel/rail contact parameters (contact stress, creepage) on wheel/rail adhesion and damage behavior should be explored. Also, the action mechanism of FM should be systematically clarified. Then, the optimal application parameters could be selected based on the test results, which could provide guidance on the field application strategy [36–38].

Therefore, this paper firstly will explore the influences of application amount of FM and wheel/rail contact parameters (contact stress and creepage) on the wheel/rail adhesion behaviors including the minimum adhesion coefficient and holding time. After that, the influences of FM on the wear rate, plastic deformation and surface damages of wheel/rail materials under different contact stresses will be studied with different initial surface damages. Finally, the abnormal propagation mechanism of rail cracks under large contact stress will be discussed.

2. Experiment details

The tests were carried out on the MJP rolling-sliding wear and contact fatigue apparatus (MJP is the equipment type which is given by the manufacturer) [39]. Two groups of tests were conducted: one group aimed at exploring the influence of FM application conditions (contact stress, creepage and application amount) on the wheel/rail adhesion coefficient. The second group focuses on the effect of applying FM under different contact stresses on the wheel/rail wear and damage behaviors.

The wheel and rail rollers used in the tests were taken from the CL65 wheel tread and the U75V hot-rolled rail head, respectively. The diameters of the rollers were 60 mm and the contact width between two rollers was 5 mm. The sampling position and the sample schematic are shown in Fig. 1. Before the test, the surface roughness (R_a) of the wheel/rail sample was about 0.3 μm, and the values of initial hardness on the circumferential surface of the wheel and rail samples were $330HV_{0.5}$ and $315HV_{0.5}$, respectively. The chemical compositions of the wheel and rail materials are shown in Table 1.

The color of FM product used in this study is charcoal grey, as shown in Fig. 2(a). It is a non-Newtonian fluid and a water-based suspension [16]. The compositions of FM are shown in Table 2.

This FM product is a lubricating material with water as the dispersion medium, which is required to have fluidity and degradability. The volatilization of the water and a small amount of additives in the FM after the application makes it environmentally friendly. In general, the main function of each FM composition is as following: (i) The lubricant, mainly consists of molybdenum disulfide, graphite and polytetrafluoroethylene. They are used to reduce the wheel/rail adhesion coefficient; (ii) The function of the FM granules is to adjust the wheel/rail adhesion coefficient to a medium level, and the main components are magnesium carbonate, talc (magnesium silicate), bentonite (natural clay), kaolinton (aluminum silicate), and various metal oxides; (iii) The function of anticoagulant is to reduce the freezing point of this product and ensure good performance in low temperature environment. The main components of anticoagulant are glycerin, alcohols (propylene glycol or composition); (iv) The rheology agent is mainly consist of bentonite (montmorillonite), carboxymethyl cellulose (CMC), hydroxypropyl methyl cellulose (HPMC) and starch, aiming to increase the suspension performance of various particles and reduce the sedimentation phenomenon; (v) The retaining agent can increase the holding time of adhesion coefficient after using FM. The main components are acrylic acid, polyvinyl alcohol, polyvinyl chloride, acrylic emulsion, acrylic epoxy resin mixture (resin and curing agent); (vi) Defoamers can reduce the bubbles of lubricating materials. The wetting agent can effectively prevent the internal particles from polymerizing and further increase the particle suspension performance.

MoS_2 and $MgSiO_3$ are the main components of lubricant and FM particles, respectively. They play an important role in the performance of FM. Fig. 2 (b) and (c) show the morphology of MoS_2 and $MgSiO_3$ particles, respectively. MoS_2 particles have a lamellar structure, which makes them have good lubrication performance; $MgSiO_3$ particles have irregular particle shape. They can appropriately adjust the low wheel/rail adhesion coefficient to a medium level.

For the first group of tests, they were carried out under four contact stresses (800, 1100, 1250 and 1500 MPa). According to the field measurement and model calculation, the wheel/rail creepage is usually limited in a small range (around 0–5%) in straight and curved sections [40,41]. 1% is the common creepage value obtained from field test [18]. Therefore, five creepages (0.3%, 1%, 2%, 3%, 5%) were chosen for in the test in the present study. Five application amounts (5, 10, 20, 40, 80 μl) were applied under each contact condition. The effects of contact stress, creepage and application amount of FM on the wheel/rail adhesion coefficient (the minimum adhesion coefficient and holding time) were summarized. As shown in Fig. 3, the minimum adhesion coefficient is the minimum value of the adhesion coefficient curve in the whole process from the FM applying moment to the moment when the

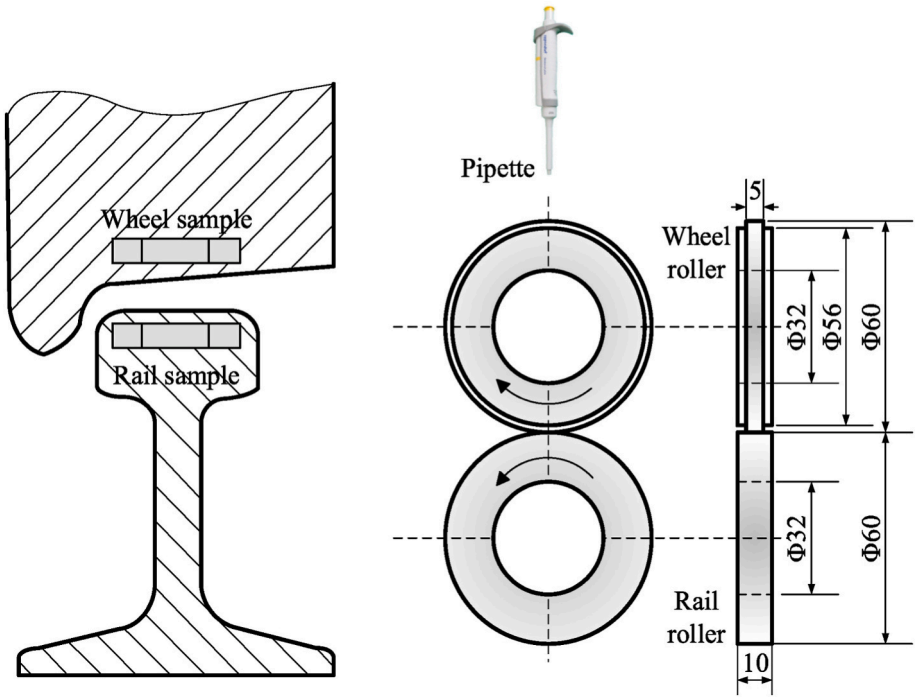

Fig. 1. Sampling positions and sizes of wheel and rail rollers.

Table 1
Chemical compositions of wheel and rail materials (%wt).

Roller	C	Si	Mn	P	S
CL65	0.57–0.67	0.15–1.00	0.60–1.20	≤0.025	≤0.020
U75V	0.65–0.75	0.15–0.58	0.70–1.20	≤0.025	≤0.025

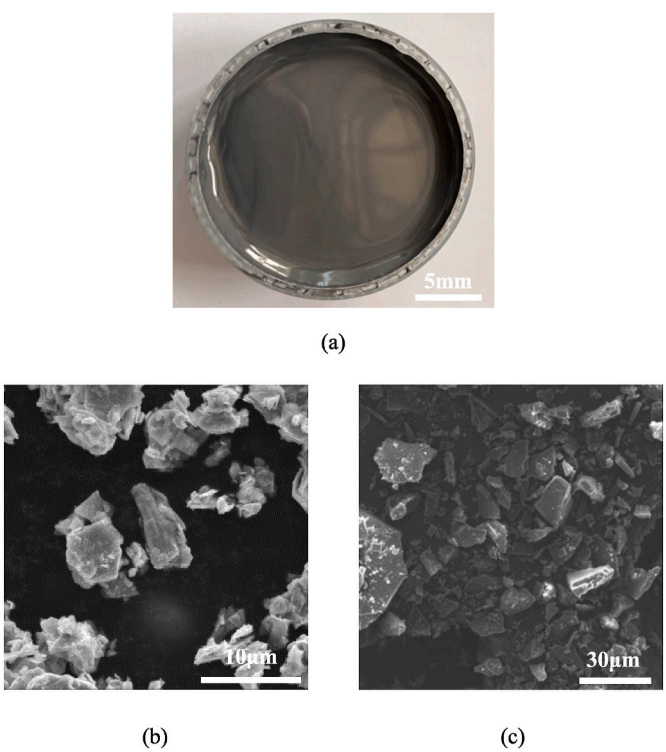

Fig. 2. SEM morphology of FM solid particles: (a) Photograph of FM; (b) MoS_2; (c) $MgSiO_3$.

Table 2
Compositions and contents of the selected FM [16].

Composition	Content (wt%)
Water	50–80%
Lubricant	1–13%
FM granules	1–5%
Anticoagulants	14–21.54%
Rheology agent	1–10%
Defoamer	0.06%
Retention agent	1–16%
Wetting agent	0.002–2%
Antioxidants	0.5–2%

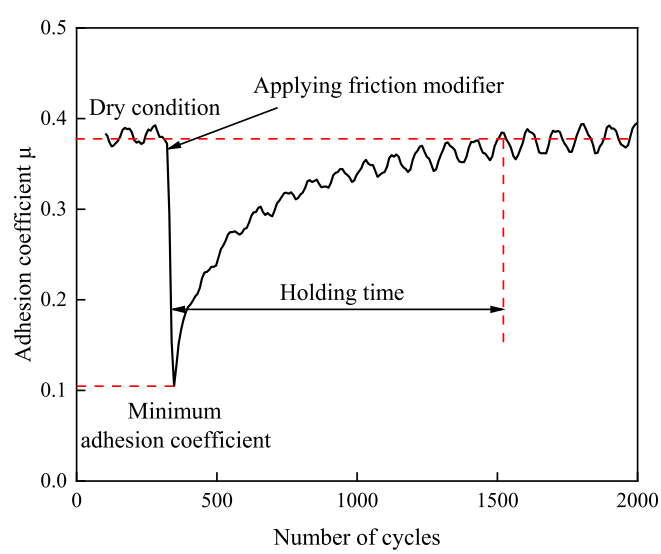

Fig. 3. Adhesion coefficient evolution after FM application.

adhesion coefficient returns to stable states. And the holding time is defined as the total number of revolutions from the FM applying moment to the moment when the adhesion coefficient returns to stable states. The specific test parameters are shown in Table 3. These tests were repeated twice.

For the second group of tests, tests were conducted for 35,000 cycles to investigate the wear and damage of wheel and rail material. Three contact stresses, 800, 1100 and 1500 MPa, were adopted. And, the creepage of 1% (the common creepage value obtained from field test [18]) was set in the test. Furthermore, under actual working conditions, there are certain wear and surface damage on the wheel and rail surfaces [42,43]. However, the finished wheel and rail samples before tests are smooth (no damages). In order to be closer to the actual working conditions, pre-worn test was performed to obtain the worn wheel and rail rollers in this study, which can simulate the surface state of on-site wheel and rail. Therefore, some tests (such as test 2-2# in Table 4) run 10,000 cycles in dry condition to produce cracks and then FM was added for 25,000 cycles; the other tests (such as test 2–3#), FM was added on the wheel/rail rollers without pre-worn. Meanwhile, tests without FM (such as test 2-1#) were conducted as comparison. During the tests with FM, FM was applied again when the wheel/rail adhesion coefficient recovered to 0.3. All the tests in this part were repeated twice, and the test parameters are shown in Table 4.

3. Results

3.1. Wheel/rail adhesion behaviors

3.1.1. Adhesion coefficient

Fig. 4 shows the wheel/rail adhesion coefficient curves under different application amounts of FM (5, 10, 20, 40 and 80 μl) under the conditions of 1100 MPa contact stress and 1% creepage. Because the tests were repeated twice, the error bar represents the true values and the average value of the two groups of test data. Fig. 4(a) shows the recovery process of wheel/rail adhesion coefficient. The minimum adhesion coefficients under five application amounts of FMs are shown in Fig. 4(b). It can be indicated that with the increase in the application amount of FM, the minimum adhesion coefficient showed a downward trend. In addition, it can be found that under this wheel/rail contact parameter, the application amount of FM in the range of 5–80 μl would not cause low adhesion risk (i.e., adhesion coefficient is less than 0.1) for the MJP rolling-sliding wear and contact fatigue apparatus. Thus the 5–80 μl per time could be suggested for the on-site FM application.

Although there was no low adhesion phenomenon happened on the wheel/rail contact interface during the increase in the application amount of FM from 5 to 80 μl, the wheel/rail contact parameters (contact stress and creepage) under dry conditions would affect the contact state of the metal micro-convex body on the wheel/rail interface and thus influence the wheel/rail adhesion coefficient [44]. Therefore, it is necessary to study the influence of wheel/rail contact parameters on the adhesion coefficient, so as to reach the optimal FM friction control performance (not only reducing the friction, but also meeting the adhesion coefficient requirement for normal traction and braking of the wheel and rail).

The minimum adhesion coefficients under various wheel/rail contact parameters (contact stress and creepage) are shown in Fig. 5. It can be seen that with the increase in the application amount of FM, the minimum adhesion coefficient showed a downward trend. Changing the wheel/rail contact parameters cannot vary the effect of application amount of FM on the adhesion coefficient. When the application amount of FM was fixed, the change of wheel/rail contact parameters would have a significant impact on the minimum adhesion coefficient. With the increase in the contact stress, the minimum adhesion coefficient showed a decreasing trend. With the increase in the creepage, the wheel/rail minimum adhesion coefficient showed a rising trend. This result was consistent with the result about the influence of contact stress and creepage on the wheel/rail adhesion coefficient under dry condition in reference [45].

In addition, quantitative analysis of the results indicated that the increase in the contact stress would cause low adhesion risk after the FM was applied to the wheel/rail contact interface. Specifically, when the application amount of FM was 80 μl and the contact stress increased from 800 to 1500 MPa, the minimum adhesion coefficient would decrease from 0.13 to the value lower than 0.1, leading to the low adhesion phenomenon. The reduction of the creepage would also cause low adhesion risk. When the creepage was 0.3% and the application amounts of FM were 20, 40 and 80 μl, the minimum adhesion coefficient would reduce to the value lower than 0.1, and the low adhesion phenomenon occurred.

The above results have fully proved that the changes of the contact stress and creepage of the wheel/rail contact interface could lead to the wheel/rail low adhesion phenomenon. In order to further investigate the effect of different contact stresses and creepages on the minimum adhesion coefficient, Fig. 6 shows the minimum adhesion coefficient of the wheel/rail with different contact stresses and creepages when the application amounts of FM were 5, 10, 20, 40 and 80 μl, respectively. It can be seen from the figures that when the application amount of FM was 5 μl, the low adhesion risk under the given parameters would not occur. When the application amounts of FM were 10 and 20 μl, the minimum adhesion coefficient would drop to the value lower than 0.1 with the creepage of 0.3%. When the application amount of FM was 40 μl, the minimum adhesion coefficient reduced to the value lower than 0.1 under the creepage 0.3%. When the application amount of FM was 80 μl, the risk of low adhesion was further exacerbated.

3.1.2. Holding time

The statistical results of the holding time under the five application amounts were shown in Fig. 7. It can be seen from the test results that with the increase in the application amount of FM, the holding time presented a gradually rising trend. There was a negative correlation between the minimum adhesion coefficient and the holding time.

Figs. 8 and 9 were the results of the holding time after applying different amounts of FM under different wheel/rail contact parameters. It can be seen from Figs. 8 and 9 that with the increase in the contact stress, the holding time showed a decreasing trend. With the increase in the creepage, the holding time also showed a decreasing trend. The holding time showed an upward trend when the application amount increases.

3.2. Wheel/rail wear and damage behaviors

According to the above results, the contact stress and creepage of wheel/rail contact interface have significant effects on the minimum adhesion coefficient and holding time. However, the wheel/rail

Table 3
Tests parameters for group one (adhesion).

No.	Contact stress (MPa)	Creepage (%)	Application amount (μl)	Rotation speed (r/min)
1-1#	800	0.3, 1, 2, 3, 5	5, 10, 20, 40, 80	500
1-2#	1100	0.3, 1, 2, 3, 5	5, 10, 20, 40, 80	500
1-3#	1250	0.3, 1, 2, 3, 5	5, 10, 20, 40, 80	500
1-4#	1500	0.3, 1, 2, 3, 5	5, 10, 20, 40, 80	500

Table 4
Tests parameters for group two (wear and damage).

No.	Contact stress (MPa)	Creepage (%)	Rotation speed (r/min)	Working condition	Application amount (μl)	Dry pre-worn (cycle)	Test revolution (cycle)
2-1#	800	1	500	Dry condition	–	0	35,000
2-2#	800			FM	20	10,000	25,000
2-3#	800			FM	20	0	35,000
2-4#	1100			Dry condition	–	0	35,000
2-5#	1100			FM	20	10,000	25,000
2-6#	1100			FM	20	0	35,000
2-7#	1500			Dry condition	–	0	35,000
2-8#	1500			FM	20	10,000	20,000
2-9#	1500			FM	20	0	35,000

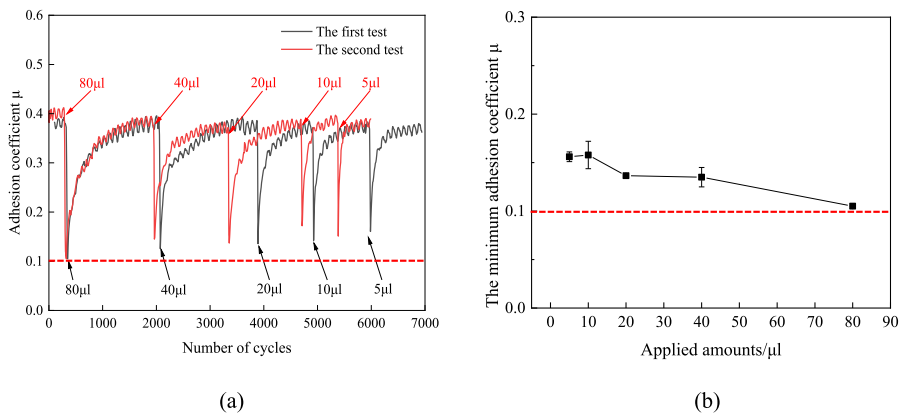

Fig. 4. Adhesion coefficient: (a) as a function of cycle number; (b) the minimum values.

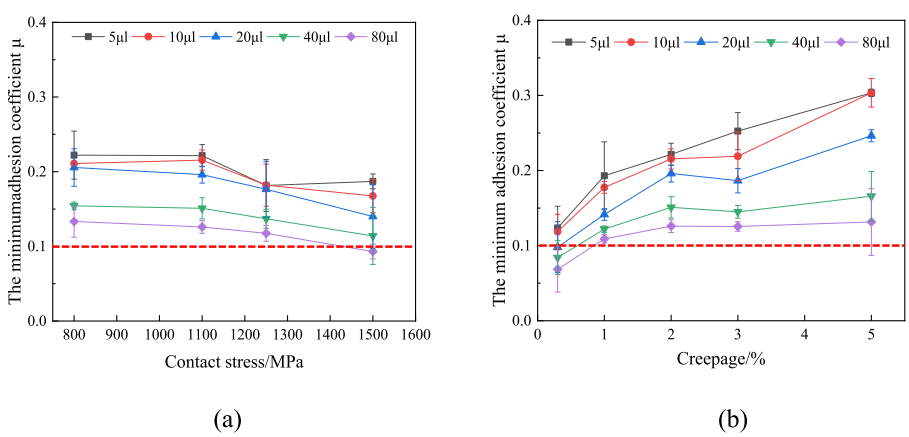

Fig. 5. Minimum adhesion coefficients under different contact parameters: (a) Different contact stresses (Creepage 2%); (b) Different creepages (Contact stress 1100 MPa).

adhesion coefficient is also closely related to its damage behavior. Fig. 10 shows the wheel/rail adhesion coefficient with or without applying FM under three contact stresses of 800, 1100 and 1500 MPa. It can be seen that under dry condition without FM, the adhesion coefficient showed a decreasing trend with the increase in the contact stress, which was the same as the previous research results [45]. Applying the FM can control the wheel/rail adhesion coefficient lower than 0.3, because the FM was applied once when the adhesion coefficient recovers to 0.3.

When the FMs were applied to the pre-worn rollers under three contact stresses, it can be seen that with the increase in the contact stress, the FM holding time decreased significantly, which was the same as the result in section 3.1. Compared with 800 MPa, the minimum adhesion coefficient was further reduced under 1100 MPa, but there was no further decrease under 1500 MPa. When the FMs were applied to the rollers without pre-worn, compared with 800 MPa, the minimum adhesion coefficient and the holding time of the FMs under 1100 MPa was further decreased. Under 1500 MPa, the minimum adhesion coefficient was increased after 10,000 cycles. This might be because the surface cracks were generated on the wheel and rail rollers as the test progresses. Part of FMs entered the surface cracks, but the amount of FM participated in the lubrication of wheel/rail contact interface was reduced, making the minimum adhesion coefficient higher than that in the first 10,000 revolutions.

3.2.1. *Wear rate*

Fig. 11 shows the effect of FM on the wear rates of wheel and rail rollers. Under dry conditions, with the increase in the contact stress, the wear rates increased gradually. Specifically, when the contact stress changed from 800 to 1500 MPa, the wear rates of the wheel and rail

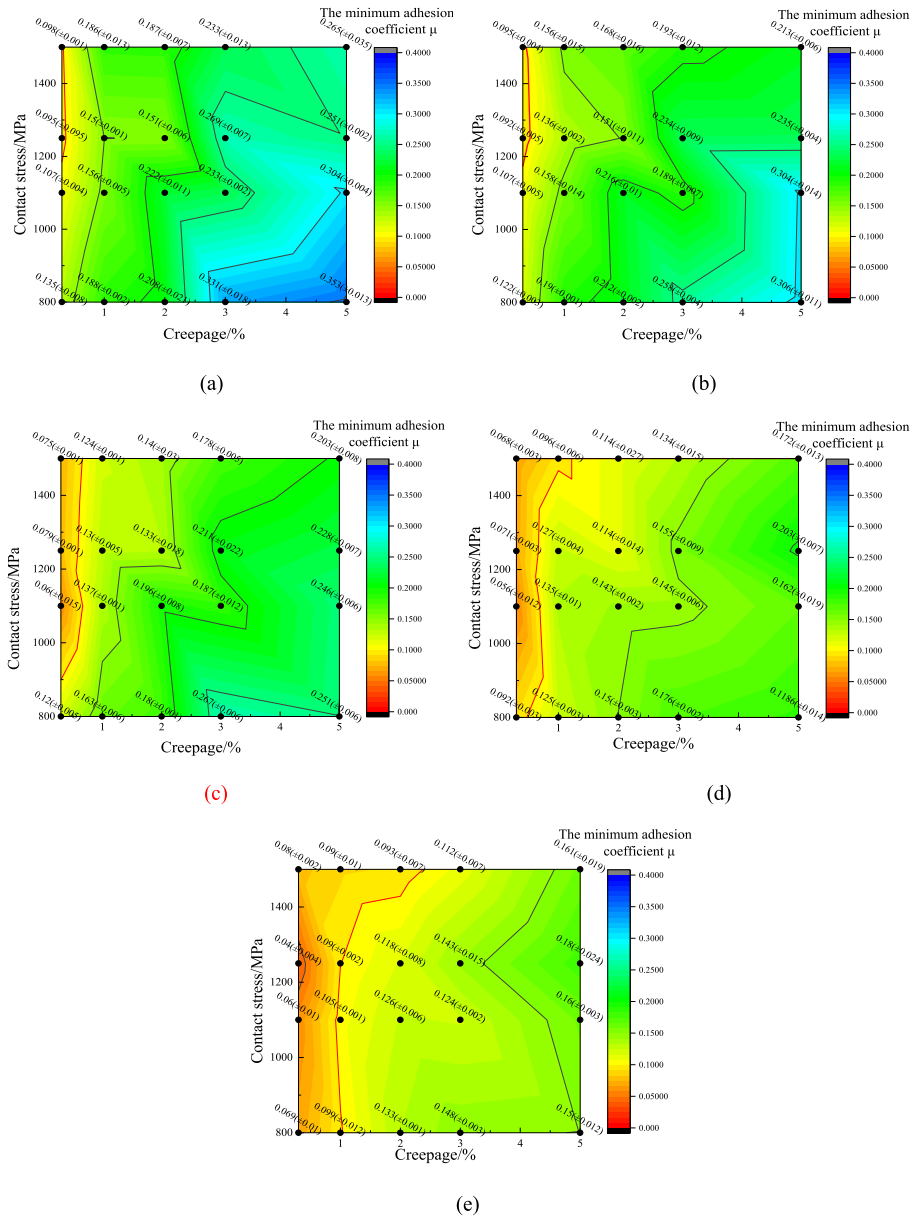

Fig. 6. Contour diagram of minimum adhesion coefficient under different application amount of FMs: (a) 5 μl; (b) 10 μl; (c) 20 μl; (d) 40 μl; (e) 80 μl.

rollers under dry condition increased by 2.34 times and 2.99 times, respectively.

In order to be closer to the actual working conditions, in this part of the tests, the FM was applied to the pre-worn rollers. Compared with the dry condition, the wear rates of the wheel and rail rollers with FM applied were respectively reduced by 87.6% and 39.4% when the contact stress was 800 MPa. The wear rates were reduced by 54.4% and 10.1% under 1100 MPa. When the contact stress was 1500 MPa, the wear rate of the wheel roller reduced by 53.3%, but the wear rate of the rail roller increased by 2.87 times. Contrary to the previous results, applying FM under 1500 MPa would cause abnormal wear of the rail roller (with significant wear rate).

In order to further analyze the reasons for the abnormal wear of the rail samples, this part of the tests applied the FM to the rollers without pre-worn. It could be found that when the contact stresses were 800 and 1100 MPa, the wear rates of the wheel and rail rollers were further reduced compared with the pre-worn wheel and rail rollers. When the contact stress was 1500 MPa, the wear rate of the wheel and rail rollers was reduced by 90.6% and 42.7% compared with the pre-worn wheel and rail rollers. The decreasing trend of the wheel wear rate was consistent with that of other contact stress conditions. But the wear rate of rail roller was still higher than that under dry condition (without FM), and it was still in an abnormal wear state. The above results showed that when the wheel/rail contact parameters remain unchanged, the surface state of the wheel/rail sample would also affect the friction control performance of the FM. Applying FM on the wheel/rail rollers without initial cracks can better exert its friction modification effect.

3.2.2. Surface damages

Figs. 12 and 13 showed the damage morphologies of the wheel and rail surfaces under three contact stresses. There were obvious surface damages under dry conditions. With the increase in the wheel/rail contact stress, the surface damage gradually changed from cracks to peeling and spalling, and the overall damage level gradually increased.

Compared with the dry condition, when the FM was used, the surface damages of the pre-worn wheel and rail rollers were significantly reduced under the contact stresses of 800 and 1100 MPa. There were only a small amount of slight cracks on the surface (Fig. 12(b) and (e),

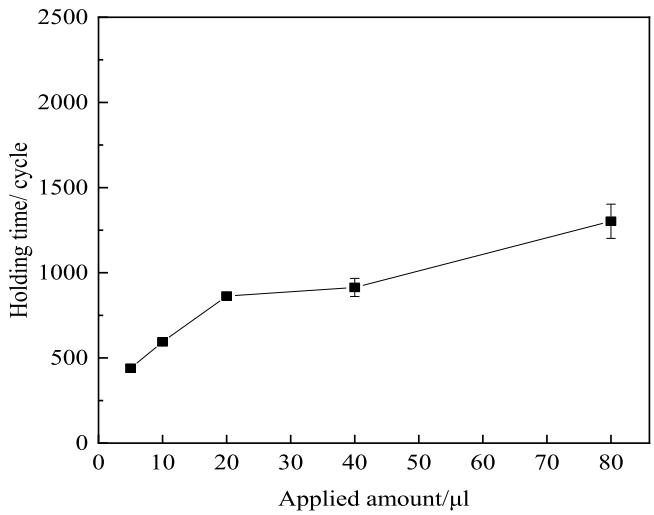

Fig. 7. Holding time under different application amounts of FM (1100 MPa, 1%).

Fig. 13(b) and (e)), and the FM had an obvious effect on inhibiting wheel and rail damages. While the FM was applied under the contact stress of 1500 MPa, although the surface damage of the wheel sample was reduced (only a small amount of microcracks were generated), the surface damage of the rail sample was more serious than those in the dry condition. Severe peeling damage occurred on the rail surface (Fig. 12 (h) and Fig. 13(h)).

When the contact stresses were 800 and 1100 MPa, compared with the pre-worn wheel and rail rollers (Fig. 12(b) and (e)), the surface damage level on the wheel and rail rollers without pre-worn was lightened, and the damages were mainly micro-cracks. This was consistent with the wear rates (Fig. 11). When the contact stress was 1500 MPa, the micro-crack damage on the wheel sample was also further reduced, and the surface peeling damages of the rail sample were still serious (Fig. 12 (i) and Fig. 13(i)).

3.2.3. Plastic deformation

The plastic deformation layers (PDLs) observed on the cross sections of the wheel and rail sample (along the rolling direction) were shown in Fig. 14. The PDL thickness was the largest under the dry condition. With the increase in the contact stress from 800 to 1500 MPa, the PDL thicknesses of wheel and rail rollers were increased from around 99 μm–281 μm and from around 140 μm–339 μm, respectively. The cross section of rail roller appeared many long cracks and the crack opening was large (Fig. 14(h) and (i)).

Table 5 gives the reduction rates of PDL thickness of wheel/rail sample with FM applied. When the FM was applied on the pre-worn rollers, the PDL thicknesses were significantly reduced compared with those without FM. Although the application of FM under 1500 MPa can effectively reduce the work hardening phenomenon of the wheel and rail rollers. When the FM was directly applied on the rollers without pre-worn, the PDL thicknesses of was further reduced compared with those on the pre-worn rollers.

Based on the results in section 3.1, it can be seen that the FM can play a role in reducing friction under heavy load condition (1500 MPa), but the damage was serious accompanied with many long cracks. This was similar to the surface damage of the rail under the application of lubricating oil and grease in previous studies [37], which indicated that the application of FM under heavy load conditions might aggravate the damage of the rail roller due to the “oil wedge effect”.

3.2.4. Surface damage morphology on cross section

Fig. 15 shows the SEM images of surface damage on the cross sections. The crack angle means the angle between the sample surface and the crack develop direction, the crack depth means the depth of the crack tip from the sample surface, and the crack length means the length of the crack propagation path, as shown in Fig. 15(g). The statistical results of the crack length and depth were given in Fig. 16. Under the dry conditions, cracks mainly propagated in a small angle along the direction of the plastic deformation curve. With the increase in contact stress, the surface damages of wheel and rail samples became more serious. Specifically, the crack depth and length increased gradually. The crack angle slightly increased. Under the heavy load condition (1500 MPa), the crack depth, crack length and the number of cracks were the largest, which corresponded to the significant peeling damage observed on the surface.

After the FM was applied under 800 and 1100 MPa, no matter whether added on the rollers with or without pre-worn, the surface cracks propagated at a small angle, the crack length was short, and the degree of surface damage was proportional to the contact stress.

After the FM was applied under the heavy load condition (1500 MPa), damages of the wheel and rail samples showed a significant difference. Compared with the dry condition, the slight damages (mainly shallow cracks) occurred on the wheel sample with the FM applied, and the propagation length and angle of the cracks were significantly reduced (Fig. 15(h) and (i)). This indicated that the FM had obvious effect on reducing wheel damage. On the contrary, after the FM was applied, there were significant surface damages on the rail roller. Surface cracks grew at a small angle first, and then expanded to the inside of the material with a large angle when it extended to a certain length. This expansion type led to a significant increase in the depth and length of the crack. Further observation found that there were branch cracks in the middle of the crack and at the crack tip, and these branch cracks

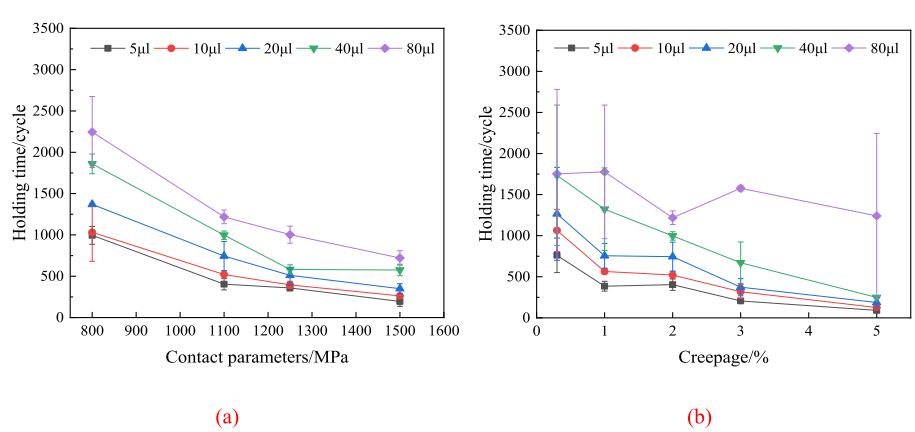

Fig. 8. Holding time under different wheel/rail contact parameters: (a) Creepage (2%); (b) Contact stress (1100 MPa).

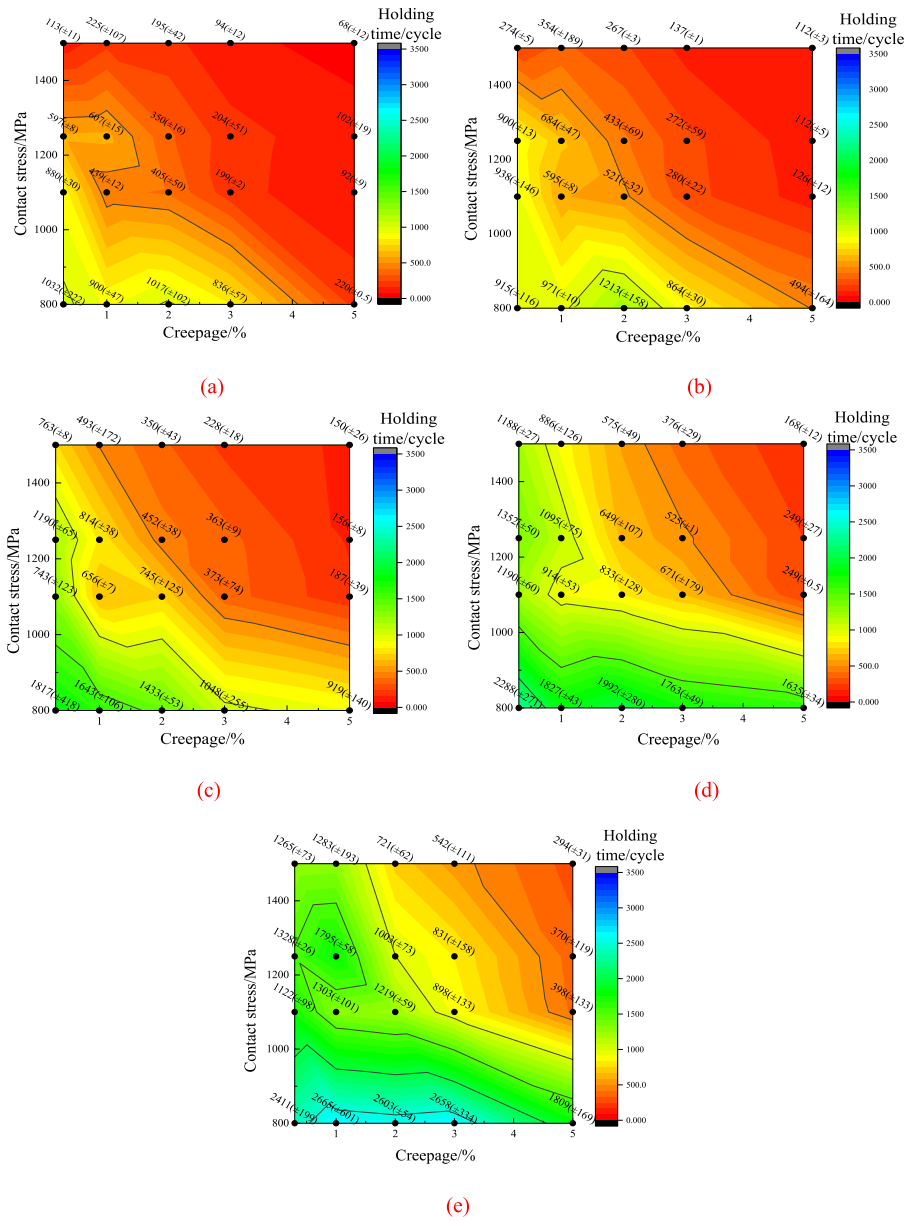

Fig. 9. Contour diagram of FM holding time under different contact stresses, creepages and application amounts: (a) 5 μl; (b) 10 μl; (c) 20 μl; (d) 40 μl; (e) 80 μl.

extended to the inside of the material with a larger angle, thereby further aggravating the surface damage of the rail.

Under 800 and 1100 MPa, the application of FM can effectively reduce the wear rate, surface damages and plastic deformation of wheel and rail rollers. Under heavy load conditions (1500 MPa), the application of FM can only effectively reduce the wear rate, surface damage, plastic deformation and surface damages of wheel rollers, while the wear rate, damage of rail rollers were significantly increased. Although the above series of test results showed that the application of FMs under heavy load conditions would aggravate the surface damage of rail, this doesn't mean that it is not suitable to apply FMs for wear reduction modification under heavy load conditions. On the contrary, heavy haul lines and curve lines on site are the most urgent conditions for friction control from the field investigation. Thus, it is necessary to analyze the mechanism of abnormal wear of rails with FMs under heavy load conditions, and then optimize the application parameters of FMs to prevent rail surface crack propagation into rapid growth stage, so as to obtain the optimal friction control performance, and then provide guidance for the field application.

4. Discussion

4.1. Effects of contact conditions and application parameters of FM on wheel/rail adhesion behaviors

With the increase in the application amount of FM and contact stress, the minimum adhesion coefficient reduced (Figs. 4 and 5(a)). And with the increase in the creepage, the minimum adhesion coefficient rose (Fig. 5(b)). With the increase in the application amount of FM and the wheel/rail contact stress and the decrease in the creepage, low adhesion phenomenon was easy to occur (Fig. 6). When the application amount of the FM increased, the thickness of the formed third body layer increased, the normal load borne by the third body layer increased, and the normal load borne by the metal micro-convex bodies decreased accordingly. Since the shear resistance of the third body layer of the FM was lower than that of the metal micro-convex bodies, the minimum adhesion coefficient would show a downward trend. With the increase in the contact stress, more metal micro-convex bodies participated in the contact. However, according to the Hertz contact theory, the increase

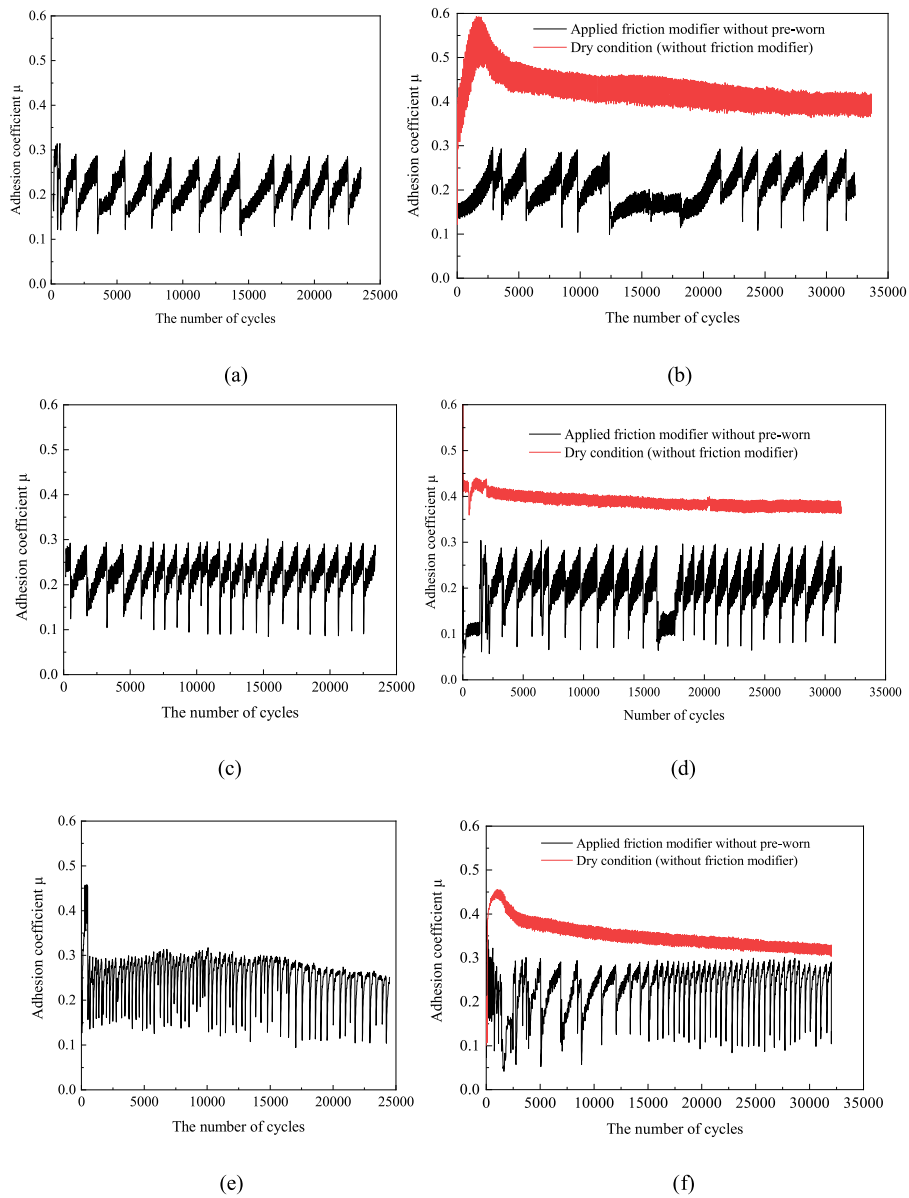

Fig. 10. Wheel/rail adhesion coefficient under different contact stresses: (a) Apply FM (800 MPa); (b) Dry and apply FM without pre-worn (800 MPa); (c) Apply FM (1100 MPa); (d) Dry and apply FM without pre-worn (1100 MPa); (e) Apply FM (1500 MPa); (f) Dry and apply FM without pre-worn (1500 MPa).

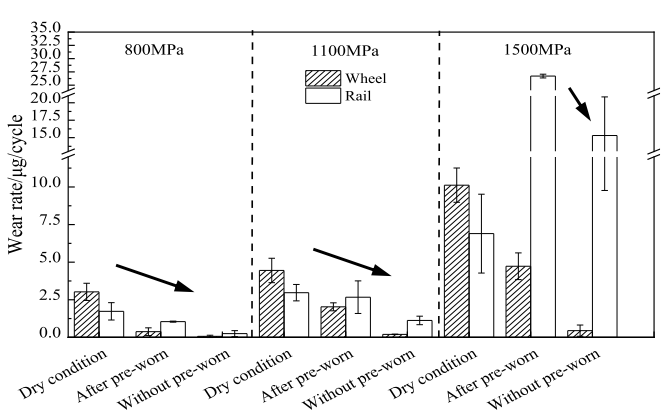

Fig. 11. Wear rate of wheel and rail rollers under different application conditions of FM.

rate of the contact spot area was far less than that of the vertical load. So, the increase of the axle load was greater than the increase of the tangential force, and the minimum adhesion coefficient showed a downward trend. This was consistent with the reason why the adhesion coefficient decreased when the contact stress of the wheel/rail contact interface increased under the dry condition. When the application amount of FM was constant, with the increase in creepage, the solid lubricating layer adhering to the wheel/rail interface was removed more quickly under the action of mechanical shearing, which led to significant increase in the minimum adhesion coefficient.

With the increase in the application amount, the holding time of FM was increased (Fig. 7). With the increase in the contact stress and creepage, the holding time reduced (Fig. 8). The increase in the application amount of FM would raise the thickness of the third body layer on the wheel/rail contact interface. It is natural that the holding time would be longer if the application amount of FM was higher. In addition, with the wheel/rail adhesion coefficient reducing, the consumption rate of the third body layer was reduced, leading to the rise of the holding time. The increase in the contact stress and creepage would raise the

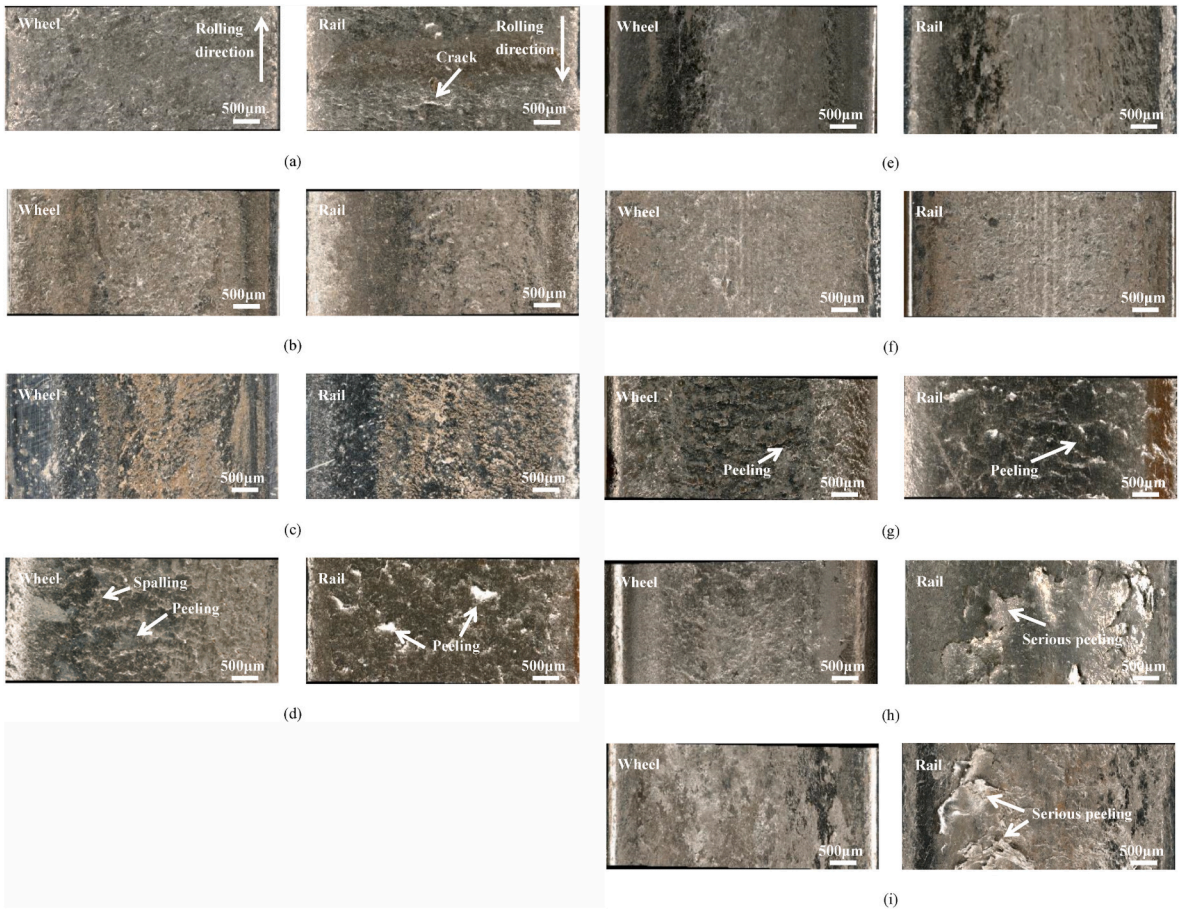

Fig. 12. OM morphologies of wheel and rail rollers under different application conditions of FM: (a) Dry condition (800 MPa); (b) Apply FM after pre-worn (800 MPa); (c) Apply FM without pre-worn (800 MPa); (d) Dry condition (1100 MPa); (e) Apply FM after pre-worn (1100 MPa); (f) Apply FM without pre-worn (1100 MPa); (g) Dry condition (1500 MPa); (h) Apply FM after pre-worn (1500 MPa); (i) Apply FM without pre-worn (1500 MPa).

consumption of the solid lubricant layer between the wheel/rail interface, which would lead to a significant decrease in the holding time.

In Fig. 4, it can be seen that the adhesion coefficient recovered nonlinearly. This phenomenon was mainly related to the consumption of FM and the state of wheel/rail interface (contact pressure, wheel/rail surface wear state). The adhesion coefficient curve was obtained on a new wheel and rail rollers (without pre-worn). Since the consumption of FM was not linear, the consumption of FM was large at the beginning, so the adhesion coefficient changed rapidly. As the number of cycles increased, the amount of remaining FM decreased, and its consumption would slow down, resulting in the slow change of adhesion coefficient. Therefore, the adhesion coefficient showed a nonlinear recovery.

4.2. Influence mechanism of FM on wheel/rail damage under different contact pressures

Under contact pressure of 1500 MPa, significant rail surface damage was produced after applying the FM, and the rail damage was significantly different from that of the wheel rollers on which no obvious surface damages were observed. Even if the FM was added into the wheel/rail interface (without initial cracks), surface cracks would still be formed on the surface of the rail roller as the test progresses. In the rolling-sliding test using the wheel and rail rollers under the dry condition, the rail roller damage was slight [17,46,47]. In this study, the rail damage was serious in the case of the third fluid medium condition. Thus, it can be inferred that the existence of the third fluid medium aggravated the rail damage. Previous studies have proved that the third fluid medium could cause the "oil wedge effect" [37,38], which aggravated the rail damage. Therefore, "oil wedge effect" was considered as the main reason for serious rail damage. Fig. 17 showed a hypothesis illustration of damage propagation progress of wheel and rail cracks after applying FM under the contact pressure of 1500 MPa. The crack propagation process of rail was mainly divided into three stages: initial stage, transition stage and rapid propagation stage.

At the initial stage: in the test, the wheel roller was the driving wheel, and the rail roller was driven wheel which was located above the wheel roller (Fig. 1). After the FM was applied to the contact interface of the rollers without pre-worn (no initial crack), the crack propagation process first entered the initial stage. At this stage, there was no crack on the surface of the wheel and rail rollers. After the FM was applied, the internal water dispersion medium in FM would evaporate rapidly. Furthermore, a solid lubricating film on the contact surface was formed, so that the FM could fully exert its anti-wear effect (Fig. 17(a)).

At the transition stage: as the increase in the number of cycles, the wheel and rail cracks began to initiate and expand under the action of the cyclic contact stresses. Affected by the wheel/rail tangential force, the direction of the plastic deformation curve was more consistent with the direction of the wheel/rail tangential force, as shown in Fig. 17(a). In the process of wheel/rail rolling contact, cracks would be formed on the wheel/rail roller surface, as shown in Fig. 17(b). At this time, the "oil wedge effect" occurred. The FM was squeezed into the rail roller. During the wheel/rail rolling contact process, the wheel roller first compressed and closed the crack on rail surface, and then rolled on the closed crack, causing the medium in the closed crack to generate greater hydraulic pressure (thus producing "oil wedge effect"), which further aggravated the rail damage. Since the number and length of the rail cracks were

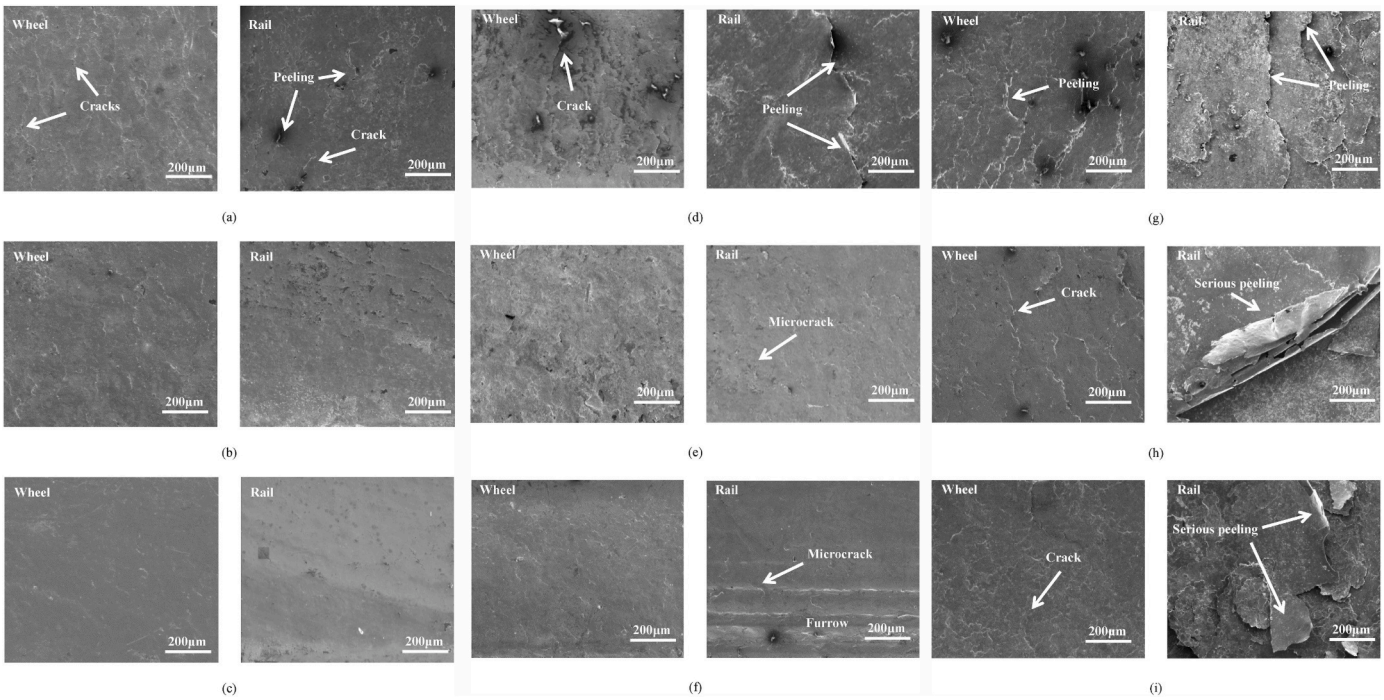

Fig. 13. SEM morphologies of wheel and rail surface rollers under different application conditions of FM: (a) Dry condition (800 MPa); (b) Apply FM after pre-worn (800 MPa); (c) Apply FM without pre-worn (800 MPa); (d) Dry condition (1100 MPa); (e) Apply FM after pre-worn (1100 MPa); (f) Apply FM without pre-worn (1100 MPa); (g) Dry condition (1500 MPa); (h) Apply FM after pre-worn (1500 MPa); (i) Apply FM without pre-worn (1500 MPa).

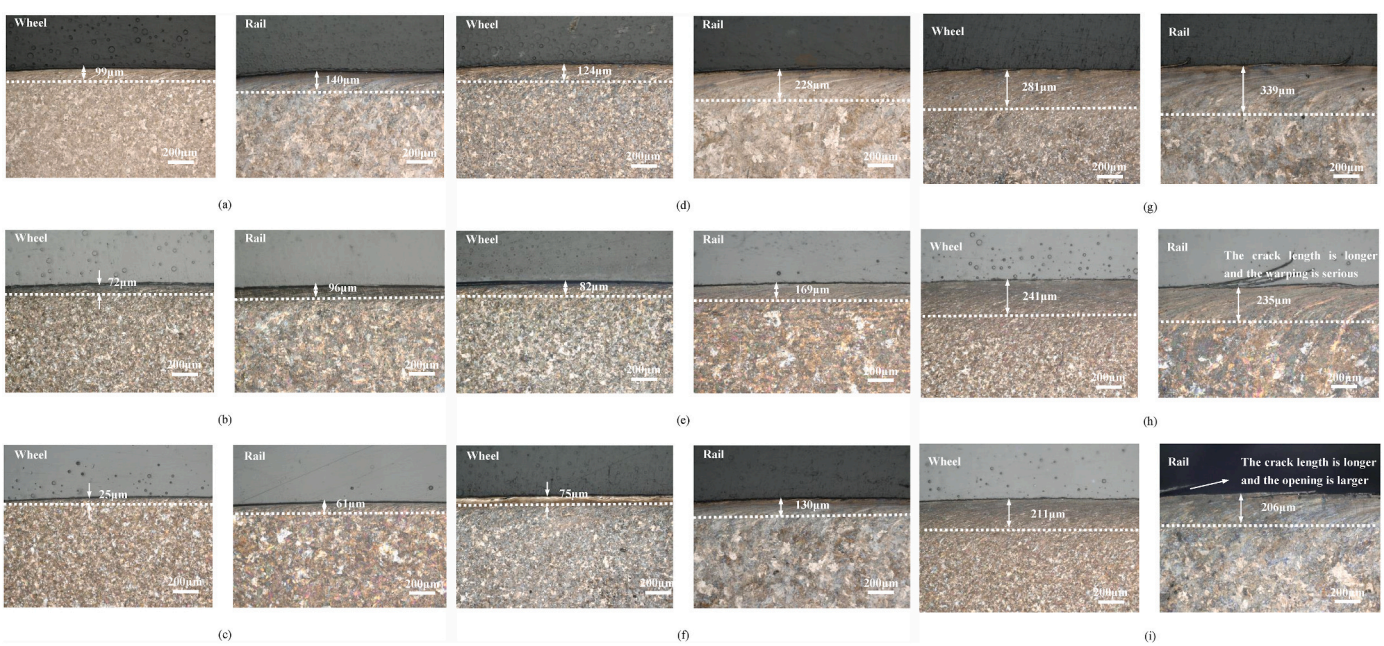

Fig. 14. OM morphology of plastic deformation under different contact stresses: (a) Dry condition (800 MPa); (b) Apply FM after pre-worn (800 MPa); (c) Apply FM without pre-worn (800 MPa); (d) Dry condition (1100 MPa); (e) Apply FM after pre-worn (1100 MPa); (f) Apply FM without pre-worn (1100 MPa); (g) Dry condition (1500 MPa); (h) Apply FM after pre-worn (1500 MPa); (i) Apply FM without pre-worn (1500 MPa).

relatively small at this stage, the rail surface damages were relatively slight (Fig. 17(b)).

At the rapid propagation stage: when the length, number and angle of the rail cracks expanded to a certain extent, the amount of the FM squeezed into the rail crack was increased. Consequently, serious "oil wedge effect" occurred, and only a small part of the FM had the effect of reducing friction on the wheel/rail contact surface. Due to the "oil wedge effect", the cracks of the rail rollers rapidly expanded in a large-angle expansion mode. Long cracks were easily curled under heavy-load cyclic contact stresses and eventually peeled off in the form of large pieces of wear debris, resulting in a sharp increase in the wear rate of the rail roller (Fig. 17(c)). Therefore, the FM cannot exert its friction reduction effect under heavy load conditions.

The propagation mechanism of wheel and rail cracks under 800 and 1100 MPa was as following: only a small part of the FM was squeezed into the crack at the moment of application, and the contact stress was

Table 5
Reduction rates of PDL thickness with FM applied.

Contact stress	FM applied on pre-worn rollers		FM applied on rollers without pre-worn	
	Wheel	Rail	Wheel	Rail
800 MPa	27.3%	31.4%	74.7%	56.4%
1100 MPa	33.9%	25.9%	39.5%	43%
1500 MPa	14.2%	30.7%	24.9%	39.2%

not enough to cause serious "oil wedge effect" under this contact condition. The FM quickly dried up and formed a solid lubricant layer after being applied to the wheel/rail contact interface. Because the fluidity of the solid lubricating layer was poor, the application of FMs under 800 and 1100 MPa could not only exert the effect of reducing friction and lubrication, but also avoided the serious surface damages of the rail caused by the "oil wedge effect".

For the wheel roller, it was a driving wheel and located below the rail roller. According to the stress relationship, the FM was extruded from the wheel roller during the wheel/rail rolling process, so the "oil wedge effect" of the wheel roller was significantly weakened, and the wear and damage of the wheel roller were significantly less than those of the rail roller. Therefore, compared with the dry condition, the application of FM could fully exert its friction reduction effect, and the damage of wheel rollers was significantly reduced under 800, 1100 and 1500 MPa.

Additionally, there was a difference in the amplitude of the adhesion coefficient between Fig. 10(a)–(d) and (e)-(f). With the increase in contact stress, the wheel/rail adhesion coefficient had a downward trend under dry condition (Fig. 10 (b), (d) and (f)). In the tests with FM applied, the upper amplitude of adhesion coefficient was 0.3 because the FM was applied once when the adhesion coefficient recovered to 0.3. When the FM was applied to the pre-worn wheel and rail rollers, the minimum adhesion coefficient gradually decreased with the increase in contact stress, as shown in Fig. 10 (a) and (c). For Fig. 10 (e), when the contact stress reached 1500 MPa, surface cracks occurred on the wheel and rail rollers. At the moment of applying the FM, part of the FM was squeezed into the wheel/rail sample along the crack. However, the amount of FM involved in lubrication was relatively small, so the minimum adhesion coefficient did not continually decrease with the increase in contact stress. When the FM was applied to wheel and rail rollers without pre-worn, as shown in Fig. 10 (b) and (d), the minimum adhesion coefficient decreased with the increase in contact stress. But as shown in Fig. 10 (f), when the contact stress reached 1500 MPa, before 10,000 cycles, the minimum adhesion coefficient gradually decreased with the increase in contact stress, and after 10,000 cycles, cracks were formed on the surface of the wheel and rail samples. Similarly, at the moment of applying the FM, some of the FM entered into the wheel and rail sample along the cracks, while the amount of FM involved in lubrication was relatively small, so the minimum adhesion coefficient did not decline continually. On the other hand, due to the increased wear and damage of the wheel and rail samples, the surface roughness of the wheel and rail would increase, and the adhesion coefficient would also rise [48]. This further explains why the minimum adhesion coefficient did not continuously decrease when the contact stress reached 1500 MPa compared with 800 and 1100 MPa.

Overall, compared with the dry condition, the FM could adjust the wheel/rail adhesion coefficient to the "medium adhesion coefficient level" under 800 and 1100 MPa, and can effectively reduce wheel and rail wear, plastic deformation and surface damages. Under heavy load conditions (1500 MPa), FM could effectively inhibit the wear rate, plastic deformation and surface damages of wheel samples, but it would aggravate the wear and surface damages of rails with initial cracks. Therefore, it should be cautious to use FM directly on rails with initial surface damage such as oblique cracks, etc.

5. Conclusion

The influences of the application amount of FM and wheel/rail

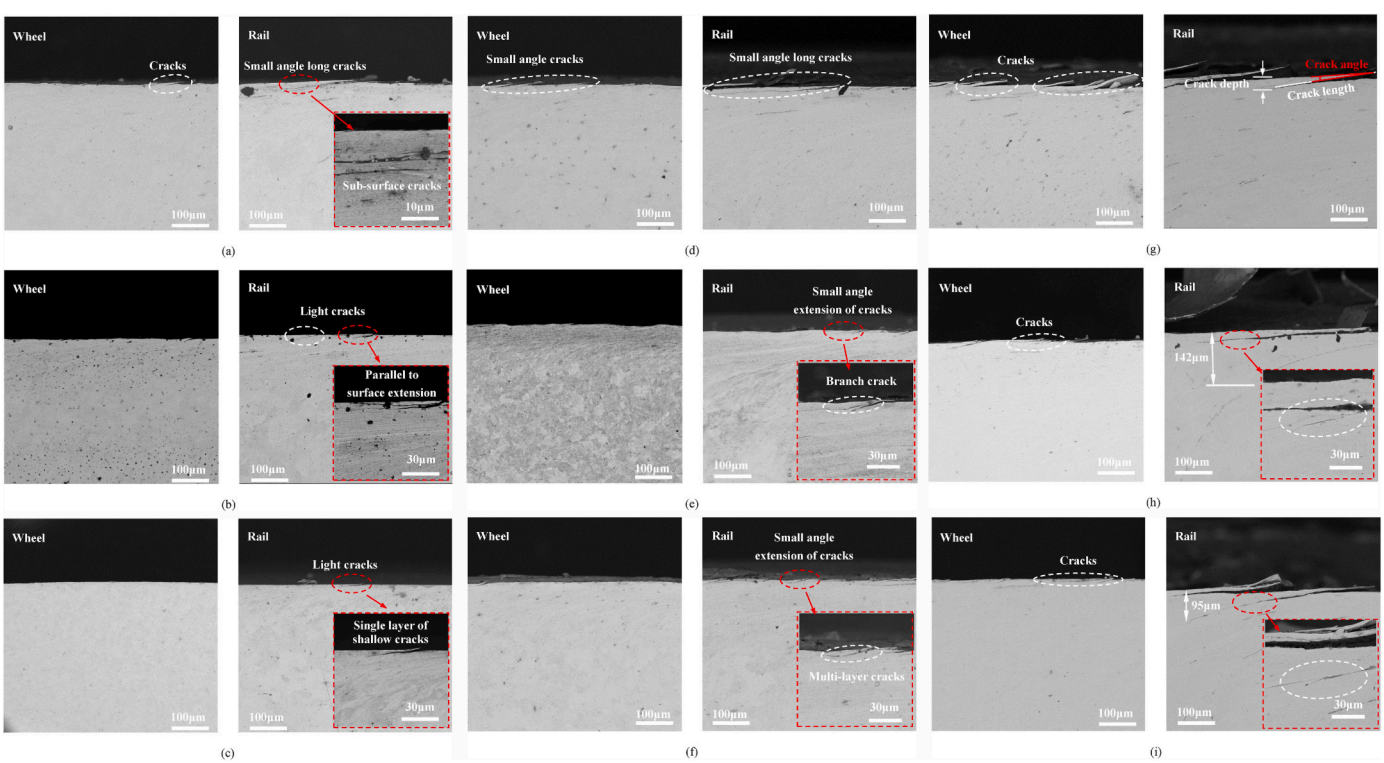

Fig. 15. SEM morphology of wheel and rail section damages under different contact stresses: (a) Dry condition (800 MPa); (b) Apply FM after pre-worn (800 MPa); (c) Apply FM without pre-worn (800 MPa); (d) Dry condition (1100 MPa); (e) Apply FM after pre-worn (1100 MPa); (f) Apply FM without pre-worn (1100 MPa); (g) Dry condition (1500 MPa); (h) Apply FM after pre-worn (1500 MPa); (i) Apply FM without pre-worn (1500 MPa).

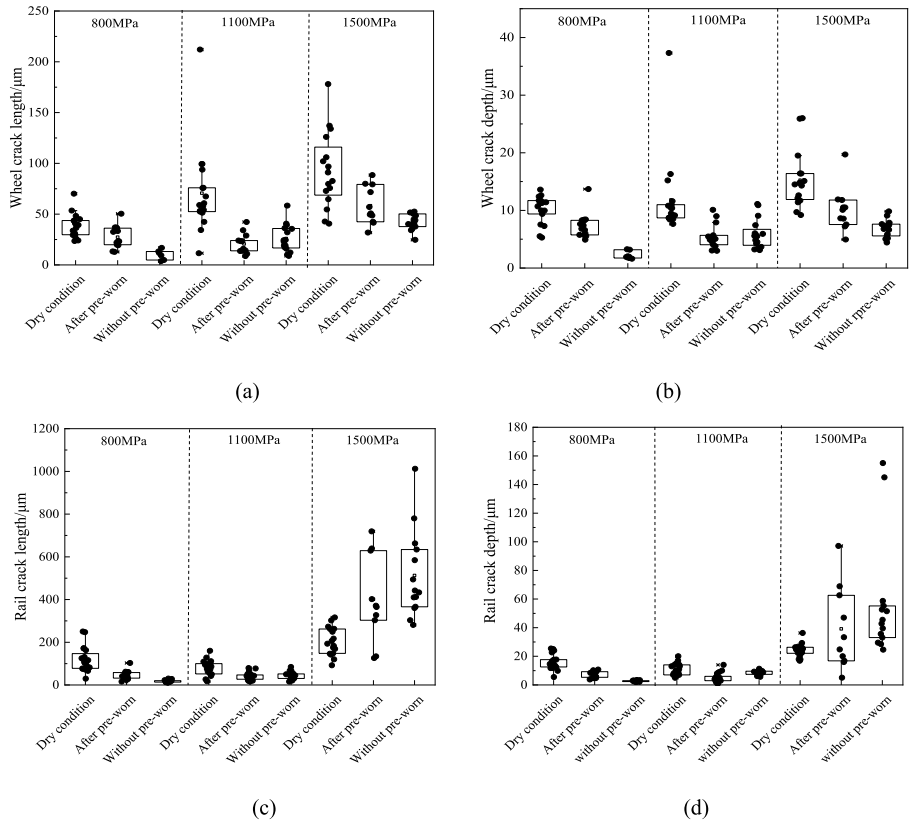

Fig. 16. Propagation length and depth of wheel and rail surface cracks under different contact stresses: (a) Wheel crack length; (b) Wheel crack depth; (c) Rail crack length; (d) Rail crack depth.

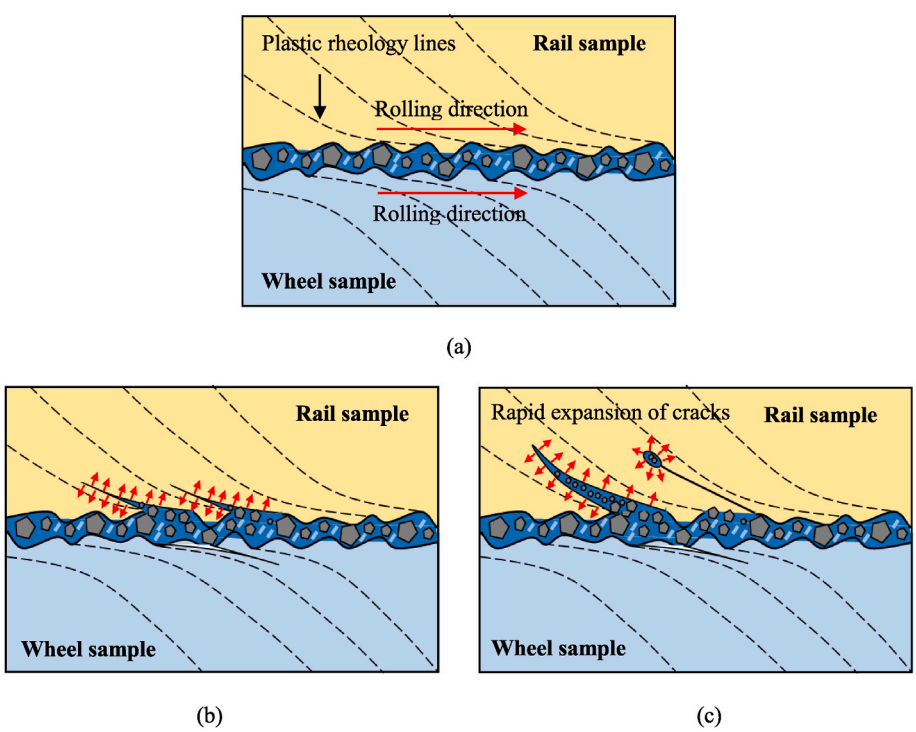

Fig. 17. Schematic diagram of damage mechanism of rail under different contact stresses: (a) Initial stage; (b) Transition stage; (c) Rapid expansion stage.

contact parameters (contact stress and creepage) on the minimum adhesion coefficient and holding time were first studied. Then, the effects of FMs on wheel and rail damages under different contact stresses were explored. The following conclusions can be drawn.

(1) With the increase in the application amount of FM, the minimum adhesion coefficient was reduced and the holding time of FM was increased. The increase in the contact stress reduced the minimum adhesion coefficient and the holding time. The increase in creepage increased the minimum adhesion coefficient and decreased the holding time.
(2) Under 800 and 1100 MPa, the FM could modify the adhesion coefficient to the "medium adhesion coefficient level" (0.1–0.3), and alleviate the wheel and rail wear, plastic deformation and surface damage.
(3) Under the heavy load condition (1500 MPa), the FM could alleviate the wear and damages of the wheel samples, but cause serious surface damages to the rail with initial surface cracks. The crack propagation process on rail mainly included three stages: initial stage, transition stage and rapid propagation stage. The "oil wedge effect" was the main mechanism to aggravate the rail damage.

Author statement

Wenjian Wang: conceived and designed the experiments, performed the sample preparation, carried out the experiments and materials characterization and prepared the manuscript. Shengjie Li: conceived and designed the experiments, analyzed the results. Haohao Ding: conceived and designed the experiments, analyzed the results. Qiang Lin: conceived and designed the experiments, analyzed the results and prepared the manuscript. Radovan Galas: analyzed the results and prepared the manuscript. Milan Omasta analyzed the results. Enrico Meli: analyzed the results. Jun Guo: analyzed the results. Qiyue Liu: analyzed the results.

Declaration of competing interest

The authors declare that they have no known competing financial interests or personal relationships that could have appeared to influence the work reported in this paper.

Acknowledgements

The work was supported by National Natural Science Foundation of China (Nos.52272443, 52027807), Natural Science Foundation of Sichuan Province (No.2022NSFSC0036) and 2022 China-Central and Eastern European University Joint Education Project (No.2022153).

References

[1] Y. Hu, L. Zhou, H.H. Ding, R. Lewis, Q.Y. Liu, J. Guo, W.J. Wang, Microstructure evolution of railway pearlitic wheel steels under rolling-sliding contact loading, Tribol. Int. 154 (2021), 106685.
[2] S.Y. Zhang, Q.Y. Liu, W.J. Wang, M. Spiryagin, Q. Lin, H.H. Ding, Q. Wu, Z. R. Zhou, Implications of water medium for the evolution of rolling contact fatigue under rail surface defect conditions, Tribol. Int. 175 (2022), 107870.
[3] Y. Zhu, W.J. Wang, R. Lewis, W.Y. Yan, S.R. Lewis, H.H. Ding, A review on wear between railway wheels and rails under environmental conditions, J. Tribol. Trans. ASME 141 (2019), 120801.
[4] H.H. Ding, X.P. Mu, Y. Zhu, W.B. Yang, Q. Xiao, W.J. Wang, Q.Y. Liu, J. Guo, Z. R. Zhou, Effect of laser claddings of Fe-based alloy powder with different concentrations of WS2 on the mechanical and tribological properties of railway wheel, Wear 488–489 (2022), 204174.
[5] S.Y. Zhang, M. Spiryagin, H.H. Ding, Q. Wu, J. Guo, Q.Y. Liu, W.J. Wang, Rail rolling contact fatigue formation and evolution with surface defects, Int. J. Fatig. 158 (2022), 106762.
[6] S.Y. Zhang, M. Spiryagin, Q. Lin, H.H. Ding, Q. Wu, J. Guo, Q. Liu, W.J. Wang, Study on wear and rolling contact fatigue behaviours of defective rail under different slip ratio and contact stress conditions, Tribol. Int. 488–489 (2022), 204174.
[7] D. Kvarda, S. Skurka, R. Galas, M. Omasta, L.B. Shi, H.H. Ding, W.J. Wang, I. Krupka, M. Hartl, The effect of top of rail lubricant composition on adhesion and rheological behaviour, Engineering Science and Technology, Int. J. 35 (2022), 101100.
[8] Y. Suda, T. Iwasa, H. Komine, M. Tomeoka, H. Nakazawa, K. Matsumoto, T. Nakai, M. Tanimoto, Y. Kishimoto, Development of onboard friction control, Wear 258 (2005) 1109–1114.
[9] D. Kvarda, R. Galas, M. Omasta, L.B. Shi, H.H. Ding, W.J. Wang, I. Krupka, M. Hartl, Asperity-based model for prediction of traction in water-contaminated wheel-rail contact, Tribol. Int. 157 (2021), 106900.
[10] R. Stock, L. Stanlake, C. Hardwick, M. Yu, D. Eadie, R. Lewis, Material concepts for top of rail friction management-classification, characterization and application, Wear 366–367 (2016) 225–232.
[11] Q. Li, B.N. Wu, H.H. Ding, R. Galas, D. Kvarda, Q.Y. Liu, Z.R. Zhou, M. Omasta, W. J. Wang, Numerical prediction on the effect of friction modifiers on adhesion behaviours in the wheel-rail starved EHL contact, Tribol. Int. 170 (2022), 107519.
[12] R. Galas, D. Kvarda, M. Omasta, I. Krupka, M. Hartl, The role of constituents contained in water-based friction modifiers for top-of-rail application, Tribol. Int. 117 (2017) 87–97.
[13] M. Omasta, M. Machatka, D. Smejkal, M. Hartl, I. Krupka, Influence of sanding parameters on adhesion recovery in contaminated wheel/rail contact, Wear 322–323 (2015) 218–225.
[14] R. Galas, M. Omasta, I. Krupka, M. Hartl, Laboratory investigation of ability of oil-based friction modifiers to control adhesion at wheel/rail interface, Wear 368–369 (2016) 230–238.
[15] K. Chiddick, Solid lubricants and friction modifiers for heavy loads and applications, US Patent 6136757 (2000).
[16] J. Cotter, Friction control composition with enhanced retentivity, US Patent 6759372 (2004).
[17] C. Hardwick, R. Lewis, R. Stock, The effects of friction management materials on rail with pre-existing RCF surface damage, Wear 384 (2017) 50–60.
[18] M. Tomeoka, N. Kabe, M. Tanimoto, E. Miyauchi, M. Nakata, Friction control between wheel and rail by means of on-board lubrication, Wear 253 (2002) 124–129.
[19] D.T. Eadie, M. Santoro, Top-of-rail friction control for curve noise mitigation and corrugation rate reduction, J. Sound Vib. 293 (2006) 747–757.
[20] D.T. Eadie, M. Santoro, J. Kalousek, Railway noise and the effect of top of rail liquid friction modifiers: changes in sound and vibration spectral distributions in curves, Wear 258 (2005) 1148–1155.
[21] J.I. Egana, J. Vinolas, N. Gil-Negrete, Effect of liquid high positive friction (HPF) modifier on wheel/rail contact and rail corrugation, Tribol. Int. 38 (2005) 769–774.
[22] M. Messaadi, M. Oomen, A. Kumar, Friction modifiers effects on tribological behaviour of bainitic rail steels, Tribol. Int. 140 (2019), 105857.
[23] Z. Li, O. Arias-Cuevas, R. Lewis, E.A. Gallardo-Hernández, Rolling-sliding laboratory tests of friction modifiers in leaf contaminated wheel-rail contacts, Tribol. Lett. 33 (2009) 97–109.
[24] O. Arias-Cuevas, Z. Li, R. Lewis, E.A. Gallardo-Hernández, Rolling-sliding laboratory tests of friction modifiers in dry and wet wheel-rail contacts, Wear 268 (2010) 543–551.
[25] J. Lundberg, M. Rantatalo, C. Wanhainen, J. Casselgren, Measurements of friction coefficients between rails lubricated with a friction modifier and the wheels of an IORE locomotive during real working conditions, Wear 324–325 (2015) 109–117.
[26] M. Harmon, R. Lewis, Review of top of rail friction modifier tribology, Tribol. Mater. Surface Interfac. 10 (2016) 150–162.
[27] D.T. Eadie, D. Elvidge, K. Oldknow, R. Stock, P. Pointner, J. Kalousek, P. Klauser, The effects of top of rail friction modifier on wear and rolling contact fatigue: full-scale rail-wheel test rig evaluation, analysis and modelling, Wear 265 (2008) 1222–1230.
[28] W.J. Wang, T.F. Liu, H.Y. Wang, Q.Y. Liu, M.H. Zhu, X.S. Jin, Influence of friction modifiers on improving adhesion and surface damage of wheel/rail under low adhesion conditions, Tribol. Int. 75 (2014) 16–23.
[29] D.T. Eadie, M. Santoro, K. Oldknow, Y. Oka, Field studies of the effect of friction modifiers on short pitch corrugation generation in curves: changes in sound and vibration spectral distributions in curves, Wear 265 (2008) 1212–1221.
[30] R. Galas, M. Omasta, M. Klapka, S. Kaewunruen, I. Krupka, M. Hartl, Case study: the influence of oil-based friction modifier quantity on tram braking distance and noise, Tribol. Int. 39 (2017) 198–206.
[31] D.T. Eadie, M. Santoro, W. Powell, Local control of noise and vibration with KELTRACK friction modifier and Protector trackside application: an integrated solution, J. Sound Vib. 267 (2003) 761–772.
[32] A. Matsumoto, Y. Sato, H. Ohno, M. Tomeoka, K. Matsumoto, T. Ogino, M. Tanimoto, Y. Oka, M. Okano, Improvement of bogie curving performance by using friction modifier to rail/wheel interface Verification by full-scale rolling stand test, Wear 258 (2005) 1201–1208.
[33] K. Matsumoto, Y. Suda, T. Iwasa, T. Fujii, M. Tomeoka, M. Tanimoto, Y. Kishimoto, T. Nakai, A method to apply friction modifier in railway system, JSME Int. J. Ser. C 47 (2004) 482–487.
[34] C. Wang, L.B. Shi, H.H. Ding, W.J. Wang, R. Galas, J. Guo, Q.Y. Liu, Z.R. Zhou, M. Omasta, Adhesion and damage characteristics of wheel/rail using different mineral particles as adhesion enhancers, Wear 477 (2021), 203796.
[35] P.L. Morgado, J.E. Otero, J.B.S.P. Lejarraga, J.L.M. Sanz, A.D. Lantada, J. M. Munoz-Guijosa, Models for predicting friction coefficient and parameters with influence in elastohydrodynamic lubrication, Proc. IME J. J. Eng. Tribol. 223 (2009) 949–958.
[36] L.E. Buckley-Johnstone, G. Trummer, P. Voltr, A. Meierhofer, K. Six, D.I. Fletcher, R. Lewis, Assessing the impact of small amounts of water and iron oxides on adhesion in the wheel/rail interface using High Pressure Torsion testing, Tribol. Int. 135 (2019) 55–64.

[37] W.J. Wang, R. Lewis, M.D. Evans, Q.Y. Liu, Influence of different application of lubricants on wear and pre-existing RCF cracks of rail materials, Tribol. Lett. 65 (2017) 4–15.
[38] D.I. Fletcher, P. Hyde, A. Kapoor, Modelling and full-scale trials to investigate the fluid pressurization of rolling contact fatigue cracks, Wear 265 (2008) 1317–1324.
[39] L.B. Shi, Q. Li, D. Kvarda, R. Galas, M. Omasta, W.J. Wang, J. Guo, Q.Y. Liu, Study on the wheel/rail adhesion restoration and damage evolution in the single application of alumina particles, Wear 426–427 (2019) 1807–1819.
[40] X.S. Jin, Analysis of the creepages and creep forces of wheelset/rail rolling contact, J. China Railw. Soc. 20 (1998) 38–44 (in Chinese).
[41] K. Nagase, A study of adhesion between the rails and running wheels on main lines: results of investigations by slipping adhesion test bogie, Proc. Inst. Mech. Eng. F J. Rail Rapid Transit 203 (1989) 33–43.
[42] H.C. Shi, L.B. Shi, H.H. Ding, Influence of laser strengthening techniques on anti-wear and anti-fatigue properties of rail welding joint, Eng. Fail. Anal. 101 (2019) 72–85.
[43] H.H. Ding, J.Y. Yang, W.J. Wang, J. Guo, Q.Y. Liu, Characterization and formation mechanisms of rail chips from facing grinding by abrasive wheel, J. Manuf. Process. 73 (2022) 544–554.
[44] L.B. Shi, Q. Li, J. Guo, W.J. Wang, Q.Y. Liu, Adhesion-creep curve characteristics of wheel/rail under various conditions, J. Mech. Eng. 55 (2019) 151–157 (in Chinese).
[45] X.Y. Jin, Q.Y. Liu, X.Q. Wang, The experimental study on the adhesion-creep behavior of wheel/rail system, J. China Railw. Soc. 22 (2000) 36–39 (in Chinese).
[46] P.J. Bolton, P. Clayton, Rolling-sliding wear damage in rail and tyre steels, Wear 93 (1984) 145–165.
[47] R. Stock, R. Pippan, RCF and wear in theory and practice-The influence of rail grade on wear and RCF, Wear 271 (2011) 125–133.
[48] Y. Zhu, U. Olofsson, A. Söderberg, Adhesion modeling in the wheel-rail contact under dry and lubricated conditions using measured 3D surfaces, Tribol. Int. 61 (2013) 1–10.

Wear 523 (2023) 204796

Contents lists available at ScienceDirect

Wear

journal homepage: www.elsevier.com/locate/wear

Wear and damage behaviours of wheel and rail materials: Effects of friction modifier and environmental temperature

J.X. Li [a], B.N. Wu [a], H.H. Ding [a], R. Galas [b], M. Omasta [b], Z.F. Wen [a], J. Guo [a], W.J. Wang [a,*]

[a] Tribology Research Institute, Traction Power State Key Laboratory, Southwest Jiaotong University, Chengdu, 610031, China
[b] Faculty of Mechanical Engineering, Brno University of Technology, Technicka 2896/2, 616 69, Brno, Czech Republic

ARTICLE INFO

Keywords:
Friction modifier
Low temperature
Wheel and rail
Wear
Rolling contact fatigue

ABSTRACT

Low temperature conditions can aggravate the wear and fatigue damage of the wheel and the rail materials. Friction modifier (FM) is used to control the adhesion and alleviate the wear and damage. However, the wear and damage behaviours of wheel and rail with the application of FM under low temperature have not been revealed. Therefore, the present study aims to investigate the effect of FM on the wear and the rolling contact fatigue (RCF) damage of the wheel and the rail under low temperature conditions. Tests were conducted on a rolling-sliding wear testing apparatus with the samples enclosed in a temperature-controlled chamber. The results indicated that the effect of FM on the wear and the RCF damage of the wheel and the rail was influenced by the temperature significantly. Compared with the dry condition, the wear rate of the wheel decreased obviously at all temperature conditions when using FM. Meanwhile, the RCF damage of the wheel was relatively slight. Besides, there was no significant difference among the RCF damage of the wheel at different temperatures both under the dry and the FM conditions. At room temperature, the application of FM could alleviate the RCF damage of the rail. Under the low temperature condition, the performance of FM would fail, which would result in a severe oil wedge effect on the rail specimen. Therefore, the application of FM could induce a higher wear rate and severe RCF damages on rail material at the low temperature condition. The results of the present study could provide guidance for the development and design of FMs used in cold regions.

1. Introduction

With the rapid development of rail transport, the running speed of railway vehicles has gradually increased, which has put forward higher requirements for the safety and stability of railway systems [1–3]. After a period of service, the wheel would suffer from the wear, the polygons, and the RCF damage [4,5], while the rail would suffer from the wear, the rail corrugation, and the RCF [6]. Various methods such as rail grinding [7,8] and laser cladding [9,10] were used in the field to solve the above problems. In recent years, the reduction of the wear and the RCF damage of the wheel and the rail materials can also be achieved by the adhesion control method (control the adhesion coefficient at the wheel-rail interface to a target level by some means) [11–13]. The method of adhesion control of the wheel-rail contact interface has the advantages of the low cost, easy operation, and environmental protection [14]. It was found that the wheel-rail RCF damages, such as the wheel polygons, the rail corrugation, the vibration, and the noise can be effectively inhibited through the adhesion control [15]. Therefore, in recent years, the adhesion control at the wheel-rail interface has become a hot research topic in the wheel-rail research field.

Friction modifier (FM) is used as a wheel-rail adhesion control product to reduce the wear of the wheel and the rail materials, inhibit the wheel polygon and the rail corrugation, and the noise. FMs are suspensions those contain complex components, which can be classified into three types: the water-based FM, the oil-based FM, and the water-oil hybrid FM [16,17]. At present, water-based FM is the most widely used because it is environmentally friendly. After the application at the wheel-rail interface, water-based FM dries rapidly and forms a third body layer at the wheel-rail interface. The formed third body layer can control the adhesion coefficient within the target level [18].

Plenty of studies have been conducted to investigate the effect of FMs on the adhesion and the RCF damage behaviours of the wheel and the rail materials. The results showed that the water-based FM could provide a suitable adhesion coefficient (0.2–0.3) [19]. It was found out that the wear of the wheel-rail was significantly reduced when using FMs, so as to the surface and the subsurface damages [20,21]. In addition,

* Corresponding author.
E-mail address: wwj527@swjtu.cn (W.J. Wang).

https://doi.org/10.1016/j.wear.2023.204796
Received 18 September 2022; Received in revised form 5 January 2023; Accepted 16 January 2023
Available online 23 March 2023
0043-1648/© 2023 Elsevier B.V. All rights reserved.

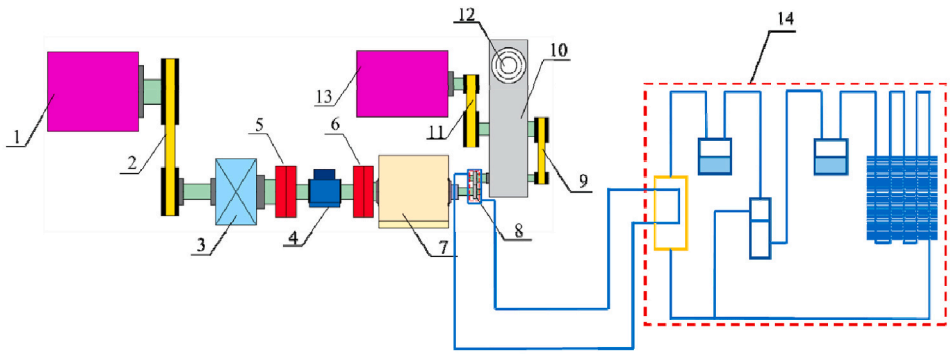

1,13: servo motor; 2,9,11: drive belt; 3,7: bearing; 4: torque sensor; 5,6: coupling; 8: test specimen; 10: lever; 12: hydraulic loading device; 14: cooling system;

Fig. 1. Schematic diagram of MJP-30A wheel-rail test apparatus and low-temperature system.

Table 1
The chemical components (%wt) and hardness of the wheel and the rail materials.

Material	C	Si	Mn	P	S	Hardness/$HV_{0.5}$
ARR-B wheel	0.67–0.77	0.15–1.00	0.60–0.90	≤0.030	0.005–0.040	320
U75V rail	0.71–0.80	0.50–0.80	0.70–1.05	≤0.030	≤0.030	315

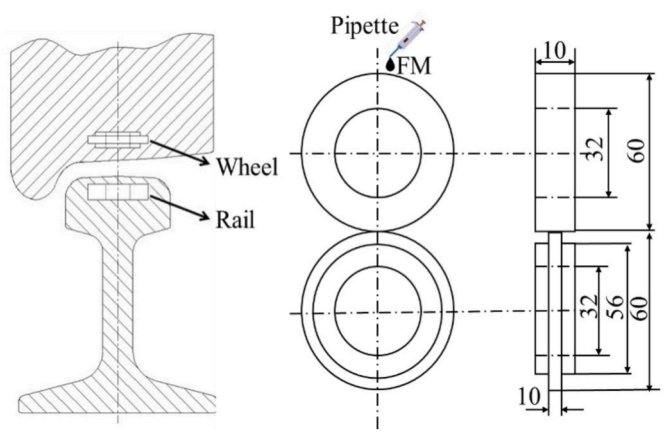

Fig. 2. Sampling position and dimensions of the wheel and the rail specimens.

Table 2
Test parameters.

Test	Temperature/ °C	Contact condition	Hertzian pressure/ MPa	Wear cycles
1	25	Dry	1100	25,000
2	0	Dry	1100	25,000
3	−40	Dry	1100	25,000
4	25	Friction modifier	1100	25,000
5	0	Friction modifier	1100	25,000
6	−40	Friction modifier	1100	25,000

studies on the oil-based FM showed that, depending on the amount of oil-based FM, the application of oil-based FM could also achieve adhesion coefficient control. Furthermore, the content of the metal particles in the oil-based FM was the main factor that affected the wheel-rail RCF damage. It was also found out that the oil-based FMs containing higher hard solid particles could provide higher adhesion coefficients but were more likely to aggravate the wheel-rail RCF damages [22]. However,

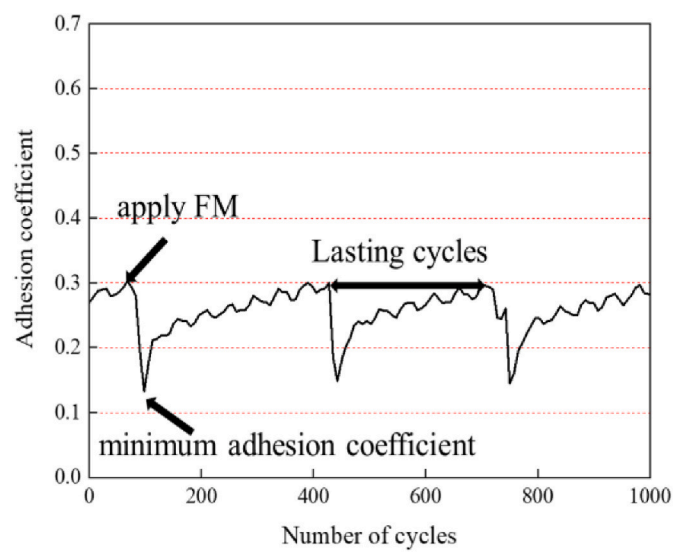

Fig. 3. Schematic diagram of minimum adhesion coefficient and lasting cycles of FM.

some studies also showed that using FMs could cause severe wheel-rail RCF damage due to some FM entering into the cracks and resulting in the "oil wedge effect" [23,24].

Serving in an open environment, the wheel and the rail always face low temperature condition. Plenty of studies have found that the low temperature environment significantly affected the wheel-rail adhesion and aggravated the wheel-rail wear and RCF damage [25,26]. The current investigations on the performance of FM at the wheel-rail interface were mainly conducted at room temperature. The results in the low temperature environment are lacking. In this study, the adhesion control performance of friction modifiers and the effect on the wear and RCF damage wheel-rail under the room temperature and the low temperature conditions were investigated through a twin-disk rolling-sliding wheel-rail simulation facility. In addition, the RCF damage of the wheel-rail material was analyzed by various microscopic methods.

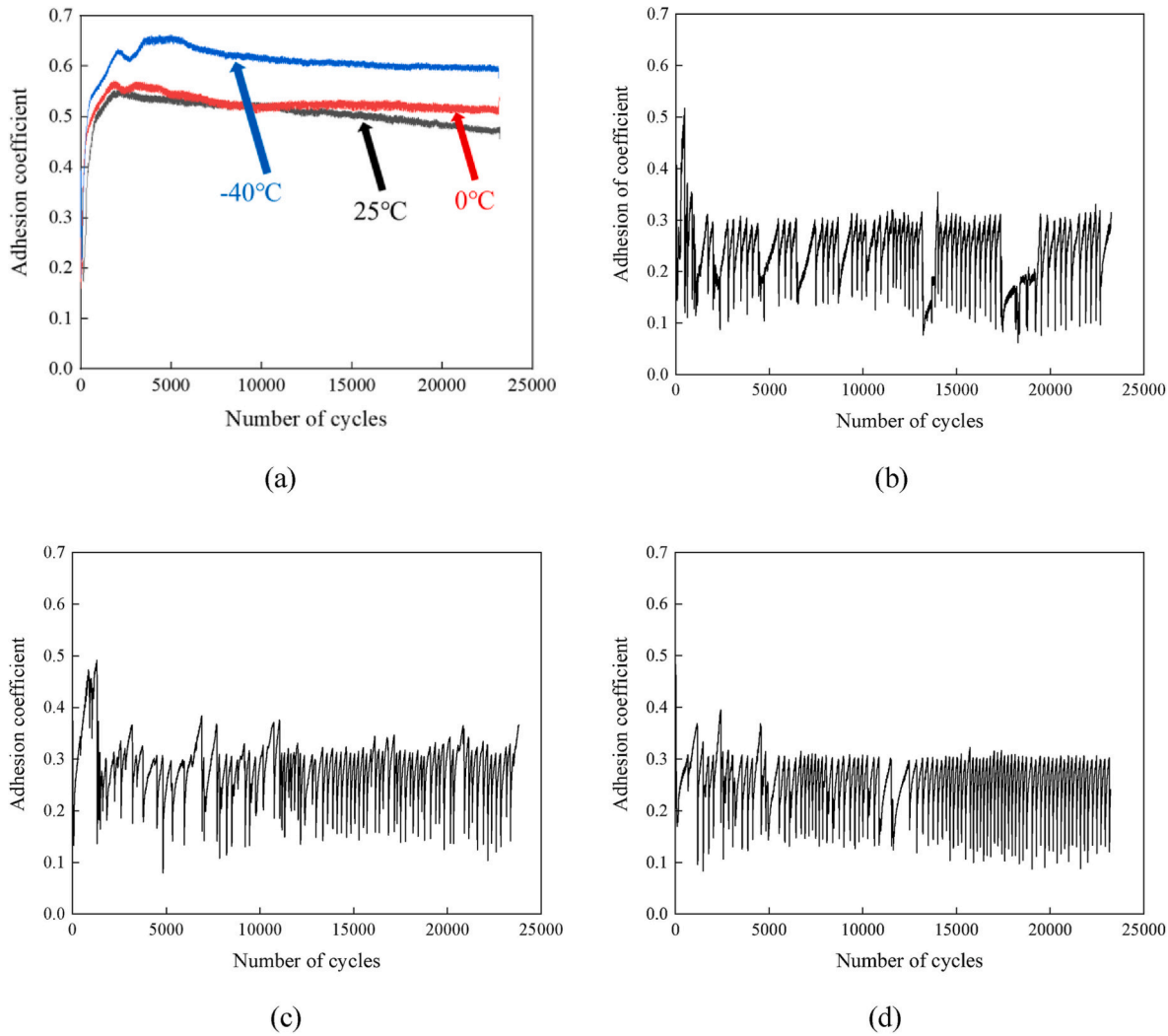

Fig. 4. Adhesion coefficient at different temperatures and conditions: (a) dry, (b) 25 °C FM, (c) 0 °C FM, (d) −40 °C FM.

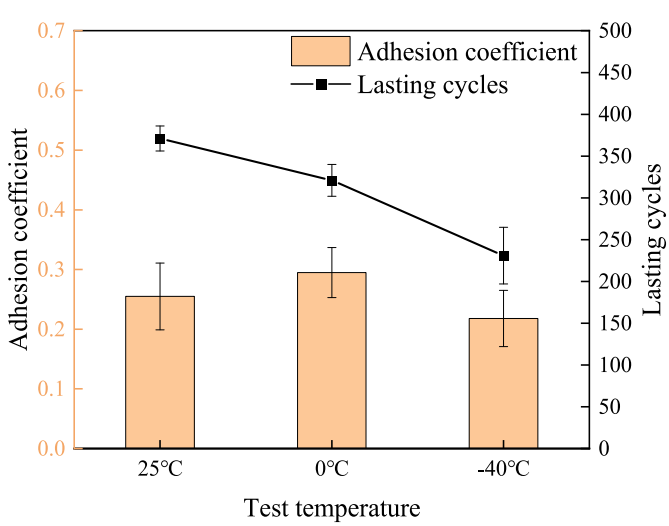

Fig. 5. Minimum adhesion coefficient and lasting cycles of FM at different temperatures.

2. Experimental details

2.1. Test equipment

All tests are conducted on a twin-disk rolling-sliding wheel-rail simulation facility equipped with a low temperature environmental simulation system. The schematic diagram of the test machine is shown in Fig. 1. The wheel specimen and the rail specimen are mounted on the upper and the lower shafts, respectively. Two separated servo motors are used to drive the two shafts. By adjusting the rotational speeds of the two motors, the wheel and the rail specimens have a rotational speed difference to achieve the control of the slip ratio. The formula for calculating the slip ratio is shown in equation (1):

$$\lambda = \frac{|V_1 - V_2|}{V_2} = \frac{|n_2 d_2 - n_1 d_1|}{n_2 d_2} \tag{1}$$

where: λ is the creep slip rate; V_1 and V_2 are the linear velocities of the wheel-rail specimens (mm/min); n_1, n_2 are the rotational speeds of the wheel and rail specimens (r/min); d_1, d_2 are the diameters of the wheel and rail specimens (mm);

The normal load is loaded through a hydraulic loading system and measured through a load sensor. A torque sensor is installed on the lower shaft, which is used to measure the torque. Wheel-rail adhesion coefficient (tangential force/normal force) is a term used to describe the friction behavior between the wheel-rail contact interface. The adhesion

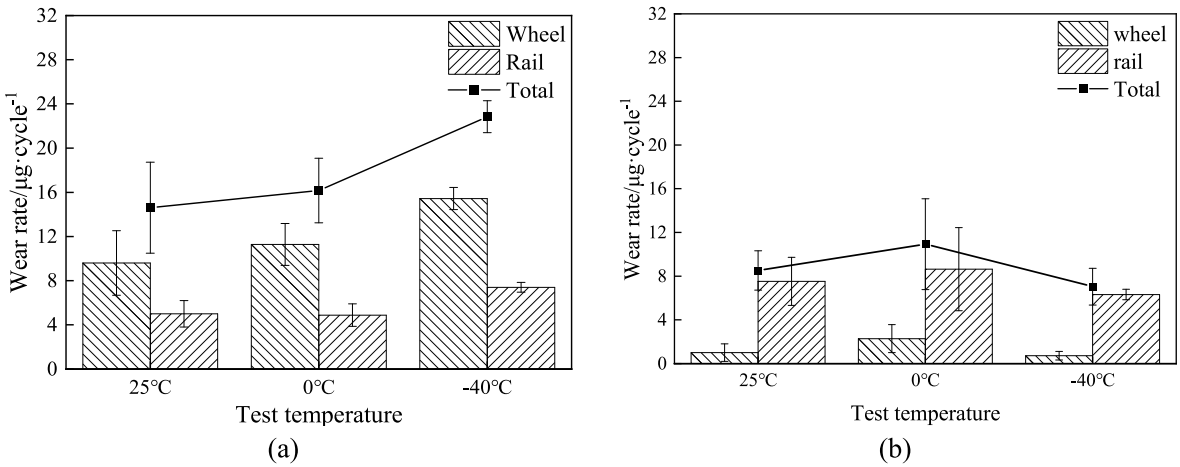

Fig. 6. Wear rates under the dry and the FM application at different temperatures: (a) dry, (b) FM.

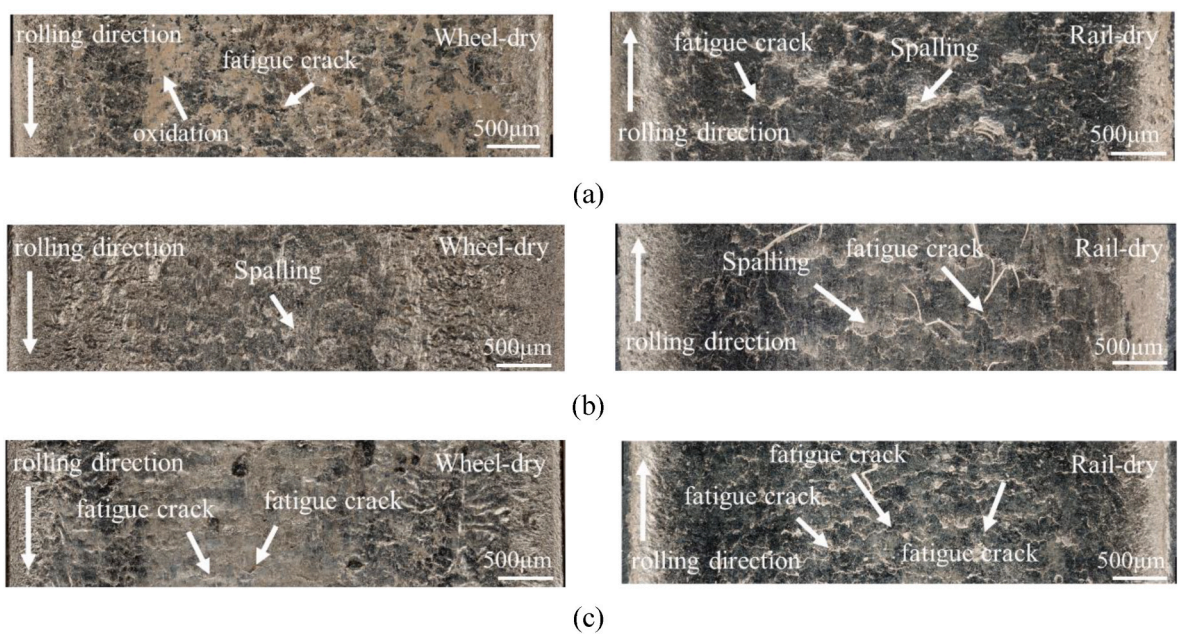

Fig. 7. OM image of surface damage morphology of wheel-rail sample under dry condition: (a) 25 °C, (b) 0 °C, (c) −40 °C.

coefficient is used to represent the change in the degree of train traction or braking force transmitted to the rail. The adhesion coefficient is always used to judge the adhesion level between the wheel-rail contact interface. The traction and braking process of the train during operation depends on the adhesion coefficient of the wheel-rail interface. The adhesion coefficient is calculated through dividing the torque by the radius of the specimen, as shown in equation (2):

$$\mu = \frac{M_1}{rF_N} \tag{2}$$

where: μ is the wheel-rail adhesion coefficient during the test; M_1 is the friction torque detected by the torque sensor (N × m); r is the radius of the specimen (m); F_N is the normal load between the simulated wheel and the rail specimens (N).

The cooling system can provide a cold medium of −60 °C for the low temperature environmental chamber. The cooling system is mainly composed of a secondary refrigeration compressor. The cooling medium is compressed by the compressor into a high-pressure coolant, then flow through the environmental chamber to cool the wheel and the rail specimens. In addition, a PID controller is used to achieve accurate control of the temperature inside the environmental chamber.

2.2. Materials

The wheel specimens and the rail specimens are taken from the ARR-B wheel tread and the U75V railhead, respectively. The chemical compositions and the hardness of the wheel and the rail materials are listed in Table 1. The wheel and the rail specimens are turned into a cylinder shape with a diameter of 60 mm. The contact width between the wheel specimen and the rail specimen is 5 mm. The sampling locations and dimensions of specimens are shown in Fig. 2.

The water-based FM product is provided by Xi'an Kaifeng Railway Mechanical and Electrical Equipment Co., Ltd and it is used in Chinese railway lines currently. The water-based FM is composed of about 60%–70% water, 20%–25% molybdenum disulfide, 5% resin, 5% alcohol and other small amounts of functional additives. The rotational viscosity of the FM is measured by the NDJ-8S rotational viscometer of Shanghai Lichen. The viscosity is 15,920 mPa s at 25 °C and 119,600 mPa s at −40 °C. The moment the water-based FM was applied to the wheel-rail contact area. After the liquid FM was squeezed, a part of the FM would

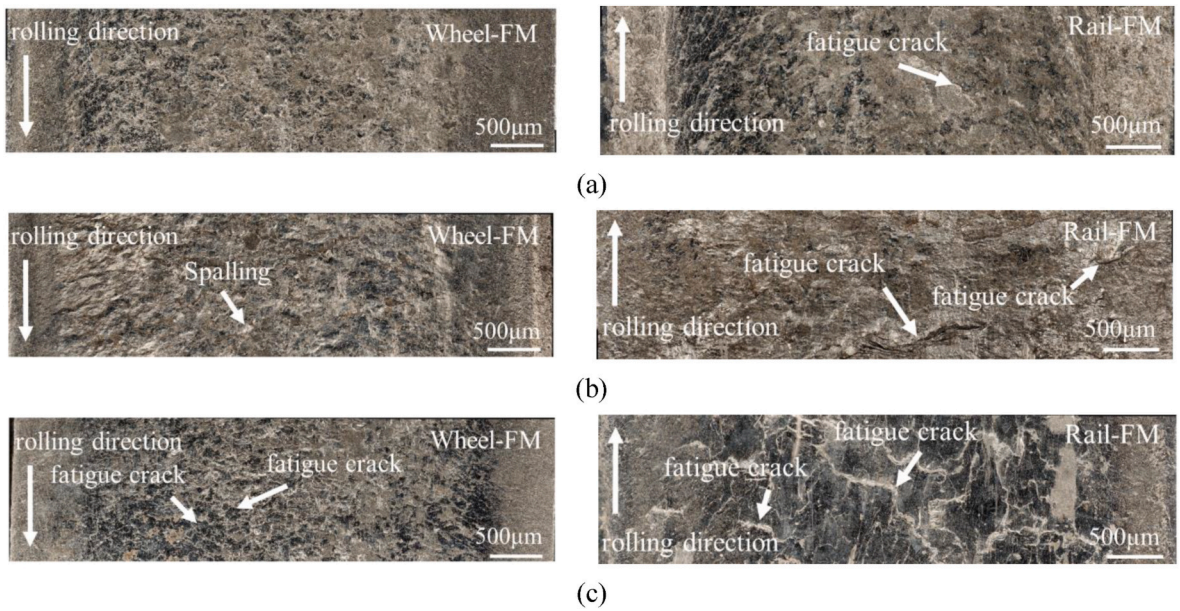

Fig. 8. OM observations of surface damage morphologies of the wheel and the rail specimens under the FM condition: (a) 25 °C, (b) 0 °C, (c) −40 °C.

remain in the wheel-rail contact area and formed a liquid lubricating film. Subsequently, the water in the FM in the wheel-rail contact area evaporated rapidly, gradually forming a solid film, which can control the adhesion coefficient of the wheel-rail [27].

2.3. Test parameters procedures

In the present study, the rotational speeds of the wheel specimen and the rail specimen are 500 r/min and 490 r/min, respectively, which lead to a slip ratio of 2%. The normal load is 2520 N, which is corresponded to the maximum contact stress of 1100 MPa according to the Hertzian contact theory. The test parameters are shown in Table 2.

The wheel-rail specimens are pre-run for 5000 cycles under room temperature and dry conditions, which produce slight RCF damage on wheel-rail specimens to correspond to the actual service condition. Previous studies show that in the twin disc testing, 17,000 to 20,000 cycles are needed to reach a stable statement of the wear and the RCF damage of the wheel and the rail materials. Therefore, 25,000 cycles are selected in the present study.

2.4. Test procedures

Tests are conducted at 25 °C, 0 °C, and −40 °C under the dry contact condition or the FM condition to study the wear and the RCF damage of wheel and rail materials. All the tests are conducted at least twice.

Since the typical way of the application of FM in the field is the roadside, the FM is added into the wheel-rail contact interface 20 μl/time using a pipette in the present study. The FM is applied again when the adhesion coefficient increases to 0.3. The adhesion coefficient under dry condition for the same test parameters is about 0.5 even higher, so this application method ensures that the friction modifier is always present between the wheel-rail contact interfaces.

At the end of each test, small specimens are cut from the worn wheel and rail discs along the longitudinal direction and then polish and etched by 4% Nital to observe the plastic deformation and the subsurface RCF damages. The surface and subsurface morphologies are observed via an optical microscope (OM) (KEYENCE VHX-6000, Japan) and a scanning electron microscope (SEM) (Phenom pro, the Netherlands).

When the FM is applied to the wheel-rail contact interface, the wheel-rail adhesion coefficient will decrease to a minimum point, which is called the minimum adhesion coefficient of the FM in this condition. As the number of cycles increases, the adhesion coefficient will gradually increase. The number of cycles from the application of FM to the recovery of the adhesion coefficient to 0.3 is called the lasting cycles, as shown in Fig. 3.

3. Results

3.1. Adhesion coefficient and wear rate

The curves of adhesion coefficient of the wheel-rail with and without FM are shown in Fig. 4. Under the dry condition (i.e., without FM), as the environmental temperature decreases from 25 °C to −40 °C, the adhesion coefficient gradually increases from 0.5 to 0.6, as shown in Fig. 4a. The adhesion coefficient under the dry contact condition in the present study is consistent with the results in previous studies [25]. This is due to the fact that the decrease in the humidity induced by the low temperature could increase the adhesion coefficient of the wheel-rail.

For the tests with FM, the number of the applied FM gradually increases with the decrease in temperature due to the changing of the performance of FM at low temperature. The minimum adhesion coefficient and the lasting cycles of FM at these three temperatures are plotted, as shown in Fig. 5. It can be observed that the minimum adhesion coefficient under FM conditions increases first and then decreases with the decrease in the environmental temperature. Furthermore, the number of lasting cycles decreases with the decrease in the temperature, which is coincided with the adhesion coefficient results of the dry condition.

The wear rates of the wheel and the rail specimens are shown in Fig. 6. It can be observed that the wear rates of the wheel and the rail specimens increase with the decrease in the temperature under the dry condition (Fig. 6a). Under the FM condition (Fig. 6b), the wear rates of the wheel and the rail specimens increase first and then decrease, which is consistent with the change of the adhesion coefficient under FM condition. The larger adhesion coefficient indicates a larger tangential force at the wheel-rail interface, which might cause a higher wear rate. Furthermore, under the dry condition, the wear rate of the wheel specimen is higher than that of the rail specimen at these three temperatures. The wear rate of the wheel decreases significantly after the FM is applied, while the wear rate of the rail increases. Therefore, the application of the FM both in the room and the low temperatures can

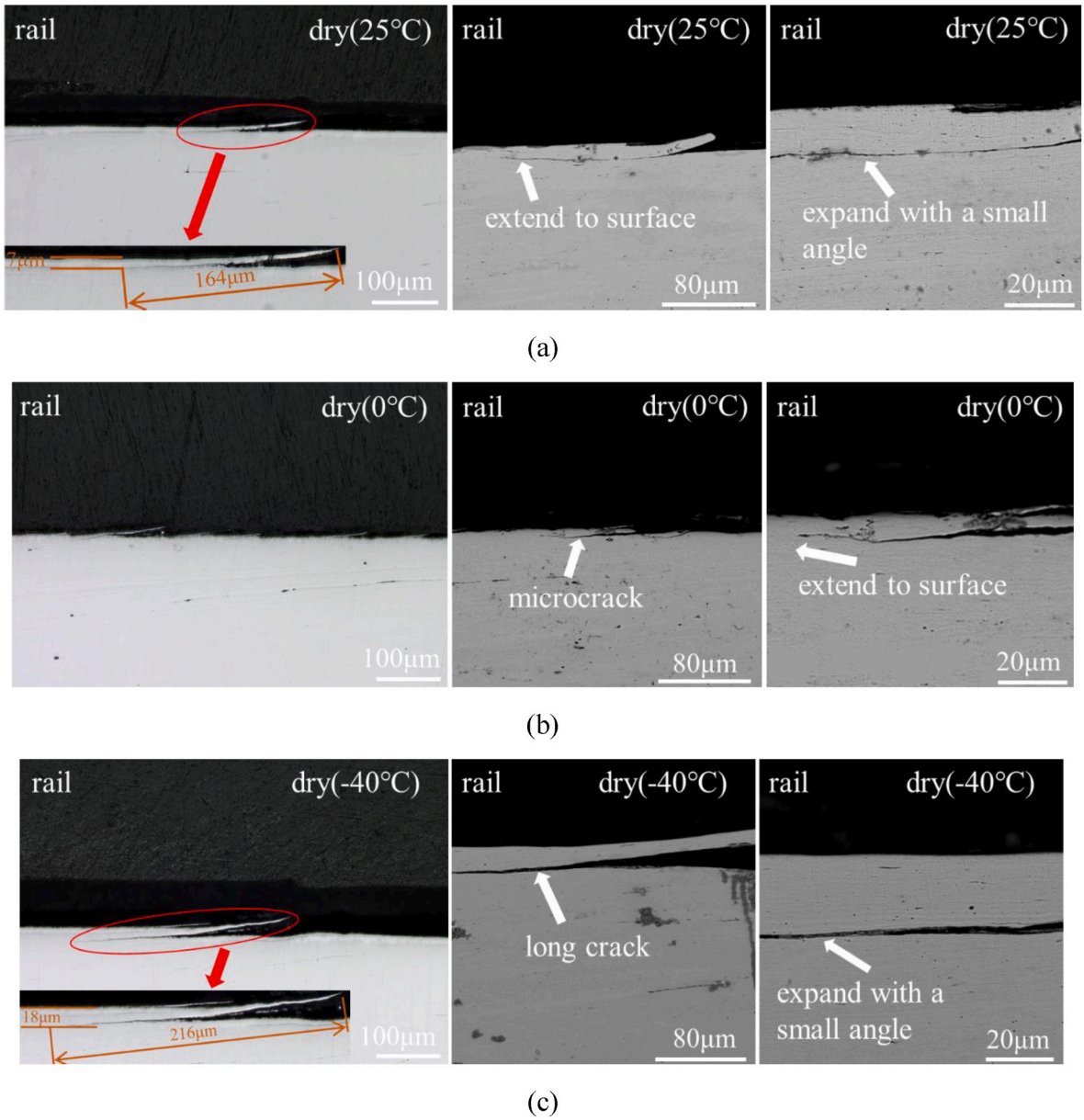

Fig. 9. OM and SEM images of wheel and rail specimen profile damage after dry condition test: (a) 25 °C, (b) 0 °C, (c) −40 °C.

significantly reduce the wheel wear. However, compared with the dry condition, the total wear rate of the wheel and the rail specimens decreases under the FM condition.

3.2. Surface damage

The surface morphologies of the wheel and the rail specimens after testing under the dry and the FM conditions are shown in Figs. 7 and 8, respectively. Under the dry condition, the content of the iron oxide on the surface of the wheel specimen decreases gradually with the decrease in the temperature, as shown in Fig. 7. This is due to the fact that the formation of the iron oxide on the surface under the low temperature is suppressed because of the low humidity. Meanwhile, the RCF damage of the wheel surface at these three temperatures is slight and similar. Concerning the rail specimen, at 25 °C, the rail surface is dominated by the slight fatigue crack and small spalling. At 0 °C, the surface of the rail specimen is dominated by slight fatigue cracks, while severe fatigue cracks and large spalling at −40 °C.

Under the FM conditions (Fig. 8), with the decrease in the environmental temperature, the wheel surface is dominated by slight RCF damage and small amounts of spalling. However, the decrease in the temperature has no obvious effect on the wheel surface morphology. Concerning the rail specimen, with the decrease in the environmental temperature, the surface RCF damage of the rail becomes severer. Compared with the dry condition, the application of FM has a different influence on the rail surface morphologies at these three temperatures. At 25 °C and 0 °C, the application of FM has no visible influence on the rail surface. At −40 °C, compared with the dry contact condition, the application of FM aggravates the RCF damage on the rail surface. The ability of surface damage to reflect RCF damage is limited. It is not advisable to evaluate wheel-rail RCF damage only by surface damage. To reflect the wheel-rail RCF damage more accurately, a more detailed analysis of the subsurface damage is required. Moreover, the application of FM at these three temperatures has a more important influence on the rail specimens than that on the wheel specimens. Therefore, the subsurface RCF damage of the rail specimen is analyzed in detail.

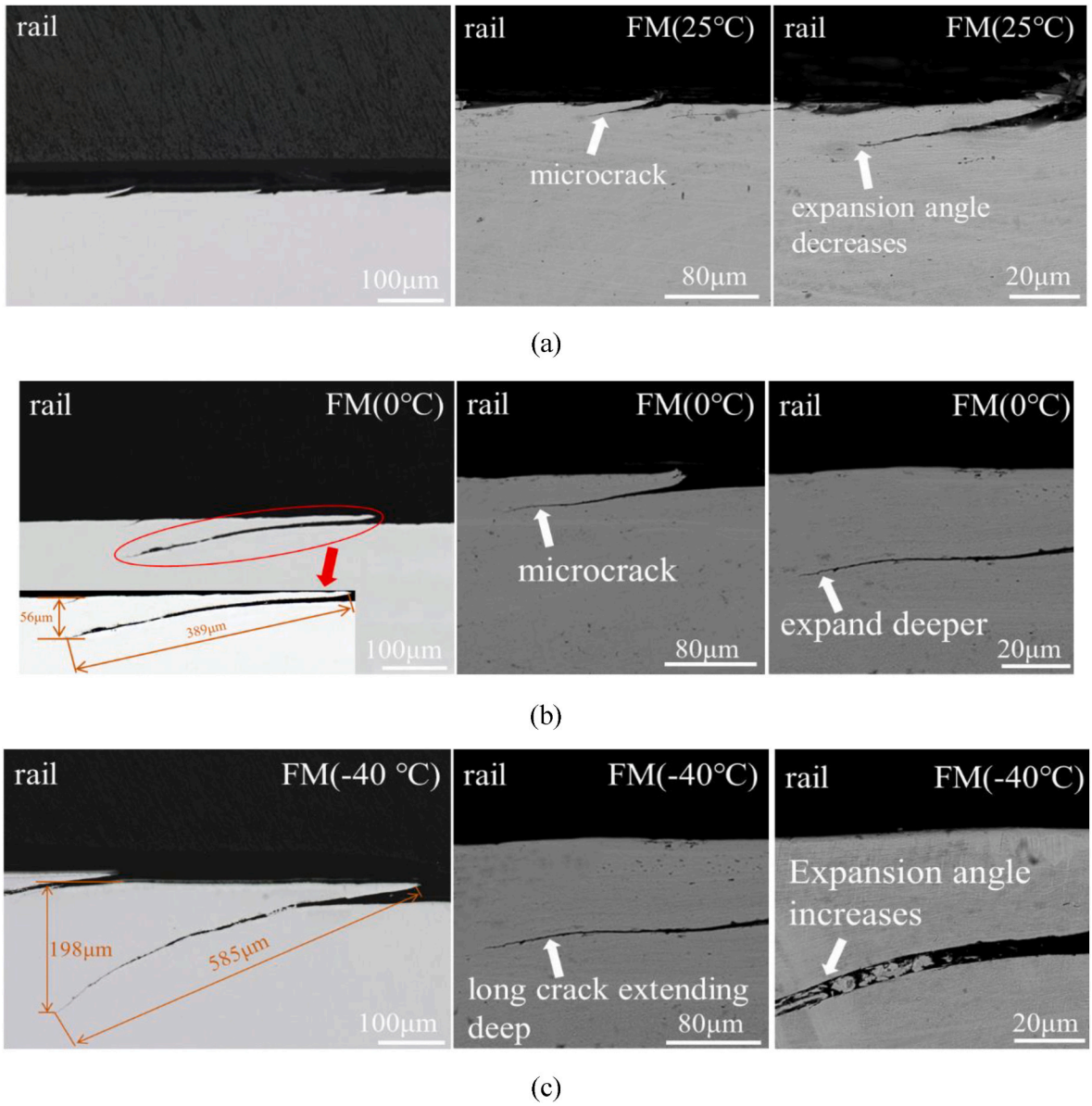

Fig. 10. OM and SEM images of wheel and rail specimen profile damage after FM condition test: (a) 25 °C, (b) 0 °C, (c) −40 °C.

3.3. Subsurface damage

The rail subsurface RCF damages after testing are shown in Figs. 9 and 10. It can be observed that, under the dry contact condition, the crack at 25 °C is short in length and shallow in depth (Fig. 9a). These fatigue cracks of are almost parallel with the running surface. Compared with the 25 °C, both of the crack length and the crack depth at 0 °C are reduced (Fig. 9b). Furthermore, the crack length at −40 °C increases significantly while the crack depth increases slightly (Fig. 9c), which is consistent with the surface RCF damage (Fig. 7).

Under the FM condition, it can be observed that the fatigue cracks under 25 °C are dominated by the micro-crack (Fig. 10a). Compared with the 25 °C condition, the length and the depth of fatigue cracks at 0 °C increased significantly, and more obvious fatigue cracks have been formed, and the RCF damage has slightly increased (Fig. 10b). Compare with the 25 °C and 0 °C conditions, the length and the depth of fatigue cracks increased significantly at −40 °C condition. Meanwhile, the fatigue cracks at −40 °C are dominated by large fatigue cracks (Fig. 10c). Furthermore, these fatigue crack propagates into the material with a large angle which shows a "C-shaped" propagation.

To compare the RCF crack of the rail specimens objectively, the fatigue crack length and the crack depth of the rail specimens after the test of the dry condition and the FM condition were statistically analyzed, as shown in Fig. 11 and Fig. 12 respectively. Compared with the dry contact condition, it can be observed that, at 25 °C, the fatigue crack length decreases significantly under the FM condition. At 0 °C, both of the fatigue crack length and the fatigue crack depth increase under the FM condition. At −40 °C, both of the fatigue crack length and the fatigue crack depth increase dramatically under the FM condition and are nearly four times larger than those under the dry contact condition, which indicates a severe RCF damage.

4. Discussion

4.1. Effect of temperature on FM lasting cycles

The lasting cycles of FM were mainly divided into two stages: (1) FM liquid-solid conversion (rapid evaporation of water within FM to form a solid FM film) stage; (2) solid FM film wear stage. The decrease in the temperature caused the decrease in the ambient humidity, which could

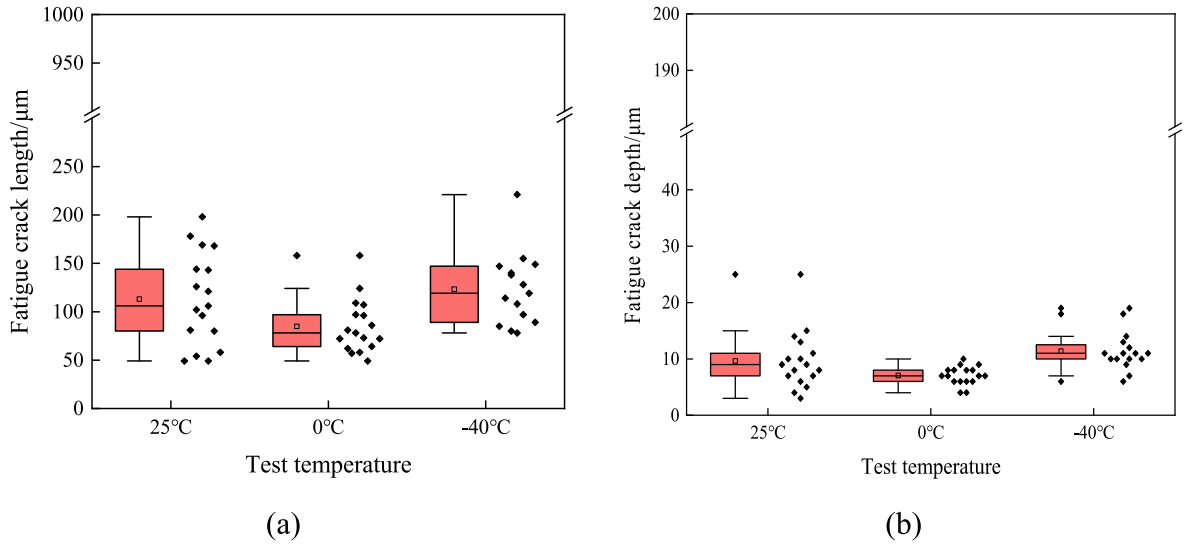

Fig. 11. Fatigue crack statistics of rail specimens after dry condition test: (a) Fatigue crack length, (b) Fatigue crack depth.

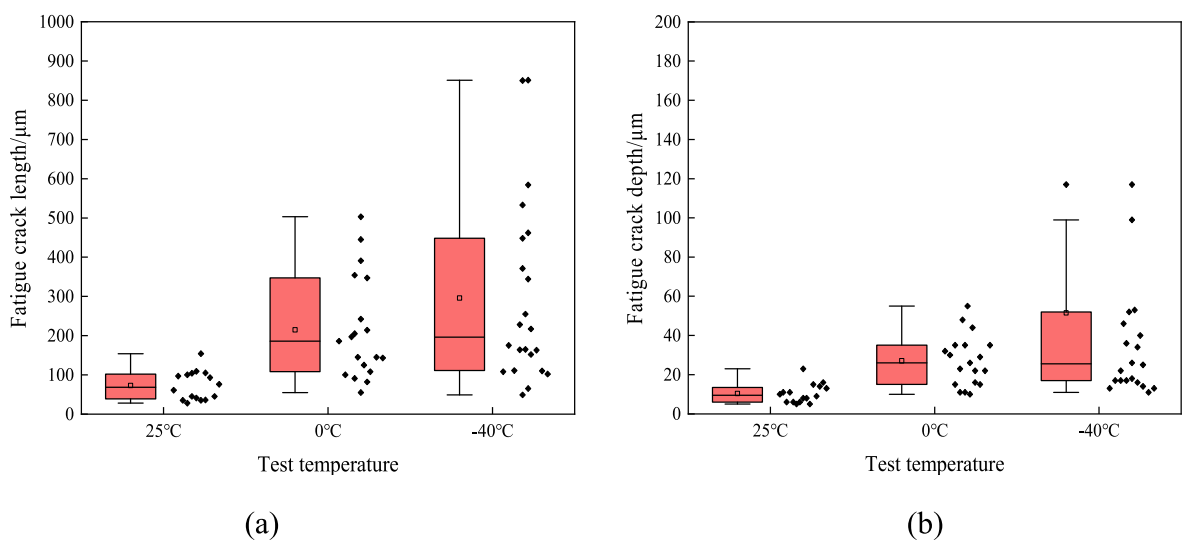

Fig. 12. Fatigue crack statistics of rail specimens under the FM condition: (a) Fatigue crack length, (b) Fatigue crack depth.

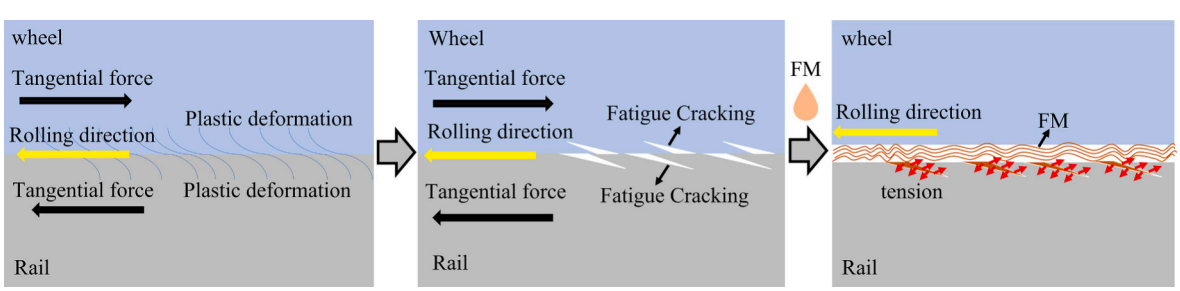

Fig. 13. Schematic diagram of the "oil wedge effect".

accelerate the speed of FM liquid-solid conversion. Therefore, as the temperature decreased, the liquid-solid conversion of FM was gradually accelerated, resulting in a gradually decreased in the lasting cycles of the first stage (FM liquid-solid conversion). In addition, according to the Moore-Coulomb law shown in equation (3), as the temperature decreases, the cohesive force (C) of the solid FM film gradually decreased, resulting in a decrease in the shear strength (T) of the solid FM film under the low temperature condition.

$$T = C + \sigma \tan \varphi \tag{3}$$

where σ is the positive stress, and φ is the angle of internal friction.

As the temperature decreased, the shear resistance of solid FM film gradually decreased and became more susceptible to abrasion. Therefore, as the temperature decreased, the wear rate of solid FM film gradually increased, leading to a gradually decreased in the number of

lasting cycles of the second stage (solid FM film wear). In summary, the decrease in the temperature enlarged the recovery rate of the two FM action stages, which resulted in a decrease in lasting cycles.

4.2. Effect of FM on wheel-rail RCF damage

From the above results, it could be concluded that the use of FM at room temperature could significantly reduce the wheel-rail wear rate and the RCF damage (Figs. 6, 8a and 10a). The application of FM at the low temperatures could effectively reduce the wheel-rail wear but would significantly cause a severe rail RCF damage. The mechanism of the effect of FM on the wheel-rail RCF damage was analyzed, as shown in Fig. 13.

The liquid FM was applied to the wheel-rail contact interface, and some FM would enter into the existing fatigue cracks. As the rolling contact continued, the fatigue cracks were closed due to the contact stress. Meanwhile, the FM in the fatigue cracks was squeezed by the stress and induced a tension state inside the fatigue cracks, which could accelerate the crack propagation (the "oil wedge effect" [25,26]).

Many studies [28–30] have shown that as the ambient temperature decreased, the wheel-rail material would undergo a ductile-brittle transition. When the temperature was higher than −15 °C, the toughness of the material was more obvious and played a leading role in the mechanical properties. When the temperature was lower than −15 °C, the material completed the ductile-brittle transition with the refinement of the grains of the wheel-rail materials. Meanwhile, the brittleness of the material was the main reason affecting the material performance. The increase of material brittleness was easy to aggravate the development of wheel-rail fatigue cracks. In addition, some studies [31] have also found that under normal temperature conditions, the pearlite structure of rail materials was mainly arranged in strips and linear arrangements, and the fatigue cracks at this time mainly expanded along the ferrite. As the temperature decreased, the pearlite structure of the rail material changed into a mixture of long linear distribution and short and small irregular arrangement, resulting in more diversified directions of fatigue crack propagation. At this time, the change of material microstructure would affect the RCF performance of the material. When the temperature dropped to −40 °C, the pearlite structure of the rail material was shorter and more irregularly arranged, and the brittleness of the material increased, which would lead to the subsurface cracks and were easy to merge with the cracks on the surface, forming more obvious fatigue cracks, causing severe wheel-rail RCF damage.

Due to the reduction of the lasting cycles of FM under the low temperature condition, more FM was added to achieve the same adhesion conditions. Therefore, the amount of FM entered into the fatigue cracks increased. The "oil wedge effect" was enhanced, which aggravated the wheel-rail RCF damage under the low temperature condition. The "oil wedge effect" also occurred under room temperature conditions. The fatigue cracks direction of the wheel specimen was opposite to the rolling direction, while the rail specimen was the same. Therefore, it was easier for FM to enter into the fatigue cracks of the rail specimen, which was the main reason why the wear rate and the RCF damage of the rail were higher than the wheel under FM conditions.

5. Conclusions

The wear rate and the RCF damage of the wheel and the rail under three temperature conditions were investigated under the dry and FM conditions via a twin-disc test machine. The following conclusions were drawn.

(1) Under the dry condition without FM, as the temperature decreases, the adhesion coefficient, wear rates, and the RCF damages of wheel-rail showed an increase trend.
(2) The application of FM under the condition of 25 °C can effectively reduce the wheel-rail RCF damage. However, the application of FM at the temperature of 0 °C and −40 °C will aggravate the wheel-rail RCF damages.
(3) The decrease in the temperature will affect the minimum adhesion coefficient and the lasting cycles of FM. The minimum adhesion coefficient has an effect on the wear while the lasting cycles has an effect on the RCF damage of the wheel.

Declaration of competing interest

The authors declare that they have no known competing financial interests or personal relationships that could have appeared to influence the work reported in this paper.

Acknowledgments

The work was supported by National Natural Science Foundation of China (Nos.U21A20167, 52027807), Autonomous Research Project of State Key Laboratory (No.2022TPL-T04) and 2022 China-Central and Eastern European University Joint Education Project (No.2022153).

References

[1] F. Sadeghi, B. Jalalahmadi, T.S. Slack, N. Raje, N.K. Arakere, A review of rolling contact fatigue, J TRIBOL-T. 131 (2009) 75–79.
[2] S.Y. Zhang, M. Spiryagin, Q. Lin, H.H. Ding, Q. Wu, J. Guo, Q.Y. Liu, W.J. Wang, Study on wear and rolling contact fatigue behaviors of defective rail under different slip ratio and contact stress conditions, Tribol. Int. 169 (2022), 107491.
[3] S.Y. Zhang, M. Spiryagin, H.H. Ding, Q. Wu, J. Guo, Q.Y. Liu, W.J. Wang, Rail rolling contact fatigue formation and evolution with surface defects, Int. J. Fatig. 158 (2022), 106762.
[4] R. Stock, D.T. Eadie, D. Elvidge, K. Oldknow, Influencing rolling contact fatigue through top of rail friction modifier application-A full scale wheel-rail test rig study, Wear 271 (2011) 134–142.
[5] K.S. Baek, K. Kyogoku, T. Nakahara, An experimental study of transient traction characteristics between rail and wheel under low slip and low speed conditions, Wear 265 (2008) 1417–1424.
[6] T. Nakahara, K.S. Baek, H. Chen, M. Ishida, Relationship between surface oxide layer and transient traction characteristics for two steel rollers under unlubricated and water lubricated conditions, Wear 271 (2011) 25–31.
[7] K. Zhou, H.H. Ding, M. Steenbergen, W.J. Wang, J. Guo, Q.Y. Liu, Temperature field and material response as a function of rail grinding parameters, Int. J. Heat Mass Tran. 175 (2021), 121366.
[8] H.H. Ding, J.Y. Yang, W.J. Wang, Q.Y. Liu, J. Guo, Z.R. Zhou, Wear mechanisms of abrasive wheel for rail facing grinding, Wear 504–505 (2022), 204421.
[9] H.H. Ding, X. Mu, Y. Zhu, W.B. Yang, Q. Xiao, W.J. Wang, Q.Y. Liu, J. Guo, Z. R. Zhou, Effect of laser claddings of Fe-based alloy powder with different concentrations of WS_2 on the mechanical and tribological properties of railway wheel, Wear 488–489 (2022), 204174.
[10] Y. Hu, L. Zhou, H.H. Ding, R. Lewis, Q.Y. Liu, J. Guo, W.J. Wang, Microstructure evolution of railway pearlitic wheel steels under rolling-sliding contact loading, Tribol. Int. 154 (2021), 106685.
[11] X. Lu, J. Cotter, D.T. Eadie, Laboratory study of the tribological properties of friction modifier thin films for friction control at the wheel/rail interface, Wear 259 (2005) 1262–1269.
[12] X. Liu, P.A. Meehan, Investigation of squeal noise under positive friction characteristics condition provided by friction modifiers, J. Sound Vib. 371 (2016) 393–405.
[13] D.T. Eadie, M. Santoro, K. Oldknow, Y. Oka, Field studies of the effect of friction modifiers on short pitch corrugation generation in curves, Wear 265 (2008) 1212–1221.
[14] M. Tomeoka, N. Kabe, M. Tanimoto, E. Miyauchi, M. Nakata, Friction control between wheel and rail by means of on-board lubrication, Wear 253 (2002) 124–129.
[15] S. Jung-Won, J. Hyun-Kyu, K. Seok-jin, L. Dong-kyeong, Effect of friction modifier on rolling contact fatigue and wear of wheel and rail materials, Tribol. 61 (2018) 19–30.
[16] R. Galas, D. Kvarda, M. Omasta, I. Krupka, M. Hartl, The role of constituents contained in water-based friction modifiers for top-of-rail application, Tribol. Int. 117 (2018) 87–97.
[17] J. Guegan, M. Southby, H. Spikes, Friction modifier additives, synergies and antagonisms, Tribol. Lett. 67 (2019) 83.
[18] D.T. Eadie, D. Elvidge, K. Oldknow, R. Stock, P. Pointner, J. Kalousek, P. Klauser, The effects of top of rail friction modifier on wear and rolling contact fatigue: full-scale rail-wheel test rig evaluation, analysis and modelling, Wear 265 (2008) 1222–1230.
[19] O. Arias-Cuevas, Z. Li, R. Lewis, E.A. Gallardo-Hernández, Rolling-sliding laboratory tests of friction modifiers in dry and wet wheel-rail contacts, Wear 268 (2010) 543–551.

[20] L. Buckley-Johnstone, M. Harmon, R. Lewis, C. Hardwick, R. Stock, A comparison of friction modifier performance using two laboratory test scales, P I MECH ENG 233 (2018) 201–210.
[21] F. Cyriac, T.X. Yi, S.K. Poornachary, P.S. Chow, Boundary lubrication performance of polymeric and organic friction modifiers in the presence of an anti-wear additive, Tribol. Int. 165 (2022), 107256.
[22] R. Galas, M. Omasta, I. Krupka, M. Hartl, Laboratory investigation of ability of oil-based friction modifiers to control adhesion at wheel-rail interface, Wear 368 (2016) 230–238.
[23] M. Kaneta, H. Yatsuzuka, Y. Murakami, Mechanism of crack growth in lubricated rolling/sliding contact, A S L E Transactions 28 (2008) 407–414.
[24] S. Bogdański, P. Lewicki, M. Szymaniak, Experimental and theoretical investigation of the phenomenon of filling the rcf crack with liquid, Wear 258 (2005) 1280–1287.
[25] L. Ma, W.J. Wang, J. Guo, Q.Y. Liu, Rolling wear and fatigue damage behavior of high-speed wheel materials at low temperature, CHIN J MECH ENG-EN. 53 (2017) 113–120.
[26] Y. Lyu, E. Bergseth, U. Olofsson, The effect of subzero temperature and snow on the tribology of wheel-rail contact, Data Brief 5 (2015) 208–212.
[27] S. Richard, S. Louisa, H. Chris, Y. Marcia, E. Donald, L. Roger, Material concepts for top of rail friction management – classification, characterisation and application, Wear 366–367 (2016) 225–232.
[28] K. Valtonen, V. Ratia, K.R. Ramakrishnan, M. Apostol, J. Terva, V. Kuokkala, Impact wear and mechanical behavior of steels at subzero temperatures, Tribol. Int. 129 (2019) 476–493.
[29] Y.Q. Wang, W. Xi, Y.J. Shi, Experimental study of the impact toughness of rail steel at low temperatures, Tsinghua Sci. Technol. 47 (2007) 1414–1417.
[30] Y. Lyu, E. Bergseth, U. Olofsson, Open system tribology and influence of weather condition, Sci. Rep. 6 (2016), 32455.
[31] L. Ma, J. Guo, Q.Y. Liu, W.J. Wang, Fatigue crack growth and damage characteristics of high-speed rail at low ambient temperature, Eng. Fail. Anal. 82 (2017) 802–815.

Vol. 44, No. 3 (2022) 361-373, DOI: 10.24874/ti.1211.11.21.02

Tribology in Industry

www.tribology.rs

RESEARCH

Wheel Squeal Noise in Rail Transport: The Effect of Friction Modifier Composition

Václav Navrátil[a,*], Radovan Galas[a], Milan Klapka[a], Daniel Kvarda[a], Milan Omasta[a], Lubing Shi[b], Haohao Ding[c], Wen-Jian Wang[c], Ivan Křupka[a], Martin Hartl[a]

[a]*Faculty of Mechanical Engineering, Brno University of Technology, Technicka 2896/2, 616 69 Brno, Czech Republic,*
[b]*Zhengzhou Research Institute of Mechanical Engineering Co., Ltd., Zhengzhou 450001, China,*
[c]*Tribology Research Institute, State Key Laboratory of Traction Power, Southwest Jiaotong University, Chengdu 610031, China.*

Keywords:

Wheel squeal noise
Noise mitigation
Friction management
Friction modifier
Wheel-rail tribology

* Corresponding author:

Václav Navrátil
E-mail: Vaclav.Navratil@vutbr.cz

Received: 5 November 2021
Revised: 17 December 2021
Accepted: 21 February 2022

A B S T R A C T

This study aimed to find an appropriate content of water-based friction modifier that will be able to reduce squeal noise without a significant impact on the coefficient of adhesion. A twin-disc machine was used, and the angle of attack of 4 ° simulates sharp curve conditions. The frictional behavior of nine water-based compositions was investigated for dry and wet films. During these experiments, the sound pressure level and the coefficient of adhesion were monitored. The results showed that the presence of solid lubricant in the composition is needed to achieve a long retentivity; however, its higher content can cause low adhesion. The composition with lower solid lubricant content and particles for friction modification with lower Mohs hardness was found to be suitable for further experiments. Moreover, comparison of recorded signals revealed that there is a bilinear dependence between the coefficient of adhesion and the sound pressure level.

© 2022 Published by Faculty of Engineering

1. INTRODUCTION

Noise pollution is one of the most unpleasant side effects of rail transport. Thompson [1] divided railway noise according to its origin mechanism into rolling noise, curve squeal, which can be further divided into wheel squeal and flanging noise, aerodynamic noise, bridge noise, and ground-borne noise. In cities, wheel squeal noise, which occurs in sharp curves and tram reversing loops, is probably the most severe because of its strong tonal character. In addition to that, the radiated sound pressure level (SPL) of squeal noise is usually higher than that of other railway noises [2]. In urban areas, increases in noise levels are problematic. Müller's [2] calculations show that in densely populated areas, up to 1000 inhabitants can be influenced within a radius of 250 m from the source of wheel squeal noise.

There are several ways to mitigate wheel noise. Damping of wheels [3,4] is an effective method; however, retrofitting vehicles is expensive. Friction modifiers (FM) represent a cheaper

alternative to mitigate noise. The purpose of using FMs is to achieve the so-called intermediate level of adhesion in wheel-rail contact. At this level of adhesion, there is no frictional instability in contact, which is considered to cause squeal noise on the wheel [5,6]. Moreover, the use of FM suppresses the initiation and growth of corrugation, which has an impact on wear, dynamic loads, passenger comfort, and rail transport safety [7].

Since 1996, when the liquid form of FM was developed [8], research in the mitigation of wheel-rail noise has focused mainly in this direction. The composition of FM has gradually evolved [8–10], but in general, FM is a water-based composition that contains a binding agent, particles for friction modification, and a solid lubricant [11]. After application, the base medium evaporates leaving only a thin dry friction layer. This layer provides an intermediate level of adhesion and a positive adhesion trend, which plays an important role in reducing wheel noise.

Several field studies have been conducted to investigate the effect of FM on noise. Eadie [12,13] states that FMs can reduce wheel squeal noise and flanging noise by 12 dB in various European mass transit systems. In addition to the effect of oil-based FM on noise, Galas [14] monitored the effect on the braking distance of the vehicle. The results showed that it is difficult to reduce the SPL without significantly affecting the braking distance. Several studies [15,16] also showed the effect of FMs on corrugation formation, another common problem that occurs in sharp curves on tram lines. In critical cases, corrugation can develop tens of micrometers per month [16]. It was observed that the presence of FM on the rail can reduce or prevent the development of corrugation.

Simultaneously, laboratory research of FMs was carried out. The ability of FMs to change the negative trend of the creep force characteristic to positive was confirmed by Matsumoto [17], who used a 1/5 scaled roller stand. The positive effect on the creep force characteristic and noise was confirmed in a twin-disc machine by Li and Arias-Cuevas [18,19]. The influence of individual FM components on adhesion and wear was discussed by Galas et al. [7]. Namely, the effect of bentonite, talc, zinc oxide, molybdenum disulfide (MoS_2), graphite, and their various complex compositions was investigated. Using a twin-disc test rig and a mathematical model, Meehan and Liu [20] showed that water-based FMs eliminate squeal only at a lower angle of attack (AoA). Effective reduction of SPL occurs only after the critical low coefficient of adhesion (CoA) level is exceeded, below which squeal noise is eliminated for all AoAs. Meehan and Liu [21,22] have also been modeling and simulating contact with modified friction properties in recent years.

This study builds on previous research by Galas et al. [7] that dealt with the role of individual constituents of FM and their combination on frictional behavior and wear. As the work is motivated by wheel squeal, it mainly evaluates the influence of the friction modifier composition on the radiated SPL and its relation to CoA. The main goal of this work is to find an appropriate composition of a water-based friction modifier that will be able to reduce the SPL below 90 dB, above which noise normally occurs [2]. At the same time, the composition should not reduce CoA below the critical value of 0.09 for reliable braking and should not cause significant traction problems, for which the limit value can be up to 0.20 [23]. In addition, the dependence between CoA and SPL will be analyzed. For this purpose, compositions with different degrees of complexity in both dry and wet forms are investigated to describe the effect of the drying effect on noise and adhesion, which is usually neglected in similar studies.

2. MATERIAL AND METHODS

2.1 Adhesion measurements

A twin-disc machine was used to simulate wheel-rail contact; see Fig. 1(a). The main part of the machine is a pair of discs with a diameter of 80 mm. The test discs are made of 100CrMn6 bearing steel with roughness of Ra = 0.4 μm and a hardness of 60 HRC. This material is more resistant to wear than the real materials for wheels and rails. Changes in the contact area should be less significant in the case of bearing steel; thus, a better repeatability of experiments should be achieved. The upper disc representing the wheel is cylindrical, the lower disc is rounded with a radius of 50 mm. This configuration leads to the elliptical contact area; see Fig. 1(b). This shape of the contact area is typical for the real wheel-rail contact.

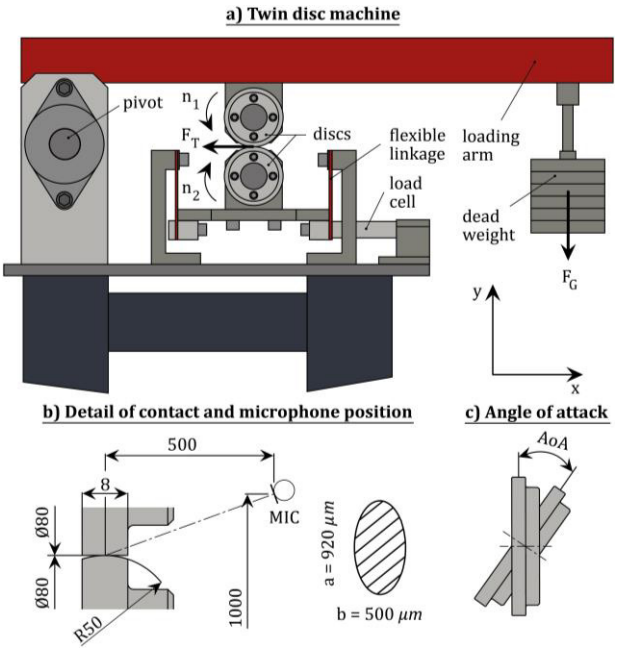

Fig. 1. (a) Twin-disc machine, (b) detail of contact and microphone position, (c) AoA.

Both discs are independently driven by an AC motor with a shaft encoder, which enables setting the slide-to- roll ratio (SRR) accurately and controlling the SRR according to Equation (1):

$$SRR = 2\frac{u_1 r_1 - u_2 r_2}{u_1 r_1 + u_2 r_2} \tag{1}$$

where r_1 and r_2 are the diameters of the discs and u_1 and u_2 are the angular speeds of the discs. The mean speed can be managed in the range of 0 to 2 m/s. The contact load is realized by a lever and a dead weight that is placed at the end of the loading arm. The lower disc is mounted on a steel plate suspended with flexible linkages. This technical solution allows a transfer of friction force from the contact to the load cell measuring the friction force. Based on these data, the CoA is calculated using Equation (2):

$$CoA = \frac{F_T}{F_N} \tag{2}$$

where F_T is the friction force in the direction of the x-axis and F_N is the normal force. As is evident from Fig. 1(c), the twin-disc machine enables setting the AoA in the range of -10° to 10°, to simulate the passage of a vehicle through a sharp curve.

2.2 Sound measurements

The measuring chain consisting of a calibrated measuring microphone t.bone MM-1, an external sound card Focusrite Scarlett 2i2, and a laptop was used to perform sound level measurements. Noise was measured in the frequency range from 20 Hz to 18 kHz. The noise generated on the twin-disc machine dominates at a frequency of 3200 Hz, so the frequency range used meets Nyquist's theorem. The microphone signal was processed in DEWESoft X3 software. The experiments were performed in a standard laboratory. The microphone was mounted 100 cm above the floor (10 cm above the contact of the discs), 50 cm from the contact in the horizontal direction, and was oriented toward the contact of the discs during the experiments; see Fig. 1(b). SPL was evaluated from the moment the twin-disc machine was launched until the moment the adhesion coefficient was recovered to dry conditions.

2.3 Experimental procedure

During all measurements, CoA and SPL were monitored. In this study, two sets of experiments were performed to describe different situations that may occur in real operation due to the use of FMs. The first set of experiments was called 'wet' tests because the experiments were started immediately after the application of FMs. Under these conditions, both CoA and SPL were affected by the presence of the base medium. This situation can typically occur immediately after the application of FMs, especially when FMs are applied by trackside applicators. The second set of experiments was called 'dry' tests. In this case, the water was fully evaporated before the beginning of the experiment; thus, the friction film consisted only of solid particles. Both sets of experiments aimed to clarify the ability of FMs to mitigate unpleasant squeal noise, which occurs at a nonzero AoA. In addition to this, the ability of FMs to maintain CoA above the minimum values required for traction and braking was assessed.

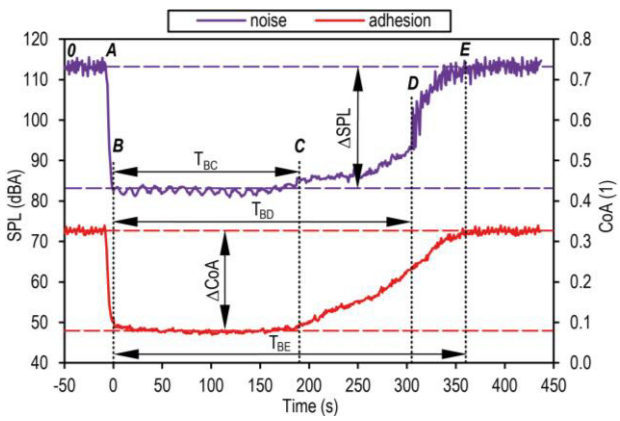

Fig. 2. Parameters evaluated during experiment

The scheme of the experiment is depicted in Fig. 2. Experiments with 'wet' films started immediately after the run-in phase (0-A). The moment of application of the composition is indicated by point A. The difference in 'dry' film preparation lies in stopping the twin-disc machine at point B (approx. 5 s after application point A) for 10 min. During this time, the base medium is fully evaporated and a continuous 'dry' film is formed. Point B is the beginning of the experiment from which all data are recorded and this point is considered to be the point t = 0 s of each experiment. Due to the interruption of the experiment to prepare the dry film, the decrease between points A and B is not shown in the resulting figures. All experiments were terminated after reaching point E. This point represents the moment at which the measured values stabilize at the reference level.

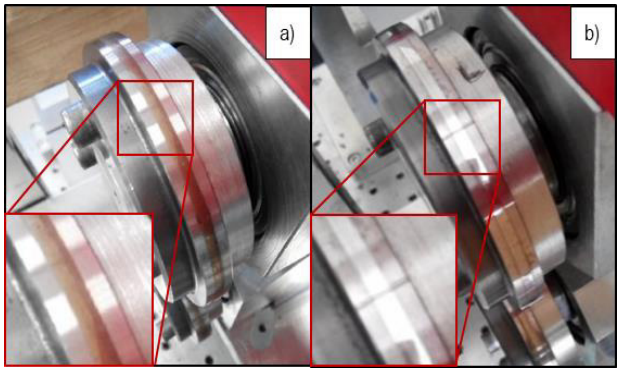

Fig. 3. (a) Acetone-cleaned disc, (b) phase-cleaned disc.

All experiments were carried out twice and under the following experimental conditions: contact pressure p_h = 0.8 GPa simulating the axle load of the light rail system, mean speed u_m = 1 m/s, *SRR* = 0.05 and *AoA* was set at 4 °. These values represent typical conditions in top-of-rail wheel-rail contact in reversing loops with a radius of 25-30 m. At point A, 40 µl of the composition tested was applied to the upper disc using the micropipette (accuracy ± 0.04 µl). In the case of the reference test under wet conditions (without FM), water was applied continuously with a flow rate of 10 µl/s. This flow rate was chosen to achieve stable conditions without contact starvation.

Cleaning the discs with acetone was shown to be insufficient; see Fig. 3(a). Therefore, two-phase cleaning was used in this study. First, the discs were cleaned with acetone and then a continuous feed of water was used to finish the cleaning process. The contact path can be perfectly cleaned using this method; see Fig. 3(b). Furthermore, the width of the contact path increased with the number of experiments. Therefore, the path width was measured before each test and the loading force was adjusted to achieve the required contact pressure.

2.4 Tested compositions

Considering the results of Galas' study [7], the following compositions were selected for twin-disc testing. In the present study, nine water-based compositions with different components and their different contents, listed in Table 1, were investigated in terms of the effect on SPL and CoA. The following components were used: water, binding agent, particles for friction modification, and solid lubricant. No other addi¬tives, e.g. preservatives, were used.

Table 1. Overview of tested compositions.

Composition	Base medium	Binding agent	Friction modifier	Solid lubricant
W	100 wt.% water	/	/	/
C1	92.5 wt.% water	7.5 wt.% bentonite	/	/
C2	92.5 wt.% water	/	7.5 wt. % talc	/
C3	92.5 wt.% water	/	7.5 wt.% zinc oxide	/
C4	85 wt.% water	7.5 wt.% bentonite	7.5 wt.% talc	/
C5	85 wt.% water	7.5 wt.% bentonite	7.5 wt.% zinc oxide	/
C6	83 wt.% water	7.5 wt.% bentonite	7.5 wt.% talc	2 wt.% MoS_2
C7	80 wt.% water	7.5 wt.% bentonite	7.5 wt.% talc	5 wt.% MoS_2
C8	83 wt.% water	7.5 wt.% bentonite	7.5 wt.% zinc oxide	2 wt.% MoS_2
C9	80 wt.% water	7.5 wt.% bentonite	7.5 wt.% zinc oxide	5 wt.% MoS_2

Together with water, the bentonite particles form a colloidal suspension, hence the apparent viscosity increases, as previously observed by Dangler [24]. A previous study [7] showed that the application of 5 wt.% bentonite could be associated with the risk of reaching low adhesion values. On the other hand, when 10 wt.% bentonite is used, the composition becomes a viscous paste, creating a problem with the composition application. Therefore, an amount of 7.5 wt.% bentonite was used. Detail information about the particles is listed in Table 2. The tested compositions were divided according to the number of components into three groups: two-component (comp. C1-3), three-component (comp. C4-5), and four-component compositions (comp. C6-9).

Table 2. Technical specifications of the used FM components [7].

Particle	Size (μm)	Mohs hardness	Shape	Role
bentonite	5.5	1	flake	binding agent
talc	D50: 4.7 D90: 2.3	1	flake	friction modifier
zinc oxide	<5	4–5	granule	friction modifier
MoS_2	D50: 4.2	1–1.5	flake	solid lubricant

An analytical laboratory balance and a laboratory mixer guaranteeing the homogeneity of the compositions were used to prepare the compositions. The components were added and mixed in the following order: water, binding agent, particles for friction modification, and solid lubricant. For compositions containing solid lubricant, the other components were first mixed separately before the solid lubricant was added. To prevent the heterogeneity of the composition due to sedimentation, each composition was prepared just before the experiment.

2.5 Data evaluation

All compositions were primarily evaluated based on noise measurements where three time intervals were found and identified as important parameters for test evaluation; see time interval T_{BC}, T_{BD}, and T_{BE} in Fig. 2. The first interval T_{BC} expresses the ability of a composition to maintain noise and adhesion at almost constant reduced levels. The second parameter T_{BD} expresses the period for which the composition reduces noise and adhesion levels effectively. Behind point D, the friction film breakdown occurs. However, the composition still affects the reduction of SPL and CoA, as is evident in Fig. 2. The T_{BE} parameter expresses the period until SPL stabilizes at the reference value, which is called the 'retentivity' of a composition. Wheel squeal noise does not occur during this period.

In addition to the time parameters, two other parameters were introduced to evaluate the ability of the composition to reduce noise and adhesion. The ΔSPL parameter, defined as the difference between the steady state level of noise in the final stage of the experiment and the average level of noise in the BC stage, expresses the ability of a composition to reduce the level of noise. Similarly, the ΔCoA parameter expresses the difference between the steady-state level of adhesion in the final stage of the experiment and the average level of adhesion in the BC stage. This parameter describes the ability of a composition to reduce the level of adhesion. The experiments were repeated; therefore, all parameters are expressed as mean and standard deviation.

3. RESULTS

3.1 Reference measurements

Before the experiment with the compositions, reference measurements were made. The purpose of the tests was to determine the reference levels of SPL and CoA for subsequent monitoring of the effect of individual compositions on these parameters.

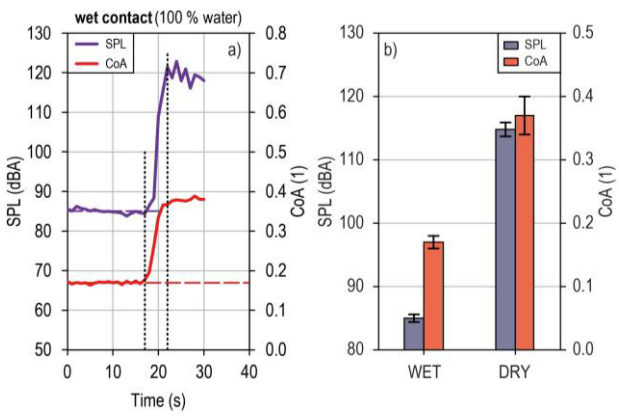

Fig. 4. (a) Wet contact experimental data; (b) reference values for dry and wet contact

Reference levels of SPL and CoA were measured at an AoA of 4 °. The SPL and CoA values of 85 ± 0.6 dBA and 0.17 ± 0.01 were determined as the reference for wet contact; see Fig. 4 (a-b). SPL and CoA reference values of 114.8 ± 1.1 dBA and 0.37 ± 0.03 were determined for dry contact; see Fig. 4(b).

3.2 Wet film measurements

As can be seen in Fig. 5(a), composition C1 was unable to maintain SPL and CoA values at constant levels during the tests. The composition had a moderate effect on the reduction of SPL and CoA levels during the first seconds of the experiment. The dry reference values of SPL and CoA were reached after 15 s. Composition C2 reduced SPL and CoA below the wet contact reference values for 15 s; see Fig. 5(b). The SPL level was reduced by 33.2 dBA and CoA by 0.30. The retentivity of the composition C2 was around 65 s. Composition C3 showed a similar behaviour to composition C1, but the retentivity of composition C3 was longer. The dry contact reference values were reached after approx. 30 s; see Fig. 5(c).

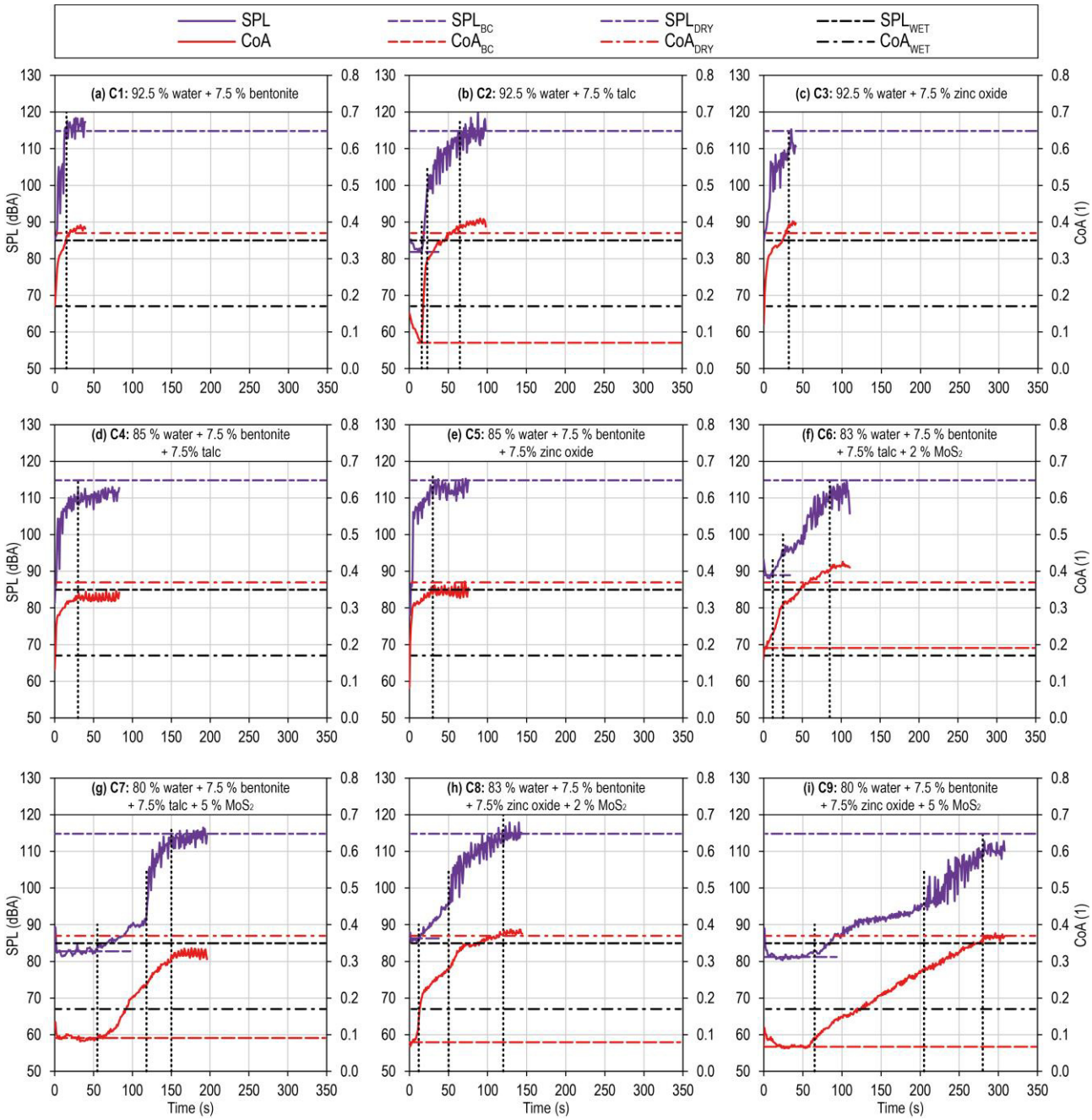

Fig. 5. Wet film results: (a) composition C1; (b) composition C2; (c) composition C3; (d) composition C4; (e) composition C5; (f) composition C6; (g) composition C7; (h) composition C8; (i) composition C9.

As can be seen in Fig. 5(d-e), both three-component compositions reported similar behaviour. None of the tested compositions was able to maintain the SPL and CoA values at constant levels during the experiments. The effect of the compositions on SPL and CoA was almost negligible, and both compositions reached the dry reference values after approx. 30 s. Compared to the two-component compositions, no significant changes in the measured values were found when the third component was added to the composition.

The results of four-component compositions are shown in Fig. 5(f-i). In contrast to previous results, all four component compositions were able to reduce SPL and CoA, and a significant difference occurred in the parameters T_{BC}, T_{BD}, and T_{BE} between the individual compositions. Composition C6 reduced SPL and CoA levels for only the first few seconds, the friction film broke after about 25 s, and the dry reference values were reached in 90 s, see Fig. 5(f). SPL and CoA were reduced by 25.7 dBA and 0.19, respectively. As the amount of MoS_2 increased in the case of composition C7, the monitored time intervals also increased, see Fig. 5(g). Composition C7 maintained constant levels of SPL and CoA for 55 s, the friction film broke after 110 s, the retentivity of the composition was 150 s long, and the composition was able to reduce SPL and CoA by 31.1 dBA and 0.29. Differences due to the content of MoS_2 were also observed for compositions containing zinc oxide. Like composition C6, composition C8 maintained constant SPL and CoA levels for only the first few seconds; see Fig. 5(h). Friction film breakdown occurred after 60 s and dry reference values were reached after 120 s. The reduction in SPL and CoA achieved 28.7 dBA and 0.26. Composition C9 was able to maintain constant levels of SPL and CoA for the longest time of the four-component compositions; specifically for 65 s, see Fig. 5(i). The friction film breakdown occurred after 220 s, the retentivity of the composition was 300 s long, and SPL and CoA were reduced by 33.0 dBA and 0.31.

3.3 Dry film measurements

As can be seen in Fig. 6(a-c), none of the tested two-component compositions was able to maintain SPL and CoA values at constant levels. Composition C1, composed of water and bentonite, did not affect SPL and CoA. SPL and CoA were almost at dry reference values since the beginning of the experiment. The other two compositions already had a moderate effect on SPL and CoA levels. The retentivity of composition C2 was approx. 50 s long. In the case of composition C3, the dry reference values of SPL and CoA were reached after about 40 s.

The results of the dry film experiments for three-component compositions are depicted in Fig. **6**(d-e). As in previous dry film experiments, none of the three-component compositions provided constant levels of SPL and CoA, but the compositions had a moderate effect on SPL and CoA levels. In the case of composition C4, the dry reference values of SPL and CoA were reached after 40 s. The retentivity of composition C5 was 35 s long. In comparison to the results of two-component compositions, it is evident that the addition of bentonite shortens the retentivity of the composition.

Similarly to the wet film experiments, all four-component compositions were able to reduce SPL and CoA significantly, see Fig. 6(f-i). However, a substantial difference in the monitored time intervals T_{BC}, TBD, and T_{BE} occurred again. Composition C6 had the shortest effect on SPL and CoA levels. Constant levels of SPL and CoA were maintained only for the first couple of seconds; see Fig. 6(f). The friction film was broken after 85 s, the dry reference values were reached in 130 s, and the composition was able to reduce SPL and CoA by 29.6 dBA and 0.25. Increasing the amount of MoS_2 had the same effect as in the case of wet films, specifically prolonging the time parameters. Composition C7 was able to maintain constant levels of SPL and CoA for 80 s, the friction film breakdown occurred after 140 s, and the retentivity of the composition was 190 s long; see Fig. 6(g). SPL and CoA were reduced by 31.6 dBA and 0.27. The monitored time intervals of compositions containing zinc oxide were up to twice as long as the intervals of compositions containing talc. Composition C8 maintained constant levels of SPL and CoA for 105 s; see Fig. 6(h). The friction film broke after about 190 s, and the dry reference values were reached in 270 s. The composition was able to reduce SPL and CoA by 33.2 dBA and 0.30. Composition C9 was able to maintain constant levels of SPL and CoA for the longest time, specifically for 160 s, see Fig. 6(i). The friction film breakdown occurred after 300 s, and the retentivity of the composition was 370 s long. SPL and CoA

reduction achieved 32.7 dBA and 0.31. The data confirmed previous observations of the amount of the effect of MoS_2 amount on the monitored time parameters. Moreover, clear differences in the time parameters between talc- and zinc oxide-containing compositions were observed. Wider statistical data for both wet and dry experiments are listed in the Supplementary material.

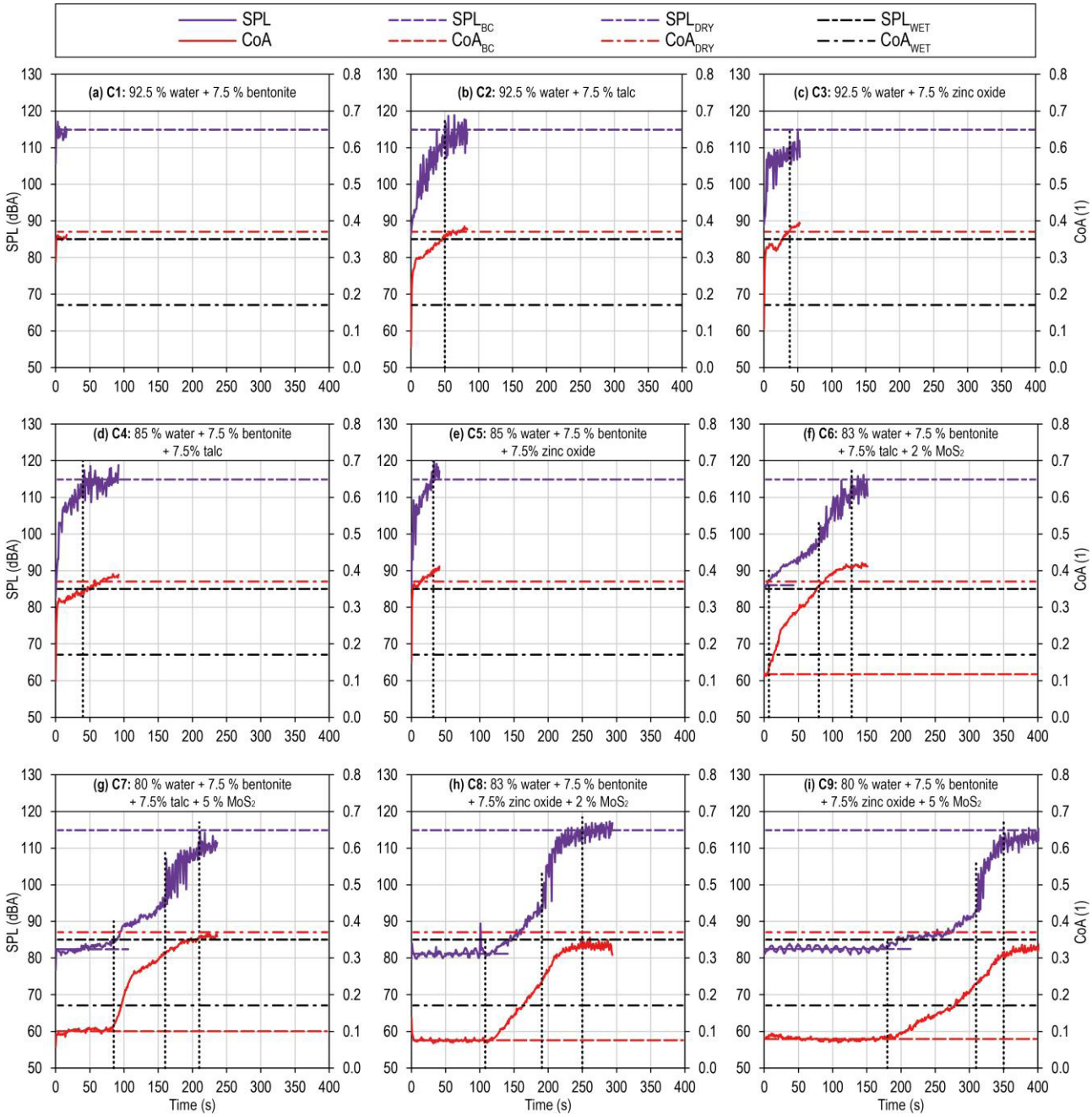

Fig. 6. Dry film results: (a) composition C1; (b) composition C2; (c) composition C3; (d) composition C4; (e) composition C5; (f) composition C6; (g) composition C7; (h) composition C8; (i) composition C9.

3.4 Noise frequency analysis

Fig. 7 shows the frequency analysis of the signal recorded during the dry film experiment of composition C9. The figure shows that the dominant noise is in the frequency band around 3150 Hz. The higher frequency bands indicated by the dashed line are harmonic multiples of this frequency. The dominant frequency band falls into the 1-5 kHz band, in which, according to Eadie [12], squeal noise ranges. After application of the product, SPL decreases by 35 dB at this frequency. The frequency composition of the signal is the same for all compositions and for wet and dry films.

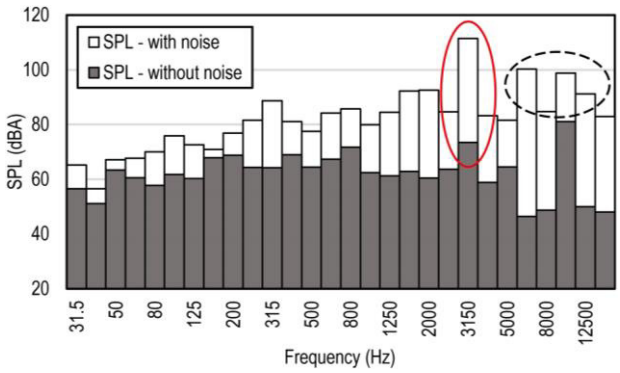

Fig. 7. Frequency analysis of measured noise

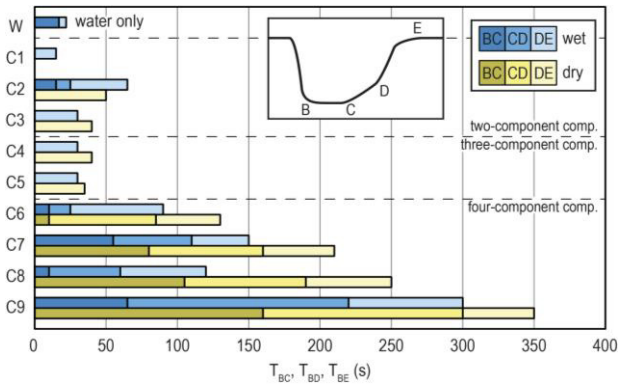

Fig. 8. Comparison of compositions time parameters.

4. DISCUSSION

4.1 General discussion of the results obtained

In the beginning, reference tests were carried out to investigate the level of SPL and CoA for wet and dry contact. It should be noted that water was applied to the contact continuously throughout the experiment, while a single application was used for other compositions. The data from all the experiments performed are summarized in Fig. 9. These data show that water itself could be considered as a solution for curve squeal mitigation. A significant drop in SPL at the noise frequency was observed immediately after the water application. Furthermore, water lubrication did not cause the appearance of very low adhesion, which can occur depending on other conditions (such as applied amount, presence of other contamination, etc.) for both water-based and oil-/grease-based top-of-rail products [14,21,25–27]. On the other hand, the water retentivity in contact was up to several times shorter compared to the complex compositions C6-C9; see Fig. 9. These conclusions correspond to the observations of Oertli [28], who studied the effect of water spraying on a real track and concluded that water was able to reduce squeal noise in 86% of cases. Except for noise reduction, the major benefit is that insufficient adhesion is not achieved. It should also be emphasized that water could represent a simple, cheap and environmentally friendly option for lubricating the wheel-rail interface. From that perspective, frequent spraying of water directly from a passing vehicle could be a promising way to combat squeal noise. In addition to pure water, bentonite thickened water was tested in this study; see composition C1 in Fig. 8.

Composition with this lubricated by wayside (stationary) lubrication systems, which are still the most common way for top-of-rail friction modification in many countries. The study by the previous authors [7] revealed that this composition, which contains only water and bentonite as a thickener, can provide the intermediate level of adhesion required without the risk of very low adhesion, but the effect of this composition on SPL has not been studied yet. The present study investigated that no stable noise reduction was achieved with this composition and was the retentivity that even shorter than was found for pure water. Furthermore, there was no evident effect of the composition on SPL and CoA after water evaporation (dry film), which is one of the key requirements for friction modifiers when a wayside lubrication system is used. In that case, water acts mainly as a transport medium, ensuring a better spread of the composition along the track. Its ability to reduce SPL and CoA should be present even after water evaporation. Regarding these requirements, only composition C2 showed satisfactory results, although the retentivity of this composition was still rather limited. The other two- and three-component compositions did not achieve the required noise reduction.

Based on the comparison of three- and four-component compositions in Fig. 8, it is obvious that the retentivity of the compositions is significantly affected by the solid lubricant and its content for both dry and wet films. This behaviour was also observed by Galas [7] and Hou [29]. The comparisons in Fig. 9 show that although a stable and long phase of SPL reduction on noise frequency (phase B-C in Fig. 8) was achieved for compositions containing 5 wt.% solid lubricant, CoA was significantly compromised in this phase. According to Fulford [23], CoA of 0.09 is required for reliable braking.

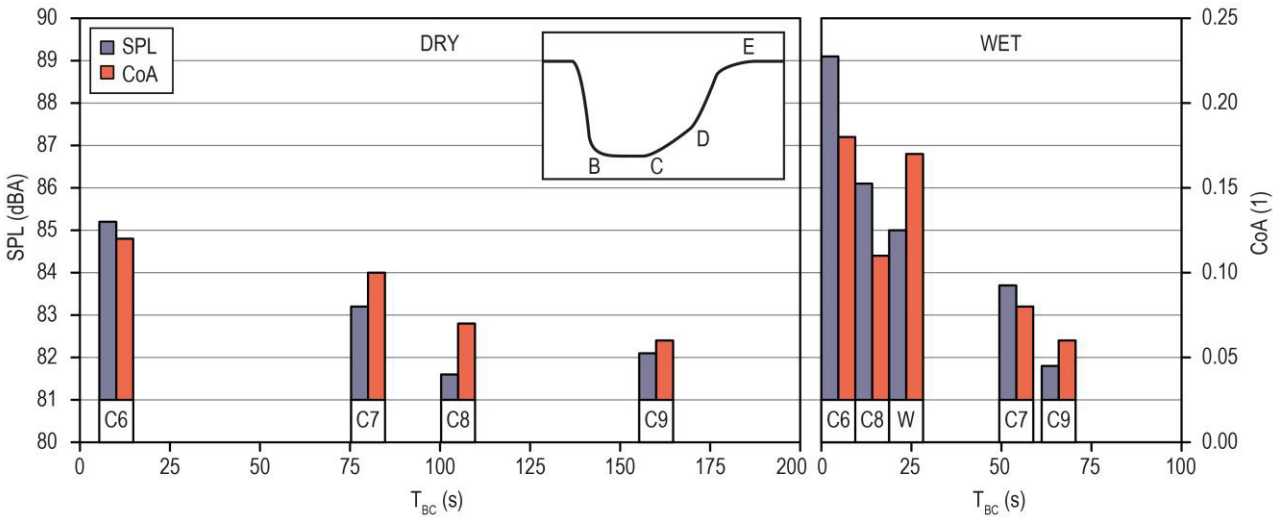

Fig. 9. Comparison of wet and dry experiments results.

Fig. 9 also show the most evident difference between compositions containing talc (C6 and C8) and zinc oxide (C7 and C9), which is the retentivity of the composition. The difference is attributed to the different Mohs hardness of the talc and zinc oxide particles. As a result of the lower Mohs hardness of talc, the abrasion resistance of the friction film containing talc particles is lower than in the case of the film containing zinc oxide particles. Thus, the friction film containing talc loses the ability to reduce SPL and CoA earlier than that of the film containing zinc oxide.

Regarding these results, composition C6 appears to be the most suitable composition because there was a significant reduction in noise and CoA was sufficient for braking under both dry and wet films. This composition contained only 2 wt.% solid lubricant and 7.5 wt.% bentonite and talc particles as friction modification particles. Based on these findings, it could be suggested that compositions with a lower content of solid lubricant can be suitable for application in track sections where intensive braking and traction are expected. Furthermore, it could be assumed that this composition can also be beneficial in terms of surface wear and damage of contact bodies because all solid particles contained in composition C6 have low Mohs hardness values (from 1 to 1.5).

4.2 Relationships between SPL and CoA

Fig. 10 shows the dependence of SPL on CoA during experiments with four-component compositions. A strong correlation between CoA and SPL was observed. Up to a CoA value of approx. 0.24, the SPL and CoA gradually increase. After these values are reached, the slope of the curve changes, and both measured parameters increase rapidly. It is obvious that there is a bilinear dependence for all of the compositions tested. This phenomenon can be interpreted as a point where the effect of the wet/dry film becomes insignificant, and both CoA and SPL are mainly given by the properties of the dry surfaces of contact bodies.

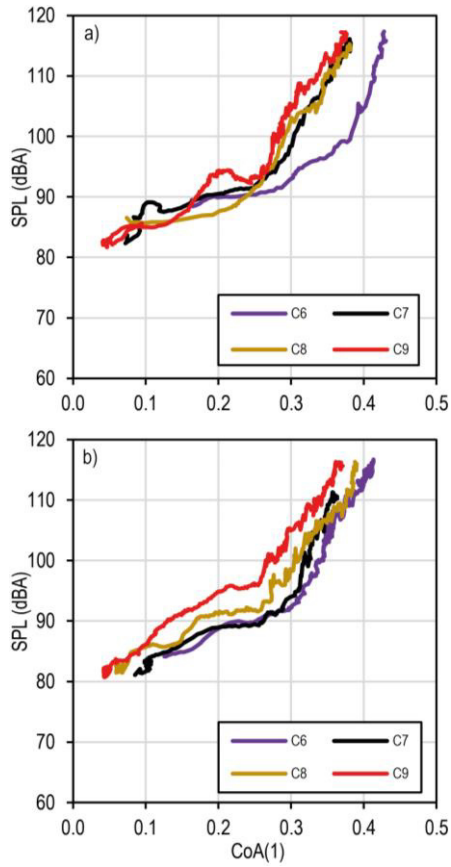

Fig. 10. Dependence of SPL on CoA (a) wet; (b) dry film.

As can be seen in the Supplementary material, all SPL values at point D, behind which the rapid increase of CoA and SPL occurs, fall within a given range of 90-96 dBA. This behaviour could be the subject of further research because potential findings could be useful in the design of the control units of the lubrication system on the side. On the basis of the monitored SPL, it would be possible to control the activation of the FM application in wheel-rail contact to avoid a sudden increase in unpleasant squeal noise. Currently, wayside lubrication systems are mostly controlled on the basis of interval application. Application management based on SPL monitoring could make the process more effective.

4.3 Future study

We expect the compositions to show the same behaviour during experiments on the test rig with full-scale wheel and on the real track. Therefore, most attention should be paid to pure water and FM composition with low solid lubricant content. Future experiments should be focused especially on noise in individual frequency bands, in combination with the use of methods of capturing and mapping a transient acoustic event (e. g., NS-STSF). For this purpose, the experiments should be conducted using a full-scale test rig with real contact geometry to study the noise from two-point contact that occurs in curves. The second possibility is to perform more accurate field experiments. Both possible approaches can reveal how a sound spectral distribution is changed when a railhead is lubricated by a friction modifier or water. Furthermore, more realistic SPL mitigation values could be investigated using these approaches. In the present study, the reduction in SPL was unrealistically high (up to 35 dBA), and generally the mitigation of noise in the field reaches values of the order of decibels [12,13]. The results also showed the dependence of SPL on CoA, which is bilinear. Further experiments should also take into account the way the products are applied. If the study is focused on the wayside application, it will be necessary to further investigate the distribution of the product along the rail, which means a move from the laboratory to the real track. It would be possible to monitor the noise threshold at which the friction film breaks on a real track. This knowledge could be used to control the application of products to avoid noise. In the case of an on-board application, it will be necessary to change the way the product is applied to spray the product on the disc.

5. CONCLUSION

A twin-disc machine was used to study the behaviour of water-based FMs in terms of noise and adhesion in the contact between the wheel and the rail. The ability to reduce SPL and CoA of nine different water-based compositions for AoA of 4 °, which simulates the conditions that occur in tram reversing loops, was investigated. Dry and wet films were prepared and tested for each composition. The main conclusions of this study are as follows:

- The spraying of water seems to be a promising method for reducing squeal noise without the risk of low adhesion.
- To achieve long retentivity, a solid lubricant is needed in the composition, but a high content of solid lubricant results in low adhesion, which could be risky for braking. In this study, 2 wt.% solid lubricant appears to be the optimal content.
- The most appropriate results were achieved for a composition containing bentonite, talc, and molybdenum disulphide. This composition provided the required behaviour in both wet and dry forms.
- There is a strong correlation between CoA and SPL. The dependence between these parameters is bilinear. This dependence could be used in the control systems of wayside lubrication systems to make them more effective and to avoid a sudden increase in SPL.

Acknowledgement

This research was supported by the Czech Science Foundation (Project No. 20-23482S). The authors also thank the support by National Key R&D Program Intergovernmental Key Items for International Scientific and Technological Innovation Cooperation (No.2018YFE0109400) and the Sichuan Science and Technology Program (No.2020YFH0057).

REFERENCES

[1] D. Thompson, *Curve Squeal Noise*, in: Railway Noise and Vibration, Elsevier, pp. 315–342, 2009, doi: 10.1016/B978-0-08-045147-3.00009-8

[2] B. Müller, J. Oertli, *Combating Curve Squeal: Monitoring existing applications*, Journal of Sound and Vibration, vol. 293, iss. 3–5, pp. 728–734, 2006, doi: 10.1016/j.jsv.2005.12.005

[3] J. Han, Z. Wen, R. Wang, D. Wang, X. Xiao, G. Zhao, X. Jin, *Experimental study on vibration and sound radiation reduction of the web-mounted noise shielding and vibration damping wheel*, Noise Control Engineering Journal, vol. 62, no. 3, pp. 110–122, 2014, doi: 10.3397/1/376211

[4] J.F. Brunel, P. Dufrénoy, F. Demilly, *Modelling of squeal noise attenuation of ring damped wheels*, Applied Acoustics, vol. 65, iss. 5, pp. 457–471, 2004, doi: 10.1016/j.apacoust.2003.12.003

[5] D.T. Eadie, J. Kalousek, K.C. Chiddick, *The role of high positive friction (HPF) modifier in the control of short pitch corrugations and related phenomena*, Wear, vol. 253, iss. 1–2, pp. 185–192, 2002, doi: 10.1016/S0043-1648(02)00098-4

[6] D.T. Eadie, M. Santoro, W. Powell, *Local control of noise and vibration with KELTRACK™ friction modifier and Protector® trackside application: An integrated solution*, Journal of Sound and Vibration, vol. 267, iss. 3, pp. 761–772, 2003, doi: 10.1016/S0022-460X(03)00739-9

[7] R. Galas, D. Kvarda, M. Omasta, I. Krupka, M. Hartl, *The role of constituents contained in water–based friction modifiers for top–of–rail application*, Tribology International, vol. 117, pp. 87–97, 2018, doi: 10.1016/j.triboint.2017.08.019

[8] K. Chiddick, *Solid lubricants and friction modifiers for heavy loads and rail application*, US Patent 6.136.757, 2000.

[9] D.T. Eadie, X. Lu, J. Cotter, *Modified friciton control compositions*, US Patent 7.939.476 B2, 2011.

[10] K. Chiddick, A. Medrano, R. Krinker, K. Wilson, D. Birdwell, *Positive friction control composition for railways*, US Patent 9.617.498 B2, 2017.

[11] M. Harmon, R. Lewis, *Review of top of rail friction modifier tribology*, Tribology – Materials, Surfaces & Interfaces, vol. 10, iss. 3, pp. 150–162, 2016, doi: 10.1080/17515831.2016.1216265

[12] D.T. Eadie, M. Santoro, J. Kalousek, *Railway noise and the effect of top of rail liquid friction modifiers: Changes in sound and vibration spectral distributions in curves*, Wear, vol. 258, iss. 7–8, pp. 1148–1155, 2005, doi: 10.1016/j.wear.2004.03.061

[13] D.T. Eadie, M. Santoro, *Top-of-rail friction control for curve noise mitigation and corrugation rate reduction*, Journal of Sound and Vibration, vol. 293, iss. 3–5, pp. 747–757, 2006, doi: 10.1016/j.jsv.2005.12.007

[14] R. Galas, M. Omasta, M. Klapka, S. Kaewunruen, I. Krupka, M. Hartl, *Case study: The influence of oil-based friction modifier quantity on tram braking distance and noise*, Tribology in Industry, vol. 39, no. 2, pp. 198–206, 2017, doi: 10.24874/ti.2017.39.02.06

[15] J.I. Egana, J. Vinolas, N. Gil-Negrete, *Effect of liquid high positive friction (HPF) modifier on wheel-rail contact and rail corrugation*, Tribology International, vol. 38, iss. 8, pp. 769–774, 2005, doi: 10.1016/j.triboint.2004.11.006

[16] D.T. Eadie, M. Santoro, K. Oldknow, Y. Oka, *Field studies of the effect of friction modifiers on short pitch corrugation generation in curves*, Wear, vol. 265, iss. 9–10, pp. 1212–1221, 2008, doi: 10.1016/j.wear.2008.02.028

[17] A. Matsumoto, Y. Sato, H. Ono, Y. Wang, M. Yamamoto, M. Tanimoto, Y. Oka, *Creep force characteristics between rail and wheel on scaled model*, Wear, vol. 253, iss. 1–2, pp. 199–203, 2002, doi: 10.1016/S0043-1648(02)00100-X

[18] Z. Li, O. Arias-Cuevas, R. Lewis, E.A. Gallardo-Hernández, *Rolling-sliding laboratory tests of friction modifiers in leaf contaminated wheel-rail contacts*, Tribology Letters, vol. 33, pp. 97–109, 2009, doi: 10.1007/s11249-008-9393-3

[19] O. Arias-Cuevas, Z. Li, R. Lewis, E.A. Gallardo-Hernández, *Rolling-sliding laboratory tests of friction modifiers in dry and wet wheel-rail contacts*, Wear, vol. 268, iss. 3–4, pp. 543–551, 2010, doi: 10.1016/j.wear.2009.09.015

[20] P.A. Meehan, X. Liu, *Wheel squeal noise control under water-based friction modifiers based on instantaneous rolling contact mechanics*, Wear, vol. 440–441, pp. 1–9, 2019, doi: 10.1016/j.wear.2019.203052

[21] X. Liu, P.A. Meehan, *Investigation of squeal noise under positive friction characteristics condition provided by friction modifiers*, Journal of Sound and Vibration, vol. 371, pp. 393–405, 2016, doi: 10.1016/j.jsv.2016.02.028

[22] P.A. Meehan, X. Liu, *Modelling and mitigation of wheel squeal noise under friction modifiers*, Journal of Sound and Vibration, vol. 440, pp. 147–160, 2019, doi: 10.1016/j.jsv.2018.10.025

[23] C. R. Fulford, *Engineering Review of Low Adhesion Research*, Report published by Rail Safety and Standards Board, UK, 2004.

[24] E. Dangler, *Comparative rheological behaviour of suspended clays with varying ionic composition,* PhD thesis, Honolulu (USA): University of Hawaii, 1973.

[25] H. Chen, S. Fukagai, Y. Sone, T. Ban, and A. Namura, *Assessment of lubricant applied to wheel/rail interface in curves*, Wear, vol. 314, iss. 1–2, pp. 228–235, 2014, doi: 10.1016/j.wear.2013.12.006

[26] R. Galas, M. Omasta, I. Krupka, M. Hartl, *Laboratory investigation of ability of oil-based friction modifiers to control adhesion at wheel-rail interface*, Wear, vol. 368–369, pp. 230–238, 2016, doi: 10.1016/j.wear.2016.09.015

[27] L. Buckley-Johnstone, M. Harmon, R. Lewis, C. Hardwick, R. Stock, *A comparison of friction modifier performance using two laboratory test scales*, Proceedings of the Institution of Mechanical Engineers, Part F: Journal of Rail and Rapid Transit, vol. 233, iss. 2, pp. 201–210, 2019, doi: 10.1177/0954409718787045

[28] J. Oertli, *Combating Curve Squeal Phase II*, Final report published by Swiss Federal Railways, Bern, 2005.

[29] K. Hou, J. Kalousek, E. Magel, *Rheological model of solid layer in rolling contact.* Wear, vol. 211, iss. 1, pp. 134–40, 1997, doi: 10.1016/S0043-1648(97)00097-5

Supplementary material

WET									
Composition	**C1**	**C2**	**C3**	**C4**	**C5**	**C6**	**C7**	**C8**	**C9**
T_{BC} (s)	/	15	/	/	/	10	55	10	65
σ (s)	/	5	/	/	/	2	5	2	5
T_{BD} (s)	/	25	/	/	/	25	110	60	220
σ (s)	/	5	/	/	/	2	5	7	10
T_{BE} (s)	15	65	30	30	30	90	150	120	300
σ (s)	2	5	5	5	5	5	5	5	25
ΔSPL (dB)	/	/	/	/	/	25.6	31.1	28.7	33.0
σ (dB)	/	/	/	/	/	0.4	1.5	0.3	0.9
ΔCoA (1)	/	/	/	/	/	0.19	0.28	0.26	0.31
σ (1)	/	/	/	/	/	0.02	0.01	0.05	0.02
SPL_D (dB)	/	/	/	/	/	93.1	93.2	94.8	94.3
σ (dB)	/	/	/	/	/	0.8	1.2	1.2	1.1
CoA_D (1)	/	/	/	/	/	0.30	0.26	0.28	0.27
σ (1)	/	/	/	/	/	0.01	0.04	0.01	0.02
DRY									
Composition	**C1**	**C2**	**C3**	**C4**	**C5**	**C6**	**C7**	**C8**	**C9**
T_{BC} (s)	/	/	/	/	/	10	80	105	160
σ (s)	/	/	/	/	/	3	5	10	15
T_{BD} (s)	/	/	/	/	/	85	140	190	300
σ (s)	/	/	/	/	/	5	20	2	10
T_{BE} (s)	/	50	40	40	35	130	190	270	370
σ (s)	/	5	5	5	3	25	20	20	20
ΔSPL (dB)	/	/	/	/	/	29.6	31.5	33.1	32.7
σ (dB)	/	/	/	/	/	1.7	1.2	0.7	0.5
ΔCoA (1)	/	/	/	/	/	0.25	0.26	0.30	0.31
σ (1)	/	/	/	/	/	0.01	0.01	0.01	0.02
SPL_D (dB)	/	/	/	/	/	96.5	93.1	93.9	93.9
σ (dB)	/	/	/	/	/	0.7	2.6	0.1	1.3
CoA_D (1)	/	/	/	/	/	0.34	0.27	0.26	0.25
σ (1)	/	/	/	/	/	0.02	0.07	0.03	0.02

Vol. 46, No. 3 (2024) 418-431, DOI: 10.24874/ti.1579.11.23.01

Tribology in Industry

www.tribology.rs

RESEARCH

Wheel Squeal Mitigation Under Water Lubrication

Václav Navrátil[a,*], Radovan Galas[a], Milan Klapka[a], Daniel Kvarda[a], Milan Omasta[a]

[a]*Faculty of Mechanical Engineering, Brno University of Technology, Technicka 2896/2, 616 69 Brno, Czechia.*

Keywords:

Wheel squeal noise
Noise mitigation
Friction management
Water lubrication
Wheel-rail tribology

* Corresponding author:

Václav Navrátil
E-mail: Vaclav.Navratil@vutbr.cz

Received: 13 November 2023
Revised: 14 December 2023
Accepted: 26 January 2024

A B S T R A C T

This study investigates the potential of applying water to the wheel-rail contact to reduce squealing noise. For this purpose, a twin-disc device with a single tram wheel and real wheel suspension stiffnesses was developed. Three types of tests were performed. During the tests, adhesion coefficient, sound pressure level and wheel axial vibration were measured. The tests under dry conditions were carried out to describe the frequency spectrum of wheel vibration and to establish reference values for further measurements. The tests under wet conditions were carried out to investigate the ability of water to reduce adhesion and noise. Finally, tests with varying amounts of water in contact were carried out because of the low adhesion risk. The experimental results showed that the twin-disc device was able to reproduce both the adhesion and noise properties of the contact. Tests with different amounts of water showed that the application of water can be a promising way to reduce squealing noise from wheel-rail contact.

© 2024 Published by Faculty of Engineering

1. INTRODUCTION

One of the most unpleasant downsides of railway transport is the curve squealing noise that occurs when rolling stock negotiates a sharp curve. This is mainly due to frictional instabilities in the wheel-rail contact [1] which can occur in several ways [2]. Lateral slip, or creepage, of the wheel tread on the top of the rail plays an important role. This noise, known as a top-of-rail squeal, has a strong tonal character and is very loud, usually exceeding 90 dB [3]. It typically occurs in the 400 – 5000 Hz frequency range [4,5]. Recently, the longitudinal slip has also been shown to influence the occurrence of top-of-rail squeal [6], with the noise occurring in the 3.5 – 6 kHz frequency band [7]. Frictional instabilities can also arise from the interaction of the wheel flange with the gauge face of the rail [3]. Such noise is called flanging noise and is present at higher frequencies over a wide band of 5 – 10 kHz [8,9]. Both types of squeal occur in a largely random, chaotic manner [10–12], and this is mainly due to the large number of parameters that influence the noise generation - e.g. operating parameters such as rolling speed or angle of attack [13], railway track dynamics [14,15], longitudinal creepage [7], etc.

Curve squeal noise is very annoying in densely populated areas, where squealing noise can, according to Müller and Oertli [16], affect up to 1,000 inhabitants within 250 m of the noise source. For this reason, it is important to reduce noise, which can be done in several ways: by passive [17–

19] or active vibration control [20,21], or by adjusting the frictional properties of the wheel-rail contact [22,23]. With wheel vibration damping, the sound pressure level can be reduced by up to 15 dB [24], but this solution is limited by the narrow frequency band to which the damping is tuned. Active wheel vibration control is a new approach that involves mounting actuators on the wheel that damp frequencies based on signals from piezoelectric sensors. This method has been shown to be effective in reducing squeal noise by up to 12 dB in the near field [20], but the system has not yet been used in real-world applications.

Modification of the contact friction properties is possible through the application of various products to the top of the rail head. Top-of-rail (TOR) products include water-based friction modifiers and oil-based TOR lubricants. These products allow the positive trend of the traction curve and the adhesion coefficient to be maintained at an intermediate level. When used on real tracks, sound pressure levels can be reduced by up to 12 dB [8,25]. Recently it has been shown that the application of water to the wheel-rail contact can lead to lower wear [26–28] and noise [29] in addition to reduced adhesion. Several authors show that water can reduce the coefficient of adhesion at levels between 0.2 – 0.45 [30–33] depending on quantity and temperature, or velocity. Water spraying could represent a simple, cheap, and environmentally friendly option for wheel-rail interface lubrication. However, research to date has mainly been carried out on scaled twin discs without a focus on noise reduction, so further research is needed under conditions that more closely resemble real contact.

As it is difficult to control experiments on the real track, test rigs are set up for laboratory research. Naeimi [34] compiled an overview of different approaches and designs but in general, it can be said that due to the ease of slip control and compact dimensions, the twin disc concept is the most common approach to study a single wheel-rail contact. Hsu et al. [4] developed a device which was used to study the adhesion-noise relationship and to validate theoretical models. A similar device was developed at TNO-TPD Delft and used to study the effect of longitudinal creepage together with lateral creepage [35,36]. Another device was built at the University of Queensland. The primary motivation for building the device was to study corrugation formation and wear [37], but later, it was used by Meehan and Liu [13,38,39] to experimentally validate the developed simulation models and predictions of squealing noise generation. The device was further modified and Liu [40] used it to investigate the effect of contact angle on noise generation.

This study aims to investigate the potential reduction of wheel squeal noise through the application of water into the wheel-rail contact area. For this purpose, the twin-disc test rig with a real tram wheel was designed and used, see Fig. 1. During the design process, emphasis was placed on maintaining the realistic stiffness of the wheel fit in the tram chassis. Detailed information regarding the design of this device can be found in the paper [41]. The analysis of the effects of water application on wheel-rail interaction is intended to contribute to the knowledge of noise reduction techniques and a better understanding of the factors influencing wheel squeal.

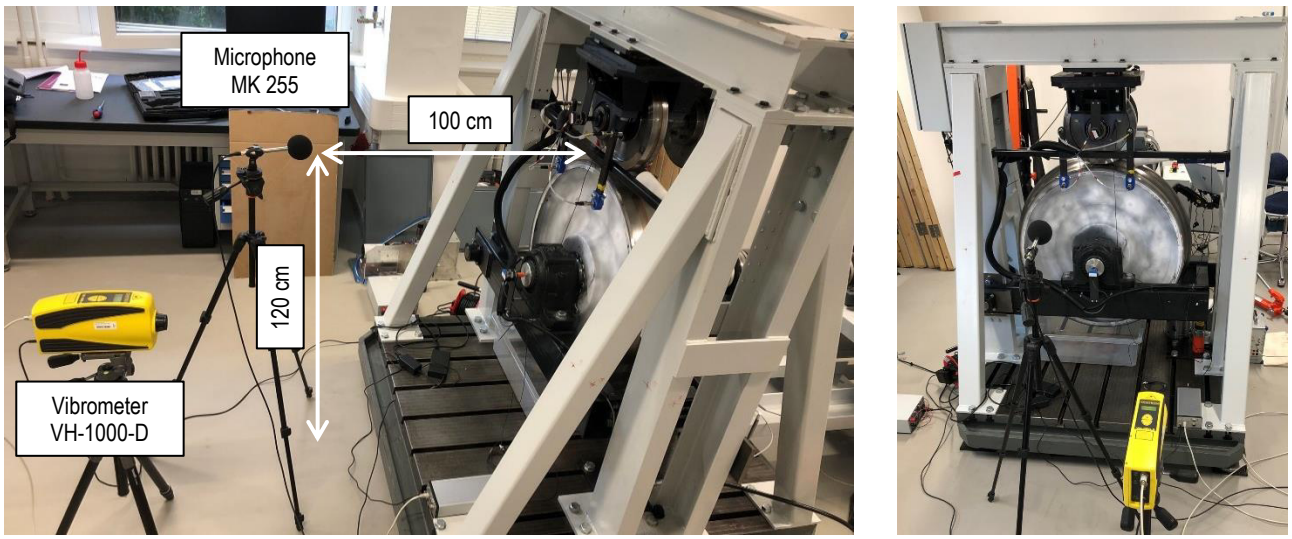

Fig. 1. Experimental twin-disc device.

2. MATERIAL AND METHODS

2.1 Experimental methods

The main parts of the device in Fig. 1 are tram wheel with ORE S 1002 profile with a diameter of 800 mm and 320 mm diameter rail disc. The disc is made of C55E steel. This material does not correspond to the actual rail material but was chosen for higher wear resistance and longer maintenance of stable conditions during testing. The wheel is mounted on a structure that is pivotally attached to the main frame and the contact loading is thus realized by a lever using a hydraulic cylinder and a compression coil spring. The disc is mounted on a support that allows the disc to be rotated to change the angle of attack, and the disc to be moved to change the lateral position of the disc thanks to a pair of linear guideways. The 11 kW AC electric motor with a gearbox, which drives the wheel, is mounted on an independent frame. The test rig was designed with the required dynamic characteristics in mind. To achieve the required dynamic properties of the wheel and suspension disc, the stiffness of certain elements in the support frame was optimised. By optimising the stiffness of the bridging beams at the top of the rig, the normal stiffness of the rail disc was determined. This, together with the lateral stiffness of the positioning system, also influences the lateral stiffness of the rail disc. The normal stiffness of the wheel was determined by selecting a compression spring in the loading mechanism with the appropriate stiffness. The lateral stiffness of the wheel corresponds to the stiffness of the beams that make up the wheel lever. The stiffness of the elements was designed using FEM software and analytical calculations. The parameters of the twin-disc device can be found in Table 1. A more detailed description of the device can be found in the paper [41].

An integral part of the equipment is the measuring system. To evaluate the lateral adhesion coefficient, it is necessary to measure the load and lateral force. Two load cells are used for this purpose. The first one is part of the load mechanism and reads the force in the range of 0 – 10 kN. The second is mounted in the disc support and measures the lateral force in the range of 0 – 5 kN. The sampling frequency of 500 Hz for the force measurements is set. Lateral adhesion coefficient can be calculated according to Hsu [4]:

$$\mu = 0{,}5196\frac{F_2}{F_1} \tag{1}$$

where F_2 is the lateral force and F_1 is the load force.

Table 1. Parameters of twin-disc device.

Parameter	Value	Unit
Outer dimensions	1340 x 3020 x 1690	mm
Weight	2270	Kg
Wheel diameter	800	mm
Wheel profile	ORE S 1002	-
Rail disc diameter	320	mm
Rail disc profile radius	100	mm
Maximum velocity	4	m/s
Wheel drive torque	1000	Nm
Wheel drive power	11	kW
Ange of attack range	±5	°
Wheel normal suspension	0.172	kN/mm
Wheel lateral suspension	5.21	kN/mm
Rail disc normal suspension	124	kN/mm
Rail disc lateral suspension	6	kN/mm

The numerical coefficient expresses the ratio of the oversteer because the load force is not measured in the axis of contact but at the end of the arm on which the wheel is mounted.

Another important parameter to evaluate is the lateral creepage. According to Meehan and Liu [30], the quasi-static value of lateral creepage equals the angle of attack. Two ultrasonic sensors SICK UM12-1172271 are used to read the position of the disc and the resulting angle of attack can be calculated according to the scheme in Fig. 2 using the equation:

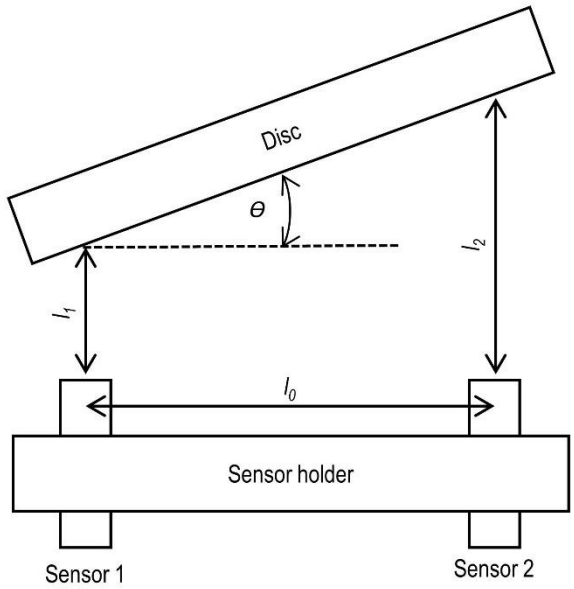

Fig. 2. Angle of attack evaluation scheme.

$$\theta = tan^{-1}\left(\frac{l_2 - l_1}{l_0}\right) \quad (2)$$

where l_1 and l_2 are measured distance to the disc from sensor no. 1 and 2, respectively, l_0 is the distance between sensors, which for the device used is 286 mm. The sampling frequency for distance measurements is set to 500 Hz.

2.2 Noise and vibration measurements

The twin-disc is not equipped with any vibration and noise measuring equipment; therefore, the use of external equipment is necessary. For noise measurements, a Svantek 911 sound meter with MK 255 microphone and SV 12L preamplifier was used to record the noise data. The noise was recorded in the frequency range 20 Hz – 20 kHz and no weighting filter was used. The microphone was placed 100 cm from the wheel-disc contact at contact height (120 cm), see Fig. 1.

To correctly identify the frequencies at which only the wheel emits noise, wheel vibration was also measured. An Ometron VH-1000-D industrial laser Doppler vibrometer connected to Brüel & Kjær PULSE™ data acquisition system was used to measure wheel vibration. The vibration was scanned in the axial direction with the laser aimed at the edge of the wheel tyre. Data was acquired in the frequency range of 20 Hz – 22 kHz. Fast Fourier transform analysis was used to obtain the frequency spectrum of vibration.

2.3 Data validation

Finite Element Method (FEM) modal analysis was carried out using ANSYS to gain a comprehensive understanding of the dynamic behaviour of the wheel. This analysis provided insight into the structural response of the wheel, revealing its natural frequencies, and associated modal shapes. By simulating the vibrational behaviour, we identified critical modes of vibration, such as those that could lead to resonant conditions, and assessed their impact on the wheel's performance.

To ensure the accuracy and reliability of the adhesion values measured in this study, a validation procedure was required. The validation procedure involved a comparison of the measured adhesion data with simulations obtained from the established model developed by de Beer [35], see equation (3):

$$\mu = \begin{cases} \mu_K\left\{\zeta' - \frac{1}{3}\zeta'^2 + \frac{1}{27}\zeta'^3\right\} & \text{for } \zeta' \leq 3 \\ \mu_K & \text{for } \zeta' > 3 \end{cases} \quad (3)$$

where μ_K is the realistic friction characteristic defined in [42]as:

$$\mu_K = \mu_0\left\{1 - 0.5e^{-0.138/|\zeta V_0|} - 0.5e^{-6.9/|\zeta V_0|}\right\} \quad (4)$$

where μ_0 is static friction coefficient, V_0 is rolling speed, ζ is nominal lateral creepage calculated according to equation (5):

$$\zeta = \frac{\theta}{\cos\theta_C} \quad (5)$$

using angle of attack θ and contact angle θ_C, ζ' is normalised creepage which can be obtained from equation (6):

$$\zeta' = \frac{\zeta k_\zeta}{N} \quad (6)$$

where k_ζ is the contact parameter and N is the load. Using this validated simulation model, we aimed to confirm the consistency of our experimental results with the expected results based on established theoretical frameworks. This approach not only increases the robustness of our results but also allows us to assess the validity of our measurement techniques and their agreement with theoretical predictions.

2.4 Experimental procedure

Three types of tests were performed in this study. The purpose of tests under dry conditions was to describe the frequency spectrum of wheel vibration and to establish reference values for subsequent comparison with wet contact. The tests were carried out at two speeds, 2 and 4 m/s. The lower speed is the speed at which trams normally travel through the loop and the higher speed is close to the limit at which trams are allowed to travel through the loop. The contact force was chosen to be 1,000 N (≈ 600 MPa) according to Meehan [43]. In the loop, the angle of attack reaches values of around 2° (≈ 35 mrad), so tests were carried out in the range 0 – 35 mrad. The experiments were performed at room temperature (25 °C). In addition to adhesion, sound pressure and vibration levels were also recorded, see sections 2.1 and 2.2. All tests were repeated three times and traction curves for each speed were made from the average of three measurements for each angle of attack. Before each test, the wheel and disc were cleaned with paper towels, acetone and water as in the previous study [29].

The tests under wet conditions were carried out under the same conditions as the tests under dry conditions. Water was continuously applied to the contact at a rate of 5 ml/s for 20 s. Before each test, the wheel and disc were cleaned in the same way as for the tests under dry conditions tests. A traction curve was also constructed in the same way and the sound pressure level and wheel vibration were measured.

The final part of the experiments focused on the effect of the amount of water applied to the wheel-rail contact. The motivation was to see if the amount of water in contact influenced the development of low adhesion (μ < 0.1). The tests were carried out under a uniform setup with a speed of 4 m/s, a contact load of 1,000 N, an angle of attack of 20 mrad, and at room temperature. Amounts of 1, 2, 5 and 10 ml were used for the experiments. Each test was repeated three times. Three parameters were monitored during the tests: the change in adhesion ($\Delta\mu$), the change in sound pressure level (ΔSPL) and the retentivity (Δt), i.e., the time between the application of water and the achievement of the reference values, see Fig. 3.

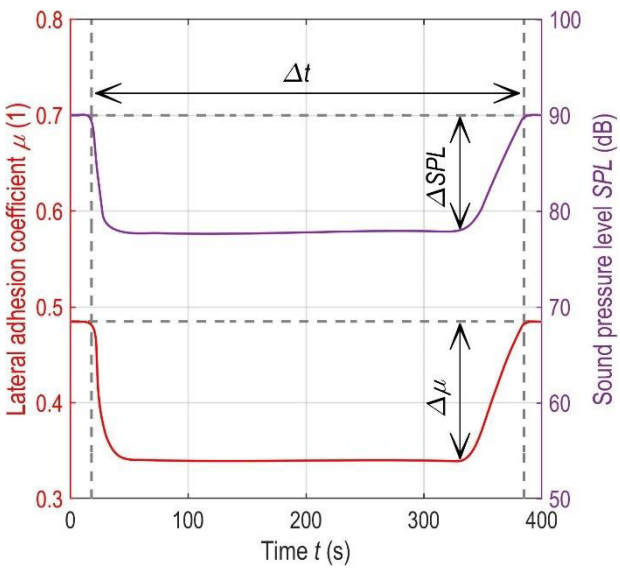

Fig. 3. A typical development of μ and SPL over time.

3. RESULTS AND DISCUSSION

3.1 Modal analysis

The results of the analysis revealed six dominant frequencies in the 0 – 5 kHz range at which wheel oscillations can be expected, see Table 2. The resulting frequencies are similar to those reported by Liu [13] in his paper. The largest differences are at frequencies below 1 kHz, but these are due to the use of a different wheel profile. The agreement with Liu's results for the (3,0) mode, see Fig. 4, is important, as this mode is described by the authors as prone to squeal. The FEM analysis showed that modes exist in pairs, i.e., two modes have identical natural frequencies and modal shapes with phase shift between them, which is the typical feature of an axisymmetric structure [4].

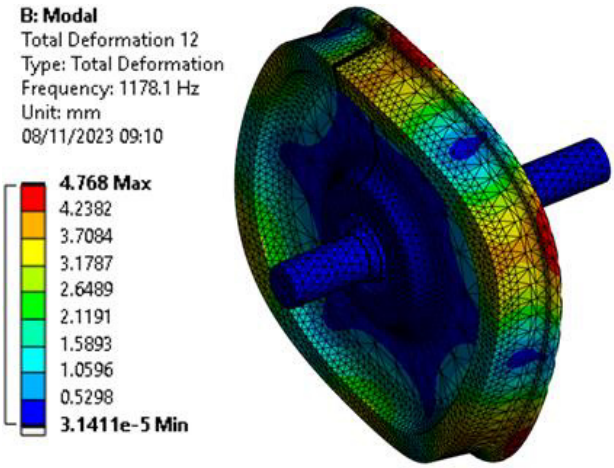

Fig. 4. Visualization of wheel modal shape (3,0) - 1178 Hz.

Table 2 Results of FEM modal analysis.

Dominant frequency (Hz)	Vibration mode (*n,m*)	Mode shape
295	(1,0)	
475	(2,0)	
1178	(3,0)	
2013	(4,0)	
3125	(5,0)	
4202	(6,0)	

3.2 Measurements under dry conditions

The results of the experiments under dry conditions in Fig.5 show that the measured adhesion coefficient at the saturation point of the traction curve is around 0.5, which is

expected value [44]. After fitting the data with the simulation model of de Beer [35] with parameter settings according to Meehan [43], it can be concluded that the measured data fit the simulation well. The deviation of the measured data from the simulation is due to a combination of uncertainties in the load and lateral force measurements. According to Hsu [4], uncertainty in the measurement of the adhesion coefficient can be expressed as:

$$\delta\mu = \sqrt{(\delta F_1/F_1)^2 + (\delta F_2/F_2)^2} \quad (7)$$

Both load cells were used to measure with an error of 5 %. Substituting this value into the formula gives an uncertainty in the lateral adhesion coefficient of approximately 7 %. Converted to adhesion coefficient values, an error of ±0.04 can be expected. This band is shown in Fig. 5 by error lines. All results, which are listed in Table A1 in the Supplementary Material, are within this tolerance.

The measured sound pressure levels increased with increasing angle of attack and also with higher rolling velocity, see Table A2 in the Supplementary Material, which was expected given the results of Meehan [13,38]. The frequency composition of the measured noise is shown in Fig. 6. In the figure, peaks can be observed at frequencies that correspond to the simulation, but the signal is significantly affected by noise from other components of the twin-disc device, e.g. the rail disc.

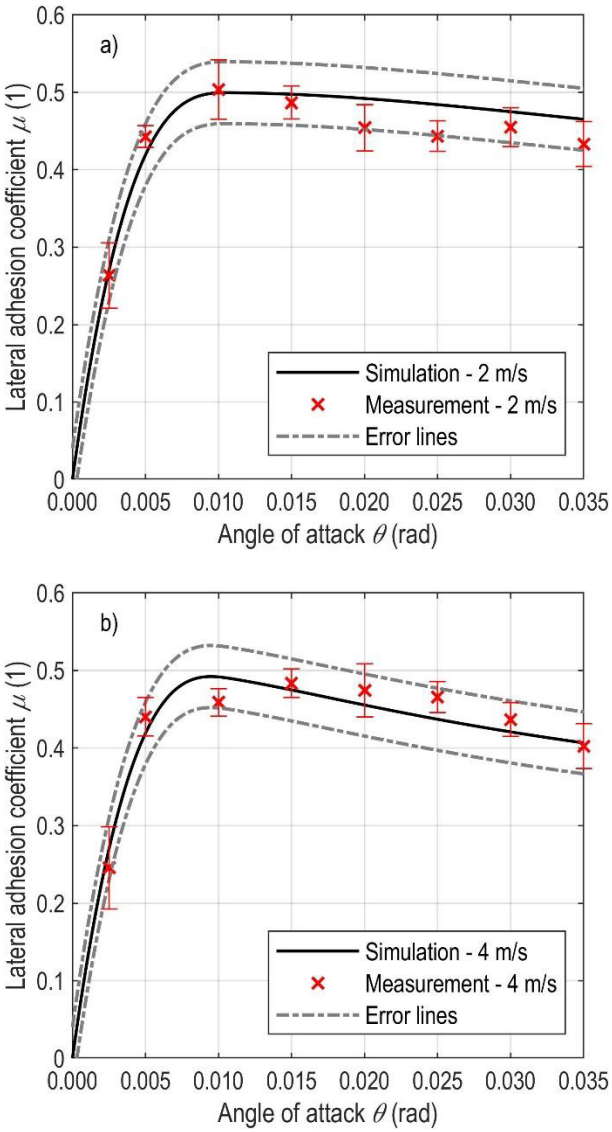

Fig. 5. Results of experiments under dry conditions for speed: (a) 2 m/s, (b) 4 m/s.

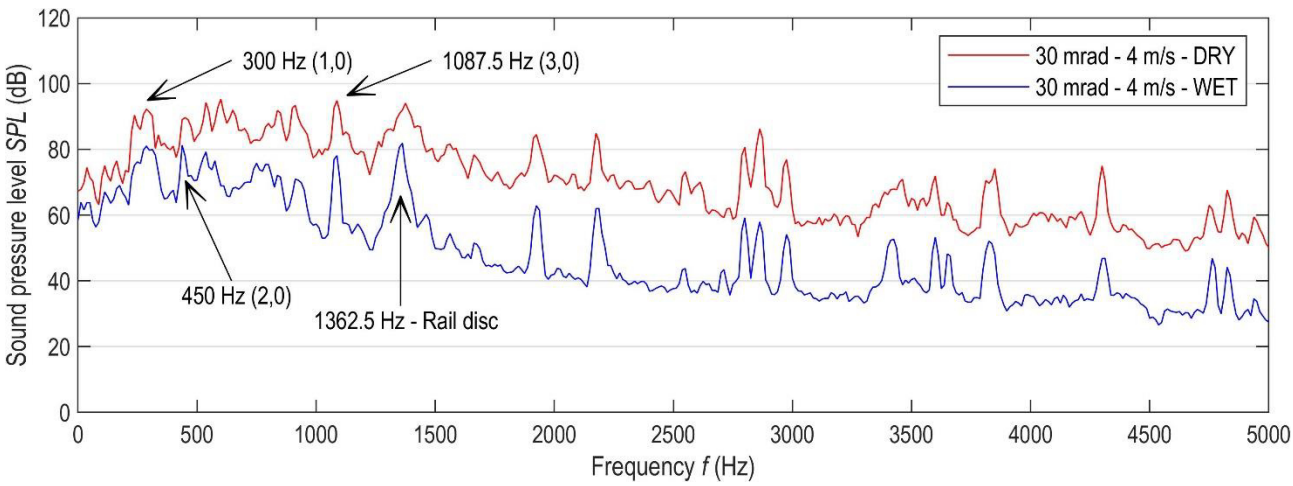

Fig. 6. Frequency composition of measured noise under dry (red) and wet (blue) conditions.

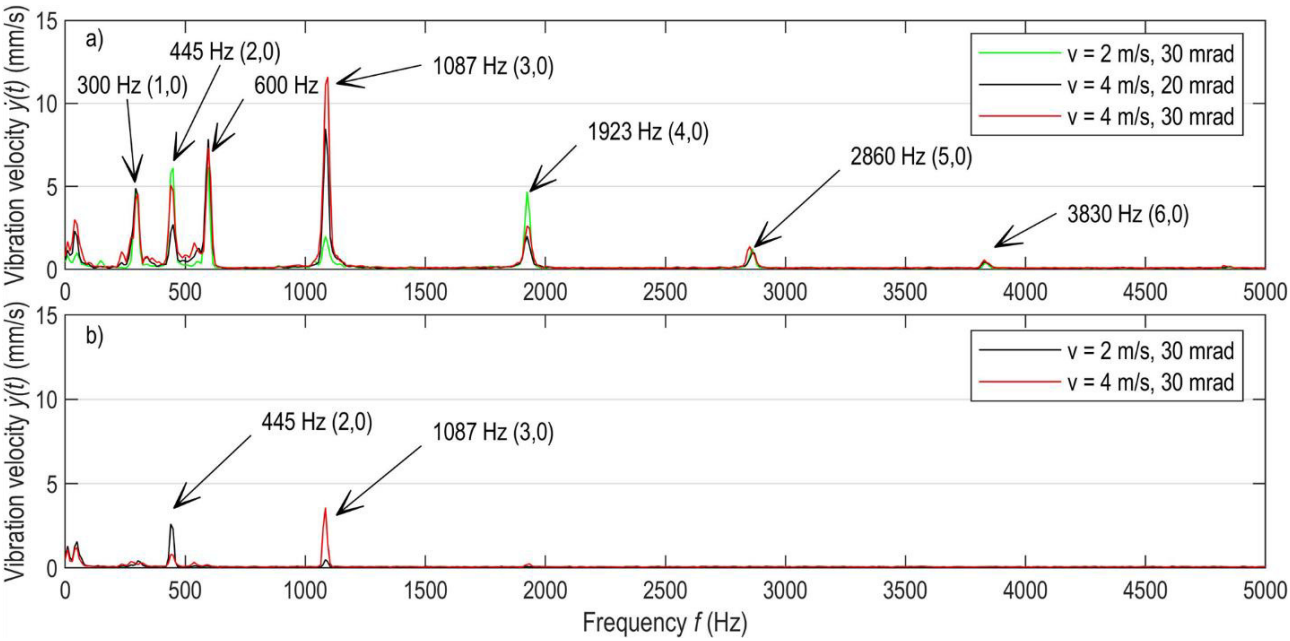

Fig. 7. Frequency composition of measured vibrations in (a) dry contact, and (b) wet contact.

Therefore, the vibration spectrum is more suitable for validating the noise manifestations as it is not as affected by any other component of the twin-disc device as the noise spectrum. The results of the vibration frequency analysis of the measurements under dry conditions are shown in Fig. 7(a) and listed in Tables A3 – A5 in the Supplementary Material. The frequencies of the wheel vibration modes can be identified in the graph, namely 300, 445, 1087, 1923, 2860 and 3830 Hz. These frequencies agree with the results of the modal finite element analysis in ANSYS, although there are minor differences of a few units of Hz for the lower frequencies and low hundreds of Hz for the higher frequencies. This inaccuracy is due to the simplification of the wheel geometry and mounting for the FEM analysis. A frequency of 600 Hz still appears in the frequency spectrum, which does not correspond to the FEM analysis. Control measurements showed that this frequency corresponds to the lateral vibration of the wheel mounting structure. Essentially all the modes identified by FEM analysis appear in the frequency spectrum, but the most dominant vibration mode is at 1100 Hz and is mainly excited at the higher speed of 4 m/s. Meehan and Liu [13,38–40] or Ding [45] also work with this frequency mode in their models. It is important to note that the study is focused on the tram wheel. Different frequency modes are expected for the larger railway wheels used, for example, on freight trains. The results also confirm the findings of Meehan and Liu [13] who state that the vibration velocity amplitude increases with increasing rolling velocity and angle of attack. Interestingly, at lower velocities, the vibration modes at 445 and 1923 Hz are more excited than the mode at 1087 Hz. These findings may lead to the idea of excitation of the vibration modes according to the operating conditions, i.e. which vibration mode becomes dominant depends on what operating conditions prevail. This hypothesis should be the subject of further research.

3.3 Measurements under wet conditions

The results of the tests under wet conditions are shown in Fig. 8 and listed in Table A1 in the Supplementary Material. It can be seen from the graphs that the lateral adhesion coefficient decreases after the application of water by up to 20 % compared to simulation under dry conditions in angle of attack range of 5 – 20 mrad. The values of the lateral adhesion coefficient range from 0.3 to 0.4 for angles of attack of 5 mrad and above, which is within the expected range of 0.2 to 0.45 [31]. The experimental results for both rolling speeds are rather constant after passing the saturation point. After the application of water to the contact, there is probably no increase in contact temperature with increasing slip. Water probably acts as a cooling medium and may prevent the formation of oxide layers that reduce the adhesion coefficient, thus

keeping the trend of the traction curve neutral [46,47]. Therefore, the traction curves in Fig. 8 were obtained by modifying equation (3) according to Shen [48]:

$$\mu = \begin{cases} \mu_0 \left\{ \zeta' - \frac{1}{3}\zeta'^2 + \frac{1}{27}\zeta'^3 \right\} & \text{for } \zeta' \leq 3 \\ \mu_0 & \text{for } \zeta' > 3 \end{cases} \quad (8)$$

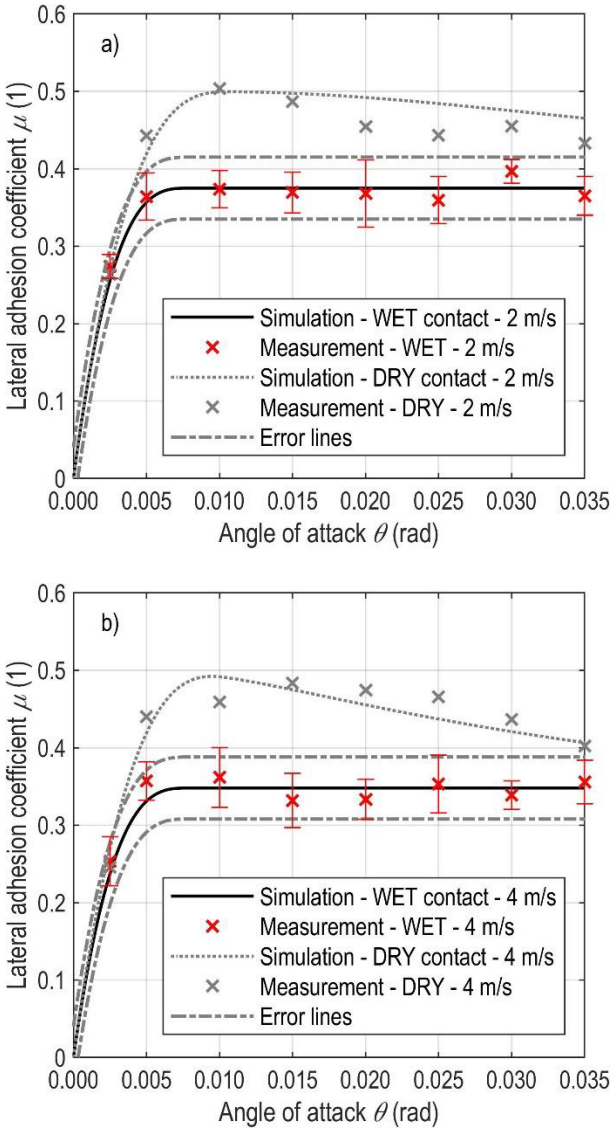

Fig. 8. Results of experiments under wet conditions for speed: (a) 2 m/s, (b) 4 m/s.

To fit the measured data to the simulation curve, it was necessary to determine the value of the static coefficient of friction. This value was estimated using the method of least squares, the aim being to find the smallest deviation of the simulation curve from the data. Using this method, the value of the static coefficient of friction was determined to be 0.375 for rolling speed 2 m/s and 0.348 for 4 m/s. The lateral adhesion coefficient appears to decrease slightly as the rolling speed increases to 4 m/s. This is contrary to the general conclusions drawn by Liu and Meehan in their study [30]. On the other hand, after analyzing their results, it is clear that the increase in the lateral adhesion coefficient is not linear and only occurs at high speeds, up to 25 m/s in the case of the study [30]. It can therefore be assumed that the lateral adhesion coefficient decreases with increasing speed up to a certain speed, after which the trend is reversed. This hypothesis could be the subject of further research.

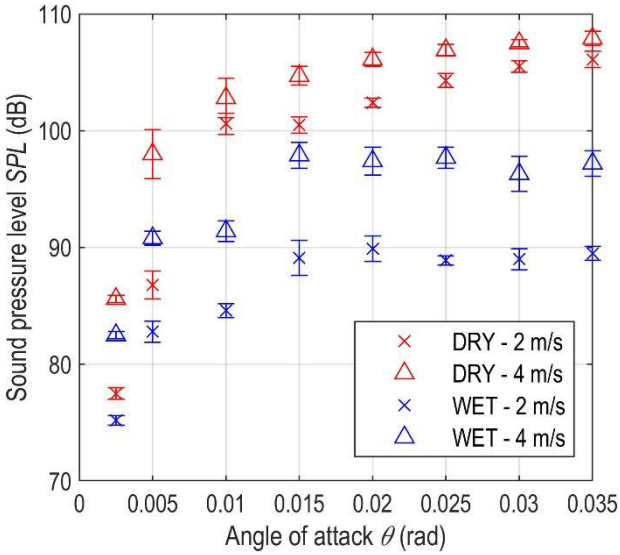

Fig. 9 Evolution of SPL with increasing speed and angle of attack.

Looking at the frequency spectrum of the measured noise in Fig. 6, it can be seen that there is a reduction in noise over a wide range of frequencies. Fig. 9 and Table A2 in the Supplementary Material also show that noise reduction in wet conditions is dependent on rolling speed. At 2 m/s there are reductions of up to 11 – 17 dB beyond the saturation point, while at 4 m/s the reductions are lower, up to 9 – 11 dB. The explanation is that greater dynamic effects at higher rolling speeds lead to an increase in stored acoustic energy and hence a higher overall SPL. The frequency spectrum of the vibration in dry (Fig. 7(a)) and wet (Fig. 7(b)) contact shows that applying water significantly reduces the overall amplitude of the vibration velocity across the entire spectrum, thus reducing the squealing noise. Again, it was observed that at a lower speed of 2 m/s, the 445 Hz frequency is excited. This again raises the idea of excitation of the vibration modes according to the operating conditions. All results are listed in Tables A3 – A5 in the Supplementary Material. The mechanism

by which water reduces noise and vibration in contact is related to the fact that the water can form a lubricating film with the oxides and wear particles in contact similar to the boundary lubrication film that TOR products create [32]. However, as it does not contain all the typical components of a TOR product, it does not reduce adhesion as much as has been observed with TOR products. Such a film is still able to reduce the number of peaks and valleys that interact with each other, thereby reducing the lateral force. This then leads to a reduction in the out-of-plane vibration of the wheel and hence a reduction in the amplitude of sound pressure levels [49].

3.4 Effect of the applied amount of water

The experimental results show that the amount of water applied can affect the adhesion conditions in contact, see Fig. 10. In the case of 1 ml of water applied, there was a large variance in the reduction in adhesion in the tests compared to the other amounts. This may be due to the method of water application, which was from a syringe into the contact area. With such a small amount, even a noticeable deviation from the contact patch may play a role. It is also interesting to note that an amount of 10 ml reduced adhesion the least. This may be related to the fact that in a fully flooded contact, water may wash out debris, which, together with iron oxides, may reduce the resulting adhesion to lower values, as has been observed by other authors [50–52]. The results of the experiments are listed in Table A6 in the Supplementary Material.

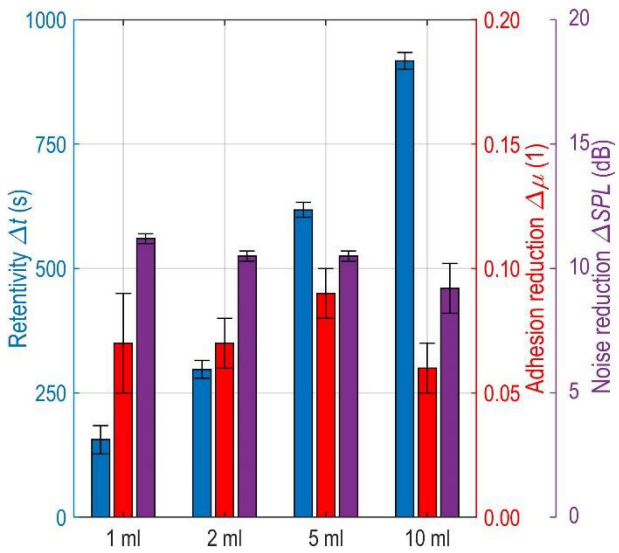

Fig. 10. Comparison of retentivity, adhesion and noise reduction for different amounts of water.

A look at noise reduction shows similar conclusions to the adhesion results. The application of 1, 2 and 5 ml of water resulted in a stable noise reduction of up to 11 – 12 dB. For the 10 ml application, the noise reduction was lower, only around 9 dB. Again, this is attributed to the fact that larger amounts of water are more effective at washing off oxides, which could lead to greater reductions, than smaller amounts of water. A significant difference was observed in the case of the retentivity of water in wheel-rail contact. The retentivity increased significantly with increasing amounts of water applied, which was expected and corresponds with Galas' results [50]. This is because more water takes longer to evaporate from the contact path. In addition, larger volumes of water will also flood the area around the contact, allowing further flooding of the contact and thus increasing the retentivity. When comparing the results, the dependence of retentivity on the amount of water applied appears to be linear.

These data show that water itself could be considered as a solution for reducing wheel squeal noise. An important finding is that the amount of water does not lead to low adhesion that can occur with an incorrect dosage of water-based and oil/grease-based top-of-rail products [49,53–57]. These results are in line with previous work [29]. It can be expected that more frequent applications will be required compared to a water- and oil-based top-of-rail product; on the other hand, the application of clean water represents an environmentally friendly way to achieve similar noise reductions, which are up to 12 dB on a real track [8,25].

3.5 Future study

The next study should focus on the problem of low adhesion. It turns out that the interaction of water with contaminants can lead to the formation of a highly viscous paste that causes this phenomenon [58,59]. This can then cause problems when starting and breaking rolling stock. From an operational safety point of view, this phenomenon should be avoided. The study should be carried out on a twin-disc rig with a real railway wheel to make the contact conditions as close as possible to real track conditions. Also, further research should focus on the idea of excitation of the vibration modes depending on the operating conditions. The

acoustic measurements should be extended to include acoustic emission measurements, which could provide a deeper insight into the coupling of friction film and noise manifestations. If conditions can be found that guarantee noise reduction without risking low adhesion, these conditions should be tested on a real track.

4. CONCLUSIONS

Our research seeks to provide solutions to mitigate wheel squeal noise. One of these solutions may be the application of water to the wheel-rail contact. This solution could lead to an improvement in the overall environmental quality. A newly developed twin-disc device was used to study the effect of water application on squeal noise. The main results of this work are:

- The twin-disc device, designed to simulate as closely as possible the actual wheel-rail contact on a tram track, can produce data that is consistent with current theory and the results of other authors. It can therefore be considered valid.
- The results of the experiments under dry and wet conditions lead to the idea of excitation of the vibration modes depending on the operating conditions, which should be further investigated.
- Applying water to the wheel-rail contact significantly reduces the excitation of the wheel's frequency modes, thereby reducing the squeal noise. At the same time, it does not cause low adhesion problems. The total reduction of emitted noise is up to 9 – 17 dB depending on rolling velocity and angle of attack.
- The amount of water applied does not affect noise reduction and more water does not increase the risk of low adhesion. The only difference observed was an increase in noise and adhesion reduction time as the amount of water applied increased.

Acknowledgement

This research was supported by the Czech Science Foundation (Project No. 20-23482S). The authors would also like to thank the Faculty of Mechanical Engineering at the Brno University of Technology for support within the F22-12 project.

ORCID iDs

Václav Navrátil 0000-0002-5248-4487
Radovan Galas 0000-0001-7364-899X
Milan Klapka 0000-0002-6503-6085
Daniel Kvarda 0000-0002-5386-2486
Milan Omasta 0000-0002-1448-3731

REFERENCES

[1] P.J. Remington, "Wheel/rail squeal and impact noise: What do we know? What don't we know? Where do we go from here?," *Journal of Sound and Vibration*, vol. 116, no. 2, pp. 339–353, Jul. 1987, doi: 10.1016/S0022-460X(87)81306-8.

[2] D. Alarcao, J.L. Bento Coelho, "An experimental assessment on the performance of fixed rail lubricators for curve squealing noise mitigation," *Noise Control Engineering Journal*, vol. 61, no. 6, pp. 567-577, Nov. 2013, doi: 10.3397/1/3761050 .

[3] D. Thompson, "Curve Squeal Noise," in: *Railway Noise and Vibration*, *Elsevier eBooks*, 2009, pp. 315–342. doi: 10.1016/b978-0-08-045147-3.00009-8.

[4] S.S. Hsu, Z. Huang, S.D. Iwnicki, D.J. Thompson, C.J.C. Jones, G. Xie, P.D. Allen, "Experimental and theoretical investigation of railway wheel squeal," *Proceedings of the Institution of Mechanical Engineers, Part F: Journal of Rail and Rapid Transit*, vol. 221, no. 1, pp. 59–73, Jan. 2007, doi: 10.1243/0954409jrrt85.

[5] J.F. Brunel, P. Dufrénoy, J. Charley, F. Demilly, "Analysis of the attenuation of railway squeal noise by preloaded rings inserted in wheels," *Journal of the Acoustical Society of America*, vol. 127, no. 3, pp. 1300 – 1306, Mar. 2010, doi: 10.1121/1.3298433.

[6] D.J. Fourie, P.J. Gräbe, P.S. Heyns, R.D. Fröhling, "Experimental characterisation of railway wheel squeal occurring in large-radius curves," *Proceedings of the Institution of Mechanical Engineers, Part F: Journal of Rail and Rapid Transit*, vol. 230, no. 6, pp. 1561–1574, Oct. 2015, doi: 10.1177/0954409715605142.

[7] D.J. Fourie, P.J. Gräbe, P.S. Heyns, R.D. Fröhling, "Frequency domain model for railway wheel squeal resulting from unsteady longitudinal creepage," *Journal of Sound and Vibration*, vol. 445, pp. 228–246, Apr. 2019, doi: 10.1016/j.jsv.2018.12.014.

[8] D.T. Eadie, M. Santoro, J. Kalousek, "Railway noise and the effect of top of rail liquid friction modifiers: Changes in sound and vibration spectral distributions in curves," *Wear*, vol. 258, no. 7–8, pp. 1148–1155, Mar. 2005, doi: 10.1016/j.wear.2004.03.061.

[9] Y.-K. Luo, L. Zhou, Y.-Q. Ni, "Towards the understanding of wheel-rail flange squeal: In-situ experiment and genuine 3D profile-enhanced transient modelling," *Mechanical Systems and Signal Processing*, vol. 180, p. 109455, Nov. 2022, doi: 10.1016/j.ymssp.2022.109455.

[10] C. Glocker, E. Cataldi-Spinola, R.I. Leine, "Curve squealing of trains: Measurement, modelling and simulation," *Journal of Sound and Vibration*, vol. 324, no. 1–2, pp. 365–386, Jul. 2009, doi: 10.1016/j.jsv.2009.01.048.

[11] Z. Yang, Z. Li, "Numerical modeling of wheel-rail squeal-exciting contact," *International Journal of Mechanical Sciences*, vol. 153–154, pp. 490–499, Apr. 2019, doi: 10.1016/j.ijmecsci.2019.02.012.

[12] P.A. Meehan, "Investigation of chaotic instabilities in railway wheel squeal," *Nonlinear Dynamics*, vol. 100, no. 1, pp. 159–172, Feb. 2020, doi: 10.1007/s11071-020-05493-x.

[13] X. Liu, P.A. Meehan, "Wheel squeal noise: A simplified model to simulate the effect of rolling speed and angle of attack," *Journal of Sound and Vibration*, vol. 338, pp. 184–198, Mar. 2015, doi: 10.1016/j.jsv.2014.10.031.

[14] B. Ding, G. Squicciarini, D. Thompson, "Effect of rail dynamics on curve squeal under constant friction conditions," *Journal of Sound and Vibration*, vol. 442, pp. 183–199, Mar. 2019, doi: 10.1016/j.jsv.2018.10.027.

[15] V.-V. Lai, O. Chiello, J.-F. Brunel, P. Dufrénoy, "The critical effect of rail vertical phase response in railway curve squeal generation," *International Journal of Mechanical Sciences*, vol. 167, p. 105281, Feb. 2020, doi: 10.1016/j.ijmecsci.2019.105281.

[16] B. Müller, J. Oertli, "Combating Curve Squeal: Monitoring existing applications," *Journal of Sound and Vibration*, vol. 293, no. 3–5, pp. 728–734, Jun. 2006, doi: 10.1016/j.jsv.2005.12.005.

[17] J.F. Brunel, P. Dufrénoy, F. Demilly, "Modelling of squeal noise attenuation of ring damped wheels," *Applied Acoustics*, vol. 65, no. 5, pp. 457–471, May 2004, doi: 10.1016/j.apacoust.2003.12.003.

[18] J. Han, Z. Wen, R. Wang, D. Wang, X. Xiao, G. Zhao, X. Jin, "Experimental study on vibration and sound radiation reduction of the web-mounted noise shielding and vibration damping wheel," *Noise Control Engineering Journal*, vol. 62, no. 3, pp. 110–122, May 2014, doi: 10.3397/1/376211.

[19] Y.-S. Yun, J.-C. Kim, "Reducing Curve Squeal Noise Using Composite Materials Based on Experimental Investigation," *International Journal of Precision Engineering and Manufacturing*, vol. 22, no. 9, pp. 1573–1582, Jun. 2021, doi: 10.1007/s12541-021-00540-y.

[20] S.R. Marjani, D. Younesian, "Active Vibration Control for the Mitigation of Wheel Squeal Noise Based on a Fuzzy Self-Tuning PID Controller," *Shock and Vibration*, vol. 2022, pp. 1–17, Jul. 2022, doi: 10.1155/2022/3978230.

[21] W. Kropp, J. Theyssen, A. Pieringer, "The application of dither to mitigate curve squeal," *Journal of Sound and Vibration*, vol. 514, p. 116433, Dec. 2021, doi: 10.1016/j.jsv.2021.116433.

[22] R. Stock, L. Stanlake, C. Hardwick, M. Yu, D. Eadie, R. Lewis, "Material concepts for top of rail friction management – Classification, characterisation and application," *Wear*, vol. 366–367, pp. 225–232, Nov. 2016, doi: 10.1016/j.wear.2016.05.028.

[23] D.T. Eadie, M. Santoro, W. Powell, "Local control of noise and vibration with KELTRACK™ friction modifier and Protector® trackside application: An integrated solution," *Journal of Sound and Vibration*, vol. 267, no. 3, pp. 761–772, Oct. 2003, doi: 10.1016/s0022-460x(03)00739-9.

[24] J.T. Nelson, "Wheel/Rail Noise Control Manual." Transit Cooperative Research Program (TCRP) Report 23, published by Transportation Research Board, Washington, 1997.

[25] D.T. Eadie, M. Santoro, "Top-of-rail friction control for curve noise mitigation and corrugation rate reduction," *Journal of Sound and Vibration*, vol. 293, no. 3–5, pp. 747–757, Jun. 2006, doi: 10.1016/j.jsv.2005.12.007.

[26] C. Hardwick, R. Lewis, D.T. Eadie, "Wheel and rail wear—Understanding the effects of water and grease," *Wear*, vol. 314, no 1-2, pp. 198–204, Jun. 2014, doi: 10.1016/j.wear.2013.11.020.

[27] W.J. Wang, R. Lewis, B. Yang, L.C. Guo, Q.Y. Liu, M.H. Zhu, "Wear and damage transitions of wheel and rail materials under various contact conditions," *Wear*, vol. 362–363, pp. 146–152, Sep. 2016, doi: 10.1016/j.wear.2016.05.021.

[28] H. Lee, "The effect of water lubricant on reducing the generation of airborne wear particles from wheel–rail contacts under various train velocities," *Tribology International*, vol. 150, p. 106393, Oct. 2020, doi: 10.1016/j.triboint.2020.106393.

[29] V. Navrátil, R. Galas, M. Klapka, D. Kvarda, M. Omasta, L. Shi, H. Ding, W.-J. Wang, I. Krupka, M. Hartl, "Wheel Squeal Noise in Rail Transport: The Effect of Friction Modifier Composition," *Tribology in Industry*, vol. 44, no. 3, pp. 361–373, Sep. 2022, doi: 10.24874/ti.1211.11.21.02.

[30] X. Liu, C. Xiao, P.A. Meehan, "The effect of rolling speed on lateral adhesion at wheel/rail interface under dry and wet condition," *Wear*, vol. 438–439, p. 203073, Nov. 2019, doi: 10.1016/j.wear.2019.203073.

[31] H. Chen, M. Ishida, A. Namura, K.-S. Baek, T. Nakahara, B. Leban, M. Pau, "Estimation of wheel/rail adhesion coefficient under wet condition with measured boundary friction coefficient and real contact area," *Wear*, vol. 271, no. 1–2, pp. 32–39, May 2011, doi: 10.1016/j.wear.2010.10.022.

[32] B. White, R. Lewis, "Simulation and understanding the wet-rail phenomenon using twin disc testing," *Tribology International*, vol. 136, pp. 475–486, Aug. 2019, doi: 10.1016/j.triboint.2019. 03.067.

[33] H. Chen, S. Fukagai, Y. Sone, T. Ban, A. Namura, "Assessment of lubricant applied to wheel/rail interface in curves," *Wear*, vol. 314, no. 1–2, pp. 228–235, Jun. 2014, doi: 10.1016/j.wear.2013.12.006.

[34] M. Naeimi, Z. Li, R.H. Petrov, J. Sietsma, R. Dollevoet, "Development of a New Downscale Setup for Wheel-Rail Contact Experiments under Impact Loading Conditions," *Experimental Techniques*, vol. 42, no. 1, pp. 1–17, Oct. 2017, doi: 10.1007/s40799-017-0216-z.

[35] F.G. De Beer, M.H.A. Janssens, P.P. Kooijman, "Squeal noise of rail-bound vehicles influenced by lateral contact position," *Journal of Sound and Vibration*, vol. 267, no. 3, pp. 497–507, Oct. 2003, doi: 10.1016/s0022-460x(03)00710-7.

[36] A.D. Monk-Steel, D.J. Thompson, F.G. de Beer, M.H.A. Janssens, "An investigation into the influence of longitudinal creepage on railway squeal noise due to lateral creepage," *Journal of Sound and Vibration*, vol. 293, no. 3–5, pp. 766–776, Jun. 2006, doi: 10.1016/j.jsv.2005.12.004.

[37] L. Walls, "Test Rig Design for Simulation and Identification of Rail Corrugation," Ph.D. dissertation, Faculty of Engineering, Physical Sciences and Architecture, The University of Queensland, Queensland, 2003.

[38] P.A. Meehan, X. Liu, "Modelling and mitigation of wheel squeal noise amplitude," *Journal of Sound and Vibration*, vol. 413, pp. 144–158, Jan. 2018, doi: 10.1016/j.jsv.2017.10.032.

[39] P.A. Meehan, X. Liu, "Modelling and mitigation of wheel squeal noise under friction modifiers," *Journal of Sound and Vibration*, vol. 440, pp. 147–160, Feb. 2019, doi: 10.1016/j.jsv.2018.10.025.

[40] S. Liu, U. De Silva, D. Chen, A.C. Leslie, P.A. Meehan, "Investigation of wheel squeal noise under mode coupling using two-disk testrig experiments," *Wear*, vol. 530–531, p. 205035, Oct. 2023, doi: 10.1016/j.wear.2023.205035.

[41] M. Omasta, V. Navrátil, T. Gabriel, R. Galas, M. Klapka, "Design and Development of a Twin Disc Test Rig for the Study of Squeal Noise from the Wheel – Rail Interface," *Applied Engineering Letters: Journal of Engineering and Applied Sciences*, vol. 7, no. 1, pp. 10–16, Jan. 2022, doi: 10.18485/aeletters.2022.7.1.2.

[42] E. Schneider, K. Popp, H. Irretier, "Noise generation in railway wheels due to rail-wheel contact forces," *Journal of Sound and Vibration*, vol. 120, no. 2, pp. 227–244, Jan. 1988, doi: 10.1016/0022-460x(88)90431-2.

[43] P.A. Meehan, "Prediction of wheel squeal noise under mode coupling," *Journal of Sound and Vibration*, vol. 465, p. 115025, Jan. 2020, doi: 10.1016/j.jsv.2019.115025.

[44] Y.A. Areiza, S.I. Garcés, J.F. Santa, G. Vargas, A. Toro, "Field measurement of coefficient of friction in rails using a hand-pushed tribometer," *Tribology International*, vol. 82, pp. 274–279, Feb. 2015, doi: 10.1016/j.triboint.2014.08.009.

[45] B. Ding, G. Squicciarini, D. Thompson, R. Corradi, "An assessment of mode-coupling and falling-friction mechanisms in railway curve squeal through a simplified approach," *Journal of Sound and Vibration*, vol. 423, pp. 126–140, Jun. 2018, doi: 10.1016/j.jsv.2018.02.048.

[46] E.A. Gallardo-Hernandez, R. Lewis, "Twin disc assessment of wheel/rail adhesion," *Wear*, vol. 265, no. 9–10, pp. 1309–1316, Oct. 2008, doi: 10.1016/j.wear.2008.03.020.

[47] H. Chen, S. Fukagai, Y. Sone, T. Ban, A. Namura, "Assessment of lubricant applied to wheel/rail interface in curves," *Wear*, vol. 314, no. 1–2, pp. 228–235, Jun. 2014, doi: 10.1016/j.wear.2013.12.006.

[48] Z.Y. Shen, J.K. Hedrick, J.A. Elkins, "A Comparison of Alternative Creep Force Models for Rail Vehicle Dynamic Analysis," *Vehicle System Dynamics*, vol. 12, no. 1–3, pp. 79–83, Jul. 1983, doi: 10.1080/00423118308968725.

[49] X. Liu, P.A. Meehan, "Investigation of squeal noise under positive friction characteristics condition provided by friction modifiers," *Journal of Sound and Vibration*, vol. 371, pp. 393–405, Jun. 2016, doi: 10.1016/j.jsv.2016.02.028.

[50] R. Galas, M. Omasta, L. Shi, H. Ding, W. Wang, I. Krupka, M. Hartl, "The low adhesion problem: The effect of environmental conditions on adhesion in rolling-sliding contact," *Tribology International*, vol. 151, p. 106521, Nov. 2020, doi: 10.1016/j.triboint.2020.106521.

[51] C. Hardwick, R. Lewis, U. Olofsson, "Low adhesion due to oxide formation in the presence of salt," *Proceedings of the Institution of Mechanical Engineers, Part F: Journal of Rail and Rapid Transit*, vol. 228, no. 8, pp. 887–897, Jul. 2013, doi: 10.1177/0954409713495666.

[52] L.E. Buckley-Johnstone, G. Trummer, P. Voltr, A. Meierhofer, K. Six, D.I. Fletcher, R. Lewis, "Assessing the impact of small amounts of water and iron oxides on adhesion in the wheel/rail interface using High Pressure Torsion testing," *Tribology International*, vol. 135, pp. 55–64, Jul. 2019, doi: 10.1016/j.triboint.2019.02.024.

[53] R. Galas, M. Omasta, M. Klapka, S. Kaewunruen, I. Krupka, M. Hartl, "Case study: The influence of oil-based friction modifier quantity on tram braking distance and noise," *Tribology in Industry*, vol. 39, no. 2, pp. 198–206, Jun. 2017, doi: 10.24874/ti.2017.39.02.06.

[54] L. Buckley-Johnstone, M. Harmon, R. Lewis, C. Hardwick, R. Stock, "A comparison of friction modifier performance using two laboratory test scales," *Proceedings of the Institution of Mechanical Engineers, Part F: Journal of Rail and Rapid Transit*, vol. 233, no. 2, pp. 201–210, Sep. 2018, doi: 10.1177/0954409718787045.

[55] R. Galas, M. Omasta, I. Krupka, M. Hartl, "Laboratory investigation of ability of oil-based friction modifiers to control adhesion at wheel-rail interface," *Wear*, vol. 368–369, pp. 230–238, Dec. 2016, doi: 10.1016/j.wear.2016.09.015.

[56] D. Kvarda, S. Skurka, R. Galas, M. Omasta, L. Shi, H. Ding, W. Wang, I. Krupka, M. Hartl, "The effect of top of rail lubricant composition on adhesion and rheological behaviour," *Engineering Science and Technology, an International Journal*, vol. 35, p. 101100, Nov. 2022, doi: 10.1016/j.jestch.2022.101100.

[57] R. Galas, S. Skurka, M. Valena, D. Kvarda, M. Omasta, H. Ding, Q. Lin, W. Wang, I. Krupka, M. Hartl, "A benchmarking methodology for top-of-rail products," *Tribology International*, vol. 189, p. 108910, Nov. 2023, doi: 10.1016/j.triboint.2023.108910.

[58] S. Skurka, R. Galas, M. Omasta, B. Wu, H. Ding, W.-J. Wang, I. Krupka, M. Hartl, "The performance of top-of-rail products under water contamination," *Tribology International*, vol. 188, p. 108872, Oct. 2023, doi: 10.1016/j.triboint.2023.108872.

[59] M. Moreno-Ríos, E.A. Gallardo-Hernández, M. Vite-Torres, A. Peña-Bautista, "Field and laboratory assessments of the friction coefficient at a railhead," *Proceedings of the Institution of Mechanical Engineers, Part F: Journal of Rail and Rapid Transit*, vol. 230, no. 1, pp. 313–320, May 2014, doi: 10.1177/0954409714536383.

Supplementary material

Table A1 – traction curves – Measured lateral adhesion coefficient.

Angle of attack (mrad)	**2,5**	**5**	**10**	**15**	**20**	**25**	**30**	**35**
μ (1) - 2 m/s - DRY	0.2634	0.4429	0.5036	0.4869	0.4544	0.4434	0.4552	0.4332
σ (1)	0.0423	0.0142	0.0383	0.0214	0.0300	0.0197	0.0251	0.0291
μ (1) - 4 m/s - DRY	0.2457	0.4404	0.4588	0.4837	0.4745	0.4658	0.4367	0.4025
σ (1)	0.0529	0.0249	0.0176	0.0183	0.0342	0.0201	0.0218	0.0290
μ (1) - 2 m/s - WET	0.2739	0.3642	0.3736	0.3695	0.3680	0.3595	0.3966	0.3652
σ (1)	0.0153	0.0304	0.0240	0.0264	0.0436	0.0305	0.0154	0.0250
μ (1) - 4 m/s - WET	0.2534	0.3572	0.3618	0.3318	0.3335	0.3531	0.3388	0.3558
σ (1)	0.0318	0.0247	0.0386	0.0351	0.0259	0.0372	0.0184	0.0282

Table A2 – Sound pressure levels during tests under dry and wet conditions.

Angle of attack (mrad)	**2,5**	**5**	**10**	**15**	**20**	**25**	**30**	**35**
SPL (dB) - 2 m/s - DRY	77.5	86.8	100.6	100.5	102.4	104.3	105.5	106.1
σ (dB)	0.5	1.2	0.9	0.7	0.4	0.6	0.5	0.7
SPL (dB) - 4 m/s - DRY	85.6	98.0	102.8	104.7	106.1	106.9	107.5	107.9
σ (dB)	0.3	2.1	1.7	0.8	0.6	0.5	0.3	0.6
SPL (dB) - 2 m/s - WET	75.2	82.8	84.6	89.1	89.9	88.9	89.0	89.5
σ (dB)	0.4	0.9	0.6	1.5	1.1	0.4	0.9	0.6
SPL (dB) - 4 m/s - WET	83.5	90.8	91.4	97.9	97.4	97.7	96.3	97.2
σ (dB)	0.3	0.6	0.9	1.1	1.2	0.9	1.5	1.1

Table A3 – Vibration velocities during tests under dry and wet conditions at 445 Hz.

Angle of attack (mrad)	**2,5**	**5**	**10**	**15**	**20**	**25**	**30**	**35**
$\dot{y}$ (mm/s) - 2 m/s - DRY	0.20	0.30	0.72	2.87	5.71	5.97	6.10	6.35
σ (mm/s)	0.06	0.05	0.12	0.20	0.27	0.47	0.34	0.41
$\dot{y}$ (mm/s) - 4 m/s - DRY	0.48	0.57	3.77	4.34	4.47	5.14	5.08	5.20
σ (mm/s)	0.07	0.08	0.53	0.39	0.22	0.36	0.56	0.38
$\dot{y}$ (mm/s) - 2 m/s - WET	0.18	0.43	0.77	1.61	2.08	2.70	2.97	3.15
σ (mm/s)	0.04	0.06	0.12	0.16	0.15	0.20	0.26	0.31
$\dot{y}$ (mm/s) - 4 m/s - WET	0.32	0.80	0.93	1.19	1.24	1.28	1.64	1.93
σ (mm/s)	0.05	0.19	0.13	0.11	0.15	0.12	0.21	0.22

Table A4 – Vibration velocities during tests under dry and wet conditions at 1087 Hz.

Angle of attack (mrad)	**2,5**	**5**	**10**	**15**	**20**	**25**	**30**	**35**
$\dot{y}$ (mm/s) - 2 m/s - DRY	/	/	0.84	1.07	1.77	2.71	3.11	3.33
σ (mm/s)	/	/	0.13	0.11	0.25	0.33	0.19	0.25
$\dot{y}$ (mm/s) - 4 m/s - DRY	/	0.89	1.71	3.54	8.65	11.05	12.11	12.52
σ (mm/s)	/	0.11	0.38	0.33	0.62	1.23	1.52	1.34
$\dot{y}$ (mm/s) - 2 m/s - WET	/	0.22	0.67	0.87	0.76	0.82	1.07	1.18
σ (mm/s)	/	0.05	0.10	0.24	0.11	0.09	0.11	0.10
$\dot{y}$ (mm/s) - 4 m/s - WET	/	0.68	1.45	1.88	1.94	2.80	3.92	4.21
σ (mm/s)	/	0.11	0.20	0.33	0.25	0.23	0.44	0.38

Table A5 – Vibration velocities during tests under dry and wet conditions at 1923 Hz.

Angle of attack (mrad)	**2,5**	**5**	**10**	**15**	**20**	**25**	**30**	**35**
$\dot{y}$ (mm/s) - 2 m/s - DRY	/	/	0.63	0.82	3.55	3.78	4.45	4.72
σ (mm/s)	/	/	0.09	0.19	0.33	0.46	0.68	0.56
$\dot{y}$ (mm/s) - 4 m/s - DRY	/	0.30	1.58	2.50	2.44	3.37	3.70	4.12
σ (mm/s)	/	0.09	0.41	0.21	0.41	0.38	0.22	0.44
$\dot{y}$ (mm/s) - 2 m/s - WET	/	/	/	/	/	/	/	/
σ (mm/s)	/	/	/	/	/	/	/	/
$\dot{y}$ (mm/s) - 4 m/s - WET	/	/	0.24	0.25	0.27	0.28	0.22	0.29
σ (mm/s)	/	/	0.04	0.04	0.06	0.05	0.06	0.04

Table A6 – Results of experiments with different water amounts.

Amount (ml)	**1**	**2**	**5**	**10**
$\Delta\mu$ (1)	0.07	0.07	0.09	0.06
σ (1)	0.02	0.01	0.01	0.01
ΔSPL (dB)	11.2	10.5	10.5	9.2
σ (dB)	0.2	0.2	0.2	1.0
Δt (s)	156	297	618	917
σ (s)	28	18	15	17

Tribology International 151 (2020) 106521

Contents lists available at ScienceDirect

Tribology International

journal homepage: http://www.elsevier.com/locate/triboint

The low adhesion problem: The effect of environmental conditions on adhesion in rolling-sliding contact

Radovan Galas [a,*], Milan Omasta [a], Lu-bing Shi [b], Haohao Ding [b], Wen-jian Wang [b], Ivan Krupka [a], Martin Hartl [a]

[a] Faculty of Mechanical Engineering, Brno University of Technology, Technicka 2896/2, 616 69, Brno, Czech Republic
[b] Tribology Research Institute, State Key Laboratory of Traction Power, Southwest Jiaotong University, Chengdu, 610031, China

ARTICLE INFO

Keywords:
Low adhesion
Wheel-rail tribology
Environmental conditions
Contaminated contact

ABSTRACT

Low adhesion problem is one of the major problems for railways all over the world because this phenomenon can occur anytime and anywhere. To investigate when poor adhesion conditions can be expected in real operation, a ball-on-disc tribometer with a climate chamber was employed to simulate rolling-sliding contact under various environmental conditions. Clean and contaminated discs with leaf extract were used to simulate different surface conditions. Results indicate that contact operating under rolling-sliding conditions is more prone to the occurrence of low adhesion than found by others for pure sliding contact. Very low adhesion (≤0.05) were identified for contaminated and oxidized specimens operating under humid and wet conditions. For clean surfaces, low adhesion (≤0.15) were found under dew conditions.

1. Introduction

Low adhesion between rail head and wheel tread is one of the major problems for railways in many countries all over the world. This phenomenon has a negative impact on cost, performance, and safety. The term "low adhesion" or "poor adhesion" is usually associated with the autumn season when a slippery layer from crushed fallen leaves is formed on the track. Both laboratory [1–3] and field research [4,5] revealed that this layer can result in the coefficient of adhesion (CoA) lower than 0.15, in some critical cases even lower than 0.05 [6]. Although it is a well-known fact that leaf contamination causes serious problems in railways all over the world; it must be emphasized that fallen leaves are not the only cause of low adhesion incidents. Besides fallen leaves, there are other causes of low adhesion which are mainly related to environmental conditions.

Water can be considered as one of the most common contaminants influencing adhesion in the wheel-rail contact. Water in the field can be found in various forms such as morning dew, fog, and light or heavy rain. These different forms may lead to different adhesion levels. In the case of bulk water, CoA can take values between 0.05 and 0.5 [7–12] depending on speed, roughness, and other parameters. More significant adhesion drop can be expected for slightly wet conditions, which usually occurs due to dew or light rain. Beagley et al. [13] observed that a small amount of water from condensation decreased CoA to 0.22. Even more critical case was found when the rail was not free of solid particles. This combination of a small amount of water and solid particles (such e.g. wear debris) led to the formation of a viscous paste, which provided low (<0.15) [14] or even very low CoA (<0.05) [15].

In the case of weather conditions, daytime evolution of relative humidity (RH) and temperature can have a substantial impact on CoA. Beagley et al. [13] showed that CoA was reduced from 0.55 to 0.22 with increasing RH, while the effect of temperature was rather negligible during these tests. Similar findings were reported by Olofsson et al. [16] where the effect of RH on CoA was studied for dry and leaf contaminated contact using the pin-on-disc apparatus. It was found that the coefficient of friction (CoF) was reduced to 0.37 (dry) and 0.27 (leaf) when RH reached 95%. A pin-on-disc device was used also by Zhu et al. [17,18] who investigated the effect of RH and temperature on CoF for clean and rusted specimens. These complex studies showed that rusted discs generally led to lower CoF than found for clean discs; however, the lowest observed adhesion was still 0.4 or higher for both disc types. The lowest values of CoF was observed when RH reached 70%. A subsequent increase in RH did not lead to a further decrease in CoF.

Previous research works have shown that adhesion/friction is very variable depending on contaminants and current weather conditions. It means that low adhesion problem can happen anytime and anywhere.

* Corresponding author.
E-mail address: Radovan.Galas@vut.cz (R. Galas).

https://doi.org/10.1016/j.triboint.2020.106521
Received 12 May 2020; Received in revised form 15 June 2020; Accepted 19 June 2020
Available online 5 July 2020
0301-679X/© 2020 Elsevier Ltd. All rights reserved.

Although a decrease of CoA/CoF was observed in all above-mentioned studies, low CoA or CoF (<0.15) was found predominantly when contact was contaminated with leaves. However, White et al. [19] reported that many of low adhesion incidents in a real operation were not associated only with leaf contamination but there were other factors leading to low adhesion incidents. These authors suggested several reasons why these low adhesion incidents happened, such as due to the presence of water, moisture or not detectable leaf layer. The conditions and mechanisms leading to low adhesion phenomenon are not fully understood.

The main objective of this study is to reveal conditions when low adhesion ($\mu \leq 0.15$) and very low adhesion conditions ($\mu \leq 0.05$) can be expected in the wheel-rail contact. Special attention is paid to the effect of RH, temperature and leaf contamination. For this purpose, a ball-on-disc tribometer with a climate chamber is employed. This contact configuration is chosen because it enables to set typical rolling-sliding conditions occurring in the wheel-rail interface. Based on the previous studies, it is assumed that pure sliding configuration, where a pin is in permanent contact with the counterpart, is not sufficiently representative in terms of the formation and action of the third-body layer. The presence of this layer is important to study low adhesion problem.

2. Material and methods

2.1. Test setup and specimens

Adhesion measurements were conducted on the ball-on-disc tribometer (Mini–traction–Machine, PCS Instruments) where a 19.05 mm steel ball and 46 mm diameter flat steel disc was loaded against each other as is depicted in Fig. 1. Both these specimens were independently driven, thus a rolling-sliding contact (where the slip was accurately controlled) can be achieved. The slip is defined in Eq. (1), where w_{ball} and w_{disc} are the angular speeds of the ball and the disc respectively and r_{ball} and r_{disc} represent the radii of specimens. CoA was calculated as a ratio between traction and normal forces which were directly measured using embedded sensors.

$$slip = \frac{w_{ball} \cdot r_{ball} - w_{disc} \cdot r_{disc}}{w_{ball} \cdot r_{ball} + w_{disc} \cdot r_{disc}} \cdot 200\% \quad (1)$$

The material of both the ball and the disk was bearing steel AISI 52 100 with the hardness of 800–920 HV (ball) and 720–780 HV (disc). The initial roughness of the ball and the disc was Ra 0.01 μm and Ra 0.02 μm respectively. These specimens were enclosed in a climate chamber where temperature and air humidity were controlled. Heating was ensured by heaters installed in the tribometer body while cooling was provided by an external cooling unit with cooling oil circulating through the tribometer body. Air with controlled RH and ambient temperature was fed to the chamber from external humidity unit. Thanks to the method of cooling, this equipment enables to reach dew point conditions resulting in water condensation on the surface of the disc. Detail parameters of employed sensors are listed in Appendix A.

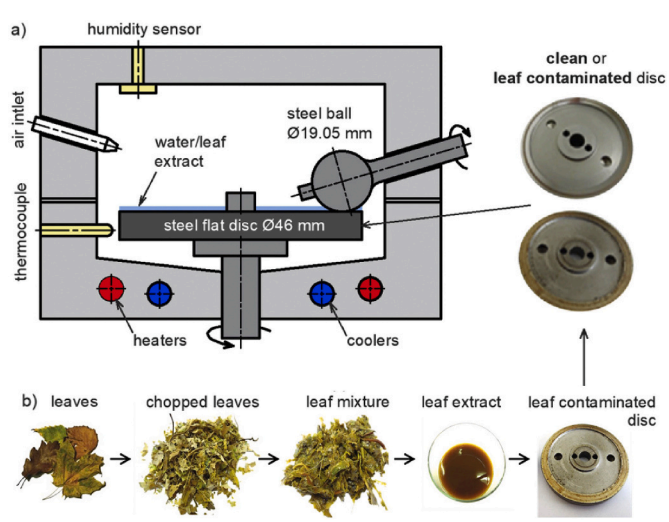

Fig. 1. (a) Scheme of the ball–on–disc apparatus with a climate chamber, (b) preparation of leaf extract and contaminated disc.

2.2. Experimental conditions and procedure

Several sets of adhesion measurements were conducted under various operating and environmental conditions, see Table 1a. For all sets, a contact pressure of 750 MPa (a normal force of 17 N) was used to achieve representative light rail system contact conditions. In the beginning, tests under dry and wet (fully-flooded) conditions were run to obtain reference CoA values for dry and wet (heavy rain) conditions. Based on these tests, adhesion characteristics for dry and wet (fully-flooded) conditions were drawn for a speed range of 0.5–3 m/s. Each point on adhesion characteristics was evaluated as the average value from a 30-s test. After the completion of these reference tests, other tests were always conducted with a fixed slip value of 5% and a speed of 1 m/s. Test sets No. 3 and 4 were focused on the effect of water (light precipitation) and leaf extract amounts on CoA. Last two test sets (No. 5 and 6) were performed under various temperature (1–50 °C) and RH values (6–100%) to investigate conditions occurring throughout the day. Moreover, the last test set was conducted with the contaminated disc (described below) to combine the effects of leaf contamination, RH, and temperature on CoA.

Leaf contamination was represented in two ways: as a liquid leaf extract and as a dry friction layer (from the extract) on the disc. The leaf extract was prepared from leaves which were gathered from fallen maple, beech, birch and oak leaves near the railway network in autumn. Subsequently, leaves were chopped into small pieces (approx. 5 μm) and soaked in water for 5 days. After that, excess water was separated and the leaf extract was obtained as shown in Fig. 1b. A dry layer from leaf extract was prepared one day before testing. The preparation of the layer proceeded in several steps. At first, 20 μl of leaf extract was applied on the disc and then, several cycles under pure rolling conditions were carried out to create a uniform friction layer around the circumference of the disc. Finally, the disc was left for several hours to ensure that all liquid contained in the friction layer was evaporated. This preparation process of dry leaf layer was needed before each particular measurement. The disc with the layer is further referred to as "contaminated disc".

Each test in Table 1, except tests with the contaminated disc, was started by a running-in to remove oxides and any other residual layers adhered on contact surfaces. This running-in was stopped when a stable and dry level of adhesion was reached. Experimental conditions of running-in (speed, slip, etc.) were the same as the conditions of the "main" test performed immediately after this running-in. As is evident from Table 1, some tests were carried out with oxidized disc. In this case, the clean disc was run under wet (fully-flooded) conditions to form the oxide layer. This wet running-in was stopped when CoA was dropped (due to the presence of oxides) and stabilized. All liquids were applied to the contact using a micropipette with a dosing accuracy of ±0.04 μl. In the case of fully-flooded conditions, the disc was immersed in water. At the end of each test, both specimens were removed from tribometer and ultrasonically cleaned with acetone. The statistics data of all tests are listed in Appendix B.

To judge the effects of tested contaminants and environmental conditions listed in Table 1, the following intervals of CoA were considered in this study: *high adhesion* $\mu > 0.4$, *intermediate adhesion* $0.4 \geq \mu > 0.15$, *low adhesion* $0.15 \geq \mu > 0.05$, and *very low adhesion* $0.05 \geq \mu$.

Table 1
Experimental conditions of the tests.

set of tests	contaminant	disc	amount (μl)	running-in	mean speed (m/s)	temp. (°C)	RH (%)	Hertz pressure (MPa)	slip	correspond Fig. No.
1r[a]	none	clean	–	dry	0.5–3	ambient	ambient	750 ± 3	0–8	2
2r[a]	water	clean	fully-flooded							3a
		oxidized		wet						3a, 3b
3	water	clean	1–10	dry	1				5	4, 5, 8
4	leaf extract		1–20							6, 7, 8
5	none		–			1–50	8–100			9, 10a, 11a, 12a, 13a
6	none	contam.	–	none			6–100			10b, 11b, 12b, 13b
overview of selected results										16

[a] Reference tests.

3. Results and discussion

3.1. Reference tests under dry and wet conditions

To obtain reference values of CoA, adhesion characteristics under dry and wet (fully-flooded) conditions were measured for four different mean speeds (Fig. 2 and Fig. 3).

Fig. 2 shows data from the tests ran in dry conditions where CoA reached the typical values for non-lubricated rolling-sliding contact operating in laboratory conditions [9,20]. The results also indicate that there was almost no significant change in CoA as the speed increased; however, the tested speed range used in this study was rather limited. As was shown in Table 1, most of the tests were carried out at 5% slip. For this particular slip value, CoA reached approximately 0.6 for all tested speeds. The value of 0.6 is considered as a reference value of CoA for dry conditions in later parts of this study.

Besides the value of CoA, the shape of the adhesion characteristic is another important factor influencing a maximum available adhesion in the contact and wear (corrugation formation especially). From the results in Fig. 2, it is obvious that a positive slope of the adhesion characteristic was found in all cases even though the negative adhesion characteristic is generally expected for non-lubricated wheel-rail contact as was found in Ref. [21]. The reason for this discrepancy may be the fact that the slip in laboratory research is usually set as a fixed value, while the slip in a real wheel-rail contact can immediately change depending on current operating conditions. This hypothesis is consistent with the findings from previous laboratory research, where the positive adhesion characteristic was also observed under dry conditions [22,23].

When tests under dry conditions were completed, the same set of experiment was conducted again with pure water under fully-flooded conditions, which ensured that the contact did not starve during the test, see the set of tests in Fig. 3a marked as "no oxide". The results give evidence that no significant drop of CoA occurred under these conditions. Even at the maximum speed, CoA reached a relatively high value

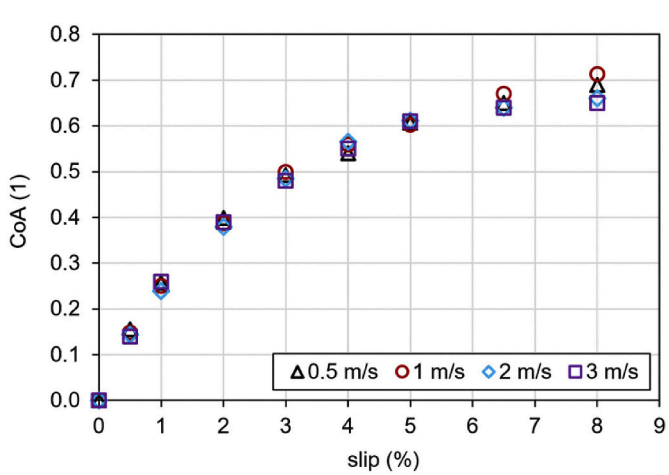

Fig. 2. Adhesion characteristics for different speeds in dry conditions.

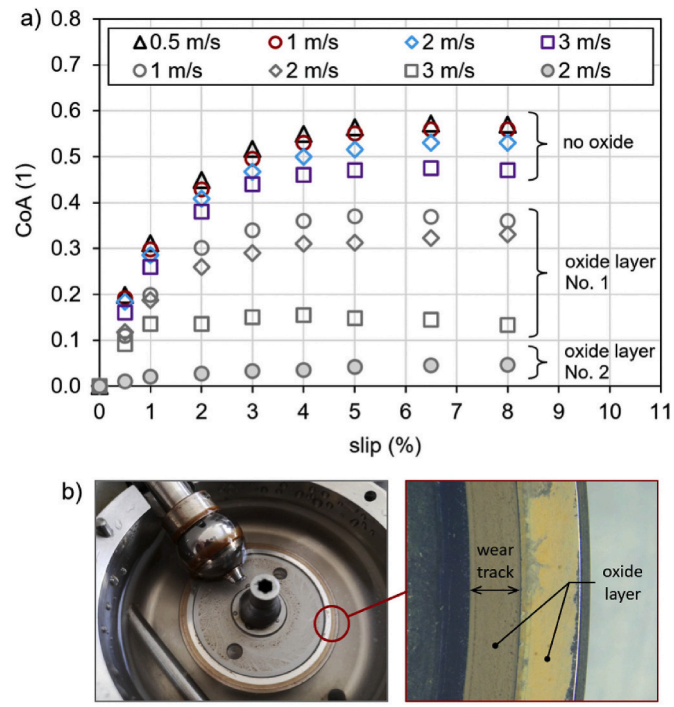

Fig. 3. (a) Adhesion characteristics in wet (fully-flooded) conditions for clean (colour points) and oxidized disc (grey points), (b) the oxide layer No. 1. (For interpretation of the references to colour in this figure legend, the reader is referred to the Web version of this article.)

of 0.47 at 5% slip which means that CoA was reduced by 28% compared to dry conditions. The fact that wet conditions did not lead to low adhesion is well correlated with lambda prediction for isoviscous-elastic lubrication regime. For the tested range of speeds (from 0.5 to 3 m/s), the lambda parameter ranged between 0.02 and 0.07 which means that the contact was operating in the boundary lubrication regime. This regime can be supposed for trams and non-high speed trains when rain is heavy and other contaminants are washed away from the rail surface. The similar findings were reported by Chen et al. [10] where CoA under wet conditions was measured by the twin-disc machine. Chen's results showed that CoA at low speed ($v < 2$ m/s) reached high values ($\mu > 0.4$). Moreover, these authors conducted the tests with a lower slip ($s = 0.7\%$) and also the roughness of specimens was approx. half in comparison with the roughness in the present study.

However, there are some publications [1,3,9] where the application of water resulted in substantially lower CoA (between 0.17 and 0.28) than found in the present study. There are two things which can explain this important difference. Firstly, other authors used lower slip values leading to lower values of CoA. Note that the slip value of 5% in this study was chosen based on the actual shape of adhesion characteristics in Fig. 2. This slip value should ensure that the contact was operating near to the saturation point as is apparent from curves in Fig. 3a. The

second thing is that in this study the material of specimens was the bearing steel AISI 52 100 which differs from common wheel and rail materials in chemical composition as well as in the hardness. Note that the bearing steel contains Cr (1.3–1.6%) which can affect an oxidation rate. These different properties of specimens could slow down the formation of the oxide body layer between contact surfaces.

Consequently, the second set of tests under wet conditions were conducted. In that case, each test was started by running-in under wet (fully-flooded) conditions to oxidize the disc. This wet run-in period of the test took approx. 30 min until a visible oxide layer has been formed on both contact surfaces, see Fig. 3b. After that, CoA was evaluated for the same experimental conditions as before, see the set of tests in Fig. 3a marked as "oxide layer No. 1". Subsequently, the same test with wet run-in period was conducted again for the speed of 2 m/s, but the duration of wet running-in was doubled compared to the previous test. This longer wet run-in period ensured that a different level of surface oxidation was reached, see the test in Fig. 3a marked as "oxide layer No. 2". By comparing the results in Fig. 3a, it can be concluded that the presence of an oxide layer under wet conditions can cause a significant adhesion decrease. At 2 m/s and 5% slip, CoA was reduced to 0.37 and 0.041 depending on the level of surface oxidation. These results imply that heavy rain does not generally cause poor adhesion conditions itself but CoA can be significantly impacted by heavy rain when contact surfaces are covered by an oxide layer. These findings are consistent with the findings in Ref. [24] where the presence of an oxide layer under wet conditions caused that CoA was reduced by up to 75% compared to a reference wet test without oxide layer.

3.2. Effect of a small amount of water on CoA

To imitate light rain, the effect of small amounts of water on CoA over time was investigated, see Fig. 4a. These friction curves show that a drop of CoA occurred immediately after water application; however, poor adhesion conditions were not observed in any of the tests. On the other hand, small amounts of water reduced CoA significantly more than found under fully-flooded conditions, see Fig. 4b. Comparing to dry (0.6) and wet fully-flooded conditions (0.55), CoA was reduced up to by 35 and 20% respectively when small amounts of water were applied into the contact. The results show that the larger the amount of water, the less significant decrease in CoA (the average value in the middle part of friction curve) and the longer drop time of CoA "*t*" (from 5 to 39 s).

Friction curves in Fig. 4a are compared to each other in detail in Fig. 4b. This figure shows that friction curves can be described by three followings points: μ_0, μ_m, μ_{min}. The first point μ_0 represents the drop of CoA occurring immediately after the application of water; so this point describes the transition between dry and wet conditions. After that, CoA usually slightly increases and CoA is more or less stable because a friction boundary layer is formed. This "middle" part of the friction curve can be described by the second point μ_m. The last point μ_{min} describes the transition between wet and dry conditions. This phenomenon is usually accompanied by a significant decrease in adhesion as can be seen in Fig. 4b for 10 μl. This is in line with Ref. [25] where a similar trend of friction curve was found for the case when water was applied continuously and then water was stopped and hot air drier was started. Note that in that study the second adhesion drop μ_{min} was observed after several cycles since stopping the water.

The data from this and the following subchapter are summarized in Fig. 6. As was mentioned above, no poor adhesion conditions were found for contact contaminated with a small amount of water. The lowest observed CoA during all tests was 0.36. Nevertheless, considering the results in the previous chapter, it can be reasonably expected that the combination of a small amount of water and oxides or other solid contaminants can lead to very low CoA. In that case, a small amount of water and solid particles can form non-Newtonian viscous mixture/paste [13] resulting in low or even very low CoA, e.g. $\mu = 0.14$ in Refs. [23], and 0.05 in Ref. [26].

3.3. Effect of leaf contamination on CoA

To investigate the conditions typical for autumn months, friction tests with different amounts of leaf extract were carried out, see Fig. 5a. It was found that all tested amounts of leaf extract caused a rapid drop in CoA leading to low adhesion conditions ($\mu \leq 0.15$), see Fig. 5b. These results are in good agreement with previous laboratory studies where CoA was lower than 0.1 for both leaves [2] and leaf extract contamination [27].

As can be seen from the comparison of Figs. 4b and 5b, there are similarities between friction curves for a small amount of water and leaf extract. For both of these tests, the same following stages of friction curves can be identified: (1) a rapid decrease of CoA occurring after the application (μ_0, μ_{0L}), (2) relatively stable middle part of CoA (μ_m, μ_{mL}), (3) the second drop in CoA related to the transition between wet and dry conditions (μ_{min}, μ_{minL}), and (4) the final rapid increase of CoA. The only exceptions are the tests with the smallest applied amount of water/leaf extract because these amounts seem to be insufficient for forming of a lubrication film around the circumference of the ball and the disc; thus, the contact quickly starved and CoA increased rapidly. Besides this, it should be emphasized that in case of tests with leaf extract, CoA was stabilized at values less than the reference value for dry adhesion, see *ΔCoA* in Fig. 5b. This difference in CoA may be due to the changes in surface conditions of specimens that occurred during the test. Furthermore, CoA may be also affected by the presence of residual components from leaf extract, which remained in the wear track.

As mentioned in Chapter 2, a leaf extract is a mixture of water and a liquid lubricant released from the chopped leaf pieces. This composition may explain the similarity of a shape of friction curves under wet and

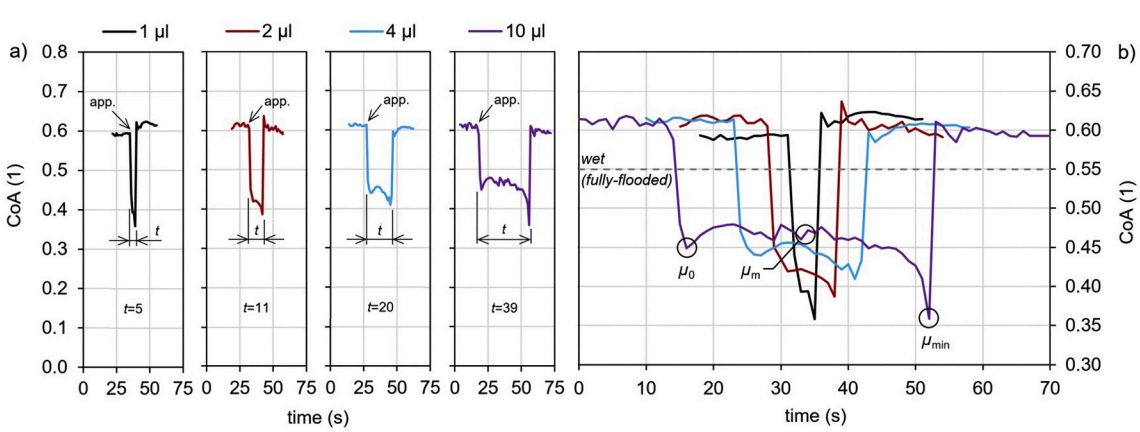

Fig. 4. (a) Friction curves for contact contaminated with a small amount of water, (b) detailed comparison of these curves.

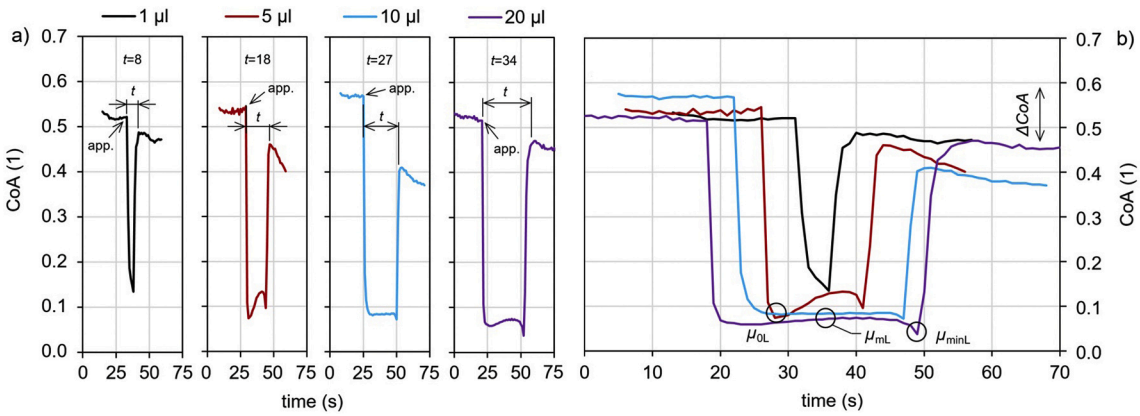

Fig. 5. (a) Friction curves for contact contaminated with different amount of leaf extract, (b) detailed comparison of these curves.

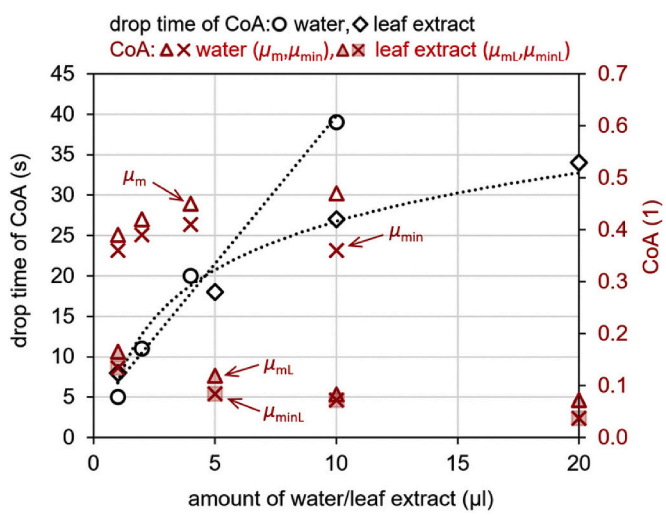

Fig. 6. The effect of the amount of water/leaf extract on drop time of CoA and on the level of "CoA".

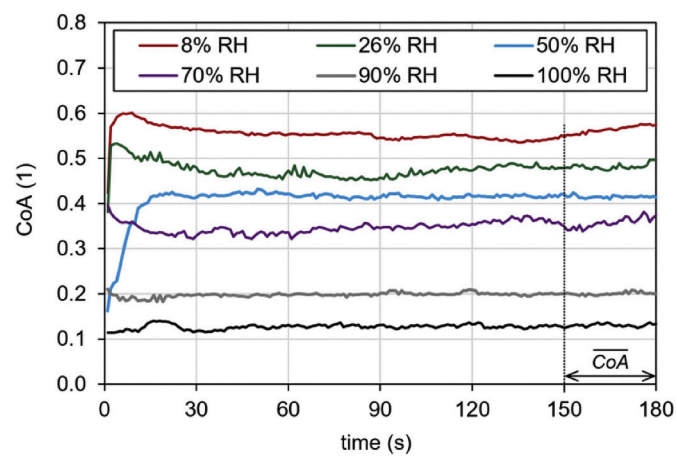

Fig. 7. Effect of RH on CoA for the clean disc at air temperature 1 °C.

leaf extract conditions. Moreover, this composition explains why CoA was even lower than 0.05, see Fig. 6. It is a well-known fact that a mixture of water and oil leads to very low CoA, even lower than for pure oil [28]. Fig. 6 also shows that there is an opposite dependence between the applied amount of leaf extract and CoA than was observed for different (small) amounts of water.

3.4. Effect of humidity and temperature on CoA

The influence of humidity and temperature on CoA was studied for the clean and contaminated disc, see Fig. 1. Fig. 7 shows an example of friction tests with a clean disc where the effect of various RH on CoA was investigated at a constant air temperature of 1 °C. The same set of tests were carried out, for both clean and contaminated disc, for various temperatures according to Table 1. Based on the data from the last 30 s of each measurement, the average CoA was calculated and Fig. 8 and Fig. 10, which describe the relationship between CoA and RH for various air temperatures, was plotted.

The results in Fig. 8 show that an increasing RH reduces CoA for all tested conditions and the trend is nearly linear. For the clean disc (Fig. 8a), it was investigated that CoA is almost insensitive to changes in RH for temperature higher than approximately 30 °C. In contrast, the effect of RH on CoA becomes substantial when the temperature drops to or below 24 °C. The combination of low temperature and high RH led to the condensation resulting in a rapid decrease of CoA, see the condensation area in Figs. 8a and 9a. Under these undesirable conditions, low adhesion conditions occurred ($\mu \leq 0.15$) when the air was fully-saturated with water (RH = 100%).

An even more significant decrease in CoA was found for the tests with the contaminated disc. The results in Fig. 8b revealed that for RH values below 10% the presence of the leaf layer on the disc decreases CoA by only 0.1 (compared to the tests with the clean disc). Once RH starts to rise, CoA falls more dramatically than for the clean disc. Unlike tests with the clean disk, a significant decrease of CoA was observed even for high temperatures. A substantial decrease of CoA was found for lower temperatures (1 and 10 °C) when RH value was higher than 60%. As expected, the lowest CoA was found when a dew point occurred, see the condensation area in Figs. 8b and 9b. Under these conditions, CoA was lower than 0.1 and at some points even lower than 0.05; so very low adhesion conditions were found. This abrupt fall of CoA could occur as a result of the softening of the leaf layer with a small amount of condensation water. This softening could lead to a decrease in the shear strength of the leaf layer; thus, the maximum achievable CoA in the contact was reduced.

The results above revealed that CoA decreases with increasing value of RH. The most considerable adhesion drop was observed for the temperature to be 24 °C and lower, once the condensation occurred. Under these conditions, CoA was reduced to 0.13 and 0.04 for clean and contaminated disc respectively. These results are well correlated with Ref. [14,16–18] where a gradual decrease of CoA with increasing RH was also observed. However, it must be noted that the lowest observed CoA in these studies was 0.22 [14], 0.28 [16], 0.41 [17], and 0.40 [18], even though the tests were performed with leaves [16], with the rusted

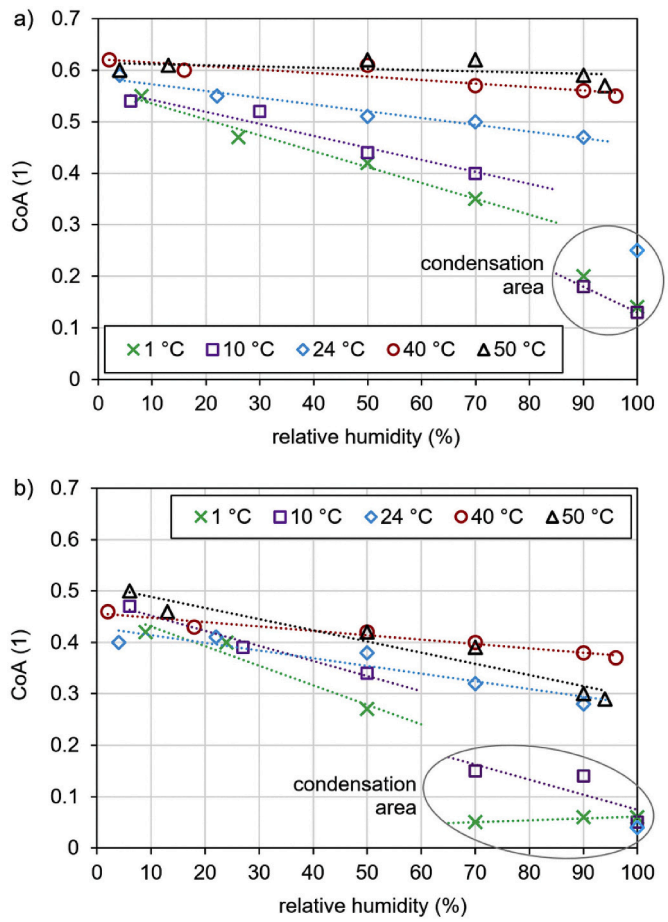

Fig. 8. Effect of RH and temperature on CoA for clean disc (a) and contaminated disc (b).

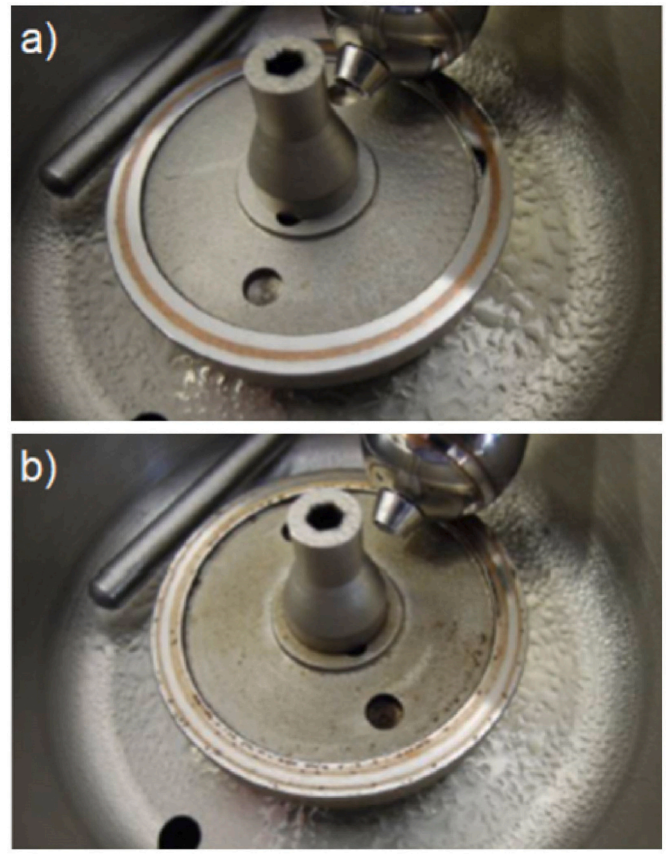

Fig. 9. Condensation during tests with the clean disc (a) and contaminated disc (b).

disc [17,18], and with the heavily rusted disc [17]. In the case of Ref. [14], a twin-disc Amsler machine was employed and the temperature range during tests was from 20 to 40 °C. Results in Ref. [14] showed the friction coefficient was almost independent of temperature; however, the tested temperature range was very limited. As was shown in the present study, the greatest decrease in CoA was found for the temperatures lower than 20 °C. In the case of Ref. [16–18], tests were conducted using a pin-on-disc tribometer operating under pure sliding conditions. Generally, these conditions can lead to a higher contact temperature and can cause severe removal of oxide layers formed on surfaces, whereby the occurrence of low adhesion associated with high RH value, or even with condensation, can be suppressed.

Finally, the data from Fig. 8 were recalculated to the absolute humidity (AH) in g/m3 with the following equation using Bolton's approximation for the saturation vapour pressure of water [29]:

$$AH = \frac{6.112 \cdot e^{\left[\frac{17.67 \cdot T}{T+243.5}\right]} \cdot RH \cdot 2.1674}{273.15 + T} \tag{2}$$

where T is a temperature in °C and RH is the relative humidity in %RH. The results in Fig. 10 show that the trend is nearly linear for each temperature; however, the data in the condensation area do not follow the trend for the specific temperature without condensation.

3.5. Analytical model for prediction of CoA

The results of CoA measurements for various temperatures and various RH values are summarized for both clean and contaminated conditions in the contour plot in Fig. 11. It should be noted that the data when condensation occurred are not included in these graphs. The experimental data were fitted to the following regression equations:

$$\mu_{clean} = 0,5461 + 0,003029 \cdot T - 0,002844 \cdot RH - 3,346 \cdot 10^{-5} \cdot T^2 + 5,401 \cdot 10^{-5} \cdot T \cdot RH \tag{3}$$

$$\mu_{contaminated} = 0,4153 + 0,001587 \cdot T - 0,001662 \cdot RH \tag{4}$$

where T is a temperature in °C and RH is the relative humidity in %RH. In the model, the dependence of CoA on temperature is a quadratic polynomial for clean conditions while for leaf-contaminated conditions is linear. The dependency on RH is linear in for both cases. This regression model leads to a very good determination coefficient of 0.962 for clean conditions and fairly good value of 0.725 for contaminated conditions. Generally, CoA for contaminated conditions is in average 25% lower than that under clean conditions. The difference is very low for the lowest adhesion that starts at app. 0.25 because the contaminated data are not included. The area of occurrence of relatively low or intermediate adhesion is larger for contaminated conditions. Larger differences can be observed for higher adhesion values where the maximum CoA 0.65 and 0.45 for clean and contaminated conditions respectively.

The analytical model for the clean disc, created as an approximation of measured data, predicts the effect of RH on CoA as a linear function with a very good determination coefficient. However, previously published studies [17,18,30–34] have reported an uneven trend. Some of them [30–32] point to a more significant drop in friction accompanied by an abrupt change in wear mechanism, although the transition level of RH varies across the studies between 15% [30], 45–55% [31] and 50 a 60% RH [33]. Other studies predict the trend as bilinear, wherein the

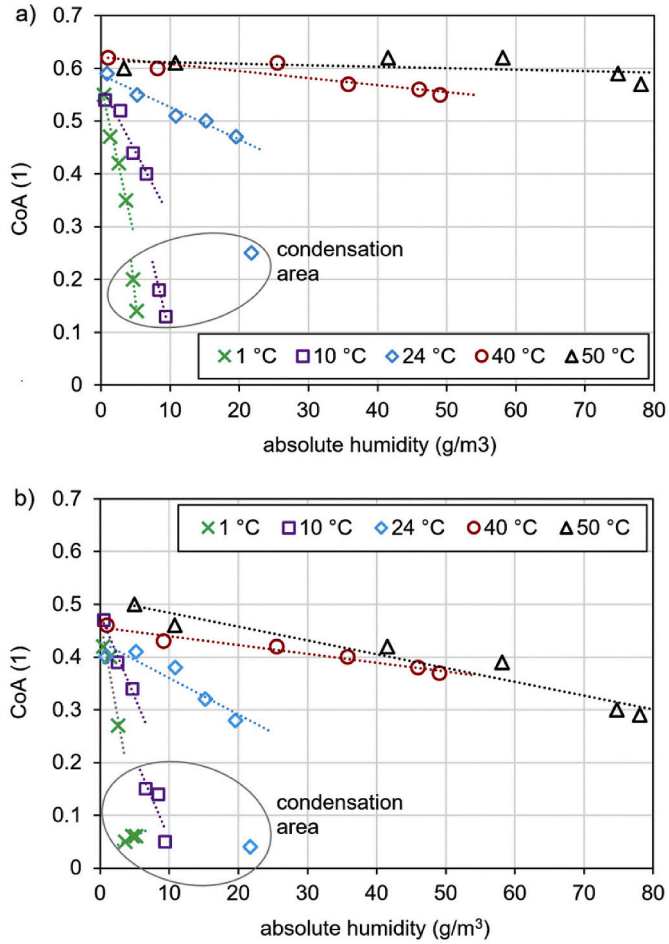

Fig. 10. Effect of AH and temperature on CoA for the clean disc (a) and contaminated disc (b).

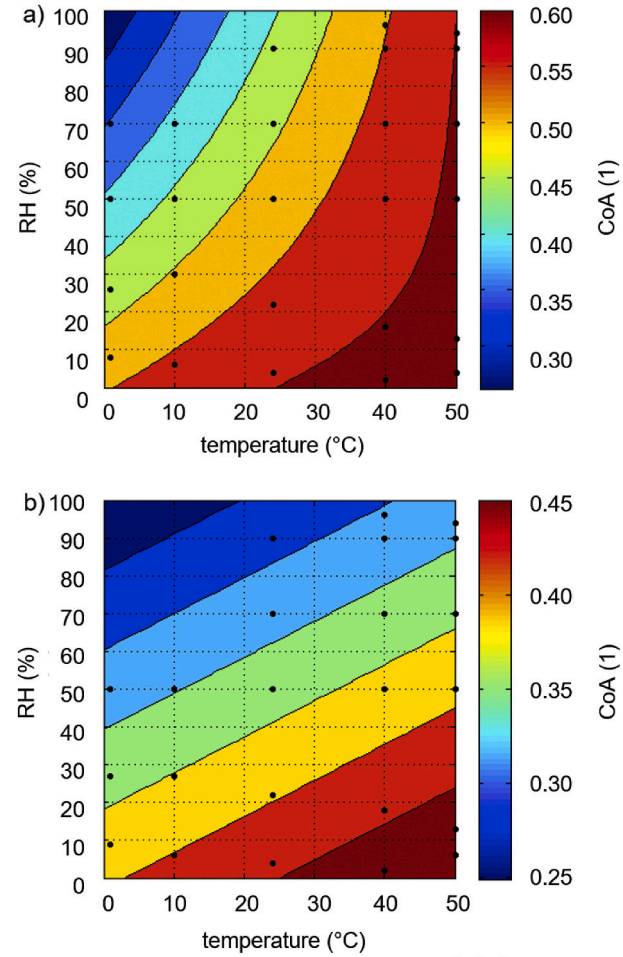

Fig. 11. Contour plot of the regression model of the effect of RH and temperature on CoA for clean conditions (a) and contaminated conditions (b).

change in behaviour occurring at 65% RH is explained by counterbalancing the effect of the boundary layer formed by the water molecules and hematite film formation at higher RH [17,18,33]. This difference in the trend can be explained by two following facts.

Firstly, the data in the present work represents CoA determined in rolling-sliding contact at a slip of 5%, whereas most of the previous studies utilized a pure sliding friction approach to measure CoF. As apparent in Figs. 2 and 3a, this slip was still before the saturation point in the ball-on-disc configuration, so the difference between CoA and CoF was substantial. The second difference is associated with the formation and retention of oxide layers between pure sliding and rolling-sliding tests. In real wheel-rail contact (rolling-sliding contact), the oxide layer usually consists of two types of oxides, magnetite (Fe3O4) and hematite (a-Fe2O3) [33,35,36]. Magnetite, known as "black oxide'', decreases friction while hematite has generally a tendency to increase friction [35]. Some hypotheses consider that under higher humidity normal atmospheric oxidation is inhibited because of the effect of water molecules in the surrounding air [37]. This could explain decreasing friction with RH when considering slowed down the formation of hematite. However, the process of oxide layer formation under pure sliding conditions can vary greatly. A pin operating under pure sliding conditions is in permanent contact with a counterpart that generally leads to higher flash temperature and heat dissipation can cause higher pin bulk temperature. Moreover, the formation of oxide layers on the pin/disc surface is prevented, as well as the access of water molecules to the wear track [38]. This is in contrast to rolling-sliding contact which provides a time for the environment to act on both surfaces during each cycle and it does not cause such an intensive removal of the formed layer.

Note that there is also a question about the effect of sample material. From this perspective, the most representative studies are those using a real rail and wheel steels [17,18,32,36,38]. Nevertheless, a fundamental discussion on the effect of relative humidity on friction and wear comes from studies using more general materials such as carbon steels [31], austenitic stainless steel [33,39] and bearing steel [30,40] and the trends are qualitatively similar. It is believed that the effect of the material is not as significant as the effect of the testing configuration.

3.6. General discussion: possible occurrence of low adhesion

The summary of the selected results is depicted in Fig. 12 where the results are categorized into different adhesion intervals. This figure gives evidence that neither heavy nor light rain does not lead to low adhesion conditions when contact surfaces are clean (free of debris). However, clean surfaces in operation can be expected very rarely such as after heavy rain when contaminants are washed away. Otherwise, rail and wheel surfaces are contaminated with dust, wear debris, their oxides, etc. These solid contaminants affect adhesion even under dry conditions; however, their impact on CoA can be much more substantial under wet conditions as was observed for oxidized surfaces operating under fully-flooded conditions, see Fig. 12. Under these conditions, even very low adhesion conditions were found when the contact was run-in under wet conditions before the test; thus, the tick and uniform oxide layer has been formed on the surfaces. With respect to these findings, it can be reasonably expected that more significant adhesion drops may occur even for light precipitation when contact surfaces are covered by the

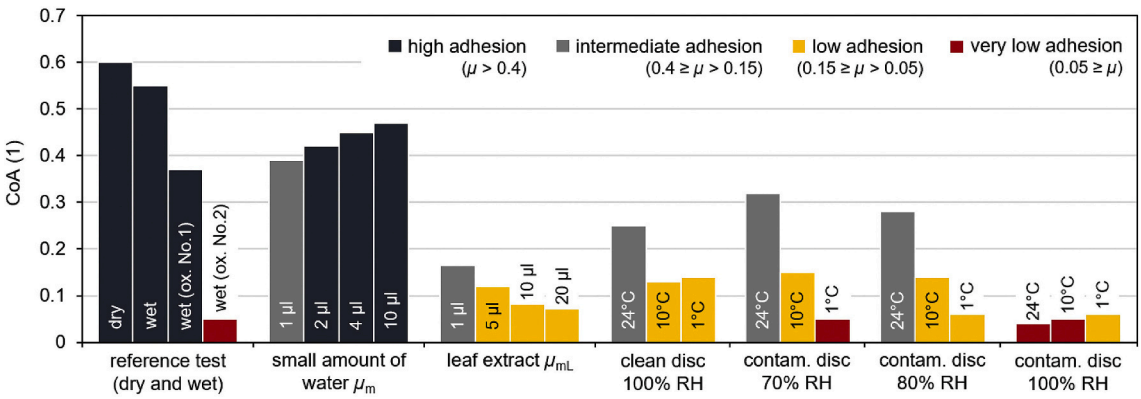

Fig. 12. Overview of selected results.

oxide layer or contaminated with free solid particles, as was observed in Ref. [13,15,23,26].

Besides water, leaves are common natural contaminants causing an annual problem for rail transportation. To study the effect of leaves on adhesion, two approaches were used in this study. In the former case, a liquid leaf extract was used as a lubricant which was applied directly into the contact, while in the latter case, a solid friction layer was prepared from the leaf extract on the disc surface. For a liquid leaf extract, low adhesion was found for all tested amounts. These results indicate that not only thick black leaf film can lead to poor adhesion conditions, as was observed before [4], but poor adhesion conditions can also occur due to the release of natural lubricant from the crushed leaves, such as pectin gel [41]. These results are in a line with Ref. [19] where a large number of low adhesion incidents have been reported for "non--contaminated" surfaces. Authors in Ref. [19] proposed these incidents can be caused by not detectable leaf layer. As was shown in the present study, the leaf extract can cause traction/braking difficulties and it can be difficult to detect this almost invisible layer on the rail surfaces.

In the last part of this study, the influence of RH and temperature on CoA was studied for the clean and contaminated disc. These results show that low adhesion can be expected especially during cold mornings and evenings when low temperature and very high RH usually occur [19, 41], see Fig. 12.

An even more critical case may occur in the autumn months when a leaf layer is formed on rail heads, see tests with the contaminated disc in Fig. 12. Under these conditions, low adhesion incidents can be anticipated more often for two reasons. First, CoA reaches critically low values when a leaf layer on the rail is wetted by a small amount of water from condensation. In such a situation, CoA can be even lower than 0.05. Second, the presence of leaf layer on the rail causes that very high RH is not needed for a rapid adhesion decrease because an adhesion drop may even occur at RH of 70% when the temperature is low (<10 °C). It means that adhesion problems can be observed even the dew point has not been reached yet.

This study showed that the most substantial adhesion drop occurs when contact is contaminated with water from condensation. This adhesion drop is much more serious than in tests with small amounts of water, see Fig. 12. Although it is difficult to quantify the amount of condensed water in the wear track, it can be assumed that the amount was similar to amounts applied during the set of tests No. 3 (1–10 µl). It means that this difference in adhesion drops is likely not attributed only to different amounts of water in the wear track, but can be the result of another phenomenon. The specimens used in sets of test No. 5 and 6 were exposed to high RH before starting the test because it was necessary to wait for RH and temperature to stabilize. It is hypothesised that the contact surfaces exposed to high RH for longer time are covered with a thin oxide layer. If RH is subsequently high enough for condensation, then a small amount of condensed water between oxidized surfaces results in low adhesion conditions. This hypothesis is contradictory to several studies that have noted that the pre-created oxides have a little effect since they are easily removed due to the contact conditions in pin-on-disc [17,18] as well as twin-disc [36] tests. So the hypothesis will be tested in the future study in detail.

4. Conclusions

In this work, the ball-on-disc tribometer with the climate chamber was used to identify conditions when low adhesion incidents can be expected in operation due to weather and season changes. The performed tests investigated the effect of several factors influencing adhesion. Unlike previously published articles dealing with the effect of environmental conditions on adhesion, the low and even very low adhesion conditions have been found for several contact conditions. These low and very low adhesion conditions were mostly associated with a high value of RH leading to the formation of oxide layer between surfaces. Based on this, the authors recommend studying "low adhesion phenomenon" under rolling-sliding conditions. This experimental approach seems to be more suitable than tests under pure sliding conditions where an oxide layer is quickly removed; thus CoA is almost unaffected by this layer. With regard to a possible occurrence of low adhesion incidents, the main conclusions of this study are as follows:

- The lowest value of CoA was found when the contaminated disc (by leaf extract) was run at RH of 70% or higher. Under these conditions, CoA fell even below 0.05. In real operation, this undesirable situation can occur especially during autumn mornings even though no visible leaf layer may be detectable on the rails.
- For leaf extract contamination, low adhesion conditions were observed for all tested amounts of extract but very low adhesion conditions did not occur.
- If contact surfaces are clean, very low adhesion conditions were not found for any tests; however, low adhesion incidents may occur under dew conditions.
- In the case of water as the most common natural contaminant, no important adhesion drops were observed for clean surfaces but very low adhesion was found when an oxide layer was formed on the surfaces.

Future work should be focused on the effect of condensate water on adhesion for various surface conditions of specimens occurring due to surface oxidation. Besides this, an interaction of condensed water and leaf residuals should be investigated to explore if these conditions may be responsible for unexpected low adhesion incidents during the autumn season.

Declaration of competing interest

The authors declare that they have no known competing financial

interests or personal relationships that could have appeared to influence the work reported in this paper.

CRediT authorship contribution statement

Radovan Galas: Conceptualization, Methodology, Investigation, Data curation, Writing - original draft. **Milan Omasta:** Conceptualization, Investigation, Methodology, Writing - review & editing, Project administration. **Lu-bing Shi:** Data curation, Writing - review & editing, Visualization. **Haohao Ding:** Writing - review & editing, Visualization. **Wen-jian Wang:** Conceptualization, Data curation, Writing - review & editing, Project administration. **Ivan Krupka:** Data curation, Writing - review & editing. **Martin Hartl:** Supervision, Funding acquisition.

Acknowledgements

The authors are sincerely grateful to European Commission for the financial sponsorship of the H2020-MSCA-RISE Project No. 691135 "RISEN: Rail Infrastructure Systems Engineering Network," which enables a global research network that tackles the grand challenge in railway infrastructure resilience and advanced sensing under extreme environments. The authors also thank the support of National Key R&D Program Intergovernmental Key Items for International Scientific and Technological Innovation Cooperation (No.2018YFE0109400).

Appendix A. Parameters of employed sensors

sensor	range	accuracy	nonlinearity
load cell for normal force	2–75 N	±0.3 N	±1% of full scale
load cell for friction force	−20 to +20 N	±0.3 N	±2% of full scale
servodrives	−4 to +4 m/s	±1 mm/s or 0.1% of speed, whichever is larger	not applicable
temperature sensor	0–150 °C	±0.5 °C	±1% of full scale
relative humidity sensor	0–100% RH (for temperature between −20 and + 60 °C)	2% RH	<1% RH

Appendix B. Mean standard deviations for sets of tests listed in Table 1

set No. 1	adhesion characteristics under dry conditions										
	stats	surface	0.5%	1%	2%	3%	4%	5%	6.5%	8%	n*
0.5 m/s	mean	clean	0.14	0.26	0.39	0.48	0.55	0.61	0.64	0.65	20
	Std Dev		0.005	0.002	0.003	0.004	0.004	0.005	0.006	0.005	20
1 m/s	mean		0.15	0.25	0.39	0.50	0.56	0.60	0.67	0.71	20
	Std Dev		0.002	0.003	0.003	0.006	0.005	0.004	0.004	0.005	20
2 m/s	mean		0.14	0.23	0.38	0.48	0.57	0.61	0.64	0.66	20
	Std Dev		0.001	0.003	0.002	0.001	0.002	0.001	0.003	0.003	20
3 m/s	mean		0.14	0.26	0.39	0.48	0.55	0.61	0.64	0.65	20
	Std Dev		0.002	0.002	0.006	0.004	0.004	0.003	0.002	0.003	20
set No. 2	**adhesion characteristics in wet conditions for different speeds and surface conditions**										
	stats	surface	0.5%	1%	2%	3%	4%	5%	6.5%	8%	n*
0.5 m/s	mean	clean	0.20	0.31	0.45	0.52	0.55	0.56	0.57	0.57	20
	Std Dev		0.006	0.005	0.002	0.002	0.001	0.001	0.001	0.003	20
1 m/s	mean		0.19	0.30	0.43	0.50	0.53	0.55	0.56	0.56	20
	Std Dev		0.003	0.003	0.003	0.001	0.001	0.004	0.002	0.001	20
2 m/s	mean		0.18	0.29	0.41	0.47	0.50	0.52	0.53	0.53	20
	Std Dev		0.003	0.002	0.003	0.002	0.001	0.002	0.003	0.002	20
3 m/s	mean		0.16	0.26	0.38	0.44	0.46	0.47	0.47	0.47	20
	Std Dev		0.005	0.006	0.003	0.002	0.002	0.004	0.008	0.002	20
1 m/s	mean	ox. layer No. 1	0.11	0.20	0.30	0.34	0.36	0.37	0.37	0.36	20
	Std Dev		0.003	0.002	0.004	0.02	0.02	0.003	0.004	0.002	20
2 m/s	mean		0.12	0.19	0.26	0.29	0.31	0.31	0.32	0.33	20
	Std Dev		0.004	0.02	0.001	0.003	0.002	0.002	0.005	0.002	20
3 m/s	mean		0.09	0.14	0.14	0.15	0.16	0.15	0.14	0.13	20
	Std Dev		0.002	0.004	0.003	0.002	0.005	0.001	0.003	0.003	20
2 m/s	mean	ox. layer No. 2	0.01	0.02	0.03	0.03	0.04	0.04	0.05	0.05	20
	Std Dev		0.003	0.001	0.003	0.001	0.003	0.004	0.002	0.003	20

set No. 3	**small amount of water**				
	stats	1 µl	2 µl	4 µl	10 µl
μ_m	mean	0.39	0.42	0.45	0.47
	Std Dev	0.029	0.012	0.006	0.006
	n*	4	6	10	10

set No. 4	**leaf extract**			
	1 µl	5 µl	10 µl	20 µl
μ_{mL}	0.17	0.12	0.08	0.07
	0.012	0.012	0.001	0.002
	3	7	10	10

set No. 5	clean disc					
	stats	8% RH	26% RH	50% RH	70% RH	90% RH	100% RH
1 °C	mean	0.56	0.48	0.43	0.36	0.23	0.15
	Std Dev	0.008	0.006	0.015	0.011	0.025	0.002
	n*	30	30	30	30	30	30
RH		**6%**	**27%**	**50%**	**70%**	**90%**	**100%**
10 °C	mean	0.57	0.52	0.46	0.40	0.18	0.14
	Std Dev	0.006	0.007	0.011	0.016	0.012	0.005
	n*	30	30	30	30	30	30

(*continued on next page*)

(*continued*)

set No. 5	clean disc						
	stats	8% RH	26% RH	50% RH	70% RH	90% RH	100% RH
RH		**4%**	**22%**	**50%**	**70%**	**90%**	**100%**
24 °C	mean	0.60	0.55	0.52	0.51	0.48	0.27
	Std Dev	0.001	0.002	0.003	0.002	0.011	0.005
	n*	30	30	30	30	30	30
RH		**2%**	**16%**	**50%**	**70%**	**90%**	**96%**
40 °C	mean	0.62	0.60	0.60	0.57	0.56	0.55
	Std Dev	0.002	0.008	0.003	0.003	0.004	0.005
	n*	30	30	30	30	30	30
RH		**6%**	**13%**	**50%**	**70%**	**90%**	**94%**
50 °C	mean	0.60	0.61	0.61	0.61	0.58	0.57
	Std Dev	0.005	0.004	0.002	0.003	0.004	0.003
	n*	30	30	30	30	30	30
set No. 6	**contaminated disc**						
	stats	**9% RH**	**24% RH**	**50% RH**	**70% RH**	**90% RH**	**100% RH**
1 °C	mean	0.42	0.38	0.28	0.06	0.06	0.06
	Std Dev	0.003	0.038	0.013	0.004	0.003	0.001
	n*	30	30	30	30	30	30
RH		**6%**	**27%**	**50%**	**70%**	**90%**	**100%**
10 °C	mean	0.48	0.38	0.35	0.14	0.17	0.06
	Std Dev	0.007	0.003	0.005	0.006	0.005	0.001
	n*	30	30	30	30	30	30
RH		**4%**	**22%**	**50%**	**70%**	**90%**	**100%**
24 °C	mean	0.41	0.38	0.38	0.33	0.28	0.04
	Std Dev	0.004	0.004	0.004	0.007	0.009	0.004
	n*	30	30	30	30	30	30
RH		**2%**	**18%**	**50%**	**70%**	**90%**	**100%**
40 °C	mean	0.45	0.43	0.43	0.40	0.38	0.35
	Std Dev	0.004	0.004	0.003	0.002	0.004	0.009
	n*	30	30	30	30	30	30
RH		**6%**	**13%**	**50%**	**70%**	**90%**	**94%**
50 °C	mean	0.50	0.46	0.42	0.39	0.32	0.29
	Std Dev	0.002	0.002	0.003	0.002	0.009	0.037
	n*	30	30	30	30	30	30

*n – sample size.

References

[1] Wang WJ, Liu TF, Wang HY, Liu QY, Zhu MH, Jin XS. Influence of friction modifiers on improving adhesion and surface damage of wheel/rail under low adhesion conditions. Tribol Int 2014;75:16–23. https://doi.org/10.1016/j.triboint.2014.03.008.

[2] Shi LB, Wang C, Ding HH, Kvarda D, Galas R, Omasta M, et al. Laboratory investigation on the particle-size effects in railway sanding: comparisons between standard sand and its micro fragments. Tribol Int 2020;146:62–70. https://doi.org/10.1016/j.triboint.2020.106259.

[3] Cann PM, Olofsson U, Persson K. The "leaves on the line" problem—a study of leaf residue film formation and lubricity under laboratory test conditions. Tribol Lett 2006;24:151–8. https://doi.org/10.1007/s11249-006-9152-2.

[4] Chen H, Furuya T, Fukagai S, Saga S, Ikoma J, Kimura K, et al. Wheel slip/Slide and low adhesion caused by fallen leaves. Wear 2020:446–7. https://doi.org/10.1016/j.wear.2020.203187.

[5] Zhu Y, Olofsson U, Nilsson R. A field test study of leaf contamination on railhead surfaces. Proc Inst Mech Eng - Part F J Rail Rapid Transit 2013;228:71–84. https://doi.org/10.1177/0954409712464860.

[6] Arias-Cuevas O, Li Z. Field investigations into the adhesion recovery in leaf-contaminated wheel–rail contacts with locomotive sanders. Proc Inst Mech Eng - Part F J Rail Rapid Transit 2011;225:443–56. https://doi.org/10.1177/2041301710394921.

[7] Broster M, Pritchard C, Smith DA. Wheel/rail adhesion: its relation to rail contamination on british railways. Wear 1974;29:309–21. https://doi.org/10.1016/0043-1648(74)90017-9.

[8] Nagase K, Pritchard C, Smith DA. A study of adhesion between the rails and running wheels on main lines: results of investigations by slipping adhesion test bogie. Proc Inst Mech Eng - Part F J Rail Rapid Transit 2016;203:33–43. https://doi.org/10.1243/PIME_PROC_1989_203_206_02.

[9] Gallardo-Hernandez EA, Lewis R. Twin disc assessment of wheel/rail adhesion. Wear 2008;265:1309–16. https://doi.org/10.1016/j.wear.2008.03.020.

[10] Chen H, Ishida M, Namura A, Baek K-S, Nakahara T, Leban B, et al. Estimation of wheel/rail adhesion coefficient under wet condition with measured boundary friction coefficient and real contact area. Wear 2011;271:32–9. https://doi.org/10.1016/j.wear.2010.10.022.

[11] Lewis SR, Lewis R, Olofsson U. An alternative method for the assessment of railhead traction. Wear 2011;271:62–70. https://doi.org/10.1016/j.wear.2010.10.035.

[12] Shi LB, Li Q, Kvarda D, Galas R, Omasta M, Wang WJ, et al. Study on the wheel/rail adhesion restoration and damage evolution in the single application of alumina particles. Wear 2019;426–427:1807–19. https://doi.org/10.1016/j.wear.2019.01.021.

[13] Beagley TM, Pritchard C. Wheel/rail adhesion — the overriding influence of water. Wear 1975;35:299–313. https://doi.org/10.1016/0043-1648(75)90078-2.

[14] Beagley TM, McEwen IJ, Pritchard C. Wheel/rail adhesion — the influence of railhead debris. Wear 1975;33:141–52. https://doi.org/10.1016/0043-1648(75)90230-6.

[15] White B, Lewis R. Simulation and understanding the wet-rail phenomenon using twin disc testing. Tribol Int 2019;136:475–86. https://doi.org/10.1016/j.triboint.2019.03.067.

[16] Olofsson U, Sundvall K. Influence of leaf, humidity and applied lubrication on friction in the wheel-rail contact: pin-on-disc experiments. Proc Inst Mech Eng - Part F J Rail Rapid Transit 2005;218:235–42. https://doi.org/10.1243/0954409042389364.

[17] Zhu Y, Olofsson U, Chen H. Friction between wheel and rail: a pin-on-disc study of environmental conditions and iron oxides. Tribol Lett 2013;52:327–39. https://doi.org/10.1007/s11249-013-0220-0.

[18] Zhu Y, Lyu Y, Olofsson U. Mapping the friction between railway wheels and rails focusing on environmental conditions. Wear 2015;324–325:122–8. https://doi.org/10.1016/j.wear.2014.12.028.

[19] White BT, Nilsson R, Olofsson U, Arnall AD, Evans MD, Armitage T, et al. Effect of the presence of moisture at the wheel–rail interface during dew and damp conditions. Proc Inst Mech Eng - Part F J Rail Rapid Transit 2017;232:979–89. https://doi.org/10.1177/0954409717706251.

[20] Arias-Cuevas O, Li Z, Lewis R, Gallardo-Hernández EA. Rolling–sliding laboratory tests of friction modifiers in dry and wet wheel–rail contacts. Wear 2010;268:543–51. https://doi.org/10.1016/j.wear.2009.09.015.

[21] Voltr P, Lata M. Transient wheel–rail adhesion characteristics under the cleaning effect of sliding. Veh Syst Dyn 2015;53:605–18. https://doi.org/10.1080/00423114.2014.961488.

[22] Galas R, Omasta M, Krupka I, Hartl M. Laboratory investigation of ability of oil-based friction modifiers to control adhesion at wheel-rail interface. Wear 2016;368–369:230–8.

[23] Shi LB, Ma L, Guo J, Liu QY, Zhou ZR, Wang WJ. Influence of low temperature environment on the adhesion characteristics of wheel-rail contact. Tribol Int 2018;127:59–68. https://doi.org/10.1016/j.triboint.2018.05.037.

[24] Hardwick C, Lewis R, Olofsson U. Low adhesion due to oxide formation in the presence of salt. Proc Inst Mech Eng - Part F J Rail Rapid Transit 2013;228:887–97. https://doi.org/10.1177/0954409713495666.
[25] Lewis R, Gallardo-Hernandez EA, Hilton T, Armitage T. Effect of oil and water mixtures on adhesion in the wheel/rail contact. Proc Inst Mech Eng - Part F J Rail Rapid Transit 2009;223:275–83. https://doi.org/10.1243/09544097JRRT248.
[26] Galas R, Kvarda D, Omasta M, Krupka I, Hartl M. The role of constituents contained in water–based friction modifiers for top–of–rail application. Tribol Int 2018;117: 87–97. https://doi.org/10.1016/j.triboint.2017.08.019.
[27] Omasta M, Machatka M, Smejkal D, Hartl M, Křupka I. Influence of sanding parameters on adhesion recovery in contaminated wheel–rail contact. Wear 2015; 322–323:218–25. https://doi.org/10.1016/j.wear.2014.11.017.
[28] Wang WJ, Shen P, Song JH, Guo J, Liu QY, Jin XS. Experimental study on adhesion behavior of wheel/rail under dry and water conditions. Wear 2011;271:2699–705. https://doi.org/10.1016/j.wear.2011.01.070.
[29] Bolton D. The computation of equivalent potential temperature. Mon Weather Rev 1980;108(7):1046–53. https://doi.org/10.1175/1520-0493(1980)108<1046:TCOEPT>2.0.CO;2.
[30] Klaffke D. On the repeatability of friction and wear results and on the influence of humidity in oscillating sliding tests of steel-steel pairings. Wear 1995;189:117–21. https://doi.org/10.1016/0043-1648(95)06672-1.
[31] Oh H-K, Yeon K-H, Yun Kim H. The influence of atmospheric humidity on the friction and wear of carbon steels. J Mater Process Technol 1999;95:10–6. https://doi.org/10.1016/S0924-0136(99)00259-9.
[32] Liew WYH. Effect of relative humidity on the unlubricated wear of metals. Wear 2006;260:720–7. https://doi.org/10.1016/j.wear.2005.04.011.
[33] Zhu Y. The influence of iron oxides on wheel–rail contact: a literature review. Proc Inst Mech Eng - Part F J Rail Rapid Transit 2017;232:734–43. https://doi.org/10.1177/0954409716689187.
[34] Chen Z, He X, Xiao C, Kim S. Effect of humidity on friction and wear—a critical review. Lubricants 2018;6. https://doi.org/10.3390/lubricants6030074.
[35] Godfrey D. Iron oxides and rust (hydrated iron oxides) in tribology. Tribol Lubric Technol 1999;55(2):33–7.
[36] Zhu Y, Chen X, Wang W, Yang H. A study on iron oxides and surface roughness in dry and wet wheel−rail contacts: a literature review. Wear 2015;328–329:241–8. https://doi.org/10.1016/j.wear.2015.02.025.
[37] Leheup ER, Pendlebury RE. Unlubricated reciprocating wear of stainless steel with an interfacial air flow. Wear 1991;142:351–72. https://doi.org/10.1016/0043-1648(91)90174-S.
[38] Zhu Y, Yang H, Wang W. Twin-disc tests of iron oxides in dry and wet wheel−rail contacts. Proc Inst Mech Eng - Part F J Rail Rapid Transit 2015;230:1066–76. https://doi.org/10.1177/0954409715575093.
[39] Bregliozzi G, Di Schino A, Kenny JM, Haefke H. The influence of atmospheric humidity and grain size on the friction and wear of AISI 304 austenitic stainless steel. Mater Lett 2003;57:4505–8. https://doi.org/10.1016/S0167-577X(03)00351-3.
[40] de Baets P, Kalacska G, Strijckmans K, Van de Velde F, Van Peteghem AP. Experimental study by means of thin layer activation of the humidity influence on the fretting wear of steel surfaces. Wear 1998;216:131–7. https://doi.org/10.1016/S0043-1648(97)00189-0.
[41] Ishizaka K, Lewis SR, Lewis R. The low adhesion problem due to leaf contamination in the wheel/rail contact: bonding and low adhesion mechanisms. Wear 2017; 378–379:183–97. https://doi.org/10.1016/j.wear.2017.02.044.

Tribology International 188 (2023) 108872

Contents lists available at ScienceDirect

Tribology International

journal homepage: www.elsevier.com/locate/triboint

The performance of top-of-rail products under water contamination

Simon Skurka [a,*], Radovan Galas [a], Milan Omasta [a], Bingnan Wu [b], Haohao Ding [b], Wen-Jian Wang [b], Ivan Krupka [a], Martin Hartl [a]

[a] Faculty of Mechanical Engineering, Brno University of Technology, Technicka 2896/2, 616 69 Brno, Czech Republic
[b] Tribology Research Institute, State Key Laboratory of Traction Power, Southwest Jiaotong University, Chengdu 610031, China

ARTICLE INFO

Keywords:
Wheel-rail tribology
Friction modification
Low adhesion
Water contamination

ABSTRACT

Top-of-rail products are commonly used for friction modification in wheel-rail contact. However, the effect of environmental conditions and contaminants on their performance remains unclear. In this study, three commercial top-of-rail products were contaminated by different amounts of water. The laboratory tribometer in ball-on-disc configuration was used to measure the coefficient of adhesion in contaminated contact. The results show that water influenced tested top-of-rail products significantly. A very low coefficient of adhesion occurred in tests with oil-based top-of-rail products suggesting that water could cause traction problems on the actual railway where friction modification is being used. Water-based top-of-rail products showed more resistance to water contamination.

1. Introduction

Friction modification presents a practical approach to dealing with high friction in railway transportation. Nowadays, top-of-rail (TOR) products are applied on railheads via trackside applicators or systems mounted on a train [1]. Initially, these products were used as solid sticks containing solid lubricants like graphite or molybdenum disulfide [2]. However, liquid-based products containing water [3] or oil with thickeners [4] as a base medium are often used. Dealing with friction is an important task to improve the energy efficiency of rail transportation and decrease maintenance costs. High friction causes rail corrugation [5] and is also the leading cause of excessive wear on both wheels and rail [6–9]. Also, friction in the wheel-rail contact and the shape of the traction curve contribute to noise pollution. According to WHO, the noise limit of 55 dB is harmful in case of long-term exposure. It is estimated that up to 113 million people in Europe (of which rail transport contributes approximately 20%) are exposed to traffic noise above this limit [10]. Various field and laboratory tests confirmed the ability of TOR products to reduce friction [11] and influence corresponding effects like wear [12–14], noise [15,16] and energy consumption [17].

On the other hand, maintaining a sufficient level of friction is required to transmit traction forces from wheel to rail to accelerate or stop the vehicle. The coefficient of adhesion (CoA) describes the effectivity of this transmission. Generally, CoA lower than 0.2 and 0.09 is considered insufficient for traction and braking, respectively [18]. Thus, TOR products often contain mineral or metal particles to secure sufficient CoA. A liquid base (water, oil or less often a combination of both) is included to carry these particles along the rail [4]. The performance of some TOR products, especially oil-based ones, strongly depends on the applied amount [19]. As shown in [20], excessive amounts of product could cause low CoA problems resulting in an extension of the braking distance. TOR products are developed and tested to reduce friction while maintaining a required level of CoA for traction/braking. This can be achieved only with a suitable composition of the product and its optimal dosing.

Both water and oil-based TOR products are commonly referred to as friction modifiers (FMs) in literature. However, the mechanism of friction modification differs significantly for both types. In the case of water-based TOR products, the base medium quickly evaporates after application, and solid particles mix with the third body layer on the rail surface, providing a shear displacement compensation mechanism [21]. On the other hand, oil-based TOR products do not dry up and rely on a mixed/boundary lubrication regime. Because the base medium stays liquid, these TOR products can be redistributed for longer distances than water-based ones. However, it also carries the risk of low CoA occurrence close to the application unit due to overdosing [20]. Following [19], this paper will refer to water-based TOR products as "friction modifiers" and oil-based TOR products as "TOR lubricants" for clarity.

As stated above, the performance of friction modifiers and TOR lubricants in dry and clean contact has been well examined. However,

* Corresponding author.
E-mail address: Simon.Skurka@vut.cz (S. Skurka).

https://doi.org/10.1016/j.triboint.2023.108872
Received 27 April 2023; Received in revised form 8 August 2023; Accepted 12 August 2023
Available online 21 August 2023
0301-679X/© 2023 Elsevier Ltd. All rights reserved.

while the coefficient of friction in dry wheel-rail contact is usually between 0.5 and 0.6 [22], in contaminated contact, the friction decreases significantly, causing also drop in CoA. It is caused by third body layers naturally occurring on the rail surface and environmental contaminants [23]. Water is one of the most common environmental contaminants. It can be found on the track from rain, morning dew, or even leakage from passing vehicles. Several laboratory studies show that water can reduce the CoA under 0.2 [23–25] and even lower depending on quantity and temperature. Also, water forms a highly viscous mixture if combined with iron oxides, leading to a CoA of 0.05 or lower [24].

Although contamination of wheel-rail contact is practically inevitable in reality, very little is known about the interaction between contaminants and TOR products. In most studies, TOR products were tested only in laboratory-clean conditions without contamination, or the effect of contamination was not considered. Chen et al. compared the lubrication performance of several lubricants on dry and wet rails [25]. They showed that the reduction of lateral forces was greater on the wet rail for all tested lubricants. Lewis et al. tested the influence of air humidity on friction modifiers. They discovered that when exposed to air with a higher % of relative humidity, CoF reaches lower values than in less humid air [26]. This phenomenon could be explained by water condensation and contamination of friction modifiers. The case study [27] shows that the combined effect of water and oil can cause traction problems on the top of the railhead. As oil is the main component in TOR lubricants, a question arises as to if a similar phenomenon can happen when a TOR product is contaminated by water. TOR products usually maintain CoA sufficient for traction/braking thanks to the balance between base medium and solid particles. However, there is a possibility that if TOR products are contaminated with water, the balance will be disturbed, product performance will decrease, and the minimum required CoA will not be kept.

This study uses three commercial TOR products. Two of them are TOR lubricants, and one is a friction modifier. All CoA tests were conducted on a laboratory tribometer in a ball-on-disc configuration. On an actual railway, contamination by water can occur, resulting in an insufficient CoA level. The degree of the contamination can differ depending on the water source (dew, rain, leakage from passing trains). Therefore, all TOR products were tested in dry and wet conditions. Small and large amounts of water were applied. Also, single and continuous water application was tested to simulate different ways of contamination. This study aims to describe the influence of water and its amount on the TOR product performance in terms of CoA.

2. Material and methods

2.1. Test setup and specimens

A laboratory tribometer MTM (Mini-Traction Machine, PCS Instruments) in a ball-on-disc configuration was used for all tests, see Fig. 1. Technical norms specify the measuring procedure on this device. However, these norms are mainly focused on traction curve evaluation. Therefore, they are unsuitable for observation of CoA drop caused by contamination. Thus, a different approach previously used in papers [3, 4] will be used in this study. The contact bodies were discs and balls of 46 mm and 19.05 mm in diameter, so the contact has a circular shape. Both specimens were made of AISI 52100 bearing steel with a Vickers macro-hardness of 800–920 HV and 720–780 HV for ball and disc. The bearing steel is not a typical rail material. However, higher hardness ensures stable conditions during experiments and better repeatability due to reduced wear compared to standard wheel/rail steel. The initial roughness of the surface of both specimens was Ra 0.01 μm; however, it grew to Ra 0.15 μm (ball) and Ra 0.3 μm (disc) after the initial wear-in and the following run-in.

Both specimens were loaded against each other and driven by independent servo motors so the required slide–roll ratio (SRR) could be achieved according to the given equation:

$$SRR = \frac{w_{ball} \bullet r_{ball} - w_{disc} \bullet r_{disc}}{w_{ball} \bullet r_{ball} + w_{disc} \bullet r_{disc}} \bullet 200\% \quad (1)$$

where w_{ball} and w_{disc} are angular speeds of specimens and r_{ball} and r_{disc} stands for its radii. The embedded sensor measures the normal force (N) with ± 0.3 N accuracy. Traction force (T) is calculated from the torque measured by the transducer attached to the disc shaft, so the adhesion coefficient (CoA) could be determined as follows:

$$CoA = \frac{N}{T} \quad (2)$$

Data from force sensors are acquired with a 1 Hz sampling frequency. However, this signal results from averaging a non-specified higher frequency input signal.

2.2. Tested TOR products and contaminants

Two commercial TOR lubricants (referred to as "TORL-A" and "TORL-B"; oil-based TOR products) and one friction modifier ("FM-A"; water-based TOR product) were used in this study. Essential information about the composition of both TOR lubricants can be read from datasheets, see Table 1.

Although water-based TOR products are meant to form a dry film after base medium evaporation, wet film lubrication occurs immediately after application. Thus FM-A was tested both before and after the evaporation of the base medium. Distilled water was used as a contaminant in all tests.

2.3. Wear-in, run-in and cleaning of specimens

Before any experiments, an initial 60-minute dry wear-in of specimens was conducted. This is because severe wear of contact surfaces occurs with a new pair of specimens. After 60 min of wear-in, the wear rate decreases significantly, and stable test conditions could be secured. According to Hertz's Theory, the diameter of the contact is calculated to be 0.2 mm for a new pair of specimens. However, due to wear and topography changes caused by the wear-in, the actual contact will differ from the theory, and the diameter will be higher. Please note that described 60-minute wear-in is performed only once at the beginning for

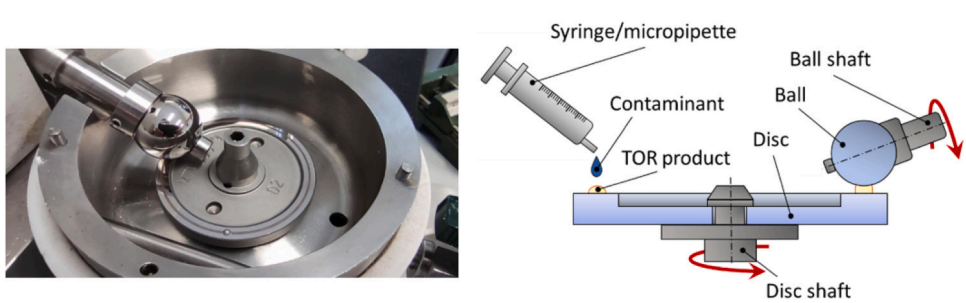

Fig. 1. Photo (left) and scheme (right) of the apparatus.

Table 1
Composition and characteristics of tested TOR lubricants.

TOR product	Structure	NLGI grade	Base oil	Thickener	Particles	Base oil viscosity at 40 °C (mm^2/s)
TORL-A	Paste	0	Biodegradable ester	Organic	Soft metal	41–53
TORL-B	Gel paste	00	Synthetic ester	Inorganic (silicate)	Soft metal	46

each new pair of specimens. The wear-in parameters (speed, load and SRR) are the same as for adhesion tests and run-ins and will be described later.

A 15-minute run-in was performed before every adhesion test to remove the oxide layer and TOR product residual from the track and to stabilize surface roughness. During this process, the CoA stabilized around 0.39 (a reference value for dry contact), ensuring that every test started from the same initial conditions. Unlike a wear-in, a run-in was performed before every adhesion test, not only at the beginning for a new pair of specimens. Specimens were cleaned manually with a paper towel and ultrasonically in an acetone bath for 10 min after each test.

The wear-in/run-in and cleaning parameters are based on a preliminary study conducted before this work in the experiment design process. The base value of 0.39 for the dry contact CoA and the duration of 60 min and 15 min for wear-in and run-in were selected based on the results of 20 tests focusing on adhesion and wear development. After the end of every test, the surface topography was checked on an optical profilometer. Also, the contact path surface was checked under a microscope to visually confirm that the cleaning process removed any remaining lubricant residue or particles.

2.4. Adhesion test: performance of water/TOR product under dry conditions

Firstly, different amounts of water and TOR products were tested in dry conditions to investigate their separate influence on CoA, see Table 2. The following parameters were set for all tests: a fixed value of 2% SRR, a mean speed of 1 m/s, and a load of 18 ± 0.01 N normal force (corresponding to 0.8 GPa Hertzian contact pressure). The same parameters were used in wear-ins and run-ins. The set SRR represents a value from the effective linear part of the traction curve near the saturation point commonly found in actual railway operations. Moreover, higher values of SRR could cause excessive wear. According to [28], the chosen value of the mean speed represents the velocity of approx. 60 km/h in actual wheel-rail contact corresponding to the light-rail system.

The performance of oil-based TOR products strongly depends on applied quantity [19]. Thus, choosing the optimal amount for tests in the main part of this work was necessary. Different amounts of each TOR product were tested to determine the optimal amount (regarding retentivity, low/intermediate CoA). The 15-minute run-in was performed before each test.

2.5. Stribeck test: water, oil and water-oil mixture under fully flooded conditions

A Stribeck test of water, oil, and a 1:1 water-oil (W/O) mixture under fully flooded conditions was conducted. TORL-A bleed oil with a viscosity of 64 mPa.s was used in this test. The set parameters for this test were 18 N of load and 2% SRR. The mean speed of specimens was 100–2500 mm/s for water and 50–2500 mm/s for oil and W/O mixture. For each tested speed, one mean value of CoA was calculated from the 6-second test. This test revealed the lubrication regime and thickness of the lubrication film and will be further discussed in the Sections Results and Discussion.

2.6. Adhesion test: performance of TOR product under wet conditions

In the main part of this work, TOR products were tested under wet conditions. Please note that water was applied to the contact only after the TOR product. The moment of application varied and is specified in Table 2. The parameters of these tests were the same as in adhesion tests under dry contact conditions (see Section 2.4). The tested amount of each product was determined regarding optimal performance in dry conditions. TOR products were applied to the disc surface using an electronic micropipette (error ± 0.04 μl). There were two types of tests: (1) single water application using a syringe/electronic micropipette and (2) continuous water application via a peristaltic pump. The procedure of all adhesion tests is summarised in Table 2.

In addition, water-based FM-A was tested both before ("wet film") and after ("dry film") base medium evaporation. To prepare a dry film, a short 30-second test immediately followed the application of FM-A to spread it on contact bodies. The parameters of this test were: 0% SRR, 300 mm/s mean speed, and 18 N load. A 10-minute pause follows to provide enough time for water evaporation. These two steps ensure the formation of an evenly distributed dry film. This procedure only applies to FM-A (dry film) tests.

In the case of single application tests, the TORL-A and FM-A (wet/dry

Table 2
Procedure of adhesion tests: dry and wet conditions (see 2.4 and 2.6).

Type of test	Water/TOR product	Run-in duration (min)	Amount of TOR product (μl)	T1–T3[a] (CoA)	Amount of water (μl)	Test duration (s)	Fig. # in Results
Dry conditions, a single water/TOR product application	TORL-A	15	1; 2; 3; 4	-	-	600	3 a)
	TORL-B	15	1; 2; 3; 4	-	-	900	3 b)
	FMA-(wet film)	15	2; 4; 6; 8	-	-	600	3c)
	FM-A (dry film)	15	4	-	-	600	3c)
	Water	15	-	-	2; 8; 32; 2000	150	3 d)
Wet conditions, a single water application	TORL-A	15	2	0.13; 0.2; 0.3	2; 8; 32; 2000	600	5
	TORL-B	15	1	0.13; 0.2; 0.3	2; 8; 32; 2000	900	6
	FM-A (wet film)	15	4	0.13; 0.2; 0.3	2; 8; 32; 2000	600	7
	FM-A (dry film)	15	4	0.3	2; 8; 32; 2000	600	8
Wet conditions, continuous water application	TORL-A	15	2	0.18	2150	2000	9
	TORL-B	15	1	0.18	2150	2000	9
	FM-A (wet film)	15	4	0.23	2150	1000	10
	FM-A (dry film)	15	4	0.32	2150	1000	10

[a] T1–T3 are defined values of CoA. When reached during the test, water was applied to the TOR product.

film) test duration was 600 s. For TORL-B, the test duration was extended to 900 s due to its longer retentivity. For the continuous application of water, the duration was 2 000 s for TOR lubricants and 1 000 s for friction modifiers.

In various tests, water was applied at different times after the start of the test. The reason for this was to observe the effect of water on TOR products at different phases of its performance. The exact moment of application was determined by the value of CoA defined in Table 2. Water was applied only once per adhesion test when CoA reached the specified value. In the Section Results, points where water was applied, are marked as T1–T3 in the graphs. These values vary for TOR lubricants and friction modifiers because both types of TOR products led to different CoA.

A typical adhesion test of TOR product with a single and continuous water application can be seen in Fig. 2a) and b). First, a 15-minute run-in was conducted before every test. Only the final parts of the run-in are shown in Fig. 2. Second, a TOR product was applied. In the FM-A (dry film) tests, the spreading and drying procedure followed (not shown in Fig. 2). After that, the adhesion test with described parameters started. The CoA development during the typical test was as follows: after a TOR product application, an initial drop caused by a large amount of TOR product occurred. However, part of the TOR product dosage was quickly pushed away from the track, and the CoA slowly rose to 0.15–0.25. When the trigger value of CoA was reached (T1–T3), water was applied either by a) a micropipette/syringe or b) a peristaltic pump. The magnitude and duration of the drop of CoA caused by the water application on the disc with the tested TOR product depended on the amount of applied water. During test b), 430 μl/min of water was continuously applied for 5 min (2 150 μl in total). Both small and large amounts of water were used to determine the influence on product performance (2–2 000 μl for a single application and 430 μl/min for a continuous application).

3. Results

3.1. Results: performance of water/TOR product under dry conditions

First, TOR products and distilled water were tested separately in a series of adhesion tests. Each TOR product was tested in different amounts to determine the best-performing amount, which was later used for the adhesion tests of TOR products in wet conditions in the main part of this work. The term "best-performing amount" means the amount of TOR product, which ensures a good ratio between the duration of the initial drop of CoA under 0.1 (which is undesired but inevitable in most cases for TOR lubricants) and the duration of a period of intermediate CoA (desired effect of TOR products). Also, the three phases after application can be distinguished: the initial rise in CoA, stabilization at the desired adhesion level, and starvation and dry contact restoration.

In the case of TORL-A (Fig. 3a), the amount of 4 μl was unsuitable for further testing as it caused over-lubrication, and the CoA restoration did not occur during the standard test duration. On the contrary, both 1 μl and 2 μl led to desired adhesion development. Finally, the amount of 2 μl was chosen because, for this amount, the product stays in effect slightly longer than for 1 μl. Also, the repeatability of the measurement was tested. Two dashed lines in Fig. 3a) represent additional measurements of 2 μl of TORL-A. After comparing all three curves, it can be said that in all three tests, very similar values of CoA were measured. The curves slightly differ only at the end when the starvation occurs, which should not be a problem as contamination will not be tested at this part of the curve.

In the case of TORL-B (Fig. 3b), 4 μl of the product led to over-lubrication of the contact. Although 2 μl did not cause the over-lubrication, the tests would be inefficiently long for this amount. As the 1 μl showed desired adhesion development in the standard test duration, this amount was chosen for the rest of the experiments.

Contrary to TOR lubricants, the over-lubrication did not occur for any tested amount of FM-A. Although it shows some adhesion-amount dependency, generally, it is much less significant than in the case of TOR lubricants. The 4 μl was chosen from all tested amounts as it led to a similar test duration compared to TORL-A and TORL-B. Afterward, this amount was also tested as dry film (red dashed line in Fig. 3c).

Four different amounts of water (2, 8, 32 μl, and 2 ml) were tested). These exact amounts were later used for adhesion tests under wet conditions. Fig. 3d) shows that with the increase of water amount, the duration of CoA drop also increases. However, there is no significant difference between 32 μl and 2 ml. The effect of the amount on the CoA level is relatively negligible. For tested amounts, the CoA ranged from 0.32 to 0.35.

3.2. Results: Stribeck test of water, oil and W/O mixture

The results of the Stribeck test are displayed in Fig. 4. Please note that each line represents the mean value calculated from three measurements. The lubrication parameter λ was calculated for water and oil to determine the lubrication regime. Value $\lambda = 1$, often used in literature as a transition between boundary and mixed lubrication regime [29], is marked for oil conditions in the figure.

For water, the boundary regime occurs for all tested speeds. For oil, the boundary regime occurs up to 280 mm/s. Above this speed, the contact operates mainly in the mixed lubrication regime. For the W/O mixture, parameter λ was not calculated. In addition, Fig. 4 shows that with the increase in speed, the CoA decreased. The highest CoA of 0.56 was measured for water. With increasing speed, the decrease of CoA was somewhat limited, and the lowest value of 0.43 was measured for a mean speed of 2 500 mm/s. On the other hand, a W/O mixture led to significantly lower CoA. The measured value for a speed of 1000 mm/s was 0.04 and 0.02 for the oil and W/O mixture, respectively. Meanwhile, the CoA of water was 0.45 at this speed.

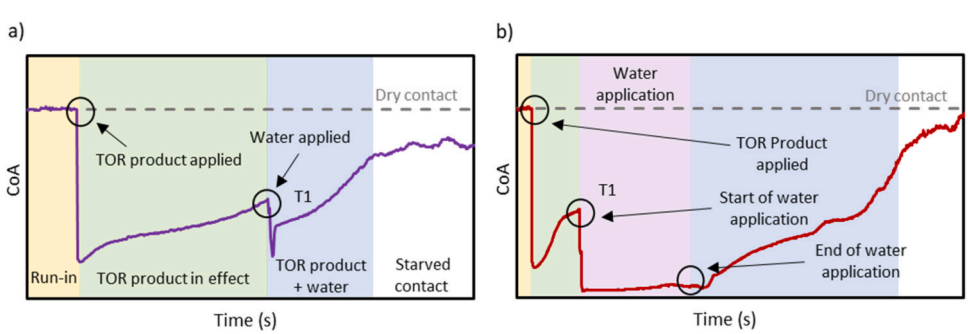

Fig. 2. (a) Adhesion test – a single application of water, (b) adhesion test – continuous application of water.

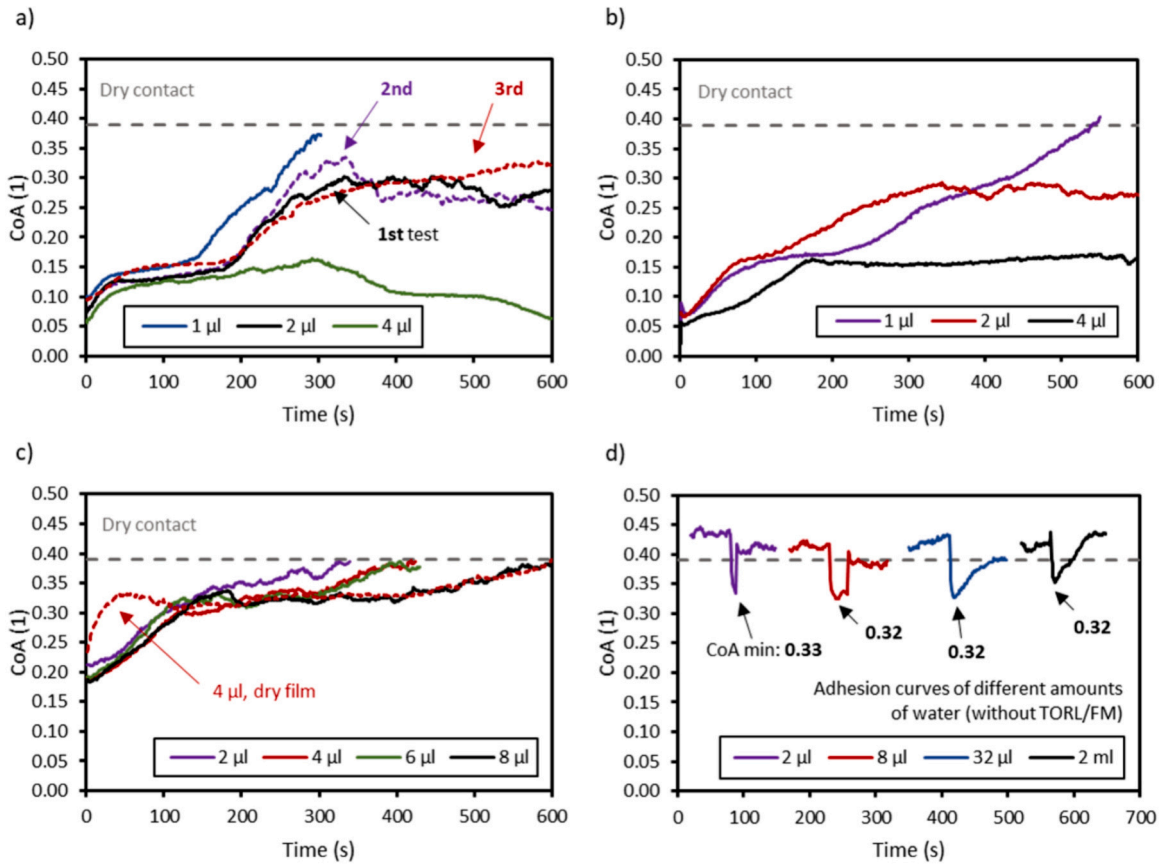

Fig. 3. Adhesion tests: different amounts of (a) TORL-A, (b) TORL-B, (c) FM-A, and (d) distilled water.

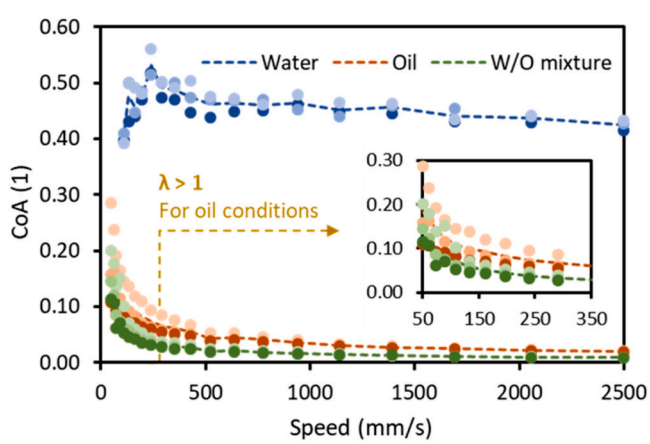

Fig. 4. Stribeck test of water, oil, and W/O mixture.

3.3. Results: performance of TOR products under a single water application

Figs. 5 and 6 represent TORL-A and TORL-B adhesion tests after a single water application. Both figures consist of four independent graphs marked as a–d). In each graph, a different amount of water was applied, see the upper left corner. There are two types of curves in these graphs. Dashed lines represent the dry contact CoA level (grey) and adhesion tests of TOR products measured under dry conditions (black). These curves are already depicted in Fig. 3a) and b). The purpose of showing them again in these graphs is to enable a quick comparison between adhesion tests with and without water application. Solid lines represent adhesion tests where water was applied into contact with TORL-A and TORL-B. Each graph includes three curves because three measurements were conducted for the same amount of water. Although each has a different color, this is only for clarity, and the test parameters for the triplet of tests were the same. The only difference was the time when water was applied to the contact. Water was applied when a specific value of CoA was reached. These values are for each TOR product listed in.

Table 2 and are marked as T1–T3 in all graphs. In addition, the minimum values of CoA reached during the initial adhesion drop are displayed. There are slight differences between curves of the same TOR product measured at different tests. These could be caused by different contact temperatures, surface topography changes as wear progresses during the experiment, or slightly different amounts of TOR product in the contact path. However, these differences are not statistically significant.

Fig. 5 shows results for TORL-A. For 2 µl of water, a drop to the lowest CoA value of 0.084 was observed when water was applied in T3. Similar drops were also observed in T1 and T2 applications. Compared to b–d), the CoA drop caused by 2 µl of water had the shortest duration. The CoA was restored to the level before water application in all three measurements. For the rest of the tests, the lowest CoA measured were: 0.037 in T3 for b); 0.035 in T3 for c) and 0.026 in T1 for d). As can be seen, with an increase in water amount, the CoA decreases to lower levels. Moreover, larger amounts of water also slow the CoA restoration after the initial drop. In c) and d), the CoA was not restored during the standard test duration (except for T3; 2 ml). The CoA stayed in the 0.05–0.1 interval until the end of the test.

The curves for TORL-B measured in dry conditions are more flattened than those of TORL-A. However, under wet conditions, they show similar behavior, see Fig. 6. With the increasing amount of water, CoA decrease, and it takes more time for CoA to reach dry contact levels. The lowest CoA measured: 0.069 in T3 for a); 0.028 in T2 for b); 0.017 in T1

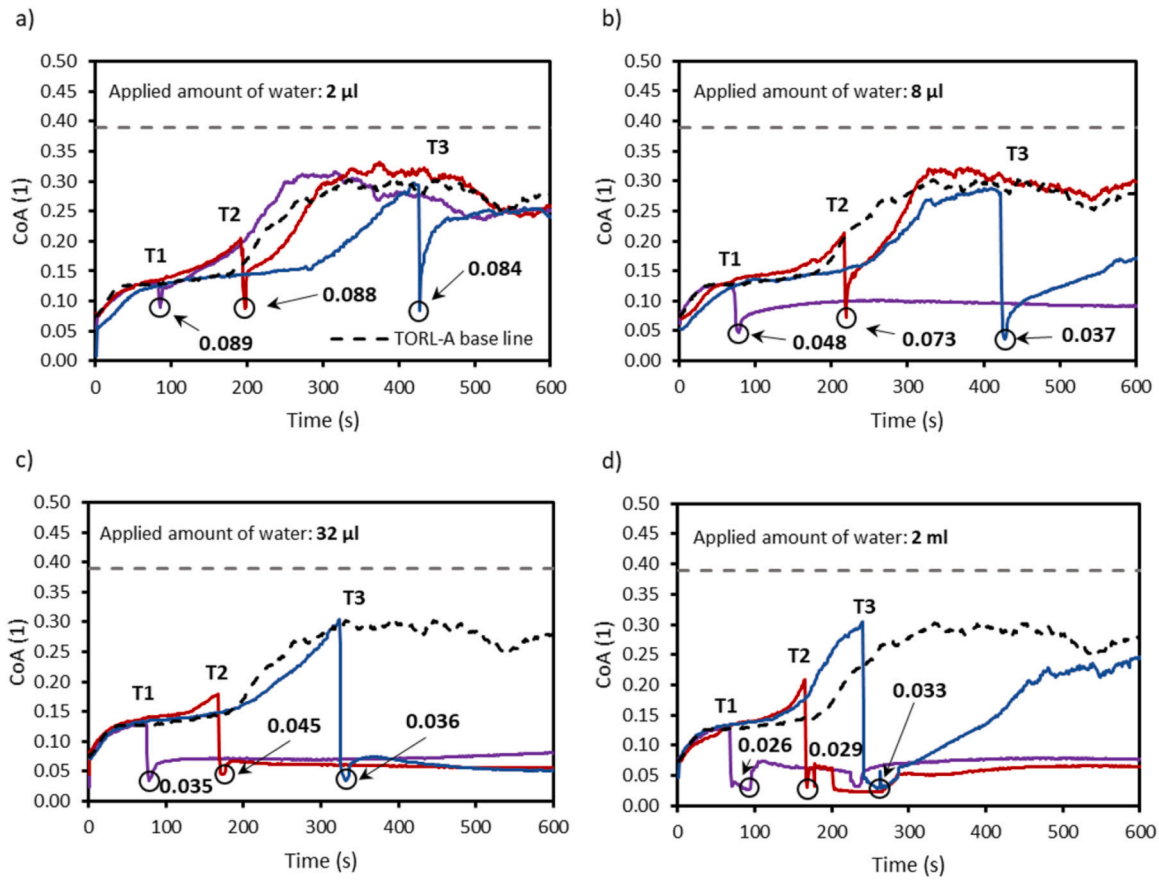

Fig. 5. Adhesion tests of TORL-A under wet conditions. Amounts of water: a) 2 µl; b) 8 µl; c) 32 µl; and d) 2 ml.

for c) and 0.026 in T1 for d). Compared to TORL-A, lower values of minimum CoA were reached after water application in the case of TORL-B. In addition, except for experiments with 2 µl of water a), the dry adhesion level restoration did not occur during the standard test duration.

Fig. 7 shows the results of tests with FM-A (wet film). Please note that points T1–T3, where water was applied, now have different values of CoA than in the case of TOR lubricants (see Table 2). This is because FM-A generally led to the different development of CoA than tested TOR lubricants. From a–c), a clear relationship between the increase in the amount of water and the magnitude of the initial drop of CoA after water was applied can be seen. The lowest reached CoA was 0.086 in T1 for a); 0.042 in T2 for b), and 0.021 in T1 for c). Moreover, the CoA restoration slows down with the increase in the amount of water. For the lowest amount, the CoA drop lasts only a couple of seconds after water application. On the contrary, CoA recovery in case c) took more than 100 s. Still, the duration of the drop is relatively short compared to tests with TOR lubricants. Case d) does not fit this trend. From all tested amounts of water, in tests where 2 ml was applied, the initial adhesion drop was the shortest, and the CoA was quickly restored to a dry level and even higher. This behavior will be further discussed in the Section Discussion.

Fig. 8 shows the results of experiments with dry friction film. Contrary to wet film experiments, water was only applied at one value of CoA marked as T1 for all tested amounts. Thus different line colors in the graph represent different amounts of water; please see the legend. Similarly to the wet film tests, the higher the amount of water applied, the lower the CoA and the longer the adhesion recovery. The only exception is the test with 2 ml of water, where CoA first rises after contamination but then decreases to 0.061. This value is higher than 0.047 in the case of 32 µl of water but lower compared to tests with 2 µl and 8 µl, with measured values of 0.151 and 0.077, respectively. The CoA drop is slow and divided into two parts – after the first initial drop, second to lower values follow. Water significantly reduces CoA compared to non-contaminated dry friction modifier film in all cases.

3.4. Results: performance of TOR products under continuous water application

Figs. 9 and 10 show the results for continuous water application, and in terms of visualization, they follow the same rules as the figures in the previous section. In Fig. 9, it can be seen that TORL-A shows a similar behavior under continuous water application as in tests with a single application of large amounts of water. The lowest reached CoA for TORL-A was 0.025. TORL-B reached an even lower value of 0.015, the same value as in the test with a single application of 2 ml of water, see Fig. 6d). In terms of CoA restoration, even though TORL-B led to lower CoA than TORL-A, approx. 100 s from the end of the water application, the CoA starts to rise, reaching dry-level CoA significantly quicker. The CoA restoration is also faster than in the tests with a single application of larger amounts of water (8 µl, 32 µl, and 2 ml). The gradient of the CoA increase in tests with TORL-A is comparable to tests with a single application of water.

Regarding water-based product FM-A, wet and dry film behaves differently compared to tests with a single application, see Fig. 10. In the case of the wet film, the lowest measured CoA was 0.073, which is lower than in tests with a single application (2 ml). Also, the CoA restoration to dry level takes longer (183 s). On the other hand, the CoA drops only to 0.168 in the case of dry film, and it takes approximately 180 s to restore CoA to dry levels. In both cases (dry/wet film), CoA was restored before the end of the water application.

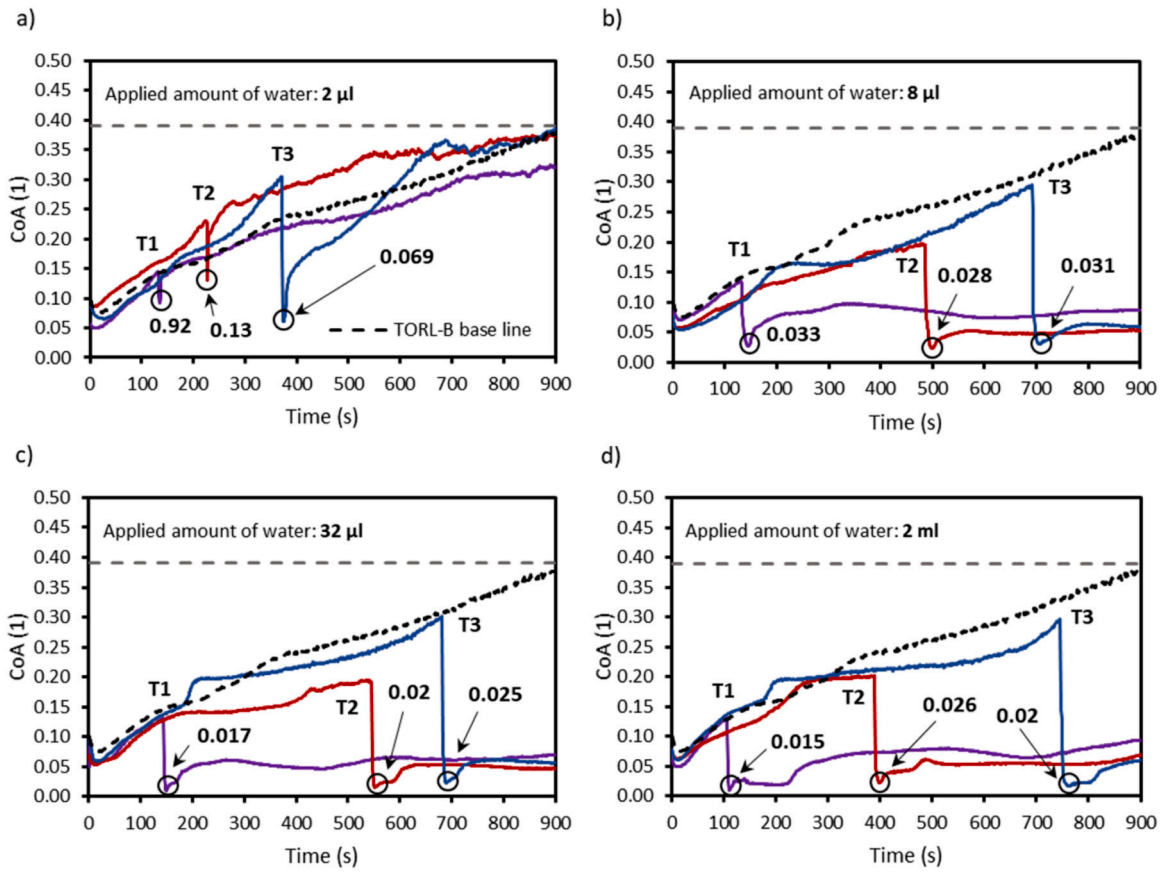

Fig. 6. Adhesion tests of TORL-B under wet conditions. Amounts of water: a) 2 µl; b) 8 µl; c) 32 µl; and d) 2 ml.

4. Discussion

4.1. The influence of the water amount on CoA

The Section Results show that water affects oil-based and water-based TOR products differently. In data evaluation, two main parameters were examined: (1) the lowest CoA reached after water was applied to the TOR product and (2) the duration of the interval of CoA < 0.1 (low adhesion). The overall results of experiments are summarised in the bar graphs in Fig. 11a) and b). Bars of different colors represent mean values evaluated from three measurements (applications in T1–T3), except FM-A (dry film), where water was applied only once at T1. Each color refers to a specific TOR product. Different shades of the same color indicate the amount of water applied, see the label of each bar. For Fig. 11a), the height of each bar represents the lowest CoA reached after water was applied to the TOR product. In Fig. 11b), the height of each bar represents the time duration in seconds for which the CoA was lower than 0.1. Note that a CoA did not drop under 0.1 in some tests. On the other hand, in some tests, the CoA restoration did not occur after water was applied, and the CoA did not reach 0.1 again during the test duration. These tests are marked with the "* " symbol in Fig. 11b). Please note that only tests with single water application were included in this evaluation. During tests with continuous water application, the CoA stays under 0.1 during the whole water application process. So, the CoA remained under the limit value for five extra minutes compared to tests with a single water application. Thus, time durations of CoA lower than 0.1 in those two types of tests cannot be compared.

For TORL-A, Fig. 11a) shows that as the amount of water increases, the CoA decreases to lower minimal values. For comparison, the mean CoA of 0.029 reached after 2 ml of water was applied is nearly three times lower than CoA of 0.086 in the case of 2 µl. TORL-B follows the same trend with an exception between 32 µl and 2 ml, where CoA decreases to a slightly lower value of 0.017 for 32 µl compared to CoA of 0.02 for 2 ml of water. For both oil-based TOR products, it can be said that the higher the amount of water, the longer the CoA stays under 0.1. In the case of a larger amount of water, the CoA restoration did not occur at all. Under continuous water application, both oil-based TOR products behaved similarly to a single application of 2 ml.

In the case of the FM-A (wet film), with an increasing amount of water, CoA reaches lower minimal values. The only exception was between 32 µl and 2 ml, which was caused due to a large amount of water flushing TOR product away from the track, causing quick CoA recovery. When water was applied to dried FM-A film, the drop of CoA was less significant compared to wet FM-A film, and the time of CoA lower than 0.1 was also shorter. Higher values of minimal CoA and shorter duration of the low adhesion period are probably caused by the absence of the evaporated base medium. An exception was the tests with 2 ml of water, where the combined effect of water and dried particles led to better lubrication than in the case of FM-A (wet film). Under continuous water application, the CoA restoration was quicker for dried FM-A film than for wet film.

In most tests, the CoA drop was not as high for water-based TOR products as for oil-based TOR products. Although the oil does not easily mix with water, contamination of oil-based TOR products poses a more significant risk in terms of low CoA. This is mainly supported by the fact that CoA stayed below 0.1 for no or very little time for water-based TOR products.

From a practical point of view, the amount of water on an actual rail can be either small (morning dew, leakage from passing train) or large (mostly rain). By comparing the approximate contact area of tested samples under set conditions to the expected size of the actual wheel-rail contact, the amounts of water tested in this paper correspond to the following amounts in the field conditions: 2 µl $\approx$ 3 ml; 8 µl $\approx$ 12 ml; 32 µl $\approx$ 46 ml; 2 ml and 2.15 ml $\approx$ 3 l. Single contamination of the

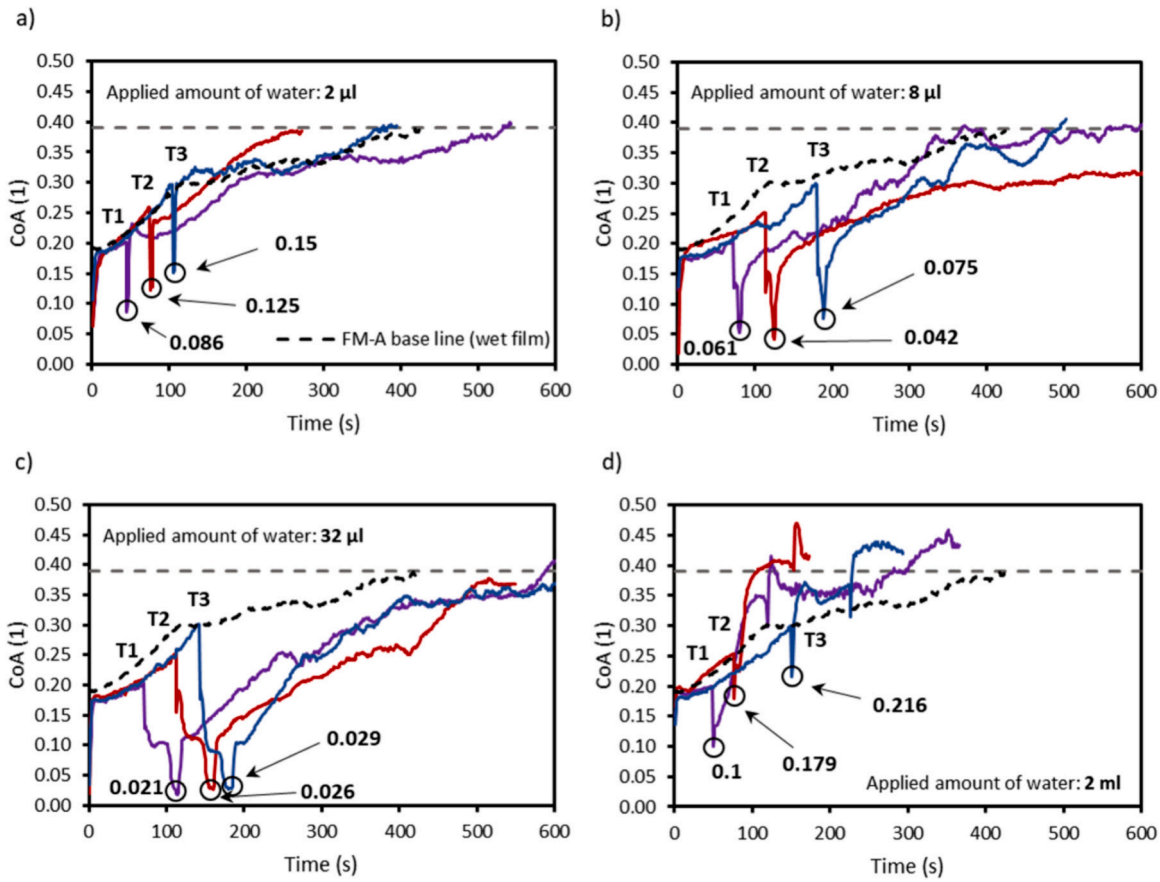

Fig. 7. Adhesion tests of FM-A (wet film) under wet conditions. Amounts of water: a) 2 µl; b) 8 µl; c) 32 µl; and d) 2 ml.

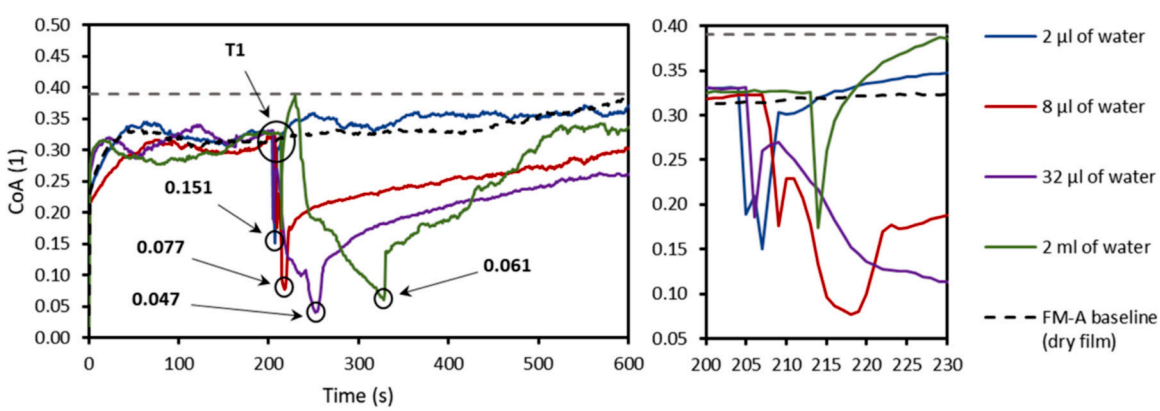

Fig. 8. Adhesion tests of FM-A (dry film) under wet conditions. Each line represents a different amount of water, see the legend.

contact by liters of water in actual railway operation seems to be unlikely. However, knowing the worst-case scenario is still necessary when dealing with passenger safety. On the other hand, it is possible for the smaller amounts in the order of milliliters to be accumulated over a short period from the rain or the overnight condensation from the humid air. Thus, tested amounts of water (especially 2 µl and 8 µl) are relevant to actual field conditions.

Results indicate that the risk of low CoA rises with the amount of water. However, this is contrary to field measurements, which suggest that it is rather a small amount of water leading to low CoA. The analysis in [5] shows that low CoA-related incidents are most probable when morning dew is on a rail. Similarly, findings in [24] show that when a small amount of water is mixed with particles of iron oxides, CoA lower than 0.05 can occur. On the other hand, several papers showed that although the exact value of CoA depends on water temperature [30], larger amounts generally lead to much higher CoA [31,32]. The effect of water also depends on the presence of the third-body layer, consisting of iron oxides, wear particles, environmental contaminants, or even TOR product residua. Thus, possible mechanisms of water contamination of TOR products will be discussed next.

4.2. Fluid-film regime / Mechanisms relevant to oil-water system

First, the question arises as to why the CoA of the W/O mixture is lower than that of bleed oil, as revealed by the Stribeck test under fully flooded conditions in Chapter 3.2. Similar observations were made in

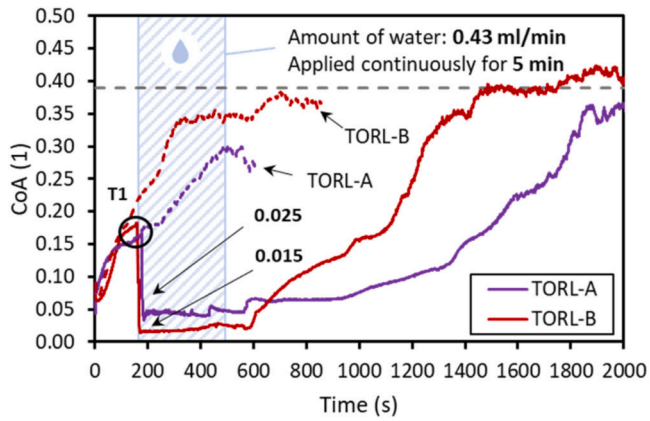

Fig. 9. Adhesion tests of TORL-A and TORL-B under wet conditions. Water was applied continuously for 5 min.

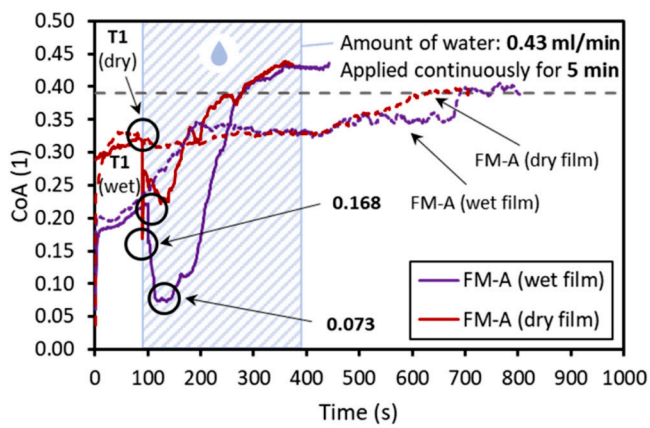

Fig. 10. Adhesion tests of FM-A (dry film) and FM-A (wet film) under wet conditions. Water was applied continuously for 5 min.

simulated wheel-rail contact [31]. Over the last decades, several theories have been proposed on the lubrication mechanism of water-in-oil (W/O) or oil-in-water (O/W) emulsions. Those theories can help to explain the behavior of water-contaminated EHL contacts.

At low speeds, the behavior can be explained by the well-accepted plate-out theory [33,34]. This theory assumes that water is excluded from the contact due to the stronger wetting ability of oil, creating an oil pool around EHL contact, see Fig. 12a). This mechanism is in accordance with the theory of energy displacement [33]. Ideally, a lubricant film in the contact is fully composed of the oil phase, and there is no negative effect on lubricant film thickness [35,36]. For larger droplets, dynamic concentration theory describing the increasing concentration of oil in the inlet zone as water is gradually excluded from the gap is more appropriate [37].

According to a starvation theory [38], the first critical speed exists, after which the oil pool becomes unstable, and lubricant film thickness in the contact decreases [39–41]. While remaining in full-film lubrication, lower film thickness means lower shear stress in lubricating film and, therefore, lower traction [40]. After the second critical speed, lubricant film thickness starts to increase. However, due to starvation, water can no longer be excluded from the contact inlet, and a certain amount of water phase, given by the dynamic concentration theory [37], passes through the contact resulting in a much lower coefficient of traction. This behavior strongly depends on the size of water droplets [42]. A single application of a water droplet may differ from the behavior of emulsified water. A large water droplet is more easily expelled from the oil. If it occurs under contact starvation, water can easily enter the contact [43]. Those theories can explain low CoA in the water-contaminated oil-lubricated contact.

4.3. Starved fluid-film regime / Mechanisms relevant to grease-water system

Oil-based TOR products are usually based on grease, i.e., they contain thickener and base oil. In this case, water influences the oil pool in the contact and structure and the rheology of bulk grease [44]. Evaluation of its water resistance is covered by industry standards [45]. Unlike lubricating oil, grease can absorb a larger amount of water due to the polar nature of its thickener and additives. This ability strongly depends on a thickener type, while some greases become stiffer and others soften [44].

Grease-lubricated contact is much more susceptible to starvation since a relatively thick grease is being pushed out of the contact track. Lubricant replenishment from the reservoirs on track sides is very slow, and the replenishment flow is inversely proportional to viscosity [46, 47]. Absorbed water influences stiffness and oil-bleeding, i.e., the ability to replenish the contacts. The effects can be positive or negative depending on the type of thickener [48,49]. If the water absorption leads to an enhanced contact replenishment, higher oil film thickness under starved conditions and lower friction in the mixed regime may occur, which is consistent with our observations. For visualization of this mechanism, please see Fig. 12b). On the other hand, oil-based TOR products intended for the open tribology system are designed as water-repellent with low water adsorption, so the "free water" should rather occur in the contact.

4.4. Mixed regime / Mechanisms relevant to TOR-water system

When severe starvation occurs, lubricant film thickness further decreases, resulting in a mixed regime, where a part of the load is transmitted by the contacts of surface asperities and CoA increases [50]. Under these conditions, boundary friction is given by the composition of the created tribological layer. TOR products contain solid lubricants like graphite or molybdenum disulfide. The frictional properties of those particles are affected by water in different ways. The coefficient of friction of graphite usually decreases in the presence of water because of the dissociative chemisorption of water. On the contrary, the lubricity of MoS_2 decreases due to oxidation and physisorption of water molecules. However, the effect may be reduced by interaction with metal particles, which are also a common component of TOR products [51].

More significant is probably the interaction of water with other components of TOR products as particles for friction modification or wear particles. When mixed with a small amount of water, solid particles create a paste that causes a transient decrease in friction. This mechanism is known as a "wet-rail" phenomenon [52] and is depicted in Fig. 12c). Since the decrease in CoA appears to be independent of the water application time during friction development, it can be assumed to be due to particles contained in the TOR products rather than wear particles.

4.5. Mechanisms relevant to water-based TOR product contamination

Regarding the water-based TOR product, a similar dependence of magnitude and duration of CoA drop on the applied amount of water exists up to 32 μl. However, large amounts (2 ml) flush the product out of the surface, quickly restoring CoA to dry contact levels. This happened for both single and continuous applications, although in dry film test single application, the results are not entirely clear. Even if a CoA lower than 0.1 occurs immediately after the contamination, it remains below this limit only for a short period and then rises.

The drop of CoA can be divided into two parts. After the first drop, the second more significant follows, see Fig. 7a-c). This behavior was already seen in the study [53], in which the authors performed various

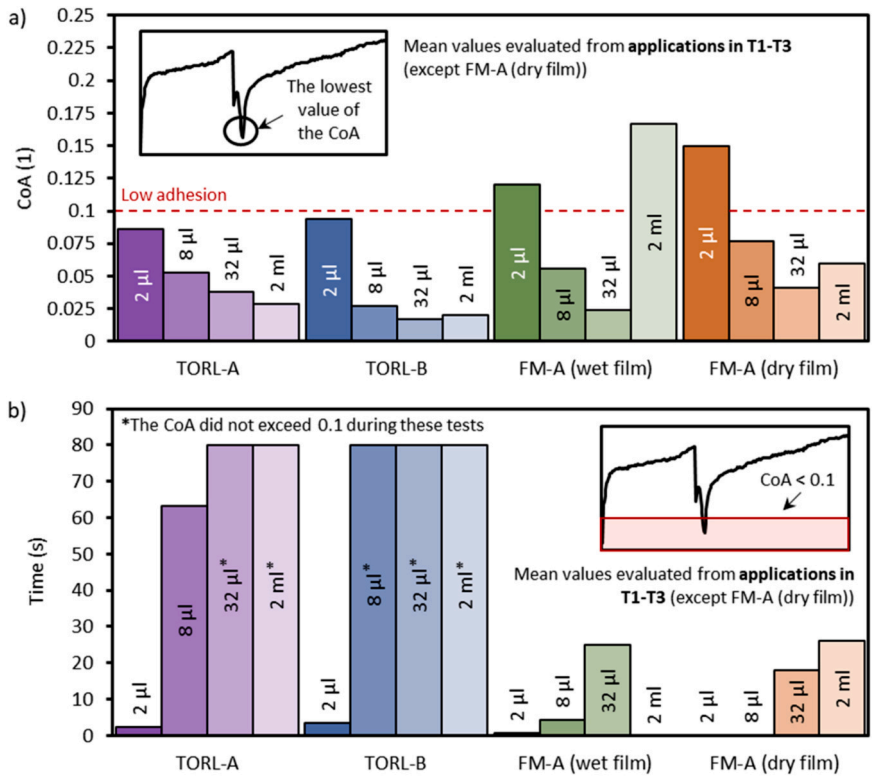

Fig. 11. Mean (a) adhesion drop after water application and (b) duration of a period when CoA was lower than 0.1.

tests with water alone. Similar behavior was also observed in a paper [3] focused on water-based TOR products. It can be assumed that this behavior relates to the water contained in the product and thus did not occur in tests with oil-based TOR products.

Results presented in this study are comparable with findings in [54], where two water-based TOR products were tested under various slips and water contamination. Although both products differ from those tested in this study in the type of particles contained, the trends in CoA development seem similar. In an extreme case, the CoA after water contamination drops to approx. 0.05, which is comparable to tests with FM-A (8 µl). In other cases, the magnitude of the drop was not as high, probably caused by different product particles. As was shown in [2], product performance strongly depends on the type of contained particles. Tested products in [54] had particles of metals with a diameter as large as 100 µm. Particles in [3] were mainly minerals like bentonite or talc, and their diameter did not exceed 10 µm. Substances with mineral particles of smaller diameters reach lower CoA comparable to one of the products used in this study. Thus, the type and scale of the particles play an essential role in achieving sufficient CoA. In both studies, it seems that water slows CoA development rather than interrupts it, contrary to the case of oil-based TOR products. As shown in Fig. 7a-c), the CoA develops similarly to the situation before contamination, only starting again from lower values.

Authors propose that the contamination mechanism of water-based TOR products lay in the refill of the evaporated base medium. After contamination, water mixes with dried particles and the mixture act as a freshly applied product. This is supported by Fig. 8, which summarises the results of dry FM-A film tests. The dry film leads to higher CoA (higher than 0.3) than the wet film. However, after contamination, water mixes with dried particles, and the CoA drops to values comparable to values of the original TOR product before base medium evaporation, see Fig. 7. After that, the mixture behaves similarly to tests with FM-A (wet film).

4.6. Limitations of the Study

The CoA values and performance of tested oil-based TOR products measured in this study follow results published in [13], which were also measured on a ball-on-disc tribometer. As was shown in [11], measured adhesion strongly depends on the measuring device. The point contact between the ball and the disc simplifies actual rail conditions. However, many previous studies on wheel-rail tribology already used universal tribometers in the ball-on-disc configuration, obtaining useful results [3,4,28]. Although conclusions from laboratory tests can be limited due to simplifications, they are suitable for preliminary studies as these tests are more controllable than field tests. Regarding used specimens, there are three main differences compared to actual wheel-rail contact: the contact shape, the surface roughness, and the material hardness.

As for the point contact, Chen et al. [30] measured the adhesion of water-contaminated contact on a twin disc machine. The use of discs as contact bodies led to line contact, and still, values obtained for given conditions correspond to values represented in Fig. 3d) or published in [53].

Pieringer et al. [55] measured the surface roughness of wheel and rail to be tens of micrometers which is significantly higher compared to Ra 0.15–0.3 µm of specimens in this study. Conversely, Chen et al. assumed that surface roughness depends on the current state of the wheel and rail (new/worn/after grinding) and can be expected in the range of 0.3–1.5 µm [56]. Previously, Galas et al. [13] used specimens with surface roughness varying from 0.05 to 0.45 µm to conduct similar experiments and achieved representative results. Furthermore, Zhu et al. [57] used discs with Ra as low as 0.2 µm to measure CoA in contaminated contact on a twin disc machine. Since surface roughness influences the lubrication regime, Stribeck tests were conducted in this study. Fig. 4 shows that the tested configuration operated in similar conditions to the actual wheel-rail contact. So, in theory, measured CoA should be representative.

Regarding hardness, sets of standard material grades were established around the world. In Europe, rail steels are typically perlitic and

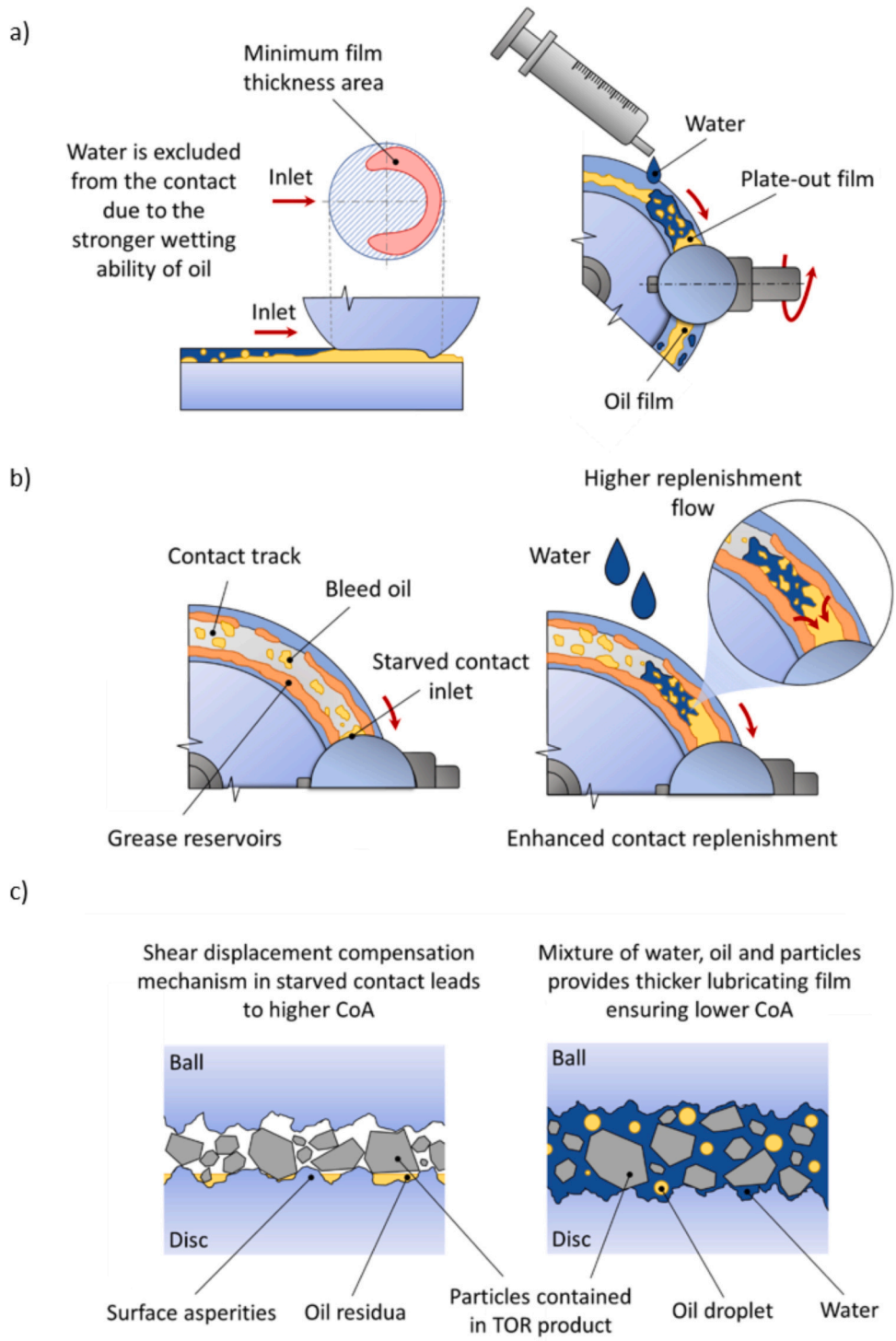

Fig. 12. Discussed mechanisms: a) Fluid-film regime, b) Starved fluid-film regime, c) Mixed regime.

could be heat-treated. Lewis et al., in their paper, compared the hardness of several materials [7]. They showed that the bulk hardness of conventional R260 steel was approx. 275 HV, and for heat-treated R350HT steel was 350 HV. It should also be noted that due to the work-hardening effect, the hardness close to the surface can be 2.5 times higher than the hardness of the bulk [58]. On the other hand, the hardness of specimens in this study was 800–920 HV and 720–780 HV for ball and disc, which is significantly higher, meaning their behavior can differ from actual rail materials. Harmon et al. showed that with a higher hardness of specimens, the slightly lower values of CoA will be measured compared to specimens made of softer materials [59].

The main purpose of choosing harder material was to reduce wear. The surface topography changes as the wear progresses during the test, causing a decrease in contact pressure. It was observed that the most severe wear occurred during the first 60 min of the test with new pair of specimens. But after this period, the wear becomes stable, and the width and depth of the contact path increased only a little. Thus, contact pressure remains relatively constant. The wear-in period was conducted on all new specimens to overcome the initial rapid wear and ensure stable test conditions. Although the actual contact pressure during tests

was probably lower than the initial 800 MPa, it remains relatively the same for all tests, so the results should be comparable.

A similar approach was used before in [3,4,13] and enabled focusing primarily on the effect of tested substances without bias from other factors that were not in the scope of the study. Measured results show a clear influence of water on TOR products. However, their transferability into railway operation could be limited and should be validated on specimens made from authentic rail material with more realistic geometry.

There is one more significant difference compared to the actual rail track. While in the laboratory tribometer, the contact between bodies occurs on the same spots as both bodies rotate, in reality, the wheel passes an exact location on the rail only once per ride. In laboratory conditions, this means that enough amount of lubricant is always present because it has nowhere to go. However, as shown in [15], the product is carried by wheels on an actual track for several hundred meters. Thus, larger amounts of lubricant are present only for a limited distance from an application unit. It is unclear if this increases or decreases the probability of low CoA. On one side, the probability of overdosing decreases with distance from the application unit. On the other, it was shown that water is most likely to cause low CoA when only a small amount is mixed with the third body layer [18,24]. From this point of view, the effect of water will be more significant if only a thin layer of TOR product is present, which could be expected farther away from the application unit. Either way, water will always influence the performance of TOR product, and the extent of this influence should be known for the safety of passengers and the efficiency of rail transport.

5. Conclusion

The ball-on-disc tribometer MTM was used in this study to investigate the influence of water contamination on TOR product performance. One commercial water-based and two oil-based TOR products were tested. The water-based TOR product was tested both before and after the base medium evaporation. Four different amounts of water were applied by syringe/electronic micropipette to TOR products. Also, continuous water application by a peristaltic pump was tested. The results could be summarized in the following points:

1) A low amount of water (2 μl) had a limited effect on tested TOR products and did not cause low CoA. However, it is important to mention that the contact surfaces of specimens were cleaned before every test. In actual railway, water could mix with third body layer particles and form a highly-viscous paste known for lowering CoA to insufficient levels.
2) Contamination of oil-based TOR products by a large amount of water resulted in a long-lasting period of low CoA (the lowest measured value was 0.015). A suggested explanation for this derives from W/O emulsion lubrication theories. Due to its low viscosity, water helped the oil to move into contact. Thus, lower values of CoA could be achieved for a prolonged time.
3) Low CoA rarely occurred in tests with water-based TOR products. Although CoA dropped after water was applied, after several dozen seconds, it was restored to the level before contamination. The water and dried solid particles formed a mixture similar to the original TOR product before the base medium evaporation. From this point of view, adding water to the dried water-based TOR product extended its lasting effect rather than causing low CoA problems. However, excessive amounts of water (2 ml) flushed the TOR product out of the contacting surfaces and significantly shortened its performance.
4) No significant difference existed between a single or continuous application of the same amount of water that contaminated oil-based TOR products. In the case of a water-based TOR product, CoA was restored slightly slower under continuous application.

The wheel-rail interface is an open system, meaning water and other contaminants can enter the contact. The presented results showed the strong influence of water contamination on the performance of TOR products. A long-lasting period of CoA lower than 0.1 occurred in several tests, suggesting that traction problems could also happen in actual railway conditions. This potential risk should be taken into account in the TOR conditioning deployment. Also, the interaction of TOR products with water should be considered in product development and testing. Although several hypotheses were proposed, the exact mechanism of the described phenomenon was not revealed and thus will be the object of the following research work.

Statement of Originality

As a corresponding author, I, Simon Skurka, hereby confirm on behalf of all authors that:

1) The authors have obtained the necessary authority for publication.
2) The paper has not been published previously, that it is not under consideration for publication elsewhere, and that if accepted it will not be published elsewhere in the same form, in English or in any other language, without the written consent of the publisher.
3) The paper does not contain material which has been published previously, by the current authors or by others, of which the source is not explicitly cited in the paper.

Upon acceptance of an article by the journal, the author(s) will be asked to transfer the copyright of the article to the publisher. This transfer will ensure the widest possible dissemination of information.

CRediT authorship contribution statement

Simon Skurka: Conceptualization, Methodology, Investigation, Data curation, Writing – original draft. **Radovan Galas:** Conceptualization, Investigation, Methodology, Writing – review & editing. **Milan Omasta:** Conceptualization, Investigation, Methodology, Writing – review & editing, Project administration. **Bingnan Wu:** Data curation, Writing – review & editing, Visualization. **Haohao Ding:** Writing – review & editing, Visualization. **Wen-Jian Wang:** Conceptualization, Data curation, Writing – review & editing, Project administration. **Ivan Krupka:** Data curation, Writing – review & editing. **Martin Hartl:** Supervision, Funding acquisition.

Declaration of Competing Interest

The authors declare that they have no known competing financial interests or personal relationships that could have appeared to influence the work reported in this paper.

Data Availability

Data will be made available on request.

Acknowledgments

This research was carried out under project EG20_321/0025198 with financial support from the Ministry of Industry and Trade of the Czech Republic and under project GA20-23482S with financial support from the Czech Science Foundation. Also, the authors thank the support of the National Natural Science Foundation of China (No. 52272443).

References

[1] Suda Y, Iwasa T, Komine H, Tomeoka M, Nakazawa H, Matsumoto K, et al. Development of onboard friction control. Wear 2005;258:1109–14. https://doi.org/10.1016/j.wear.2004.03.059.

[2] Kalousek J, Johnson KL. An investigation of short pitch wheel and rail corrugations on the vancouver mass transit system. Proc Inst Mech Eng F J Rail Rapid Transit 1992;206:127–35. https://doi.org/10.1243/PIME_PROC_1992_206_226_02.

[3] Galas R, Kvarda D, Omasta M, Krupka I, Hartl M. The role of constituents contained in water–based friction modifiers for top–of–rail application. Tribol Int 2018;117: 87–97. https://doi.org/10.1016/j.triboint.2017.08.019.

[4] Kvarda D, Skurka S, Galas R, Omasta M, Shi L, Ding H, et al. The effect of top of rail lubricant composition on adhesion and rheological behaviour. Eng Sci Technol, Int J 2022;35:101100. https://doi.org/10.1016/j.jestch.2022.101100.

[5] Valehrach J, Guziur P, Riha T, Plasek O. Assessment of rail long-pitch corrugation. IOP Conf Ser Mater Sci Eng 2017;236:012048. https://doi.org/10.1088/1757-899X/236/1/012048.

[6] Stock R, Pippan R. RCF and wear in theory and practice—The influence of rail grade on wear and RCF. Wear 2011;271:125–33. https://doi.org/10.1016/j.wear.2010.10.015.

[7] Lewis R, Christoforou P, Wang WJ, Beagles A, Burstow M, Lewis SR. Investigation of the influence of rail hardness on the wear of rail and wheel materials under dry conditions (ICRI wear mapping project). Wear 2019;430–431:383–92. https://doi.org/10.1016/j.wear.2019.05.030.

[8] Braghin F, Lewis R, Dwyer-Joyce RS, Bruni S. A mathematical model to predict railway wheel profile evolution due to wear. Wear 2006;261:1253–64. https://doi.org/10.1016/j.wear.2006.03.025.

[9] Olofsson U, Telliskivi T. Wear, plastic deformation and friction of two rail steels—a full-scale test and a laboratory study. Wear 2003;254:80–93. https://doi.org/10.1016/S0043-1648(02)00291-0.

[10] Number of Europeans exposed to harmful noise pollution expected to increase — European Environment Agency n.d. ⟨https://www.eea.europa.eu/highlights/number-of-europeans-exposed-to⟩ (accessed August 12, 2022).

[11] Lundberg J, Rantatalo M, Wanhainen C, Casselgren J. Measurements of friction coefficients between rails lubricated with a friction modifier and the wheels of an IORE locomotive during real working conditions. Wear 2015;324–325:109–17. https://doi.org/10.1016/j.wear.2014.12.002.

[12] Eadie DT, Elvidge D, Oldknow K, Stock R, Pointner P, Kalousek J, et al. The effects of top of rail friction modifier on wear and rolling contact fatigue: Full-scale rail–wheel test rig evaluation, analysis and modelling. Wear 2008;265:1222–30. https://doi.org/10.1016/j.wear.2008.02.029.

[13] Galas R, Omasta M, Krupka I, Hartl M. Laboratory investigation of ability of oil-based friction modifiers to control adhesion at wheel-rail interface. Wear 2016; 368–369:230–8. https://doi.org/10.1016/j.wear.2016.09.015.

[14] Abbasi S, Olofsson U, Zhu Y, Sellgren U. Pin-on-disc study of the effects of railway friction modifiers on airborne wear particles from wheel–rail contacts. Tribol Int 2013;60:136–9. https://doi.org/10.1016/j.triboint.2012.11.013.

[15] Han J, He Y, Xiao X, Sheng X, Zhao G, Jin X. Effect of Control Measures on Wheel/Rail Noise When the Vehicle Curves. Appl Sci 2017;7:1144. https://doi.org/10.3390/app7111144.

[16] Meehan PA, Liu X. Wheel squeal noise control under water-based friction modifiers based on instantaneous rolling contact mechanics. Wear 2019;440–441:203052. https://doi.org/10.1016/j.wear.2019.203052.

[17] Szablewski D, LoPresti J, Sultana T. Testing of latest top-of-rail friction modification materials at FAST. Railw Track Struct 2015;111:13–6.

[18] Ishizaka K, Lewis SR, Lewis R. The low adhesion problem due to leaf contamination in the wheel/rail contact: Bonding and low adhesion mechanisms. Wear 2017; 378–379:183–97. https://doi.org/10.1016/j.wear.2017.02.044.

[19] Stock R, Stanlake L, Hardwick C, Yu M, Eadie D, Lewis R. Material concepts for top of rail friction management – Classification, characterisation and application. Wear 2016;366–367:225–32. https://doi.org/10.1016/j.wear.2016.05.028.

[20] Galas R, Omasta M, Klapka M, Kaewunruen S, Krupka I, Hartl M. Case study: case study: the influence of oil-based friction modifier quantity on tram braking distance and noise. Tribol Ind 2017;39:198–206. https://doi.org/10.24874/ti.2017.39.02.06.

[21] Harmon M, Lewis R. Review of top of rail friction modifier tribology. Tribology - Mater, Surf Interfaces 2016;10:150–62. https://doi.org/10.1080/17515831.2016.1216265.

[22] Areiza YA, Garcés SI, Santa JF, Vargas G, Toro A. Field measurement of coefficient of friction in rails using a hand-pushed tribometer. Tribol Int 2015;82:274–9. https://doi.org/10.1016/j.triboint.2014.08.009.

[23] Olofsson U, Lyu Y. Open system tribology in the wheel–rail contact—a literature review. Appl Mech Rev 2017;69. https://doi.org/10.1115/1.4038229.

[24] White B, Lewis R. Simulation and understanding the wet-rail phenomenon using twin disc testing. Tribol Int 2019;136:475–86. https://doi.org/10.1016/j.triboint.2019.03.067.

[25] Chen H, Fukagai S, Sone Y, Ban T, Namura A. Assessment of lubricant applied to wheel/rail interface in curves. Wear 2014;314:228–35. https://doi.org/10.1016/j.wear.2013.12.006.

[26] Lewis SR, Lewis R, Olofsson U, Eadie DT, Cotter J, Lu X. Effect of humidity, temperature and railhead contamination on the performance of friction modifiers: pin-on- disk study. Proc Inst Mech Eng F J Rail Rapid Transit 2013;227:115–27. https://doi.org/10.1177/0954409712452239.

[27] Moreno-Ríos M, Gallardo-Hernández EA, Vite-Torres M, Peña-Bautista A. Field and laboratory assessments of the friction coefficient at a railhead. Proc Inst Mech Eng F J Rail Rapid Transit 2016;230:313–20. https://doi.org/10.1177/0954409714536383.

[28] Zhu Y, Olofsson U, Persson K. Investigation of factors influencing wheel–rail adhesion using a mini-traction machine. Wear 2012;292–293:218–31. https://doi.org/10.1016/j.wear.2012.05.006.

[29] Kalin M, Velkavrh I, Vižintin J. The Stribeck curve and lubrication design for non-fully wetted surfaces. Wear 2009;267:1232–40. https://doi.org/10.1016/j.wear.2008.12.072.

[30] Chen H, Ishida M, Namura A, Baek KS, Nakahara T, Leban B, et al. Estimation of wheel/rail adhesion coefficient under wet condition with measured boundary friction coefficient and real contact area. Wear 2011;271:32–9. https://doi.org/10.1016/j.wear.2010.10.022.

[31] Wang WJ, Zhang HF, Wang HY, Liu QY, Zhu MH. Study on the adhesion behavior of wheel/rail under oil, water and sanding conditions. Wear 2011;271:2693–8. https://doi.org/10.1016/j.wear.2010.12.019.

[32] Wang WJ, Shen P, Song JH, Guo J, Liu QY, Jin XS. Experimental study on adhesion behavior of wheel/rail under dry and water conditions. Wear 2011;271:2699–705. https://doi.org/10.1016/j.wear.2011.01.070.

[33] Kimura Y, Okada K. Lubricating properties of oil-in-water emulsions. Tribology Trans 1989;32:524–32. https://doi.org/10.1080/10402008908981921.

[34] Fujita N, Kimura Y, Kobayashi K, Amanuma Y, Sodani Y. Estimation model of plate-out oil film in high-speed tandem cold rolling. J Mater Process Technol 2015;219: 295–302. https://doi.org/10.1016/j.jmatprotec.2015.01.002.

[35] Nakahara T, Makino T, Kyogoku K. Observations of liquid droplet behavior and oil film formation in O/W type emulsion lubrication. J Tribol 1988;110:348–53. https://doi.org/10.1115/1.3261630.

[36] Benner JJ, Sadeghi F, Hoeprich MR, Frank MC. Lubricating properties of water in oil emulsions. J Tribol 2006;128:296–311. https://doi.org/10.1115/1.2164464.

[37] Wilson WRD, Sakaguchi Y, Schmid SR. A dynamic concentration model for lubrication with oil-in-water emulsions. Wear 1993;161:207–12. https://doi.org/10.1016/0043-1648(93)90471-W.

[38] Chiu YP. An analysis and prediction of lubricant film starvation in rolling contact systems. A S L E Trans 1974;17:22–35. https://doi.org/10.1080/05698197408981435.

[39] Zhu D, Biresaw G, Clark SJ, Kasun TJ. Elastohydrodynamic lubrication with O/W emulsions. J Tribol 1994;116:310–9. https://doi.org/10.1115/1.2927216.

[40] Yang H, Schmid SR, Kasun TJ, Reich RA. Elastohydrodynamic film thickness and tractions for oil-in-water emulsions. Tribol Trans 2004;47:123–9. https://doi.org/10.1080/05698190490278976.

[41] Liang H, Guo D, Ma L, Luo J. Investigation of film formation mechanism of oil-in-water (O/W) emulsions at high speeds. Tribol Int 2017;109:428–34. https://doi.org/10.1016/j.triboint.2017.01.006.

[42] Zhang F, Fillot N, Bouscharain N, Devaux N, Philippon D, Matta C, et al. Water droplets in oil at the inlet of an EHD contact: A dual experimental and numerical investigation. Tribol Int 2023;177:108015. https://doi.org/10.1016/j.triboint.2022.108015.

[43] Liu X, Wang J, Huang L, Zhang J, Xu C, Tong L, et al. Direct observation of the impact of water droplets on oil replenishment in EHD lubricated contacts. Friction 2022;10:388–97. https://doi.org/10.1007/s40544-020-0466-0.

[44] Cyriac F, Lugt PM, Bosman R. Impact of water on the rheology of lubricating greases. Tribol Trans 2016;59:679–89. https://doi.org/10.1080/10402004.2015.1107929.

[45] Gurt A, Khonsari M. An overview of grease water resistance. Lubricants 2020;8:86. https://doi.org/10.3390/lubricants8090086.

[46] Cann PME, Damiens B, Lubrecht AA. The transition between fully flooded and starved regimes in EHL. Tribol Int 2004;37:859–64. https://doi.org/10.1016/j.triboint.2004.05.005.

[47] Jacod B., Pubilier F, E. Cann P.M., Lubrecht A.A. An Analysis of Track Replenishment Mechanisms in the Starved Regime, 1999, p. 483–492. ⟨https://doi.org/10.1016/S0167–8922(99)80069–8⟩.

[48] Cyriac F, Lugt PM, Bosman R, Venner CH. Impact of water on EHL film thickness of lubricating greases in rolling point contacts. Tribol Lett 2016;61:23. https://doi.org/10.1007/s11249-016-0642-6.

[49] Hudedagaddi CB, Raghav AG, Tortora AM, Veeregowda DH. Water molecules influence the lubricity of greases and fuel. Wear 2017;376–377:831–5. https://doi.org/10.1016/j.wear.2017.02.002.

[50] Li Q, Zhang S, Wu B, Lin Q, Ding H, Galas R, et al. Analysis on the effect of starved elastohydrodynamic lubrication on the adhesion behavior and fatigue index of wheel-rail contact. Wear 2022;510–511:204506. https://doi.org/10.1016/j.wear.2022.204506.

[51] Chen Z, He X, Xiao C, Kim S. Effect of humidity on friction and wear—a critical review. Lubricants 2018;6:74. https://doi.org/10.3390/lubricants6030074.

[52] White B, Kempka R, Laity P, Holland C, Six K, Trummer G, et al. Iron oxide and water paste rheology and its effect on low adhesion in the wheel/rail interface. Tribol Lett 2022;70:8. https://doi.org/10.1007/s11249-021-01549-0.

[53] Galas R, Omasta M, Shi L bing, Ding H, Wang W jian, Krupka I, et al. The low adhesion problem: The effect of environmental conditions on adhesion in rolling-sliding contact. Tribol Int 2020;151:106521. https://doi.org/10.1016/j.triboint.2020.106521.

[54] Arias-Cuevas O, Li Z, Lewis R, Gallardo-Hernández EA. Rolling-sliding laboratory tests of friction modifiers in dry and wet wheel-rail contacts. Wear 2010;268: 543–51. https://doi.org/10.1016/j.wear.2009.09.015.

[55] Pieringer A, Kropp W. Model-based estimation of rail roughness from axle box acceleration. Appl Acoust 2022;193:108760. https://doi.org/10.1016/j.apacoust.2022.108760.

[56] Chen H, Namura A, Ishida M, Nakahara T. Influence of axle load on wheel/rail adhesion under wet conditions in consideration of running speed and surface roughness. Wear 2016;366–367:303–9. https://doi.org/10.1016/j.wear.2016.05.012.

[57] Zhu Y, Chen X, Wang W, Yang H. A study on iron oxides and surface roughness in dry and wet wheel-rail contacts. Wear 2015;328–329:241–8. https://doi.org/10.1016/j.wear.2015.02.025.
[58] Tyfour W.R., Beynon J.H., Kapoor A. The steady state wear behaviour of pearlitic rail steel under dry rolling-sliding contact conditions. vol. 180. 1995.
[59] Harmon M, Santa JF, Jaramillo JA, Toro A, Beagles A, Lewis R. Evaluation of the coefficient of friction of rail in the field and laboratory using several devices. Tribol Mater Surf Interfaces 2020;14:119–29. https://doi.org/10.1080/17515831.2020.1712111.

Tribology Letters (2024) 72:90
https://doi.org/10.1007/s11249-024-01889-7

ORIGINAL PAPER

Assessing the Performance of TOR Lubricants in Humid Environments and Under Dew Conditions

Simon Skurka[1] · Radovan Galas[1] · Milan Omasta[1] · Haohao Ding[2] · Wen-Jian Wang[2] · Ivan Krupka[1] · Martin Hartl[1]

Received: 6 May 2024 / Accepted: 3 July 2024 / Published online: 16 July 2024
© The Author(s) 2024

Abstract

Top-of-rail (TOR) lubricants are commonly used for friction control in railway operations. They aim to lower friction and reduce noise and wear while ensuring sufficient transmission of traction/braking forces. However, the wheel–rail interface is an open system, so the conditions may suddenly change due to the weather, and different contaminants may enter the contact and influence the performance of these lubricants. Thus, this study examined the effect of humidity and dew on two commercial products, as these conditions often occur on the track. A methodology based on a creep curves measurement approach was used to assess product performance under various scenarios. All measurements were conducted on a universal tribometer in the ball-on-disc configuration covered with a climate chamber. The results show a strong influence of dew on the tested products, as dew lowered their performance parameters and caused low adhesion problems. Possible mechanisms of water–oil interaction and formation of oxidic third body layers were discussed. The main findings indicate that TOR lubricants may cause traction/braking problems if used in dew conditions. The present study may be helpful in optimising friction management methods in the future.

Graphical Abstract

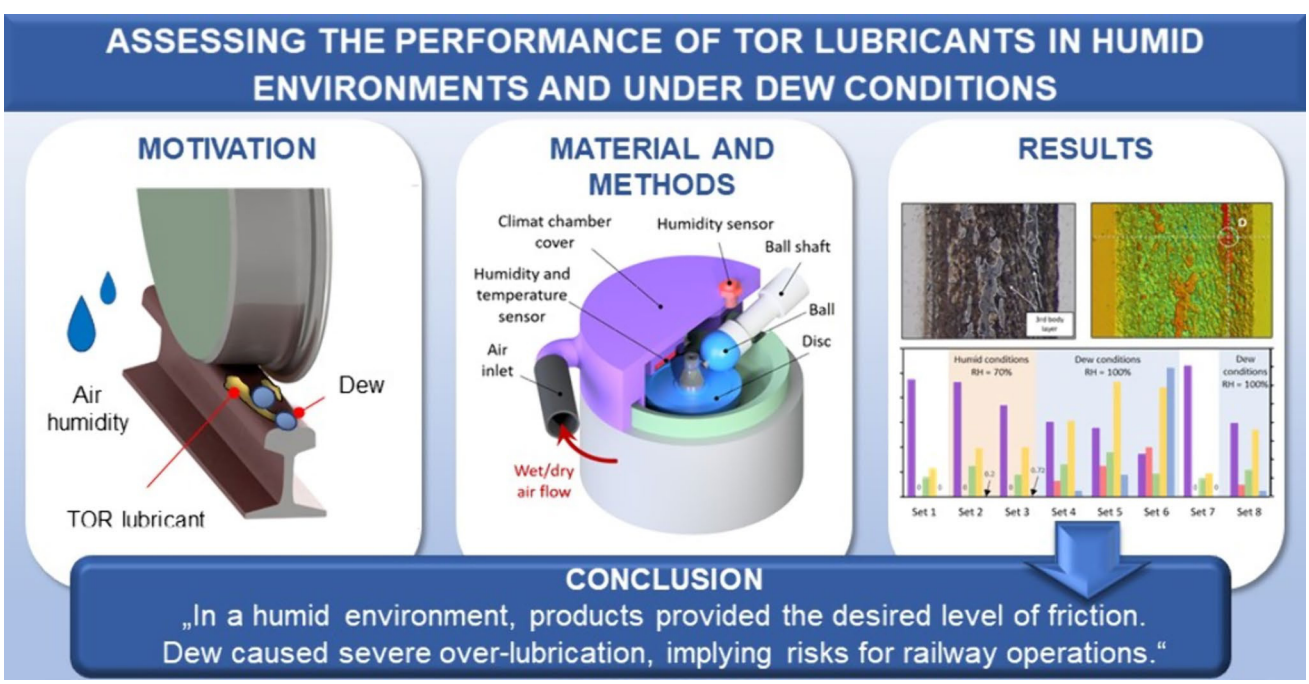

Keywords Wheel–rail tribology · Friction modification · Humidity · TOR lubricants · Dew · Contamination

Extended author information available on the last page of the article

1 Introduction

Railway transportation is an ecologically friendly way of transporting passengers and goods, and its energy efficiency can be further improved by reducing the adverse effects of friction in the wheel–rail (W/R) contact. Too high friction is the cause of excessive fuel consumption [1]. Furthermore, it causes wear of contact surfaces, leading to more frequent wheel changes and rail grinding [2, 3], increasing maintenance costs [4]. Lastly, friction is a source of noise pollution [5, 6]. At the same time, keeping a certain minimum level of friction is necessary. Otherwise, the effectivity of tangential forces transmission from the wheel to the rail will drop, which can result in the vehicle being unable to accelerate and break effectively [7]. A normal and tangential force ratio can quantify frictional conditions in the rolling–sliding contacts. In the literature, this parameter is called the traction (or sometimes adhesion) coefficient (CoT) and depends on several parameters, e.g. load and creepage. Values higher than 0.09 and 0.2 are sufficient for braking and traction, respectively [8].

Top-of-rail (TOR) products were developed to maintain friction at the desired levels, where noise and wear are reduced, but sufficient CoT for traction and braking is maintained. Initially, these products were solid sticks containing lubricants like graphite or molybdenum disulphide. They were used with great success back in the 90 s in the Vancouver mass transit system to overcome problems with corrugation [9]. Since then, TOR products have undergone intensive development, and new liquid-form types have been established. Following [10], liquid TOR products can be divided into two groups depending on their base medium type: Friction modifiers (FMs), which are water-based and TOR lubricants (grease/oil-based products). The difference between these two groups lies in the friction modification mechanism [11]: Water in FMs acts as a transport medium and helps to distribute solid lubricants on the rail head. After that, water evaporates, and the friction is reduced by the shear–displacement mechanism of solid lubricants. In the case of TOR lubricants, grease/oil forms a thin lubricating film on the rail head, contact operates in a boundary/mixed lubricating regime, and solid particles in the product composition help maintain the desired CoT levels. Please note that in general tribology, the term "friction modifier" is used for various additives added to the lubricant to modify its frictional properties. However, in W/R tribology, the term is commonly used for one specific group of TOR products to distinguish between different base-medium types [10]. So, in this paper, "friction modifier" (or "FM") always refers to the group of water-based TOR products. Intensive research over the past decade has already proven the benefits of TOR products. Field studies showed that lower friction was measured on rails where TOR products are applied [12–15], resulting in wear [16–18] and noise reduction [5, 6] and even the number of air-born particles generated from the contact decreased [18].

However, the W/R contact is an open system, which means that besides the intentionally applied TOR products, it is also influenced by various contaminants naturally present on the rail [19]. One of the most common is water. Several studies have shown that water is a good lubricant that can reduce CoT significantly and cause low adhesion problems [20–23]. Furthermore, low adhesion problems are typically linked to the so-called "wet–rail phenomenon" [24, 25]. In that case, a small amount of water mixes with iron oxides, which are inevitably present on the rail surface. Together, they form a thick layer with high viscosity, capable of reducing CoT to as low as 0.05 [25]. It was shown that low adhesion problems are most probable in the morning when dew is present on the track [8], concluding that a small amount of water rather than large amounts causes low adhesion problems. Furthermore, several tests in a climate chamber were conducted to examine the effect of humidity on friction [22, 26]. The results show that with the rise in relative humidity (RH) %, the CoT decreases.

Moreover, the study [27] found that it is even worse when the dew point is reached and water condenses on the specimen surfaces. CoT drop is significantly more substantial in that case than in the humid conditions without dew. In addition, it was shown that temperature influences this behaviour, as it determines how much water can be contained in the air before dew conditions happen. It was found that the effect of humidity is most substantial for temperatures below 24 °C. On the contrary, it is almost negligible for temperatures over 30 °C [27].

Even though contamination significantly influences CoT, little is known about the interaction between TOR products and contaminants. Although TOR products are designed to maintain the CoT required for traction/braking, their effect has been tested primarily in laboratory-clean conditions, or the effect of contaminants has not been evaluated. There are only a few studies addressing this problem. In [28], two FMs were tested under water contamination. Water influenced both products and caused a drop of CoT below 0.1 when applied. However, these products contained friction enhancers like stainless steel particles or sand with high particle diameters, which are not typically found in modern TOR products [29, 30]. It can be assumed that the influence of water on products that do not contain such particles can be even more significant. This conclusion is supported by [31], where different amounts of water were applied to three commercial TOR products (one FM and two TOR lubricants). It was shown that water mixes with the oil in TOR

lubricants and causes a long-lasting period of very low CoT. This observation is also supported by a study [32] that showed that a mixture of rail oil and water leads to even lower CoT than the oil itself. Finally, in [26], an FM mixed with iron oxide particles was tested in a climate chamber under high-humidity conditions. It was shown that with an increase in % of RH, the performance of FM was influenced, and CoT decreased. It was also noted that for a higher % of RH, FM stayed wet for a more extended period, suggesting that the base medium evaporates slowly in a humid environment. Although the increase in % of RH caused a decrease in CoT, it stayed in the interval of desired friction levels as it did not drop below 0.2.

Although testing of FMs in a humid environment did not result in low adhesion in the study [26], it must be noted that as the RH ranged between 40 and 90%, severe water condensation probably did not occur. Previously, in [27], it was shown that there is a significant drop in CoT when dew is present due to the water acting as a lubricant. Furthermore, it was shown in [31] that water influences the performance of TOR products significantly, and oil-based products even cause low adhesion problems in these conditions.

So, based on [27, 31], the question arises about what would happen if condensation occurs and dew is mixed with the product. Although this scenario may happen in the field, the interaction between dew and TOR lubricants has not yet been thoroughly examined. So, this study aims to explore the effect of humidity and dew on two commercial TOR lubricants. Experiments follow an approach based on the creep curve measurement described in [33]. A laboratory tribometer in a ball-on disc configuration equipped with a climate chamber was used for all experiments.

2 Material and Methods

2.1 Test Setup and Specimens

A laboratory tribometer MTM (Mini-Traction Machine, PCS Instruments) in a ball-on-disc configuration was used for all tests and wear-ins/run-ins, see Fig. 1. The specimens were disc with 46 mm in diameter and a ball with 19.05 mm in diameter. According to the Hertz theory, the contact area was circular at the beginning with a diameter of 0.2 mm (the Poisson's ratio of 0.33 and Elastic modulus of 205 GPa was considered for this material). Both specimens were loaded against each other and driven by independent servo motors so the required slide–roll ratio (SRR) could be achieved according to the given equation:

$$\mathrm{SRR} = \frac{w_{\mathrm{ball}} \cdot r_{\mathrm{ball}} - w_{\mathrm{disc}} \cdot r_{\mathrm{disc}}}{w_{\mathrm{ball}} \cdot r_{\mathrm{ball}} + w_{\mathrm{disc}} \cdot r_{\mathrm{disc}}} \cdot 200\% \tag{1}$$

where w_{ball} and w_{disc} are angular speeds of specimens and r_{ball} and r_{disc} stands for its radii. The embedded sensor measures the normal force (N) with ± 0.3 N accuracy with a 1 Hz sampling frequency. However, this signal results from averaging a non-specified higher frequency input signal. Traction force (T) is calculated from the torque measured by the transducer attached to the disc shaft, so the traction coefficient (CoT) could be determined as follows:

$$\mathrm{CoT} = \frac{T}{N} \tag{2}$$

The specimens were made of AISI 52100 bearing steel with a Vickers macro-hardness of 800–920 and 720–780 HV for ball and disc, respectively. Although bearing steel is not a typical rail material, its higher hardness ensures stable conditions during experiments and better repeatability

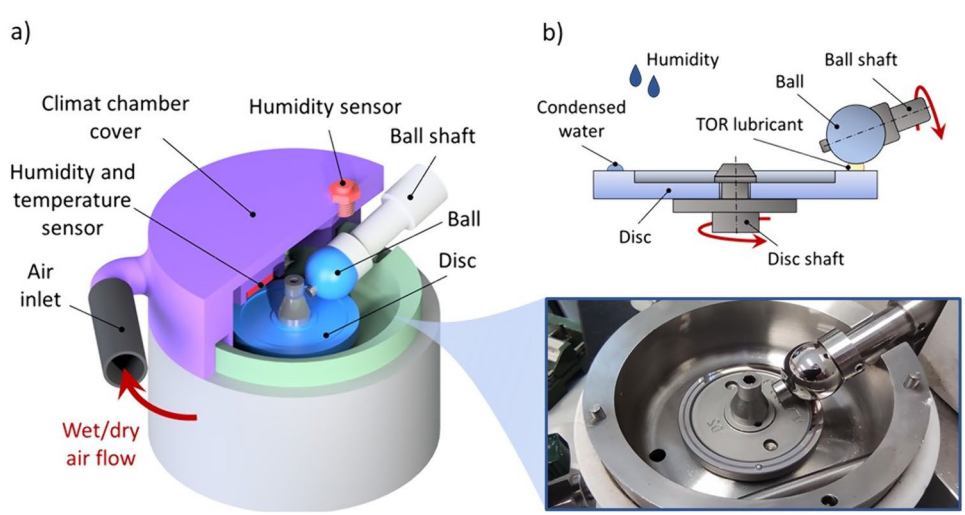

Fig. 1 Test setup: **a** climate chamber and **b** detail of the specimens inside. Part of **b** redrawn from [31] with the Publisher's permission (Elsevier)

due to reduced wear compared to standard wheel/rail steel. The choice of specimen material and geometry follows the benchmarking methodology [33] and enables results to be compared between different laboratories. The impact of the selection of bearing steal over authentic rail steal on measured results and all other study limitations derived from the simplified ball-on-disc configuration will be thoroughly discussed in Sect. "Study limitations". Before tests (after running-in), the surface roughness of specimens was checked using an optical profiler Contour GT (Bruker), and it varied around Ra 0.15 µm for the ball and Ra 0.3 µm for the disc. The same profiler was used to study topography changes and observe oxide layer formation.

The stability of the environment was ensured by a climate chamber mounted on the top of the pot of the tribometer, see Fig. 1a. The chamber had two sensors for monitoring RH and air temperature. The first sensor was mounted in the upper part of the chamber and provided feedback to the humidification unit. Based on the data from this sensor, the humidification unit runs the mixture of wet and dry air into the chamber in a specific ratio, achieving the desired value of RH. The second sensor (HTU21D) was placed near the contact area to enable online monitoring of RH and air temperature near the contact inlet. This sensor measures RH in the 5–95% range with an accuracy of ± 2%. It is also possible to measure outside these borders but with slightly lower accuracy. However, this should not affect the tests conducted since the 100% RH was achieved by running only wet air in the climate chamber. The climate chamber did not enable air temperature control, so all tests were conducted at room temperature of 22 ± 1 °C. However, due to the rise of air temperature due to heat generated in the contact during tests, the HTU21D sensor was also used for air temperature monitoring with ± 0.3 °C accuracy (declared in the range from − 40 to 125 °C).

2.2 Tested TOR Lubricants

The TOR lubricant used in most tests is referred to as "TORL-A". It is a commercially available product used for friction modification in railway operations. Additionally, several tests were conducted using a second TOR lubricant labelled "TORL-B". These tests investigated whether similar phenomena can occur for products with different compositions, indicating that they are not specific to TORL-A alone. Essential information about the composition of both products obtained from datasheets can be seen in Table 1.

2.3 Methodology

Studies on friction modification usually use time tests (CoT on time dependency) [17, 30, 31] or creep curve measurements (CoT on SRR dependency) [14, 28, 34] for testing FMs and TOR lubricants. A study [33] shows that results obtained during time tests can be influenced by the ever-changing topography of the contact surfaces. On the contrary, results based on creep curve measurements are less influenced by topography changes and enable the study of TOR lubricants in a wide range of conditions typical for railway operations. Also, a higher % of slip prevents the contact path surface smoothening effect (the major drawback of time tests), enabling the testing of TOR lubricants in higher quantities. So, in this study, the authors chose to follow a creep curve measurement approach proposed in [33] to examine the effect of humidity and dew on TOR lubricants, which is the main objective of this paper. As seen in Fig. 2, this Sect. "Methodology" is divided into four consecutive parts describing the fundamental principles of the methodology. Readers are encouraged to see the study [33], where the detailed reasoning behind each step was explained.

2.3.1 Cleaning and Running-ing

Before each test, specimens were cleaned manually with a paper towel and ultrasonically in an acetone bath for 10 min. After that, specimens were runned-in for 30 min to stabilise surface roughness and remove residual contaminants. The run-in parameters were 2% SRR, a speed of 1000 mm/s and a normal force of 18 N (corresponding to 0.8 GPa Hertz pressure for unworn specimens). For a given set of humidity/dew conditions, every test was repeated five times on the same pair of specimens to obtain results from a wide range of conditions, as the contact path width and depth changes during tests due to wear. Before each of these five tests, the run-in was conducted the same way except for the first one, which was extended to 60 min to overcome the initial rapid topography changes of unworn surfaces and form a stable contact path.

Table 1 Composition and characteristics of tested TOR lubricants

TOR lubricant	Structure	NLGI grade	Base oil	Thickener	Particles	Base oil viscosity at 40 °C (mm^2/s)
TORL-A	Paste	0	Biodegradable ester	Organic	Soft metal	41–53
TORL-B	Gel paste	00	Synthetic ester	Inorganic (silicate)	Soft metal	46

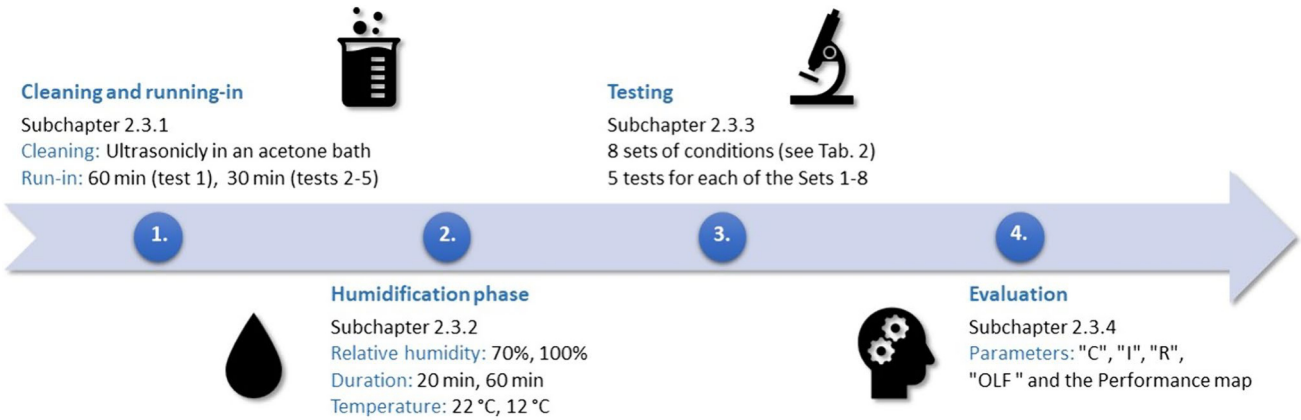

Fig. 2 The individual steps of the methodology

2.3.2 Humidification Phase

Next, TOR lubricant was applied to the contact path of the disc. Then, the tribometer pot was covered with a climate chamber, and the mixture of wet and dry air in the specific ratio was run inside to achieve the desired % of RH (this step is further referred to as the "Humidification phase"). It can be assumed that water condensation only occurred during this step since after the start of the test, the surface temperature quickly rose due to the heat generated by friction, and water could no longer condense on the specimens. The humidification phase was skipped in Sets 1 and 7 (see Table 2), where TOR lubricants were tested under laboratory ambient conditions.

2.3.3 Testing

The test starts when the Humidification phase is ended (see Table 2). One test consists of repetitive creep curve measurements with the same specimen pair, see Fig. 3a. TOR lubricant is applied only once before the first creep curve measurement. So, as the starvation progresses, every consecutive curve reaches higher values of CoT until the threshold criterion is met. This approach enables testing the product under a wide range of topography conditions and evaluating its lasting effect. Every creep curve consists of six points, each evaluated from a 30-s time test as an average CoT at a given SRR value, namely 0, 2, 5, 10, 15, and 20%. Please note that time tests with 0% SRR were only to redistribute

Table 2 The testing parameters and conditions

Set	Product	Amount (µl)	SRR (%)	Normal force[d] (N)	Speed (mm/s)	RH (%)	Humidification phase (min)	Specimen temp. (°C)
1	TORL-A	1	0–20	18	1000	Ambient[a]	–	Ambient[a]
2	TORL-A	1	0–20	18	1000	70[b]	20	Ambient[a]
3	TORL-A	1	0–20	18	1000	70[b]	20	12 ± 2
4	TORL-A	1	0–20	18	1000	100[c]	20	Ambient[a]
5	TORL-A	1	0–20	18	1000	100[c]	60	Ambient[a]
6	TORL-A	1	0–20	18	1000	100[c]	20	12 ± 2
7	TORL-B	1	0–20	18	1000	Ambient[a]	–	Ambient[a]
8	TORL-B	1	0–20	18	1000	100[c]	20	Ambient[a]

[a]Laboratory ambient conditions: RH = 34 ± 2%, temperature = 22 ± 1 °C

[b]Tests with RH = 70 ± 5% are labelled as "humid conditions" in the text

[c]Tests with RH = 100% are labelled as "dew conditions" in the text

[d]According to the Hertz theory, 18 N normal force results in 0.8 GPa contact pressure in the given configuration and unworn specimens

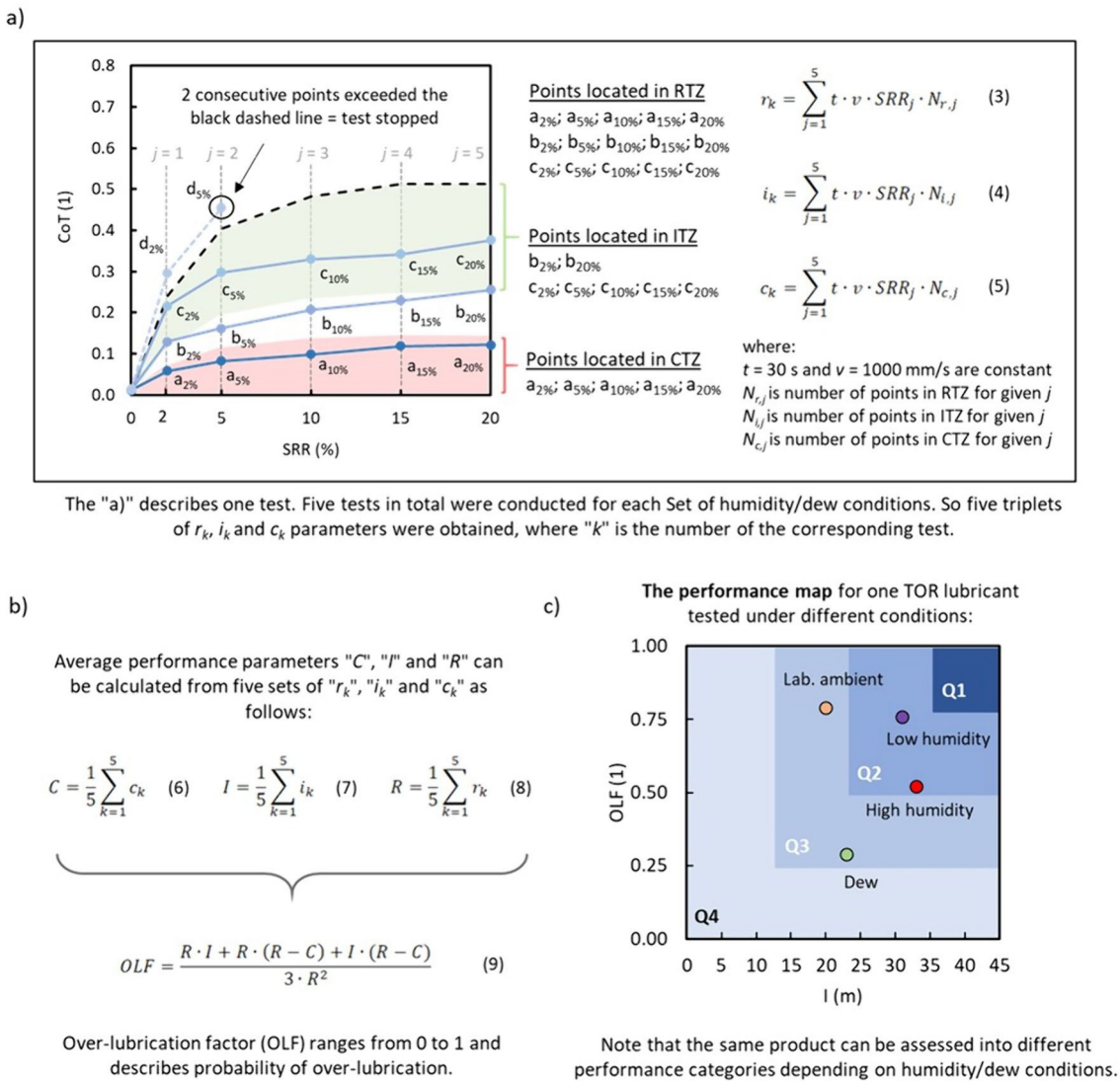

Fig. 3 **a** Model example of one test. Each test is repeated five times, so five triplets of "r", "i", and "c" parameters are obtained. **b** Average parameters "R", "I", and "C" are calculated and used for the "OLF" evaluation. **c** Product performance is assessed into four categories Q1–Q4 based on "OLF" and "I" for each set of humidity/dew conditions

TOR lubricant on the surfaces evenly, and these tests were not used in the evaluation. The threshold criterion was as follows: If two consecutive points exceeded the threshold curve (black dashed line in Fig. 3a), the test was ended. If not, another creep curve was measured. "Consecutive points" are two neighbouring SRRs from the sequence 2, 5, 10, 15 and 20% and corresponding values of CoT.

Three traction zones located under the threshold curve were defined: Critical traction zone (CTZ), Intermediate traction zone (ITZ) and Retentivity traction zone (RTZ). These zones represent different frictional levels: "CTZ" for levels insufficient for reliable traction/braking, "ITZ" represents levels desired for operating the rail vehicles, and "RTZ" which shows the distance for which the TOR lubricant has a noticeable effect on friction. If a point is placed in "CTZ" (red area in Fig. 3a), the CoT decreases to very low values for a given SRR, indicating that over-lubrication occurs. On the other hand, in "ITZ" (green area in Fig. 3a), the CoT reaches intermediate values, meaning the product performed well (that is where, on actual track, adverse effects of friction are reduced but sufficient transmission of traction/braking forces is ensured). Finally, "RTZ" is the entire area under the threshold curve and contains all points measured during the test (except those that exceeded the threshold criterion). Lastly, there is a blank area between "CTZ" and "ITZ", in which CoT acquires values that are not considered critical nor optimal. If a point is placed in this area, this does not directly benefit or penalise the product in the evaluation but influences the retentivity and prolongs test time. Exact values for the threshold

curve and "CTZ", "ITZ", and "RTZ" boundary points were calculated as a defined fraction [33] of dry and clean contact CoT for a given % of SRR and are listed in Appendix A.

2.3.4 Evaluation

From each test, three performance parameters were calculated, namely: "*c*" (critical traction parameter), "*i*" (intermediate traction parameter), and "*r*" (retentivity parameter). These parameters represent the cumulative sliding distances for which CoT stayed in "CTZ", "ITZ", and "RTZ" during the test (see Fig. 3a) Eqs. 3–5) and their unit is one meter. In other words, each parameter is calculated as a sum of weighted distances for which the contact operated in the corresponding zone, where the weight is the value of the corresponding SRR %. The ideal TOR lubricant would aim to maintain the intermediate friction level for as long as possible (represented by the high value of the "*i*" parameter) and simultaneously reduce the probability of low adhesion problems (zero or low value of the "c" parameter). The values of these parameters are limited by the product retentivity (expressed by the "*r*" parameter), which shows how long the effect of the product is noticeable (in this methodology, this parameter represents the whole test duration). Five tests were performed for each set of humidity/dew conditions, resulting in the five triplets of these parameters. From those, average parameters "C", "I", and "R" were calculated, and the over-lubrication factor ("OLF") was evaluated, see Fig. 3b) Eqs. 6–9. The "OLF" describes the probability of over-lubrication (ranges from 0 to 1; the lower the number, the higher the probability of over-lubrication). The ideal product would score "OLF" equal to 1, meaning only desirable CoT values were measured during the test duration.

Finally, a 2D Performance map was constructed in which the *x*-axis contains the value of "*I*", and the *y*-axis has the value of "OLF" for each set of humidity/dew conditions (see Fig. 3c). In this map, four performance categories Q1–Q4 were defined (these categories divide the performance map into quartiles). To be placed into Q1, both "I" and "OLF" values have to lay in the upper 25% on each axis, for Q2 in the upper 50%, for Q3 in the upper 75% and for Q4 at least one value is in the bottom 25%. If the TOR lubricant scores in Q1, that means that the risk of low adhesion problems due to over-lubrication (or condensed water, in this study) is not significant, and the product maintains the desired frictional conditions for a very long time. A change in the performance category caused by humidity/dew indicates how the product performs under different scenarios that can occur on the rail.

2.4 Test Conditions

TOR lubricants were tested in various conditions to evaluate which factors (% RH value, duration of the Humidification phase, etc.) affect their performance the most. TORL-A was chosen for the majority of experiments. However, some experiments were performed with the second lubricant, TORL-B, to ensure that observed phenomenons are not limited to the composition of TORL-A alone but can be generalised to other TOR lubricants with different compositions. All the information about humidity/dew conditions and performed tests is listed in Table 2. In this table, each set of conditions is labelled as "Set 1–8". The purpose of testing these sets is as follows:

(1) Set 1 was conducted under laboratory ambient conditions, specifically RH = 34 ± 2% and temperature of 22 ± 1 °C. This set shows how the TOR lubricant performs in "normal conditions" and was used as the base reference.
(2) In Set 2, TORL-A was exposed to "humid conditions" (specifically RH = 70 ± 5%) for 20 min.
(3) Set 3 was also conducted under "humid conditions" (RH = 70 ± 5%) for 20 min. However, specimens were first put into the refrigerator and cooled to 12 ± 2 °C (measured on the surface). A comparison between Sets 2 and 3 can highlight the importance of the temperature and the dew point.
(4) In Set 4, the TOR lubricant was exposed to RH = 100% ("dew conditions") for 20 min during the Humidification phase. A comparison between Sets 1, 2 and 4 shows how the change in RH % value influences the performance parameters.
(5) In Set 5, TORL-A was exposed to RH = 100% ("dew conditions") for a prolonged duration of 60 min. A comparison between Sets 4 and 5 reveals how the duration of exposure to the humidity will affect the performance parameters.
(6) In Set 6, TORL-A was exposed to RH = 100% ("dew conditions") for 20 min, but first, specimens were put into a refrigerator and cooled down to 12 ± 2 °C (same procedure as in Set 3). The difference in temperature between the surface and surrounding air lowers the dew point and speeds up the water condensation. Thus, more water could condense during the Humidification phase in Set 6 compared to Set 4, where the temperature of the specimens was the same as that of the surrounding air.
(7) Set 7 was conducted with TORL-B under laboratory ambient conditions, specifically RH = 34 ± 2% and temperature of 22 ± 1 °C to obtain the reference for this TOR lubricant under "normal conditions".
(8) In Set 8, the TORL-B was exposed to RH 100% ("dew conditions") for 20 min during the Humidification phase. Sets 7 and 8 were designed to validate results for TOR lubricants with different compositions.

2.5 Additional Experiments

Before the tests mentioned above, several experiments were performed to quantify how much water condenses on the disc surface during the Humidification phase for conditions defined in Table 2, Sets 2–6 (and 8). Only the Humidification phase was performed in these experiments (without any running-in or testing; the goal was to quantify the amount of water). Then, the discs were weighed, and the amount of water was calculated based on the disc weight difference before and after the Humidification phase. So, the change in TOR lubricant performance could be linked to the explicit water quantity.

3 Results and Discussion

First, experiments defined in Sect. "Additional Experiments" were performed to quantify water amounts that condense on the disc surface during the Humidification phase. The results of these experiments can be seen in Table 3 (an average value of 5 measurements). Please note that these are the quantities condensated on the entire disc surface. It is expected that most of the water did not enter the contact because it did not lay in the contact path, as can be seen in pictures from the optical microscope, see Fig. 4. So, there are two more columns in Table 3: corresponding amounts of water in the contact path and amounts of water in W/R contact. These values were calculated based on the ratio between the entire disc surface area, contact path area, and actual W/R contact area. Note that the "contact path area" was measured using an optical profiler, and an approximated value of 1 cm^2 was used as the "actual W/R contact area" based on the literature [11].

3.1 The Effect on TOR Lubricant Creep Curves

The results for Sets 1–8 are summarised in Fig. 5. From each Set, only one out of five tests was randomly selected to be displayed for the sake of clarity. However, average

Table 3 Weighed amounts of water during the Humidification phase and corresponding amounts for the contact path and actual W/R contact

Amount of water	Set 1 (7)	Set 2	Set 3	Set 4 (8)	Set 5	Set 6
On disc (µl)	–	0.2	0.72	7	30	180
In contact path (µl)[a]	–	0.007	0.03	0.26	1.2	7.2
In W/R contact (ml)[b]	–	0.01	0.04	0.37	1.7	10.3

[a]Calculated based on the disc surface and contact path area ratio

[b]Calculated based on the ratio between the MTM and the actual W/R contact areas

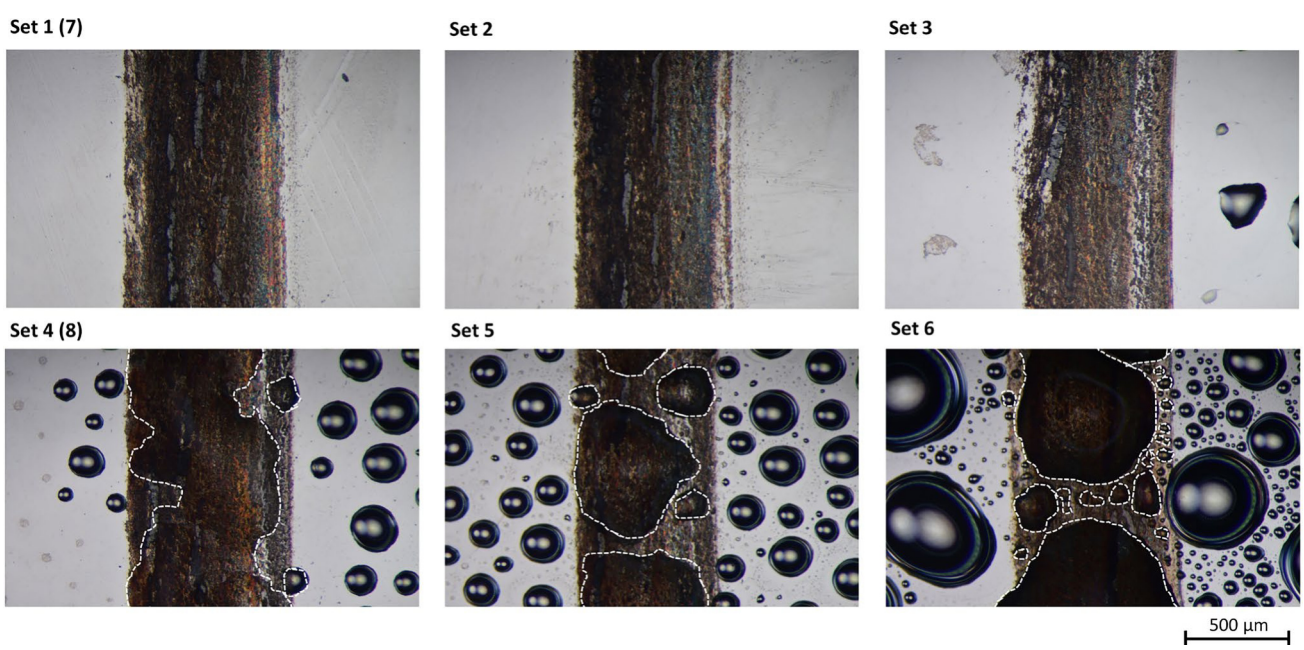

Fig. 4 Photo of the contact path after the Humidification phase in Sets 1–8. A white dashed line highlights water droplets lying in the contact path

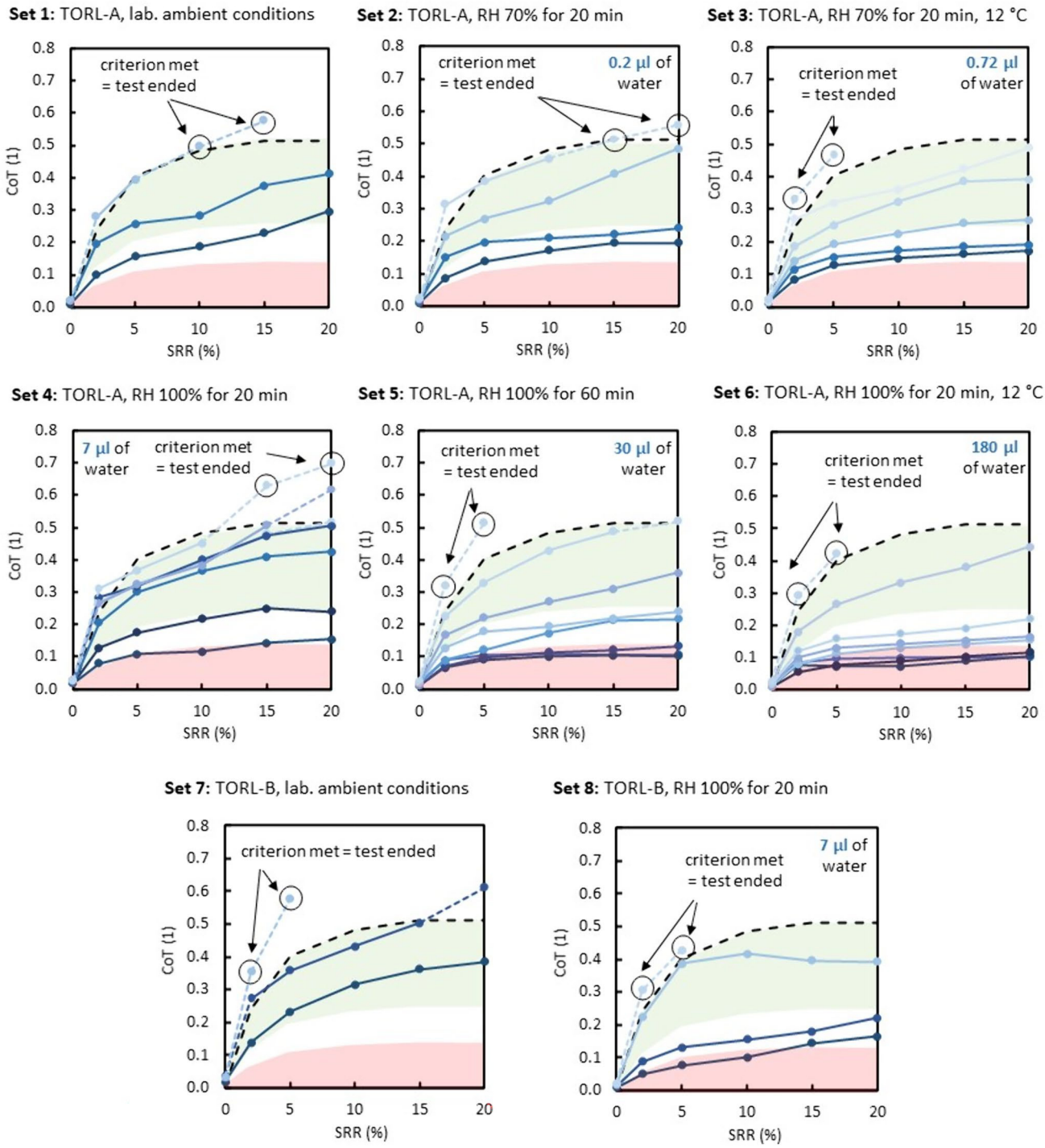

Fig. 5 One selected test for each of Sets 1–8. A black dashed line shows the threshold criterion. Creep curves are depicted in shades of blue. "CTZ" and "ITZ" are highlighted by the red and green areas, respectively

performance parameters were calculated based on all five tests and will be discussed later in the text. These charts show creep curves constructed from SRR value on the *x*-axis and CoT on the *y*-axis. Each creep curve has six points (the last creep curve in each chart may be an exception). The threshold limit is displayed in these charts by a dashed black line. Creep curves are shown by solid lines in shades of blue. If some point of the creep curve is placed outside the black threshold curve, this point is excluded from the evaluation and connected with other points by a dashed line of the

same colour. If two consecutive points are placed outside the threshold line, the criterion for ending the test was met, and the test was stopped (which is why the last creep curve in each test may consist of less than six points). Furthermore, the red area highlights the "CTZ", and the green area highlights "ITZ" in these charts.

First, the effect of humidity/dew on TORL-A creep curves will be discussed. After linking the results for Sets 1–6 from Fig. 5 to corresponding amounts of water from Table 3, it is clear that with increased water amount, more creep curves are measured during the single test, and CoT decreases to lower values. During the displayed test for Set 1, in which measurements were conducted under laboratory ambient conditions to obtain the reference, only two creep curves lay entirely under the threshold, and the test was stopped during the third one. In the beginning, when the TOR lubricant is applied, the contact is flooded. A uniform layer of oil may be formed for sufficient speeds, preventing direct contact between surface asperities, resulting in low CoT for a given % of SRR. However, at some point, starvation occurs, and the load is transmitted partly by the oil film and partly by the direct contact between the surface asperities, which is typical for mixed/boundary lubrication regimes. At this point, higher values of CoT are measured until the threshold criterion is finally met.

During the displayed test for Set 2, where specimens were exposed to RH 70% for 20 min, one extra creep curve was measured compared to the previous test. However, as shown in Fig. 4, no water was present in the contact path after the Humidification phase. This slight difference is not out of the range in which this product performs under normal conditions (topography changes and precision of application play a role), concluding that RH 70% had no significant effect on the TORL-A. On the contrary, a noticeable effect was seen during Set 3, where precooling of the specimen led to higher water condensation compared to Set 2, see Table 3. In this test, not only were more creep curves measured, but some of these curves also approached boundaries of the "CTZ".

The most significant effect was observed during Sets 4–6 with RH 100% when dew conditions occurred. During Set 4, some points fell into the "CTZ" for the first time, meaning very low CoT was measured for these SRRs. Furthermore, the situation worsens in Set 5 when the Condensation period is extended to 60 min. Finally, the highest number of creep curves placed in "CTZ" were measured during Set 6, where precooling of the specimens led to the condensation of excessive amounts of water of 180 µl on the disc surface.

Lastly, Sets 7 and 8 were performed with TORL-B to see if this behaviour is exclusive to TORL-A or may occur for products with different compositions and rheological properties. Although the number of creep curves did not rise dramatically under the dew conditions, significantly lower values of CoT were measured, and points for some of the SRRs were moved from "ITZ" to the "CTZ", showing an apparent effect of water on TORL-B, as in the case of TORL-A.

It is clear that water interacts with the product and mixes with its base medium, which is grease/oil in this case. The interaction between oil and water can be described based on Oil-in-water (O/W) emulsion theories, especially the plate-out theory (valid for lower running speeds). This theory says that in the case of O/W emulsion, contact is predominantly lubricated by the oil as it has stronger wetting abilities [35, 36]. This means that even if the mixture consists mainly of water, the oil forms a pool before the contact inlet and prevents water from entering the contact. Thus, the lubricating film is entirely composed of oil, and water does not negatively influence film thickness in the contact [37]. Furthermore, the study [32] experimentally confirmed that water may even improve the lubricating abilities of oil in some cases, as an oil and water mixture provided lower CoT than pure oil in experiments conducted in the study. This scenario may describe the situation in the contact during a couple of first points of the creep curve(s).

At some point, starvation occurs, meaning water can no longer be excluded from the contact [38]. Without water, CoT would rise at this point (as was seen in Sets 1, 2 and 7). However, in this case, water can refill starved contact and maintain low CoT. It is important to note that the base medium of tested TOR lubricants also contains thickeners and other additives, and the lubricating mechanism may differ from O/W emulsions. So, in this case, water will influence not only the oil pool formed before the contact inlet but also the rheology and structure of the grease itself. It was shown that grease bulk can absorb water due to the polar nature of the thickener [39]. Usually, grease tends to be pushed to the sides of the contact path, and then, the contact replenishment is inversely proportional to viscosity [40, 41]. Water may influence stiffness and oil-bleeding ability, which could lead to higher contact replenishment and prolong the duration of low CoT. So, a higher number of creep curves is measured in Sets 4–6 compared to those with lower amounts or no water at all.

3.2 The Effect on TOR Lubricant Performance Parameters

The values of average performance parameters "C", "I", and "R" were computed using Eqs. 3–8 (Fig. 3) from five triplets of "c", "i", and "r" for each of the Set 1–8. Together with "OLFs" and corresponding amounts of water, they are summarised in Table 4 and depicted in Fig. 6. In this figure, the x-axis is divided into eight parts, one for each Set 1–8. The

purple *y*-axis is for "OLF", and the black *y*-axis is for sliding distances of "*C*", "*I*", and "*R*". Finally, the blue *y*-axis on the right stands for water amounts that condensated. Furthermore, tests under humid and dew conditions are differentiated by brown and blue, respectively.

A clear relation between the change in "OLF" and the amount of water can be seen: with an increase in water amount, "OLF" gradually decreases between Sets 1–6 and 7–8, which means that the risk of low adhesion problems is dependent on the water amount, which follows findings in [8]. This trend is also valid for "*C*" and "*R*" parameters (with a slight exception for "*R*" between Sets 5 and 6)—the higher the water amount, the longer the duration of critical traction and the longer the retentivity. On the other hand, parameter "*I*" did not show any clear trend, which can be interpreted as follows: water does not strongly influence the

Table 4 The exact values of "C", "I", and "R" parameters and "OLF" for Sets 1–8

	Set 1	Set 2	Set 3	Set 4	Set 5	Set 6	Set 7	Set 8
C (m)	0	0	0	16	31	50	0	12
I (m)	20	31	22	33	45	23	19	27
R (m)	29	49	50	77	116	111	24	68
OLF (1)	0.79	0.76	0.63	0.52	0.47	0.29	0.88	0.51

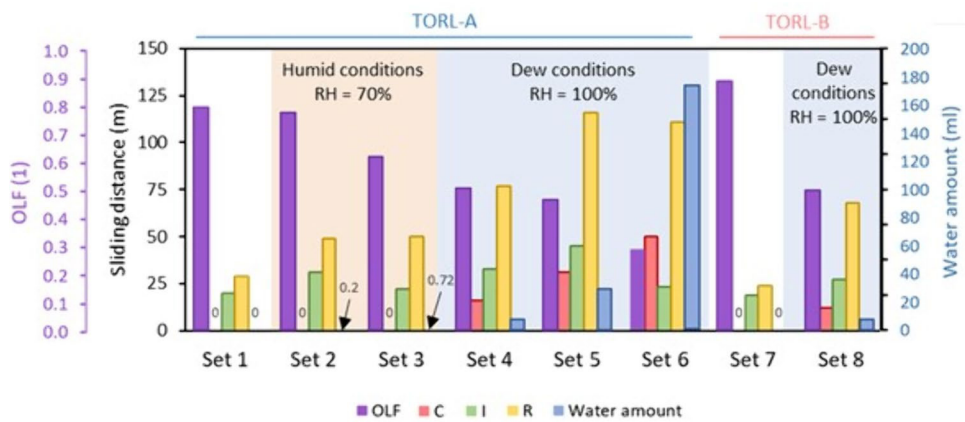

Fig. 6 The final results: Summary of "OLF", "*C*", "*I*", and "*R*" parameters and corresponding amounts of water

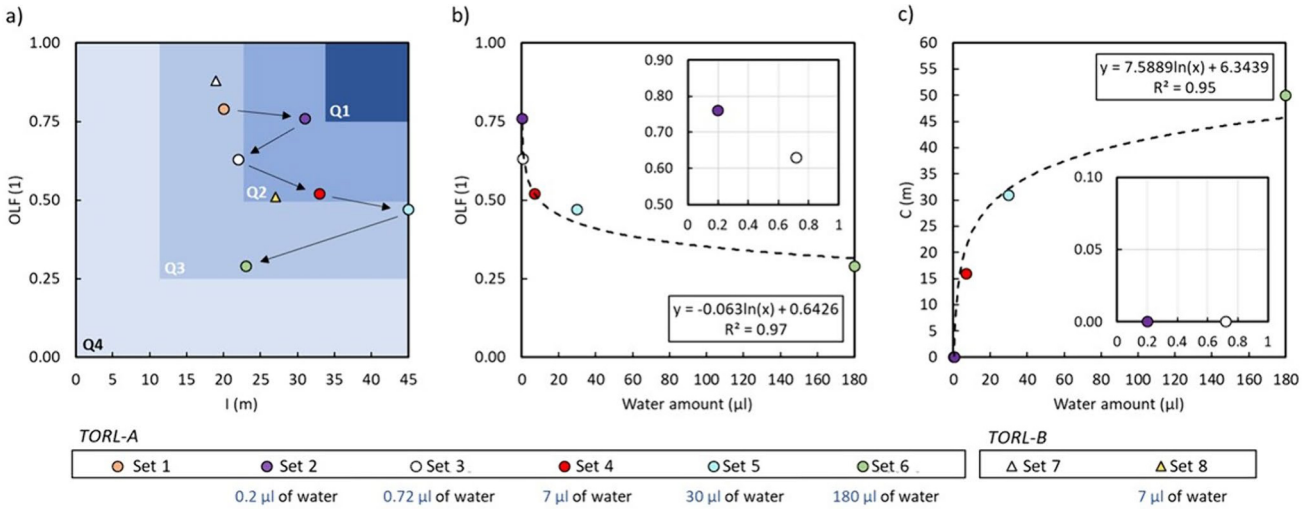

Fig. 7 The final results: **a** performance map, **b** the dependency of "OLF" on water amount for TORL-A and **c** the dependency of average critical traction parameter "C" on water amount for TORL-A

duration of positive effects of TOR lubricants. However, it enhances the time of undesirable critical traction, which also prolongs retentivity and, in the end, lowers "OLF". To sum it up, water does not influence the desired effects of TOR lubricants but enhances their adverse effects.

Next, the performance map was constructed. In Fig. 7a, four performance classes Q1–Q4 are highlighted in shades of blue. Placing in the best-performing class (Q1) requires scoring high values for both parameters. This requirement was met under no set of conditions. Although in Sets 1, 2 and 7, the "OLF" of TORL-A and TORL-B was sufficient for the Q1 class, their "I" parameter was good enough only for the Q2 or Q3 class, resulting in a lower product overall assessment, meaning that in these tests, products provided desired frictional levels, but only for a limited sliding distance. In Sets 2, 4 and 8, tested products provided a good compromise between the provided CoT and the duration of its performance and were assessed in the Q2 class. In Sets 1, 3, 5 and 6, products lacked sufficient duration, or low adhesion problems occurred, and Q3 class was assessed.

TORL-A performed the worst in Set 6, where a large amount of water nearly caused a drop from Q3 to the worst Q4 category. In the performance map, arrows between points show the direction in which the performance class changed with increased water amount.

Furthermore, "OLF" on water amount dependency was plotted in Fig. 7b. Please note that the results are shown only for TORL-A, and only Sets 2–6 in which the water amount was non-zero are displayed. There is a clear trend that with increased water amount, "OLF" decreases to lower values. However, this behaviour is not linear—a slight increase in small amounts of water leads to a significant "OLF" change. On the other hand, with larger amounts of water, a further increase leads only to a negligible change in "OLF". This behaviour can be explained by the fact that there is a limit to the amount of water that can enter the contact, depending on the contact size. The reference logarithmic curve is plotted as a black dashed curve over measured results. However, there is not enough evidence to state that the "OLF"—water amount dependency is logarithmic. More tests should be conducted to support this conclusion, and the logarithmic curve is displayed only to highlight that the severity of the impact of the change in water amount differs for small and large amounts.

In addition, parameter "C" on water amount dependency was plotted in Fig. 7c). A similar trend can be seen in this case as for lower amounts of water, a slight increase in water amount causes a significant increase in the sliding distance in the "CTZ". However, when larger amounts of water are present, further increase leads only to a slight rise in parameter "C", which is probably also linked to the contact size area and the fact that only a limited amount of water can enter the contact with TOR lubricant.

3.3 The General Discussion and Implications for Railway Operation

To better understand the results, it is necessary to put them in the context of the rest of the scientific work. The Fig. 8 shows a selection of published papers on this topic.

The *y*-axis has the value of CoT/CoF measured in dry conditions (grey bars), under humid/water/dew conditions (blue bars) and a combination of humidity/water/dew and TOR products (brown bars). Moreover, essential parameters (e.g. measuring configuration, range of RH or temperature, etc.) are noted, and the "CTZ" for 20% SRR used in this study is highlighted in red.

The left part of Fig. 8 shows that in dry contact, CoT (or CoF in case of pure sliding contact) usually vary from 0.4 to 0.8 depending on the presence of third body layers and also measurement method, as studies with different measurement configurations (rail tribometer, ball-on-disc and twin-disc) were chosen on purpose to gain a broader overview. Studies in the middle show that under humid conditions, CoT decreases slightly compared to dry contact. However, the decrease is not significant. A more substantial effect was shown in [42], where RH 60% and water caused the reduction of CoT to 0.3. This value was measured also in [27] under RH 70%. However, in the same study, the author raised RH further to 100%, which caused severe condensation, lowering CoT to 0.13. A comparison between grey and blue bars shows that although humidity somewhat reduces CoT, a more substantial CoT drop occurs only when water is introduced to the contact through direct application [42] or condensation [27]. The right part of Fig. 8 shows that the situation worsens when TOR products come into play. First, a study [26] tested the effect of humidity and iron oxides on FM. Although very low CoT was not measured, another study [31] showed that FMs are generally more resistant to contamination (in terms of low adhesion), and the problem arises when oil contained in TOR lubricants mixes with water. In that case, CoT as low as 0.015 was measured in [31], even lower than in the present study. However, as different tests were performed in both studies, the comparison of the results is slightly limited. Also, different amounts of water were tested, from which the most comparable are results for 8 µl of water, which caused a long-lasting period of very low CoT in [31], similar to the effect of 7.2 µl of water in Set 6 in the present study.

Another critical factor is the presence of a third body layer. A study [8] suggests that low adhesion problems are more probable in the morning when dew is present, as a

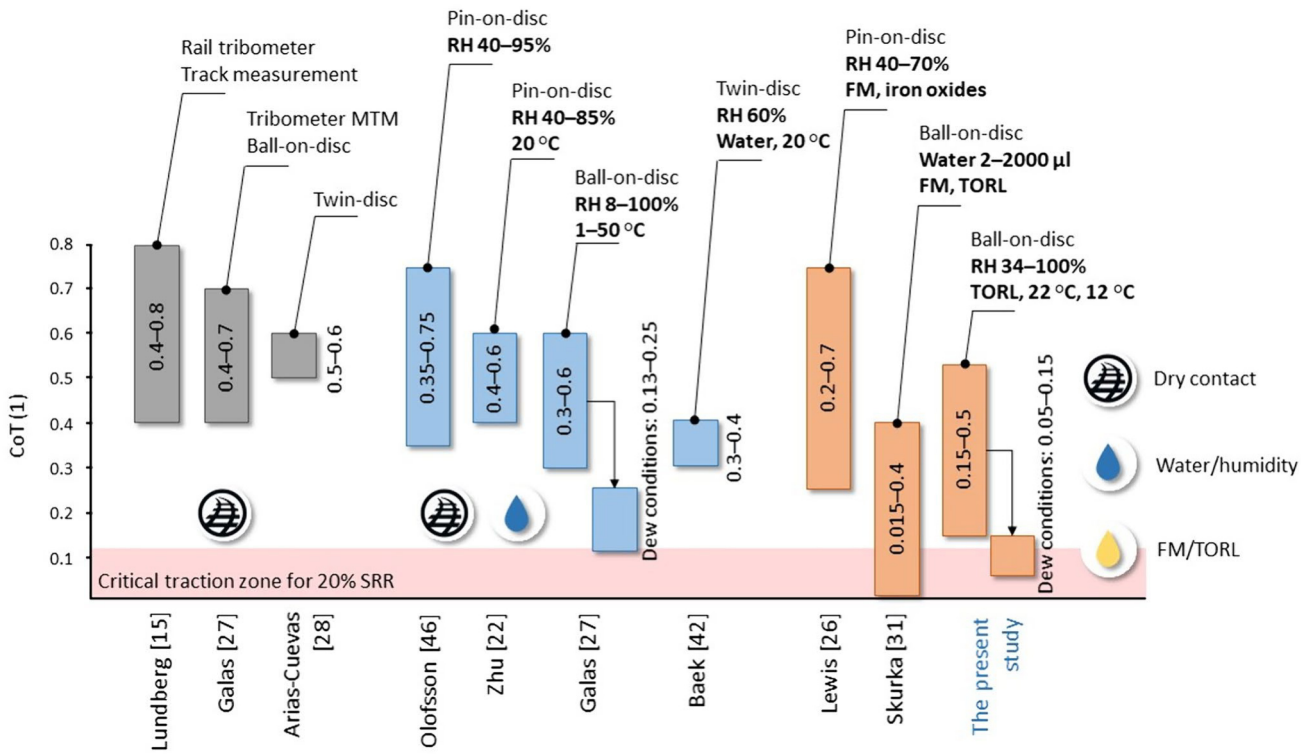

Fig. 8 The comparison of measured CoT/CoF under humid/water/dew conditions across different studies

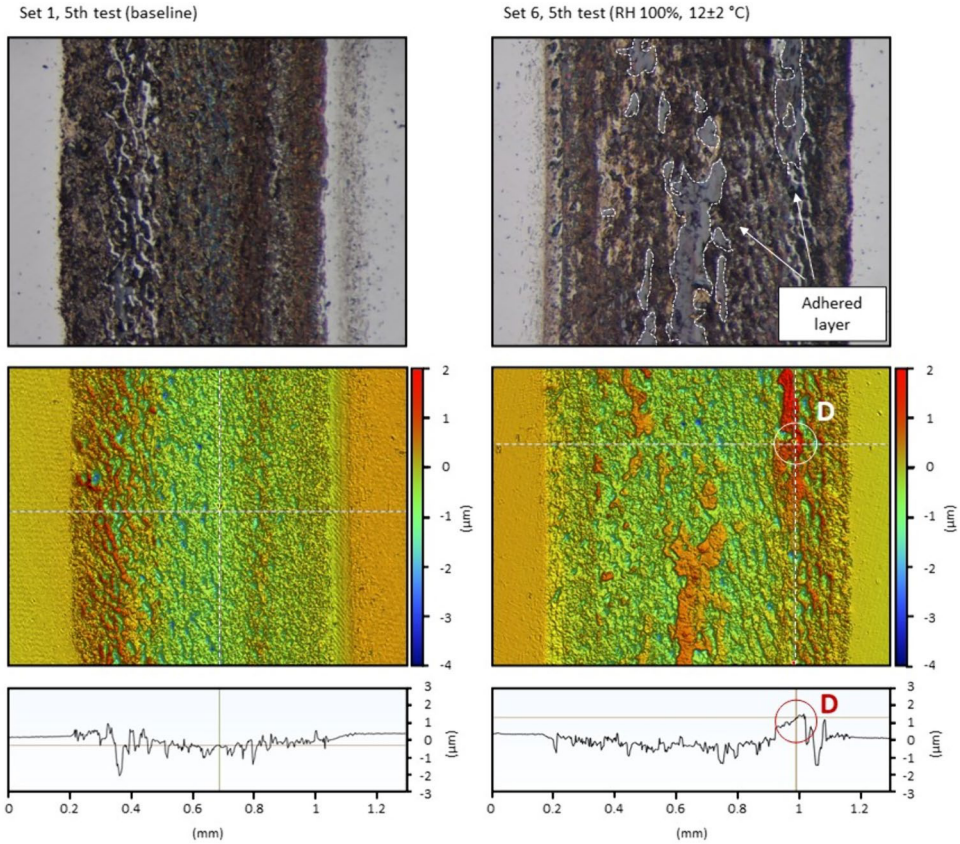

Fig. 9 The images of the contact path surface after the 5th test of Sets 1 and 6. The white dashed line highlights the thick adhered layer

small amount of water is mixed with particles and wear debris [25]. This follows the results of the presented study, where low adhesion problems occurred only under dew conditions, where water droplets on the specimen surfaces were eye-visible. As water–particle interaction plays a crucial role in low adhesion problems [25], the contact path surface was checked on an optical profiler after tests, during which low adhesion problems occurred. The images of the contact path after the last tests in Sets 1 and 6 can be seen in Fig. 9. These images show that at the end of Set 6, an eye-visible layer up to 2 µm thick has formed and covered part of the contact path. The highest amount of water was weighed during these tests, and its influence on "OLF" was the most significant.

On the contrary, at the end of Set 1, the contact path was covered by wear particles, but there was no sign of the "thick adhered layer" as in Set 6. The difference in the third body layer formed in those two Sets was that the wear particles (found in both Sets 1 and 6) could be easily removed by simply cleaning the surface with a paper towel and acetone. However, the thick layer found in Set 6 (and also other Sets where the dew conditions occurred) firmly adhered to the surface, and removing it requires increased effort (e.g. sandpaper, but it was tested that this layer was completely removed during the run-in process). This layer probably consists of iron oxides, which could explain low "OLF" scores in these tests, as the mixture of water and iron oxides is known for reducing CoT. This behaviour was previously observed in [43], where an adhered layer of Fe_2O_3 was mixed with condensed water and caused a stable period of low CoT. Several factors may influence the formation of the oxidic layer, and temperature is one of them. Based on numerical calculations computed in [33], the highest temperature in the contact should not exceed 95 °C (and the average temperature will be significantly lower), which does not seem very high at first glance. Still, the oxides can form under sliding conditions even at room temperature when metal surfaces are exposed to the air and in the absence of water, as these factors may alter/enhance the oxidation but are not the necessary conditions for oxides to be formed. As iron oxides are naturally present on the railhead, mixing them with TOR lubricants is inevitable. On the other hand, water seems more likely to pose a risk to TOR lubricants in terms of low adhesion, as these problems were observed only in tests where severe condensation occurred.

Unlike in the case of iron oxides, water contamination can be potentially avoided by carefully planned friction management, depending on weather conditions, and by avoiding applying TOR lubricant when dew is on the railhead in the morning. A possible benefit of contamination is that water prolonged retentivity, as in the tests where the highest quantities were present, the "*R*" parameter scored the highest values, which can help to extend the carry distance on the actual track.

When transferring results to the actual track, the drop of CoT is expected to be less significant for *W/R* contact (larger area compared to the one between specimens in the ball-on-disc configuration) and farther distances from the application unit (as every pass of the wheel remove TOR lubricant and redistribute it further). Even if a low CoT occurs, this should not pose a considerable risk to passengers' safety on a straight, long track where braking is not expected. However, this may be an issue on tram loops, where, after completing the ride, vehicles are parked one after another. There are reported cases from Brno, Czechia, in which vehicles experience braking problems on tram loops due to low adhesion, and collisions between vehicles often occur. As TOR product application units are commonly placed in front of these loops to reduce friction when the tram is driving into the curve, there is a real risk of TOR lubricants being contaminated by morning dew or rainwater, which may further worsen this issue. In the future continuation of this work, the focus should be on the actual track measurements in these loops.

3.4 Study Limitations

Regarding laboratory testing, measurements in humid conditions were previously performed in several studies. Shen [44] used a twin-disc device to measure CoT in the 5–99% RH range. Baek [42] tested 60% RH under different air temperatures. Zhu [22] also tested under different air temperatures but used a 40–95% RH, and Lyu [45] performed experiments under 40–85% RH. Next, Olofsson [46] tested two different levels of RH: 40% and 95%. Finally, Galas [27] conducted tests in the 8–100% RH range. In all these studies, higher humidity always led to a decrease in measured friction/CoT, supporting the validity of the presented results. Regarding testing conditions, 34 and 70% of RH used in this study fit into these ranges and represent normal and higher humidity conditions (e.g. in tunnels), and 100% RH was chosen to achieve dew conditions.

The most significant study limitation lies in simplified apparatus, as the ball-on-disc configuration leads to point contact rather than the elliptical, which is standard on the actual track. The measured CoT values are firmly dependent on the device and method of measurement [15]. Thus, adapting a universal benchmarking methodology and a commercial tribometer MTM with certified specimens is the most suitable option for laboratory CoT measurement to compare

results between different workplaces [33]. The MTM tribometer allowed precise control over test parameters in a wide range and was used in several studies focusing on W/R tribology before [29–31]. Although the transferability of laboratory results into actual W/R contact may be slightly challenging due to measuring configuration limitations, these measurements are useful in preliminary testing to identify the most reasonable conditions and parameters, as laboratory tests are fast and cost-effective. However, these results should be verified using a testing rig with more realistic geometry and conditions.

Together with measuring configuration, the most significant difference from the actual track conditions lies in the material of specimens. Specimens used in this study were made of AISI 52100 bearing steel with macrohardness of 820–920 and 720–780 HV for ball and disc, respectively. These values are significantly higher than those of typical rail materials. For example, one of the most common rail steel used in Europe is R260, with a bulk hardness around 275 HV, although there are also special heat-treated steels with bulk hardness as high as 350 HV [47]. It is also estimated that due to the work-hardening effect, the hardness close to the surfaces can be up to 2.5 times higher [48]. The AISI 52100 steel was chosen for two reasons. First, these specimens are provided directly by the tribometer manufacturer, enabling comparability of contact conditions across different workplaces. The second reason is that due to the higher hardness, the surfaces of the specimens were more resistant to wear, so topography changes of contact path groove were reduced, and relatively stable conditions could be maintained for all tests. However, it is necessary to remember that wear debris oxidises and forms a third body layer on the rail. Thus, less wear debris means the third body layer formed in these tests was less developed compared to field conditions. Furthermore, when interpreting results, it is essential to note that lower CoT values can usually be measured for specimens with higher hardness than those with lower hardness [12].

It is important to note that although the bearing steel experiences lower wear than the rail materials, it still occurs to some extent and influences contact conditions. The wear-in was always conducted on a new pair of specimens to create a stable contact path with an initial width of around 0.6 mm, which is sufficient for particles in TOR products to enter the contact, as their diameter typically ranges in tens of micrometres [29]. However, as the wear progresses, the contact path becomes wider. The width was measured at the end of the fifth test from each of the Sets 1–8, and the results (average from three values measured on different cross-sections of the disc) in order from the first to the eighth are as follows: 0.85 ± 0.01, 0.92 ± 0.02, 0.93 ± 0.02, 1.09 ± 0.08, 1.00 ± 0.02, 1.03 ± 0.06, 0.92 ± 0.01, and 1 ± 0.05 mm. The contact path's width increases with the experiment's length, although the increase is not proportional. This is probably caused by the fact that in the experiments with longer duration, the extra creep curves are measured in the areas of low CoT, in which a lower wear rate is also expected. However, the last couple of creep curves in each test have the most significant effect on wear as they reach higher values of CoT.

On the other hand, a larger contact area and more conformal contact results in a decrease in contact pressure. Evaluating the change in contact pressure is not an easy task, as during the assembly of specimens at the start of each test, specimens may be positioned slightly differently due to small clearances in the mounting mechanism. The contact is then realised on different radii in each test, which means that the size of the contact is not equal to the width of the contact path but is smaller. This is a limitation of the measuring device and means that the initial conditions for each of the five tests in the set will inevitably differ. However, from one perspective, this may be seen as beneficial because the final parameters are computed as an average and thus can be related to a broader range of conditions like on the actual track, where the ever-changing topography of surfaces also leads to a variety of contact conditions after each pass of the wheel.

In addition, the transfer mechanism of TOR lubricant under this configuration differs from the situation on the actual track. The contact is in a ball-on-disc configuration realised repeatedly on the same pair of points on both surfaces, and lubricant cannot easily leave the contact path, resulting in delayed starvation. On the railhead, TOR lubricant is spread at a longer distance [34]. Thus, after several dozen meters from the application unit, a significantly smaller amount of TOR lubricant is present, meaning that the effect on CoT will probably be less severe than in the MTM case. The recently published second part of the methodology [49] utilises a more realistic testing device, which incorporates a piece of actual rail, a scaled wheel and a hand-pushed tribometer. In this configuration, TOR products are tested in conditions close to the actual track, as the lubricant transfer mechanism is more realistic and the contact area is larger. The same TOR products were tested in both studies [33, 49]. Although the exact numerical values of CoT differed due to the different measuring methods and apparatus, strong correlations were found in the behaviour of the tested TOR products. Testing under contamination was not part of the study. However, the results imply that

a similar correlation may exist for testing under humidity/dew conditions, and these tests will be the next step in our future research.

4 Conclusion

This study investigated the influence of air humidity and dew on the performance of TOR lubricants. The universal methodology based on creep curve measurement was adapted to enable comparability of results across different workplaces. This methodology uses the coefficient of traction (CoT) and several performance parameters to evaluate the risk of low adhesion problems and the retentivity of TOR lubricants. Based on these parameters, TOR lubricants are assessed into four performance classes: Q1–Q4. The tribometer MTM in a ball-on-disc configuration was used for all measurements. The pot of the tribometer was covered with a climate chamber to control RH %. Tested TOR lubricants were exposed to three RH levels: laboratory ambient (34%), 70%, and 100%, simulating different situations on the track, e.g., morning dew, tunnels, etc. In some tests, specimens were precooled to create a temperature gradient and lower the dew point. The findings can be summarised as follows.

In tests with RH 70%, the effect of humidity on TOR lubricant was insignificant, as there was almost no water condensation. Although humidity influences friction in nonlubricated contacts, the effect is negligible compared to the effect of TOR lubricant. The cooling of specimens enhanced water condensation, resulting in worse product performance in terms of CoT. However, the product still performed sufficiently well, showing that TOR lubricants can be safely used in humid environments without significant risk of low adhesion problems.

A substantial effect was observed in tests under dew conditions. There is a clear relationship between the amount of water and its impact on performance. With the increase in water amount, the severity of low adhesion problems also increases, and lower values of CoT are measured. However, this behaviour is not linear, as a slight change in water amount causes a significant change for small amounts of water, but a substantial change in water amount causes only a slight difference for larger water amounts. This may be related to the fact that only a limited amount of water/lubricant can enter the contact area. The second TOR lubricant with a different composition was tested to confirm that this behaviour is not exclusive to the first product. The effect of dew was even more significant in this case, meaning that the resistance to contamination, besides others, depended on the product composition.

Results presented in this study imply that without significant water condensation, humidity has a less substantial effect on TOR lubricants. If the dew point is not reached, the low adhesion problems are more likely to occur due to the other impacts, e.g. contact over-dosing. However, when the dew point is reached and water condenses, it can significantly affect the performance of the TOR lubricant. This study showed that dew severely worsens the performance of tested TOR lubricants and, in some cases, can even cause low adhesion problems. These findings can be used to optimise friction management methods.

Appendix A

See Table 5.

Table 5 The limits of traction zones and the threshold curve

SRR (%)	0[a]	2	5	10	15	20
Dry contact CoT	0.008	0.361	0.605	0.724	0.769	0.773
CTZ upper limit CoT	0.001	0.060	0.101	0.121	0.128	0.128
ITZ lower limit CoT	0.002	0.120	0.202	0.241	0.256	0.256
ITZ upper limit[b] CoT	0.003	0.240	0.403	0.483	0.513	0.513

[a]Values for SRR 0% were not used in the evaluation

[b]ITZ Upper limit was also used as a threshold curve

Author contributions Simon Skurka: Conceptualization, Methodology, Investigation, Data curation, Writing—original draft. Radovan Galas: Conceptualization, Investigation, Methodology, Writing—review & editing. Milan Omasta: Conceptualization, Investigation, Methodology, Writing—review & editing, Project administration. Haohao Ding: Writing—review & editing. Wen-Jian Wang: Project administration. Ivan Krupka: Data curation, Writing—review & editing. Martin Hartl: Supervision, Funding acquisition.

Funding Open access publishing supported by the National Technical Library in Prague. This work was carried out in the framework of the project "Bozek Vehicle Engineering National Center of Competence" (TN02000054), which was co-financed from the state budget by the Technology Agency of the Czech Republic within the programme "National Centres of Competence". The work was also supported by the National Natural Science Foundation of China (No. 52320105007) and the 2024 Excellent Youth Team Training Program of Southwest Jiaotong University.

Declarations

Conflict of interests The authors declare that they have no known competing financial interests or personal relationships that could have appeared to influence the work reported in this paper.

Open Access This article is licensed under a Creative Commons Attribution 4.0 International License, which permits use, sharing, adaptation, distribution and reproduction in any medium or format, as long as you give appropriate credit to the original author(s) and the source, provide a link to the Creative Commons licence, and indicate if changes were made. The images or other third party material in this article are included in the article's Creative Commons licence, unless indicated otherwise in a credit line to the material. If material is not included in the article's Creative Commons licence and your intended use is not permitted by statutory regulation or exceeds the permitted use, you will need to obtain permission directly from the copyright holder. To view a copy of this licence, visit http://creativecommons.org/licenses/by/4.0/.

References

1. Szablewski, D., LoPresti, J., Sultana, T.: Testing of latest top-of-rail friction modification materials at FAST. Railway Track and Struct. **111**, 13–16 (2015)
2. Wang, R.X., Zhou, K., Yang, J.Y., Ding, H.H., Wang, W.J., Guo, J., et al.: Effects of abrasive material and hardness of grinding wheel on rail grinding behaviors. Wear. pp 454–455 (2020). https://doi.org/10.1016/j.wear.2020.203332.
3. Niu, L., Yang, F., Deng, X., Zhang, P., Jing, G., Qiang, W., et al.: An assessment method of rail corrugation based on wheel–rail vertical force and its application for rail grinding. J. Civ. Struct. Health Monit. **13**, 1131–1150 (2023). https://doi.org/10.1007/s13349-023-00700-w
4. Krishna, V. V., Hossein-Nia, S., Casanueva, C., Stichel, S.: Long term rail surface damage considering maintenance interventions. Wear, pp 460–461 (2020). https://doi.org/10.1016/j.wear.2020.203462.
5. Han, J., He, Y., Xiao, X., Sheng, X., Zhao, G., Jin, X.: Effect of control measures on wheel/rail noise when the vehicle curves. Appl. Sci. **7**, 1144 (2017). https://doi.org/10.3390/app7111144
6. Meehan, P.A., Liu, X.: Wheel squeal noise control under water-based friction modifiers based on instantaneous rolling contact mechanics. Wear **440–441**, 203052 (2019). https://doi.org/10.1016/j.wear.2019.203052
7. Galas, R., Omasta, M., Klapka, M., Kaewunruen, S., Krupka, I., Hartl, M.: Case Study: the Influence of Oil-based Friction Modifier Quantity on Tram Braking Distance and Noise. Tribol. Ind. **39**, 198–206 (2017). https://doi.org/10.24874/ti.2017.39.02.06.
8. Ishizaka, K., Lewis, S.R., Lewis, R.: The low adhesion problem due to leaf contamination in the wheel/rail contact: bonding and low adhesion mechanisms. Wear **378–379**, 183–197 (2017). https://doi.org/10.1016/j.wear.2017.02.044
9. Kalousek, J., Johnson, K.L.: An Investigation of short pitch wheel and rail corrugations on the Vancouver mass transit system. Proc. Inst. Mech. Eng. F. J. Rail Rapid Transit. **206**, 127–135 (1992). https://doi.org/10.1243/PIME_PROC_1992_206_226_02
10. Stock, R., Stanlake, L., Hardwick, C., Yu, M., Eadie, D., Lewis, R.: Material concepts for top of rail friction management—classification, characterisation and application. Wear **366–367**, 225–232 (2016). https://doi.org/10.1016/j.wear.2016.05.028
11. Harmon, M., Lewis, R.: Review of top of rail friction modifier tribology. Tribol. Mater. Surf. Interfaces **10**, 150–162 (2016). https://doi.org/10.1080/17515831.2016.1216265
12. Harmon, M., Santa, J.F., Jaramillo, J.A., Toro, A., Beagles, A., Lewis, R.: Evaluation of the coefficient of friction of rail in the field and laboratory using several devices. Tribol. Mater. Surf. Interfaces **14**, 119–129 (2020). https://doi.org/10.1080/17515831.2020.1712111
13. Moreno-Ríos, M., Gallardo-Hernández, E.A., Vite-Torres, M., Peña-Bautista, A.: Field and laboratory assessments of the friction coefficient at a railhead. Proc. Inst. Mech. Eng. F J. Rail Rapid Transit. **230**, 313–320 (2016). https://doi.org/10.1177/0954409714536383
14. Areiza, Y.A., Garcés, S.I., Santa, J.F., Vargas, G., Toro, A.: Field measurement of coefficient of friction in rails using a hand-pushed tribometer. Tribol. Int. **82**, 274–279 (2015). https://doi.org/10.1016/j.triboint.2014.08.009
15. Lundberg, J., Rantatalo, M., Wanhainen, C., Casselgren, J.: Measurements of friction coefficients between rails lubricated with a friction modifier and the wheels of an IORE locomotive during real working conditions. Wear **324–325**, 109–117 (2015). https://doi.org/10.1016/j.wear.2014.12.002
16. Eadie, D.T., Elvidge, D., Oldknow, K., Stock, R., Pointner, P., Kalousek, J., et al.: The effects of top of rail friction modifier on wear and rolling contact fatigue: full-scale rail–wheel test rig evaluation, analysis and modelling. Wear **265**, 1222–1230 (2008). https://doi.org/10.1016/j.wear.2008.02.029
17. Galas, R., Omasta, M., Krupka, I., Hartl, M.: Laboratory investigation of ability of oil-based friction modifiers to control adhesion at wheel-rail interface. Wear **368–369**, 230–238 (2016). https://doi.org/10.1016/j.wear.2016.09.015
18. Abbasi, S., Olofsson, U., Zhu, Y., Sellgren, U.: Pin-on-disc study of the effects of railway friction modifiers on airborne wear particles from wheel–rail contacts. Tribol. Int. **60**, 136–139 (2013). https://doi.org/10.1016/j.triboint.2012.11.013
19. Olofsson, U., Lyu, Y.: Open system tribology in the wheel–rail contact—a literature review. Appl. Mech. Rev., 69 (2017). https://doi.org/10.1115/1.4038229.
20. Wang, W.J., Shen, P., Song, J.H., Guo, J., Liu, Q.Y., Jin, X.S.: Experimental study on adhesion behavior of wheel/rail under dry and water conditions. Wear **271**, 2699–2705 (2011). https://doi.org/10.1016/j.wear.2011.01.070
21. Gallardo-Hernandez, E.A., Lewis, R.: Twin disc assessment of wheel/rail adhesion. Wear **265**, 1309–1316 (2008). https://doi.org/10.1016/j.wear.2008.03.020
22. Zhu, Y., Lyu, Y., Olofsson, U.: Mapping the friction between railway wheels and rails focusing on environmental conditions. Wear

324–325, 122–128 (2015). https://doi.org/10.1016/j.wear.2014.12.028
23. Chen, H., Ban, T., Ishida, M., Nakahara, T.: Experimental investigation of influential factors on adhesion between wheel and rail under wet conditions. Wear **265**, 1504–1511 (2008). https://doi.org/10.1016/j.wear.2008.02.034
24. Kempka, R., Falconer, R., Gutsulyak, D., Lewis, R.: Effects of oxide and water on friction of rail steel–new test method and friction mapping. Tribol. Mater. Surf. Interfaces **15**, 80–91 (2021). https://doi.org/10.1080/17515831.2020.1765611
25. White, B., Lewis, R.: Simulation and understanding the wet-rail phenomenon using twin disc testing. Tribol. Int. **136**, 475–486 (2019). https://doi.org/10.1016/j.triboint.2019.03.067
26. Lewis, S.R., Lewis, R., Olofsson, U., Eadie, D.T., Cotter, J., Lu, X.: Effect of humidity, temperature and railhead contamination on the performance of friction modifiers: Pin-on-disk study. Proc. Inst. Mech. Eng. F J. Rail Rapid Transit. **227**, 115–127 (2013). https://doi.org/10.1177/0954409712452239
27. Galas, R., Omasta, M., Shi, L., Ding, H., Wang, W., Krupka, I, et al.: The low adhesion problem: the effect of environmental conditions on adhesion in rolling-sliding contact. Tribol. Int. **151**, 106521 (2020). https://doi.org/10.1016/j.triboint.2020.106521.
28. Arias-Cuevas, O., Li, Z., Lewis, R., Gallardo-Hernández, E.A.: Rolling–sliding laboratory tests of friction modifiers in dry and wet wheel–rail contacts. Wear **268**, 543–551 (2010). https://doi.org/10.1016/j.wear.2009.09.015
29. Kvarda, D., Skurka, S., Galas, R., Omasta, M., Shi, L., Ding, H., et al.: The effect of top of rail lubricant composition on adhesion and rheological behaviour. Eng. Sci. Technol. Int. J. **35**, 101100 (2022). https://doi.org/10.1016/j.jestch.2022.101100
30. Galas, R., Kvarda, D., Omasta, M., Krupka, I., Hartl, M.: The role of constituents contained in water–based friction modifiers for top–of–rail application. Tribol. Int. **117**, 87–97 (2018). https://doi.org/10.1016/j.triboint.2017.08.019
31. Skurka, S., Galas, R., Omasta, M., Wu, B., Ding, H., Wang, W.J., et al.: The performance of top-of-rail products under water contamination. Tribol. Int. 188 (2023). https://doi.org/10.1016/j.triboint.2023.108872.
32. Wang, W.J., Zhang, H.F., Wang, H.Y., Liu, Q.Y., Zhu, M.H.: Study on the adhesion behavior of wheel/rail under oil, water and sanding conditions. Wear **271**, 2693–2698 (2011). https://doi.org/10.1016/j.wear.2010.12.019
33. Galas, R., Skurka, S., Valena, M., Kvarda, D., Omasta, M., Ding, H., et al.: A benchmarking methodology for top-of-rail products. Tribol. Int. **189**, 108910 (2023). https://doi.org/10.1016/j.triboint.2023.108910
34. Valena, M., Omasta, M., Kvarda, D., Galas, R., Krupka, I., Hartl, M.: An approach for the creep-curve assessment using a new rail tribometer. Tribol. Int. 191 (2024). https://doi.org/10.1016/j.triboint.2023.109153.
35. Kimura, Y., Okada, K.: Lubricating properties of oil-in-water emulsions. Tribol. Trans. **32**, 524–532 (1989). https://doi.org/10.1080/10402008908981921
36. Fujita, N., Kimura, Y., Kobayashi, K., Amanuma, Y., Sodani, Y.: Estimation model of plate-out oil film in high-speed tandem cold rolling. J. Mater. Process. Technol. **219**, 295–302 (2015). https://doi.org/10.1016/j.jmatprotec.2015.01.002
37. Nakahara, T., Makino, T., Kyogoku, K.: Observations of Liquid Droplet Behavior and Oil Film Formation in O/W Type Emulsion Lubrication. J. Tribol. **110**, 348–353 (1988). https://doi.org/10.1115/1.3261630
38. Wilson, W.R.D., Sakaguchi, Y., Schmid, S.R.: A dynamic concentration model for lubrication with oil-in-water emulsions. Wear **161**, 207–212 (1993). https://doi.org/10.1016/0043-1648(93)90471-W
39. Cyriac, F., Lugt, P.M., Bosman, R.: Impact of water on the rheology of lubricating greases. Tribol. Trans. **59**, 679–689 (2016). https://doi.org/10.1080/10402004.2015.1107929
40. Cann, P.M.E., Damiens, B., Lubrecht, A.A.: The transition between fully flooded and starved regimes in EHL. Tribol. Int. **37**, 859–864 (2004). https://doi.org/10.1016/j.triboint.2004.05.005
41. Jacod, B., Pubilier, F., Cann, P.M., Lubrecht, A.A.: An analysis of track replenishment mechanisms in the starved regime. In: Dowson, D. et al (eds) Lubrication at the frontier, tribology series, 36,. Elsevier, Amsterdam, pp 483–492 (1999). https://doi.org/10.1016/S0167-8922(99)80069-8.
42. Baek, K.S., Kyogoku, K., Nakahara, T.: An experimental investigation of transient traction characteristics in rolling-sliding wheel/rail contacts under dry-wet conditions. Wear **263**, 169–179 (2007). https://doi.org/10.1016/j.wear.2007.01.067
43. Shi, L.B., Ma, L., Guo, J., Liu, Q.Y., Zhou, Z.R., Wang, W.J.: Influence of low temperature environment on the adhesion characteristics of wheel-rail contact. Tribol. Int. **127**, 59–68 (2018). https://doi.org/10.1016/j.triboint.2018.05.037
44. Shen, M., Li, J., Li, L., Li, S., Ma, C.: Adhesion and damage behaviour of wheel-rail rolling–sliding contact suffering intermittent airflow with different humidities and ambient temperatures. Tribol. Lett. **72**, 18 (2024). https://doi.org/10.1007/s11249-023-01817-1
45. Lyu, Y., Zhu, Y., Olofsson, U.: Wear between wheel and rail: a pin-on-disc study of environmental conditions and iron oxides. Wear **328–329**, 277–285 (2015). https://doi.org/10.1016/j.wear.2015.02.057
46. Olofsson, U., Sundvall, K.: Influence of leaf, humidity and applied lubrication on friction in the wheel-rail contact: pin-on-disc experiments. Proc. Inst. Mech. Eng. F J. Rail Rapid Transit. **218**, 235–242 (2004). https://doi.org/10.1243/0954409042389364
47. Lewis, R., Christoforou, P., Wang, W.J., Beagles, A., Burstow, M., Lewis, S.R.: Investigation of the influence of rail hardness on the wear of rail and wheel materials under dry conditions (ICRI wear mapping project). Wear **430–431**, 383–392 (2019). https://doi.org/10.1016/j.wear.2019.05.030
48. Tyfour, W.R., Beynon, J.H., Kapoor, A.: The steady state wear behaviour of pearlitic rail steel under dry rolling-sliding contact conditions. Wear. **180**, 79–89 (1995).
49. Galas, R., Valena, M., Jordan, T., Kvarda, D., Omasta, M., Skurka, S., et al.: A benchmarking methodology for top-of-rail products: Carry distance and retentivity. Tribol. Int. **197**, 109810 (2024). https://doi.org/10.1016/j.triboint.2024.109810

Publisher's Note Springer Nature remains neutral with regard to jurisdictional claims in published maps and institutional affiliations.

Authors and Affiliations

Simon Skurka[1] · Radovan Galas[1] · Milan Omasta[1] · Haohao Ding[2] · Wen-Jian Wang[2] · Ivan Krupka[1] · Martin Hartl[1]

✉ Simon Skurka
Simon.Skurka@vut.cz

[1] Faculty of Mechanical Engineering, Brno University of Technology, Technicka 2896/2, 616 69 Brno, Czech Republic

[2] State Key Laboratory of Rail Transit Vehicle System, Tribology Research Institute, Southwest Jiaotong University, Chengdu 610031, China

Tribology International 189 (2023) 108910

Contents lists available at ScienceDirect

Tribology International

journal homepage: www.elsevier.com/locate/triboint

A benchmarking methodology for top-of-rail products

Radovan Galas [a,*], Simon Skurka [a], Martin Valena [a], Daniel Kvarda [a], Milan Omasta [a], Haohao Ding [b], Qiang Lin [b], Wen-jian Wang [b], Ivan Krupka [a], Martin Hartl [a]

[a] Faculty of Mechanical Engineering, Brno University of Technology, Technicka 2896/2, 616 69 Brno, Czech Republic
[b] Tribology Research Institute, State Key Laboratory of Traction Power, Southwest Jiaotong University, Chengdu 610031, China

ARTICLE INFO

Keywords:
Rail-wheel tribology
Rolling-sliding
Friction modifier
Top-of-rail lubricants

ABSTRACT

Top-of-rail (TOR) products are designed to optimize adhesion, reduce wear and mitigate noise from the wheel-rail interface. Prior to testing these products in field conditions, a laboratory approach is suitable because it is not time-consuming and expensive. This study aims to design a benchmarking methodology to investigate the performance of TOR products using a standard tribometer in a ball-on-disc configuration. The resulting methodology is based on a multi-parameter approach enabling the assessment of TOR products from multiple perspectives. The core of the methodology is formed by traction tests and a robust evaluation phase resulting in a performance map dividing TOR products into four performance classes, Q1-Q4, based on which a suitable TOR product can be chosen for further testing.

1. Introduction

TOR products represent a progressive approach to modification of friction between the wheel tread and the rail head. In contrast with other conventional methods, such as sanding and flange lubrication, TOR products are designed to control friction at a desired level, referred to as an intermediate level of friction [1]. Besides that, the presence of TOR product in the contact should avoid a negative slope of the creep curve occurring in untreated contact [2]. According to the state of matter, TOR products are classified into solid and liquid. Solid TOR products are usually called “solid sticks” or “HPF solid sticks”, while there are different, sometimes confusing, terms for liquid products. Water-based products (drying products) are called friction modifiers (FMs), while oil- or grease-based products (non-drying products) are called TOR lubricants (TORLs). There is also a third category of TOR products containing both water and oil/grease. These products are called TOR hybrids [1,2].

The possible benefits of TOR products have been intensively studied since 1992, when Kalousek et al. [3] published a pilot study on railway friction management. This study was conducted on the Vancouver mass transit system line, where severe short pitch wheel and rail corrugation developed only a few months after its opening. This investigation showed that applying a solid stick to the wheel tread prevented corrugation formation as roll-slip oscillations were eliminated due to a positive creep curve. The ability to reduce or completely avoid the corrugation growth for different mass transit systems was later confirmed for FMs [4–7]. Other field studies [7–11] showed that suppression of roll-slip oscillations via solid or liquid TOR products reduced curve squeal noise. Moreover, these studies clarified the benefits of TOR products for several transit systems that differ in curve radii, track structures and track conditions. Besides this, it was shown that reducing the coefficient of traction (CoT) to the intermediate level brings other benefits, such as saving fuel consumption [12], reducing the risk of derailment [13,14], and no risk of isolation of track circuits [15] as can occur for sanding [16].

Although field studies have proved many benefits of TOR products, some negative effects related to their application have been revealed as well. One of the most severe drawbacks is the risk of a very low CoT compromising traction and braking. This undesirable phenomenon was observed for both FM [17] and TOR lubricants [18–20]. FMs may cause a very low CoT immediately after their application when a high amount of FM enters the contact [21]. In addition, a significant drop in the CoT was observed during the drying of FM when a viscous film was formed between the contacting surfaces [22]. In the case of TOR lubricants as oil or grease-based products, the applied amount strongly affects product performance [23,24]. A high amount of these non-drying products (TORLs and TORHs) in the contact can lead to the extension of braking distance and can promote the growth of pre-existing cracks and spalling formation [19,25]. Besides these security risks, recently published studies [26–28] showed that the expected benefits of TOR products, such as squeal noise reduction and long carry distance, cannot be

* Corresponding author.
E-mail address: Radovan.Galas@vut.cz (R. Galas).

https://doi.org/10.1016/j.triboint.2023.108910
Received 3 May 2023; Received in revised form 25 July 2023; Accepted 28 August 2023
Available online 29 August 2023
0301-679X/© 2023 Elsevier Ltd. All rights reserved.

Nomenclature

CTZ	critical traction zone
FM	friction modifier
HPF	high positive friction
ITZ	intermediate traction zone
LTZ	low traction zone
MTM	mini-traction machine
PT, PT_1-PT_5	performance test
Q1-Q4	performance classes
RCF	rolling contact fatigue
RTZ	retentivity traction zone
S1-S6	steps of the experimental phase
S7-S9	steps of the evaluation phase
TOR	top-of-rail
TORP	model TOR product
TORL	TOR lubricant
c, c_1-c_5	critical traction parameter for individual PT (m)
C	average critical traction parameter (m)
CoT	coefficient of traction (1)
F_N	normal force (N)
F_T	traction force (N)
i, i_1-i_5	intermediate traction parameter for individual PT (m)
I	average intermediate traction parameter (m)
j	index representing different values of SRR (1)
k	index representing the number of PT (1)
n, n_1-n_5	number of creep curves within individual PT (1)
N	average number of creep curves for five PTs (1)
$N_{c,j}$, N_{c1}- N_{c5}	number of points of the creep curve(s) for a specific SRR in the CTZ (1)
$N_{i,j}$, N_{i1}- N_{i5}	number of points of the creep curve(s) for a specific SRR in the ITZ (1)
$N_{r,j}$, N_{r1}- N_{r5}	number of points of the creep curve(s) for a specific SRR in the RTZ (1)
OLF	over-lubrication factor (1)
r, r_1-r_5	retentivity for individual PT (m)
r_b	ball radius (m)
r_d	disc radius (m)
R	average retentivity (m)
Sa	average Roughness (m)
S_i	area defining the ideal product (m^2)
S_p	area defining the tested TOR product (m^2)
Sq	root mean square roughness (m)
SRR	slide/roll ratio (1)
t	duration of friction test (s)
t_r	duration of the run-in process (s)
t_w	duration of the wear-in process (s)
v	mean speed (m/s)
w	disc path width (m)
ω_b	ball angular speed (1/s)
ω_d	disc angular speed (1/s)

achieved.

These negative findings indicate that several aspects should be considered before implementing the friction modification method into real operation. One of the most important aspects is the purpose for which the TOR product is used. This factor should be considered together with the type of transit system because the performance of the same product may substantially vary for different systems. Another aspect relates to the application strategy that covers application amount, application interval, and application method. Two methods are currently used to apply TOR products: wayside units along the tracks and on-board vehicle units. Moreover, both methods enable applying TOR products on one or both wheels/rails.

It is evident that the successful implementation of friction management methods into operation involves many aspects that should be considered beforehand. Then, however, the question arises: How to choose a suitable product and its application strategy? One of the options represents field tests that provide reliable results but are costly and time-consuming. Therefore, this approach seems reasonable as a final step of testing. In contrast, laboratory tests seem suitable for comparing different TOR products in different aspects. These tests are inexpensive, time-saving, and usually can be performed under well-controlled conditions, which are difficult to achieve for field tests.

Several experimental approaches have been used to study TOR products in laboratory conditions. Full-scale devices were used to investigate the effect of TOR products on wear, rolling contact fatigue (RCF) [29,30] and bogie-curving performance [31]. In the case of small-scale devices, several types of devices were utilised to study TOR products: pin-on-disc tribometer [32,33], ball-on-disc tribometer [22,24,34], twin-disc machine [19,35–40], plate-on-plate tribometer [41], high-pressure torsion (HPT) tribometer [23,42], pendulum tester [43,44] and hand-push tribometer [44,45]. Note that the latter two approaches are mainly used in field measurements; thus, they can represent an intermediate step between operational and laboratory tests. This literature review showed that the adhesion/friction/traction level, retentivity, and creep curve are the most frequently evaluated parameters to assess the performance of TOR products in laboratory conditions. However, comparing the results across these studies is difficult, sometimes even impossible, because most studies on TOR products utilise non-commercial devices. It means that the contact bodies differ in many aspects, such as size, material, hardness, roughness, etc. Furthermore, the test procedure and parameters can also vary significantly, which further complicates the comparison of results. Based on these findings, it is clear that a unified testing methodology is required to standardize the design and assessment of TOR products under laboratory conditions. Recently published standard no. CEN/TS 15427–2–2:2021 [46] partially deals with this topic for a twin-disc machine and a Mini-Traction machine (MTM). This standard defines two types of tests for twin-disc machines whose result is product retentivity, CoT, and the creep curve. In addition, the test for creep curve investigation is described for MTM. This approach to determining product suitability relies on a single, basic criterion that provides limited insight into the product's behaviour, indicating a need for a more comprehensive testing methodology that can assess TOR products from multiple perspectives.

This study proposes a benchmarking methodology for assessing the performance of various TOR products under rolling-sliding conditions. A standard MTM tribometer in a ball-on-disc configuration was employed to ensure the future transferability and comparability of the results across different laboratories. A robust evaluation phase is an integral part of the comparative test methodology to ensure clarity of the assessment. This approach enables the complex assessment of TOR products from multiple perspectives and improves the reliability and accuracy of TOR product testing. In order to validate the proposed benchmarking methodology, the performance of three TOR products and one bleed oil (the oil separated from the TOR product) is tested and compared within the case study.

2. Material and methods

2.1. Introduction to the methodology development process

The methodology presented in this paper is based on the following assumptions:

I. **Single device:** A single widely used device is utilized to assess TOR products from various perspectives.
II. **Multi-parametric approach:** The product assessment is based on a combination of several important parameters of TOR products:
   - o Retentivity: time, number of cycles or sliding distance for which the product influences the CoT.
   - o Performance parameters: Parameters that express the duration for which a TOR product causes insufficient CoT level and the duration for which it provides a desired intermediate CoT level. These parameters are expressed as a function of sliding distance.
   - o These parameters are considered together to provide a single parameter expressing the product's relative performance.
III. **Traction zones:** Several zones of CoT, defined as a fixed ratio to the baseline (dry) CoT, are used to cover the changing CoT from product application until the moment when its effect is negligible.
IV. **Variable creep:** Benchmarking performance tests are done under different creep to assess product behaviour in different regions on the creep curve (CoT-SRR dependency).
V. **Amount dependence:** Some TOR products, especially oil- and grease-based, are strongly amount-dependent. It is not possible to compare the products regardless of the applied amount. This means that one product may perform better at a specific amount while another product may perform better at a different amount. A final assessment should clearly show which of the tested amount is appropriate for the tested TOR products and identify the TOR product that has the best potential for further testing using full-scale devices or in the field.
VI. **Run-in/wear-in process:** These processes were established specifically to provide the same initial state for all tests and to avoid excessive wear that negatively affects test repeatability.
VII. **Consecutive tests using the same specimens:** A number of consecutive tests are required to cover the variability of the results and gradual changes in the surface topography of the specimens.

2.2. Instruments and specimens

The MTM tribometer in a ball-on-disc configuration was used to develop and validate a benchmarking methodology for assessing TOR products. This tribometer was chosen because it simulates rolling-sliding conditions, similar to the real wheel-rail contact, and is widely used for tribological testing, including the above-mentioned CEN/TS standard [46]. The MTM tribometer and its scheme are depicted in Fig. 1. This configuration consists of a steel ball and a steel disc leading to non-conformal point contact. Both these standard specimens are independently driven; thus, desired slide/roll ratio (SRR) can be set. The SRR value is calculated according to Eq. (1), where ω_b and ω_d are the angular speeds of the ball and the disc, and r_b and r_d represent their radii. To investigate the CoT (Eq. (2)) the tribometer is equipped with load and traction sensors providing information about the normal force F_N and the traction force F_T. Detailed information about the specimens and sensors is listed in Table 1 and Appendix A, respectively.

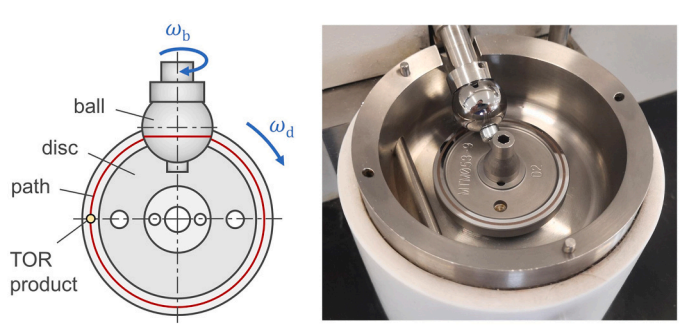

Fig. 1. MTM in ball-on-disc configuration.

$$\mathrm{SRR} = \frac{\omega_b \cdot r_b - \omega_d \cdot r_d}{\omega_b \cdot r_b + \omega_d \cdot r_d} \cdot 200\% \tag{1}$$

$$\mathrm{CoT} = \frac{F_T}{F_N} \tag{2}$$

2.3. Initial tests: methodology input parameters investigation

Several parameters had to be investigated as input parameters to the proposed methodology. These input parameters included: (1) the duration of the wear-in process, (2) the duration of the run-in process, (3) the creep curve for dry conditions (baseline), and (4) the traction zones and threshold curve. These input parameters are an integral part of the methodology, and the initial tests to investigate them are described in this Subchapter, while the proposed methodology is presented in Subchapter 2.4.

Two sets of tests were conducted under dry conditions to investigate the required input parameters. The experimental conditions of these initial tests are described in Table 2. This table shows that all tests were performed with a load of 18 N, corresponding to a maximum Hertzian pressure of 800 MPa. A mean speed was chosen to be 1 m/s because this value is frequently used for tribological testing on small-scale devices [38,39,47]. This relatively low speed was used because of the device limitation and the stability of tests. According to [48], a speed of 1 m/s on MTM corresponds to a higher train speed (tens of km/h) based on comparing the lambda parameter between MTM and the train.

Set no. 1 in Table 2 aimed to find a suitable duration of the wear-in and run-in process. The wear-in process is always performed when new contact pair is used to overcome excessive wear occurring when new bodies come into contact. In contrast, the run-in process is designed to stabilize the CoT and the surface roughness of worn contact pairs that were already used for TOR product testing. Suitable durations of wear-in process t_w and run-in process t_r were investigated based on the 20 consecutive 30-minute friction tests (CoT-time dependency) under dry conditions (600 min in total), see Table 2. All these friction tests were carried out at 2% SRR, which is a representative value for real wheel-rail contact. After each friction test, both specimens were cleaned in a solvent, and then the surface roughness (Sq and Sa) and the width of the contact path w were analysed for both contact specimens using an optical profilometer. The required time for the wear-in process t_w was chosen based on the evolution of the path width over time. The aim was to select a time at which excessive wear had already occurred. It means that the contact path became more stable for subsequent testing with TOR products. In the case of the run-in process, the required time t_r was chosen as the time needed to stabilise the CoT during the 20 friction tests mentioned above.

Set no. 2 in Table 2 was performed to investigate a creep curve (baseline) for dry conditions. This baseline was subsequently used as a reference curve to design the traction zones and the threshold curve, which are important for the evaluation phase of the proposed methodology (described below). While the maximum Hertzian pressure and mean speed of this set are consistent with set no. 1, SRR varied from 0% to 20%. However, there are two ranges of SRR listed in Table 2. Initially, a range of SRR from 0% to 50% was tested, but it was revealed that SRR values higher than 20% might not be appropriate for testing TOR products. The reason for this SRR limitation is described in the

Table 1
Detailed information about MTM specimens.

	diameter (mm)	material	hardness (HV)	roughness (μm)
ball	19.05	AISI 52100	800 – 920	0.01
disc	46		720 – 780	0.01

Table 2
Experimental conditions of initial tests: friction and traction tests.

set no.	conditions	Hertzian pressure	mean speed	SRR (%)	test duration	measured parameters	evaluated parameters	Fig. No.
1	dry (no TOR product)	800 MPa	1 m/s	2%	20 × 30 min	CoT, *Sq*, *w*	t_w, t_r	6
2				0–20% (0–50%)	6x (8 ×25 s)[a]	CoT	traction zones and threshold	7

[a] 60-minute wear-in process was carried out before this test.

discussion. Therefore, the SRR range was limited to 0–20% (specifically: 0%, 2%, 5%, 10%, 15%, and 20%) for all other tests in this study. As noted in Table 2, the creep curve for dry conditions was measured six times consecutively. These creep curves were obtained based on the series of friction tests (CoT-time dependency). Finally, the average baseline was determined.

The next step was to design the threshold curve and the traction zones. While the threshold curve is important for the measurement phase, the traction zones play a crucial role in the evaluation phase, see Fig. 3. As shown in Fig. 2, the following four traction zones have been defined for the proposed methodology: critical traction zone (CTZ), low traction zone (LTZ), intermediate traction tone (ITZ), and retentivity traction zone (RTZ).

The CTZ is marked in red because it represents a zone with very low CoT that may not provide enough traction and braking capability for vehicles. In contrast, the ITZ (the green zone) represents the range of CoT optimal for traction and braking while reducing significant wear occurring under dry conditions (baseline). As evident from Fig. 2, there is another zone labelled as the LTZ. The CoT values in the LTZ are no longer critical for traction and braking but are not optimal. The presence of this zone between CTZ and ITZ is meaningful because it prevents a sudden transition between critical CoT values and optimal ones. Moreover, this "transition" zone between CTZ and ITZ is commonly considered in the literature [30,49].

The last zone is the RTZ, which is important for evaluating the so-called retentivity parameter. This parameter is usually defined as the interval from product application until the product becomes ineffective regarding expected benefits [46]. Note that this parameter is typically expressed in the number of cycles. Based on its value, different TOR products can be compared in terms of expected carry distance representing one of the key parameters assessed in TOR products [46]. The carry distance defines how far the product is spread in real operation.

Considering the above, the RTZ is defined by zero at the lower boundary and by the upper limit of the ITZ at the upper boundary, as shown in Fig. 2. This upper limit of ITZ and RTZ is simultaneously considered as a threshold value for stopping the performance test (PT, described below) because, beyond this limit, the behaviour of the contact becomes similar to that of dry contact. In other words, the effect of TOR products becomes negligible beyond this limit.

The traction zones mentioned above have been defined as percentage values of the baseline, see Fig. 2. The percentage values were chosen according to [50,51], where the dry level of friction was considered 0.6,

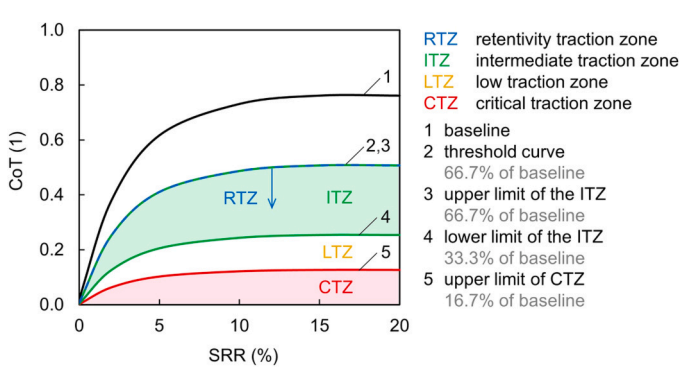

Fig. 2. Baseline, traction zones and threshold curve.

and the intermediate and low friction levels were 0.2–0.4 and 0.1, respectively. With respect to these values, the lower and upper intermediate limits were calculated to be 33.3% and 66.7% of the dry CoT. The limit value of a critical traction zone (CTZ) was 16.7% of the dry CoT.

Note that the specific values on the y-axis in Fig. 2 were obtained from the initial tests conducted under dry conditions (set no. 2 according to Table 2). Detailed descriptions of these test results can be found in Subchapter 3.1. This subchapter includes not only information about traction zones and the threshold curve but also describes other important input parameters for the proposed methodology, specifically the duration of the wear-in and run-in process. Once these parameters were determined in Subchapter 3.1, they were used as fixed values for all subsequent tests with TOR products described in Subchapter 3.2.

2.4. The proposed methodology and its steps

Fig. 3 provides a schematic representation of the proposed benchmarking methodology. The methodology consists of the experimental and evaluation phases, as shown in Fig. 3(a) and (b). The experimental phase includes five consecutive PTs (PT1-PT5), which are required to investigate the performance of one TOR product for one specific applied amount. It is important to note that all five PTs are carried out using the same contact pair. It means that the initial conditions (such as the path width, roughness, pressure, etc.) are not the same for individual PTs due to wear from the previous PT(s). This approach is beneficial because it enables the investigation of the performance of TOR products under a wide range of conditions, and the resulting product assessment is thus more representative.

Each of the five PTs is composed of a preparation phase (indicated by blue colour) and the measurement phase (indicated by red colour), as shown in Fig. 3(a). These two phases comprise six consecutive steps (S1-S6), but only step S4 (traction test) is considered as the measurement step. In this step (S4), The CoT is measured for six SRR values ranging from 0% to 20% (the detailed test procedure is described below). The result of this traction test is plotted to form the creep curve, as depicted in Fig. 4. This figure provides a detailed view of steps S4 and S5. Once the traction test S4 is completed and the creep curve is obtained, checkpoint S5 must be performed. Depending on the result of checkpoint S5, the PT continues by S6 or is finished, and another PT can start by S1. If PT continues, more creep curves are obtained within one PT. It indicates that several creep curves can be obtained during one PT, as in the example in Fig. 4 – step S5, where three creep curves are obtained before checkpoint S5 is met. This procedure is repeated until the fifth PT is completed.

As was mentioned in the previous paragraph, the experimental phase is completed after the fifth PT. Subsequently, the evaluation phase begins with step S7, as illustrated in Fig. 3(b). It should be emphasized that the traction zones depicted in Fig. 2 are crucial for the first evaluation step (S7). This step focuses on the calculation of the performance parameters noted in Table 3.

At first, three performance parameters denoted with lowercase letters (c, i, and r) are evaluated for each PT. As evident from Table 3, each of these parameters is named according to the related traction zone (CTZ, ITZ, and RTZ). These parameters are calculated as the cumulative sliding distance over which the contact was operating in the related traction zone. It means that a total of fifteen parameters (c_1-c_5, i_1-i_5, and

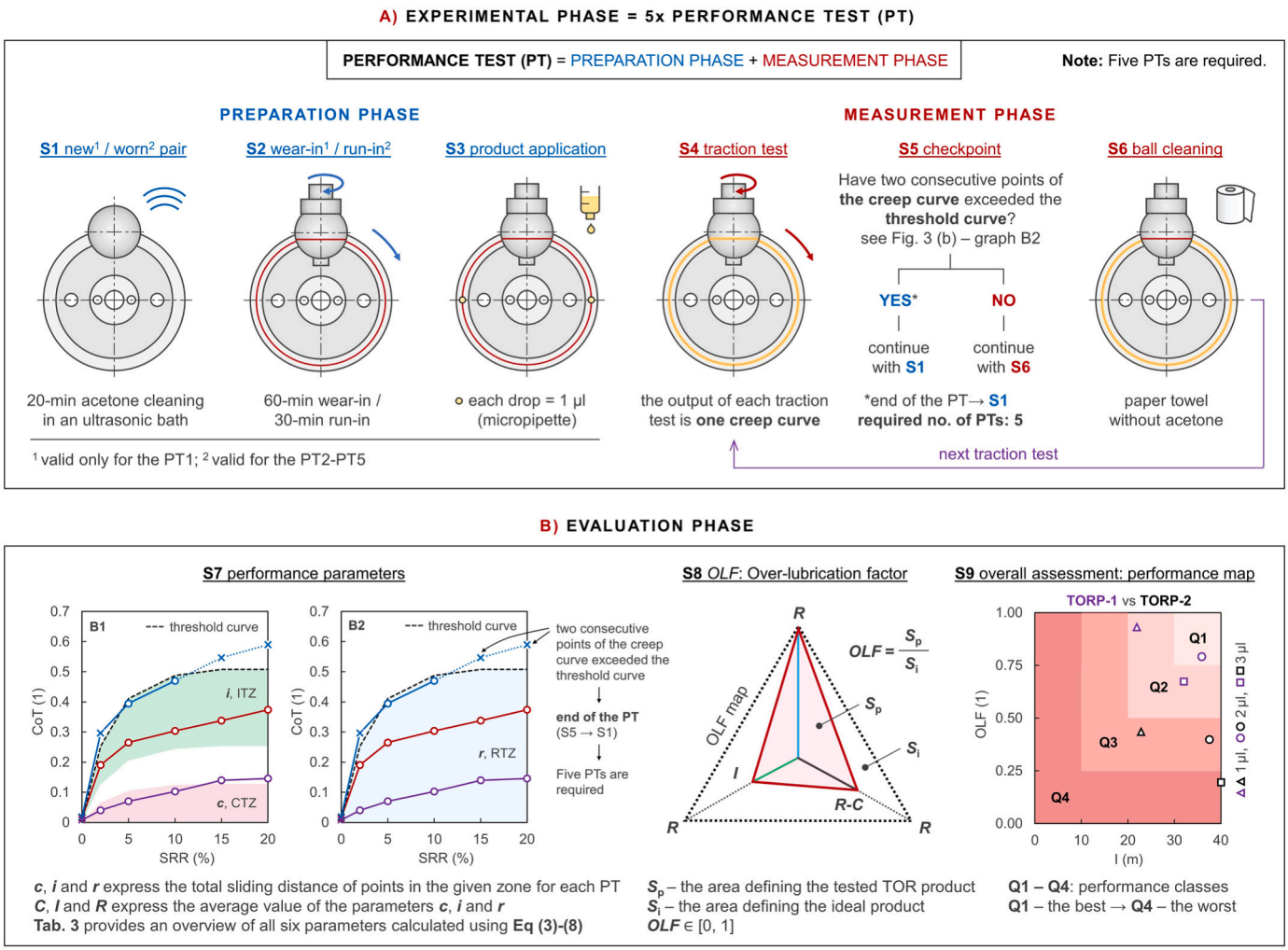

Fig. 3. A benchmarking methodology for assessing the performance of TOR products: (a) experimental phase and (b) evaluation phase.

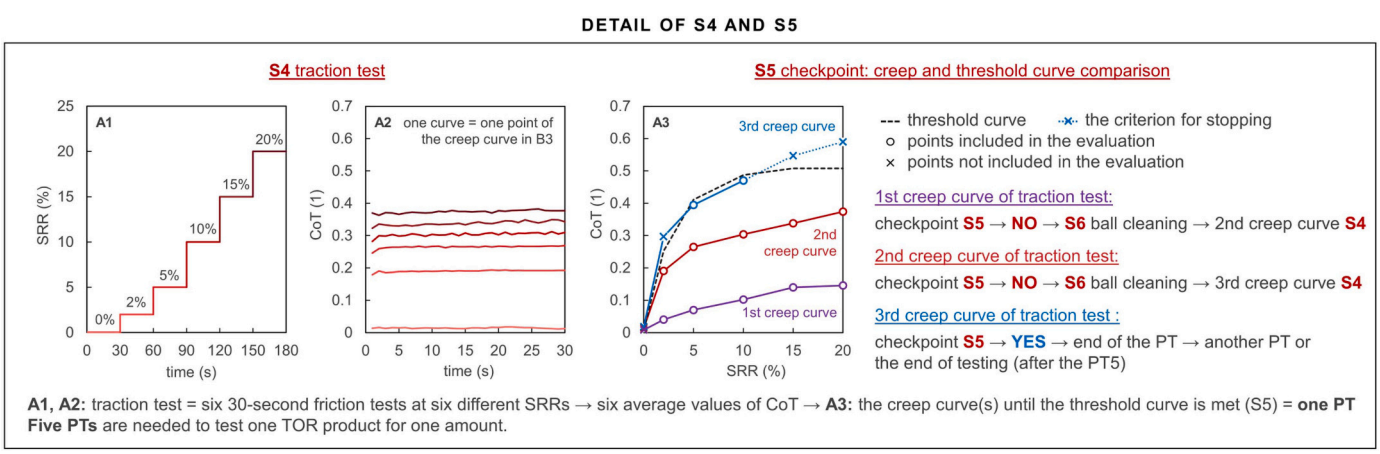

Fig. 4. Detailed information about methodology steps S4 and S5.

r_1-r_5) are obtained for the five required PTs. Subsequently, these sets of parameters are used to determine the average performance parameters denoted by capital letters (C, I, and R). A more detailed description of the parameter calculations is provided below.

Individual PT test parameters (c, i, and r) are calculated according to Eqs. (3)–(5), where index k represents the number of PTs ($k = 1$–5). Note that it is necessary to know the values of the traction zones to calculate these parameters. As noted earlier, each performance parameter expresses the cumulative sliding distance over which the contact was operating in the related traction zone. It is important to emphasize that the sliding distance is calculated as cumulative, using the sum, because the individual points of the creep curve are measured for different SRRs. Each of these individual points of the creep curve is determined based on a 30-second friction test (CoT-time dependency, see Fig. 4); thus, the

Table 3
Overview of the performance parameters evaluated in step S7.

	symbol	related traction zone	related Eq. no.
Critical traction parameter	c, (c_1-c_5)	CTZ	3
Intermediate traction parameter	i, (i_1-i_5)	ITZ	4
Retentivity	r, (r_1-r_5)	RTZ	5
Average critical traction parameter	C	CTZ	6
Average intermediate traction parameter	I	ITZ	7
Average retentivity	R	RTZ	8

time t in Eqs. (3)–(5) is equal to 30 s and remains constant. In addition, the velocity $v = 1$ m/s also remains constant for calculating all parameters.

On the contrary, each point of the creep curve is measured for different SRR values; therefore, a summation with an index j is included in the equations. This index describes the variation in SRR during the measurement of individual points (friction tests) of the creep curves. The index j ranges from 1 to 5, corresponding to the SRR values in the table in Fig. 5. Note that an SRR of 0% is not included in the calculation because the sliding distance equals zero for this SRR value (pure rolling conditions).

The last parameters in Eq. (3)-(5), $N_{c,j}$, $N_{i,j}$, $N_{r,j}$, represent the number of points of the creep curve(s) (obtained for one PT) within a given traction zone and at a given SRR. In other words, the first character of the index determines from which traction zone the points of the creep curve(s) are selected, while the second character further narrows down the selection of points based on the desired SRR value. This desired SRR value ranges from 2% to 20%, as defined by the summation index j and table in Fig. 5.

Fig. 5 provides an example of how $N_{c,1}$-$N_{c,5}$ can be determined. For simplicity, Fig. 5 depicts only one traction zone (CTZ) and two creep curves. The red points represent the points belonging to the related traction zone (CTZ, based on the first character of the index). If the second character of the index equals "3", for example, then only the points corresponding to a 10% SRR are counted, resulting in $N_{c,3} = 2$. The same procedure also applies to ITZ and RTZ.

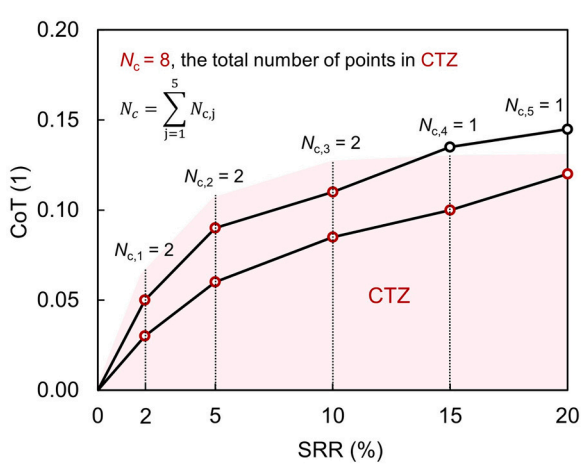

j_1	j_2	j_3	j_4	j_5
$N_{c,1}$	$N_{c,2}$	$N_{c,3}$	$N_{c,4}$	$N_{c,5}$
SRR_1	SRR_2	SRR_3	SRR_4	SRR_5
0.02	0.05	0.10	0.15	0.20

Fig. 5. Example illustrating the determination of $N_{c,j}$ points.

$$c_k = \sum_{j=1}^{5} t \cdot v \cdot SRR_j \cdot N_{c,j} \tag{3}$$

$$i_k = \sum_{j=1}^{5} t \cdot v \cdot SRR_j \cdot N_{i,j} \tag{4}$$

$$r_k = \sum_{j=1}^{5} t \cdot v \cdot SRR_j \cdot N_{r,j} \tag{5}$$

When the performance parameters are evaluated for each PT, three sets of parameters are obtained: c_1-c_5, i_1-i_5, and r_1-r_5. These sets are subsequently used to calculate the average performance parameters C, I, and R using Eqs. (6)-(8).

$$C = \frac{1}{5} \sum_{k=1}^{5} c_k \tag{6}$$

$$I = \frac{1}{5} \sum_{k=1}^{5} i_k \tag{7}$$

$$R = \frac{1}{5} \sum_{k=1}^{5} r_k \tag{8}$$

When S7 is completed, performance parameters C, I, and R are used to assess the overall performance of TOR products. The overall performance is based on two parameters. The first one is the average intermediate traction parameter I described above. This parameter is crucial because it expresses the average sliding distance over which the TOR product provides the desired intermediate level of CoT. As the second parameter, the aim was to use a parameter that would not only indicate whether a tested TOR product may be risky in terms of low (LTZ) and critical CoT (CTZ) but also quantify the degree of this risk. For this purpose, an Over-Lubrication Factor (OLF) was defined. As can be seen in see Fig. 3(b) – step S9 and Eq. (9), the OLF is defined as the ratio of the triangle area of the tested TOR product S_p (the red triangle) to the area of the ideal product S_i (the black dotted triangle).

$$OLF = \frac{S_p}{S_i} = \frac{R \cdot I + R \cdot (R - C) + I \cdot (R - C)}{3 \cdot R^2} \tag{9}$$

The pair of triangles in Fig. 3(b) is further referred to as the OLF map. Note that the OLF ranges between 0 and 1 depending on the values of the average performance parameters C, I, and R. It means that the calculation of the OLF includes data from all proposed traction zones, including the LTZ. Although the LTZ does not have a corresponding average performance parameter, its data are included in the RTZ, contributing to the parameter R. It should be pointed out that the angles between the directions in which the parameters of triangles are plotted are 120°.

Fig. 3 shows that the triangle representing the tested product is defined by the following vertices: R, R-C, and I. The vertex R was chosen because it directly represents the retentivity of the tested product. The second vertex is defined as the difference between R and C. This vertex ensures that with an increase in the "undesirable" parameter C, the triangle size decreases, resulting in a lower OLF value. The last vertex is defined by the average performance parameter I expressing the sliding distance over which the product provides the desired intermediate level of CoT. As evident from Fig. 3(b) – S8, this red triangle is compared with the black triangle defining the ideal product. This black triangle is drawn solely based on the parameter R (all vertices). The term "ideal" is used because $C = 0$ and $R = I$, which means that the product provides only the desired intermediate level of CoT (all points of creep curves lie within the ITZ, $R = I$) without any risk of low and critical CoT ($C = 0$).

Because OLF is defined as the ratio of the above-described triangles, the OLF value represents the deviation of the test TOR product's performance from the ideal product's performance. The closer the OLF

value is to 1, the better the behaviour of the TOR product can be expected in real operation. In contrast, lower OLF values indicate a risk of over-lubrication, which may lead to traction and braking issues. Once the OLF is calculated, the overall performance of the tested TOR product can be evaluated by considering both the OLF and parameter *I*.

The overall assessment is built on the I-OLF map defined in this study. This map represents the final step of the proposed methodology, Fig. 3(b) – step S9. This I-OLF map, further referred to as a "performance map", is plotted to compare the performance of different TOR products under varying applied amounts. An example of this performance map is in Fig. 3(b) – step S9, where the performances of two model TOR products (TORP-1 and TORP-2) are plotted for three different amounts. These different amounts are represented using different shapes of data points/markers.

When the performance map is plotted, the graph is divided into four equidistantly ranked performance classes/quartiles Q1-Q4, ranked from the best to the worst. If the tested TOR product reaches group Q1, it shows its ability to provide a long effective carry distance without a high risk of over-lubrication. Note that the effective carry distance is defined as the carry distance where the CoT lies within the intermediate traction zone. Compared to the Q1 class, reaching the Q4 class for the TOR product is likely to result in a significantly shorter effective carry distance and/or a higher risk of over-lubrication. Using these four performance classes makes it possible to compare and select the optimal TOR product and its amount for further testing. It should be noted that the y-axis range (OLF) is fixed from 0 to 1, representing absolute categorization. In contrast, the x-axis is relative, as the best tested TOR product (in terms of the parameter *I*) determines its range. However, it should be noted that future studies should set the x-axis range based on the best-performing TOR product obtained so far. If not, the classification of products into classes Q1-Q4 may be significantly affected.

The individual steps of the proposed methodology are summarized in the following points:

- S1 new/worn pair: Cleaning the specimens in a solvent ultrasonic bath for 20 min to remove any preservative oil (for the new pair) or TOR product residue (for the already used pair).
- S2 wear-in/run-in process: The wear-in process is performed only before the first PT when the new pair is used. The run-in process is performed instead of the wear-in process for the second and subsequent PTs. The wear-in and run-in process duration is 60 and 30 min, respectively.

Note: These durations represent the input parameters investigated during the initial tests (set no. 1 in Table 2). These tests and their results are described in the following chapter.

- S3 product application: All tested products are applied to the disc path using an electronic micropipette with a tip volume of 0.1 ml. This configuration allowed for the maintenance of systematic and random errors below ± 1.6% and ± 2.5%, respectively, while also ensuring a minimum dosage of 1 μl. Note that an application jig can be employed with the micropipette to increase the accuracy of the product application. All applications are made at zero speed of samples immediately after finishing the wear-in/run-in process. As depicted in Fig. 3(a) – step S3, the lubricant dose is split into a series of 1 μl drops, which are distributed evenly around the circumference of the contact path to achieve uniform application.
- S4 traction test: Each traction test includes six 30-second friction tests (CoT-time dependency at a specific SRR). Fig. 4 shows that each of these 30-second friction tests is conducted at a different specific SRR value, ranging from 0% to 20%. These tests result in six friction curves for six different SRR values describing the evolutions of the CoT over time, see Fig. 4 – graph A2. Based on these friction curves, six average values of CoT are calculated for each tested SRR. These average values of CoT are used to plot a single creep curve, see Fig. 4 – graph A3. When the creep curve is completed, checkpoint S5 must follow.
- S5 checkpoint: An obtained creep curve from S4 is compared with the threshold curve (depicted in Fig. 2 and described in detail below), and the following criterion is checked: "Have two consecutive points of the creep curve exceeded the threshold curve?" Please note that it requires two consecutive points on a single creep curve, as depicted in Fig. 3(b) – graph B2. As a result of checkpoint S5, there are two following possibilities:

  - o NO (the criterion has not been met): No two consecutive CoT points on a single creep curve exceeded the threshold curve (e.g. purple and red creep curves in Fig. 4 – graph A3). In this case, the PT continues at step S6.
  - o YES (the criterion has been met): Two or more consecutive CoT points on a single creep exceeded the threshold curve (e.g. blue curve in Fig. 4 – graph A3). After that, another PT should begin with step S1 if the fifth traction test has not been completed yet.

- S6 ball cleaning: When the traction test S4 has been completed, and criterion S5 has not been met, the ball path is cleaned with a paper towel without solvents. The subsequent traction test S4 begins after this cleaning, as indicated by the purple arrow in Fig. 3(a). This cycle of steps S4 and S6 is repeated until criterion S5 is met. Note that there are two reasons for ball cleaning. Firstly, the cleaning decreases the amount of TOR product in the contact path, which leads to the shortening of the traction test. This shortening helps avoid the undesired smoothing effect described in the Discussion. This aspect is important because it enables testing larger applied amounts of TOR products without the risk of smoothing. The second reason is to simulate a situation in the field where a product covers only one surface, and the second is "fresh" without any TOR product. White et al. [49] used a similar cleaning approach where the retentivity of traction gels was studied.
- S7 performance parameters: Based on the results of PTs and designed traction zones, the *c*, *i*, and *r* parameters are calculated according to Eqs. (3)–(5) for each PT. Subsequently, the average performance parameters *C*, *I*, and *R* are evaluated using Eqs. (6)-(8).
- S8 OLF: The average performance parameters are plugged into Eq. (9) to calculate the OLF.
- S9 performance map: This map is drawn based on the OLF and the parameter *I*, where each point on the map corresponds to the performance of the TOR product at a specific tested amount. This approach enables a comprehensive comparison of the performance of TOR products for various amounts.

2.5. Case study

The proposed methodology was verified using a case study where two TOR lubricants (TORL-A and TORL-B) and one FM were tested for different amounts. It should be pointed out that FM was tested for both wet and dry conditions (the terms wet-FM and dry-FM are used below) to describe the possible change in its performance due to the evaporation of the base medium. In addition, the performance of TORL-A bleed oil was investigated for two amounts to show the difference between the behaviour of TORL and bleed oil. The experimental conditions of this case study are listed in Table 4. Note that the maximum Hertzian pressure, mean speed, and SRR range were the same as in the initial tests described in Subchapter 2.4.

3. Results

3.1. Results of the initial tests

Fig. 6 shows the results of set no. 1 according to Table 2, which aimed to find necessary methodology input parameters. These input

Table 4
Experimental conditions of the case study: traction tests.

set no.	TOR product	applied amount	Hertzian pressure	mean speed	SRR	test duration	measured param.	evaluated param.	Fig. No.
3	wet-FM	1, 2, 3, 12 µl	800 MPa	1 m/s	0–20%	to threshold value[1]	*CoT*	*5x (c, i, r),*	8, 10
4	dry-FM	12 µl						*C, I, R*	8, 10
5	TORL-A	1, 2, 3, 5 µl						*OLF*	9, 10
6	TORL-B	1, 2, 3 µl							9, 10
7	TORL-A	1, 3 µl							10
	bleed oil								
	overview of all results using the performance map of TOR products								11

[1] 60-minute wear-in process was carried out before the application of the TOR product.

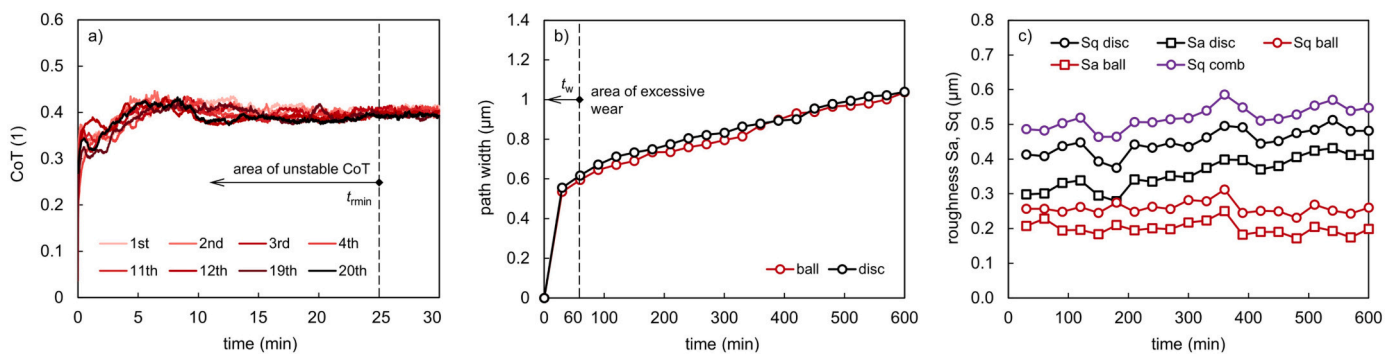

Fig. 6. The results of initial tests under dry conditions (set no. 1 according to Table 2): (a) the examples of friction tests, (b) the development of the ball and disc path during twenty consecutive friction tests, (c) the evaluation of disc and ball roughness during twenty consecutive friction tests.

parameters included the time needed for the run-in and wear-in process, which were determined based on twenty consecutive friction tests (CoT-time dependency) that were measured for various SRRs. Examples of these friction tests are depicted in Fig. 6(a), where only eight curves are drawn for clarity. These curves indicate that the CoT is unstable in the first hundreds of seconds and becomes stable after approximately 1 500 s. Therefore, a time of 1 800 s (t_r =30 min) was finally chosen as the required time for the run-in process. After each friction test, the path width of both contact bodies was evaluated to identify the time needed for the initial wear-in process of the new contact pair, see Fig. 6(b). The results show that excessive wear occurred during the first 40–60 min; after that, the path width grew steadily. Therefore, the time required for the wear-in process t_w was chosen to be 60 min. This wear-in time ensured that the path width was around 0.6 mm before the traction test with the TOR product (step S4). Fig. 6(c) shows the development of surface roughness of both specimens. It is evident that the ball roughness remained almost the same, whereas a gradual increase in the disc roughness was observed. As a result, the calculated combined roughness of the ball and the disc fluctuated between 0.46 and 0.59 µm.

Fig. 7 shows the results of set no. 2 according to Table 2. The purpose of this set was to investigate a creep curve (baseline) under dry conditions and to design the traction zones, which are crucial for the evaluation phase of the methodology. Six creep curves under dry conditions were evaluated for eight different SRR values, see Fig. 7(a). It can be seen that there is no substantial difference among these creep curves. CoT saturates at SRR values between 10% and 20% in all cases. However, a further SRR increase led to a gradual CoT reduction accompanied by an interfacial layer formation, see Fig. 7(c). This layer covered most of the contact path, and its thickness reached up to 2.5 µm. Therefore, the range of SRR was limited to 20% for other tests to mitigate interfacial layer formation. A threshold curve and adhesion zones were then designed for the SRR range from 0% to 20% according to the proposed percentage values of the creep curve under dry conditions. The resulting threshold curve and traction zones are plotted in Fig. 7(b), and CoT values of individual points and related performance parameters are given in Table 5.

3.2. Results of the case study

After initial tests under dry conditions, the measurement phase (steps

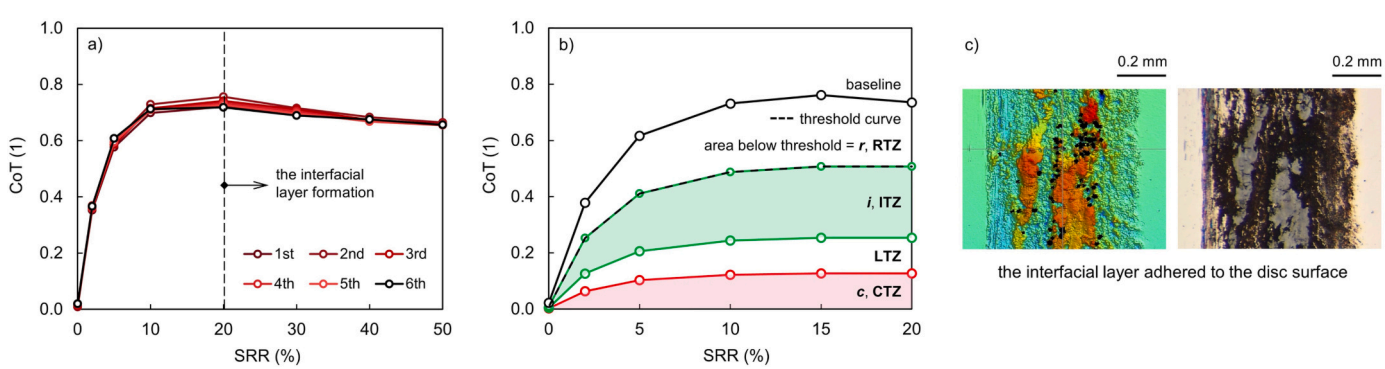

Fig. 7. The results of initial tests under dry conditions (set no. 2 according to Table 2): (a) reference creep curves (baselines) under dry conditions, (b) designed traction zones and threshold curve, (c) the disc surface covered by an interfacial layer after the test at high SRR.

Table 5
Baseline, traction zones, threshold curve and performance parameters.

Traction zones	SRR	0%	2%	5%	10%	15%	20%	perform. param.
	% of dry CoT							
baseline	100%	0.022	0.379	0.617	0.731	0.762	0.736	-
threshold curve; retentivity	66.7%	0.015	0.253	0.411	0.487	0.508	0.508[1])	*r*, *R*
intermediate zone upper limit	66.7%	0.015	0.253	0.411	0.487	0.508	0.508[1])	*i*, *I*
intermediate zone lower limit	33.3%	0.007	0.126	0.206	0.244	0.254	0.254[1])	
very low zone (upper limit)	16.7%	0.004	0.063	0.103	0.122	0.127	0.127[1])	*c*, *C*

[1]) The same value as for 15% SRR was used to avoid the negative trend of the creep curve behind the saturation point occurring under dry conditions.

S4-S6) and the evaluation phase (step S7) were performed to calculate the individual and average performance parameters. These tests correspond with set no. 3–7 in Table 4, where one FM, two TOR lubricants and one bleed oil of one TORL were tested for different applied amounts. Investigating the effect of applied amounts for several products resulted in many large data sets; therefore, only some of them are presented in the following paragraphs. It is important to note that only the points that are included in the evaluation of performance parameters (prior to checkpoint S6 being met) are displayed in the graphs below. Complete results for all products and tested amounts are summarised in Fig. 11. Appendix B lists the performance parameters for all tested conditions.

Fig. 8 presents the results of wet-FM (a-c) and dry-FM (d-f) for the amount of 12 μl (set no. 3 and 4 according to Table 4). The left and middle graphs show examples of PTs, specifically the third and fifth, which were performed according to steps S4 and S5 in Figs. 3 and 4. A summary of the result of all five PTs, which were required to assess the performance of one product, is shown in the graphs to the right (c,f). These bar charts show the values of the performance parameters *c*, *i* and *r* obtained for individual PTs. Moreover, this figure also includes their average values *C*, *I*, and *R*, which define the performance of the tested product throughout the whole testing. Besides this, parameters n_1-n_5 represent the number of traction tests performed in each PT, and the *N* parameter was calculated as an average value. The results in Fig. 8 give evidence that wet-FM provides a longer period of intermediate CoT (the *I* parameter) and a longer retentivity (the *R* parameter) compared to dry-FM. In these cases, the *I* parameter is equal to the *R* parameter because there are no points of creep curves in the very low (the *C* parameter) and low traction zones.

Fig. 9 shows the results of TORL-A (a-c) and TORL-B (d-f) for the lowest tested amount of 1 μl (set no. 5 and 6 according to Table 4). As in the case of FM results, the left and middle graphs show the results of the 3rd and 5th PTs, based on which the individual and average performance parameters were evaluated and displayed in the bar charts on the right. The results revealed that both TOR lubricants provided longer retentivity than FM, even though the applied amount was twelve times smaller. However, for TORL-A and TORL-B, only 40% and 55% of the parameter *R* is made up of the points in the intermediate zone (the *I* parameter). The rest of the *R* parameter is given mainly by points in the low traction zone because parameter *C* was negligible for both tested TOR lubricants.

After the completion of steps S1-S7, the OLF was calculated to reveal the tendency of tested TOR products for different amounts to over-lubricate the contact. The example of OLF maps for tests depicted in Figs. 8 and 9 are shown in Fig. 10. Moreover, Fig. 10 also includes the OLF maps for two tested amounts of the TORL-A bleed oil in order to show the difference between the behaviour of TORL and its bleed oil. It

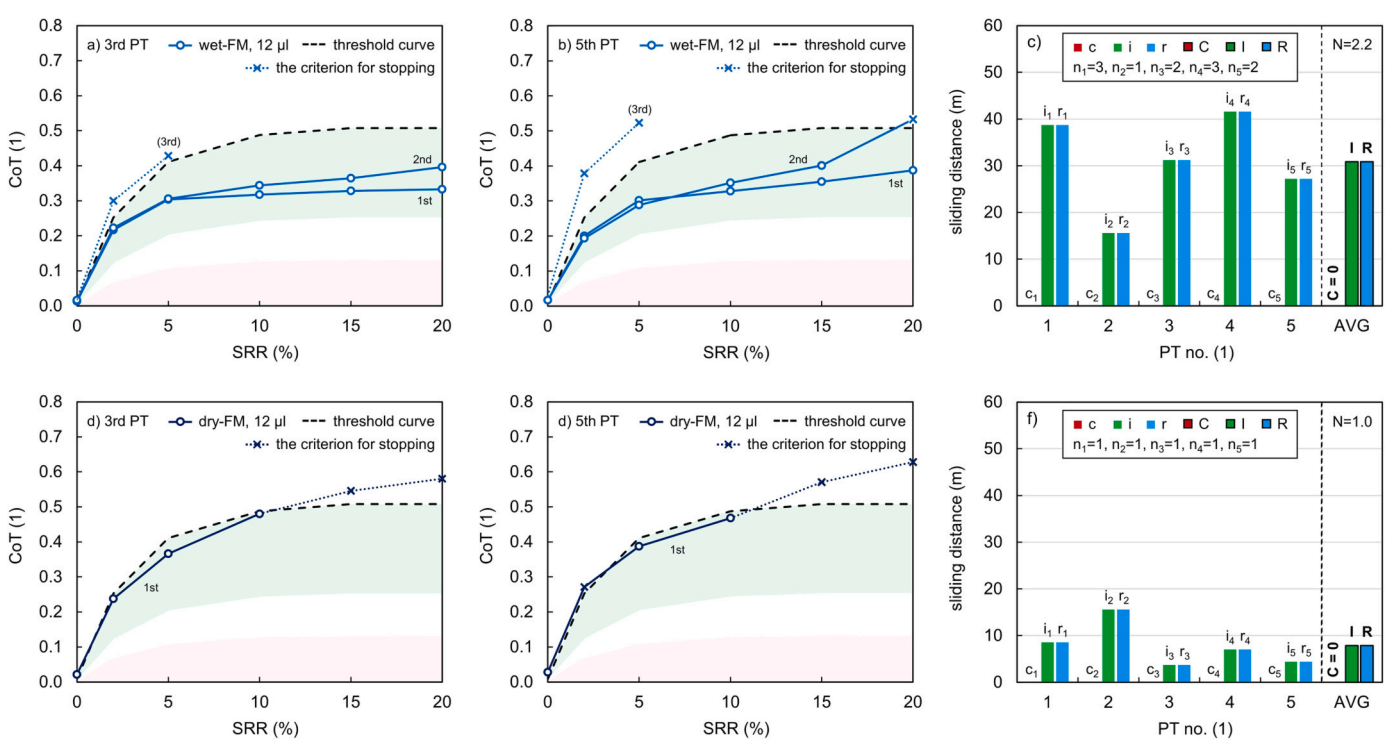

Fig. 8. The results of FM (set no. 3 and 4 according to Table 4, 12 μl): (a) the 3rd PT of wet-FM, (b) the 5th PT of wet-FM, (c) the performance parameters of wet-FM, (d) the 3rd PT of dry-FM, (b) the 5th PT of dry-FM, (c) the performance parameters of dry-FM.

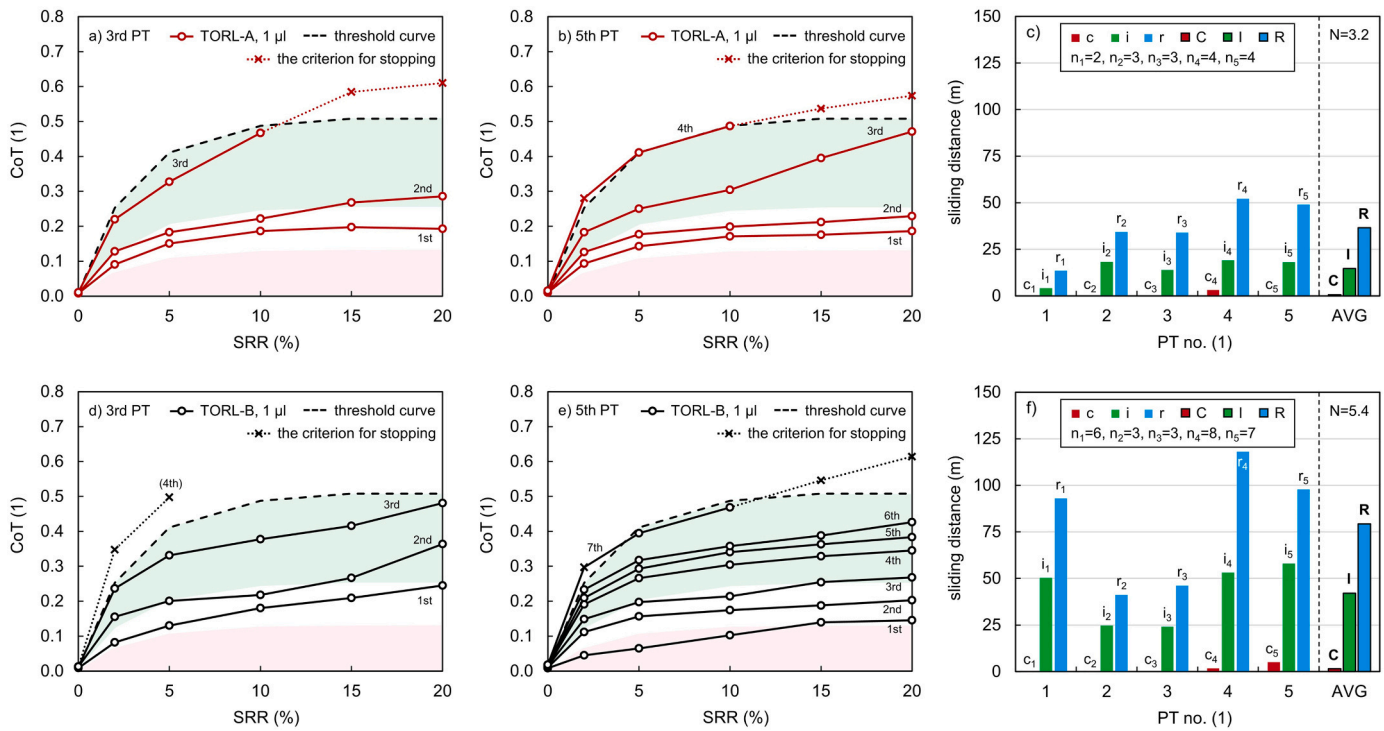

Fig. 9. The results of TORL-A and TORL-B (set no. 5 and 6 according to Table 4, 1 µl): (a) the 3rd PT of TORL-A, (b) the 5th PT of TORL-A, (c) the performance parameters of TORL-A, (d) the 3rd PT of TORL-B, (b) the 5th PT of TORL-B, (c) the performance parameters of TORL-B.

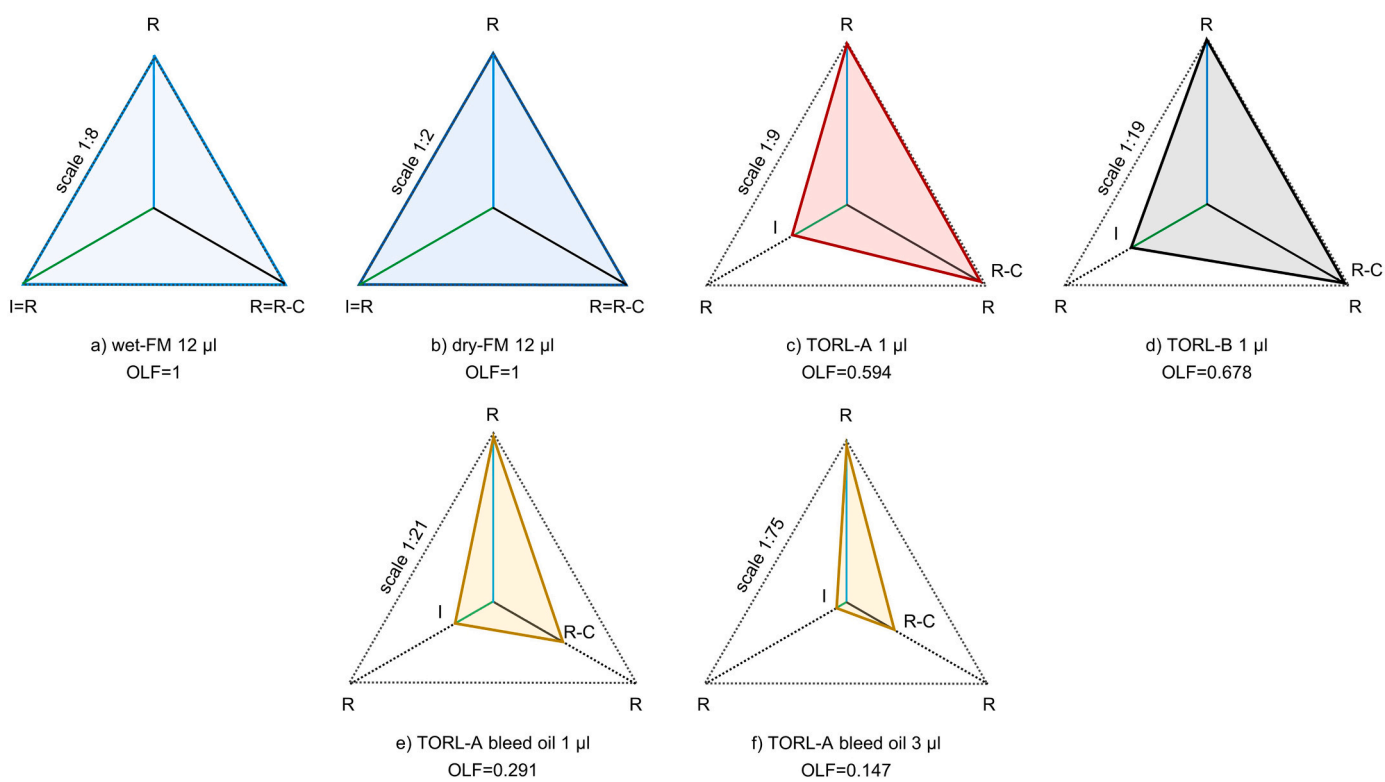

Fig. 10. OLF maps: (a) wet-FM, (b) dry-FM, (c) TORL-A, (d) TORL-B, (e) and (f) TORL-A bleed oil.

should be pointed out that the triangles are drawn at different scales because the tested products achieved significantly different retentivity (the *R* parameter). The first two maps (a) and (b) demonstrate the performance of wet-FM and dry-FM for 12 µl. In both cases, the triangle defining the product performance is identical to the triangle representing the best possible score; therefore, the OLF equals 1. Maps (c) and (d) show the results of TORL-A and TORL-B for the applied amount of 1 µl. As was mentioned above, TORL lubricants caused low and even very low CoT, which indicates that the *R* and *I* parameters are not equal. Therefore, the OLF parameters are lower than 1, specifically

0.594 for TORL-A and 0.678 for TORL-B. The last pair of OLF maps (e) and (f) show the results of TORL-A bleed oil. Comparing the scales with the other maps, it is evident that the bleed oil provided much longer retentivity, as expected. However, the *C* parameter significantly reduced the OLF, resulting in values of 0.291 and 0.147 for 1 μl and 3 μl, respectively. When comparing the performance triangles of tested products with those representing the best possible scores, it is evident that TOR products achieve a significantly better result in preventing over-lubrication than bleed oil.

Fig. 11 (a) shows the performance map and amount-OLF relationship representing the final assessment of tested products. None of the tested products was classified as Q1, the highest-performing class. Wet-FM (12 μl) and TORL-B (1 μl) were the top performers in this study, achieving a Q2 performance class. The rest of the products/amounts fell into the performance classes in Q3 and Q4. As is evident from Fig. 11 (a), FM is limited by very short retentivity, whereas a worse rating of oil-based products results from the low values of OLF. Fig. 11 (b) shows that the higher the amount of oil-based products, the lower the OLF. In contrast, no effect of the applied amount on OLF was observed for FM. Fig. 11 also illustrates the contrasting frictional behaviour between TOR lubricant and its bleed oil. It was revealed that bleed oil led to significantly lower OLF values for both tested amounts compared to TORL.

4. Discussion

This section is divided into four parts. In the first part (4.1), the individual steps of the experimental phase of the proposed methodology are discussed. Moreover, the discussion of initial tests dealing with the input parameters is included in this part. Note that the evaluation steps are omitted because they have been described and explained in Subchapter 2.4. The second part (4.2) focuses on analysing and interpreting the performance of tested products investigated according to the proposed methodology. In addition, the reliability of the methodology is discussed. In the third part (4.3), the proposed methodology is discussed in relation to the CEN/TS standard [46]. Finally, the last part of the discussion (4.3) describes possible future extensions of the methodology.

4.1. Discussion of the methodology: experimental phase

S1 new/worn pair and cleaning: both the new and worn pairs were cleaned in an ultrasonic bath with solvent for 20 min. It should be pointed out that Areiza et al. [45] revealed that solvent cleaning could not completely remove strongly-adhered oxide layers forming during the tests. Therefore, an effective cleaning method was introduced by Navrátil et al. [39], where solvent cleaning was combined with water and mechanical cleaning/grinding with sandpaper. This cleaning method resulted in a clean surface without any visible residue, and the required time for a subsequent run-in process was reduced. Although this method has proven very effective, applying it to MTM samples is difficult because of their narrow contact paths. Therefore, in this study, solvent cleaning in an ultrasonic bath was always followed by a relatively long run-in process to remove the residue of tested products and the interfacial layer.

The material of the contact bodies was bearing steel AISI 52100 100Cr6, which differs in chemical composition and hardness compared to rail and wheel steel. However, the use of these original specimens, offered directly by the tribometer manufacturer, allows future comparison and transferability of the results across laboratories, which is one of the main requirements for any methodology and standard. Furthermore, higher hardness and higher wear resistance of AISI 52100 lead to milder wear and less surface damage than in the case of softer wheel and rail steels. It means that the tests with bearing steel are less affected by changes in surface topography and contact pressure, and the impact of wear debris on the test is not so substantial. This behaviour is crucial for the stability and repeatability of tests, especially for small point contact, as in the case of the MTM tribometer. Therefore, the high carbon-chromium steel seems suitable for friction tests, where the effect of TOR products or another material on friction is investigated. Due to these material properties, this type of steel has been commonly utilized in many previous studies [22,23,47,48,52]. As demonstrated by Harmon et al. [44] for rail materials with varying hardness, higher hardness in specimens may result in slightly lower CoT values compared to softer materials.

S2 wear-in/run-in process: the primary purpose of the run-in process is to stabilize the CoT and roughness. In addition, this process is important to remove residual layers that were formed on the surfaces during tests with TOR products or as a consequence of solvent cleaning. The required time of the run-in process was determined based on the shape of the curves in Fig. 6(a). These data showed that at least 25 min (finally chosen 30 min) was necessary to stabilize the CoT. After 30 min, the CoT was stable and reached almost the same value for all tests. The shape of the curves in Fig. 6(a) is typical for non-lubricated steel-on-steel contact because this type of contact needs some time to stabilise roughness and surface conformity [53]. Optical analysis showed that the combined roughness Sq of specimens was almost the same at the end of each test. The average value of combined Sq was 0.52 ± 0.03 μm, which is in the expected range of wheel/rail roughness [54].

The wear-in process aims to overcome the initial excessive wear occurring when new specimens are rubbed against each other. This process ensures that subsequent tests with TOR products are not significantly affected by the effect of wear debris and related changes in contact geometry. The results revealed that a suitable wear-in process length is 60 min. This length also ensured that the width of the contact path increased to 0.6 mm. This path width allows the solid particles contained in TOR products to come into contact because the typical

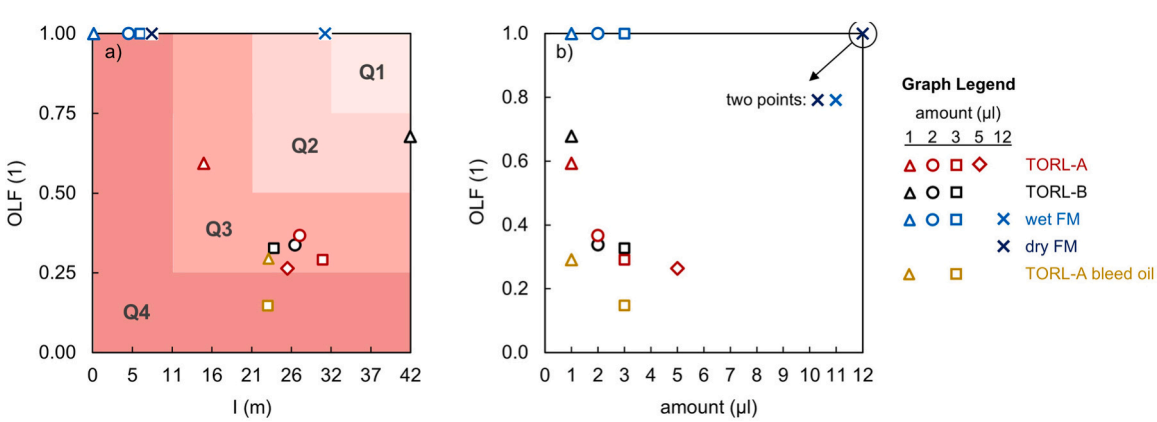

Fig. 11. The final assessment: (a) performance map, (b) amount-OLF relationship.

particle size is in the units to tens of micrometres. Moreover, the wider path allows for a more accurate application of TOR products to the centre of the contact path, compared to a narrow path (without a wear-in process).

S3 product application: there are several methods for the application of TOR products: brush, nozzle, syringe or micropipette. While brush and nozzle were used mainly for field testing [13,45], syringe and micropipette were typically utilized for laboratory testing [34,55]. This is because the required doses are very small in the laboratory, and also high application accuracy is needed. It means that a relatively narrow contact path between the ball and the disc does not allow the application of TOR products using a brush or nozzle.

The micropipette used in this study enables the application of a minimum dosage of 1 μl with a low error guaranteed by the manufacturer. However, since the tested TOR products were viscous liquids containing many solid particles, the application accuracy might have been compromised. Therefore, additional tests focused on application accuracy were conducted where the applied amounts were weighed using a precise analytical balance. These measurements showed that the application error was not higher than 6% except for 12 μl of FM, where the error reached 12%. This larger error resulted from the accumulation of smaller errors due to the application of twelve doses of 1 μl (same as in the PTs). Although this error is not negligible, the application accuracy is still sufficient to study the effect of the applied amount.

As mentioned above, all tested amounts were applied using several 1 μl doses. This application strategy was chosen because it ensures that almost the whole product dose ends up in contact. Note that the application was always performed when both contact bodies were stopped. These conditions are beneficial because it is possible to check whether the application was accurate (based on the position of each drop relative to the centre of the contact path). If not, the whole test has to be repeated. The authors recommend using the application jig to achieve a higher application accuracy. This jig precisely sets the position of the micropipette tip relative to the centre of the contact path.

S4 traction test: this step is a crucial part of the measurement phase in the proposed methodology. This step includes several 180-second tests with different SRR values based on which tested product performance is evaluated. A similar approach to studying TOR products was used in previous studies [19,35]. However, there is also a second and more often used approach to investigate the performance of TOR products in laboratory conditions. Traditionally, the performance of TOR products has been evaluated by measuring the CoT over time at a specific SRR. This friction test begins with the application of TOR product and ends with contact starvation. Note that this test typically has a duration of a few minutes to tens of minutes. Although this experimental approach was previously used in many studies dealing with TOR products [55–60], this approach was found to be unsuitable for tests using the MTM tribometer.

The authors of this study performed these friction tests during the initial testing phase; however, the results were not fully satisfactory. Fig. 12 (a) schematically shows some selected results of these friction tests. The results were acceptable for some kinds of TOR products and very small amounts; see curves no. 1a-1c in Fig. 12 (a). However, the repeatability of these tests was not always good enough to evaluate the performance parameters of TOR products, such as retentivity [24,58] or CoT rate (ratio between CoT difference and time difference) [61]. An unexpected change in the trend of the friction curve was observed for small and medium applied amounts of TOR product (mainly TOR lubricants); see curve no. 2 in Fig. 12 (a). The surface analyses revealed that these unexpected changes occurred due to surface smoothing. A comparison between Fig. 12 (b) and (c) highlights this effect. This smoothing effect was previously described as one of the consequences of applying TOR products [4,30]. This effect was even more significant for tests on the MTM tribometer because of the small contact area and a relatively high amount of TOR product in the contact path compared to real contact. As a consequence of roughness smoothing, the lambda parameter defining the lubrication regime was considerably changed; thus, the test conditions were also changed. Therefore, this result could not be considered relevant because the retentivity was much longer for the lower roughness [62]. Similar behaviour was observed for large amounts of TOR products (curve no. 3 in Fig. 12), where the CoT was very low throughout the whole test, similar to Sánchez et al. [59].

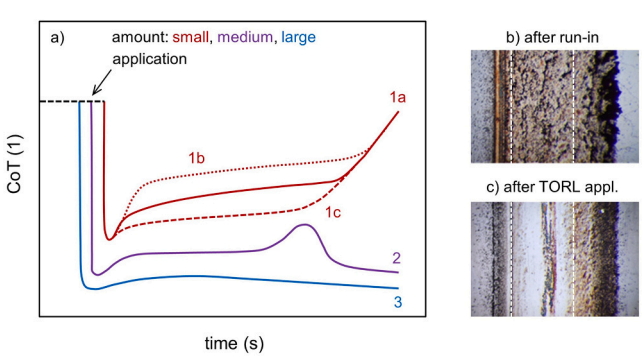

Fig. 12. (a) Schematic results of friction tests, (b) rough path after run-in process, and (c) smooth path after test with higher amount of TOR lubricant and at a low SRR value.

With respect to the findings, a traction test with the range of SRR from 0% to 20% was finally chosen as a suitable approach to investigate the performance of TOR products. Increasing the SRR to higher values raises the shear stress in the TOR product layer; thus, the smoothing effect is suppressed by the gradual starvation of the contact. This approach enables investigating the performance of TOR products for a wider range of applied amounts compared to fixed friction tests at a specific SRR value. The ability to test the performance of TOR products depending on the applied amount is one of the objectives of the proposed methodology.

S5 checkpoint: the creep curve obtained in step S4 was always compared with the threshold curve. This threshold curve was designed as a percentage value of the CoT for a given SRR under dry conditions, see Table 5. The PT was stopped when two neighbouring points of the tested TOR product were above the threshold curve. The reason for choosing two neighbouring points, as a criterion for stopping the PT, instead of one point was that there were many tests where the threshold value was exceeded at lower SRR values. However, the following points of the creep curve were below the threshold curve. Therefore, the criterion was extended to two neighbouring points to ensure that the PT was not stopped too early (before the contact starvation).

If the criterion for stopping the PT has been met, another PT follows. As was mentioned above, five consecutive PTs on the same specimens are needed to investigate the performance of one TOR product for one tested amount. This approach ensures that the performance of each tested product is investigated for a wide range of conditions; thus, the obtained results are more valuable. The most significant change occurs for the geometry of the contact path, while the combined roughness remains almost the same due to the wear-in process between the PTs. The width of the contact path was between 0.6 (after the run-in process) and 0.9 mm (after the fifth PT). This increase in the path width caused a drop in pressure leading to an increase in the value of the Lambda ratio. This ratio defines the lubrication regime and extends the consumption time of TOR products as the load decreases [63]. Moreover, a wider contact path can slightly increase the amount of TOR product which comes into contact while the rest of the dose is pushed out of the contact [64]. These facts explain why the parameter n usually grew with the number of PTs, see Figs. 9(c) and 8 (f).

S6 ball cleaning: the ball is cleaned with a paper tissue without any solvent before the next traction test if the criterion for stopping the test has not been met, see Fig. 3(a). However, it is important to note that this cleaning introduces certain uncertainties in the experiment, as it cannot be easily checked and quantified. Therefore, the cleaning must be

carried out with great precision, using a wipe that does not leave any residues on the surface. It is recommended to check the surface using a microscope. It is important to note that a solvent is not suitable for ball cleaning as it affects the CoT.

As mentioned in Subchapter 2.4, the primary aim of cleaning is to enable testing of higher product amounts without the risk of the smoothing effect depicted in Fig. 12. However, if these higher amounts (e.g. higher than 4 μl) are not being tested, it is possible to omit the ball cleaning and simplify the measurement phase in Fig. 3(a). In that case, the PT will be continued to S4 instead of S6 if the criterion in S5 has not been met. However, it is necessary to decide at the beginning of the testing whether cleaning will be performed or not, as it is essential to maintain the same testing methodology for all tests. The omission of cleaning simplifies the test procedure but can also limit the comparability with this or future studies that employ the proposed methodology (including ball cleaning).

4.2. Case study discussion

In the beginning, the traction tests under dry conditions were performed to evaluate the creep curve under dry conditions. The traction zones and the threshold curve were designed based on this creep curve under dry conditions. The creep curve under dry conditions was found to have a negative trend beyond the saturation point. Although this negative trend is expected under dry conditions, the saturation point should occur at significantly lower slip values [65,66]. This contrast can be explained by different slip conditions in contacts. Whereas MTM contact operates at a fixed SRR, real wheel-rail contact operates at a variable SRR dependent on CoT. At higher SRR/slip, the contact shifts into the unstable region of the creep curve, where sliding may occur. Under these conditions, significant thermal effects arise, and the creep curve declines [23,67].

The results of the presented study are in good agreement with the previous authors' study [24], where no saturation point was observed for SRR values up to 10%. The negative trend of the creep curve in Fig. 7 (a) was not caused primarily by the thermal effects. According to Ertz et al. [68], the calculation revealed that the mean and maximum temperature in the contacts did not exceed 55 °C and 95 °C, respectively. The decline of the creep curve mainly occurred due to the formation of a higher amount of wear debris that adhered to the disc surface; see the interfacial layer in Fig. 7(c). Therefore, the range of SRR was limited to values from 0% to 20% to avoid the formation of this interfacial layer that would affect the results of the test with the TOR product.

The traction test results for several TOR products and one bleed oil are summarized in Fig. 11. These results clearly display a difference in frictional behaviour between water-based (FM) and oil-based TOR products (TORL-A and TORL-B). While increasing the applied amount of FM does not affect the OLF, a significant drop in OLF is found for both TORLs as the amount increases. This result indicates that the application of FM is not risky in terms of a very low CoT, even if the applied amount is large. In contrast, the performance of TORLs is very sensitive to the applied amount, and even a slight increase can lead to a very low CoT. These findings are consistent with Ref. [1], where the dependence of the coefficient of friction on application rate was plotted for both water-based and oil-based products. Besides that, a very low CoT occurrence after the application of TORL was previously reported in both laboratory [20,24] and field studies [18,69].

The second difference between water-based and oil-based products lies in the *I* parameter defining the "effective" retentivity. The results show that the *I* parameter is much more sensitive to the applied amount for TORLs than FM. It means that oil-based products can provide a longer retentivity than water-based products. Moreover, the behaviour of water-based products is extremely influenced by product drying, as observed in the laboratory [22] and field tests [27].

Although the results of the presented study generally agree with previously published studies, it should be noted that the proposed methodology was designed as a comparative test whose aim is to choose a suitable product for further testing. Therefore, the results are divided into four performance groups Q1-Q4 that define the performance class of TOR product for a given amount. Based on the performance map in Fig. 11, TORL-B and FM could be used for further testing because these TOR products were able to reach the performance class Q2 while the class Q3 and Q4 were found for the other two tested products. It is essential to note that class Q3 and Q4 do not necessarily mean that unsatisfactory results will be achieved on the track, but it mainly says that there is a better TOR product or a more suitable amount for its application. On the other hand, recently published studies [44,70] have shown a reasonable correlation between small and full-scale tests.

Finally, the performance of the bleed oil of TORL-A was investigated to verify the sensitivity of the proposed methodology. When comparing the results, it can be seen that TORL-A achieved a higher performance group for both tested amounts (Q2, Q3) than was found for bleed oil (Q3, Q4). Therefore, the proposed methodology can be considered reliable based on these results. Note that some of the tests were repeated to evaluate the repeatability. It was difficult to achieve the same performance parameters because many factors affect the results of traction tests, such as the width of the contact path, surface topography, roughness, etc. However, the same performance group was always achieved for the original and the repeated test. Therefore, it can be concluded that the proposed methodology is robust enough because the final product assessment (Q1-Q4) is not affected by parameters that cannot be precisely controlled during testing.

4.3. Comparison of the proposed methodology and CEN/TS standard

The main parameters of the proposed methodology, further referred to as the I-OLF methodology, and CEN/TS standards [46] are listed in Appendix C. Both methods utilize the MTM tribometer in a ball-on-disc configuration, where specimens are manufactured from AISI 52100. Both approaches involve an initial wear-in process before TOR product testing using traction tests. The CEN/TS standard prescribes only one set of traction tests for one contact pair, while in the I-OLF methodology, five consecutive tests (PTs) are conducted using the same pair. This allows the I-OLF methodology to provide more reliable and representative results, as the individual PTs are performed for a wider range of contact conditions. It should be noted that the higher number of tests in the case of the I-OLF methodology results in a significantly longer total test time, as shown in Appendix C. Therefore, the CEN/TS standard may be suitable when there is a need for rapid testing of a higher number of TOR products.

Another significant difference between the I-OLF methodology and the CEN/TS standard lies in the evaluation phase. While CEN/TS uses only one simple criterion to decide whether the product's performance is good or not in terms of a low CoT, the I-OLF methodology employs four traction zones to evaluate several performance parameters based on which the performance map is plotted. This performance map provides a more comprehensive assessment of TOR products and categorizes them, based on the applied amounts, into four performance classes Q1-Q4.

In terms of individual test parameters, the approaches differ mainly in the contact pressure and the SRR range, see Appendix C. Both contact pressures, used in the I-OLF methodology and CEN/TS standard, represent typical pressure in the wheel tread-rail head contact. The lower pressure in the I-OLF methodology was chosen to reduce wear since the contact pair is used for several consecutive PTs. The higher range of SRRs was selected in the I-OLF methodology to enable testing larger amounts of TOR products and mitigate the smoothing effect depicted in Fig. 12.

4.4. Possible future extension of the methodology

There are several possibilities to extend the proposed methodology in the future. Possible extensions of the methodology may be the

following:

- Test the performance of TOR products together with a representative natural interfacial layer which must be prepared on the surface in advance.
- Test the performance of TOR products for different temperatures, air humidity and various contaminants because all these factors can limit the usage of TOR products.
- Connect the ultrafine particle counter to investigate the number of airborne particles generated from the contact. These particles, mainly ultrafine particles, are dangerous for human health.
- Design a circuit for measuring contact impedance that is crucial to shunting.
- Implementing an optical method to evaluate the film thickness of TOR products could provide valuable insights for modelling and clarifying friction mechanisms.
- Modify the methodology to investigate wear rate, surface and subsurface damage, and RCF propagation. This task could be the most challenging because representative materials of specimens are needed. Therefore, manufacturing samples from wheel and rail steel seems to be necessary. Note that the pin-on-disc configuration (possible for MTM) may be considered in case of manufacturing difficulties of the ball from wheel steel.
- The performance parameters can be redefined to apply the methodology for evaluating oil and grease performance (e.g., products used for wheel flange lubrication).

5. Conclusions

This paper introduced a novel benchmarking methodology for assessing the performance of TOR products, which are applied in rail transportation to manage friction, noise and wear. The methodology was proposed for the MTM tribometer in ball-on-disc configuration to allow future comparison of results across different laboratories. The proposed methodology consists of nine consecutive steps describing the testing from the initial wear-in process to the final assessment of TOR products. A core of the methodology is formed by traction tests and a robust evaluation phase resulting in a performance map that compares different TOR products and their amounts. It should be highlighted that this performance map is plotted based on several performance parameters that are crucial for ensuring traffic safety and reaching the expected benefits associated with TOR products. This multi-parametric approach makes the assessment of TOR products highly representative. The resulting performance map shows the performances of tested TOR products depending on the applied amount and categorizes them into four performance classes Q1-Q4. Based on this, a suitable TOR product can be chosen for further testing because the proposed comparative test is considered the first step towards applying the product to real operation. Therefore, full-scale and operational tests should follow this initial testing with a small-scale tribometer.

The suitability of the proposed methodology was confirmed by testing three TOR products (1x FM and 2x TOR lubricants) and one bleed oil using varying amounts. The results led to the following conclusions:

- Increasing the applied amount of FM did not lead to any risks related to a very low CoT. In contrast, both tested TOR lubricants caused a very low CoT when increasing the amount applied.
- The retentivity of TOR lubricants was affected by the applied amount more notably than was found for FM.
- The previous two points show that the performance of oil-based TOR products is much more sensitive to applied amounts than water-based products.
- The retentivity of FM is significantly shortened if the base medium is evaporated before the test. However, the evaporation of the base medium did not influence the product behaviour regarding the occurrence of a very low CoT.
- Based on the case study results, the most suitable TOR products for further testing have been identified.
- TOR lubricant reached a higher performance class for both tested amounts than its bleed oil. This conclusion gives evidence that the methodology is appropriately designed.

Declaration of Competing Interest

The authors declare that they have no known competing financial interests or personal relationships that could have appeared to influence the work reported in this paper.

Data availability

Data will be made available on request.

Acknowledgements

The work was supported by the project LTACH19001 with financial support from the Ministry of Education, Youth and Sports of the Czech Republic.

Appendix A. Sensors parameters

sensor	range	accuracy	nonlinearity
load cell for normal force	2–75 N	±0.3 N	±1% of full scale
load cell for friction force	–20 to + 20 N	±0.3 N	±2% of full scale
servo-drives	–4 to + 4 m/s	±1 mm/s or 0.1% of speed, whichever is larger	not applicable

Appendix B. – Overview of performance parameters for all tested conditions

set	TOR product	amount (μl)	*C* (m)	*I* (m)	*R* (m)	*N* (1)*	*OLF* (1)	Class (1)
3	wet-FM	1	0	0.1	0.1	0.4	1	Q4
		2	0	4.8	4.8	1.0	1	Q4
		3	0	6.3	6.3	1.0	1	Q4
		12	0	30.9	30.9	2.2	1	Q2
4	dry-FM	12	0	7.9	7.9	1	1	Q4
5	TORL-A	1	0.6	14.7	36.6	3.2	0.594	Q3
		2	35.3	27.5	98.7	6.8	0.367	Q3

(*continued on next page*)

(*continued*)

set	TOR product	amount (μl)	*C* (m)	*I* (m)	*R* (m)	*N* (1)*	*OLF* (1)	Class (1)
		3	62.6	30.5	128.8	9.0	0.291	Q3
		5	82.6	25.8	200.1	13.2	0.264	Q3
6	TORL-B	1	1.5	42.1	79.2	5.4	0.678	Q2
		2	41.6	26.9	104.7	7.2	0.338	Q3
		3	40.5	24.1	103.6	7.0	0.328	Q3
7	TORL-A	1	45.6	23.2	88.3	6.4	0.291	Q3
	bleed oil	3	201.2	21.6	308.7	20.2	0.147	Q4

* N – average value of n_1-n_5

Appendix C. Comparison of the proposed methodology (I-OLF methodology) and CEN/TS standard

I-OLF methodology	pressure (GPa)	speed (m/s)	SRR (%)	duration (min)
wear-in	0.8	1	2	60
run-in			2	30
TOR product testing			0–20	~25[1])
type of test for TOR product testing	traction test (creep curves)			
more tests using the same pair	yes (5 in total)			
total test time	~5–7 h[1])			
comparative methodology	YES			
assessment based on	traction zones and several performance parameters			
overall assessment	performance map (classes Q1-Q4)			
CEN/TS standard	pressure (GPa)	speed (m/s)	SRR (%)	duration (min)
wear-in (run-in)[2])	1	0.1	50	30
TOR product testing		1, 3.8	0.25–10	22
type of test for TOR product testing	traction test (creep curves)			
more tests using the same pair	no			
total test time	~1 h[1])			
comparative methodology	YES			
assessment based on	CoT value at 10% SRR			
overall assessment	good/bad			

[1]) It is only an estimate of the duration as it depends on the number of creep curves.
[2]) Only the term "run-in" is used in the CEN/TS standard.
[3]) Time needed for specimens cleaning is not included as this information is not provided.

References

[1] Stock R, Stanlake L, Hardwick C, Yu M, Eadie D, Lewis R. Material concepts for top of rail friction management – Classification, characterisation and application. Wear 2016;366–367:225–32. https://doi.org/10.1016/j.wear.2016.05.028.

[2] Harmon M, Lewis R. Review of top of rail friction modifier tribology. Tribology - Mater, Surf Interfaces 2016;10:150–62. https://doi.org/10.1080/17515831.2016.1216265.

[3] Kalousek J, Johnson KL. An Investigation of Short Pitch Wheel and Rail Corrugations on the Vancouver Mass Transit System. Proc Inst Mech Eng, Part F: J Rail Rapid Transit 1992;206:127–35. https://doi.org/10.1243/PIME_PROC_1992_206_226_02.

[4] Eadie DT, Kalousek J, Chiddick KC. The role of high positive friction (HPF) modifier in the control of short pitch corrugations and related phenomena. Wear 2002;253:185–92. https://doi.org/10.1016/S0043-1648(02)00098-4.

[5] Egana JI, Vinolas J, Gil-Negrete N. Effect of liquid high positive friction (HPF) modifier on wheel-rail contact and rail corrugation. Tribol Int 2005;38:769–74. https://doi.org/10.1016/j.triboint.2004.11.006.

[6] Eadie DT, Santoro M, Oldknow K, Oka Y. Field studies of the effect of friction modifiers on short pitch corrugation generation in curves. Wear 2008;265:1212–21. https://doi.org/10.1016/j.wear.2008.02.028.

[7] Eadie DT, Santoro M. Top-of-rail friction control for curve noise mitigation and corrugation rate reduction. J Sound Vib 2006;293:747–57. https://doi.org/10.1016/j.jsv.2005.12.007.

[8] Eadie DT, Santoro M, Kalousek J. Railway noise and the effect of top of rail liquid friction modifiers: changes in sound and vibration spectral distributions in curves. Wear 2005;258:1148–55. https://doi.org/10.1016/j.wear.2004.03.061.

[9] Kwong M, Frossinakis R, Makowsky T, Yu M, Lu X, O'Grady J. Wayside top of rail friction control: an embedded track solution in a high density tram. Netw, Ausrail 2019;2019:1–14.

[10] FUKAGAI S, BAN T, OGATA M, ISHIDA M, NAMURA A. Development of wheel/rail friction moderating system (FRIMOS). Q Rep Rtri 2008;49:26–32. https://doi.org/10.2219/rtriqr.49.26.

[11] Anderson D, Wheatley N. Mitigation of wheel squeal and flanging noise on the australian rail network. Noise Vib Mitig Rail Transp Syst 2008:399–405. https://doi.org/10.1007/978-3-540-74893-9_56.

[12] Davis K, Stickland W. Eval a Top–rail Lubr Syst 1999:1–120.

[13] Suda Y, Iwasa T, Komine H, Tomeoka M, Nakazawa H, Matsumoto K, Nakai T, Tanimoto M, Kishimoto Y. Development of onboard friction control. Wear 2005;258:1109–14. https://doi.org/10.1016/j.wear.2004.03.059.

[14] Matsumoto K, Suda Y, Fujii T, Komine H, Tomeoka M, Satoh Y, Nakai T, Tanimoto M, Kishimoto Y. The optimum design of an onboard friction control system between wheel and rail in a railway system for improved curving negotiation. Veh Syst Dyn 2006;44:531–40. https://doi.org/10.1080/00423110600875294.

[15] Ishida M, Ban T, Iida K, Ishida H, Aoki F. Effect of moderating friction of wheel/rail interface on vehicle/track dynamic behaviour. Wear 2008;265:1497–503. https://doi.org/10.1016/j.wear.2008.02.041.

[16] Lewis R, Dwyer-Joyce RS, Lewis J. Disc machine study of contact isolation during railway track sanding. Proc Inst Mech Eng, Part F: J Rail Rapid Transit 2003;217:11–24. https://doi.org/10.1243/095440903762727311.

[17] Lundberg J, Rantatalo M, Wanhainen C, Casselgren J. Measurements of friction coefficients between rails lubricated with a friction modifier and the wheels of an IORE locomotive during real working conditions. Wear 2015;324–325:109–17. https://doi.org/10.1016/j.wear.2014.12.002.

[18] Galas R, Omasta M, Klapka M, Kaewunruen S, Krupka I, Hartl M. Case Study: the Influence of Oil-based Friction Modifier Quantity on Tram Braking Distance and Noise. Tribology Ind 2017;39:198–206. https://doi.org/10.24874/ti.2017.39.02.06.

[19] D.V. Gutsulyak, L.J.E. Stanlake, H. Qi, Twin disc evaluation of third body materials in the wheel/rail interface, 15 (2021) 115–126. ⟨https://doi.org/10.1080/17515831.2020.1829878⟩.

[20] Liu X, Meehan PA. Investigation of squeal noise under positive friction characteristics condition provided by friction modifiers. J Sound Vib 2016;371:393–405. https://doi.org/10.1016/j.jsv.2016.02.028.

[21] Li Q, Wu B-nan, Ding H-hao, Galas R, Kvarda D, Liu Q-yue, Zhou Z-rong, Omasta M, Wang W. Numerical prediction on the effect of friction modifiers on adhesion behaviours in the wheel-rail starved EHL contact. Tribol Int 2022;170. https://doi.org/10.1016/j.triboint.2022.107519.

[22] Galas R, Kvarda D, Omasta M, Krupka I, Hartl M. M. The role of constituents contained in water–based friction modifiers for top–of–rail application. Tribology Int 2018;117:87–97. https://doi.org/10.1016/j.triboint.2017.08.019.

[23] D. Kvarda, R. Galas, M. Omasta, M. Hartl, I. Krupka, M. Dzimko, Shear properties of top-of-rail products in numerical modelling, Proceedings Of The Institution Of Mechanical Engineers, Part F: Journal Of Rail And Rapid Transit. ⟨https://doi.org/10.1177/09544097221138374⟩.

[24] Galas R, Omasta M, Krupka I, Hartl M. Laboratory investigation of ability of oil-based friction modifiers to control adhesion at wheel-rail interface. Wear 2016;368–369:230–8. https://doi.org/10.1016/j.wear.2016.09.015.

[25] Hardwick, Lewis R, Stock R. The effects of friction management materials on rail with pre existing rcf surface damage. Wear 2017;384–385:50–60. https://doi.org/10.1016/j.wear.2017.04.016.

[26] Curley D, Anderson DC, Jiang J, Hanson D. Field trials of gauge face lubrication and top-of-rail friction modification for curve noise mitigation. Noise Vib Mitig Rail Transp Syst 2015:449–56. https://doi.org/10.1007/978-3-662-44832-8_54.

[27] Khan SA, Lundberg J, Stenström C. Carry distance of top-of-rail friction modifiers. Proc Inst Mech Eng, Part F: J Rail Rapid Transit 2018;232:2418–30. https://doi.org/10.1177/0954409718772981.

[28] Chen H, Fukagai S, Sone Y, Ban T, Namura A. Assessment of lubricant applied to wheel/rail interface in curves. Wear 2014;314:228–35. https://doi.org/10.1016/j.wear.2013.12.006.

[29] Eadie DT, Elvidge D, Oldknow K, Stock R, Pointner P, Kalousek J, Klauser P. The effects of top of rail friction modifier on wear and rolling contact fatigue: Full-scale rail–wheel test rig evaluation, analysis and modelling. Wear 2008;265:1222–30. https://doi.org/10.1016/j.wear.2008.02.029.

[30] Stock R, Eadie DT, Elvidge D, Oldknow K. Influencing rolling contact fatigue through top of rail friction modifier application – A full scale wheel–rail test rig study. Wear 2011;271:134–42. https://doi.org/10.1016/j.wear.2010.10.006.

[31] Matsumoto A, Sato Y, Ohno H, Mizuma T, Suda Y, Tanimoto M, Oka Y. Study on curving performance of railway bogies by using full-scale stand test. Veh Syst Dyn 2006;44:862–73. https://doi.org/10.1080/00423110600907402.

[32] Abbasi S, Olofsson U, Zhu Y, Sellgren U. Pin-on-disc study of the effects of railway friction modifiers on airborne wear particles from wheel–rail contacts. Tribology Int 2013;60:136–9. https://doi.org/10.1016/j.triboint.2020.106566.

[33] Lewis SR, Lewis R, Olofsson U, Eadie DT, Cotter J, Lu X. Effect of humidity, temperature and railhead contamination on the performance of friction modifiers: Pin-on-disk study. Proc Inst Mech Eng, Part F: J Rail Rapid Transit 2013;227:115–27. https://doi.org/10.1177/0954409712452239.

[34] Kvarda D, Skurka S, Galas R, Omasta M, Shi L-bing, Ding H, Wang W-jian, Krupka I, Hartl M. The effect of top of rail lubricant composition on adhesion and rheological behaviour. Eng Sci Technol, Int J 2022;35. https://doi.org/10.1016/j.jestch.2022.101100.

[35] Tomeoka M, Kabe N, Tanimoto M, Miyauchi E, Nakata M. Friction control between wheel and rail by means of on-board lubrication. Wear 2002;253:124–9. https://doi.org/10.1016/S0043-1648(02)00091-1.

[36] Liu X, Meehan PA. Investigation of squeal noise under positive friction characteristics condition provided by friction modifiers. J Sound Vib 2016;371:393–405. https://doi.org/10.1016/j.jsv.2016.02.028.

[37] Vélez JC, Cornelio JAC, Sierra RB, Santa JF, Hoyos-Palacio LM, Nevshupa R, Toro A. Development of a composite friction modifier with carbon nanotubes for applications at the wheel–rail interface. Adv Compos Lett 2020;29. https://doi.org/10.1177/2633366X20930019.

[38] Buckley-Johnstone L, Harmon M, Lewis R, Hardwick C, Stock R. A comparison of friction modifier performance using two laboratory test scales. Proc Inst Mech Eng, Part F: J Rail Rapid Transit 2019;233:201–10. https://doi.org/10.1177/0954409718787045.

[39] Navrátil V, Galas R, Klapka M, Kvarda D, Omasta M, Shi L, Ding H, Wang W-J, Krupka I, Hartl M. Wheel Squeal Noise in Rail Transport: The Effect of Friction Modifier Composition. Tribology Ind 2022;44:361–73. https://doi.org/10.24874/ti.1211.11.21.02.

[40] Song J, Shi L, Ding H, Galas R, Omasta M, Wang W, Guo J, Liu Q, Hartl M. Effects of solid friction modifier on friction and rolling contact fatigue damage of wheel-rail surfaces. Friction 2022;10:597–607. https://doi.org/10.1007/s40544-021-0521-5.

[41] Harmon M, Lewis R. New laboratory methodologies to analyse the top of rail friction modifier performance across different test scales. Proc Inst Mech Eng, Part F: J Rail Rapid Transit 2021;235:191–200. https://doi.org/10.1177/0954409720913759.

[42] Evans M, Skipper WA, Buckley-Johnstone L, Meierhofer A, Six K, Lewis R. The development of a high pressure torsion test methodology for simulating wheel/rail contacts. Tribology Int 2021;156. https://doi.org/10.1016/j.triboint.2020.106842.

[43] Lewis SR, Lewis R, Olofsson U. An alternative method for the assessment of railhead traction. Wear 2011;271:62–70. https://doi.org/10.1016/j.wear.2010.10.035.

[44] M. Harmon, J.F. Santa, J.A. Jaramillo, A. Toro, A. Beagles, R. Lewis, Evaluation of the coefficient of friction of rail in the field and laboratory using several devices, 14 (2020) 119–129. ⟨https://doi.org/10.1080/17515831.2020.1712111⟩.

[45] Areiza YA, Garcés SI, Santa JF, Vargas G, Toro A. Field measurement of coefficient of friction in rails using a hand-pushed tribometer. Tribology Int 2015;82:274–9. https://doi.org/10.1016/j.triboint.2014.08.009.

[46] CEN/TS 15427–2-2:2021. Railway applications - Wheel/Rail friction management - Part 2–2: Properties and Characteristics - Top of Rail materials, 2021.

[47] Cann PM. The "leaves on the line" problem—a study of leaf residue film formation and lubricity under laboratory test conditions. Tribology Lett 2006;24:151–8. https://doi.org/10.1007/s11249-006-9152-2.

[48] Zhu Y, Olofsson U, Persson K. Investigation of factors influencing wheel–rail adhesion using a mini-traction machine. Wear 292- 2012;293:218–31. https://doi.org/10.1016/j.wear.2012.05.006.

[49] White B, Hyland-Knight J, Lewis R. Assessing the effectiveness of traction gels using full-scale and field testing. Proc Inst Mech Eng, Part F: J Rail Rapid Transit 2021;235:690–9. https://doi.org/10.1177/0954409720953943.

[50] Kalousek J, Magel E. Modifying and managing friction. Railw Track Struct 1997;93:31–6.

[51] Arias-Cuevas O. Low Adhesion in the Wheel-Rail Contact, PhD Thesis. Netherlands: Delft University of Technology,; 2010.

[52] Oomen MA, Bosman R, Lugt PM. Characterization of friction and wear behavior of friction modifiers used in wheel-rail contacts. Int J Progn Health Manag 2017;8. https://doi.org/10.36001/ijphm.2017.v8i3.2663.

[53] Blau PJ. On the nature of running-in. Tribol Int 2005;38:1007–12. https://doi.org/10.1016/j.triboint.2005.07.020.

[54] Chen H, Namura A, Ishida M, Nakahara T. Influence of axle load on wheel/rail adhesion under wet conditions in consideration of running speed and surface roughness. Wear 2016;366–367:303–9. https://doi.org/10.1016/j.wear.2016.05.012.

[55] Li Z, Arias-Cuevas O, Lewis R, Gallardo-Hernández EA. Rolling–Sliding Laboratory Tests of Friction Modifiers in Leaf Contaminated Wheel–Rail Contacts. Tribology Lett 2009;33:97–109. https://doi.org/10.1007/s11249-008-9393-3.

[56] Wang W, Li S, Ding H, Lin Q, Galas R, Omasta M, Meli E, Guo J, Liu Q. Wheel/rail adhesion and damage under different contact conditions and application parameters of friction modifier. Wear 2023. https://doi.org/10.1016/j.wear.2023.204870.

[57] Li JX, Wu BN, Ding HH, Galas R, Omasta M, Wen ZF, Guo J, Wang WJ. Wear and damage behaviours of wheel and rail materials: Effects of friction modifier and environmental temperature. Wear 2023. https://doi.org/10.1016/j.wear.2023.204796.

[58] Arias-Cuevas O, Li Z, Lewis R, Gallardo-Hernández EA. Rolling–sliding laboratory tests of friction modifiers in dry and wet wheel–rail contacts. Wear 2010;268:543–51. https://doi.org/10.1016/j.wear.2009.09.015.

[59] Sánchez JC, Jaramillo JA, Santa JF, Toro A. Twin-disc assessment of the effect of top-of-rail friction modifiers on the tribological response of er8-r370ht pairs for use in wheel-rail systems. Rev Latinoam De Metal Y Mater 2019;39:2–15.

[60] Trummer G, Lee ZS, Lewis R, Six K. Modelling of Frictional Conditions in the Wheel–Rail Interface Due to Application of Top-of-Rail Products. Lubricants 2021;9. https://doi.org/10.3390/lubricants9100100.

[61] Omasta M, Galas R, Knapek J, Hartl M, Krupka I. Development of an adaptive top-of-rail friction modification system. In: Stephenson Conference: Research For Railways 2017. London: Institution of Mechanical Engineers; 2017. p. 325–32.

[62] Lewis SR, Lewis R, Evans G, Buckley-Johnstone LE. Assessment of railway curve lubricant performance using a twin-disc tester. Wear 2014;314:205–12. https://doi.org/10.1016/j.wear.2013.11.033.

[63] Aldajah S, Ajayi OO, Fenske GR, Kumar S. Investigation of Top of Rail Lubrication and Laser Glazing for Improved Railroad Energy Efficiency1. J Tribology 2003;125:643–8. https://doi.org/10.1115/1.1537745.

[64] White B, Lee ZS, Lewis R. Towards a Standard Approach for the Twin Disc Testing of Top-Of Rail Friction Management Products. Lubricants 2022;10. https://doi.org/10.3390/lubricants10060124.

[65] Polach O. Creep forces in simulations of traction vehicles running on adhesion limit. Wear 2005;258:992–1000. https://doi.org/10.1016/j.wear.2004.03.046.

[66] Six K, Meierhofer A, Müller G, Dietmaier P. Physical processes in wheel–rail contact and its implications on vehicle–track interaction. Veh Syst Dyn 2015;53:635–50. https://doi.org/10.1080/00423114.2014.983675.

[67] Vollebregt E, Six K, Polach O. Challenges and progress in the understanding and modelling of the wheel–rail creep forces. Veh Syst Dyn 2021;59:1026–68. https://doi.org/10.1080/00423114.2021.1912367.

[68] Ertz M, Knothe K. A comparison of analytical and numerical methods for the calculation of temperatures in wheel/rail contact. Wear 2002;253:498–508. https://doi.org/10.1016/S0043-1648(02)00120-5.

[69] Khan SA, Lundberg J, Stenström C. The effect of third bodies on wear and friction at the wheel-rail interface. Proc Inst Mech Eng, Part F: J Rail Rapid Transit 2022;236:662–71. https://doi.org/10.1177/09544097211034688.

[70] Buckley-Johnstone L, Harmon M, Lewis R, Hardwick C, Stock R. A comparison of friction modifier performance using two laboratory test scales. Proc Inst Mech Eng, Part F: J Rail Rapid Transit 2019;233:201–10. https://doi.org/10.1177/0954409718787045.

Tribology International 191 (2024) 109153

Contents lists available at ScienceDirect

Tribology International

journal homepage: www.elsevier.com/locate/triboint

An approach for the creep-curve assessment using a new rail tribometer

Martin Valena *, Milan Omasta, Daniel Kvarda, Radovan Galas, Ivan Krupka, Martin Hartl

Faculty of Mechanical Engineering, Brno University of Technology, Technicka 2896/2, 616 69 Brno, Czech Republic

ARTICLE INFO

Keywords:
Wheel-rail tribology
Portable tribometer
Creep curve
Coefficient of traction

ABSTRACT

The friction properties of the wheel-rail contact are characterized by a coefficient of traction (CoT), which can be affected by many contaminants. Numerous devices for assessing CoT are available; however, only a small number of them are capable of recording creep curves. This work introduced a rail-mounted tribometer that uses controlled changes in braking torque on a measuring wheel to induce creep in the contact. A methodology for assessing creep curve parameters was proposed, utilizing both analytical and numerical models of the contact. The experiments were performed both in the field and in the laboratory to investigate the effect of railhead conditions under various contact pressures and to track the evolution of the CoT during a measurement.

1. Introduction

A coefficient of traction (CoT) is one of the most important parameters characterizing the conditions in the wheel-rail contact. A high CoT value leads to excessive wear, high rolling resistance and corrugation making the operation more expensive [1]. On the other hand, low value causes problems with traction and braking, such as increased braking distance. The CoT is mainly affected by conditions of a wheel and a rail surface, 3rd body layers, environmental conditions, etc. High humidity, iron oxides, flange lubricants and leaves reduce the CoT, while sanding is used to increase it [2]. In addition to CoT, the wheel-rail contact is characterised by a creep curve, which is a CoT dependency on creep. In the low creep region, CoT rises steeply, then saturates and continues to rise slowly or starts to fall. “Dry” conditions usually show a falling creep curve, leading to stick-slip oscillations that may cause corrugation and generate squeal noise [3–5]. To prevent these phenomena, top-of-rail (TOR) products are applied to the contact to reduce the CoT to an intermediate value (0.2 – 0.4) [6] and provide a positive friction characteristic. Exact values may vary depending on the rail system. These parameters are measured in the laboratory using test rigs or in the field using instrumented trains or tribometers.

The laboratory provides well-controlled conditions for experiments, which is a major advantage over field measurements; however, with lower representativeness. There are many types of laboratory test rigs and tribometers available for studying wheel-rail contact. High-pressure torsion test rig (HPT) allows a simple 3rd body characterisation [7,8], pin-on-disc tribometers provide basic friction and wear data [9,10] and ball-on-disc tribometers like Mini-Traction Machine (MTM) are used to determine creep curve in the rolling-sliding contact [11,12]. The most widely used is a small-scale twin-disc concept that provides an optimal ratio between contact representativeness and testing costs. Rolling-sliding contact can be achieved with a controlled slip [13–17] or a torque [18,19]. Small-scale test rigs with a disc in rotation on a circular rail are also used [20,21]. The most realistic configuration is provided by full-scale tribometers using a train wheel and another disc representing the rail [22,23] or the rail itself [24–26].

There are several ways to determine the friction level on a railway. The simplest way is to measure the coefficient of friction using a simple sliding tribometer such as the Pendulum that is based on the energy loss measuring principle [27,28]. On the other side, the most representative is the measurement of the CoT with a locomotive equipped with a measuring system that records the traction forces and sliding velocities of all the bogies when the sliding occur [29,30]. These experiments are very expensive. A less expensive option is to use rolling-stock brake testing, especially together with low adhesion simulants [25,31] or TOR products [14].

A compromise is to use field tribometers inducing a rolling-sliding contact between a measuring wheel and the rail. Several generations of such devices were developed during the last decades. One of them is a car-pushed tribometer TriboRailer [32], where the creep is induced by rotating the measuring wheel around the yaw axis. A widely used device is the hand-pushed tribometer from Salient Systems [29,32,33]. This device utilizes an application of ramping braking force to the measuring wheel by an electromagnetic brake to determine when the measuring wheel begins to slip. The corresponding braking torque is then used to determine the coefficient of friction. The TriboMetro FR 101 hand-pushed tribometer works on a similar principle, but provides the

* Corresponding author.
E-mail address: Martin.Valena@vut.cz (M. Valena).

https://doi.org/10.1016/j.triboint.2023.109153
Received 16 August 2023; Received in revised form 7 October 2023; Accepted 2 November 2023
Available online 1 December 2023
0301-679X/© 2023 Elsevier Ltd. All rights reserved.

Nomenclature

A	Ratio of CoT at zero and infinity slip velocity
a, b	half-axes of the contact ellipse
B	Coefficient of exponential friction decrease
C	Proportionality coefficient characterising the contact shear stiffness
CoT	Coefficient of traction
CoT_e	Effective CoT
D	Diameter of measuring wheel
F	Tangential contact force
I	Momentum of inertia
k_A	Reduction factor in the area of adhesion
k_S	Reduction factor in the area of slip
L_1	Kalker's contact flexibility
L_e	Elastic flexibility of 3rd body layer
L_p	Plasticity parameter
M_B	Braking torque
p	Contact pressure
Q	Wheel load
s	Rigid slip
T	Traction force
u	Surface displacement
v	Rolling velocity
v_L	Longitudinal speed of measuring module
v_R	Tangential speed of measuring wheel
w	Total creep (slip) velocity
α	Angular acceleration
ε	Gradient of the tangential stress in the area of adhesion
μ_0	Maximum CoT at zero slip velocity
μ_{c1}	Elasticity limiting coefficient of friction
μ_{c2}	Plasticity limiting coefficient of friction
τ	Shear stress
τ'	Shear stress in the previous calculation step

entire creep curve [34]. Hand-pushed tribometers give an average value of friction coefficient from a longer section of the track (e.g. 30 m in the case of TriboMetro FR 101 [34]) and generally overestimate the coefficient of friction [29]. Because of the averaging, the results are rather rough and these devices are not suitable for determining the traction curve at a specific place on the rail.

The latest generation of field tribometers includes the Hand-operated (HO) tribometer [35–37], also called OnTrak [38]. In this device, creep is induced in the lateral direction by rotating the measuring wheel with a certain angle of attack (AoA), i.e. in a similar way to the TriboRailer. The measurement can be performed with a constant or a changing AoA that can be set to achieve approx. 16% creep according to [37,38], so the HO tribometer operates in a low-creep regime. Changing AoA allows the creep curve to be evaluated in one pass, but this mode is not reliable. Use of controlled slip in a lateral direction to build a traction curve may be considered less representative.

Various lab-scale contact simulators, field tribometers and instrumented wheels differ from each other in the way they simulate the rolling-sliding contact, in the measurement principle, in the contact geometry and materials and in the representativeness of the friction layer studied. Typically, lab-scale measurements give higher friction under dry conditions due to a stronger formation of wear and oxide particles. Rail tribometers tend to give lower values depending on the conditioning of the counter body. In all the scaled tests, the formation of the friction layer is of a transient nature, which should be considered when interpreting the results under dry conditions. Moreover, the results vary greatly depending on the cleaning procedure, a common part of laboratory tribological tests.

Time-consuming and costly measurements using the instrumented train, the difficult use of complex track tribometers and the low representativeness of simple portable devices make a fast assessment of frictional properties on the rail head challenging. Since it is nearly impossible to simulate the formation of a real friction layer in the laboratory, an experimental device with rolling-sliding contact enabling measurement on the rail in both field and laboratory conditions is required. Comparison of results using the same methodology in the field and in the laboratory will provide a better understanding of the real friction layer formation.

This work aims to introduce an approach utilizing a new portable rail tribometer with a controlled traction force to evaluate the creep curve. Fitting a creep force model to the experimental data allows for a simple and fast assessment of the tribological properties of the 3rd body layer formed on the rail. This approach can be used in both laboratory and field research into the wheel-rail interface and in the implementation of friction-management techniques etc.

2. Material and methods

2.1. Experimental device

A new tribometer (BUT rail tribometer), shown in Fig. 1, has been developed to study adhesion conditions on a rail in the field or in the laboratory. The main part of the tribometer is a horizontal linear unit with a timing-belt drive and a carriage. The ends of the unit are embedded in bases equipped magnets to fix the device to the rail. A stepper motor is used to drive the linear unit and to move the carriage with a measuring module along the rail. Its linear position is determined using a rotary encoder on the drive. The device is powered by a battery.

The measuring module, shown in Fig. 1, is attached to the carriage by a linear guide allowing free movement in the vertical direction to allow

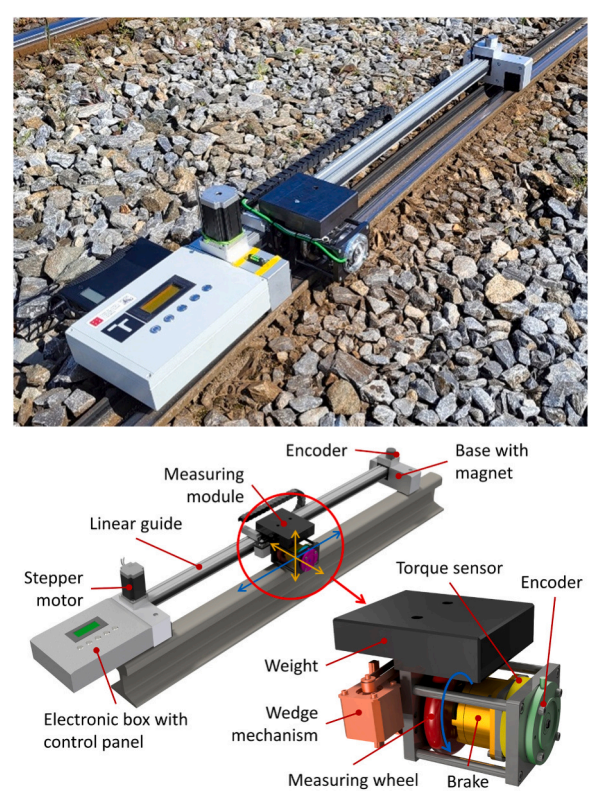

Fig. 1. BUT rail tribometer and the measuring module detail.

loading using a dead weight. Moreover, there is a wedge mechanism with a stepper motor to provide automatic positioning of the module in lateral direction, allowing measurements to be made on different contact paths. The measuring wheel is fixed on a shaft and attached to the rotor of the electromagnetic brake. Braking torque is measured with a torque transducer and shaft speed is recorded by the encoder. The measuring wheel is made of bearing steel and has a diameter of 100 mm and a transverse radius of 10 mm. The dimensions correspond to a scale of the contact width in the lateral direction of 1:10. The normal contact force is developed by the mass of the measuring module and additional weights, resulting in the theoretical Hertzian contact pressure of 0.8, 0.9 or 1 GPa. All parameters of the BUT rail tribometer are summarised in Table 1.

2.2. Data acquiring and processing

The relationship between the traction coefficient and creep is analysed by processing multiple signals to obtain a typical creep curve. The traction coefficient is calculated using data from the torque transducer attached to the brake, while the creep value is computed based on the values of the longitudinal module speed and the tangential wheel speed. Both these speeds are determined using rotary shaft encoders (see Fig. 1). Based on this data, a typical creep curve is plotted, as depicted in Fig. 2b. The stepper motor of the linear unit drives the measuring module along the rail. After reaching a constant speed of 260 mm/s, the brake starts to apply a braking torque according to the measuring mode described below. During a measurement, the wheel is rolling due to the traction force in the contact. When the brake develops sufficient torque, the creep starts to increase rapidly resulting in a blocking of the wheel and pure sliding in the contact. At the end of each measurement pass the data from the encoders and the torque transducer are post-processed automatically and the position-creep and position-braking torque curves (Fig. 2a) and the corresponding creep curve (b) are plotted.

The tribometer can operate in three measuring modes controlled by the three following parameters – initial and final braking torques and a number of steps. In the first mode, "Constant" (Fig. 3a), the measuring module runs over a rail section with constant braking torque. It is useful when some rail head sections have significantly different CoT and are too short to be investigated separately (e.g. TOR product spots) or when low-adhesion occurs as a transition phenomenon (e.g. during water evaporation). In the second one called "Step ramp" (b-c) the torque is gradually increased or decreased according to the set values and the steps are evenly distributed along the pass. Its main characteristic is the ability to make a creep curve in a single pass, while assuming adhesion conditions to be equal along the pass. The last mode (d) is called "Pulse" and alternates between two braking torques. The number of steps indicates the number of braking torque changes. It can be used when several transitions between rolling and sliding are required. In this study, only the Step ramp mode was used for all measurements.

The Gaussian filter is applied to a record of positions from the wheel and drive encoders, from which the velocities are calculated by using numerical derivation. Creep is given by Eq. (1) and pure sliding conditions correspond to 100%. The tangential force in the contact is obtained from an equilibrium of momentum (Eq. 2). The normal force is not measured directly; it is assumed to be a constant that was determined from the actual mass of the measuring module and weights. The CoT is defined as the ratio of the tangential and the normal forces (Eq. 3).

$$creep = \frac{v_L - v_R}{v_L} \cdot 100\% \tag{1}$$

$$T = \frac{2}{D}(I\alpha + M_B) \tag{2}$$

$$CoT = \frac{T}{Q} \tag{3}$$

Table 1
Parameters of the BUT rail tribometer.

Dimensions (mm)	1635 × 270×210
Weight (without battery and laptop) (kg)	21
Maximal evaluated distance (mm)	700
Minimal evaluated distance (mm)	200
Total stroke length (mm)	800
Range of lateral position (mm)	8
Speed of measuring module (mm/s)	260
Maximal Hertz pressures (GPa)	0.8, 0.9, 1
Normal force (N)	76, 110, 152
Measuring modes	Constant, step ramp, pulse
Contact	Elliptical
Main and transverse radii (mm)	50 and 10
CoT range (1)	0.02 – 0.7

2.3. Assessment of creep curve parameters

The raw data from the measurement is a point cloud, as shown in Fig. 2b, that is further processed. Three methods have been proposed to properly compare the traction curves and quantify their parameters.

The first one is the simplest and it only determines the effective CoT (CoT_e), i.e. a value at which the initial steep curve part transforms into the flat part that can slightly rise, fall or stay neutral. The braking torque is the controlled parameter and is used to calculate the CoT, so it can be said that the CoT is indirectly controlled; therefore, it must be evaluated in relation to the creep. The data from the passes are combined and only those that are within 5–15 per cent of the creep are selected to calculate a median CoT value. The 5% reliably separates points in the initial steep part of the curve, while the 15% provides enough points to calculate the median CoT.

The second method is based on the data approximation by Polach's model [39]. The tangential force in the contact F is calculated using Eqs. 4–7, where μ_0, A, B, k_A, k_S are sought parameters. The fit of the unadjusted data cannot achieve the same steepness in the low creep region as the measured data, so the following procedure has been proposed. The points are divided into three regions: – 10–5, 5–8 and 8–100 (Fig. 4a). The points in region *I* are approximated by the linear function passing through the origin (the black solid line in region *I*). This function is used to calculate new points (red points) that are equally distributed from the CoT minimum to the median. The median is computed from points in region *II*. The new dataset (Fig. 4b), which is subsequently fitted by Polach's model, consists of the calculated points in region *I* and the original points in regions *II* and *III*.

$$\mu = \mu_0\left[(1-A)e^{-Bw} + A\right] \tag{4}$$

$$\varepsilon = \frac{2}{3}\frac{C\pi a^2 b}{Q\mu}s \tag{5}$$

$$F = \frac{2Q\mu}{\pi}\left(\frac{k_A\varepsilon}{1+(k_A\varepsilon)^2} + \arctan(k_S\varepsilon)\right) \tag{6}$$

$$C = 3.2893 + \frac{0.975}{\frac{b}{a}} - \frac{0.012}{\left(\frac{b}{a}\right)^2} \tag{7}$$

The third method uses the modified FASTSIM model based on publication [40]. The model calculates shear stresses across a discretized contact area. This model assumes an elasto-plastic 3rd body layer on contacting surfaces, that affects the initial slope of the creep curve and limits CoT. The initial slope is reduced by adding the 3rd body layer flexibility coefficient L_e to Kalker's flexibility coefficient L_1 into FASTIM calculation, as seen in Eq. 8. The τ' represents shear stress from the previous calculation step that is located with a step difference Δa across the longitudinal strip. When the calculation exceeds the elastic limit $\mu_{c1}p$ a pseudo-plastic material model published by Voce [41] is used. Shear

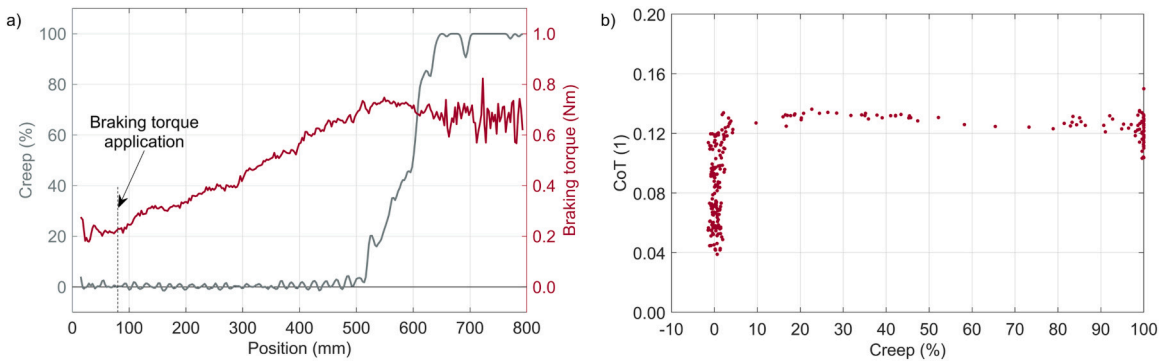

Fig. 2. a) Position-creep and position-braking torque curves of one pass obtained under step ramp measuring mode, b) corresponding creep curve.

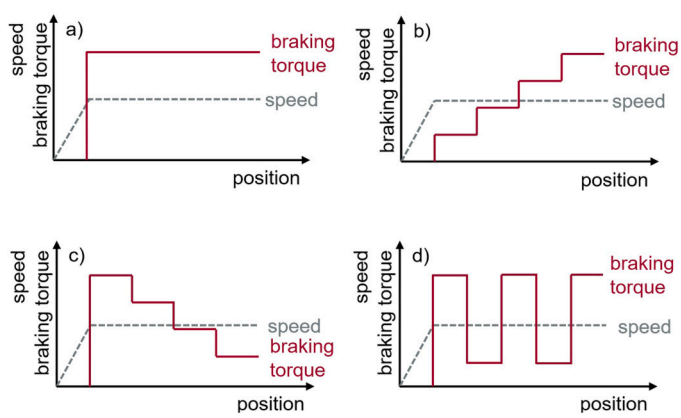

Fig. 3. Measuring modes: a) Constant, b) Step ramp - increasing c) Step ramp - decreasing, d) Pulse.

stresses in the pseudo-plastic region are defined by Eq. (9). The displacement value u is calculated using the equation from the elastic region. In these equations, the normal stress p is calculated in each discretized point using Hertzian contact theory. The resulting CoT is a ratio between shear stresses and normal stresses.

$$\tau = \tau' - \frac{2\Delta a}{v}\frac{s}{L_1 + L_e} \tag{8}$$

$$\tau = \mu_{c1}p + (\mu_{c2}p - \mu_{c1}p)(1 - e^{(-u+\mu_{c1}pL_e)/L_p}) \tag{9}$$

2.4. Conditions of experiments

The tests in this study were carried out in the laboratory on UIC60 rail under ambient temperature and relative humidity of 25 °C and 38%, respectively, and in field on the rail of a light rail transit at the temperature and relative humidity of 6 °C and 50%, respectively. The measuring wheel was cleaned with acetone before each series of passes to normalise its conditions and to make the results comparable. Three series of tests were carried out as follows and as indicated in Table 2.

The aim of the first test series consisting of 12 measurements was to investigate the effect of railhead conditions under various contact pressure on the CoT and a creep curve shape in laboratory-controlled conditions. The individual measurements involved a certain number of passes of the measuring module on the same contact path, while the resulting creep curves were derived from all the passes. The measurements were made for Hertzian contact pressure of 0.8, 0.9 and 1.0 GPa. The following contact conditions were simulated:

- The "clean" conditions are considered to represent the initial state of the rail after the cleaning. The rail was cleaned with acetone to remove any dirt and lubricant residues, but the presence of naturally occurring oxide layers has been assumed. During the measurement, the number of passes was limited to one or two due to the rapid increase in friction on repeated passes.
- The "run-in" conditions represent a 3rd body layer produced by a normal traffic. This layer was simulated using a wheel-rail contact device consisting of a cylindrical disc rolling along the tested rail with 2% slip and 0.8 GPa contact pressure. The run-in process has included 100 passes of the "conditioning" disc conducted before each test. After the run-in the rail surface was not cleaned to keep oxides and wear particles in place for the test.
- The water condition simulates heavy rain. The rail was cleaned with a solvent followed by a run-in process. Subsequently, the contact path was wiped with a dry cloth to remove excessive wear debris. Before the test, 20 ml of water was applied evenly along the length of the tested part of the rail.
- The TORL conditions correspond to the presence of a TOR lubricant (TORL) residual layer on a rail after several overruns. The tested part

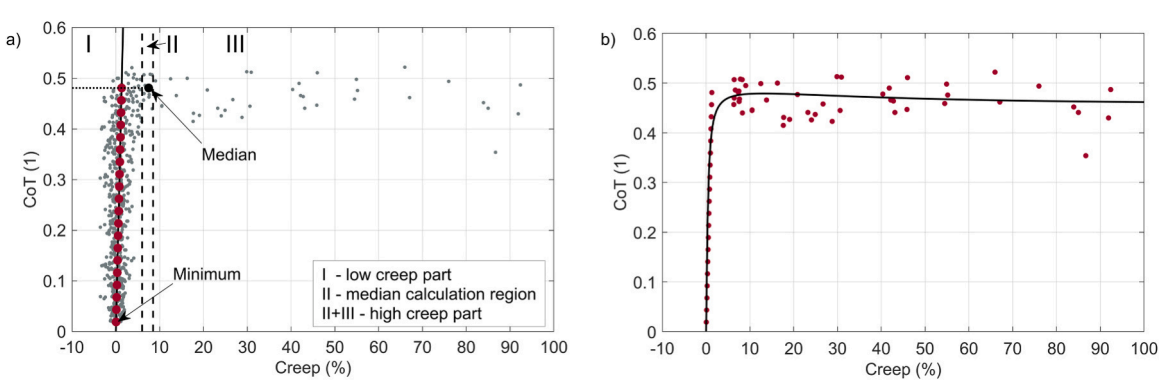

Fig. 4. Data adjustment for fitting (a) the original dataset and new point in the region *I*, b) a new dataset fitted by Polach's model).

Table 2
Conditions of tests.

Test series	Rail conditions	Contact pressure (GPa)	Number of passes	Rail run-in	Rail cleaning
1	Clean	0.8	2	no	yes
		0.9	1	no	yes
		1	2	no	yes
	Run-in	0.8	13	yes	no
		0.9	7	yes	no
		1	9	yes	no
	Water	0.8	12	yes	yes
		0.9	11	yes	yes
		1	14	yes	yes
	TORL	0.8	7	yes	no
		0.9	11	yes	no
		1	11	yes	no
2	Oil-based lubricant	0.9	30	no	no
3	laboratory	0.9	37	no	yes
	field	0.9	20	no	yes
	field	0.9	20	no	no

of the rail was evenly covered with 100 μl of conventional grease-based TORL, which was then wiped out with a paper towel as much as possible to create a thin layer that corresponds to the condition of the rail in real operation when TORL is used.

The second test series was aimed to demonstrate the repeatability of measurements. For this purpose, the rail was coated with a conventional oil-based lubricant (WD-40) to ensure stable friction conditions during individual passes. The measuring wheel was cleaned as for the previous measurements. The tribometer parameters were set so that the entire creep curve could be recorded during one pass, allowing the CoT_e to be evaluated and compared for each pass. A total of 30 passes were made at 0.9 GPa contact pressure.

The last set of measurements was carried out in the laboratory and in the field to investigate the effect of evolution of CoT. The contact pressure of 0.9 GPa was selected and the tribometer parameters were set to record the entire creep curve in one pass. In the laboratory, the rail was cleaned with a solvent to remove contaminants, while a run-in process was not included. In the field, a visibly clean section of the track, free of contaminants, was chosen. The intention was to observe the CoT evolution under real conditions, therefore the rail was not cleaned with a solvent and a run-in process was not performed.

3. Results and discussion

3.1. Effect of railhead conditions and contact pressure

Fig. 5 shows creep curves recorded under three contact pressures and four rail conditions. Each graph contains points from all measuring passes, further fitted by Polach's model (solid yellow) and modified FASTSIM model (dashed black). The parameters of the modified FASTSIM model are listed in Table 3. The agreement between the models is very good in almost all cases, only the run-in conditions show larger differences around the saturation point and at higher creep values but still show the same curve trend. The traction curves determined using the tribometer are relatively steep in the elastic area. The intersection of the linear region with the friction coefficient occurs at a creep of 1–2%, which is much closer to a prediction compared to other field tribometer [37].

The creep curves (Fig. 5) show a relatively low scatter that depends mainly on the number of measuring passes. The lowest scatter of the points is reported for the clean conditions (graph a-c), where only one or two passes were made. On the other hand, the run-in conditions (graph d-f) show the highest scatter of the points due to the device dynamics at higher CoT and creep. Slight variability in frictional conditions along the pass may also play a role, as further discussed.

The creep curves in Fig. 5a-c were recorded after the rail had been cleaned to remove all contaminants and residual grease. The curve trends change from slightly increasing to slightly decreasing with increasing the contact pressure, but the CoT_e values vary between 0.20 and 0.23, which is an intermediate friction value [6]. The run-in process shifts the CoT_e values to 0.4–0.5 (graph d-f) and the curves show a decreasing tendency for all contact pressures.

Water reduces the CoT_e to 0.35 – 0.4 and maintains the same curve trend (graph g-i) but the slope of the high creep part is not as steep as for the run-in conditions. The last three creep curves (graph j-l) represent the measurement after the application of TORL. The CoT_e reaches the lowest values, between 0.13 and 0.16. The trends of the curves at high creep are slightly increasing in two cases and slightly decreasing in the third (l).

The clean and the run-in conditions are considered as "dry" because no artificial contaminants are present, but they result in totally different creep curves in terms of the CoT and shape. It is assumed that the rail surface is covered with a thin oxide layer that reduces adhesion under the clean conditions. This layer is very easy to remove, so when more passes were made, the creep curve has a strong upward tendency in the high creep region as a result of energy dissipation due to the frictional work. This phenomenon will be discussed below. The run-in process has a cleaning effect removing the oxide layer. On the other hand, it promotes the formation of another layer consisting mainly of Magnetite (Fe_3O_4). This oxide tends to increase CoT [42].

In the case of water contamination, the CoT value is strongly dependent on the actual state of the resulting 3rd body layer. Relatively high values obtained in this study are consistent with previous data measured on MTM with samples made from the same material [43]. Lower values occur mainly in the field due to the interaction with other naturally occurring contaminants. Prolonged exposure to water also leads to the formation of hydrates [44], which usually reduce adhesion.

TORL should maintain an intermediate level of friction and ensure positive friction characteristics [5,6]. This statement cannot be fully approved because the trends of the curves are slightly increasing in two cases (Fig. 5j, k) and slightly decreasing in the third case (l). Although the residual layer containing a small amount of TORL was measured, the CoT values fall within the low friction band where lubricant should act, but TOR products should result in higher CoT. Studies [29,34] carried out in the field with the hand-pushed tribometer report similar CoT values, but a larger amount of TOR product was applied with a brush. On the other hand, different contact sizes affect the absolute CoT value compared to full-scale [24]. More TOR product ends up in a small contact, while less TOR product ends up in the actual contact because the excess is pushed away.

Fig. 6 shows the effect of the Hertzian contact pressure on the CoT under different conditions on the top of the rail head. The median (first) method was chosen for the evaluation, so the bars and error whiskers indicate the median of the selected points and the standard deviations, respectively.

The CoT decreases with increasing contact pressure for all conditions, while it is most evident for the run-in and the water conditions. The largest decrease was observed between 0.8 and 0.9 GPa in all cases, namely 10%, 12%, 8% and 13% for the clean, the run-in, the water and the TORL conditions, respectively. The results are consistent with other laboratory and field studies [18,32,34,45]. Studies using rail tribometers also report a significant decrease in the CoT for dry conditions, approximately 12% and 9% for a 0.1 GPa increase in contact pressure in the case of [34] and [45], respectively. The reduction depends on the conditions in contact as well as on the curvatures of the measuring wheel, roughness, and speed.

3.2. Comparison of evaluating methods

Three methods of evaluating the creep curve parameters have been

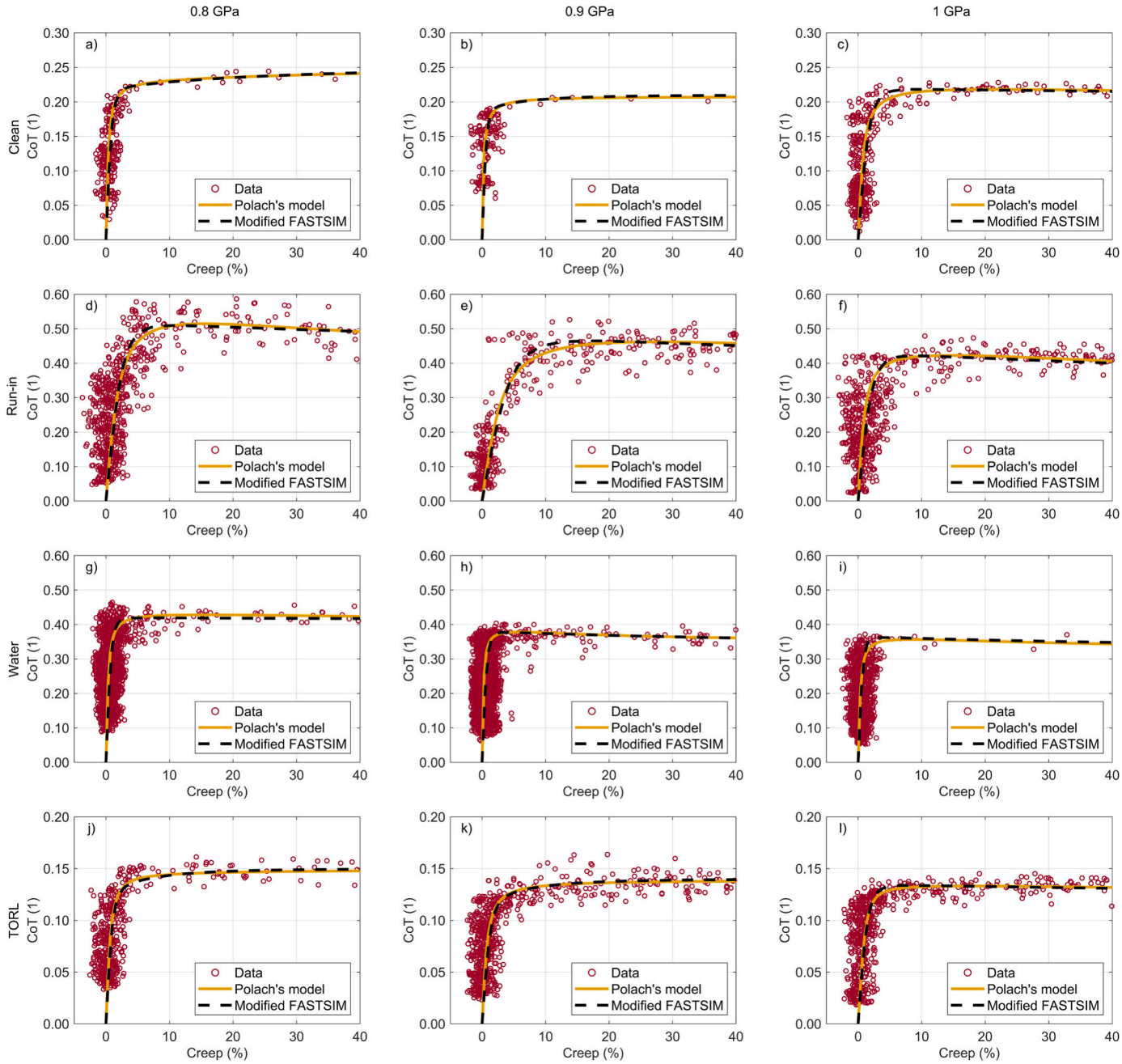

Fig. 5. Creep curves for clean, run-in, water and TORL conditions under contact pressure of 0.8, 0.9 and 1 GPa.

Table 3
Modified FASTSIM model parameters.

Conditions	Clean			Run-in			Water			TORL		
Contact pressure (GPa)	0.8	0.9	1	0.8	0.9	1	0.8	0.9	1	0.8	0.9	1
μ_1 (1)	0.22	0.19	0.22	0.52	0.48	0.43	0.42	0.38	0.365	0.13	0.12	0.135
μ_2 (1)	0.25	0.21	0.21	0.45	0.35	0.3	0.41	0.34	0.33	0.15	0.14	0.125
L_e ($*10^{-6}$)	250	200	500	300	600	300	100	100	100	500	700	700
L_p ($*10^{-3}$)	1.8	0.5	4	5	10	10	8	4	4	0.5	0.5	5

proposed. To compare the median method with the other two, the 10% creep was chosen to calculate the CoT values using Polach's and the modified FASTSIM models. The comparison of these methods for 0.9 GPa contact pressure is shown in Fig. 7. Despite the different complexity of the methods, the results are almost identical for all conditions except the run-in conditions, where the modified FASTSIM model gives a higher value of 0.033, which is 7%. The difference between the maximum and minimum values for the clean, water and the TORL conditions is 0.5%, 1.5% and 3.4% respectively. The median method gives good results, so it can be used for quick estimation of CoT_e,

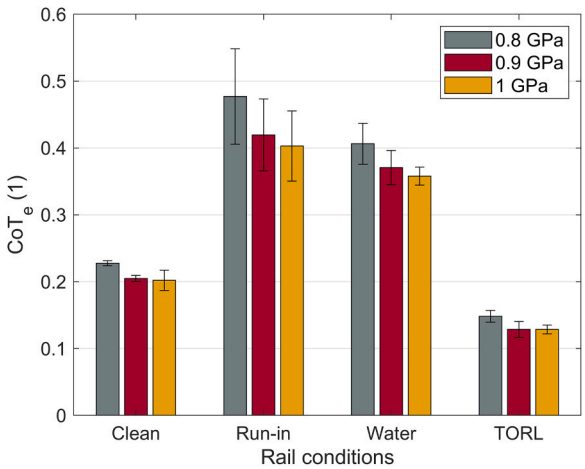

Fig. 6. Influence of contact pressure under clean, run-in, water and TORL conditions.

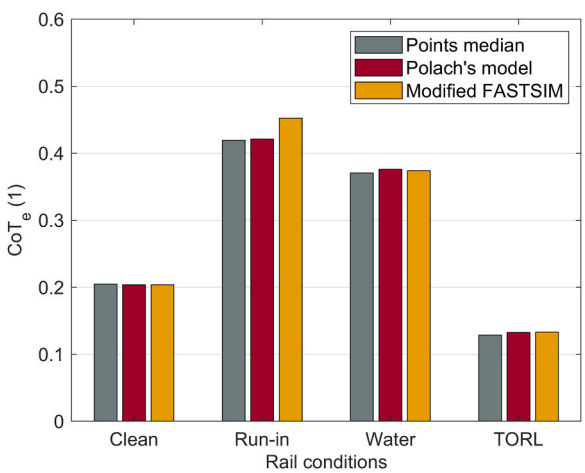

Fig. 7. Comparison of evaluation methods.

but it does not characterise the whole creep curve.

3.3. Repeatability of measurement

One of the important parameters of tribometers is the repeatability of the measurement, therefore a test under the stable friction conditions was carried out to define it. For better clarity, only some of the 30 passes are shown in Fig. 8a). The passes together form a creep curve without any large deviations caused by subsequent passes because the rail was coated with a conventional lubricant to maintain stable, unchanging conditions. The CoT$_e$ values of all 30 passes with standard deviations are shown in Fig. 8b).

The mean CoT$_e$ value is 0.1352 and the standard deviation is 0.0039 calculated for all passes. The maximum difference between individual passes and the mean is 0.0052 for the fifth and sixth passes. The most of further passes are slightly shifted higher thus the differences are smaller, around 0.0032, but there are still passes with a lower CoT$_e$.

3.4. The effect of subsequent passes

The final test series was carried out to define the effect of repeating passes along the same contact path when an evolution in friction conditions is assumed. The first measurement was made in the laboratory under clean conditions. It shows a strong upward trend with an increasing number of passes (Fig. 9). For the first 20 passes, the maximum braking torque applied was increased before each pass to record the entire creep curve. In some of the passes, the measuring wheel was blocked at the end of the pass resulting in 100% creep. Between passes 21 and 26 the maximum braking torque was not high enough, so the number of points in the high creep region was lower but the CoT$_e$ remained similar. The maximum braking torque was gradually increased in the last ten passes, otherwise the entire creep curve would not be recorded. The last pass reached 0.55 CoT$_e$ which corresponds to the creep curve in Fig. 5e).

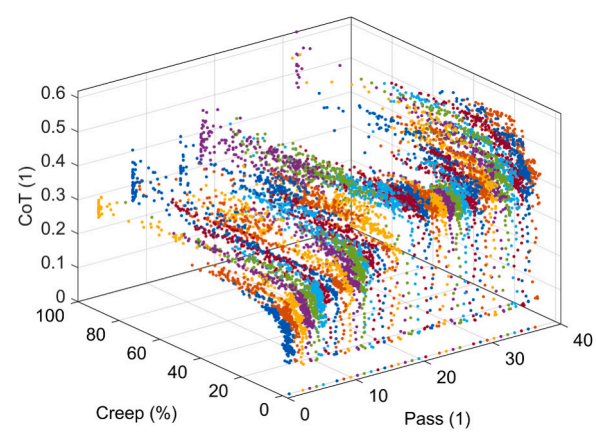

Fig. 9. Creep curve development with a rising number of passes.

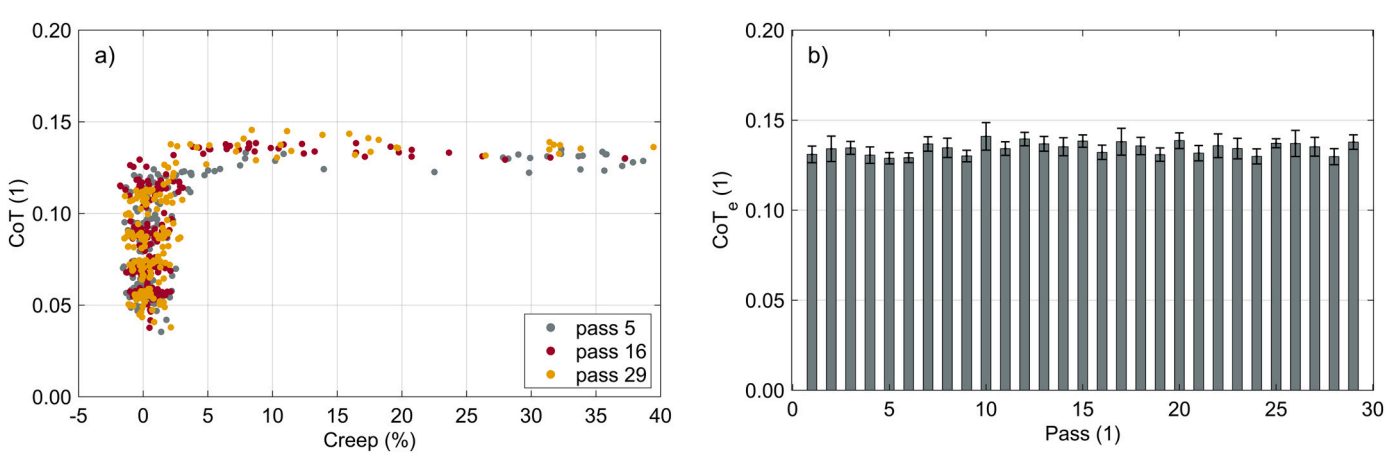

Fig. 8. a) Creep curves of repeatability test, b) CoT development with an increasing number of passes.

A similar measurement was carried out in the field to compare the laboratory results with the real conditions. The comparison is shown in Fig. 10. In the case of the solvent-cleaned rail, the same trend and CoT_e gradient as in the laboratory was achieved, while the value of CoT_e was about 0.04 lower in the field. Once the solvent was not used for rail cleaning, a stable CoT_e of 0.25 occurred even after 20 passes. This indicates the presence of a durable 3rd body layer. The layer is made up of substances capable of absorbing the frictional work without changing the contact conditions despite the high creep achieved in each pass. However, the substances are easily soluble in acetone, resulting in much weaker 3rd body layer. It can be concluded, that although the solvent is often used in a laboratory to obtain reference conditions, it is not suitable when a real layer is studied. The cleaning process has significant effect not only to the instantaneous value of CoT but also on the durability of the 3rd body layer.

The previous study [46] reported an increasing CoT during a braking test. The following wheelsets reach a higher CoT than the previous one, which is caused by the cleaning effect. The following wheelsets can be represented by successive measuring passes [47]; therefore, the CoT should increase within the passes, but this did not happened in our case when the rail was not cleaned. A possible explanation is that the BUT rail tribometer does not deliver sufficient energy to the contact to induce the cleaning effect. This phenomenon should be further investigated.

The number of passes is a critical parameter with the ability to alter the results, so it should be respected during a measurement. A small number of passes should be selected to measure the current condition of the rail, e.g. oxide layer or easily removable layers. This will ensure that there is no degradation of the layer. On the other hand, a large number should be selected to evaluate wear resistance of the friction layer, which can be an important parameter e.g. for lubricants and TOR products.

3.5. Limitation in the study

The main uncertainties have been assessed (Table 4) to define a deviation of the measurement using the tribometer. Uncertainties such as the non-repeatability of the torque transducer and bearing losses are independent of the exact CoT value and they are two orders of magnitude smaller. A further uncertainty arises from the error between the actual and set diameters of the measuring wheel. This error is linearly dependent on the diameter deviation (e.g. a deviation of 0.2 mm corresponds to 0.2% of CoT). The largest uncertainty is caused by the normal force variation due to friction losses in vertical linear guides. The losses occur as the measuring wheel moves vertically and reacts to irregularities on the rail. It has been estimated to be up to 4% at a contact pressure of 0.9 GPa.

Another possible uncertainty lies in the clearances in the measuring module and its guide. The traction force may cause a slight inclination of the module due to the clearances. The non-zero angle of attack creates a lateral creep which influences and reduces the longitudinal creep being evaluated [32]. Based on the investigations carried out, this deviation can be considered negligible.

Table 4
Uncertainties of measurement.

Non-repeatability of torque transducer	0.00091 CoT
Bearing loses	0.00023 CoT
Diameter deviation	0.2 mm corresponds to 0.2% of CoT
Loses in vertical guides	Up to 4% of CoT

In the addition to these uncertainties affecting CoT, there is also an error in creep measurement. This error is caused by the finite resolution of the encoders and it is directly responsible for the scatter of points in the low creep region (e.g. Fig. 8a), where the difference between the longitudinal and circumferential velocities is very small. It is also the reason for the negative creep values, as can be seen in the position data (Fig. 2a). This problem is overcome by the proposed fitting methods described in chapter 2.3.

The results may be affected by the material of the measuring wheel that is made of bearing steel with a higher hardness compared to regular wheel steel. Bearing steel was chosen for technological reasons, particularly because it provides much stable conditions. Moreover, lower wear of the measuring wheel has less effect on the real contact conditions.

3.6. Comparison with other tribometers

Several tribometers have been developed for assessing the CoT in the field, some of them are also suitable for laboratory use, see Fig. 11. These results indicate that all devices provide the highest traction coefficients under dry conditions. In the case of TOR products, the results cannot be directly compared because different TOR products were used, and the applied amounts were not the same. The effect of water also varies, which may be attributed to the amount or duration of water on the specimen surfaces. Furthermore, significant differences exist among these devices, including variations in contact body size, material, and roughness. It's also important to note that these devices differ significantly in terms of kinematics. While the BUT tribometer achieves typical rolling-sliding conditions, the pendulum tribometer operates under pure sliding conditions. Other devices, such as the HO tribometer, employ an angle of attack to simulate rolling-sliding conditions. Simultaneously, it is necessary to mention that the measurements were conducted at various locations and in different environments. Therefore, a straightforward comparison of values between tribometers can be misleading. Similarly, it is quite challenging to compare these values with data collected by an instrumented train if the measurements did not take

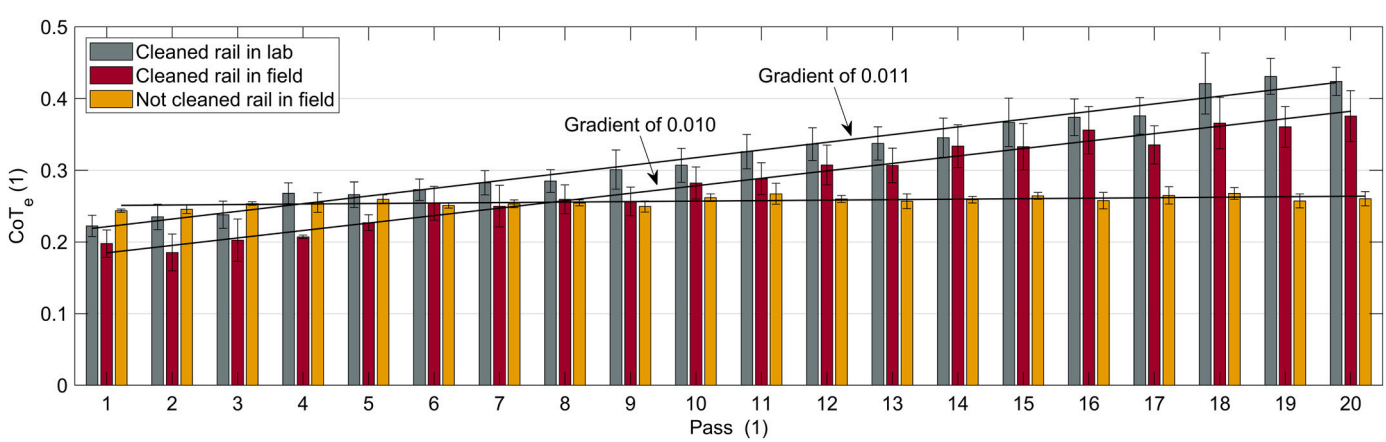

Fig. 10. CoT development in the field and in the laboratory.

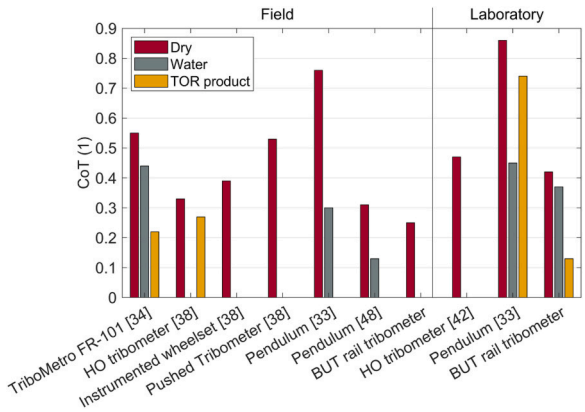

Fig. 11. The comparison of tribometers [33,34,38,42,48].

place simultaneously, on the same track, and under the same environmental conditions. Despite these limitations, these tribometers still enable comparative measurements, which can be very useful prior to testing using an instrumented train. Individual tribometers and their benefits are discussed below.

The Hand-pushed Tribometer [32], TriboMetro FR 101 [34] and HO tribometer [35] can measure the friction also at the gauge corner of the rail, whereas the Pendulum [33,48] and the BUT rail tribometer can only measure the CoT at the top of the rail. The extension of BUT rail tribometer will be made in future work.

TriboMetro FR 101, HO tribometer and BUT rail tribometer allow to assess the entire creep curve. The TriboMetro FR 101 and the BUT rail tribometer record the creep while the measuring wheel is braked, meanwhile, the HO tribometer yaws the wheel to induce lateral creep. The first method is closer to the actual wheel-rail contact. With the TriboMetro FR 101, measurements are taken over several metres of the rail, which can distort the resulting creep curve due to varying friction conditions along the measured section. The HO tribometer and the BUT rail tribometer are fixed to the rail and measure a shorter section of the rail, so the resulting creep curve is not as affected by changing friction conditions. These devices can also be advantageously used in a laboratory environment. When set up appropriately, the entire traction curve can be measured in one pass, so the negative effect of friction changes during repeated passes can be suppressed.

4. Conclusion

The new approach to the creep curve assessment using the new rail tribometer was presented. The measurement on the fixed part of the rail allows to study tribology of the wheel-rail interface in both, the laboratory and field. The controlled traction force approach has been chosen to simulate conditions of the real wheel-rail contact. Several approaches were implemented to evaluate the creep curve parameters. The creep curve measurement usually consists of several passes of the measuring module; nevertheless, if the control parameters are set correctly, the entire creep curve may be evaluated in one pass. The approach provides a useful tool to evaluate parameters of TOR products such as redistribution, carry distance, retentivity and others. Thanks to the high creep induced by the tribometer, and the ability to measure the entire traction curve in one pass, the tribometer can be used to investigate the wear resistance of the friction layer. This is especially important when developing friction layer models, implementing friction management techniques, etc.

The specific findings and conclusions from the application of the methodology are as follows:

- Effective coefficient of traction (CoT_e) decreases with increasing contact pressure.
- Traction curves were fitted by Polach's analytical model and modified FASTSIM model. Despite the different complexity of the methods, the results of CoT_e vary within 2% compared to the models describing the entire creep curve.
- The running-in of the rail increases CoT significantly and provides negative creep-curve characteristics. This conditioning technique is suitable to provide "reference" conditions in the laboratory.
- Using a solvent to clean the rail in the field significantly reduces the durability of the real 3rd body layer.

Statement of originality

As a corresponding author, I Martin Valena, hereby confirm on behalf of all authors that:

1) The authors have obtained the necessary authority for publication.
2) The paper has not been published previously, that it is not under consideration for publication elsewhere, and that if accepted it will not be published elsewhere in the same form, in English or in any other language, without the written consent of the publisher.
3) The paper does not contain material which has been published previously, by the current authors or by others, of which the source is not explicitly cited in the paper.

Upon acceptance of an article by the journal, the author(s) will be asked to transfer the copyright of the article to the publisher. This transfer will ensure the widest possible dissemination of information.

Declaration of Competing Interest

The authors declare that they have no known competing financial interests or personal relationships that could have appeared to influence the work reported in this paper.

Data availability

Data will be made available on request.

Acknowledgements

This work was carried out in the framework of the projects "Josef Bozek National Center of Competence for Surface Vehicles" (TN01000026) and "Bozek Vehicle Engineering National Center of Competence" (TN02000054) that were co-financed from the state budget by the Technology Agency of the Czech Republic within the programme "National Centres of Competence".

References

[1] Harmon M, Lewis R. Review of top of rail friction modifier tribology. Tribol - Mater Surf Interfaces 2016;10:150–62. https://doi.org/10.1080/17515831.2016.1216265.
[2] Olofsson U, Lyu Y. Open system tribology in the wheel-rail contact-a literature review. Appl Mech Rev 2017;69:1–10. https://doi.org/10.1115/1.4038229.
[3] Eadie DT, Santoro M. Top-of-rail friction control for curve noise mitigation and corrugation rate reduction. J Sound Vib 2006;293:747–57. https://doi.org/10.1016/j.jsv.2005.12.007.
[4] Eadie DT, Elvidge D, Oldknow K, Stock R, Pointner P, Kalousek J, et al. The effects of top of rail friction modifier on wear and rolling contact fatigue: Full-scale rail–wheel test rig evaluation, analysis and modelling. Wear 2008;265:1222–30. https://doi.org/10.1016/j.wear.2008.02.029.
[5] Stock R, Stanlake L, Hardwick C, Yu M, Eadie D, Lewis R. Material concepts for top of rail friction management – classification, characterisation and application. Wear 2016;366–367:225–32. https://doi.org/10.1016/j.wear.2016.05.028.
[6] White B, Lee ZS, Lewis R. Towards a standard approach for the twin disc testing of top-of rail friction management products. Lubricants 2022;10:124. https://doi.org/10.3390/lubricants10060124.
[7] Evans M, Skipper WA, Buckley-Johnstone L, Meierhofer A, Six K, Lewis R. The development of a high pressure torsion test methodology for simulating wheel/rail contacts. Tribol Int 2021;156:106842. https://doi.org/10.1016/j.triboint.2020.106842.

[8] Kvarda D, Skurka S, Galas R, Omasta M, Shi L, Ding H, et al. The effect of top of rail lubricant composition on adhesion and rheological behaviour. Eng Sci Technol Int J 2022;35:101100. https://doi.org/10.1016/j.jestch.2022.101100.
[9] Lewis SR, Lewis R, Olofsson U, Eadie DT, Cotter J, Lu X. Effect of humidity, temperature and railhead contamination on the performance of friction modifiers: pin-on-disk study. Proc Inst Mech Eng Part F J Rail Rapid Transit 2013;227: 115–27. https://doi.org/10.1177/0954409712452239.
[10] Khalladi A, Elleuch K. Tribological behavior of wheel-rail contact under different contaminants using pin-on-disk methodology. J Tribol ASME 2017;139. https://doi.org/10.1115/1.4033051.
[11] Galas R, Omasta M, Krupka I, Hartl M. Laboratory investigation of ability of oil-based friction modifiers to control adhesion at wheel-rail interface. Wear 2016; 368–369:230–8. https://doi.org/10.1016/j.wear.2016.09.015.
[12] Cann PM. The "leaves on the line" problem - a study of leaf residue film formation and lubricity under laboratory test conditions. Tribol Lett 2006;24:151–8. https://doi.org/10.1007/s11249-006-9152-2.
[13] Arias-Cuevas O, Li Z, Lewis R, Gallardo-Hernandez EA, Gallardo-Hernández EA. Rolling-sliding laboratory tests of friction modifiers in dry and wet wheel-rail contacts. Wear 2010;268:543–51. https://doi.org/10.1016/j.wear.2009.09.015.
[14] Galas R, Omasta M, Klapka M, Kaewunruen S, Krupka I, Hartl M. Case study: the influence of oil-based friction modifier quantity on tram braking distance and noise. Tribol Ind 2017;39:198–206. https://doi.org/10.24874/ti.2017.39.02.06.
[15] Zhu Y, Chen X, Wang W, Yang H. A study on iron oxides and surface roughness in dry and wet wheel-rail contacts. Wear 2015;328–329:241–8. https://doi.org/10.1016/j.wear.2015.02.025.
[16] Shrestha S, Spiryagin M, Harisson H, Persson I, Meehan P, Wu Q, et al. Introduction of rail cleaning effect into locomotive traction study based on tribometer measurements. ICRT 2021 - Proc. 2nd Int. Conf. Rail Transp, vol. 15. Reston, VA: American Society of Civil Engineers,; 2022. p. 41–51. https://doi.org/10.1061/9780784483886.006.
[17] Chen H, Kimura S, Ikoma K, Ishizaka K, Suzumura J, Hibino S. Evaluation test of tangential force coefficient under different types of fallen leaves. Wear 2023: 205072. https://doi.org/10.1016/j.wear.2023.205072.
[18] Chen H, Namura A, Ishida M, Nakahara T. Influence of axle load on wheel/rail adhesion under wet conditions in consideration of running speed and surface roughness. Wear 2016;366–367:303–9. https://doi.org/10.1016/j.wear.2016.05.012.
[19] Bosso N, Magelli M, Zampieri N. Investigation of adhesion recovery phenomenon using a scaled roller-rig. Veh Syst Dyn 2021;59:295–312. https://doi.org/10.1080/00423114.2019.1677922.
[20] Guidoum S, Merino P, Saulot A, Berthier Y, Hervieu S. Experimental study of the influence of the relative humidity of leaves and their link to adhesion losses in the wheel-rail contact. Mech Ind 2022;23:23. https://doi.org/10.1051/meca/2022017.
[21] Zhang P, Li Z. Experimental study on the development mechanism of short pitch corrugation using a downscale V-Track test rig. Tribol Int 2023;180:108293. https://doi.org/10.1016/j.triboint.2023.108293.
[22] Voltr P, Lata M. Transient wheel-rail adhesion characteristics under the cleaning effect of sliding. Veh Syst Dyn 2015;53:605–18. https://doi.org/10.1080/00423114.2014.961488.
[23] Zhang W, Chen J, Wu X, Jin X. Wheel/rail adhesion and analysis by using full scale roller rig. Wear 2002;253:82–8. https://doi.org/10.1016/S0043-1648(02)00086-8.
[24] Buckley-Johnstone L, Harmon M, Lewis R, Hardwick C, Stock R. A comparison of friction modifier performance using two laboratory test scales. Proc Inst Mech Eng Part F J Rail Rapid Transit 2019;233:201–10. https://doi.org/10.1177/0954409718787045.
[25] White B, Hyland-Knight J, Lewis R. Assessing the effectiveness of traction gels using full-scale and field testing. Proc Inst Mech Eng Part F J Rail Rapid Transit 2021;235:690–9. https://doi.org/10.1177/0954409720953943.
[26] Lewis SR, Riley S, Fletcher DI, Lewis R. Optimisation of a railway sanding system: adhesion tests. Int J Railw Technol 2017;6:87–98. https://doi.org/10.4203/ijrt.6.2.5.
[27] Lewis SR, Lewis R, Olofsson U. An alternative method for the assessment of railhead traction. Wear 2011;271:62–70. https://doi.org/10.1016/j.wear.2010.10.035.
[28] Lewis R, Lewis SR, Zhu Y, Abbasi S, Olofsson U. The modification of a slip resistance meter for measurement of railhead adhesion. Proc Inst Mech Eng Part F J Rail Rapid Transit 2013;227:196–200. https://doi.org/10.1177/0954409712455147.
[29] Lundberg J, Rantatalo M, Wanhainen C, Casselgren J. Measurements of friction coefficients between rails lubricated with a friction modifier and the wheels of an IORE locomotive during real working conditions. Wear 2015;324–325:109–17. https://doi.org/10.1016/j.wear.2014.12.002.
[30] Meierhofer A, Trummer G, Bernsteiner C, Six K. Vehicle tests showing how the weather in autumn influences the wheel–rail traction characteristics. Proc Inst Mech Eng Part F J Rail Rapid Transit 2020;234:426–35. https://doi.org/10.1177/0954409719863643.
[31] Lanigan JL, Krier P, Johnstone LB, White B, Ferriday P, Lewis R. Field trials of a methodology for locomotive brake testing to assess friction enhancement in the wheel/rail interface using a representative leaf layer. Proc Inst Mech Eng Part F J Rail Rapid Transit 2021;235:1053–64. https://doi.org/10.1177/0954409720973135.
[32] Harrison H, McCanney T, Cotter J. Recent developments in coefficient of friction measurements at the rail/wheel interface. Wear 2002;253:114–23. https://doi.org/10.1016/S0043-1648(02)00090-X.
[33] Harmon M, Santa JF, Jaramillo JA, Toro A, Beagles A, Lewis R. Evaluation of the coefficient of friction of rail in the field and laboratory using several devices. Tribol - Mater Surf Interfaces 2020;14:119–29. https://doi.org/10.1080/17515831.2020.1712111.
[34] Areiza YA, Garcés SI, Santa JF, Vargas G, Toro A. Field measurement of coefficient of friction in rails using a hand-pushed tribometer. Tribol Int 2015;82:274–9. https://doi.org/10.1016/j.triboint.2014.08.009.
[35] Harrison H. Development of a Third Generation Tribometer. CM2015–0130 2015; September.
[36] Spiryagin M, Persson I, Hayman M, Wu Q, Sun YQ, Nielsen D, et al. Friction measurement and creep force modelling methodology for locomotive track damage studies. Wear 2019;432–433:202932. https://doi.org/10.1016/j.wear.2019.202932.
[37] Persson I, Spiryagin M, Casanueva C. Influence of non-dry condition creep curves in switch negotiation. Veh Syst Dyn 2023;61:892–904. https://doi.org/10.1080/00423114.2022.2037668.
[38] Eadie DT, Harrison H, Kempka R, Lewis R, Keylin A, Wilson N. Field assessment of friction and creepage with a new tribometer. 2018 Proc 11th Int Conf Contact Mech Wear Rail/Wheel Syst C 2018;vol. 17:208–17.
[39] Polach O. Creep forces in simulations of traction vehicles running on adhesion limit. Wear 2005;258:992–1000. https://doi.org/10.1016/j.wear.2004.03.046.
[40] Kvarda D, Galas R, Omasta M, Shi L, Ding H, Wang W, et al. Asperity-based model for prediction of traction in water-contaminated wheel-rail contact. Tribol Int 2021;157:106900. https://doi.org/10.1016/j.triboint.2021.106900.
[41] Voce E. The relationship between stress and strain for homogeneous deformation. J Inst Met 1948;74:537–62.
[42] Harrison H. Producing and measuring the 3rd body layer. Jt. Rail Conf, 2020. American Society of Mechanical Engineers,; 2020. p. 1–7. https://doi.org/10.1115/JRC2020-8095.
[43] Galas R, Omasta M, Shi L bing, Ding H, Wang W jian, Krupka I, et al. The low adhesion problem: the effect of environmental conditions on adhesion in rolling-sliding contact. Tribol Int 2020;151. https://doi.org/10.1016/j.triboint.2020.106521.
[44] White BT, Lewis R, Olofsson U, Lyu Y. The contribution of iron oxides to the wet-rail phenomenon. Civ-Comp Proc 2016;vol. 110. https://doi.org/10.4203/ccp.110.154.
[45] Harrison H. The development of a low creep regime, hand-operated tribometer. Wear 2008;265:1526–31. https://doi.org/10.1016/j.wear.2008.03.028.
[46] Bosso N, Gugliotta A, Magelli M, Oresta IF, Zampieri N. Study of wheel-rail adhesion during braking maneuvers. Procedia Struct Integr 2019;24:680–91. https://doi.org/10.1016/j.prostr.2020.02.060.
[47] Shrestha S, Spiryagin M, Harisson H, Persson I, Meehan P, Wu Q, et al. Introduction of rail cleaning effect into locomotive traction study based on tribometer measurements. ICRT 2021 - Proc 2nd Int Conf Rail Transp 2022:41–51. https://doi.org/10.1061/9780784483886.006.
[48] Folorunso MO, Lewis R, Lanigan JL. Effects of temperature and humidity on railhead friction levels. Proc Inst Mech Eng Part F J Rail Rapid Transit 2022. https://doi.org/10.1177/09544097221148236/ASSET/IMAGES/LARGE/10.1177_09544097221148236-FIG8.JPEG.

Tribology International 197 (2024) 109810

Contents lists available at ScienceDirect

Tribology International

journal homepage: www.elsevier.com/locate/triboint

A benchmarking methodology for top-of-rail products: Carry distance and retentivity

Radovan Galas [a,*], Martin Valena [a], Tomas Jordan [a], Daniel Kvarda [a], Milan Omasta [a], Simon Skurka [a], Bingnan Wu [b], Haohao Ding [b], Wen-jian Wang [b], Ivan Krupka [a], Martin Hartl [a]

[a] Faculty of Mechanical Engineering, Brno University of Technology, Technicka 2896/2, 616 69 Brno, Czech Republic
[b] Tribology Research Institute, State Key Laboratory of Traction Power,Southwest Jiaotong University, Chengdu 610031, China

ARTICLE INFO

Keywords:
Wheel–rail contact
Friction modifier
Top-of-rail lubricant
Portable tribometer

ABSTRACT

Top-of-rail (TOR) products are used in railways to reduce wear and noise by providing an intermediate friction level and a positive creep curve. In addition to these general requirements, retentivity and carry distance are important for their effectiveness on the track. This study aims to determine these track performance parameters for three commercial TOR products. A contact simulator and portable tribometer were used to simulate track conditions. The results show that carry distance is the most limiting performance parameter of TOR products, especially for water-based products. TOR lubricants, on the other hand, caused a more significant drop in friction after application. A predictive model simulating product redistribution along the track was introduced for the best-performing product.

1. Introduction

Top-of-rail (TOR) products are used to achieve an intermediate level of friction and a positive creep in the wheel tread-rail head contact [1]. These friction properties enable the reduction of squeal noise [2,3] wear [4,5] corrugation [6,7] fatigue crack generation [8,9], fuel consumption [10], and derailment risk [11]. However, this approach has some limitations, including a negative effect on pre-existing cracks [12] and an amount-dependent effect [13,14], which may result in failure to achieve the desired benefits [15] or braking issues [16]. Furthermore, the performance of TOR products can vary across different railway systems [17] and may be influenced by contaminants and weather conditions [18,19]. Lastly, the performance may significantly differ based on the type of TOR product. Currently, several types of products are distinguished on the market [20], namely friction modifiers (FMs, water-based products), TOR lubricants (oil or grease-based products), and solid sticks (resin-based products).

Finding a suitable TOR product and determining its optimal amount for a particular track may be challenging. In general, the performance of TOR products can be investigated using field and laboratory testing. Field testing provides realistic results but is time-consuming and expensive. Moreover, ensuring consistent conditions during ongoing experiments may be extremely difficult. In contrast, laboratory testing is usually more cost-effective and can be conducted under well-controlled conditions. One of the challenges of this test is the transferability of the results to field conditions. Another problem is that it is difficult to compare results obtained in different laboratories due to differences in the equipment and conditions used.

Considering these facts, the author has recently introduced a benchmarking methodology [21], categorising TOR products into four performance classes (Q1-Q4). The methodology utilises a commercial tribometer, the Mini-Traction machine, with standard specimens to ensure the transferability and comparability of results across different laboratories. This methodology, further referred to as the Lab-to-Lab methodology, enables the identification of the most suitable TOR product for subsequent, more comprehensive testing.

However, the experimental conditions should be designed to closely simulate conditions occurring on a track for subsequent laboratory testing. Achieving these conditions is important for studying the transfer mechanisms of TOR products as they significantly affect product performance. Trummer et al. [22] described three key transfer mechanisms: (1) the pick-up of the product by the wheel, (2) the repeated transfer of the product between the wheel and rail, and (3) the consumption of the product. These transfer mechanisms determine the performance parameters of TOR products, such as carry distance [1] and product retentivity [23]. The carry distance expresses the distance from the point of application to the point at which the effect of the TOR product

* Corresponding author.
E-mail address: Radovan.Galas@vut.cz (R. Galas).

https://doi.org/10.1016/j.triboint.2024.109810
Received 11 March 2024; Received in revised form 9 May 2024; Accepted 21 May 2024
Available online 25 May 2024
0301-679X/© 2024 Elsevier Ltd. All rights are reserved, including those for text and data mining, AI training, and similar technologies.

Nomenclature

AP	application point of TOR product (the zero imprint)
CTZ	critical traction zone
FM	friction modifier
ITZ	intermediate traction zone
LTZ	low traction zone
Q1-Q4	performance classes of TOR products
RTZ	retentivity traction zone
TOR	top-of-rail
TORL	top-of-rail lubricant
TORL-A	top-of-rail lubricant A
TORL-B	top-of-rail lubricant B
THV	threshold value
0	zero TOR product imprint after wheel pass
0_{bp}	zero TOR product imprint before wheel pass
α	angular acceleration (s^{-2})
CoT	coefficient of traction (1)
C	critical traction parameter (m)
D	measuring wheel diameter (m)
i	imprint number (1)
I	intermediate traction parameter (m)
I_R	inertia moment (kgm^2)
k_d	product division factor (1)
k_0	product residue factor (1)
m_a	TOR product applied amount (μl; μg)
M_B	braking torque (Nm)
m_r	amount of TOR product on the rail (μg)
m_w	amount of TOR product on the wheel (μg)
N_i	number of effective imprints (1)
n_r	number of passes required for run-in process (1)
OLF	over-lubrication factor (1)
Q	normal force (N)
R	retentivity traction parameter (m)
R_{i0}	retentivity of imprint i_0 (the imprint at the AP) (1)
T	traction force (N)
v_L	longitudinal speed of measuring module (ms^{-1})
v_R	tangential speed of measuring wheel (ms^{-1})

becomes negligible, while the product retentivity expresses the number of wheel passes over which a TOR product is effective at a given track location. Rail segments and a scaled wheel may offer a promising configuration to study these performance parameters in laboratory conditions, as introduced in [24]. Another option is to use rail segments in combination with a portable tribometer, which is a method commonly used to test TOR products [16,25].

This work extends the research carried out by the same authors in two previous studies, which introduced a benchmarking methodology for TOR products (the Lab-to-Lab methodology) [21] and a new portable tribometer (further referred to as the BUT tribometer) [26]. This study aims to develop the second phase of the benchmarking methodology, further referred to as the Lab-to-Field methodology, which will enable the track performance parameters of TOR products, such as carry distance and retentivity, to be determined under conditions that closely simulate track conditions. Moreover, the study determines the optimal amount of TOR product, as its performance is usually highly amount-dependent. The developed methodology is demonstrated by investigating the performance of three TOR products previously tested in the Lab-to-Lab methodology [21] to introduce and simultaneously verify the results of this two-phase testing of TOR products. For this Lab-to-Field methodology, a new contact simulator with rail segments was developed to create a representative TOR product layer, which was then analysed using the BUT tribometer. This second phase of the

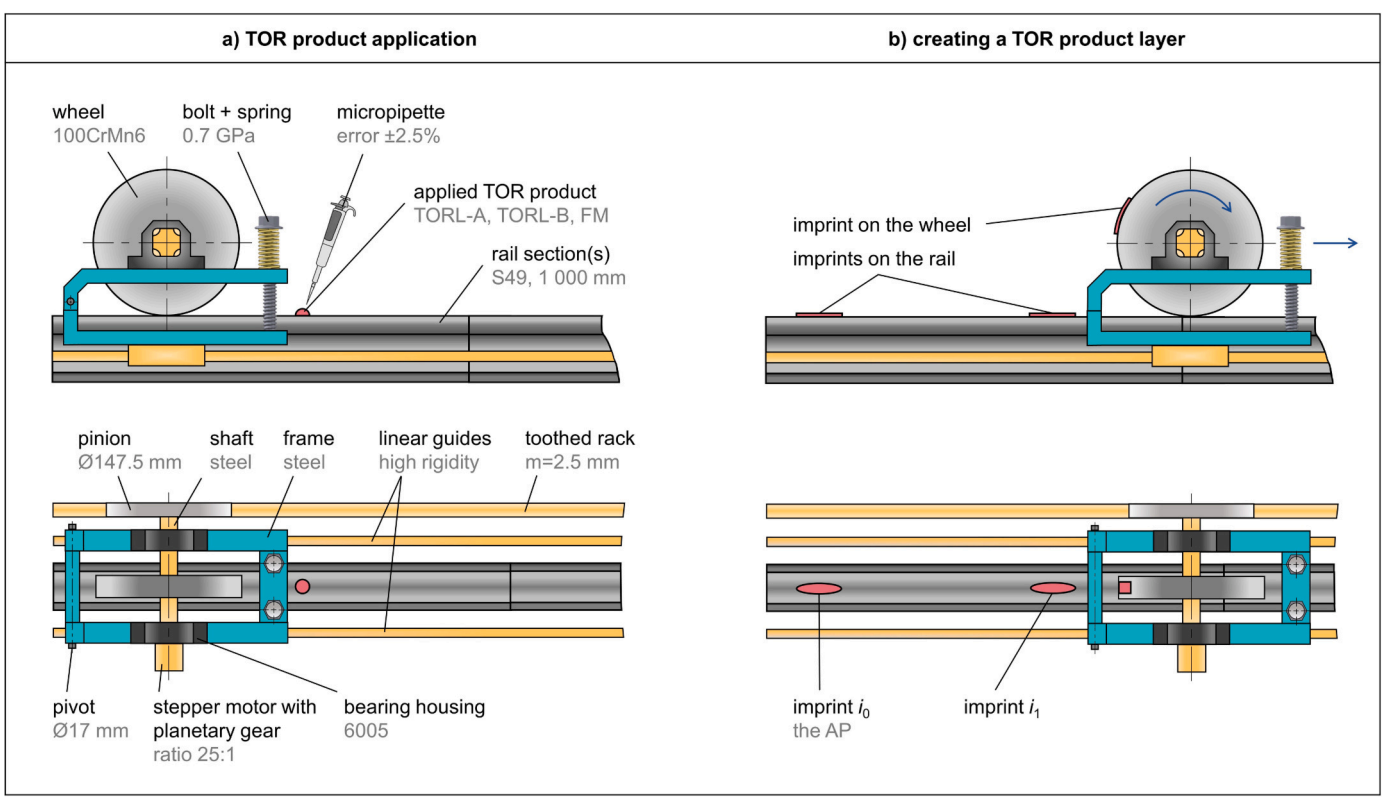

Fig. 1. Contact simulator: (a) TOR products application, (b) creating a TOR product layer.

benchmarking methodology for TOR product testing is considered to be the final step in laboratory testing, allowing the number of field tests to be minimised before the TOR product is put into service.

2. Material and methods

2.1. Contact simulator: run-in process and creating a TOR product layer

A contact simulator shown in Fig. 1 was employed to create a TOR product layer on a railheadt. The main components of this simulator include three interchangeable segments of the S49 rail, each measuring 1 m in length (3 m in total), and a cylindrical wheel made of bearing steel with a diameter of 150 mm. If experiments require a longer rail track, all segments can be easily replaced to extend it. Furthermore, this change can be made repeatedly. In this study, all rail segments were changed three times (a total of twelve rail segments were used) to ensure sufficient track length.

The cylindrical wheel is pressed against the rail by a bolt and spring. This loading mechanism is placed on the lever, enabling it to achieve a contact pressure of 0.7 GPa. The wheel is propelled by a stepper motor with a planetary gearbox, while the linear movement (0.2 m/s) of the frame with the wheel is ensured by linear guides. To induce creep in the contact, a pinion is mounted at the end of the shaft, engaging with the toothed rack during forward movement. This configuration maintains a constant creep of 1.67 % between the cylindrical wheel and rail segments.

The running-in of contact specimens was initially conducted before the application of TOR products (the running-in is not included in Fig. 1). The run-in process consisted of multiple passes of the contact simulator wheel over rail segments (all twelve segments were gradually run in) used in the subsequent experiments with TOR products. Furthermore, the run-in process included periodic measurements of the coefficient of traction (CoT) using the BUT tribometer, taken after every twenty passes. The run-in process was completed when the CoT stabilised at the expected values for dry contact conditions. Depending on the creep value and the device used, these values typically range between 0.4 and 0.6 [26,27]. The run-in process also helps to stabilise the surface roughness of the contact bodies. When the run-in process was completed, the contact surfaces became smoother; however, some manufacturing surface irregularities (e.g., small pits and shallow scratches) were still visible on the rail surfaces. The average surface roughness of the rail segments and the wheel of the contact simulator (measured in the contact path using a portable surface roughness tester) was 0.83 ± 0.20 and 0.52 ± 0.06 μm, respectively. After that, the tested TOR product was applied to the top of the rail using an electronic micropipette with a 0.2 ml tip volume, as shown in Fig. 1(a). This setup ensured that systematic errors remained below ± 1.6 % and random errors below ± 2.5 % while maintaining a minimum dosage of 1 μl. Subsequently, a single pass of the wheel of the contact simulator over the rail segments is conducted to create several imprints of the TOR product (further referred to simply as imprints) on both the wheel and the rail surfaces, as depicted in Fig. 1**(b)**. After that, the rail segments were changed and another pass of the wheel was conducted. No additional TOR product was then applied, but only the TOR product remaining on the wheel surface (after the previous pass) was distributed by the wheel movement along the replaced rail segments. As mentioned above, this change of rail segment was carried out three times. It means that an initially applied amount of TOR product was gradually spread along the twelve rail segments. It should be noted that the length of the track, consisting of twelve rail segments (twenty-four imprints in total), was sufficient for all the conditions tested in this study. After a tested TOR product was spread along twelve rail segments, the wheel of the contact simulator was cleaned with a solvent. After the imprints were analysed using the tribometer, the rail segments were also cleaned with a solvent. The subsequent procedure varies depending on the specific type of the experiment, as detailed in Section 2.3.

2.2. BUT tribometer: analysing frictional properties on the railhead

The BUT tribometer is a portable tribometer developed to evaluate the railhead friction for the creep range of 0 to 100 % [26]. Fig. 2(a) shows the BUT tribometer fixed on one rail segment using bases with magnets. A key part of this tribometer is a measuring module whose linear movement (a speed of 0.26 m/s) is ensured by a stepper motor, belt drive, and linear guide. This measuring module consists of a measuring wheel made of bearing steel, with a diameter of 100 mm and a transverse radius of 10 mm, an electromagnetic brake, a torque sensor, and a shaft encoder. Furthermore, there is a weight (steel block) and wedge mechanism to achieve the required contact pressure of 0.9 GPa and set the horizontal position of the measuring wheel, see yellow arrows in Fig. 2(a). The wedge mechanism also ensures the guidance of the measuring wheel in the vertical direction (red arrows). A specific vertical position of the measuring wheel is given by the surface of the rail. The control of the tribometer data acquisition is ensured by an electronic unit placed at the end of the tribometer. It is important to emphasise that the BUT tribometer can measure extremely low values of the CoT, reaching as low as 0.02 [26], so it does not introduce any important limitations to this study.

Fig. 2(a) depicts a typical setup where the BUT tribometer is fixed on the rail to analyse the friction properties of the imprint on the run-in rail. Different braking torque values (M_B) were applied to the wheel of the tribometer as it moved over the imprint. It means that creep was not a controlled variable, but its value changed in response to the braking torque and the friction properties of the imprint, as in the case of real wheel-rail contact. Creep values were then calculated using data from a pair of encoders, Eq. (1). CoT was calculated based on the traction and normal forces in contact obtained from the weight and data from the torque sensor, see Eqs. (2) and (3). A combined dataset allowed for plotting a point cloud, based on which the creep curve is obtained using the Polach model [28], as illustrated in Fig. 2(b).

$$\text{creep} = \frac{v_L - v_R}{v_L} 100\% \tag{1}$$

$$T = \frac{2}{D}(I_R \alpha + M_B) \tag{2}$$

$$\text{CoT} = \frac{T}{Q} \tag{3}$$

It should be noted that several passes of the measuring wheel over the imprint were sometimes required to obtain enough points to plot the creep curve. The number of required passes depends on the friction properties of the imprint and the braking torque setting. Another important note is that the obtained data were sorted according to linear position before plotting the creep curve. This sorting ensured that only the data corresponding to the imprint were chosen for creep curve visualisation. This sorting process was skipped for measurements under dry conditions (without TOR product). As indicated in Fig. 2**(b)**, several parameters were evaluated for each analysed imprint:

- CoT_1 – the average CoT calculated using the data obtained within the creep range of 5 % to 20 %,
- CoT_2 – the average CoT calculated using the data obtained within the creep range of 60 % to 90 %,
- the trend/shape of the creep curve (fitted by a Polach model),
- the Over-lubrication factor (OLF),
- visual aspect of the imprint.

The OLF was defined in a previous study [21] as one of the key parameters describing the behaviour of TOR products. This factor expresses how close the behaviour of a tested TOR product is to the ideal TOR product, which has been defined as a product that provides only the intermediate level of CoT from application until the effect of the TOR

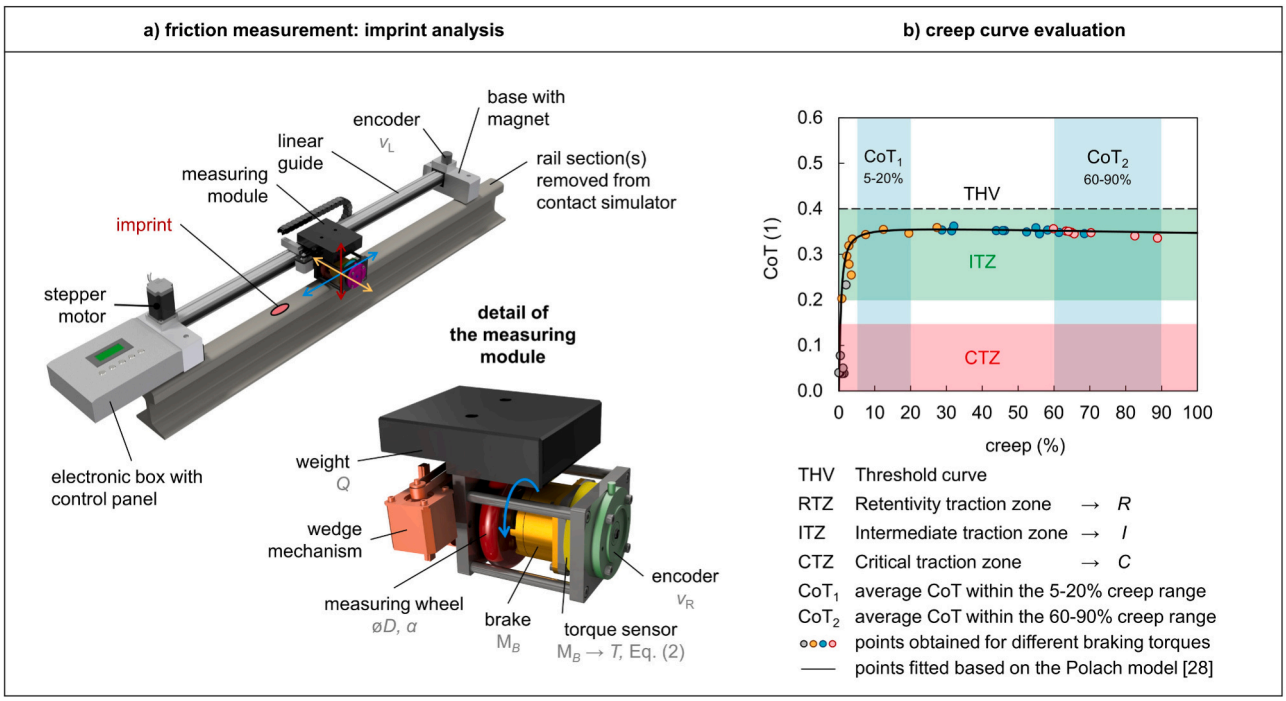

Fig. 2. BUT tribometer: (a) friction measurement: imprint analysis, (b) creep curve evaluation.

product becomes insignificant. In other words, this product does not cause low or even critically low CoT. The OLF can take values from 0 to 1. The closer the OLF value is to 1, the better the behaviour of the TOR product can be expected in terms of the desired friction properties (ideal TOR product). In contrast, a lower OLF value can indicate a risk of contact over-lubrication, which can cause traction and braking problems.

For the OLF calculation, the following three traction zones of the CoT must first be defined: the critical traction zone (the CTZ; insufficient CoT for vehicle acceleration and deceleration), the intermediate traction zone (the ITZ; required traction zone to achieve expected benefits) and the retentivity zone (the RTZ; zone covering the distance over which the TOR product affects the CoT). Note that the RTZ includes all points below the threshold value (the THV), which is considered to be the same value as the upper level of the ITZ, as shown in Fig. 2**(b)**. The specific values of all these zones and the THV were defined based on the CoT values for dry conditions, and their specific values are described in Section 3.1.

Once the required traction zones are known, the points of the creep curve obtained for a particular imprint are then categorised into these zones. Based on this, the cumulative sliding distance is calculated for each individual traction zone; thus, the three traction parameters are obtained: critical traction parameter C, intermediate traction parameter I and retentivity traction parameter R. Then, the OLF can be calculated using Eq. (4). A detailed derivation of this equation is given in the study [21].

$$\mathrm{OLF} = \frac{RI + R(R-C) + I(R-C)}{3R^2} \tag{4}$$

2.3. Type of experiments

Two types of experiments were carried out in this study to evaluate the track performance parameters of the TOR products under conditions similar to field conditions. The first type of experiment is further referred to as the carry distance test, as its objective was to evaluate the ability of TOR products to spread along the rail. After the above-described preparation of the TOR layer (Section 2.1), each imprint was sequentially analysed using the BUT tribometer (Section 2.2). Each imprint was analysed individually during the evaluation process until the CoT_1 and/or CoT_2 values exceeded the THV. When this situation occurred, the imprint no longer provided the desired friction properties, allowing the number of effective imprints N_i to be evaluated. This parameter can then be used to calculate the carry distance for a particular vehicle type depending on the diameter of the wheels. Due to the time demands of this test, only every fourth imprint (labelled 0, 4, 8, 12, 16, and 20) was sequentially analysed. Note that imprint labels such as '0' represent the point of application of the TOR product (the AP). The other imprints (4−20) represent the sequence of imprints analysed along the rail.

Based on the results of the carry distance tests, this test was extended to investigate the transfer behaviour of the best-performing TOR product. This investigation involved wiping the imprints on the rail with a paper towel, which was subsequently weighed using an analytical balance with a resolution of 0.1 mg. The residual amount of TOR product on the wheel surface was similarly assessed at the end of the test.

The second type of experiment aimed to evaluate the retentivity of the TOR products; therefore, this experiment is referred to as the retentivity test, as its objective was to determine how long an analysed imprint was able to provide the required friction properties. Similar to the previous test, this test began with the run-in process followed by the creation of a TOR product friction layer (Section 2.1).

However, in the case of the retentivity test, only the zero imprint '0' (at the AP) was analysed using the BUT tribometer (the other imprints were not analysed). If CoT_1 or CoT_2 did not exceed the THV, the contact simulator wheel and the BUT tribometer wheel were cleaned with a paper towel. Subsequently, another pass using the contact simulator was performed over this imprint, followed by another analysis of the imprint using the BUT tribometer. This process was repeated until either CoT_1 or CoT_2 exceeded the THV. When this situation occurred, the imprint no longer provided the desired friction properties, allowing the retentivity of the analysed imprint R_{i0} to be evaluated. This parameter expresses the number of driven wheelsets for which the analysed imprint provided the desired friction properties. This parameter thus expresses the number of driven wheelsets over which the imprint has maintained the desired friction properties. Due to the time demands of this test, the zero imprint

was analysed after a certain number of passes, specifically after 1, 10, 20, 30, 60, 100, and 150 passes. In addition, more frequent imprint analyses would reduce retentivity due to the effect of measurement, making the results less representative.

2.4. Experimental conditions and tested TOR products

The experiments conducted in this study are categorised into four sets. Sets no. 1 and 2 were carried out to investigate the CoT values under dry conditions, the number of passes required for the run-in process, and the optimum amount of TOR product. The obtained results were used as input parameters for experimental set no. 3 and 4, in which the performance of TOR products was investigated. The experimental conditions for these sets are listed in Table 1.

Table 1 shows that set no. 1 was performed under dry conditions (without TOR product) to determine the optimal duration of the run-in process. The run-in process duration refers to the required number of passes of the contact simulator wheel over the rail segments, denoted as n_r, required to stabilise the CoT at the expected values for dry contact conditions. This number of passes is determined based on CoT_1, CoT_2, and CoT_{max} values. The last parameter expresses the maximum value of the CoT recorded during the experiment. This parameter is used only for this particular experimental set, providing a valuable reference for comparing the dry level of the CoT with existing literature. Additionally, creep curves were plotted to differentiate between non-run-in and run-in contact. These data, collected for the run-in contact, were subsequently used to establish CTZ, ITZ, and THV (Section 3.1), as mentioned above.

Set no. 2 aimed to determine the optimal amount of TOR product for subsequent testing. This set was included in this study because the performance of TOR products, mainly TOR lubricants, can be highly dependent on the applied amount [21,29]. Therefore, TOR lubricant (specifically TORL-B) was used for this experimental set, where the carry distance test was performed for four different amounts. Based on this testing, 80 μl was identified as the most appropriate amount for set no. 3 and 4, as described in Section 3.2.

Note that the amounts tested in set no. 2 were chosen based on the maximum amount recommended by the manufacturer for the wayside application of TORL-B. However, a contact analysis revealed that the contact area for the used configuration was approximately ten times smaller than that for the chosen reference tram (Skoda 15 T with a maximum axle load of 75 kN and a new wheel diameter of 666 mm). This analysis suggested that the tested amount of TORL-B for the Lab-to-Field configuration should not exceed 80 μl. Therefore, the tested amount range of TORL-B was adjusted to 4–80 μl.

The tests conducted within sets no. 3 and 4 aimed to investigate the most important performance parameters of three commercial TOR products, see Table 1. These sets involved testing two TOR lubricants (TORL-A and TORL-B) and one friction modifier (FM). It is important to note that all of these TOR products are primarily designed to reduce curve squeal. TORL-A and TORL-B are TOR lubricants based on biodegradable ester oil, with a thickener and soft metal particles. The NLGI consistency number of TORL-A and TORL-B is 0 and 00, respectively. In contrast, the tested FM is a pure water-based product without oil or grease. This product is designed to create a thin dry friction layer as the base medium (water) evaporates.

The objective of set no. 3 was to investigate the carry distance, the OLF, and the transfer behaviour of the best-performing TOR products, while set no. 4 focused on the retentivity and creep curves. As mentioned above, both these sets employed a fixed amount of 80 μl and continued the tests until reaching the THV. It is important to note that the run-in process preceded each of these tests, and each test was repeated twice.

3. Results and discussion

3.1. Initial tests under dry conditions: determining the run-in process duration (set no. 1)

The development of the CoT over the number of passes is depicted in Fig. 3(a). This figure shows that the CoT for non-run-in surfaces ranged between 0.2 and 0.3. After a mild decrease, the CoT increased with the growing number of passes. The CoT stabilised around 0.5 for both low (CoT_1; creep from 5 to 20 %) and high creep (CoT_2; creep from 60 to 90 %) regions after 100 passes, with the CoT_{max} reaching a value of 0.56. Subsequent passes mainly showed a gradual increase in CoT_2 and CoT_{max}, reaching 0.56 and 0.59, respectively. The higher values of CoT_2 compared to CoT_1 imply a positive trend in the creep curve, as shown in Fig. 3(b). This figure illustrates the creep curves for non-run-in and run-in contacts (after 100 passes) obtained using the Polach model. Both creep curves exhibit a positive trend across the entire tested creep range, reaching the saturation point at a creep level between 5 % and 10 %.

A similar trend in the creep curve under dry conditions was observed in [30–32], where portable tribometers were employed. These studies and the present study imply that capturing the falling friction effect, typically occurring when a vehicle operates on a track under dry conditions [33–35], might be challenging when using a portable tribometer. This phenomenon was recently described by Eadie et al. [32], who proposed two hypotheses to explain this unexpected shape of the creep curve under dry conditions. The first hypothesis suggests that this unexpected shape can be associated with the tribometer used in their study, which operated with low longitudinal and high lateral creep. However, this hypothesis can be falsified as the falling friction effect was not observed even in the present study, where the BUT tribometer operated at high longitudinal creep. The second hypothesis proposes that the absence of falling friction may be associated with low sliding speed, which is a limitation evident even in this study. Although high creep values were achieved, the sliding speed was still notably lower than in real operation. This means that the temperature in the contact did not reach such high values, which may explain the absence of the falling friction effect. Another significant aspect may be attributed to the substantial difference in the moment of inertia of the wheel of the tribometer and the wheel of a vehicle.

The development of the CoT over the number of passes in Fig. 3 is in good agreement with previously published results from both laboratory [26,30] and field conditions where the rail cleaning effect was

Table 1
Experimental conditions of initial tests (sets no. 1–2) and TOR product performance tests (sets no. 3–4).

set no.	TOR product	applied amount	test duration	measured param.	evaluated param.	Fig. No.
1	none (dry conditions)	-	to stabilise the CoT	CoT, creep	CoT_1, CoT_2, CoT_{max}, n_r, creep curve	3
2	TORL-B	4, 10, 20, 80 μl	to THV	CoT, creep	CoT_1, CoT_2, N_i	4
3	TORL-B TORL-A FM	80 μl	to THV	CoT, creep	N_i transfer behaviour[a] OLF	5-8
4	TORL-B TORL-A FM				R_{i0} creep curves	9-11
	Overall performance assessment of TOR products					12

[a] The transfer behaviour was studied only for the best-performing TOR product (TORL-B) regarding the carry distance.

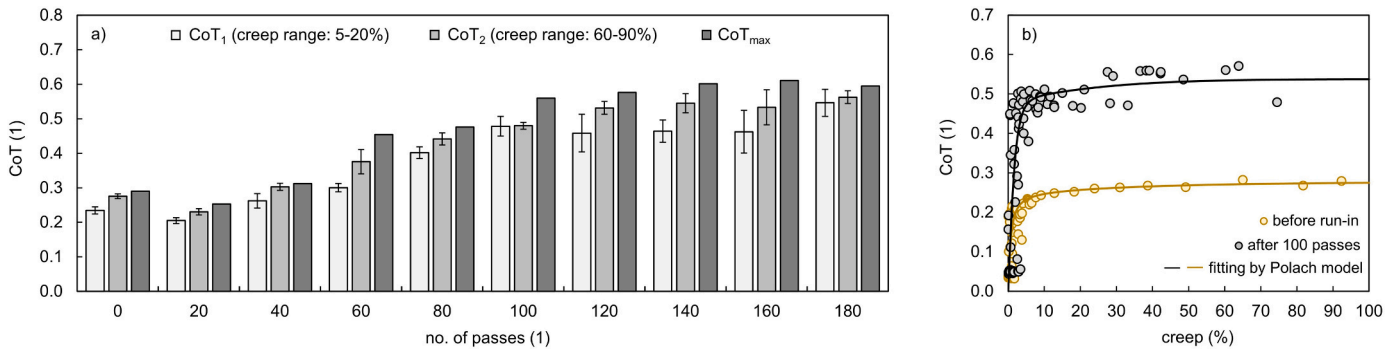

Fig. 3. (a) Development of the CoT over the number of passes, (b) creep curves for non-run-in and run-in contact.

introduced [36]. This cleaning effect/run-in process removes the third body layer that naturally forms on the contact surfaces. Moreover, the run-in process also removes an 'artificial' third body layer, which was formed on the surfaces as a result of solvent cleaning. This 'artificial' third body layer can reduce the CoT as was observed in [21]. This rail cleaning/running process increased the CoT from 0.2–0.3 to almost 0.6, as shown in Fig. 3(b). This value approaches the upper limit of values measured using portable tribometers (0.35–0.65) [30,37,38]. This wide range of the CoT is likely associated with the naturally occurring third body layer on rails [31], which is not formed in the same way under laboratory conditions. Therefore, higher CoT values are obtained under laboratory conditions.

Based on this initial testing, it was determined that a run-in process of 120 passes is required before each experiment in step no. 2–4. This slightly extended number of passes was chosen to ensure proper conditioning of both surfaces before conducting experiments with TOR products.

The data obtained for these run-in conditions were subsequently used to design CTZ, ITZ, and THV, which are crucial for the performance assessment of the TOR product. With CoT_{max} reaching almost 0.6, the range for ITZ was set at 0.2–0.4, consistent with the values in [39], [40]. CoT values required for traction and braking vary significantly across different railway systems; however, a selected value of 0.15 seems optimal for most of these systems. THV value was set to be identical to the upper limit of ITZ, specifically at 0.4, as the impact of TOR products becomes negligible above this limit. The same strategy for selecting THV was used in the previous work [21]. For graph clarity, the graphs below display only the CTZ and ITZ zones, as THV aligns with the upper limit of ITZ.

3.2. Initial tests with TOR lubricant: determining an optimal amount (set no. 2)

Fig. 4 shows the development of the carry distance for four different amounts of TORL-B. These findings suggest that the carry distance increases with a higher amount of TOR product, but the relationship is not linear. It can be seen that the same carry distance was observed for both 4 μl and 10 μl. However, it can be anticipated that the carry distance might be slightly longer for 10 μl if the performance of each imprint was evaluated individually rather than just every fourth, as mentioned in Section 2.3. In contrast, Chen et al. [41] revealed in their field study that increasing the amount of the TOR product, specifically two and a half times, did not affect the carry distance.

An increasing amount of TORL-B also influenced the average CoT for each analysed imprint. In Fig. 4, the lowest average CoT was consistently observed for the zero imprint (at the AP), where the highest amount of TOR product remained on the rail, as discussed and shown below. As the product amount increased from 4 μl to 80 μl, the CoT value at the the zero imprint decreased from 0.22 to 0.16. This finding indicates that a twenty-fold increase in the TOR product amount resulted in a 27 % reduction in the CoT at the AP while the carry distance doubled. Based on these results, 80 μl was chosen for further testing of various TOR products due to its ability to achieve the longest carry distance among the tested amounts while still maintaining the CoT above the critical value of 0.15 (even at the AP).

These results indicate that the influence of the amount on the performance of TOR products is less significant than previously reported in laboratory studies [13,23]. This difference can be mainly attributed to the specific devices employed for TOR product testing. This study utilised a configuration more closely simulating real track conditions, with one surface being TOR product-free. In contrast, many previous studies employed small-scale devices where both surfaces were uniformly covered with TOR product almost immediately after the experiment began. This condition often resulted in lower CoT values.

Another potential difference lies in experimental conditions, as small-scale tests are usually conducted at higher speeds and lower surface roughness. This combination can lead to a change in the lubrication regime. Moreover, contact starvation occurs more slowly when both surfaces are covered with a TOR product. Unlike small-scale devices that typically operate at a fixed creep value (usually less than 5 %), this study

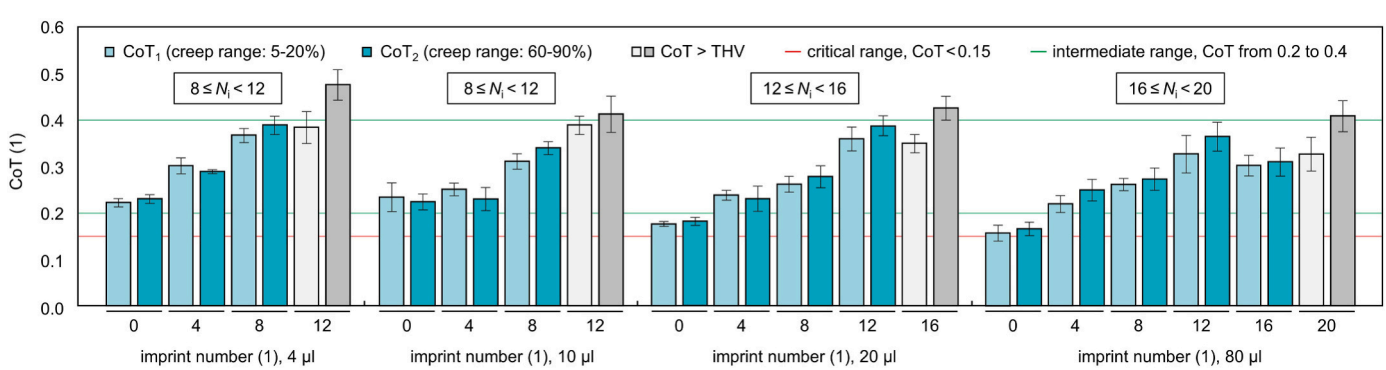

Fig. 4. The carry distance test for four different amounts of TORL-B.

covers a wide creep range from 0 % to 100 %, resulting in a faster removal of the TOR product layer and consequently leading to a faster increase in the CoT during imprint analysis.

3.3. Carry distance test, transfer behaviour, and OLF: comparison of tested TOR products (set no. 3)

The results of carry distance tests for three different TOR products, applied in the same amount of 80 μl, are shown in Fig. 5(a)-(c). These results show that both tested TOR lubricants provided significantly longer carry distances than FM. While TORL-B and TORL-A effectively affected friction properties up to 16 and 8 imprints, respectively, FM exhibited the required friction properties in only one imprint. This difference might be mainly attributed to the difference in tackiness influencing the carry distance [29]. Another reason could also be associated with the drying behaviour of FM.

The number of passes can be approximately converted into the carry distance in meters using the circumference of the vehicle wheel (e.g. 666 mm for the mentioned tram Skoda 15 T). According to these calculations, the carry distances for tested TOR products TORL-B, TORL-A, and FM are 33–42 m, 16–25 m, and 2 m, respectively. The carry distances for both tested TOR lubricants are presented as ranges, as the imprint analysis was conducted for every fourth imprint.

These results highlight a limitation of TOR products in carry distance compared to manufacturer claims that often state carry distance in kilometres. Similar findings were reported in [42], where the carry distance achieved 70 m and 450 m for rapidly and slowly drying products, respectively. Nevertheless, it is important to note that the carry distance in [42] was evaluated using an energy-dispersive X-ray analysis of the cotton swab collecting the third-body layer from the rail. However, it can be expected that the carry distance assessed through CoT measurements would be shorter than that determined using an energy-dispersive X-ray analysis. This is because this method is able to detect even small residual amounts of product on the rail, with a negligible influence on friction.

In terms of the CoT, it is evident that, except for the zero imprints, all analysed imprints of the tested products met the targeted CoT value within the ITZ. FM nearly met the required ITZ even at the AP, while the other two TOR products exhibited the CoT lower than 0.2, likely due to their oil-based nature. These values are consistent with track measurements using portable tribometers, where the CoT ranged between approximately 0.11 and 0.22 [16,25,43]. Unlike experiments using small-scale laboratory devices, where the CoT often falls below 0.15 [44–46], the present study shows a less significant drop in the CoT. The higher CoT values observed here may be attributed to the fact that the average CoT values for the analysed imprint are used rather than the frequently used minimum CoT in other laboratory studies.

Fig. 6 shows that after the wheel passes over the puddle of TOR product (the AP), the product spreads in the travel direction, and the remaining part is squeezed out laterally to the sides. This phenomenon arises due to the inability of the product to withstand the high pressure in the central part of the contact, as previously described for water-based products [47] and traction gels [48]. Consequently, only a minimal amount of TOR products remains within the contact band [49], especially in the case of TORL-A and FM. This can result in surfaces appearing unlubricated, as also observed on a real track [50]. However, it can be expected that the rail surface is still coated by a very thin friction layer, calculated to be less than 1 μm [50], consisting of solid particles from TOR products. The formation of this extremely thin, visually invisible layer is supported by a study [47], which describes the potential transfer of solid particles (without base medium) between contact surfaces. These facts can explain why visually unlubricated rails, depicted in Fig. 6(b) (4th and 8th imprint) and Fig. 6(c) (1st and 2nd imprint), could provide the intermediate CoT level.

Fig. 7(a) illustrates the transfer behaviour of TORL-B, which was tested as the final test of set no. 3 focused on investigating the transfer behaviour of the best-performing TOR product (TORL-B) in relation to the results of the carry distance tests. Note that '0_{bp}' and '0' represent the zero imprint (at the AP) before the wheel pass (index 'bp') and after the wheel pass (without index), respectively. The obtained results showed that as the number of imprints increased, the amount of TORL-B on the rail and wheel surfaces decreased exponentially. Besides this, it was observed that after the wheel passes over the AP, the product puddle was divided between the rail and the wheel in a ratio of 45:55. This ratio is in good agreement with Lee et al. [29], who reported a ratio of approximately 50:50 for FM. Note that the data from the fifth and subsequent imprints were not included in the evaluation because the weight of the wiped layer was already below the detection limit of the used analytical balance. However, there was a high residual amount of TOR product on the sides of the wheel contact band, as depicted in Fig. 7 (a). Particularly, the wheel picked up 66 mg from the rail during the first pass; however, 29 mg (44 % of the picked-up amount) remained on the sides of the wheel contact band after the fifth pass. This residual amount did not re-enter the contact band during subsequent passes. A similar residual amount of TOR products was found on the sides of the wheel contact band at the end of the carry distance tests, see Fig. 8(a)-(c).

Utilising the knowledge of the residual amount on the sides of the wheel contact band, the data from Fig. 7(a) were recalculated to the effective amount of TOR product that was directly in the contact band, see Fig. 7(b). These recalculated data were then used to develop a prediction model simulating the redistribution of TOR product applied to the top of the rail. Firstly, the product is transferred from the rail surface to the wheel, and then after every turn of the wheel, the redistribution occurs from the wheel to the rail. The product division factor k_d represents the redistribution effect. This factor defines how much of the product is transferred from the lubricated surface to the clean surface when they come into contact. In both real and laboratory conditions, part of the applied lubricant is initially squeezed out of the contact and

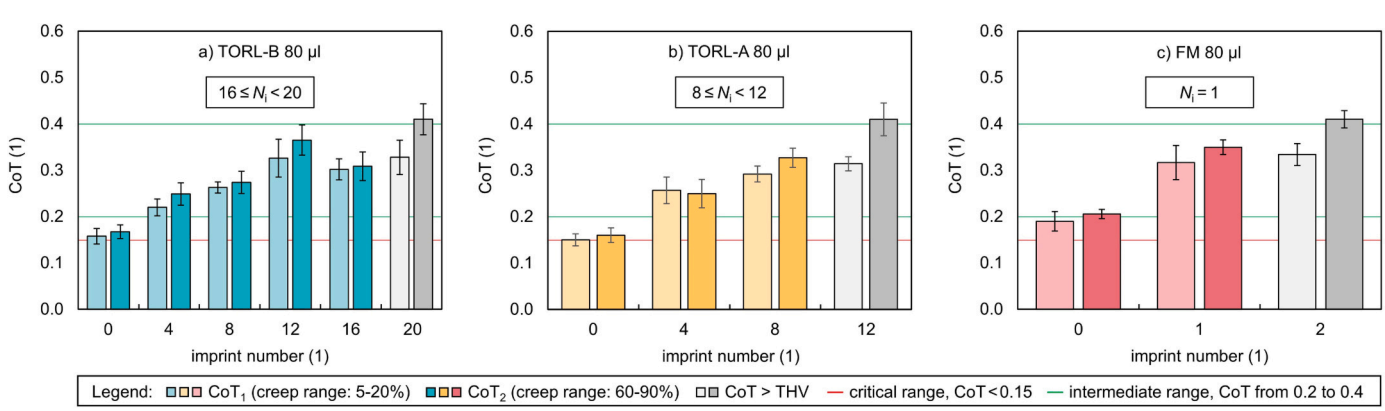

Fig. 5. Results of the carry distance tests for tested TOR products.

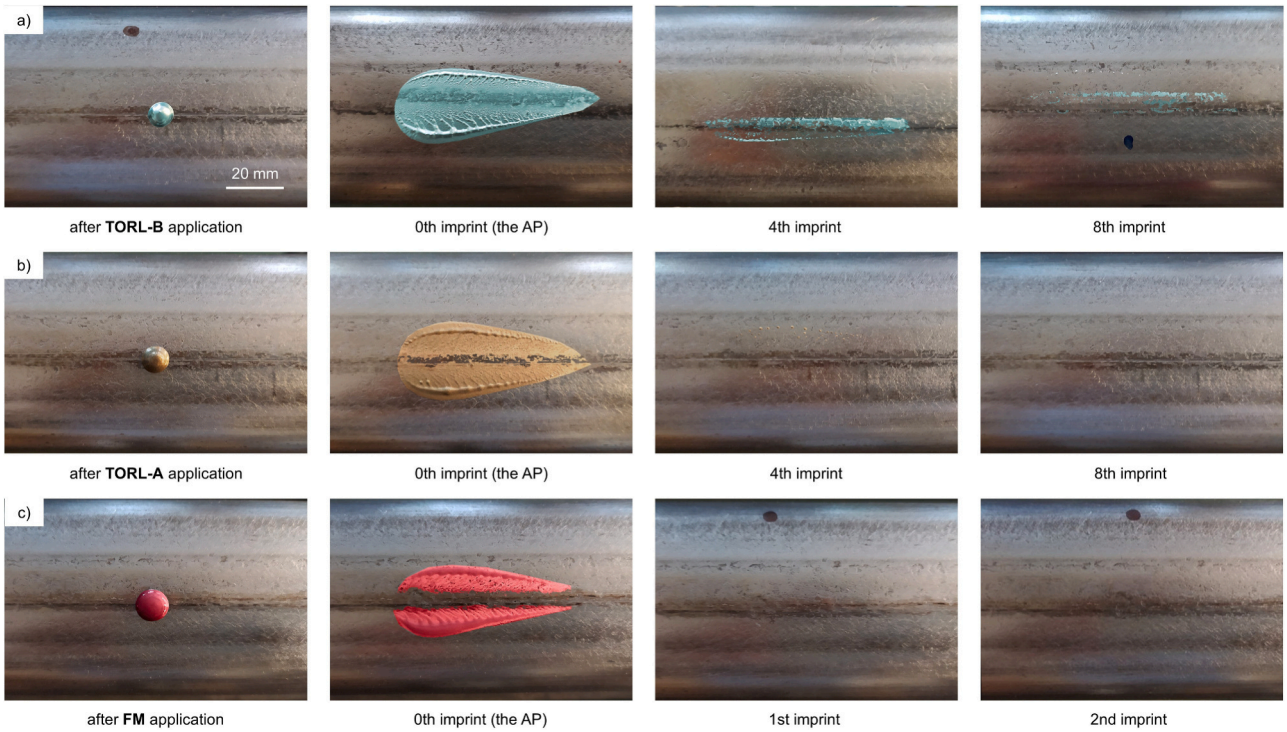

Fig. 6. Imprints of the tested TOR products on the rail surface produced by the contact simulator during the carry distance tests: (a) TORL-B, (b) TORL-A, and (c) FM.

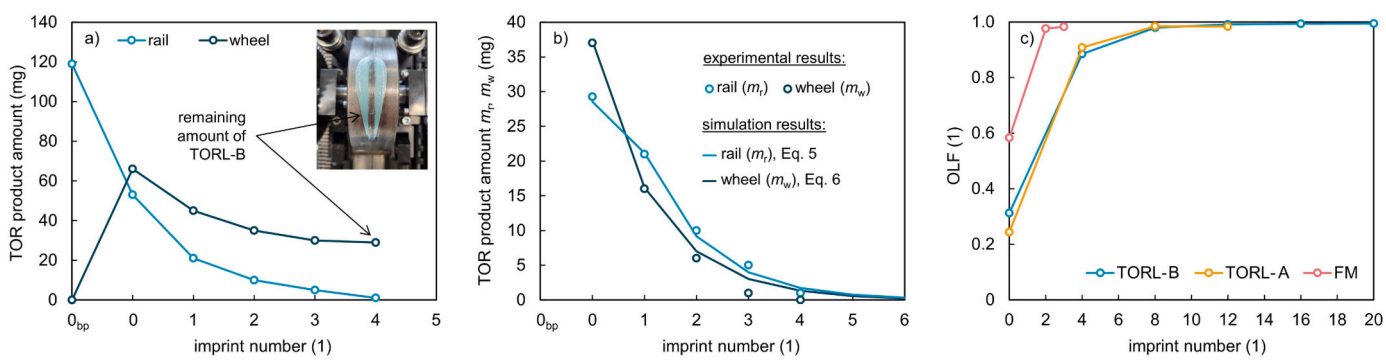

Fig. 7. Effect of increasing imprint on (a) the amount of TOR product on the rail and wheel, (b) the amount of TOR product on the rail and wheel in the contact band, (c) OLF.

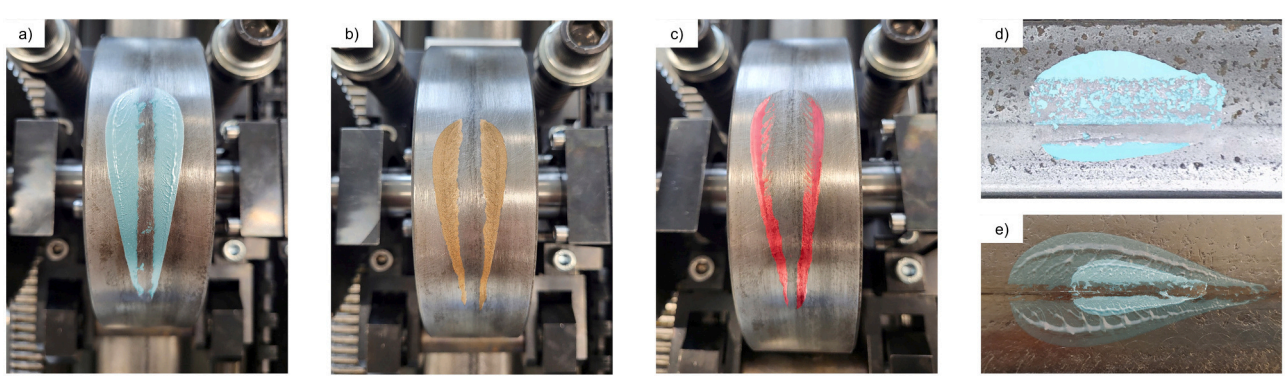

Fig. 8. Picked-up TOR products from the rail onto the wheel of the contact simulator for (a) TORL-B, (b) TORL-A, and (c) FM; (d) Imprint of TORL-B on the rail in the field, (e) Comparison of imprints at the AP for 4 μl and 80 μl.

becomes ineffective in controlling the friction in contact. This effect is taken into account by the residue factor k_0, which defines how much of the applied amount is effective in contact after the initial squeezing-out action of the contact bodies. The amount of TOR product in the contact band as a function of the number of imprints can be calculated using Eqs. (5) and (6) for the rail and the wheel, respectively.

$$m_{r,i} = \begin{cases} m_a k_0 (1 - k_d), \text{ for } i = 0 \\ m_{w,i-1} k_d, \text{ for } i \geq 1 \end{cases} \tag{5}$$

$$m_{w,i} = \begin{cases} m_a k_0 k_d, \text{ for } i = 0 \\ m_{w,i-1} - m_{r,i}, \text{ for } i \geq 1 \end{cases} \tag{6}$$

For the tested TOR product (TORL-B), the product division factor k_d was 0.5667, while the residue factor k_0 was 0.5533. Using these values, a strong correlation between experimental and simulation data was achieved, as can be seen in Fig. 7**(b)**. These curves are consistent with the previously published fact that when the TOR product layer reaches a critically low thickness, its further transferability is significantly limited [29]. This fact may explain why some TOR products provide only a very short carry distance, especially in the case of water-based products, where the layer can easily thin, which can significantly limit or completely prevent the subsequent product transfer.

A comparison of Fig. 6 and Fig. 8(d) proves that the laboratory rail imprints generated using a contact simulator sufficiently represent those observed on the rail in the field. The flattened shape of the laboratory imprints results from the different geometry of the wheel. Further imprint exploration is provided in Fig. 8(e), illustrating how the applied amount (4 μl and 80 μl) influences the size and shape of the imprints at the AP for the Lab-to-Field methodology. This figure demonstrates consistent imprint formation across this wide range of applied amounts, indicating the suitability of this methodology for imprint creation. A similar approach to studying TOR products was recently used in [24].

Finally, the OLF was calculated for each imprint of all tested TOR products to investigate whether the tested TOR products tend to over-lubricate the contact. Fig. 7(c) illustrates the OLF development with an increasing number of imprints. These findings show that the lowest value of the OLF was always observed for the zero imprints at the AP (further labelled as the OLF_{i0}), where the greatest amount of TOR products entered the contact. At this point, FM exhibited an OLF_{i0} value of 0.6, while TORL-A and TORL-B, as oil-based products, provided substantially lower values of 0.24 and 0.31, respectively. Although these values are quite low, especially for TOR lubricants, it can be seen that OLF increases sharply as the number of imprints increases. This means that there is no risk of contact over-lubrication except for the AP. Therefore, only the OLF_{i0} parameter was used further for the overall performance assessment of TOR products (Section 3.5).

3.4. Retentivity test and creep curves: comparison of tested TOR products (set no. 4)

Fig. 9 depicts the results of the retentivity tests. Similar to the carry distance test, no critical CoT values were identified in any analysed imprints, including the zero imprints. Moreover, most of the analysed imprints exhibited the required values of the CoT in the ITZ. These results indicate that TORL-B provided a considerably longer retentivity than the two other tested TOR products. Previous studies [19,21] revealed that water-based products typically exhibit lower retentivity for the same amount than oil-based TOR products due to their drying behaviour. The significant difference in retentivity between the two tested TOR lubricants may be mainly attributed to different particle concentrations [13] and particle types [51]. Additionally, different resistances to the high pressure in contact may also influence the retentivity.

The results of the retentivity test provide valuable information for determining the optimal application interval for TOR products. Specifically, TOR product consumption (the effect of TOR product becomes negligible) occurs after passing 13–19 vehicles (TORL-B) and 4–8 vehicles (TORL-A and FM) for a tram with eight driven wheelsets. These intervals can be extended further for vehicles with a lower number of driven wheelsets, as the minimal creep of non-driven wheelsets has a negligible impact on the TOR product layer. It should be noted that the TOR product layer consumption was accelerated during tests due to BUT tribometer measurements, where the creep reached up to 100 %. Therefore, it can be assumed that the actual application interval would likely approach the upper limit of the intervals mentioned above.

Fig. 10(a)-(c) depicts the development of the creep curves, fitted by the Polach model [28], over the number of passes. Fig. 10(d)-(f) shows these creep curves within the 0–15 % creep range to illustrate the initial slope of the curves. Variations in the slopes of some curves are attributed to measurement rather than data processing. It must be emphasized that the creep is not a controlled parameter but its value changes over time based on the frictional conditions in the contact. Consequently, more data points may be captured for lower creep values, affecting the slope of the fitted curve. In addition, the data points are also affected by the error of encoders. However, the differences in the slope of the creep curves are relatively minor. Further details on data processing are described in [26].

The creep curves in Fig. 10 demonstrate that when applying TOR products, neutral or positive friction is predominantly achieved. Nevertheless, a positive trend of the creep curve was observed even under dry conditions, as mentioned in Section 3.1. Therefore, discussing the influence of TOR products on the creep curve trend becomes highly challenging, which indicates the need for future research in this field.

Fig. 11 shows a visual evolution of the imprint for the zero imprint (at the AP) resulting from the increasing number of passes. It is evident that the shape of imprints remains almost unchanged after the initial

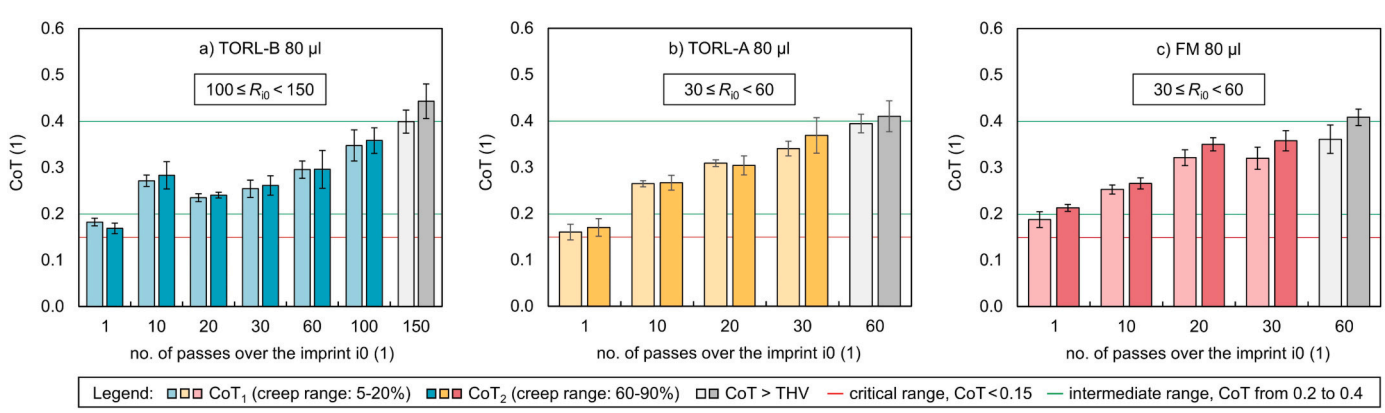

Fig. 9. Results of the retentivity tests for tested TOR products.

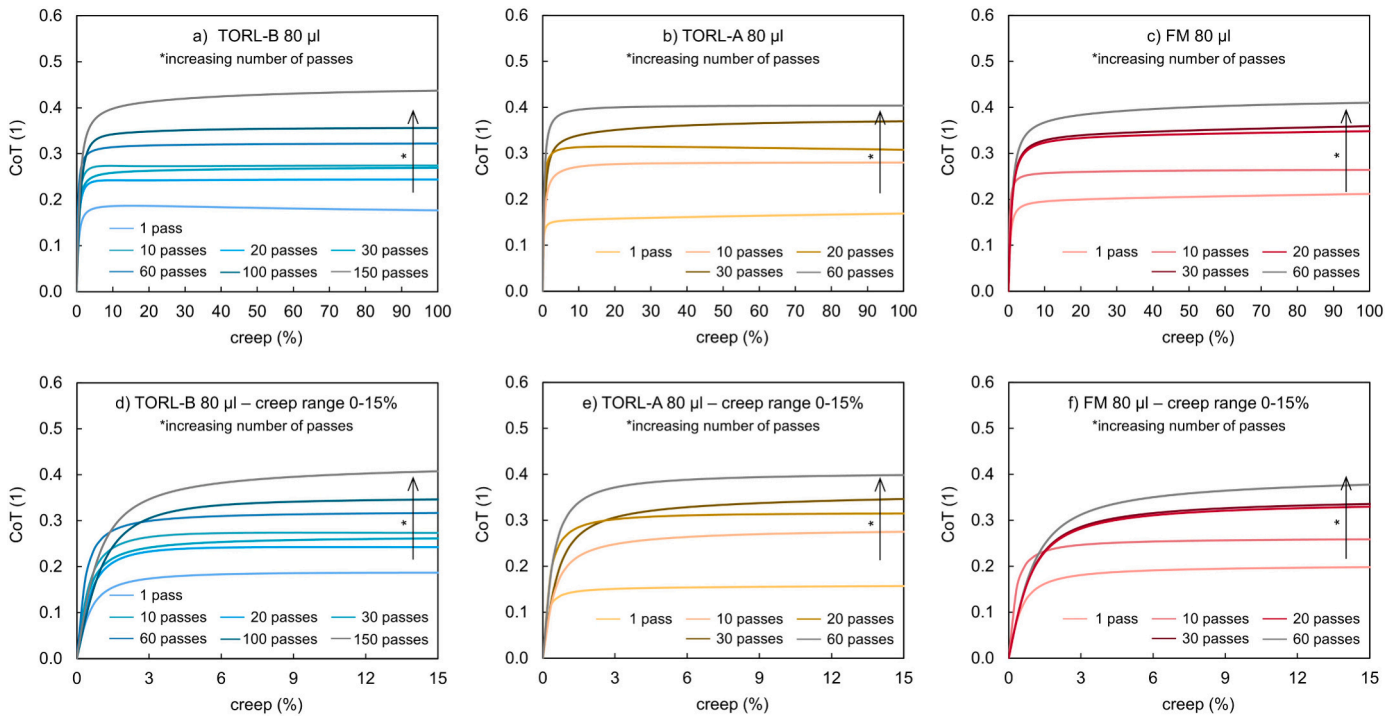

Fig. 10. Development of creep curves with an increasing number of passes and the detail on creep curves in the creep range 0–15 %.

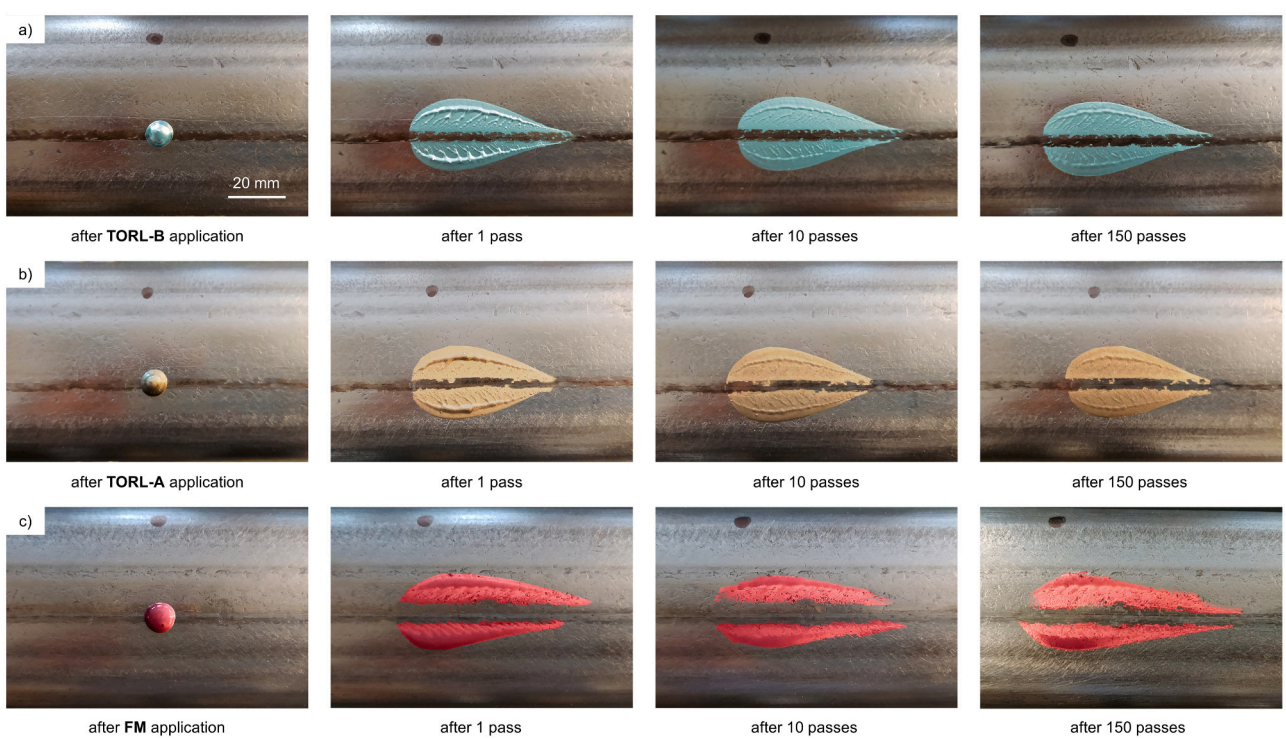

Fig. 11. Development of the imprint at the AP during the retentivity tests: (a) TORL-B, (b) TORL-A, and (c) FM.

pass when the imprint is created from a TOR product puddle. After this initial pass, the TOR product is squeezed to the sides of the contact band and does not re-enter the contact area during subsequent passes. It should be noted that due to the precise guidance of the contact simulator wheel and the BUT tribometer, there is no lateral movement of the wheel during the simulation of movement along a straight track. However, a slight lateral movement may occur even when the vehicle travels along a straight track in real operation. In that case, some previously squeezed TOR products may re-enter the contact band.

Besides this, the imprints in Fig. 11 show that the contact band appears wider (in the vertical direction) for FM than for TOR lubricants, likely due to the evaporation of the base medium. Furthermore, it can be seen that the contact band is visually almost free of TOR product, especially for FM, or contains only a minimal residual amount of TOR

lubricants. On the other hand, it was revealed that a TOR product layer might appear invisible to the naked eye despite measurements confirming the associated benefits of TOR products, such as noise reduction [50].

3.5. Overall performance assessment of TOR products using the two-phase methodology

The overall performance of TOR products is depicted in Fig. 12. This figure includes the parameters described above, namely the carry distance, retentivity, and OLF_{i0} (the OLF at the AP). Note that the creep curve trend was not included in this overall assessment due to inconclusive evidence from this study. The overall results show that TORL-B exhibited the longest carry distance and retentivity for the tested amount of 80 μl. The only weakness of this TOR product is its low OLF_{i0} value (at the AP), which can result in a longer braking distance [15] or reduced braking capacity [43] of the first wheelset. Nevertheless, as the distance from the AP increases, the sharp increase in the OLF value, as shown in Fig. 7**(c)**, should prevent any braking or traction problems. With respect to this fact, TORL-B can be classified as the best-performing TOR product among tested products. It is noteworthy that FM achieved notably better performance in the aspect of the OLF_{i0} due to its oil-free nature.

These findings align with a previous study conducted by the authors [21], where the Lab-to-Lab methodology was introduced as the initial step of the two-phase testing methodology to select the most suitable TOR product. This selection is further intended for testing using the Lab-to-Field methodology, as the whole procedure of the benchmarking methodology is depicted in Fig. 13. The focus of this second phase primarily involves assessing the track performance parameters of the TOR product and determining the optimal application amount and strategy under conditions similar to track conditions. In this study, however, the track performance parameters were evaluated for all three TOR products tested in [21], not only for the best-performing one, to validate both these experimental approaches (Lab-to-Lab and Lab-to-Field methodology). As mentioned earlier, the results obtained from both approaches exhibit a strong correlation, with TORL-B identified as the best-performing product according to both methodologies.

While this study addressed the impact of the tested amount, it did not investigate various application strategies. These strategies might involve applying the product on the rail to simulate wayside units (including different application patterns) or on the wheel to simulate application using onboard vehicle units. Moreover, studying the difference between a single application and frequent application of a small amount could be considered because it can further mitigate the drop in the CoT near the AP [22,52]. This finding could be significant mainly for TOR lubricants, as they cause quite low CoT values after application. Additionally, it can be expected that this change in the application strategy can affect other performance parameters.

3.6. Limitations of the study and future work

Although the Lab-to-Field methodology enables the study of the performance of TOR products under conditions close to real operations, some limits need to be considered. Regarding the transfer mechanism of TOR products, this study does not consider the effect of multiple wheels. This more complex scenario could allow for a deeper study of the transfer mechanism, potentially revealing effects that might not be evident after a single wheel pass. One example could be the additional drop in the CoT that occurs after multiple passes, as observed in laboratory [29] and field studies [15].

Another example can be associated with the tackiness of TOR products, which plays a key role in the transfer mechanism. As was reported in [53], TOR products that are too tacky may not transfer easily between the rail and the wheel, whereas products with low tackiness may run off the rail after their application (before the vehicle passes). Moreover, Lee et al. [29] suggested that the effect of tackiness can be even more important for the second and subsequent wheels [29].

This study did not investigate the effect of multiple passes over imprints because these experiments are time-consuming and may lead to low repeatability. When considering multiple passes and non-driven wheelsets, product retentivity may be higher than depicted in Fig. 9. This is because non-driven wheelsets operate almost under pure-rolling conditions, making their effect on imprint consumption negligible. Furthermore, a further reduction in rail imprint consumption can be expected when a lubricated wheel (the one with the imprint, shown in Fig. 1(b)) comes into contact with the rail imprint.

Knowledge of the effect of multiple passes on carry distance is still limited and should be the subject of future research. Although this phenomenon has not yet been studied, based on the research by Trummer et al. [22], it can be expected that the effect of multiple passes on carry distance would be negligible. However, the multiple passes can lead to the formation of a more continuous product layer along the rail. This phenomenon may occur because each wheel operates under slightly different creep, resulting in the positions of new imprints on the rail being different to those previously formed. This effect can be even more significant when vehicles with different wheel diameters pass over the imprints or when a vehicle has wheels of different diameters.

Another important aspect to consider is that the carry distance was measured only based on the imprint on the rail, without considering the TOR product residue on the side of the contact band on the wheel. According to [50], this residue amount may re-enter the contract band when the vehicle negotiates a curve, even if the distance from the AP is measured in kilometres. Furthermore, as previously mentioned, this

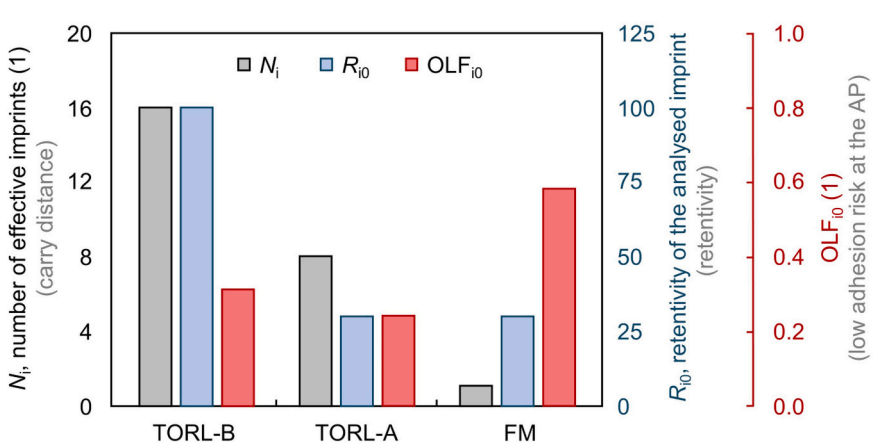

Fig. 12. The overall assessment of TOR products using Lab-to-Field methodology.

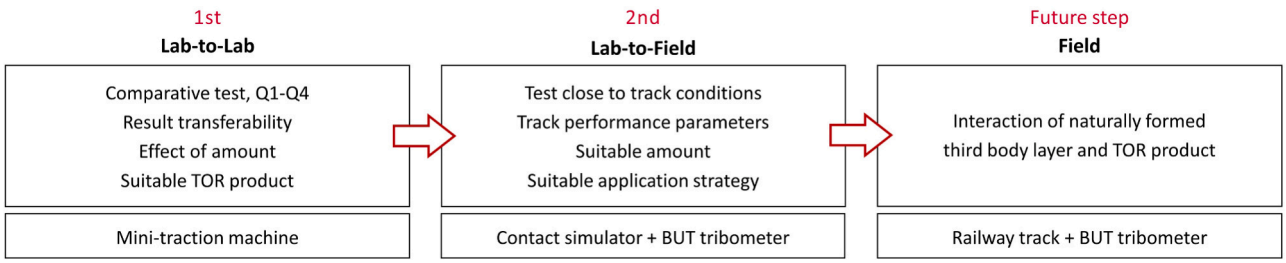

Fig. 13. Two-phase benchmarking methodology for TOR product testing and possible future step.

lateral movement may help the product re-enter the contact band even on the straight track. These findings suggest that the total carry distance may not be continuous, and assessing it on a real track by analysing individual points could lead to misleading conclusions [54]. Moreover, surface irregularities can significantly affect a product amount trapped in the contact band, as these irregularities help keep the product there [55]. This phenomenon is demonstrated by the imprint from a real track depicted in Fig. 8(d).

Other limitations of the study are associated with the operational conditions of the experiment, where speed likely represents the most significant limit. The BUT tribometer operates at a fixed speed of 0.26 m/s, while speeds in a real operation can reach up to tens of meters per second. That substantially higher speed can result in a more notable decrease in the CoT due to a change in the lubrication regime. When combined with a larger wheel, a higher speed can also influence the transfer mechanism of TOR products. Specifically, the higher speed can cause the product string, as described by Lee et al. [29], to partially or completely re-enter the contact band, resulting in extended retentivity and carry distance. Due to the low speed and small wheel size of the contact simulator and BUT tribometer, these strings were not observed during the experiments.

The performance parameters of TOR products are also impacted by axle loads. This study used a contact pressure of 0.9 GPa, which is common in many railway systems. However, heavy haul systems often operate at notably higher contact pressures. It was revealed that this increased pressure can decrease both the retentivity of TOR products and the CoT value [25,29,45]. Furthermore, higher pressure was found to potentially reduce the transfer of TOR products between contact bodies [47]; thus, the carry distance may also decrease.

Finally, it should be emphasised that all experiments were conducted within a controlled laboratory environment, ensuring that temperature, relative humidity, and typical contaminants (such as water or dust) did not affect the results. While TOR products are designed to interact with a naturally occurring third body layer, reproducing this layer in laboratory conditions may be an extremely complicated and challenging task, as many factors influence the composition of the layer. Moreover, the resulting composition may significantly differ across various track locations [56]. Concerning this fact, forming this natural layer was not included in this study.

Future field tests utilising a portable tribometer could offer a suitable approach to investigate the interaction of selected TOR products with this natural third body layer. This third phase of the methodology is suggested as a potential future step in TOR product testing, as illustrated in Fig. 13. Note that the objective of this future study should not be to replicate the current experiment, as field experiments are costly and time-consuming. Instead, the focus should be on investigating potential changes in the CoT when the TOR product interacts with a natural third body layer, e.g. at the AP.

Furthermore, the authors recommend focusing on the following points:

- Investigate friction behaviour under dry conditions to understand situations leading to the falling friction conditions.
- Explore the impact of various application methods of TOR products on performance parameters. Moreover, the wheel imprints should be analysed.
- Investigate how multiple passes over imprints affect the transfer mechanisms and related performance parameters.
- Use optical or spectroscopy analysis for an in-depth study of the contact band. This analysis can help differentiate whether an invisible layer, influencing the intermediate level of friction, originates from particles in TOR products or from a general tribological layer formed as a consequence of TOR product application.
- In this experimental setup, the interaction of TOR products with water, the most common contaminant, should be studied. A preliminary study using a small-scale tribometer [19] revealed the potential risks associated with water contamination when using TOR lubricants.

4. Conclusions

This study introduced the second phase of a benchmarking methodology for TOR product testing, called the Lab-to-Field methodology. This approach allows a comprehensive assessment of TOR product performance under conditions simulating real track conditions. These conditions enable the investigation of track performance parameters such as carry distance, transfer behaviour, OLF, product retentivity, and creep curves. The proposed methodology was demonstrated by testing three commercial TOR products (two TOR lubricants and one FM) before being tested using the Lab-to-Lab methodology [21].

The main finding is the strong correlation between the results of the Lab-to-Field methodology and the results of the previously published Lab-to-Lab methodology [21]. This correlation is crucial for validating the proposed two-phase benchmarking methodology for TOR product testing, designed to minimise the number of tests needed before the TOR product is put into service. Other important conclusions from this study are summarised in the following points:

- The run-in process is crucial for achieving typical CoT values under dry conditions.
- The proposed methodology allows the creation of representative imprints of TOR products on the rail, similar to those observed on tracks.
- Carry distance represents the most significant limit of tested TOR products. Moreover, FM showed limited product retentivity, while TOR lubricants caused a significant drop in CoT at the AP.
- The experimental configuration used in this study showed that a problem associated with insufficient CoT as a result of TOR product application is less severe than that found using a small-scale tribometer.
- The transfer behaviour of the best-performing TOR lubricant was investigated, and the predictive model simulating the redistribution of this product was proposed.

- Although the rail surface appeared visually free of TOR product, achieving the desired level of the CoT implies that the surface was lubricated. This suggests that it is not possible to identify the TOR product layer on the surfaces with the naked eye.

CRediT authorship contribution statement

Wen-jian Wang: Writing – review & editing, Supervision. **Ivan Krupka:** Writing – review & editing, Supervision, Resources. **Martin Hartl:** Writing – review & editing, Supervision, Resources. **Radovan Galas:** Writing – original draft, Visualization, Methodology, Investigation, Conceptualization. **Martin Valena:** Methodology, Investigation, Formal analysis, Conceptualization. **Tomas Jordan:** Methodology, Investigation. **Daniel Kvarda:** Writing – review & editing, Validation, Formal analysis. **Milan Omasta:** Writing – review & editing, Project administration, Conceptualization. **Simon Skurka:** Writing – review & editing, Investigation. **Bingnan Wu:** Methodology, Formal analysis. **Haohao Ding:** Writing – review & editing, Methodology, Conceptualization.

Declaration of Competing Interest

The authors declare that they have no known competing financial interests or personal relationships that could have appeared to influence the work reported in this paper.

Data availability

Data will be made available on request.

Acknowledgements

This publication was supported by the project 'Bozek Vehicle Engineering National Center of Competence' (TN02000054) that was co-financed from the state budget by the Technology Agency of the Czech Republic within the programme 'National Centres of Competence'. The work was also supported by the National Natural Science Foundation of China (No. 52320105007) and 2024 Excellent Youth Team Training Program of Southwest Jiaotong University.

References

[1] Stock R, Stanlake L, Hardwick C, Yu M, Eadie D, Lewis R. Material concepts for top of rail friction management – classification, characterisation and application. Wear 2016;366-367:225–32. https://doi.org/10.1016/j.wear.2016.05.028.
[2] Eadie DT, Santoro M. Top-of-rail friction control for curve noise mitigation and corrugation rate reduction. J Sound Vib 2006;293:747–57. https://doi.org/10.1016/j.jsv.2005.12.007.
[3] Eadie DT, Santoro M, Kalousek J. Railway noise and the effect of top of rail liquid friction modifiers: changes in sound and vibration spectral distributions in curves. Wear 2005;258:1148–55. https://doi.org/10.1016/j.wear.2004.03.061.
[4] Eadie DT, Elvidge D, Oldknow K, Stock R, Pointner P, Kalousek J, et al. The effects of top of rail friction modifier on wear and rolling contact fatigue: Full-scale rail–wheel test rig evaluation, analysis and modelling. Wear 2008;265:1222–30. https://doi.org/10.1016/j.wear.2008.02.029.
[5] Vélez JC, Cornelio JAC, Sierra RB, Santa JF, Hoyos-Palacio LM, Nevshupa R, et al. Development of a composite friction modifier with carbon nanotubes for applications at the wheel–rail interface. Adv Compos Lett 2020;29. https://doi.org/10.1177/2633366×20930019.
[6] Egana JI, Vinolas J, Gil-Negrete N. Effect of liquid high positive friction (HPF) modifier on wheel-rail contact and rail corrugation. Tribology Int 2005;38:769–74. https://doi.org/10.1016/j.triboint.2004.11.006.
[7] Eadie DT, Santoro M, Oldknow K, Oka Y. Field studies of the effect of friction modifiers on short pitch corrugation generation in curves. Wear 2008;265:1212–21. https://doi.org/10.1016/j.wear.2008.02.028.
[8] Stock R, Eadie DT, Elvidge D, Oldknow K. Influencing rolling contact fatigue through top of rail friction modifier application – a full scale wheel–rail test rig study. Wear 2011;271:134–42. https://doi.org/10.1016/j.wear.2010.10.006.
[9] Song J, Shi L, Ding H, Galas R, Omasta M, Wang W, et al. Effects of solid friction modifier on friction and rolling contact fatigue damage of wheel-rail surfaces. Friction 2022;10:597–607. https://doi.org/10.1007/s40544-021-0521-5.
[10] K. Davis, W. Stickland, Evaluation of a top-of-rail lubrication system, (1999) 1–120.
[11] Matsumoto K, Suda Y, Fujii T, Komine H, Tomeoka M, Satoh Y, et al. The optimum design of an onboard friction control system between wheel and rail in a railway system for improved curving negotiation. Veh Syst Dyn 2006;44:531–40. https://doi.org/10.1080/00423110600875294.
[12] Hardwick, Lewis R, Stock R. The effects of friction management materials on rail with pre existing rcf surface damage. Wear 2017;384–385:50–60.
[13] Galas R, Omasta M, Krupka I, Hartl M. Laboratory investigation of ability of oil-based friction modifiers to control adhesion at wheel-rail interface. Wear 2016;368-369:230–8. https://doi.org/10.1016/j.wear.2016.09.015.
[14] Li Q, Wu B-nan, Ding H-hao, Galas R, Kvarda D, Liu Q-yue, et al. Numerical prediction on the effect of friction modifiers on adhesion behaviours in the wheel-rail starved EHL contact. Tribology Int 2022:170. https://doi.org/10.1016/j.triboint.2022.107519.
[15] Galas R, Omasta M, Klapka M, Kaewunruen S, Krupka I, Hartl M. Case Study: the influence of oil-based friction modifier quantity on tram braking distance and noise. Tribology Ind 2017;39:198–206. https://doi.org/10.24874/ti.2017.39.02.06.
[16] Lundberg J, Rantatalo M, Wanhainen C, Casselgren J. Measurements of friction coefficients between rails lubricated with a friction modifier and the wheels of an IORE locomotive during real working conditions. Wear 2015;324-325:109–17. https://doi.org/10.1016/j.wear.2014.12.002.
[17] Anderson D, Wheatley N. Mitigation of wheel squeal and flanging noise on the Australian rail network. Noise Vib Mitig Rail Transp Syst 2008:399–405. https://doi.org/10.1007/978-3-540-74893-9_56.
[18] Li JX, Wu BN, Ding HH, Galas R, Omasta M, Wen ZF, et al. Wear and damage behaviours of wheel and rail materials: effects of friction modifier and environmental temperature. Wear 2023;523. https://doi.org/10.1016/j.wear.2023.204796.
[19] Skurka S, Galas R, Omasta M, Wu B, Ding H, Wang W-J, et al. The performance of top-of-rail products under water contamination. Tribology Int 2023;188. https://doi.org/10.1016/j.triboint.2023.108872.
[20] Harmon M, Lewis R. Review of top of rail friction modifier tribology. Tribol Mater Surf Interfaces 2016;10:150–62. https://doi.org/10.1080/17515831.2016.1216265.
[21] Galas R, Skurka S, Valena M, Kvarda D, Omasta M, Ding H, et al. A benchmarking methodology for top-of-rail products. Tribology Int 2023;189. https://doi.org/10.1016/j.triboint.2023.108910.
[22] Trummer G, Lee ZS, Lewis R, Six K. Modelling of frictional conditions in the wheel–rail interface due to application of top-of-rail products. Lubricants 2021;9. https://doi.org/10.3390/lubricants9100100.
[23] White B, Lee ZS, Lewis R. Towards a standard approach for the twin disc testing of top-of rail friction management products. Lubricants 2022;10. https://doi.org/10.3390/lubricants10060124.
[24] Del Negro Tayer P., Stoeterau R., FERRERB.R.U.N.O., Zuin A., Biazon Cavalcanti L., cousseau tiago. Laboratory test rig to measure carry-down, retentivity, splash and pickup of lubricant in wheel-rail lubrication system. Proceedings Of The 26Th International Congress Of Mechanical Engineering 2021:-. ⟨https://doi.org/10.26678/ABCM.COBEM2021.COB2021–1739⟩.
[25] Areiza YA, Garcés SI, Santa JF, Vargas G, Toro A. Field measurement of coefficient of friction in rails using a hand-pushed tribometer. Tribology Int 2015;82:274–9. https://doi.org/10.1016/j.triboint.2014.08.009.
[26] Valena M, Omasta M, Kvarda D, Galas R, Krupka I, Hartl M. An approach for the creep-curve assessment using a new rail tribometer. Tribology Int 2024;191. https://doi.org/10.1016/j.triboint.2023.109153.
[27] Gallardo-Hernandez EA, Lewis R. Twin disc assessment of wheel/rail adhesion. Wear 2008;265:1309–16. https://doi.org/10.1016/j.wear.2008.03.020.
[28] Polach O. Creep forces in simulations of traction vehicles running on adhesion limit. Wear 2005;258:992–1000. https://doi.org/10.1016/j.wear.2004.03.046.
[29] Lee Z.S., Trummer G., Harmon M., White B., Six K., Lewis R. Studying the transfer mechanisms of water based top-of-rail products in a wheel/rail interaction. Proceedings Of The Institution Of Mechanical Engineers, Part F: Journal Of Rail And Rapid Transit. ⟨https://doi.org/10.1177/09544097231187679⟩.
[30] Harrison H. Producing and Measuring the 3rd Body Layer. Proceedings of the Joint Rail Conference. St. Louise, USA: American Society of Mechanical Engineers; 2020. p. 208–16. https://doi.org/10.1115/JRC2020-8095.
[31] White B., Lewis R., Fletcher D., Harrison T., Hubbard P., Ward C. Rail-wheel friction quantification and its variability under lab and field trial conditions. Proceedings Of The Institution Of Mechanical Engineers, Part F: Journal Of Rail And Rapid Transit. ⟨https://doi.org/10.1177/09544097231209483⟩.
[32] Eadie, D.T.; Harrison, H.; Kempka, R.; Lewis, R.; Keylin, A.; Wilson, N. Field assessment of friction and creepage with a new tribometer. In Proceedings of the 11th International Conference on Contact Mechanics and Wear of Rail/Wheel Systems, Delft, The Netherlands, 24–27 September 2018, 208–217.
[33] Logston CF, Itami GS. Locomotive friction-creep studies. J Eng Ind 1980;102:275–81. https://doi.org/10.1115/1.3183865.
[34] Meierhofer A, Trummer G, Bernsteiner C, Six K. Vehicle tests showing how the weather in autumn influences the wheel–rail traction characteristics. Proc Inst Mech Eng, Part F J Rail Rapid Transit 2020;234:426–35. https://doi.org/10.1177/0954409719863643.
[35] Six K, Meierhofer A, Müller G, Dietmaier P. Physical processes in wheel–rail contact and its implications on vehicle–track interaction. Veh Syst Dyn 2015;53:635–50. https://doi.org/10.1080/00423114.2014.983675.
[36] Shrestha S, Spiryagin M, Harisson H, Persson I, Meehan P, Wu Q, et al. Introduction of rail cleaning effect into locomotive traction study based on tribometer measurements. ICRT 2021 Proc 2nd Int Conf Rail Transp 2022:41–51.

[37] Lewis SR, Lewis R, Olofsson U. An alternative method for the assessment of railhead traction. Wear 2011;271:62–70. https://doi.org/10.1016/j.wear.2010.10.035.
[38] Harmon M, Santa JF, Jaramillo JA, Toro A, Beagles A, Lewis R. Evaluation of the coefficient of friction of rail in the field and laboratory using several devices 2020; 14:119. https://doi.org/10.1080/17515831.2020.1712111.
[39] Kalousek J, Magel E. Modifying and managing friction. Railw Track Struct 1997; 93:31–6.
[40] O. Arias-Cuevas, Low Adhesion in the Wheel-Rail Contact, PhD Thesis, Delft University of Technology, Netherlands, 2010.
[41] Chen H, Fukagai S, Sone Y, Ban T, Namura A. Assessment of lubricant applied to wheel/rail interface in curves. Wear 2014;314:228–35. https://doi.org/10.1016/j.wear.2013.12.006.
[42] Khan SA, Lundberg J, Stenström C. Carry distance of top-of-rail friction modifiers. Proc Inst Mech Eng, Part F: J Rail Rapid Transit 2018;232:2418–30. https://doi.org/10.1177/0954409718772981.
[43] Khan SA, Rantatalo M, Asplund M. Wheel-rail squeal sound reduction using top of rail friction modifier: a case study. Int J Comadem 2020;23:69–76.
[44] Sánchez JC, Jaramillo JA, Santa JF, Toro A. Twin-disc assessment of the effect of top-of-rail friction modifiers on the tribological response of er8-r370ht pairs for use in wheel-rail systems. Rev Latinoam De Metal Y Mater 2019;39:2–15.
[45] Wang W, Li S, Ding H, Lin Q, Galas R, Omasta M, et al. Wheel/rail adhesion and damage under different contact conditions and application parameters of friction modifier. Wear 2023;523. https://doi.org/10.1016/j.wear.2023.204870.
[46] Kvarda D, Galas R, Omasta M, Hartl M, Krupka I, Dzimko M. Shear properties of top-of-rail products in numerical modelling. Proc Inst Mech Eng, Part F J Rail Rapid Transit 2023;237:796–805. https://doi.org/10.1177/09544097221138374.
[47] Hibbert MJE. Understanding the wheel/rail transfer mechanism in liquid friction modifier carry-down. Vancouver, Canada: The University of British Columbia,; 2017.
[48] White B, Hyland-Knight J, Lewis R. Assessing the effectiveness of traction gels using full-scale and field testing. Proc Inst Mech Eng Part F J Rail Rapid Transit 2021;235:690–9. https://doi.org/10.1177/0954409720953943.
[49] Neighborgall C, Mast T, Peterson A, Ahmadian M, Holton C. Development of Laser/LED-Based Instrument for Optical Detection of Railroad Top-of-Rail (ToR) Friction Modifiers and Lubricity Conditions. Proceedings of the Joint Rail Conference. Snowbird, USA: American Society of Mechanical Engineers; 2019. p. 1–7. https://doi.org/10.1115/JRC2019-1285.
[50] Eadie D. , Oldknow K. , Maglalang L. , Makowsky T. , Reiff R. , Sroba P. , et al. Implementation of Wayside Top of Rail Friction Control on North American Heavy Haul Freight Railways. In Proceedings of the 7th World Congress on Railway Research, Montreal, QC, Canada, 4–8 June 2006.
[51] Kvarda D, Skurka S, Galas R, Omasta M, Shi L-bing, Ding H, et al. The effect of top of rail lubricant composition on adhesion and rheological behaviour. Eng Sci Technol, Int J 2022;35. https://doi.org/10.1016/j.jestch.2022.101100.
[52] Pan Y, Radmehr A, Ahmadian M. Experimental evaluation of amount and repeated applications of top of rail friction modifiers on wear and adhesion. Int J Rail Transp 2023;11:855–71. https://doi.org/10.1080/23248378.2022.2119438.
[53] Harmon M, Lewis R. New laboratory methodologies to analyse the top of rail friction modifier performance across different test scales. Proc Inst Mech Eng, Part F J Rail Rapid Transit 2021;235:191–200. https://doi.org/10.1177/0954409720913759.
[54] T. Mast Y. Pan C. Holton M. Ahmadian Intermediate distance testing of optical top-of-rail (TOR) lubricity sensors on a remote-controlled rail cart 2021 Joint Rail Conference 2021 doi: 10.1115/JRC2021-58347.
[55] Rahmani H, Gutsulyak D, Stanlake L, Stoeber B, Green S. Carrydown of liquid friction modifier. Proc Inst Mech Eng, Part F: J Rail Rapid Transit 2022;236: 1124–34. https://doi.org/10.1177/09544097221076258.
[56] Lewis SR, Lewis R, Olofsson U, Eadie DT, Cotter J, Lu X. Effect of humidity, temperature and railhead contamination on the performance of friction modifiers: Pin-on-disk study. Proc Inst Mech Eng, Part F J Rail Rapid Transit 2013;227: 115–27. https://doi.org/10.1177/0954409712452239.

Article in Press

Tribology in Industry

www.tribology.rs

RESEARCH

Case Study: Correlations Between Curve Squeal, Weather Conditions, and Traction in a Tram Loop

Martin Valena [a,*], Milan Omasta [a], Milan Klapka [a], Radovan Galas [a], Vaclav Navratil [a], Ivan Krupka [a], Martin Hartl [a]

[a] *Faculty of Mechanical Engineering, Brno University of Technology, Technicka 2896/2, 616 69 Brno, Czechia.*

Keywords:

Wheel-rail tribology
Squeal and flange noise
Portable rail tribometer
Weather conditions
Coefficient of traction.

* Corresponding author:

Martin Valena
E-mail: Martin.Valena@vut.cz

Received:
Revised:
Accepted:

A B S T R A C T

This study explores the relationship between the coefficient of traction (CoT) and squeal noise parameters on a tram line loop, focusing on the influence of weather conditions. An automatic noise module was placed near a tram loop known for noise complaints. This module distinguishes between squeal and flange noise, recording their duration, root mean square (RMS) sound pressure level, and maximum sound pressure level when a threshold in the appropriate frequency band is exceeded. Concurrently, weather conditions were monitored, and the CoT on the rail was measured using a BUT rail tribometer. The findings reveal a notable correlation between the CoT and the duration of squeal noise, while the association with sound pressure levels was less pronounced. An increase in CoT was observed with rising relative humidity, which may be attributed to increasing temperature throughout a sunny April day, while absolute humidity remained almost constant. Furthermore, noise parameters rose with higher relative humidity and showed an inverse relationship with temperature. These findings suggest that weather conditions, particularly relative humidity and temperature, influence both the CoT and noise parameters on tram lines.

© 2025 Published by Faculty of Engineering

1. INTRODUCTION

Rail transport is a widely used method of transporting passengers and freight, primarily due to its low energy demands and high transport capacities. However, it also has its downsides, particularly noise. The most significant contributors to the overall noise from rail transport are rolling noise, impact noise, aerodynamic noise, and curve squeal, with their contributions varying by speed [1]. Curve squeal occurs in sharp curves with a radius of 200 m or less [2] and is particularly annoying because it is louder than rolling noise and often occurs in populated areas. The negative perception of squeal noise is amplified by ground-borne vibrations, which negatively impact the quality of life [3–6]. Therefore, considerable attention is devoted to its generation and the methods of preventing or suppressing it.

Curve squeal can be divided into squeal noise and flange noise, and both are connected to instabilities in the wheel-rail contact [7].

Flange noise is generated when the wheel flange comes into contact with a gauge face of the rail [2], usually the outer leading wheel or inner trailing wheel. The broadband noise is presented at 5-10 kHz [8]. Lateral slip (also noted as creep) between the wheel tread and the top of the rail plays an essential role in generating squeal noise, also known as top-of-rail squeal. It has a strong tonal character and study [9] identified it in interval from 400 Hz to 5 kHz. It was shown that longitudinal creep also influences squeal noise, which occurs in the frequency band of 3.5–6 kHz [10]. Many parameters, such as rolling speed, angle of attack, track geometry and dynamics influence squeal and flange noises. Therefore, they are chaotic and can be predicted only with a certain probability [11–13].

The squeal noise is mainly generated by two mechanisms: mode coupling and falling friction. Mode coupling is often caused by the coupling of modal vibrations in different directions through energy flow between them [14]. The second mechanism relates to stick-slip oscillations [15], which result from the transition between the positive and negative slopes of the creep curve. At low creep, the coefficient of traction (CoT) steeply increases with creep until it reaches the coefficient of friction. This point, known as the saturation point, typically occurs around 1-2% creep. When contact exceeds this point, slipping occurs, accompanied by thermal effects at the contact [16]. As creep returns before saturation point, the contact sticks again, and the process repeats. The negative slope of the creep curve also corresponds to negative damping; when this value exceeds the positive damping of the wheel, unstable self-excited vibrations occur [15].

The coefficient of friction and the shape of the creep curve, which affect the generation of squeal noise, strongly depend on the conditions at the wheel-rail contact. Additionally, the contact surfaces may be covered by a third-body layer that alters its friction properties, which can be classified as natural or artificial. According to Berthier [17], the natural third-body layer consists solely of particles formed during rolling-sliding motion. In contrast, Meierhofer [18] includes contaminants commonly found on the rail, such as dirt, water, snow, dust, and leaves. The artificial third-body layer contains substances intentionally added to the contact, such as sand, greases, lubricants, and top-of-rail products. These top-of-rail products are used to reduce squeal noise by providing a positive creep curve and maintaining an intermediate CoT [19–21]; however, their effectiveness depends on the amount applied, particularly for oil-based products [22,23].

In addition to contaminants affecting the frictional properties of the third-body layer, weather conditions also play a significant role [24]. The effect of relative humidity (RH) on the coefficient of friction was first observed decades ago, showing a decrease in CoT with rising RH near the surface [25]. This finding has been confirmed by numerous laboratory studies [26–29], although fewer field studies have been conducted. A field study [30] directly investigates this relationship using a pendulum tribometer with a rubber pad operating under fully sliding conditions. Measurements were taken during autumn and winter at four locations with infrequent rail operations, allowing for oxidation and leaf layer formation. Overall results support the effect, as mentioned above, of RH; however, discrepancies between individual locations and days were noted.

So far, published studies investigating curve squeal typically assess sound pressure levels (SPL) or sound power levels and frequencies while overlooking other noise parameters, such as noise duration, which can also affect noise perception. Furthermore, few studies examine the influence of weather conditions on curve squeal and friction in the field. Due to many influencing factors that change over time and the track location, it is very challenging to find correlations in larger temporal or spatial scales, as was shown, e.g. in [31]. Therefore, case studies focusing on shorter timeframes and more controlled operating conditions could yield valuable insights.

This study aims to investigate the relationship between the CoT and squeal noise parameters such as sound pressure level root mean square (SPL rms), maximum sound pressure level (max SPL), and noise duration under actual conditions on a tram line loop, accounting for variations in weather. The results will provide insights into these relationships, which may

serve as baseline data for evaluating top-of-rail products regarding changes in the coefficient of friction and noise parameters following their application. A new automatic noise module was utilized to record squeal and flange noise at their typical frequencies, while the BUT rail tribometer was employed to measure CoT on the rail head.

2. MATERIALS AND METHODS

2.1 Design of the Field Study

This field study adopts the form of a case study, in which correlations between noise, weather conditions and CoT are sought for a selected tram loop over a specified period. This work was carried out in multiple phases, as shown in Fig. 1. The main study involving the measurement of CoT took place on one sunny day at the end of April. This paper presents mainly the results from this phase of measurement. This day was preceded by a long period during which noise and weather conditions were monitored using an automatic noise module. During this phase, the noise module settings were optimised to allow independent quantification of squeal and flange noise based on analysis in the frequency domain. Various operational and external factors potentially affecting curving noise were explored. The first phase was implementing and calibrating the noise module using a standard Class I noise measurement setting.

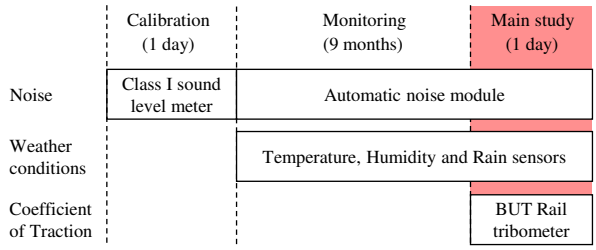

Fig. 1. Design of the field study

2.2 Vehicle, track and operation parameters

The study was carried out on a tram loop in the northwest part of Brno, Czechia, where the curve squeal occurred frequently and impacted the people living in the surroundings. The entry curve with a radius of 21 m is placed on a low-traffic road, as shown in Fig. 2. There is one-way traffic on the line, and after passing through the curve, the trams stop at a stop. The loop consists of two parallel tracks: the inner track was used for scheduled traffic during the study, while unscheduled journeys took place on the outer track. The grooved rail with an NT1 profile was commonly worn at the top and in the groove.

During the main study, the tram line was operated by a single vehicle, Tatra KT8D5, at 15-minute intervals, from 4:45 to 22:45. Entering speed was limited to 15 km/s. The tram is bi-directional and consists of three body sections connected by joints and thus can rotate each other in all directions. The body sections are mounted on four pivoting bogies (two internal and two external), each fitted with two powered wheel sets.

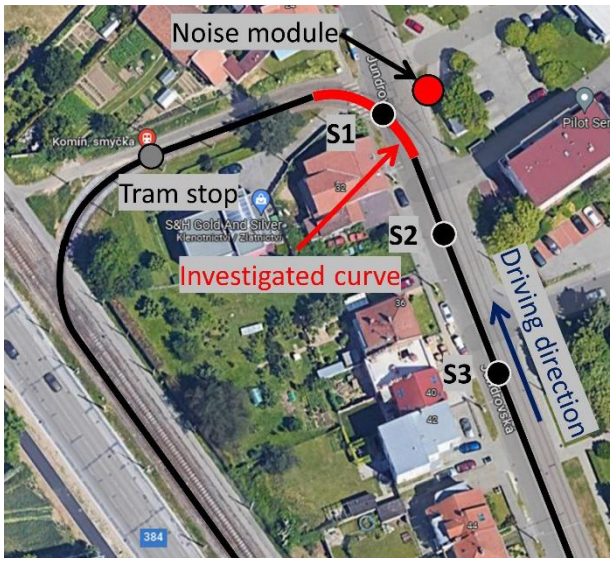

Fig. 2. Investigated tram loop

2.3 Assessment of traction conditions

The study utilised the BUT Rail Tribometer (Fig. 3) to evaluate the creep curve and CoT [32]. The BUT Rail Tribometer consists of a measuring module and a linear guide with magnetic bases that fix the tribometer to the rail. Creep is induced by adjusting the braking torque on the wheel during the measuring pass and a torque transducer simultaneously records this torque. The tangential wheel speed and longitudinal speed are measured using encoders, which are then used to compute creep. The weight of the measuring module creates a contact pressure set to 0.9 GPa, corresponding to light-rail vehicle conditions. The BUT Rail Tribometer can be operated in three modes; for this study,

the ramp mode was chosen, where the braking torque increases in several steps. The measuring wheel was cleaned with dry tissue before the first measuring pass and was not cleaned anymore.

Fig. 3. The BUT Rail Tribometer

Each measuring series counted 12 passes of the measuring module, performed in both directions (6 in each direction), but only the last few reached higher creep. Therefore, the resulting creep curve is composed of all these passes, which may be further fitted by a model of creep curve, see Fig. 4. The CoT was computed using the median method in creep interval from 5% to 15% [32], where the saturation point should occur. These values reliably separate points in the initial steep part of the curve and provide enough points to calculate the median CoT. It should be noted that the point scatter in the low creep regime is attributed to the finite resolution of the encoders. This occurs because of slight differences between the tangential wheel speed and longitudinal speed, which can alternate between positive and negative values.

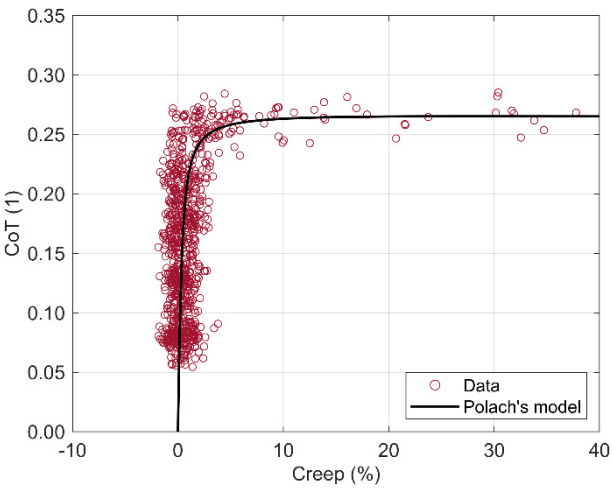

Fig. 4. Creep curve fitted by Polach's model

Main experiment: Three measurement spots, S1 – S3, were determined on the inner track at a distance of 30 m from each other, and measurement was carried out on both rails to record any differences between the inner and the outer rail. The measurement started at 7:30, repeated approximately every hour, and ended before 16:00. A total of 48 measuring series were performed from 7:30 to 16:00 (3 spots, 2 rails and 8 times). It should be emphasized that a tram passed through that location several times between each series of measurements taken at the same spot.

Reference experiment: Two measurements were conducted as the first and last measurement series of the day on the outer track at the location corresponding to S1 on the inner track. Since the outer track was not intended for use during the main study, it can be referred to as non-operated in the context of timetable traffic on the inner track. This experiment is designed solely for comparison purposes, aiming to determine whether tram operations or changes in weather conditions have a more significant effect.

2.4 Noise measurement and its evaluation

In the first phase, calibration measurements were performed to determine the frequency bands in which squeal and flange noise is pronounced on this curve. The Svantek 977 sound level meter, equipped with an MK 255 microphone and an SV 12L preamplifier, was used to record noise data from 20 Hz to 20 kHz without weighting. The microphone was positioned 1.2 m above track level next to the pole, where the noise module should be installed. A total of 10 passes were recorded and further analysed. In addition to the measurements, the subjective impression of the pass was also noted, whether it was squeal or flange noise and how severe it was. It helped to detect the correct frequencies.

The noise module was employed for autonomous long-term noise monitoring. It was placed on the pole at a distance of 11 m from the curve and a height of 4 m, see Fig. 2. It consists of a programmable logic controller with a vibration measurement module to which an IEPE outdoor microphone is connected. The noise module is equipped with temperature, humidity, and rain sensors. It is powered by a battery. The noise module performs real-time FFT analysis,

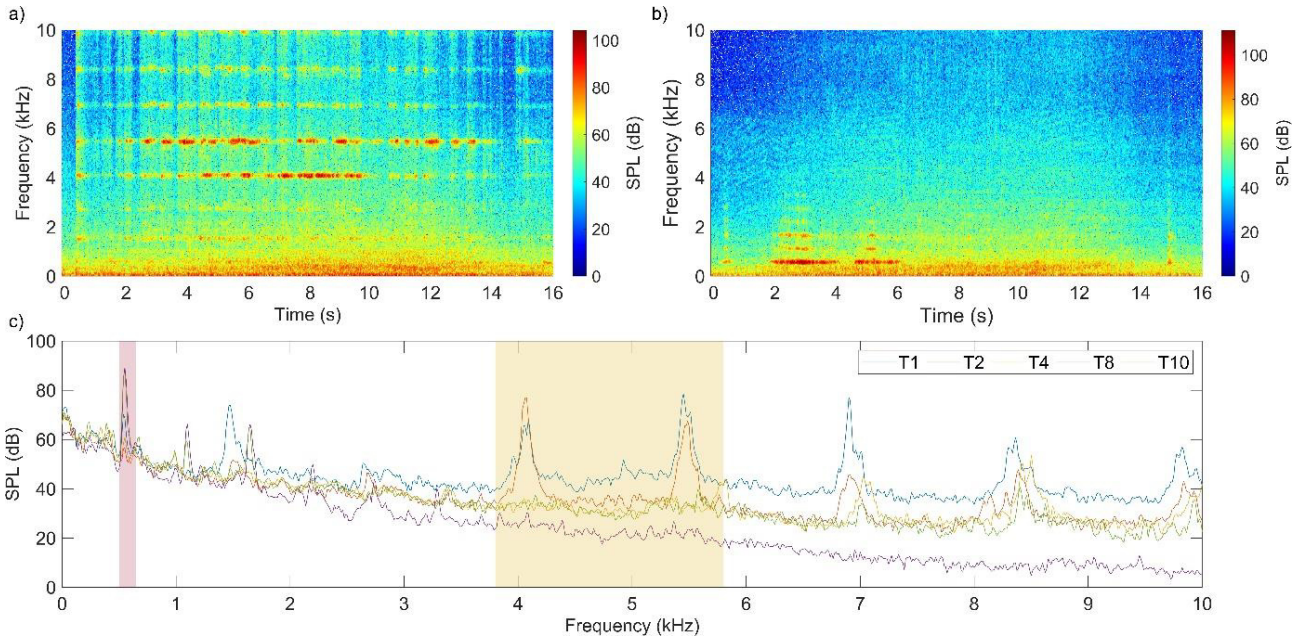

Fig. 5. Spectrograms of flange noise(a), squeal noise (b) and frequency analysis of tram passes with highlighted squeal and flange noise bands (c)

distinguishing between frequency bands characterising squeal and flange noise. Acoustic pressure was evaluated in the following frequency bands derived from preliminary measurement, the results of which are further described in chap. 3.1:

- Squeal noise: 500 – 650 Hz,
- Flange noise: 3800 – 5800 Hz.

The record in each band was created only when a threshold value was exceeded and simultaneously the noise duration was above 0.3 seconds. The threshold was set to 60 dB for squeal noise and 50 dB for flange noise. These values are high enough to suppress other noise sources, such as cars, and low enough to get a record of most tram passes. The record contains SPL rms, max SPL and noise duration. Besides acoustic parameters, the noise module records weather conditions (temperature, RH, and rain) every minute.

A single tram pass typically includes multiple noise records, as shown in Fig. 5a and b. Usually, the squeal noise is emitted intermittently as the tram wheels pass the critical points on the track where the conditions for squealing are met. The objective was to create a single record that characterizes the tram pass. The total noise duration, referred to as "duration," is calculated by summing the durations of individual records (hereinafter partial durations) during one pass. The maximum Max SPL is the highest value among the individual maximum SPLs recorded. Additionally, the SPL rms is computed using the root mean square of the individual SPL rms values. Each record is associated with a tram ID detected by a switch reading device before entering the loop.

3. RESULTS AND DISCUSSION

3.1 Definition of noise bands

The records from the first phase were analysed using FFT analysis, and the results are plotted in Fig. 5. An example of a spectrogram from the second tram pass is shown in Fig. 5a, where severe flange noise is pronounced at several higher frequencies, which is typical. The most significant frequencies are 4100 and 5500 Hz, but two lower are also essential to define correct band edges because these frequencies are exited only when flange noise is presented. In contrast, b) shows a tram pass (eighth) without any flange noise but with significant squeal noise pronounced twice between the second and sixth second of the pass. The main frequency peak is 550 Hz, but multiples up to 3300 Hz are visible, while the first three are well distinguishable. It is evident from a) and b) that the squeal and flange noise is not

continuously generated during the curve negotiation but instead emitted multiple times with short partial durations, especially the flange noise. The comparison of passes in the frequency domain is shown in c), where the typical frequencies can be seen. For clarity, only a few passes are shown.

A typical frequency of 550 Hz was observed in all cases where squeal noise occurred; therefore, the band of 500-650 Hz was chosen, which is sufficient to cover this peak (see Fig. 5c for the first highlighted area). If the upper limit is higher to include multiples, a false record of squeal noise could occur, as the peak around 1500 Hz is present when flange noise is detected. The lower limit of the flange noise was set at 3800 Hz because it reliably separates the squeal noise's last peaks while capturing the flange noise's first peaks. The upper limit of 5800 Hz is determined by noise module sampling frequency and Nyquist's theorem. The band for flange noise is highlighted in Fig. 5c, the second area. It would be better to set the upper limit higher to capture more peaks, but it might cause some difficulties with setting the SPL threshold because the SPL rms is evaluated and weak peaks might not be noticed.

3.2 Effect of weather conditions on noise

Fig. 6a and b show the typical development of noise parameters (max SPL, SPL rms and duration) corresponding to a long-term measurement, and c) weather conditions (RH, absolute humidity (AH) and temperature) recorded over the entire day. Several tram passes were silent without exceeding the thresholds; thus, the noise module could not record them, resulting in gaps in the noise records. In the case of squeal noise, max SPL and SPL rms vary around 90 and 70 dB, respectively, but neither report any noticeable trend during the day. On the other hand, the duration is longer in the morning, then decreases and increases again in the evening, which copies the development of RH over the day and has an opposite course as temperature. Similar developments can also be found in flange noise, but the main difference is that the max SPL has the same progress as the duration while the SPL rms varies around 55 dB. The duration is a suitable parameter for evaluating the severity of squeal noise because it is independent of how the sound propagates through the environment. However, it should be noted that the duration, as evaluated in this study, is still indirectly linked to SPL since SPL thresholds must be exceeded for the noise to be recorded.

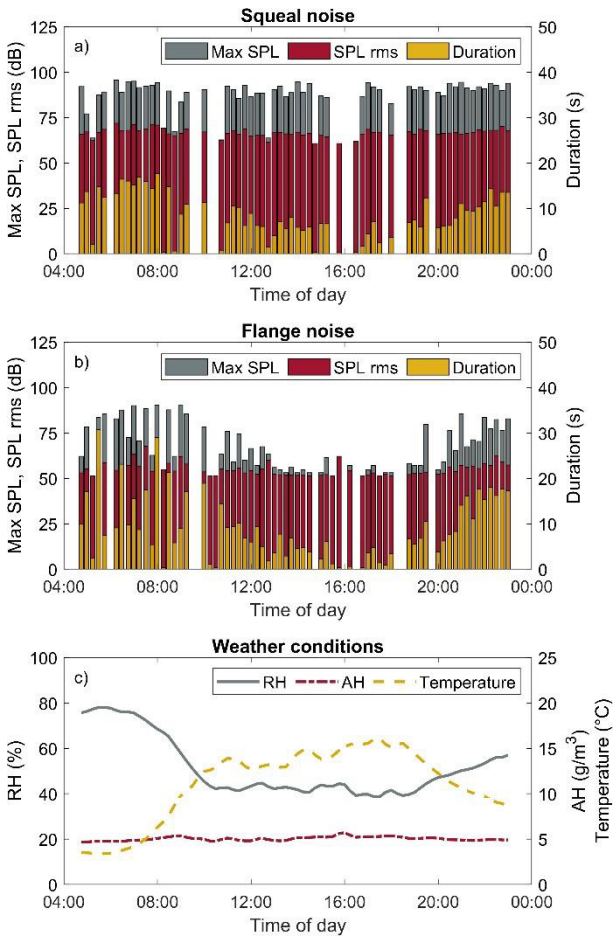

Fig. 6. Daily variation of squeal noise (a), flange noise (b), and weather conditions (c)

Parameters of squeal and flange noise are plotted in a 3D graph (Fig. 7), with temperature on the x-axis and RH on the y-axis, as these variables are interconnected. Noticeable relationships between noise parameters and weather conditions prompted a regression analysis, with Pearson correlation coefficients for squeal and flange noise presented in Table 1 and Table 2, respectively. Fig. 7a and b illustrate a clear trend: squeal duration and SPL rms decrease with lower RH and higher temperatures, while maximum SPL does not show a significant trend. The regression analysis identified the strongest correlation for squeal duration. A few points with noticeably lower values for squeal duration and maximum SPL can be observed in Fig. 7a and c; their positions in the temperature-RH plane suggest they

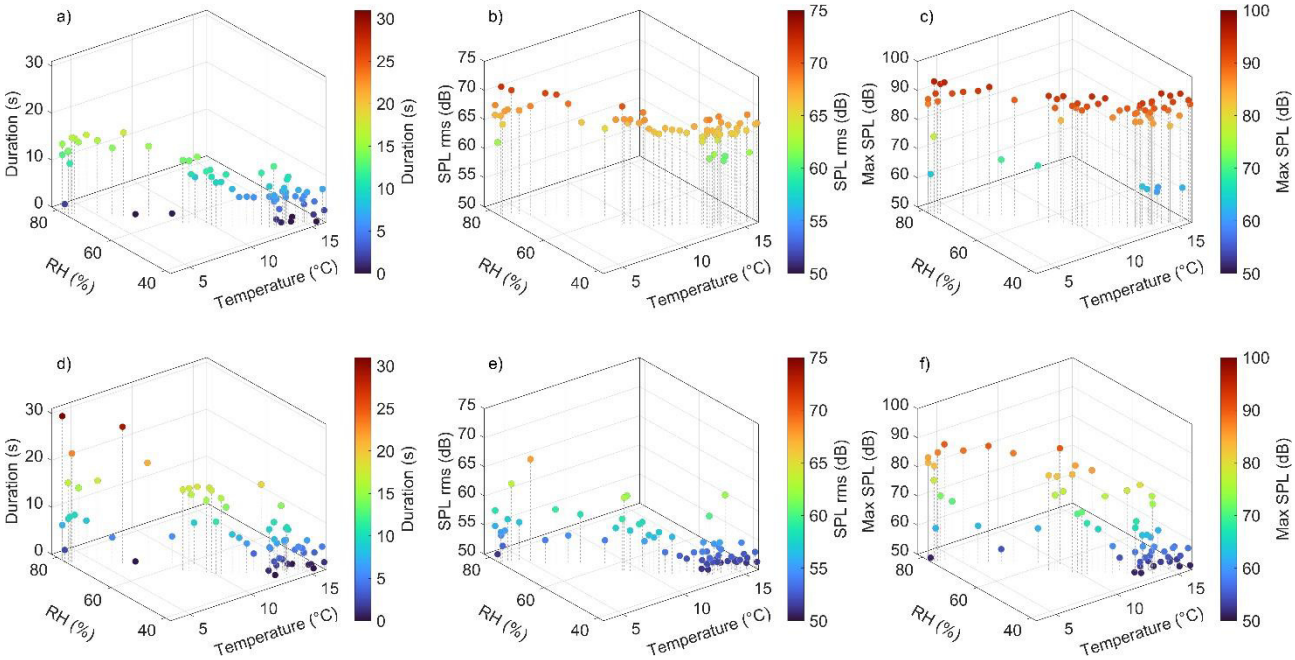

Fig. 7. The effect of temperature and RH on squeal duration (a), SPL rms of squeal noise (b), Max SPL of squeal noise (c), duration of flange noise (d), SPL rms of flange noise (e), Max SPL of flange noise (f)

correspond to each other and were recorded during the same tram passes, indicating that these passes were relatively silent and only slightly exceeded the SPL threshold. In contrast, flange noise parameters exhibit significant variability at lower or higher RH levels, with this scatter diminishing as temperature rises and RH falls (Fig. 7d-f). This indicates that higher RH or lower temperatures produce elevated noise parameters. While general trends are similar to those observed in squeal noise, the most significant correlation for flange noise was found with maximum SPL. The regression analysis shows that temperature and RH affect both squeal and flange noise, but AH has a limited impact. Most relationships are statistically significant at a 95% confidence level, although the slopes of some relationships (marked in red) may be zero.

Table 1. Pearson correlation coefficients for squeal noise (p-values in brackets)

	Temperature (°C)	RH (%)	AH (g/m³)
Duration (s)	-0.663 (<0.001)	0.626 (<0.001)	-0.506 (<0.001)
SPL rms (dB)	-0.440 (<0.001)	0.419 (<0.001)	-0.315 (0.013)
Max SPL (dB)	-0.107 (0.409)	0.061 (0.638)	-0.291 (0.022)

Increasing temperature is likely to reduce all noise parameters, as demonstrated by Maly et al. [33]. They conducted long-term measurements, recording approximately 20,000 suburban train passes under various weather conditions. Their evaluation of sound power levels showed a trend similar to that of the SPL used in this study, differing only in magnitude. Additionally, they analysed the frequency of occurrence, which exhibited the same dependency as SPL. The frequency of occurrence can be compared to the duration assessed in this study. A higher frequency of occurrence suggests that contact is more likely to produce squeal noise. Consequently, it is more probable that squeal noise will be emitted multiple times during a curve pass, leading to a longer duration. Both duration and frequency of occurrence show similar dependencies on temperature.

Table 2. Pearson correlation coefficients for flange noise (p-values in brackets)

	Temperature (°C)	RH (%)	AH (g/m³)
Duration (s)	-0.554 (<0.001)	0.511 (<0.001)	-0.368 (0.003)
SPL rms (dB)	-0.483 (<0.001)	0.481 (<0.001)	-0.067 (0.598)
Max SPL (dB)	-0.617 (<0.001)	0.593 (<0.001)	-0.272 (0.028)

The correlation coefficient between noise parameters and RH is slightly lower than that of temperature. However, the main difference is the opposite slope, meaning that all noise

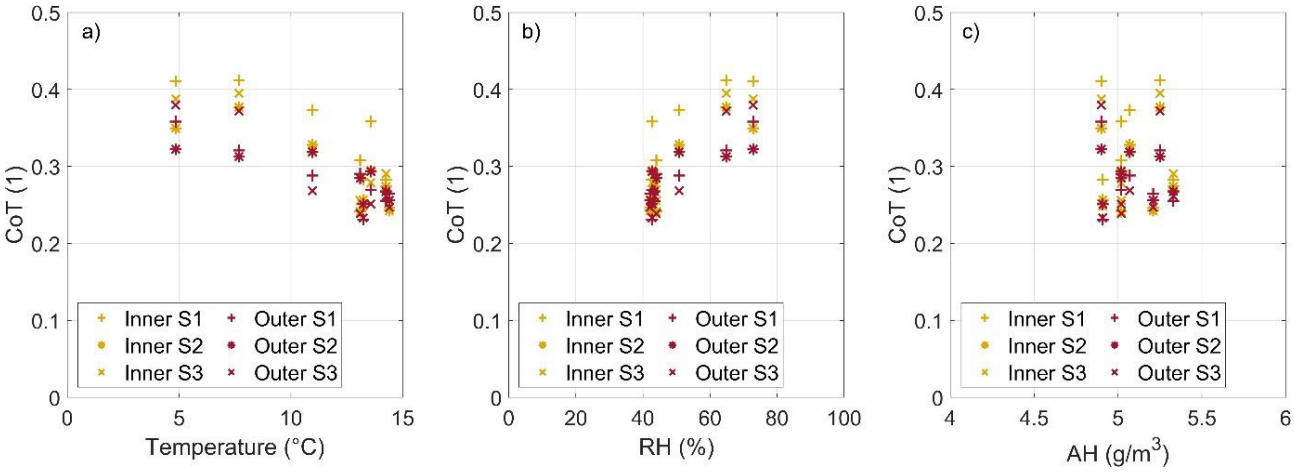

Fig. 8. The influence of weather conditions on CoT: temperature (a), RH (b) and AH (c)

parameters increase with increasing RH. This finding is consistent with a previous field study [33]. It should be noted that, according to the mentioned study, the trend also depends on the rail temperature. When the temperature is above 0 °C, the SPL increases with rising RH; when it is below 0 °C, the effect is opposite. The rail temperature was estimated to be between 0 – 10 °C based on the ambient temperature. The squeal duration can be used to compare the measured data with the publication in which the increasing probability of the squeal with increasing RH was assessed [12]. As mentioned earlier, a higher likelihood should result in a longer squeal duration, indicating that the measurement is consistent with the study [12]. Only a correlation with squeal duration was found for AH, which may be due to the limited range of AH, as the measurement was performed on a sunny day. AH varied during April between 2.77 and 11.43 g/m^3, while it reached the local minimum on the day of measurement. In this context, it might be considered as constant.

3.3 Effect of weather conditions on CoT

The friction properties of 3rd body layer presented on the rail vary with RH and temperature, as shown in Fig. 8. The colours of the points represent the inner or outer rail, and different symbols indicate the measurement place (S1-S3). Both temperature and RH significantly correlate with CoT (Table 3), although they have distinct slopes. Specifically, increasing temperatures negatively affect the CoT, while higher RH leads to an increase in CoT. In contrast, the correlation with AH is negligible, with the slope potentially being zero based on a 95% confidence interval. In all cases, the inner rail reports a higher CoT, which may be due to cleaning effect caused by the higher slip of the inner wheel while a tram negotiates the curve. A similar phenomenon was observed on the Iron Ore Line in Sweden [34] on a sunny day with an ambient temperature of 13 °C, but not under other conditions (morning dew and a frost). This was explained by different third bodies at the locations where measurements were performed, while roughness and other parameters were similar. The variation between individual spots is significant (see Fig. 8), but the overall trend remains consistent whether we consider all the data or the trend in particular spots. It may result from local friction conditions such as 3rd body layer composition, hardness, roughness and ductility [35].

The effect of temperature corresponds to findings of other papers [24,36], but the RH has an opposite effect than that described in the literature [24,26,28,30,37]. In laboratory studies, the higher RH was reached by adding steam into an enclosed chamber where the measurement was performed or using an external humidity unit. Both approaches led to an increase in AH. Besides that, experiments were carried out under constant temperature. As was mentioned before and can be seen in Fig. 8c, AH in our study is similar to the study of Zhu et al. [37]. Many field studies, for example [30] and [31], were performed in autumn under damp conditions, and the rail may be contaminated by leaves, which causes low adhesion [26]. In contrast, the presented study was performed on a regularly operated track

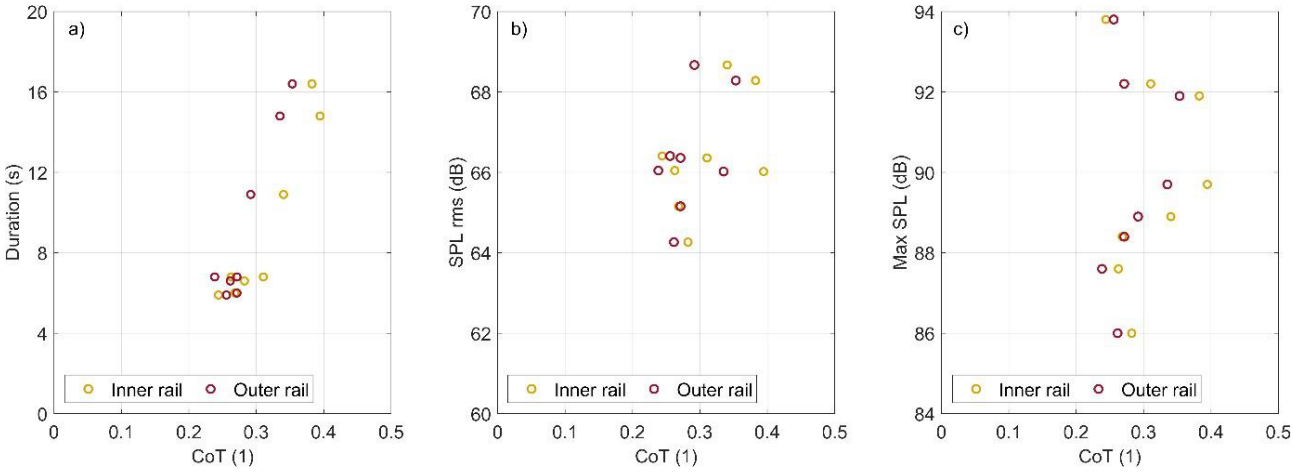

Fig. 9. The effect of CoT on squeal duration (a), SPL rms of squeal noise (b) and max SPL of squeal noise (c)

on a sunny day. The dew point fluctuated around 0 °C the previous night; however, it cannot be ruled out that some dew may have formed on the rail. Studies [37] and [38] show that haematite that increases CoT can be generated under high RH. In contrast, oxyhydroxides result from hydration [39] and decrease CoT [40]. Additionally, the wheel-rail contact operates under high pressure and a non-negligible amount of heat is generated due to wheel slip [41]. These conditions transform oxyhydroxides and iron oxides, whereas each type impacts friction differently [40]. This might explain the initial high CoT value. From another perspective, RH decreased between 6:00 and 11:00 in response to rising temperatures, which aligns with the trend observed in the CoT, as shown in Fig. 10. This suggests that direct exposure of the rail to sunlight from early morning, even before CoT measurements began, may increase the rail temperature and dry out the third body layer. Consequently, the lowest CoT values recorded in the afternoon were measured on dry rail. Therefore, it is more likely that changes in CoT are associated with temperature or daytime conditions rather than variations in RH.

The question arises as to whether the change in weather conditions or tram operations causes the change in frictional properties during the day. The highest CoT value was measured on the inner track in the morning and gradually decreased during the day, see Fig. 10. The reference experiment performed on non-operated rail also showed the highest CoT in the morning, while in the afternoon, it was lower. Based on this, it could be concluded that the change in weather conditions plays a substantial role, but creep and contact pressure should also affect the frictional properties [42]. It should be mentioned that a few trams passed on the outer track out of timetables, which might have affected the 3rd body layer similarly to the regular traffic on the inner track, where the traffic was heavier.

Table 3. Pearson correlation coefficients between CoT and weather conditions

	Pearson correlation coefficient	p-value
Temperature vs. CoT	-0.805	<0.001
RH vs. CoT	0.811	<0.001
AH vs. CoT	-0.065	0.660

Table 4. Pearson correlation coefficients between CoT and squeal noise parameters

	Pearson correlation coefficient	p-value
CoT vs. duration	0.899	<0.001
CoT vs. SPL rms	0.487	0.056
CoT vs. max SPL	0.168	0.534

3.4 Relationship between the CoT and squeal noise parameters

Combining the automatic noise module and the BUT rail tribometer enables us to investigate the relationship between squeal noise parameters and CoT. The study of the relationship between flange noise and CoT is not meaningful, as CoT was only measured at the top of the rail. Results indicate that increasing CoT increases the squeal duration and SPL rms. At the same time, the effect

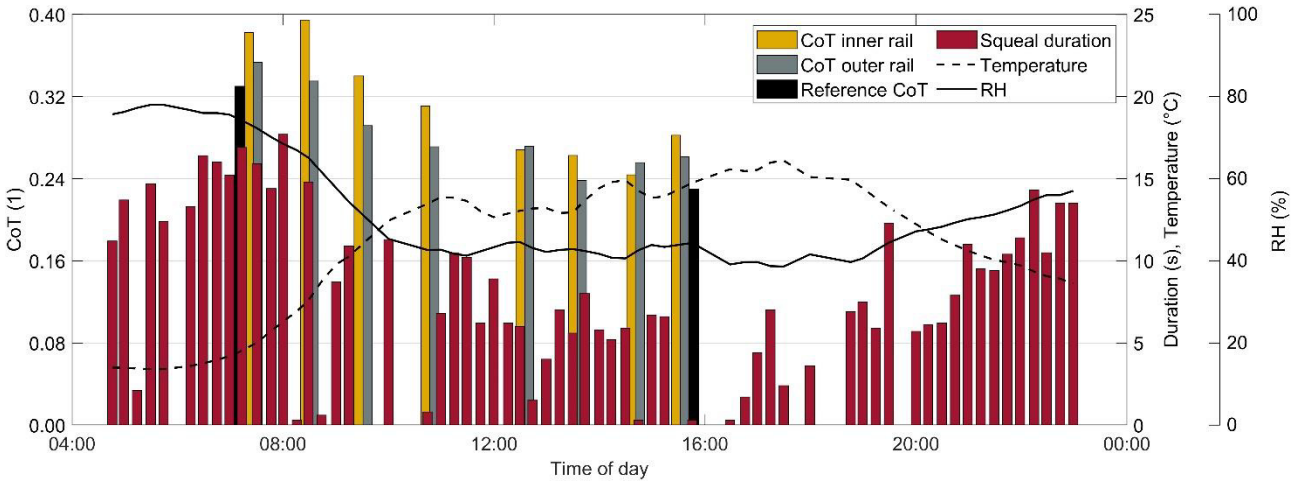

Fig. 10. Development of CoT, squeal duration and weather conditions during the daytime

of CoT on max SPL is negligible, see Fig. 9. The correlation between squeal duration and CoT is strong and statistically significant, while the SPL rms is almost statistically significant (see Table 4), but the slope may be zero according to the 95% confidence interval. Some numerical studies have shown that the coefficient of friction affects the generation of squeal noise. The study [43] claims that a higher coefficient of friction leads to higher noise intensity, which is a similar parameter to SPL. Simultaneously, a study [44] found that a higher coefficient of friction causes the wheel-rail system to be more unstable, increasing the tendency toward squeal noise. A potential explanation for the correlation between squeal duration and CoT is that the combination of an unstable system and varying instantaneous contact conditions along the curve caused the noise to be emitted multiple times, resulting in a longer squeal duration.

Fig. 10 illustrates the development of CoT and squeal duration during the daytime, highlighting the strongest correlation observed. The CoT was lower during the day compared to the morning, and a similar trend was noted in the squeal duration; however, the squeal duration increased again in the evening. While this trend in squeal duration was evident during the monitoring phase, it does not imply that low friction cannot occur in the morning or evening. Other known mechanisms, such as forming a viscous paste made up of oxides and water [45], can also contribute to low friction conditions.

These data should be expanded to include measurements under various weather conditions to enhance knowledge. This additional data could serve as baseline curves for evaluating the effectiveness of top-of-rail products.

3.5 Limitations in the Study

This study's limitation is related to the noise measurement, which was not performed and evaluated following ISO 3095:2013. This includes the approach, device, microphone position and 3rd-octave bands. While this difference may influence the exact value of SPL, it does not change the identified trends, correlations and noise duration. In particular, this standard does not cover the distinction between squeal and flange noise, which is the main purpose of the study.

A possible limitation is that the measurement of CoT was made only in one day. The previous experiments indicate that it is difficult to obtain any correlation over a long time period due to other influences that can hardly be controlled during the tests in a real tram operation. This includes the effects of the operation of different trams with different technical conditions; maintenance interventions, weather phenomena significantly affecting the condition of the rail (leaf falls, heavy rail) and many others. Although the noise data presented were recorded in a single day, they were preceded by nine months of noise monitoring to identify typical behaviours. This pattern was also observed on the day of the CoT measurements, which started early in the morning and lasted late in the evening. To better understand the relationship between CoT and squeal noise, measurements of CoT

should be made over several days at different times of the year, and measurements should last from early morning to late evening, which is a future step.

As the tribometer's measuring wheel was cleaned by dry tissue only once before the first measurement, this might have affected the value of the CoT. The CoT characterises the contact between two bodies, while only one was being investigated. Harrison [46] showed that the condition of the measuring wheel affects the CoT due to forming a 3rd body layer on it. This layer develops with the number of passes, increasing the CoT, as observed in the study [32]. The decision not to clean the measuring wheel with a cleaning agent before each measuring series was made to better represent the actual state of a tram wheel. Despite this, the CoT gradually decreased throughout the day. Therefore, we can assume that this phenomenon did not play a significant role in this study. Moreover, the measuring wheel was visually inspected after cleaning and at the end of the day, with no changes in the running band observed. However, it can be assumed that some 3rd body layer was transferred from the rail to the wheel.

The actual values of the CoT between the wheel and rail may differ from the values measured by the tribometer. The most notable is the size difference between measuring and tram wheel, making local changes in the third body layer, roughness, and hardness more pronounced. Additionally, thermal effects in smaller contacts are less significant than in larger ones, resulting in higher CoT values. Several studies [32,47] have compared different measuring approaches and demonstrated substantial discrepancies between the results of individual methods; notably, hand-pushed portable tribometers tend to overestimate friction. Nevertheless, the BUT tribometer has been shown to give reasonable values across a range of rail conditions [32]. A more important parameter that differs between tram operation and the tribometer is speed; the tribometer operates at a speed of 0.26 m/s, and research [48] has shown that higher speeds result in lower CoT values.

4. CONCLUSION

The study examined the correlation between the CoT and curve squeal produced by a tram navigating a sharp curve. This investigation utilised both an automatic noise module and a BUT rail tribometer. The noise module could distinguish between squeal noise and flange noise using real-time frequency analysis and two pre-defined frequency bands identified in the first phase. SPL rms, max SPL and duration are recorded only when the threshold in a specific band is exceeded and the noise persists for longer than 0.3 seconds. As a result, multiple records were generated during the tram's passage through the curve, which were then processed to create a single record characterizing that specific tram pass. The noise module, in combination with data from a switch, helped to identify the noisiest trams, which were removed from the operation on this line. This improved the quality of life for residents living in the surrounding area of the tram loop as occurrence of the squeal noise was reduced.

This study presents pilot results by combining this noise module and the BUT rail tribometer. The main conclusions are as follows:

- Both squeal and flange noise parameters exhibit a negative correlation with temperature and a positive correlation with RH, while the effect of AH was not observed. The strongest correlation for squeal noise is found between squeal duration and temperature, whereas it is observed between max SPL and temperature for flange noise.
- Squeal duration shows a strong positive correlation with the CoT, while the SPL rms has a weaker correlation that is not statistically significant. Additionally, max SPL does not correlate with CoT.
- CoT decreases as temperature rises and increases with higher RH. The positive correlation between CoT and RH may be attributed to the sunny day when the temperature increased throughout the day while RH decreased. AH remained almost constant compared to the rest of the month.

Acknowledgements

This work was carried out in the framework of the projects “Josef Bozek National Center of Competence for Surface Vehicles”

(TN01000026) and "Bozek Vehicle Engineering National Center of Competence" (TN02000054) that were co-financed from the state budget by the Technology Agency of the Czech Republic within the programme "National Centres of Competence".

REFERENCES

[1] R. Lewis and U. Olofsson, Wheel-rail interface handbook, 1st pub. Cambridge: Boca Raton: Woodhead: CRC Press, 2009.

[2] D. Thompson, Railway Noise and Vibration. Elsevier, 2009.

[3] A. Gidlöf-Gunnarsson, M. Ögren, T. Jerson, and E. Öhrström, "*Railway noise annoyance and the importance of number of trains, ground vibration, and building situational factors*," Noise Health, vol. 14, no. 59, pp. 190–201, 2012, doi:10.4103/1463-1741.99895.

[4] B. Griefahn, P. Bröde, A. Marks, and M. Basner, "*Autonomic Arousals Related to Traffic Noise during Sleep,*" Sleep, vol. 31, no. 4, pp. 569–577, Apr. 2008, doi: 10.1093/SLEEP/31.4.569.

[5] E. Murphy and E. A. King, Environmental Noise Pollution. Boston: Elsevier, 2014.

[6] J. Dratva *et al.*, "*Transportation Noise and Blood Pressure in a Population-Based Sample of Adults,*" Environmental Health Perspectives., vol. 120, no. 1, pp. 50–55, 2012, doi: 10.1289/ehp.1103448.

[7] P. J. Remington, "*Wheel/rail squeal and impact noise: What do we know? What don't we know? Where do we go from here?,*" Journal of Sound and Vibration, vol. 116, no. 2, pp. 339–353, 1987, doi: 10.1016/S0022-460X(87)81306-8.

[8] D. T. Eadie, M. Santoro, and J. Kalousek, "*Railway noise and the effect of top of rail liquid friction modifiers: changes in sound and vibration spectral distributions in curves*," Wear, vol. 258, no. 7–8, pp. 1148–1155, Mar. 2005, doi: 10.1016/j.wear.2004.03.061.

[9] S. S. Hsu, Z. Huang, S. D. Iwnicki, D. J. Thompson, C. J. C. Jones, G. Xie, and P. D. Allen, "*Experimental and theoretical investigation of railway wheel squeal*," Proceedings of the Institution of Mechanical Engineers, Part F: Journal of Rail and Rapid Transit, vol. 221, no. 1, pp. 59–73, 2007, doi: 10.1243/0954409JRRT85.

[10] D. J. Fourie, P. J. Gräbe, P. S. Heyns, and R. D. Fröhling, "*Frequency domain model for railway wheel squeal resulting from unsteady longitudinal creepage*," Journal of Sound and Vibration, vol. 445, pp. 228–246, Apr. 2019, doi: 10.1016/j.jsv.2018.12.014.

[11] P. A. Meehan, "*Investigation of chaotic instabilities in railway wheel squeal*," Nonlinear Dynamincs, vol. 100, no. 1, pp. 159–172, Mar. 2020, doi: 10.1007/s11071-020-05493-x.

[12] X. Liu and P. A. Meehan, "*Investigation of the effect of relative humidity on lateral force in rolling contact and curve squeal*," Wear, vol. 310, no. 1–2, pp. 12–19, Feb. 2014, doi: 10.1016/j.wear.2013.11.045.

[13] Z. Yang and Z. Li, "*Numerical modeling of wheel-rail squeal-exciting contact*," International Journal of Mechanical Sciences, vol. 153–154, pp. 490–499, 2019, doi: 10.1016/j.ijmecsci.2019.02.012.

[14] N. Hoffmann, M. Fischer, R. Allgaier, and L. Gaul, "*A minimal model for studying properties of the mode-coupling type instability in friction induced oscillations*," Mech. Res. Commun., vol. 29, no. 4, pp. 197–205, Jul. 2002, doi: 10.1016/S0093-6413(02)00254-9.

[15] D. J. Thompson, G. Squicciarini, B. Ding, and L. Baeza, "*A State-of-the-Art Review of Curve Squeal Noise: Phenomena, Mechanisms, Modelling and Mitigation*," in Notes on Numerical Fluid Mechanics and Multidisciplinary Design, vol. 139, 2018, pp. 3–41 doi: 10.1007/978-3-319-73411-8_1.

[16] O. Polach, "*Creep forces in simulations of traction vehicles running on adhesion limit*," Wear, vol. 258, no. 7–8, pp. 992–1000, 2005, doi: 10.1016/j.wear.2004.03.046.

[17] Y. Berthier, S. Descartes, M. Busquet, E. Niccolini, C. Desrayaud, L. Baillet, and M. C. Baietto-Dubourg, "*The role and effects of the third body in the wheel–rail interaction*," Fatigue & Fracture of Engineering Materials & Structures, vol. 27, no. 5, pp. 423–436, May 2004, doi: 10.1111/j.1460-2695.2004.00764.x.

[18] A. Meierhofer, C. Hardwick, R. Lewis, K. Six, and P. Dietmaier, "*Third body layer-experimental results and a model*

describing its influence on the traction coefficient," Wear, vol. 314, no. 1–2, pp. 148–154, Jun. 2014, doi: 10.1016/j.wear.2013.11.040.

[19] R. Stock, L. Stanlake, C. Hardwick, M. Yu, D. Eadie, and R. Lewis, "*Material concepts for top of rail friction management – Classification, characterisation and application*," Wear, vol. 366–367, pp. 225–232, Nov. 2016, doi: 10.1016/j.wear.2016.05.028.

[20] X. Liu and P. A. Meehan, "*Investigation of squeal noise under positive friction characteristics condition provided by friction modifiers*," Journal of Sound and Vibration, vol. 371, pp. 393–405, 2016, doi: 10.1016/j.jsv.2016.02.028.

[21] D. T. Eadie, M. Santoro, and W. Powell, "*Local control of noise and vibration with KELTRACK™ friction modifier and Protector® trackside application: an integrated solution*," Journal of Sound and Vibration, vol. 267, no. 3, pp. 761–772, Oct. 2003, doi: 10.1016/S0022-460X(03)00739-9.

[22] R. Galas, M. Omasta, I. Krupka, and M. Hartl, "*Laboratory investigation of ability of oil-based friction modifiers to control adhesion at wheel-rail interface*," Wear, vol. 368–369, pp. 230–238, Dec. 2016, doi: 10.1016/j.wear.2016.09.015.

[23] R. Galas, D. Kvarda, M. Omasta, I. Krupka, and M. Hartl, "*The role of constituents contained in water–based friction modifiers for top–of–rail application*," Tribology International, vol. 117, pp. 87–97, Jan. 2018, doi: 10.1016/j.triboint.2017.08.019.

[24] S. R. Lewis, R. Lewis, U. Olofsson, D. T. Eadie, J. Cotter, and X. Lu, "*Effect of humidity, temperature and railhead contamination on the performance of friction modifiers: Pin-on-disk study*," Proceedings of the Institution of Mechanical Engineers, Part F: Journal of Rail and Rapid Transit, vol. 227, no. 2, pp. 115–127, Mar. 2013, doi: 10.1177/0954409712452239.

[25] T. M. Beagley, I. J. McEwen, and C. Pritchard, "*Wheel/rail adhesion — the influence of railhead debris*," Wear, vol. 33, no. 1, pp. 141–152, Jun. 1975, doi: 10.1016/0043-1648(75)90230-6.

[26] R. Galas, M. Omasta , L. Shi, H. Ding, W. Wang, I. Krupka, and M.Hartl, "*The low adhesion problem: The effect of environmental conditions on adhesion in rolling-sliding contact*," Tribology International, vol. 151, no. May, p. 106521, Nov. 2020, doi: 10.1016/j.triboint.2020.106521.

[27] R. Lewis, R. S. Dwyer-Joyce, U. Olofsson, J. Pombo, J. Ambrósio, M. Pereira, C. Ariaudo, and N. Kuka, "*Mapping railway wheel material wear mechanisms and transitions*," Proceedings of the Institution of Mechanical Engineers, Part F: Journal of Rail and Rapid Transit, vol. 224, no. 3, pp. 125–137, 2010, doi: 10.1243/09544097JRRT328.

[28] Y. Zhu, Y. Lyu, and U. Olofsson, "*Mapping the friction between railway wheels and rails focusing on environmental conditions*," Wear, vol. 324–325, pp. 122–128, 2015, doi: 10.1016/j.wear.2014.12.028.

[29] Y. Zhu, H. Yang, and W. Wang, "*Twin-disc tests of iron oxides in dry and wet wheel–rail contacts*," Proceedings of the Institution of Mechanical Engineers, Part F: Journal of Rail and Rapid Transit, vol. 230, no. 4, pp. 1066–1076, May 2016, doi: 10.1177/0954409715575093.

[30] M. O. Folorunso, R. Lewis, and J. L. Lanigan, "*Effects of temperature and humidity on railhead friction levels*," Proceedings of the Institution of Mechanical Engineers, Part F: Journal of Rail and Rapid Transit, vol. 237, no. 8, pp. 1009–1024, Sep. 2023, doi: 10.1177/09544097221148236.

[31] A. Meierhofer, G. Trummer, C. Bernsteiner, and K. Six, "*Vehicle tests showing how the weather in autumn influences the wheel–rail traction characteristics*," Proceedings of the Institution of Mechanical Engineers, Part F: Journal of Rail and Rapid Transit, vol. 234, no. 4, pp. 426–435, Apr. 2020, doi: 10.1177/0954409719863643.

[32] M. Valena, M. Omasta, D. Kvarda, R. Galas, I. Krupka, and M. Hartl, "*An approach for the creep-curve assessment using a new rail tribometer*," Tribology International, vol. 191, p. 109153, Mar. 2024, doi: 10.1016/j.triboint.2023.109153.

[33] T. Maly, F. Biebl, and M. Ostermann, "*The effects of weather conditions and wheel wear on curve squeal*," Proceedings of the 23rd International Congress on Acoustics, pp. 1559–1566, 2019, doi:

10.18154/RWTH-CONV-239967.

[34] S. A. Khan, J. Lundberg, and C. Stenström, "*The effect of third bodies on wear and friction at the wheel-rail interface*," Proceedings of the Institution of Mechanical Engineers, Part F: Journal of Rail and Rapid Transit, vol. 236, no. 6, pp. 662–671, Jul. 2022, doi: 10.1177/09544097211034688.

[35] J. Kalousek, D. M. Fegredo, and E. E. Laufer, "*The wear resistance and worn metallography of pearlite, bainite and tempered martensite rail steel microstructures of high hardness*," Wear, vol. 105, no. 3, pp. 199–222, Oct. 1985, doi: 10.1016/0043-1648(85)90068-7.

[36] K. S. Baek, K. Kyogoku, and T. Nakahara, "*An experimental study of transient traction characteristics between rail and wheel under low slip and low speed conditions*," Wear, vol. 265, no. 9–10, pp. 1417–1424, 2008, doi: 10.1016/j.wear.2008.02.044.

[37] Y. Zhu, U. Olofsson, and H. Chen, "*Friction Between Wheel and Rail: A Pin-On-Disc Study of Environmental Conditions and Iron Oxides*," Tribology Letters, vol. 52, no. 2, pp. 327–339, Nov. 2013, doi: 10.1007/s11249-013-0220-0.

[38] J. L. Viesca, S. González-Cachón, A. García, R. González, A. Bernardo-Sánchez, and A. Hernández Battez, "*Influence of environmental conditions and oxidation on the coefficient of friction using microalloyed rail steels*," Proceedings of the Institution of Mechanical Engineers, Part F: Journal of Rail and Rapid Transit, vol. 235, no. 3, pp. 353–360, 2021, doi: 10.1177/0954409720925682.

[39] K. Ishizaka, S. R. Lewis, and R. Lewis, "*The low adhesion problem due to leaf contamination in the wheel/rail contact: Bonding and low adhesion mechanisms*," Wear, vol. 378–379, pp. 183–197, 2017, doi: 10.1016/j.wear.2017.02.044.

[40] B. T. White, R. Lewis, U. Olofsson, and Y. Lyu, "*The Contribution of Iron Oxides to the Wet-Rail Phenomenon*," in Proceedings of the Third International Conference on Railway Technology: Research, Development and Maintenance, 2016, vol. 110, no. September, doi: 10.4203/ccp.110.154.

[41] M. Ertz and F. Bucher, "*Improved Creep Force Model for Wheel/Rail Contact Considering Roughness and Temperature*," Vehicle System Dynamics, vol. 37, no. sup1, pp. 314–325, Jan. 2002, doi: 10.1080/00423114.2002.11666242.

[42] E. Vollebregt, K. Six, and O. Polach, "*Challenges and progress in the understanding and modelling of the wheel–rail creep forces*," Vehicle System Dynamics, vol. 59, no. 7, pp. 1026–1068, Jul. 2021, doi: 10.1080/00423114.2021.1912367.

[43] J. Wang, X. Yang, and S. Lian, "*Influence of Friction Coefficient on Wheel-rail Curve Squeal Noise*," Journal of Mechanical Engineering, vol. 54, no. 4, p. 255, 2018, doi: 10.3901/JME.2018.04.255.

[44] X. Feng, G. Chen, Q. Song, B. Dong, and W. Ren, "*A Root Cause of Curve Squeal: Self-Excited Frictional Vibration of a Wheelset–Track System*," Journal of Tribology, vol. 146, no. 6, pp. 1–20, Jun. 2024, doi: 10.1115/1.4064509.

[45] L. E. Buckley-Johnstone, G. Trummer, P. Voltr, K. Six, and R. Lewis, "*Full-scale testing of low adhesion effects with small amounts of water in the wheel/rail interface*," Tribology International, vol. 141, p. 105907, Jan. 2020, doi: 10.1016/j.triboint.2019.105907.

[46] H. Harrison, "*Producing and measuring the 3rd body layer*," in 2020 Joint Rail Conference, Apr. 2020, pp. 1–7, doi: 10.1115/JRC2020-8095.

[47] Y. A. Areiza, S. I. Garcés, J. F. Santa, G. Vargas, and A. Toro, "*Field measurement of coefficient of friction in rails using a hand-pushed tribometer*," Tribology International, vol. 82, no. PB, pp. 274–279, 2015, doi: 10.1016/j.triboint.2014.08.009.

[48] W. J. Wang, P. Shen, J. H. Song, J. Guo, Q. Y. Liu, and X. S. Jin, "*Experimental study on adhesion behavior of wheel/rail under dry and water conditions*," Wear, vol. 271, no. 9–10, pp. 2699–2705, Jul. 2011, doi: 10.1016/j.wear.2011.01.070.

APPENDIX

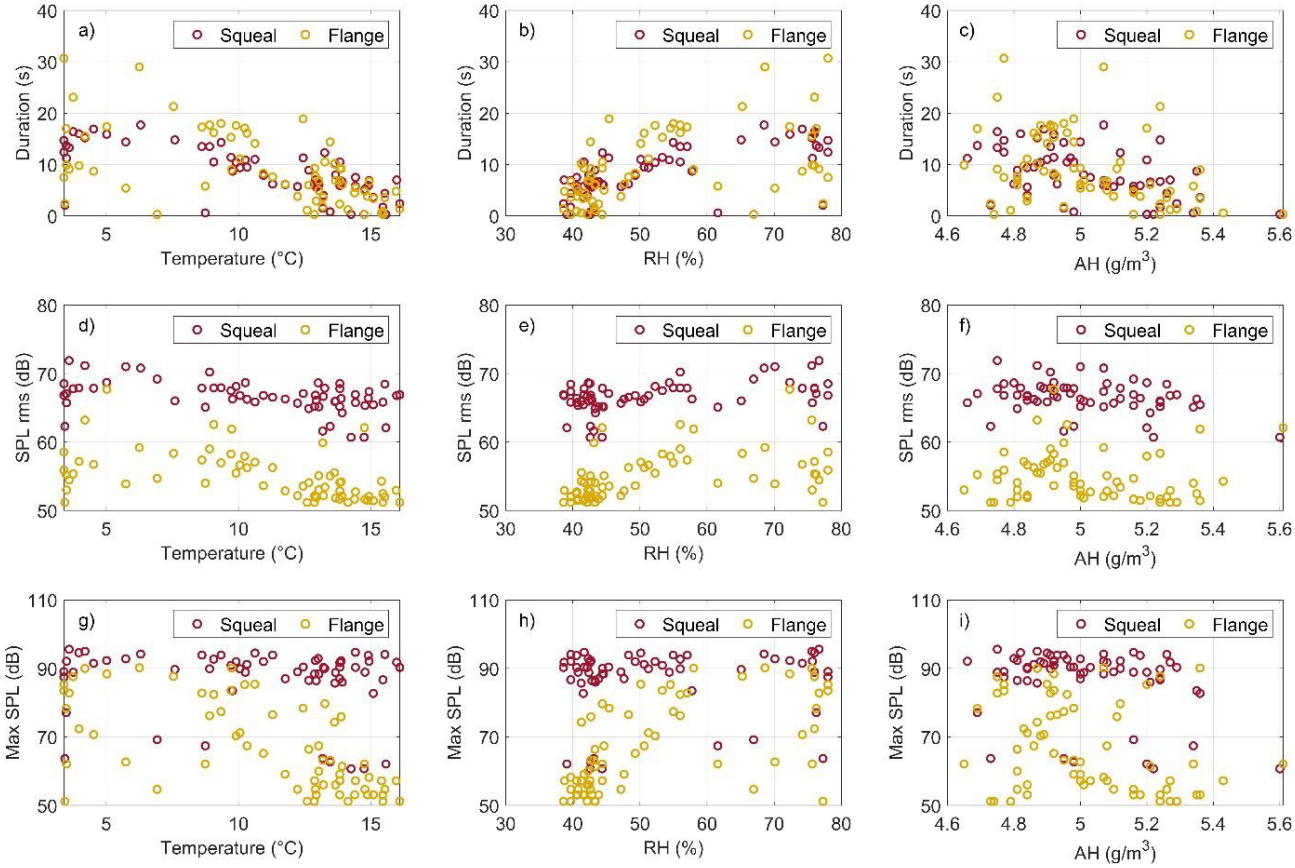

A.1 The effect of temperature, RH and AH on duration, SPL rms and max SPL for squeal and flange noise